THERMOPHYSICAL PROPERTIES OF MATERIALS

Enlarged and revised edition

G. Grimvall

North-Holland

THERMOPHYSICAL PROPERTIES
OF MATERIALS

This Page Intentionally Left Blank

THERMOPHYSICAL PROPERTIES
OF MATERIALS

Enlarged and revised edition

GÖRAN GRIMVALL

The Royal Institute of Technology
Stockholm, Sweden

1999

N·H

ELSEVIER

Amsterdam - Lausanne - New York - Oxford - Shannon - Singapore - Tokyo

This is a thoroughly revised version of my earlier (1986) book with the same title. About half the content of the previous book is kept essentially unchanged, and one quarter is rewritten and updated. The rest is replaced by completely new and extended material.

Materials science is a field with a steadily moving research front, dealing with the most modern methods and materials. At the same time, it rests on classical physics or elementary quantum mechanics that was developed a long time ago. There is also a certain amount of fashion in the choice of research problems. Many important areas of materials science were most intensely studied in the 1960's and 1970's. For instance, the investigation of phonon spectra by inelastic neutron scattering and the experimental study of properties of electrons in elemental metals peaked at that time. More recent research focuses on, e.g., new materials produced by means of "molecular engineering", and computational materials science through ab initio electron structure calculations. Another trend is the ever growing interdisciplinary aspect of both basic and applied materials science. There is an obvious need for reviews that link well established results to the modern approaches. One of the aims of this book is to provide such an overview in a specific field of materials science, namely thermophysical phenomena that are intimately connected with the lattice vibrations of solids. This includes, e.g., elastic properties and electrical and thermal transport.

Traditional textbooks in materials science or condensed matter physics often quote results in special and very simplified cases. This book attempts to present the results in such a form that the reader can clearly see their domain of applicability, for instance if and how they depend on crystal structure, defects, applied pressure, crystal anisotropy, etc. The level and presentation is such that the results can be immediately used in research. Derivations are therefore avoided.

In the selection of references one aim has been to give credit to pioneering papers, even though one often does give an explicit reference to that work in today's research. Another aim has been to quote papers that are easily accessible or of such a character that they will normally be quoted in later works and therefore are useful as a starting point in citation searches. No doubt I have failed to identify many important papers, and I apologize in advance to those authors for my lack of knowledge. Many of the figures in the book, providing illustrating examples, are taken from work done by me or in my research group. That is often for the practical reason that I already have a computer file with those figures, and it does not mean that the work of others has been ignored.

Finally, the reader I have in mind may be a graduate student in condensed matter physics, metallurgy, inorganic chemistry or geophysical materials. S/he could also be a theoretical physicist moving in the direction of applications, or a scientist in an industrial research laboratory who has to go beyond the level of undergraduate textbooks. In fact, I have been more or less involved in all these areas, and that reflects the style and choice of topics in this book.

Göran Grimvall
Stockholm, December 1998

LIST OF MOST IMPORTANT SYMBOLS

C	heat capacity
C_g	phonon group velocity
C_{har}	harmonic phonon heat capacity
$C(\mathbf{q}, s)$	sound velocity of mode $(\mathbf{q}, s)$
$C_{sound,D}$	sound velocity in the Debye model
C_D	Debye model heat capacity
C_p	heat capacity at constant pressure
C_V	heat capacity of constant volume
c	concentration of impurities, etc.
c_{ij}	elastic stiffness
$\mathbf{D}$	dynamical matrix
E	energy
E	Young's modulus
E_F	Fermi energy
e	electron charge
F	Helmholtz (free) energy
$F(\omega)$	phonon density of states
f	Fermi–Dirac distribution function
f_i	volume fraction of phase i
G	Gibbs (free) energy
G	shear modulus
H	enthalpy
K	bulk modulus
K_S	isentropic (adiabatic) bulk modulus
K_T	isothermal bulk modulus

k_B	Boltzmann's constant
$\mathbf{k}$	electron wave vector
k_F	Fermi wave number
ℓ	electron (or phonon) mean free path
M	ion (atom) mass
m	free electron mass
m_b	electron band mass
m_{th}	electron thermal mass
N	total number of atoms (ions)
N_A	Avogadro's number
$N(E)$	electron density of states
$N(E_F)$	density of states at Fermi level
n	number of electrons per unit volume
n	Bose–Einstein distribution function
p	pressure
$\mathbf{q}$	phonon wave vector
q_D	Debye wave number
$(\mathbf{q}, s)$	label on phonon state
R	position of atom (ion)
r_s	electron density parameter
S	entropy
s	label on phonon branch
s_{ij}	elastic compliance
T	temperature
T_F	Fermi temperature
T_{fus}	melting temperature
U	lattice energy
$\mathbf{u}$	displacement vector of atom (ion)
V	crystal volume
v, v_k	electron velocity
v_F	Fermi velocity
Z	ionic charge
Z	partition function

α	linear expansion coefficient
$a_{\mathrm{tr}}^2 F(\omega)$	transport coupling function
β	cubic expansion coefficient
γ	electronic heat capacity coefficient
γ_{G}	thermodynamic Grüneisen parameter
$\gamma(n)$	generalised Grüneisen parameter
$\gamma(\mathbf{q}, s)$	Grüneisen parameter of phonon mode $(\mathbf{q}, s)$
$\Delta_{2(3,4)}$	anharmonic phonon frequency shifts
$\varepsilon, \varepsilon_{\mathbf{k}}$	electron energy
$\varepsilon, \varepsilon_{ij}$	elastic strain
$\boldsymbol{\varepsilon}(\mathbf{q}, s)$	phonon eigenvector
θ_{D}	Debye temperature
$\theta_{\mathrm{D}}(n)$	generalised Debye temperature
θ_{E}	Einstein temperature
κ	compressibility
κ	label on atom in unit cell
κ	thermal conductivity
κ_S	isentropic (adiabatic) compressibility
κ_T	isothermal compressibility
κ_{el}	electron part of thermal conductivity
κ_{ph}	phonon part of thermal conductivity
$\lambda_{\mathrm{el-ph}}$	electron-phonon interaction parameter
ν	Poisson ratio
ρ	electrical resistivity
ρ	mass density of solid
σ	electrical conductivity
σ, σ_{ij}	elastic stress
τ	scattering time
τ	shear stress
Ω_{a}	atomic volume
ω	phonon frequency
$\omega(n)$	moment frequency
ω_{D}	Debye frequency
$\omega_{\mathrm{D}}(n)$	generalised Debye frequency
$\omega(\mathbf{q}, s)$	phonon frequency of mode $(\mathbf{q}, s)$

This Page Intentionally Left Blank

CONTENTS

BONDING CHARACTERISTICS

1. Introduction

Silicon and tin are elements in the same column in the Periodic Table. Silicon is known as a semiconductor, and tin is known as a metal. However, this does not imply the general rule that when silicon atoms form a condensed phase, one gets a semiconductor, and correspondingly for metallic tin. In fact, when silicon melts it becomes a metal, not very much different from liquid tin. And when ordinary (white) tin is cooled below 13 °C the stable solid phase changes from a metallic tetragonal structure to a semiconducting phase (gray tin) with the diamond structure, i.e. the same structure as that of semiconducting silicon. The dynamics of the structural change in tin is very slow, since a large energy barrier must be overcome, but the transition temperature (13 °C) is thermodynamically well defined.

Carbon is the first element of that column in the Periodic Table that contains Si and Sn. Its different properties are even more remarkable. Thermodynamically, the most stable solid phase at ambient conditions is graphite, with a lattice structure of hexagonal symmetry. The chemical bonding between the layers of carbon atoms is so weak that graphite is used as a solid lubricant. But when the carbon atoms form the diamond structure, the result is a material at the top of the hardness scale. A third form a solid carbon arises when C_{60}-molecules are stacked like balls in a lattice to form fullerenes. Many other molecules, for instance C_{72}, can also be formed.

The three examples C, Si and Sn, show how different structural arrangements of the atoms of an element can lead to very different properties. Iron is another element that occurs in different lattice structures. Below 1184 K, it has a body-centred cubic (bcc) lattice, and it is ferromagnetic below the Curie temperature $T_C = 1043$ K. Between

1

1173 K and 1660 K, the stable iron phase has a face-centred cubic (fcc) structure, and then it returns to a bcc lattice before melting at 1808 K. Many of the thermophysical properties of iron change very little when the lattice structure goes from bcc to fcc and back to bcc again. For instance, the discontinuities in the average frequency of the atomic vibrations and in the electrical resistivity are less than a few percent.

From a fundamental point of view, an account of all characteristics of a material follow from a quantum mechanical treatment of its electronic structure. In this book we will not start from such a basic level, but instead we assume that the lattice structures, the frequency spectra of atomic vibrations, etc. are known. Based on such a framework, the emphasis is on how temperature enters various physical properties. In such an approach, one also has a need to discuss some properties which refer to a static lattice at 0 K, for instance various bonding energies. We begin with those aspects.

2. Bonding and bulk modulus

Consider a certain crystal structure, with characteristic linear dimension λ, where λ can be a lattice parameter, the distance between the centres of nearest-neighbours, the cube root of the molar volume etc. The total energy $U(\lambda)$ often varies with λ as shown schematically in fig. 1.1. This curve determines three quantities which have a direct physical interpretation. The position of the minimum, λ_{min}, gives the equilibrium lattice parameter (or atomic volume etc.). The curvature at the minimum is related to the *bulk modulus K*,

$$K = -V(\partial p/\partial V) = V(\partial^2 U/\partial V^2) = V(\partial^2 U/\partial \lambda^2)(\partial \lambda/\partial V)^2,$$

$$(1.1)$$

where V is the volume of the sample and p is the pressure. In the last equality, the derivatives are evaluated at λ_{min}. The depth of the minimum gives the crystal *binding energy* U_{bind};

$$U_{bind} = U(\lambda \to \infty) - U(\lambda_{min}). \tag{1.2}$$

As an illustration, we write the energy U as a sum of a repulsive and an attractive term,

$$U(V) = AV^{-m} - BV^{-n}. \tag{1.3}$$
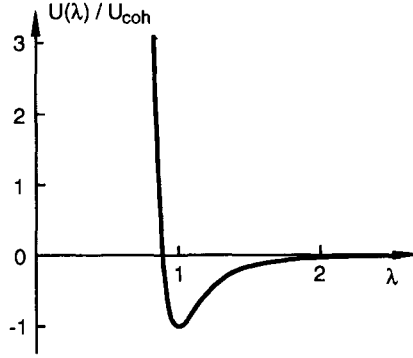
Fig. 1.1. A schematic picture of the total crystal energy $U(\lambda)$ as a function of a lattice parameter λ, here exemplified by the Lennard–Jones (1924) 6–12 potential.

Normally, the repulsive term has the most rapid variation with V, i.e. $m \gg n$. At the equilibrium volume $V = V_0$ we get

$$(\partial U / \partial V) = -mA/V^{m+1} + nB/V^{n+1} = 0, \qquad (1.4)$$

i.e. $mAV_0^n = nBV_0^m$. That yields, at $V = V_0$,

$$U_{\text{bind}} = \frac{B}{V_0^n}\left(1 - \frac{n}{m}\right) \approx \frac{B}{V_0^n}, \qquad (1.5)$$

and

$$K = V_0 \frac{Am(m-n)}{V_0^{m+2}} = V_0 \frac{Bn(m-n)}{V_0^{n+2}} \approx \frac{Bmn}{V_0^{n+1}} = \frac{Am^2}{V_0^{m+1}}. \qquad (1.6)$$

In the last steps of eqs. (1.5) and (1.6) it was assumed that $m \gg n$. The interpretation of these results is that the binding energy usually is dominated by the attractive term, i.e. it can be approximated by B/V_0^n that only contains parameters B and n from the attractive term. Analogously, the bulk modulus can be approximated by Am^2/V_0^{m+1} and is thus dominated by the repulsive term. There is also a rule of thumb that U_{bind} and K covary. From eqs. (1.5) and (1.6) we get,

$$U_{\text{bind}} \approx KV_0/(mn). \qquad (1.7)$$

This relation is not a mere coincidence (see a related discussion in Chapter 19 (§10) concerning dimensional analysis and Buckingham's

Π-theorem). The bulk modulus is further discussed in Chapters 3, 4 and 13.

In the rest of this book we will often be interested in the volume per atom (the *atomic volume*) Ω_a, rather than the specimen volume. In particular, this is convenient in the treatment of alloys and compounds, containing atoms of different sizes. The atomic volume is an averaged quantity, defined here as the total volume V of a specimen, divided by its total number of atoms N,

$$\Omega_a = V/N. \tag{1.8}$$

The *molar volume* of a compound with r atoms per formula unit is thus,

$$V_{mol} = rN_A\Omega_a, \tag{1.9}$$

where $N_A = 6.022137 \cdot 10^{23}$ mol^{-1} is Avogadro's constant.

3. Cohesive-related energies

There are no absolute values of energies in physics—only energy differences between two states, one of which can be a reference state that is given by a definition or convention. If $U(\lambda \to \infty)$ refers to separated neutral atoms of the elements, U_{bind} agrees with the normal definition of the *cohesive energy*. However, if we consider a lattice of NaCl it would be natural to let U_{bind} refer to infinitely separated ions Na$^+$ and Cl$^-$ rather than neutral atoms Na and Cl. Some authors would call that quantity the cohesive energy. It is larger than the conventional cohesive energy by the electron *ionisation energy* of Na atoms minus the *electron affinity* of Cl atoms (cf. the example below).

Another important quantity referring to binding energies is the *enthalpy of formation*, e.g. the formation of NaCl from the elements Na and Cl in their *standard states*. The standard reference state of an element is normally chosen to be in the most stable structure of that element at 298.15 K (25 °C), and at a standard pressure. Thus the standard state of Al refers to a solid in an fcc lattice, that of Hg to a liquid while that of Cl refers to the diatomic gas Cl$_2$. The standard pressure was long chosen to be 101,325 Pa (1 atm) but is now recommended to be at the slightly different value of 10^5 Pa (1 bar). Other reference temperatures than 298.15 K are occasionally used.

Thermodynamic quantities of a standard state are usually identified by the superscript °, for instance $H°$ for the enthalpy and $S°$ for the entropy. When one wants to make it clear which temperature the standard state refers to, one may use the notation $H°_{298.15}$ or $H°(298.15)$, $S°_{298.15}$ etc. Other notations for standard states are also used, for instance $°H$ or $H^{\oplus}$.

The enthalpy of formation (previously often called heat of formation) of a compound is defined as the enthalpy difference between the compound and the constituent elements, all in their standard states. It is often written $\Delta H°_f$ (or, e.g. $\Delta_f H°$). For instance,

$$\Delta H°_f(NaCl) = H°(NaCl) - H°(Na) - \frac{1}{2} H°(Cl_2). \qquad (1.10)$$

This quantity is negative since the NaCl compound is energetically more stable than the separated constituents. Obviously, the standard enthalpy of formation of an element in its standard state is zero.

The reader is warned that the conventions and reference states chosen by some authors for quantities called binding energies, cohesive energies and enthalpies (energies) of formation may not be those that are used by others. In particular, experimental values usually refer to 298.15 K or some other finite temperature, while theoretical results usually refer to 0 K.

Example: cohesive-related energies of NaCl. One of the most complete tables of thermodynamic data (Barin 1989) gives $H°_{298.15}(Na)$ = $H°_{298.15}(Cl_2) = 0$, $H°_{298.15}(NaCl) = -411.120$ kJ/mol, $H°_{298.15}(Cl) = 121.286$ kJ/mol and $H°_{298.15}(Na, gas) = 107.300$ kJ/mol, where the last two terms are for a monatomic Cl and Na gas, respectively. Another source (Tosi 1964) gives the cohesive energy $U_{coh}(NaCl) = 764.0$ kJ/mol (relative to separated ions). Furthermore, the ionisation energy for Na $\rightarrow Na^+ + e^-$ is $E_{ion} = 495.8$ kJ/mol, and the electron affinity for Cl + $e^- \rightarrow Cl^-$ is $E_{aff} = 348.7$ kJ/mol (Emsley 1989). We now write $U_{bind}(NaCl)$ as the result of a process where solid NaCl is separated into solid Na and a gas of Cl_2, then further separated into monatomic gases of Na and Cl, and a final step with ionisation of the gas atoms. Thus, $U_{bind}(NaCl) = -H°_{298.15}(NaCl) + H°_{298.15}(Cl) + H°_{298.15}(Na, gas) + E_{ion} - E_{aff} = 786.8$ kJ/mol. However, this value assumes that the (infinitely dilute) gases of Na^+ and Cl^- ions have the temperature 298.15 K,

and hence a total enthalpy $2(5RT/2) = 12.4$ kJ/mol, where R is the gas constant. Subtracting this from 786.8 kJ/mol we get $U_{bind} = 774.4$ kJ/mol at $T = 298$ K, in good agreement with the value $U_{coh} = 764.0$ kJ/mol from Tosi (1964). In fact, the calculation by Tosi follows exactly the steps of this example, but with slightly different data.

In order to predict the actual crystal structure of a solid (at $T = 0$ K), one has to compare binding energies U_{bind} (or cohesive energies U_{coh} etc.) for all conceivable lattice structures, and find the lowest U_{bind}. In practice, a comparison is often limited to the most likely structures, such as fcc, bcc, hcp and tetragonal lattices in the case of metals. At finite temperatures one should compare Helmholtz or Gibbs energies (see Chapter 7 for a treatment of temperature induced structural changes). An additional complication, that is often neglected in calculations, is that of dynamical instability. For instance, a bcc lattice may have a minimum in $U(\lambda)$ when λ corresponds to a certain value of the lattice parameter, but a further lowering of U may occur if the lattice is sheared (Chapter 4, §3). Therefore, one should consider $U(\lambda_1, \lambda_2, \ldots, \lambda_n)$, where the parameters λ_i describe all possible atomic configurations in a unit cell containing any number of atoms. Figure 1.1 corresponds to a minimum when U is a function of only one λ_i, but it does not say if this is a true minimum or, say, a saddle point in the complete λ space.

It is instructive to express some characteristic energies in the unit $k_B T_{fus}$ per atom, where T_{fus} is the melting temperature. Table 1.1 gives values for the cohesive energy $U_{coh} = H(\text{gas}) - H(\text{solid})$, relative to separated neutral atoms (Al, W, GaAs, TiC) or ions (NaCl), and the enthalpy difference ΔH_{fus} between the liquid and the solid at T_{fus} (as an example of the effect of a significant change in the atomic configuration). It also gives the quantity $E_Z \approx 9k_B\theta_D/8$ as an approximate measure of the energy associated with the zero-point lattice vibrations (Chapter 7, §2) where $\theta_D \approx \theta_D^S$ or $\theta_D(0)$ is a Debye temperature taken from the tables in Appendix I. E_{vib} is the vibrational energy if anharmonic effects are neglected, i.e. the classical value $3k_B T$ per atom at high temperatures. Data are from the JANAF thermochemical tables (1985), Barin (1989) and the above example for NaCl. The large value of ΔH_{fus} for GaAs reflects the fact the bonding in GaAs changes from covalent in the semiconducting solid state to metallic in the liquid. It should be remarked that $\Delta H_{fus}/T_{fus}$ is the entropy of fusion (see Chapter 12). The quite small variation among U_{coh} of different materials, when

Table 1.1

Some characteristic energies, expressed in the unit $k_B T_{fus}$ per atom

	U_{coh}	ΔH_{fus}	E_{vib}	E_Z
Al (T_{fus} = 933 K)	42.5	1.38	3	0.48
W (T_{fus} = 3680 K)	27.8	1.16	3	0.10
GaAs (T_{fus} = 1511 K)	25.9	3.50	3	0.24
TiC (T_{fus} = 3290 K)	25.1	1.30	3	0.28
NaCl (T_{fus} = 1074 K)	42.7[a]	1.58	3	0.29

[a] U_{coh} = 34.4 if NaCl is separated into neutral atoms instead of ions.

expressed in $k_B T_{fus}$ per atom, is a significant feature (cf. Chapter 19, §10).

4. Simple models of cohesive properties

4.1. Introduction

If we know the energy $U(\lambda)$, for instance expressed through a pairwise potential describing the interaction between the atoms (ions), we can solve for the atomic volume Ω_a at the energy minimum and also find the corresponding bulk modulus K and binding energy U_{bind}. In the early days of solid state physics, this was an important field of research. One was looking for simple mathematical descriptions, in particular for ionic compounds. Modern approaches to cohesive properties, including atomic volumes and bulk moduli, rely on large quantum mechanical calculations of the electronic structure. However, simple mathematical models may serve to give an insight into trends. We now consider such models for ionic compounds, simple (i.e. free-electron-like) and transition metals, and make a brief comment on semiconductors.

4.2. Ionic compounds

The cohesive properties of ionic compounds, in their main features, can be explained in terms of classical physics. This is in contrast to the metals, where quantum mechanics plays a major role. We assume that

two ions, i and j, interact through a potential (e.g. Born and Huang 1954),

$$\phi(r) = e^2 Z_i Z_j / r + B/r^n. \tag{1.11}$$

The first term is the Coulomb interaction between charges $Z_i e$ and $Z_j e$. When summed over the lattice, it gives the Madelung energy E_M, expressed through the *Madelung constant* α_R. (The subscript R means that $E_M \sim \alpha_R / R$, where R is the nearest-neighbour distance. One may also define a Madelung constant α_a such that $E_M \sim \alpha_a / a$, where a is the lattice parameter, or the cube root of the atomic volume Ω_a, and yet another type, α_C, is introduced in §4.3.) The last term in eq. (1.11) represents a repulsive interaction that prevents the ions from coming too close to each other. We assume that it acts only between the nearest-neighbours of unlike ions. As an example, consider diatomic compounds (e.g. NaCl, MgO). Let R be the shortest distance between anions and cations. The total energy of a lattice with ν nearest unlike neighbours is (per stoichiometric unit, and with $|Z_i| = |Z_j| = Z$)

$$U_{\text{tot}} = -\alpha_R (Ze)^2 / R + \nu B / R^n. \tag{1.12}$$

The equilibrium distance R_0 is obtained from $\partial U_{\text{tot}} / \partial R = 0$;

$$(R_0)^{n-1} = \nu B n / [\alpha_R (Ze)^2]. \tag{1.13}$$

The binding energy $U_{\text{bind}} = -U_{\text{tot}}(R_0)$ depends on three quantities; R_0, α and νB. If eq. (1.13) is used to eliminate νB, we obtain

$$U_{\text{bind}} = \frac{\alpha_R (Ze)^2}{R_0} \left(1 - \frac{1}{n} \right). \tag{1.14}$$

For many ionic compounds, the exponent $n \sim 8$ to 10, i.e. $1 - 1/n \approx 1$. The electrostatic energy, taken between point charges, is therefore by far the most important contribution to the binding energy of ionic crystals, in line with the arguments in §2. By proceeding as outlined in §2, we obtain for the bulk modulus

$$K = \frac{\alpha_R (Ze)^2 (n-1)}{18 R_0^4} = \frac{\alpha_R (Ze)^2 (n-1)}{18 \Omega_a^{4/3}}. \tag{1.15}$$
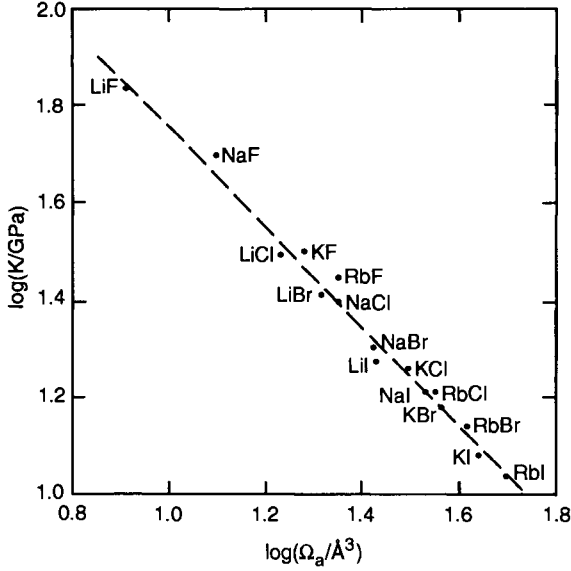
Fig. 1.2. The experimental bulk modulus K of alkali halides in the NaCl-type crystal structure, as a function of the volume per atom, Ω_a.

In the last step we specialised in the NaCl-type lattice, for which $\Omega_a = R_0^3$.

On the basis of the crude model (eq. (1.15)), we can now understand the variation of the bulk modulus of alkali halides crystallising in the NaCl-type structure, as a function of the atomic volume Ω_a, (fig. 1.2). K is obtained here as $(c_{11} + 2c_{12})/3$ with c_{ij} from the Landolt–Börnstein tables (Every and McCurdy 1992). The dashed line in the figure is just a guide to the eye. Its slope corresponds to $K \sim \Omega_a^{-1.02}$, and not $\sim \Omega_a^{-4/3}$ as suggested by eq. (1.15). Considering the crudeness of the model, for instance the neglect of interactions between next nearest-neighbours, we should not expect a better account of the bulk modulus.

4.3. Free-electron-like metals

The simplest representation of a metal is the jellium model. The ion charges are "smeared out" into a uniform positive background. The distribution of the conduction electrons is also spatially uniform. Since there is a charge neutrality everywhere, this system has no electrostatic energy. Let there be N atoms in a volume V. The only energy that varies

with the atomic volume $\Omega_a = V/N$ in this case is the kinetic energy of the electrons (Appendix B),

$$\langle E_{\text{kin}} \rangle = 2.210 Z r_s^{-2} \quad [\text{Ry}]. \tag{1.16}$$

Here, and in the rest of §4, energies refer to an average per atom. The dimensionless parameter r_s is a measure of the electron number density, $r_s a_0$ being the radius of a sphere of volume Ω_a/Z, and a_0 the Bohr radius, i.e. $(4\pi/3)(a_0 r_s)^3 = \Omega_a/Z$. Z is the number of valence electrons contributed by each ion, e.g. $Z = 1$ for the alkali metals, $Z = 3$ for Al and $Z = 4$ for Pb, in their free-electron descriptions. The energy is expressed in Rydberg units $(1 \text{ Ry} = me^4/(8\pi\epsilon_0\hbar^2); 1 \text{ mRy/atom} = 1.313$ kJ/mol). See Appendices B and H for details.

Because the energy (eq. (1.16)) is lowered if the system is allowed to expand, i.e. if r_s increases further, it represents a repulsive term. We need also an attractive term to get a minimum in the total energy, i.e. cohesion. Its essential physical origin is the fact that the positive charge is not uniformly distributed, but approximately concentrated in positive ionic charges $+Ze$ centred at the lattice points. It can not be described accurately in as simple a form as the kinetic energy. We therefore do not derive a closed-form expression for the binding energy, but turn to the bulk modulus K. Following the approach in §2, we consider only the repulsive term (eq. (1.16)) and get

$$K = \frac{\hbar^2}{4\pi(4/9\pi)^{2/3}m(r_s a_0)^5} = \left(\frac{6.13}{r_s}\right)^5 \cdot 10^9 \ [\text{N m}^{-2}]. \tag{1.17}$$

Here r_s refers to the actual value for the metal considered. Figure 1.3 shows experimental values for the bulk modulus, versus the parameter r_s, with K calculated from the single-crystal elastic coefficients c_{ij} (Every and McCurdy 1992) using the methods described in Chapter 18 (§3). For Li, Rb and Cs, low temperature c_{ij} are used to suppress the effects of anharmonic softening. The dashed line is a guide to the eye, and corresponds to $K \sim r_s^{-3.5}$. Considering the extreme simplicity of the model, with K arising entirely from the kinetic energy of a free-electron gas, we should not expect a better account of the data in fig. 1.3.

It is seen in fig. 1.3 that r_s varies considerably even among free-electron-like metals of the same valency, for instance among the alkali
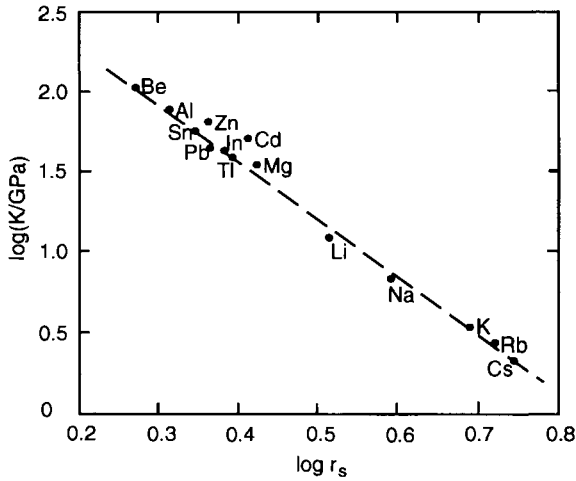
Fig. 1.3. The bulk modulus of some free-electron-like metals as a function of the electron density expressed through the parameter r_s, plotted as log K versus log r_s.

metals that are all described by $Z = 1$. Obviously, the atomic volume, Ω_a, depends crucially on the "size" of the ions (e.g. the ion Na^+, consisting of the nucleus and the filled electron shells). However, the energy does not depend much on the precise lattice configuration, for a given ion. This can be illustrated by considering the Coulomb energy E_C (per ion), when ions of charge $+Ze$ interact with a rigid uniform electron gas with a density given by r_s. Then

$$E_C = -\alpha_C Z^{5/3} Z r_s^{-1} \text{ [Ry].} \tag{1.18}$$

Here, α_C is a Madelung constant given in table 1.2. The fact that α_C depends so weakly on the configuration of the positive point charges is consistent with the experimental and theoretical result that the atomic volume is the same within about 1% for different lattice structures (e.g. bcc, fcc and hcp lattices) for a certain free-electron-like metal (Rudman 1965). The atomic volume of alloys is further discussed in Chapter 19, in connection with Vegard's (1921) rule.

Finally, it must be stressed that one cannot tell from the element alone, i.e. without a quantum mechanical calculation, what is the electron structure in the solid. For instance, tin is rather free-electron-like in the metallic tetragonal lattice structure (β-Sn or white tin), but is a semiconductor when crystallising in the diamond-type lattice struc-

Table 1.2

The Madelung constant α_C

Lattice structure		α_C
Simple cubic		1.760^a
Body-centred-cubic		1.79186^b
Face-centred-cubic		1.79172^b
Hexagonal close-packed	$(c/a = 1.633)$	1.79168^a
	$(c/a = 1.5)$	1.78998^c
	$(c/a = 1.8)$	1.78909^c
Diamond		1.671^c
Tetragonal (white tin)	$(c/a = 0.554)$	1.77302^d

[a]Carr (1961).
[b]Fuchs (1935).
[c]Harrison (1966).
[d]Ihm and Cohen (1980).

ture (α-Sn or gray tin). The atomic volume of Sn is 27% larger in the semiconducting state.

4.4. Transition metals

The d-electrons play a major role in the transition metals. We will use a simple model (Friedel 1969) that neglects the s- and p-electrons altogether. Let the d-state of an isolated atom have the energy E_d^0 relative to some reference level. When the atoms are brought together in a solid, the d-level broadens into a band described by an electron density-of-states $N_d(E)$ (per atom and spin direction). If a metal has n_d d-electrons, the cohesive energy (per atom) becomes

$$U_{\text{coh}} = n_d E_d^0 - 2 \int_{E'}^{E_F} N_d(E) E \, dE, \tag{1.19}$$

where E' is the bottom of the d-band and E_F is the Fermi level. The factor of 2 in the integral comes from summation over the two-spin directions. Friedel (1969) assumed that $N_d(E)$ is rectangular in shape, with a width W_d and a "centre of gravity" shifted from the atomic level E_d^0 to E_d (figs. 1.4 and 1.5). The total number of d-states is 10, which fixes the height of $N_d(E)$ to $5/W_d$, when $N_d(E)$ refers to one spin direction. Then
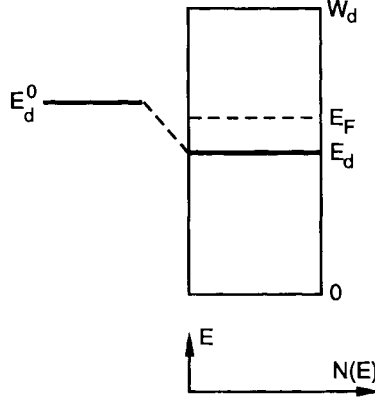
Fig. 1.4. A schematic picture of how an electron d-level shifts from its value E_d^0 in an atom and broadens into a band of width W_d in the solid.
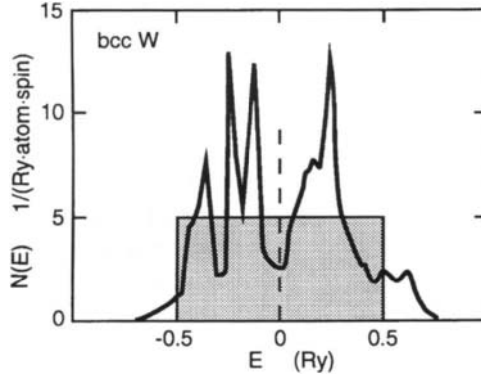
Fig. 1.5. The electron density of states $N(E)$ for a real transition metal (bcc W; from Einarsdotter et al. (1997)) and a representation through Friedel's rectangular model density of states.

$$U_{\mathrm{coh}} = (E_d^0 - E_d)n_d + (1/20)W_d n_d(10 - n_d). \tag{1.20}$$

Neglecting the fact that W_d, E_d and E_d^0 vary with n_d, which is a crude but reasonable approximation in our context, this model predicts that the cohesive energy varies parabolically with n_d, i.e. with the d-band filling. Typically, in the $4d$-transition metal series, $W_d = 0.5$ [Ry] and $E_d^0 - E_d < 0.1$ [Ry]. The model neglects any structural dependence of $N_d(E)$ but this is not too serious since U_{coh} is an integrated quantity of $N_d(E)$ and the most important factor is the width W_d of $N_d(E)$.
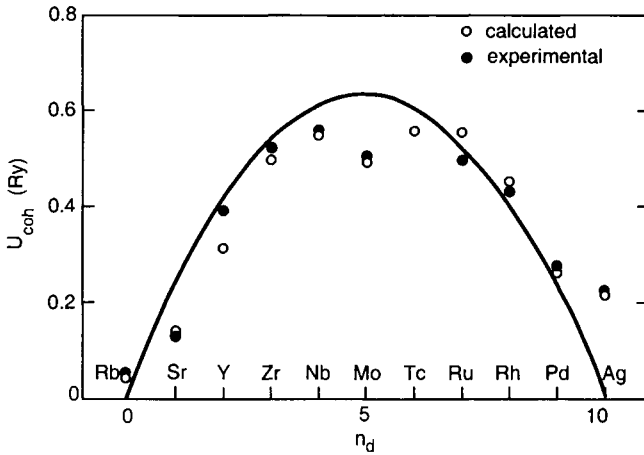
Fig. 1.6. The cohesive energy U_{coh} (solid curve) calculated from eq. (1.20) when $E_d^0 = E_d$ and $W_d = 0.5$ Ry, and plotted versus the position of the metal in the Periodic Table. Filled circles are experimental values and open circles are results from an early and very influential ab initio electron structure calculation (Moruzzi et al. 1977, 1978).

As is seen in fig. 1.6, the cohesive energy calculated in this approx-imate manner is in qualitative agreement with experiments. Since the model makes no reference to how U_{coh} changes with volume, we cannot estimate the atomic volume. Such considerations should use the fact that W_d increases with decreasing volume that corresponds to attractive forces between the atoms. This is balanced by the repulsive force arising when the conduction electrons (s- and p-electrons) are forced into the ion cores on compression. Thus, the s- and p-electrons are important in determining the atomic volume and the bulk modulus, but not for the cohesive energy, again in line with the arguments in §2. There, the balance between the repulsive and attractive forces also was found to imply a covariation between K and U_{coh}. Such a connection holds also for transition metals, as seen by comparing fig. 1.6 and 1.7. However, there is no simple correlation between the bulk modulus K and the atomic volume Ω_a in contrast to the behaviour for simple metals, ionic and covalent solids.

Example: relative stability of fcc and bcc structures. In pioneering work by Pettifor (1970), Skriver (1985) and others, the difference in cohesive energy between the fcc, hcp and bcc lattice structures of transition met-als was obtained from electron structure calculations. Such theoretical
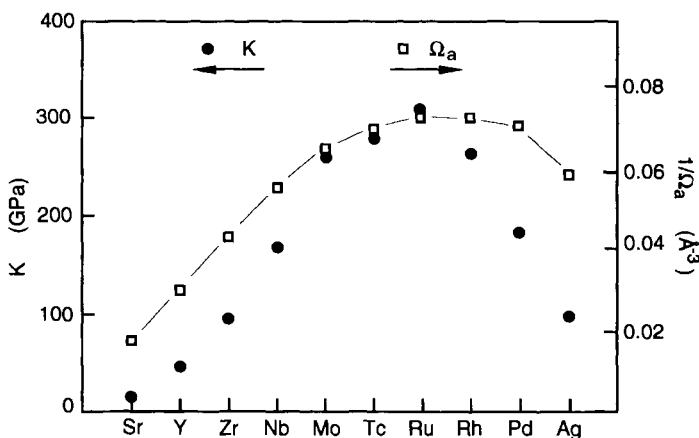
Fig. 1.7. The experimental bulk modulus K (filled symbols, left scale), obtained as in Chapter 18 with c_{ij} from Every and McCurdy (1992), plotted versus the position of the metal in the Periodic Table. The figure also shows the experimental volume per atom (open symbols, right scale), from Rudman (1965).

results were first thought to be less accurate because for some elements they seemed not to agree with the semiempirical results (cf. fig. 1.8). It is now well established that ab initio electron structure calculations can give very reliable results for the cohesive energy of transition metals in various hypothetical structures. The difference between such data and the semiempirical values that are derived, e.g. from the fitting of thermodynamic functions to alloy phase diagrams, is not physically significant. Discrepancies between the two approaches to the cohesive energy of metastable structures may arise when a metastable structure is in fact dynamically unstable (see also Chapter 4 (§3), and a review by Grimvall 1998).

It was noted above that for free-electron-like metals, the bulk modulus K varied significantly with the atomic volume Ω_a when different elements were compared, but Ω_a did not vary much for different metallic structures of the same element. As seen in fig. 1.7, there is no corresponding close relation between K and Ω_a for the transition metals. However, like the case of simple metals (§4.3) it is a good rule of thumb for the transition metals, that Ω_a does not depend much on the lattice structure as long as the electronic structure is not much changed. This is further dealt with in Chapter 19 (§2).
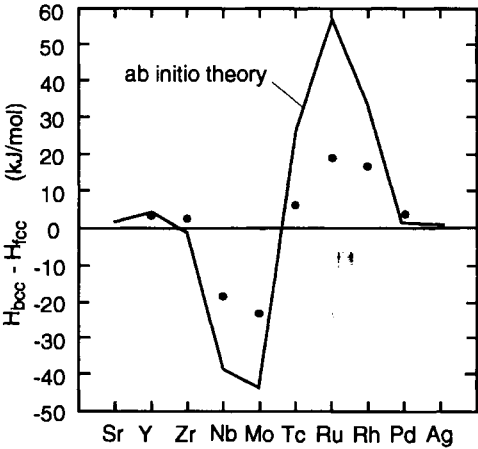
Fig. 1.8. The difference in cohesive energy between the fcc and bcc lattice structures of
4d-transition metals (solid line; after Skriver 1985) and the same quantity obtained by
the often used semiempirical estimate using Miedema's approach (symbols; Miedema
and Niessen 1983). Where the two sets of data disagree significantly, they do in fact not
reflect the same physical quantity.
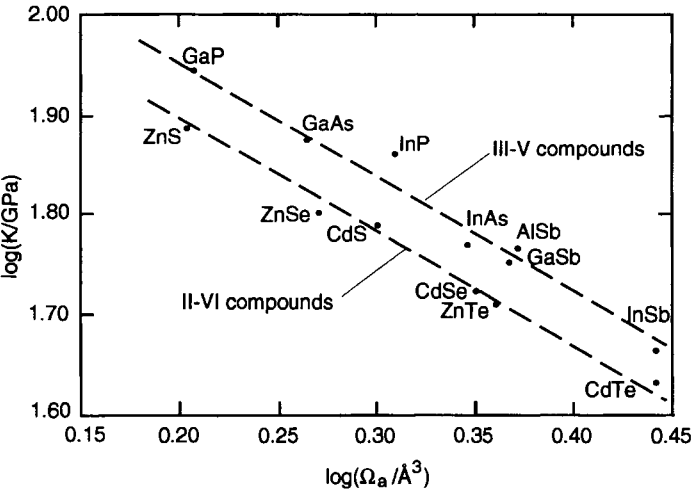
Fig. 1.9. The experimental bulk modulus $K = (c_{11} + 2c_{12})/3$, with c_{ij} from Every
and McCurdy (1992), as a function of the atomic volume Ω_a; plotted as log K versus
log Ω_a.

4.5. Semiconductors

The bonding in semiconductors cannot be described quantitatively by the simple approaches we have discussed for ionic solids, free-electron-like metals and transition metals. However, one can argue (Cohen 1985, 1988) that the bulk modulus varies approximately inversely with a power of the atomic volume. Consider the *Ansatz*

$$K = \frac{K^*}{\Omega_a^p}. \tag{1.21}$$

Figure 1.9 shows that this gives a good fit when the exponent $p \approx 7/6$. Hence, K varies as $a^{-3.5}$ within a class of materials with the same lattice structure, where a is a lattice parameter. The parameter K^* takes different values for group IV, III–V and II–VI compounds.

CRYSTAL DEFECTS

1. Introduction

Vacancies and some other point defects may be thermally generated and therefore present in thermal equilibrium. Other defects have such high formation energies that their presence depends on the detailed pre-history (cold-working, annealing etc.) of the sample. Since we are interested in the temperature dependence of phenomena related to the defects, it is illuminating to express the magnitude of some characteristic energies in units of $k_B T_{fus}$, where k_B is Boltzmann's constant and T_{fus} is the melting temperature; see table 2.1, based on Grimvall and Sjödin (1974).

Henderson (1972) has written an elementary introduction on various defects in crystalline solids, and Watts (1977) gives a somewhat more advanced account, with emphasis on non-metals, while Varotsos and Alexopoulos (1986) treat their own approach to point defects in great depth. Grain boundaries are dealt with in Chadwick and Smith (1976) and Humphreys and Hatherly (1996). There are a large number of review articles, e.g. by Seeger (1973), Kovács and El Sayed (1976) and Wollenberger (1996) who cover point defects, mainly in metals. Extended defects in materials have been reviewed by Friedel (1980).

2. General thermodynamic relations

2.1. Formation energy, enthalpy, entropy and volume

The *formation energy*, E_{def}, of a defect is the energy difference between a crystal with a defect, and a perfect crystal, containing the same number of atoms. The *formation volume* V_{def} is the difference in volume

Table 2.1

Some characteristic energies of defects in elements, in units of $k_B T_{fus}$

Vacancy formation energy	8–13
Activation energy of self-diffusion	15–19
Heat of fusion[a]	0.9–1.3
Surface energy[b]	5–10
Grain boundary energy[b]	3–6

[a] Per atom.
[b] Per area of one atom (in a monolayer).

between the two crystals. Similarly, one can define the thermodynamic quantities H_{def}, F_{def}, G_{def} and S_{def}. The usual thermodynamic relations for the enthalpy H, the Helmholtz energy F etc., are also valid for quantities like H_{def} and F_{def}, if they involve derivatives with respect to intensive variables, such as p and T. For instance, the formation volume can be written as

$$V_{def} = \left(\frac{\partial G_{def}}{\partial p} \right)_T . \tag{2.1}$$

One has to be careful in the use of relations involving derivatives with respect to extensive variables, such as the volume V (Howard and Lidiard 1964, Levinson and Nabarro 1967).

2.2. Defect concentration in thermodynamic equilibrium

The defects present in a state of complete thermodynamic equilibrium must have low formation energies E_{def}. This limits us to point defects and small aggregates of them. Let N be the number of lattice sites. The number of defects in equilibrium is

$$N_{def} = N \exp(S_{def,tot}/k_B) \exp(-H_{def}/k_B T). \tag{2.2}$$

This expression assumes that $N_{def} \ll N$ and that interactions between defects can be neglected. At ambient pressure, we can put $p = 0$ so that $H_{def} = E_{def}$. The total entropy $S_{def,tot}$ has two parts:

$$S_{def,tot} = S_{geom} + S_{def}. \tag{2.3}$$
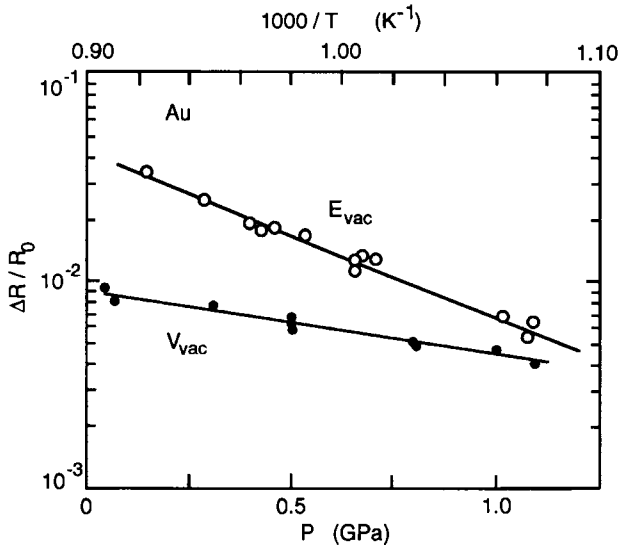
Fig. 2.1. The quenched-in electrical resistance in gold plotted as $\log(\Delta R/R_0)$ versus $1/T$ (upper scale) and p (lower scale) yields straight lines with slopes from which the vacancy formation energy E_{vac} and formation volume V_{vac} can be obtained. Data from Huebener and Homan (1963).

$S_{geom} = k_B \ln(z_{def})$ is a temperature-independent geometrical term, z_{def} being the number of configurations of a defect associated with a particular site in the lattice, and with proper consideration of double counting. We normally encounter it as a term $\exp(S_{geom}/k_B) = z_{def}$. If there are several atoms per primitive cell, one may have to assign different values H_{def}, S_{geom} and S_{def} to different configurations or lattice sites.

2.3. Defect parameters from an Arrhenius plot

A physical quantity showing an exponential temperature dependence such as in eq. (2.2) is said to obey an *Arrhenius law*. Then H_{def} (or E_{def}) can be determined from a plot of $\ln(N_{def}/N)$ versus $1/k_B T$ which yields a straight line with the slope $-H_{def}$ (cf. fig. 2.1). One has

$$-\frac{\partial \ln(N_{def}/N)}{\partial(1/k_B T)} = T^2\left(\frac{\partial S_{def}}{\partial T}\right) - T\left(\frac{\partial H_{def}}{\partial T}\right)$$
$$+H_{def} = H_{def}(T). \tag{2.4}$$

Here we have used the thermodynamic relation $T(\partial S/\partial T)_p =$ $(\partial H/\partial T)_p$. Thus, a meaningful formation enthalpy $H_{\text{def}}(T)$, or formation energy $E_{\text{def}}(T)$, can be obtained even when these quantities are temperature dependent, so that the Arrhenius plot is curved.

From eqs. (2.1) and (2.4) we obtain the formation volume

$$
V_{\text{def}} = \left(\frac{\partial G_{\text{def}}}{\partial p}\right)_T = \left(\frac{\partial (H_{\text{def}} - T S_{\text{def}})}{\partial p}\right)_T
$$
$$
= -k_B T \left(\frac{\partial \ln(N_{\text{def}}/N)}{\partial p}\right)_T. \tag{2.5}
$$

A plot of $\ln(N_{\text{def}}/N)$ versus p thus gives the formation volume V_{def} (Levinson and Nabarro 1967).

Example: temperature-dependent $H_{\text{def}}(T)$ for vacancies. We will study the variation of $H_{\text{def}}(T)$ with T and make an expansion in T near the melting temperature T_{fus}:

$$
H_{\text{def}}(T) = H_{\text{def}}(T_{\text{fus}}) + (T - T_{\text{fus}})\left(\frac{\partial H_{\text{def}}}{\partial T}\right)_{p;\,T=T_{\text{fus}}}
$$
$$
= H_{\text{def}}(T_{\text{fus}}) + (T - T_{\text{fus}})T_{\text{fus}}\left(\frac{\partial S_{\text{def}}}{\partial T}\right)_{p;\,T=T_{\text{fus}}}. \tag{2.6}
$$

For harmonic lattice vibrations, and in the high temperature limit, we have (cf. eq. (9.21))

$$
S_{\text{def}} = 3N k_B \ln[\theta(0)/\theta_{\text{def}}(0)], \tag{2.7}
$$

where $\theta_{\text{def}}(0)$ and $\theta(0)$ are "entropy Debye temperatures" for the crystal with and without a vacancy (cf. Chapter 9, §4.5). From eq. (2.7), $(\partial S_{\text{def}}/\partial T)_p = 0$. To obtain a temperature-dependent H_{def}, anharmonic effects must be included. If this is done within the quasiharmonic model, and with equal Grüneisen parameters for the perfect and the defect state, we still obtain $(\partial S_{\text{def}}/\partial T)_p = 0$. One has to go beyond such a simple description to get a temperature-dependent H_{def} (Girifalco 1967, Levinson and Nabarro 1967).

2.4. *Constant pressure and constant volume*

Sometimes it is essential to distinguish between quantities considered at constant volume (subscript V) and at constant pressure (subscript p). Experiments are usually performed at constant pressure ($p \approx 0$) but model calculations may be more conveniently carried out at constant volume. If $(V_{\text{def}})_p$ is the increase in the specimen volume when a certain defect is introduced at constant pressure, and $(p_{\text{def}})_V$ is the increase in pressure if a defect is added at constant volume, they are related by (K_T is the isothermal bulk modulus)

$$(V_{\text{def}})_p K_T = (p_{\text{def}})_V V, \tag{2.8}$$

with similar relations for other thermodynamic properties of defects (Catlow et al. 1981).

3. Vacancies

Here we mainly have in mind thermally generated vacancies in elements and alloys. The formation energy $E_{\text{def}} = E_{\text{vac}}$ of a *monovacancy* is the energy difference between a perfect lattice with N occupied lattice sites and a similar lattice with $N+1$ sites, one of which is void. The formation volume V_{def} of a monovacancy is the difference in volume between these two crystals. The concentration of monovacancies in a monatomic solid is, in thermal equilibrium and at $p = 0$,

$$c_{\text{vac}} = \exp(S_{\text{vac}}/k_B) \exp(-E_{\text{vac}}/k_B T), \tag{2.9}$$

where S_{vac} is an entropy term related to changes in the vibrational spectrum of the lattice, eq. (9.28). Since there is only one configuration (orientation etc.) for a vacancy, we have $z_{\text{def}} = 1$ and, hence, $S_{\text{geom}} = 0$. Under a pressure p, E_{vac} in eq. (2.9) is replaced by $E_{\text{vac}} + p V_{\text{vac}}$. The role of vacancy formation in the heat capacity of solids close to the melting point is considered in Chapter 11, §3.

The Landolt–Börnstein tables (Ullmaier 1991) give values of E_{vac} and S_{vac} derived by various experimental techniques. While different sources typically agree in their values for E_{vac} to within $\sim 10\%$, the values for S_{vac} are very uncertain. It is not unusual that quoted S_{vac}/k_B for a certain element range from, e.g. 1 to 2. Chapter 19 (§7) deals

Table 2.2

Vacancy defect parameters for Cu and Al

	c_{vac} $(T = T_{fus})$	E_{vac} (eV)	$E_{vac}/k_B T_{fus}$	S_{vac}/k_B
Cu	$(0.76 \pm 0.03) \times 10^{-3}$	1.19 ± 0.03	10.2	3.0 ± 0.3
Al	0.93×10^{-3}	0.75	9.3	2.4

with the estimate of E_{vac} and other defect energies from the melting temperature T_{fus}.

Example: vacancies in Cu and Al. Vacancies increase the length L of a specimen but do not affect the lattice parameter a, as measured by X-ray methods. Simmons and Balluffi (1960) used this fact to derive the vacancy formation energy of Al from the relation

$$c_{vac} = 3 \left\{ \frac{\Delta L}{L} - \frac{\Delta a}{a} \right\}. \tag{2.10}$$

Here ΔL includes the effect of vacancies as well as ordinary thermal expansion, while Δa only includes the thermal expansion. This method has been refined by Hehenkamp et al. (1992), to get c_{vac}, E_{vac} and S_{vac} with higher accuracy than obtained in other, similar or different, experiments. Table 2.2 gives some results (Hehenkamp 1994). One should note that eq. (2.10) holds even when there are relaxations around the defects (Simmons and Balluffi 1960, Seeger 1973).

Example: vacancies in gold under pressure. If a specimen is quenched from a high temperature T, the residual resistance $R_0 + \Delta R$ of the quenched sample has a part R_0 caused by impurities and a part ΔR arising from the N_{def} quenched-in thermal defects (vacancies). Since ΔR is proportional to N_{def}, a plot of $\ln(N_{def}/N)$ can be replaced by a plot of $\ln(\Delta R/R_0)$. Huebener and Homan (1963) measured ΔR for vacancies in gold at different temperatures and pressures. Figure 2.1 shows their results. From the slope of the straight lines one obtains H_{vac}

= 0.98 eV and $V_{vac} = 9.19 \times 10^{-30}$ m^3 = 0.53Ω_a, where Ω_a is the atomic volume. H_{vac} refers to $p = 0.18$ GPa. Then $pV_{vac} = 0.01$ eV is negligible.

Example: non-stoichiometric carbides and nitrides. Several transition-metal carbides and nitrides crystallise in an NaCl-type lattice with a non-stoichiometric composition VC$_x$ etc., where typically x is ~0.8–0.9. Such vacancies on the non-metal sites do not represent thermal equilibrium, even at high temperatures. Instead, the composition of the ground state, i.e. the state of lowest energy at $T = 0$ K, has $x < 1$ as was shown in total-energy electron structure calculations for VC$_x$ (Ozoliņš and Häglund 1993).

4. Divacancies and vacancy clusters

Divacancies and vacancy clusters can be treated by a direct generalisation of the approach given in §3. The concentration of *divacancies* at thermal equilibrium, in a monatomic solid, may be written

$$c_{divac} = (z/2)(c_{vac})^2 \exp(\Delta S_{divac}/k_B) \exp(E_{divac,bind}/k_B T). \quad (2.11)$$

Here c_{vac} is the monovacancy concentration, $E_{divac,bind}$ is the binding energy between two vacancies (the formation energy of a divacancy is $2E_{vac} - E_{divac,bind}$) and ΔS_{divac} is the change in the vibrational entropy when two separate vacancies form a divacancy. If a certain vacant site has z equivalent neighbouring lattice sites, one can form z differently oriented divacancies. After correction by a factor of 1/2 to avoid double counting, we obtain the prefactor $\exp(S_{geom}/k_B) = z/2$ in eq. (2.11). There may be configurations with different $E_{divac,bind}$ and S_{divac}. Then the total concentration of divacancies is a sum of terms such as the righthand side of eq. (2.11).

In a bcc lattice, the nearest sites for an adjacent vacancy are at $a(\pm 1/2, \pm 1/2, \pm 1/2)$, where a is the lattice parameter. Hence, $z = 8$ and $S_{geom} = k_B \ln 4 \approx 1.4k_B$. There may also be divacancies where the adjacent vacancy is at the second nearest-neighbour position in the lattice, i.e. at $a(\pm 1, 0, 0)$ and equivalent sites in a bcc lattice. Then $z = 6$ and $S_{geom} = k_B \ln 3 \approx 1.1k_B$. Generalisations to other configurations or lattices are obvious. For instance, in an hcp lattice one may have to distinguish between divacancies lying in, or perpendicular

to, the basal (hexagonal) lattice plane. In fcc lattices, $E_{\text{divac,bind}}$ may be so large ($\gtrsim k_B T$) for a pair of vacancies occupying the next-nearest lattice positions, that a term corresponding to this configuration must also be included in eq. (2.11). Typically, $E_{\text{divac,bind}}/k_B T_{\text{fus}} \sim 1$–2. Then, very roughly, about 0.1–0.01 of the vacant sites are associated with divacancies near $T = T_{\text{fus}}$.

Atoms may also leave their regular lattice positions and form interstitials. The thermodynamic description is similar to that of vacancies. See Smargiassi and Madden (1995) for a treatment of interstitials in sodium.

A liquid is stabilised relative to the solid phase by the large entropy of spatial disorder. There is some evidence for a similar stabilisation of a liquid-like structure surrounding vacancies or interstitials, and involving near-neighbours to the original point defect (Gösele et al. 1983, Pokorny and Grimvall 1984, Stern and Ke Zhang 1988).

5. Interactions between point defects and other defects

Consider a dilute substitutional solid solution, with concentration c_{sol} of solute atoms. The coordination number of the lattice is z. The equilibrium number of vacancies may be higher in the alloy than in the pure host, because vacancies bind to impurities and are thus associated with a lowered formation energy. The equilibrium concentration of vacancies in the alloy is given by *Lomer's equation*;

$$c_{\text{vac}} = (c_{\text{vac}})^0[1 - zc_{\text{sol}}] + (c_{\text{vac}})^0 zc_{\text{sol}} \exp[G_{\text{vac-sol}}/k_B T], \quad (2.12)$$

where $G_{\text{vac-sol}}$ is the Gibbs energy of binding between a vacancy and a solute atom. Often, the entropy term in G is neglected and G in eq. (2.12) is replaced by the binding energy $E_{\text{vac-sol}}$. We may justify eq. (2.12) as follows. The fraction $1 - zc_{\text{sol}}$ of all lattice sites is not adjacent to a solute atom. The probability for a vacant site at these lattice positions is the same as in the pure host (if interactions beyond nearest-neighbours are neglected). This gives the first term on the righthand side of eq. (2.12). The remaining sites have a vacancy bound to a solute atom, giving an extra $\exp(G_{\text{vac-sol}}/k_B T)$ in the Boltzmann factor. Thus, we obtain the second term on the righthand side of eq. (2.12). Lomer (1958), Lidiard (1960) and Burke (1972) have given more stringent arguments

for eq. (2.12). It fails if the solute atoms show clustering, and the validity is often limited to $c_{sol} < 0.01$. March and Rousseau (1971) and Seeger (1973) have reviewed various aspects of vacancy-solute interactions.

Example. vacancy-solute interactions in Al–Ag alloys. If the experiment of the Simmons–Balluffi type in the example in §3 is done on a pure element (unprimed quantities) and a dilute alloy of the same element (primed quantities), one has from eqs. (2.10) and (2.12);

$$(c_{vac})^0 c_{sol} z [\exp(E_{vac\text{-}sol}/k_B T) - 1]$$

$$= 3 \left\{ \frac{\Delta L'}{L'} - \frac{\Delta L}{L} \right\} - 3 \left\{ \frac{\Delta a'}{a'} - \frac{\Delta a}{a} \right\}. \tag{2.13}$$

Using this method for Al with 0.94 at.% Ag, Beaman et al. (1964) obtained $E_{vac\text{-}sol}/E_{vac} \approx 0.10$.

ELASTICITY. BASIC RELATIONS

1. Introduction

The elastic properties of materials can be described in different ways. The engineer usually deals with polycrystalline one- or multiphase systems which are characterised by macroscopic elastic parameters such as the bulk modulus K and the shear modulus G. The physicist is more interested in the properties of a single crystal, described by the elastic stiffness coefficients c_{ij}, and then elasticity is often considered as the special case of long-wavelength lattice vibrations. The terminology in the field is not quite clear. In this book we will adopt the following notation and terminology (Ledbetter and Reed 1973).

K = bulk modulus
$\kappa = 1/K$ = compressibility
G = shear modulus
E = Young's modulus
ν = Poisson ratio
$\left.\right\}$ elastic moduli
$\left.\right\}$ (polycrystal) engineering elastic constants

c_{ij} = elastic stiffnesses
s_{ij} = elastic compliances
$\left.\right\}$ (single crystal) elastic coefficients

$\left.\right\}$ elastic constants

Some authors use B for the bulk modulus and K for the compressibility; call our K the modulus of (hydrostatic) compression and our κ the coefficient of (hydrostatic) compression; call G the rigidity modulus and denote it μ; call s_{ij} elastic moduli and c_{ij} elastic constants; or even call s_{ij} elastic constants while c_{ij} are called elastic coefficients.

Much of the following account of elasticity is covered in monographs and articles by Nye (1957), Huntington (1958), Hearmon (1961), Fedorov (1968), Musgrave (1970) and Schreiber et al. (1973). We will

Table 3.1

Voigt's (1910) contraction scheme for indices in $c_{\alpha\beta}$ and c_{ijkl}

i, j or k, l	11	22	33	23 or 32	13 or 31	12 or 21
α or β	1	2	3	4	5	6

mainly consider those aspects which form a necessary background for our discussion of thermophysical properties in other parts of this book.

2. General considerations

The elastic strain ε_{kl} is related to the stress σ_{ij} by *Hooke's law*,

$$\sigma_{ij} = \sum_{k,l=1}^{3} c_{ijkl}\varepsilon_{kl}, \tag{3.1}$$

where i, j, k and l are indices running from 1 to 3. The elastic properties of a material are described by a fourth-rank elasticity tensor with $3^4 = 81$ elements ε_{ijkl}. Because $c_{ijkl} = c_{klij} = c_{jikl} = c_{ijlk}$, there are at most 21 different elements ε_{ijkl}. They can be arranged in a 6×6 matrix that is symmetric, i.e. with elements $c_{\alpha\beta} = c_{\beta\alpha}$. The relations between $c_{\alpha\beta}$ and c_{ijkl} are summarised in table 3.1.

We can write eq. (3.1) as

$$\sigma_\alpha = \sum_{\beta=1}^{6} c_{\alpha\beta}\varepsilon_\beta, \tag{3.2}$$

where

$$\sigma_\alpha = \sigma_{ij}; \tag{3.3}$$

$$\varepsilon_\beta = \varepsilon_{kl} \quad \text{if} \quad \beta = 1, 2 \text{ or } 3; \tag{3.4}$$

$$\varepsilon_\beta = 2\varepsilon_{kl} \quad \text{if} \quad \beta = 4, 5 \text{ or } 6. \tag{3.5}$$

Table 3.2

Parameters describing the elastic properties

Polycrystalline[a]	Any two of K, G, E and v
Cubic	c_{11}, c_{12}, c_{44}
Hexagonal	$c_{11}, c_{12}, c_{13}, c_{33}, c_{44}$
Tetragonal[b]	$c_{11}, c_{12}, c_{13}, c_{33}, c_{44}, c_{66}$
Trigonal[b,c]	$c_{11}, c_{12}, c_{13}, c_{14}, c_{33}, c_{44}$
Orthorhombic	$c_{11}, c_{12}, c_{13}, c_{22}, c_{23}, c_{33}, c_{44}, c_{55}, c_{66}$

[a] Statistically isotropic and homogeneous.
[b] A few solids in this system have a lattice structure that requires seven elastic constants.
[c] Earlier also called rhombohedral.

The *elastic stiffness tensor c* is related to the *elastic compliance tensor s* by

$$cs = I_6,\tag{3.6}$$

where I_6 is a 6×6 identity matrix. The relation (3.2) for the stresses σ expressed in the strains ε can be inverted to give the strains in terms of the stresses;

$$\varepsilon_\alpha = \sum_{\beta=1}^{6} s_{\alpha\beta}\sigma_\beta.\tag{3.7}$$

Hooke's law, (eq. (3.1)), holds for both polycrystalline and single-crystal specimens. The number of independent parameters required to specify the tensor $c_{\alpha\beta}$ depends on the symmetry of the system (cf. table 3.2). Some tetragonal and trigonal symmetry classes have additional $c_{\alpha\beta} \neq 0$ if one uses certain natural choices of coordinate axes (see, for example, Fedorov 1968).

If a material has spherically symmetric elastic properties, two parameters suffice for their description. It follows that for isotropic materials, including materials which are isotropic and homogeneous in a statistical sense, there are only two linearly independent engineering elastic constants. Then there are 12 relations between K, G, E and v;

$$K = \frac{GE}{3(3G - E)} = \frac{E}{3(1 - 2v)} = \frac{2G(1 + v)}{3(1 - 2v)},\tag{3.8}$$

$$G = \frac{3KE}{9K - E} = \frac{E}{2(1 + \nu)} = \frac{3K(1 - 2\nu)}{2(1 + \nu)}, \tag{3.9}$$

$$E = \frac{9KG}{3K + G} = 2G(1 + \nu) = 3K(1 - 2\nu), \tag{3.10}$$

$$\nu = \frac{3K - 2G}{2(3K + G)} = \frac{E}{2G} - 1 = \frac{1}{2} - \frac{E}{6K}. \tag{3.11}$$

Sometimes one prefers to take as independent elastic parameters the *Lamé constants* λ and μ, with $\lambda = K - 2G/3$ and $\mu = G$. Cubic lattices have three independent elastic coefficients. Usually one chooses them to be c_{11}, c_{12} and c_{44}. An alternative set of constants was introduced by Zener (1948);

$$K = (c_{11} + 2c_{12})/3, \quad C = c_{44}, \quad C' = (c_{11} - c_{12})/2. \tag{3.12}$$

It can be shown that K is the bulk modulus. C and C' are shear moduli for shear in the (100) and (110) planes; see eqs. (3.39) and (3.40). If the cubic lattice is elastically isotropic, $C' = C = c_{44}$ equals the shear modulus G.

3. Fundamental definitions of elastic constants

Hooke's law is a phenomenological expression of how a solid responds to an applied stress. In order to get a deeper understanding of the influence of pressure, temperature etc. on the elastic constants, we should express $c_{\alpha\beta}$ in appropriate derivatives of thermodynamic functions. The first law of thermodynamics, in most cases just written $dU = T\,dS - p\,dV$, has a generalised form when one resolves the forces and deformations into Cartesian components (a positive stress σ corresponds to a negative pressure p);

$$dU = T\,dS + V_0 \sum_{i=1}^{6} \sigma_i\,d\varepsilon_i. \tag{3.13}$$

For an isentropic (adiabatic) deformation ($dS = 0$, i.e. no heat flows in or out of the volume V_0), the components of the stress tensor can be obtained as

$$\sigma_i = (1/V_0)(\partial U/\partial \varepsilon_i)_{S,\varepsilon'}, \tag{3.14}$$

where the subscripts S, ε' mean that the derivatives are taken at constant entropy S and with all strains $\varepsilon_j \neq \varepsilon_i$ held constant. The prefactor $1/V_0$ ensures that σ_i is independent of the size of the specimen. Alternatively, we could have defined U as an energy density, i.e. energy per volume, and dropped V_0 in eq. (3.14).

The components $c_{\alpha\beta}$ of the stiffness tensor are defined by

$$(c_{\alpha\beta})_S = (\partial\sigma_\alpha/\partial\varepsilon_\beta)_{S,\varepsilon'} = (1/V_0)(\partial^2 U/\partial\varepsilon_\alpha\partial\varepsilon_\beta)_{S,\varepsilon'}. \tag{3.15}$$

Now, the subscripts S, ε' mean that S and all ε, except ε_α and ε_β, are kept constant. The $c_{\alpha\beta}$ defined by eq. (3.15) are called *isentropic* (or *adiabatic*) *elastic coefficients* since they are taken at constant entropy. We can also define *isothermal elastic coefficients*, i.e. taken at constant temperature T, if we start from the Helmholtz (free) energy F. One has

$$dF = -S\,dT + V_0 \sum_{i=1}^{6} \sigma_i\,d\varepsilon_i, \tag{3.16}$$

which leads to (Brugger 1964)

$$(c_{\alpha\beta})_T = (\partial\sigma_\alpha/\partial\varepsilon_\beta)_{T,\varepsilon'} = (1/V_0)(\partial^2 F/\partial\varepsilon_\alpha\partial\varepsilon_\beta)_{T,\varepsilon'}. \tag{3.17}$$

The isentropic (or adiabatic) *compliances* $(s_{\alpha\beta})_S$ are defined from the enthalpy H,

$$(s_{\alpha\beta})_S = (\partial\varepsilon_\alpha/\partial\sigma_\beta)_{S,\sigma'} = -(1/V_0)(\partial^2 H/\partial\sigma_\alpha\partial\sigma_\beta)_{S,\sigma'}, \tag{3.18}$$

and the isothermal *compliances* follow from the Gibbs energy G,

$$(s_{\alpha\beta})_T = (\partial\varepsilon_\alpha/\partial\sigma_\beta)_{T,\sigma'} = -(1/V_0)(\partial^2 G/\partial\sigma_\alpha\partial\sigma_\beta)_{T,\sigma'}. \tag{3.19}$$

See Brugger (1964, 1965b) for details on the definitions of $c_{\alpha\beta}$ and $s_{\alpha\beta}$ and how they are related to thermodynamics and measured elastic constants.

The isentropic (or adiabatic) and isothermal *compressibilities* κ_S and κ_T, and *bulk moduli* K_S and K_T, are of the form

$$\kappa_S = (K_S)^{-1} = \sum_{\alpha,\beta=1}^{3} (s_{\alpha\beta})_S, \tag{3.20}$$

$$\kappa_T = (K_T)^{-1} = \sum_{\alpha,\beta=1}^{3} (s_{\alpha\beta})_T. \tag{3.21}$$

These relations, valid for any crystal structure, are discussed further in Chapter 13, in connection with equations-of-state. Here we just note that $K_S/K_T = \kappa_T/\kappa_S = C_p/C_V$, eq. (13.35). There is no significant difference between isentropic and isothermal elastic constants when $T \lesssim \theta_D$ (a Debye temperature), but close to the melting temperature they may differ by 15% or more.

Example: the bulk modulus expressed in c_{ij}. As an illustration we check that the $c_{\alpha\beta}$ from eq. (3.15) are consistent with the result $K = (c_{11} + 2c_{12})/3 = -V(\partial p/\partial V)$ for cubic lattices (eq. (3.12)). We get

$$
\begin{aligned}
c_{11} + 2c_{12} &= (1/V)(\partial^2 U/\partial\varepsilon_1^2 + 2\partial^2 U/\partial\varepsilon_1\partial\varepsilon_2) \\
&= (1/V)(\partial/\partial\varepsilon_1)(\partial U/\partial\varepsilon_1 + \partial U/\partial\varepsilon_2 + \partial U/\partial\varepsilon_3) \\
&= (1/V)(\partial/\partial\varepsilon_1)(\partial U/\partial V)(\partial V/\partial\varepsilon_1 + \partial V/\partial\varepsilon_2 \\
&\quad + \partial V/\partial\varepsilon_3) \\
&= (\partial/\partial V)(-3pV) = -3V(\partial p/\partial V). \tag{3.22}
\end{aligned}
$$

Here we have used that $c_{12} = c_{13}$, $dV/V = d\varepsilon_1 + d\varepsilon_2 + d\varepsilon_3$; $p = -\partial U/\partial V$ and, in the last step, that $p \to 0$ ($c_{\alpha\beta}$ is calculated for a stress-free sample).

4. Higher-order elastic constants

The energy of a crystal can be expanded in powers of the strains ε_i as

$$
\begin{aligned}
U &= U(\varepsilon_i = 0) + V_0 \sum c_i \varepsilon_i + (1/2)V_0 \sum c_{ij}\varepsilon_i\varepsilon_j \\
&\quad + (1/6)V_0 \sum c_{ijk}\varepsilon_i\varepsilon_j\varepsilon_k + \cdots. \tag{3.23}
\end{aligned}
$$

Indices i, j, k run from 1 to 6 in the summations. The definition of the expansion coefficients is exemplified by

$$(c_{ijk})_s = (1/V_0)(\partial^3 U/\partial\varepsilon_i\partial\varepsilon_j\partial\varepsilon_k)_{S,\varepsilon'}, \tag{3.24}$$

which is called a *third-order* isentropic (or adiabatic) elastic coefficient. (Some authors call it second-order and let $c_{\alpha\beta}$ be first order.) $U(\varepsilon_i = 0)$ is the energy of the reference state from which the strains are counted. That energy is uninteresting in our discussion. All terms $c_i \varepsilon_i$ vanish if $\varepsilon_i = 0$, which refers to a stress-free equilibrium. The subscripts S, ε' have the same meaning as earlier. In addition to the isentropic third-order elastic coefficients, (eq. (3.24)), one can start from the Helmholtz energy F and define isothermal coefficients. See, for example, Brugger (1964), Thurston and Brugger (1964), Wallace (1970, 1972), Hearmon (1979, 1984) and Every and McCurdy (1992) for details and further references.

In analogy to $c_{\alpha\beta}$, symmetry reduces the number of linearly independent third-order elastic coefficients, and many of them vanish. In cubic symmetries (except for, e.g. some alums with a more complicated cubic lattice) one is left with the six coefficients

$$c_{111}, c_{112}, c_{123}, c_{144}, c_{155}, c_{456}. \tag{3.25}$$

Note that there are other conventions concerning the choice and notation of high-order elastic constants, e.g. that of Birch (1947). Furthermore, $c_{155} = c_{166}$, and hence relations below for cubic systems are sometimes quoted with c_{166} instead.

5. Hooke's law in isotropic and homogeneous polycrystalline materials

Consider a polycrystalline specimen that is isotropic and homogeneous in a statistical sense. Expressed in K and G, Hooke's law, (eq. (3.1)), takes the form

$$
\begin{pmatrix} \sigma_1 \\ \sigma_2 \\ \sigma_3 \\ \sigma_4 \\ \sigma_5 \\ \sigma_6 \end{pmatrix}
=
\begin{pmatrix}
K + 4G/3 & K - 2G/3 & K - 2G/3 & 0 & 0 & 0 \\
K - 2G/3 & K + 4G/3 & K - 2G/3 & 0 & 0 & 0 \\
K - 2G/3 & K - 2G/3 & K + 4G/3 & 0 & 0 & 0 \\
0 & 0 & 0 & G & 0 & 0 \\
0 & 0 & 0 & 0 & G & 0 \\
0 & 0 & 0 & 0 & 0 & G
\end{pmatrix}
\begin{pmatrix} \varepsilon_1 \\ \varepsilon_2 \\ \varepsilon_3 \\ \varepsilon_4 \\ \varepsilon_5 \\ \varepsilon_6 \end{pmatrix}.
$$

$$\tag{3.26}$$

We illustrate the application of eq. (3.26) by three simple cases; uniaxial stress, hydrostatic pressure and shear.

Uniaxial stress. A uniaxial stress $\sigma_{xx} = \sigma$ corresponds to $\sigma_1 = \sigma$ and all other $\sigma_i = 0$. Furthermore, only ε_1 and ε_2 ($= \varepsilon_3$) are non-zero. From eq. (3.26), we then get $\sigma = \sigma_1 = (K + 4G/3)\varepsilon_1 + (K - 2G/3)\varepsilon_2 + (K - 2G/3)\varepsilon_3$, with a similar equation for σ_2 ($= 0$). Elimination of ε_2 ($= \varepsilon_3$), and using eqs. (3.9) and (3.11), leads to

$$\varepsilon_1 = \sigma/E, \quad \varepsilon_2 = \varepsilon_3 = -\nu\sigma/E. \tag{3.27}$$

Hydrostatic pressure. A hydrostatic pressure p corresponds to $\sigma_1 = \sigma_2 = \sigma_3 = -p$, and $\sigma_4 = \sigma_5 = \sigma_6 = 0$. From eq. (3.26) we obtain $-p = \sigma_1 = (K + 4G/3)\varepsilon_1 + (K - 2G/3)\varepsilon_2 + (K - 2G/3)\varepsilon_3$, with similar equations for σ_2 and σ_3. Then

$$\varepsilon_1 = \varepsilon_2 = \varepsilon_3 = -p/3K. \tag{3.28}$$

The relative volume change, $\Delta V / V$, is

$$\Delta V / V = \varepsilon_1 + \varepsilon_2 + \varepsilon_3 = -p/K. \tag{3.29}$$

Shear. Shear, specified by $\tau_{yz} = \tau_{zy} = \tau$, has $\sigma_4 = \tau$ and all other $\sigma_i = 0$. From eq. (3.26) one obtains

$$\varepsilon_4 = \tau/G, \qquad \text{all other} \quad \varepsilon_i = 0. \tag{3.30}$$

6.   Hooke's law in single crystals with cubic symmetry

6.1.   General relations

The elastic properties of a cubic lattice may be described by the elastic stiffness coefficients c_{11}, c_{12} and c_{44}, or by the elastic compliance coefficients s_{11}, s_{12} and s_{44}. They are connected by eq. (3.6). The explicit relations are

$$s_{11} = \frac{c_{11} + c_{12}}{(c_{11} - c_{12})(c_{11} + 2c_{12})}, \tag{3.31}$$

$$s_{12} = -\frac{c_{12}}{(c_{11} - c_{12})(c_{11} + 2c_{12})}, \tag{3.32}$$

$$s_{44} = \frac{1}{c_{44}}. \tag{3.33}$$

The corresponding relations for $c_{\alpha\beta}$ expressed in $s_{\alpha\beta}$ are obtained if the symbols c and s are interchanged in eqs. (3.31)–(3.33). Equations (3.31) and (3.32) can be combined to yield two relations that more clearly show the symmetries of c_{ij} and s_{ij},

$$s_{11} + 2s_{12} = \frac{1}{c_{11} + 2c_{12}}, \tag{3.34}$$

$$s_{11} - s_{12} = \frac{1}{c_{11} - c_{12}}, \tag{3.35}$$

where we recognise, on the righthand side, the bulk modulus $K = (c_{11} + 2c_{12})/3$ and Zener's elastic constant $C' = (c_{11} - c_{12})/2$.

Hooke's law, in the case of cubic elastic symmetry, has the form

$$\begin{pmatrix} \sigma_1 \\ \sigma_2 \\ \sigma_3 \\ \sigma_4 \\ \sigma_5 \\ \sigma_6 \end{pmatrix} = \begin{pmatrix} c_{11} & c_{12} & c_{12} & 0 & 0 & 0 \\ c_{12} & c_{11} & c_{12} & 0 & 0 & 0 \\ c_{12} & c_{12} & c_{11} & 0 & 0 & 0 \\ 0 & 0 & 0 & c_{44} & 0 & 0 \\ 0 & 0 & 0 & 0 & c_{44} & 0 \\ 0 & 0 & 0 & 0 & 0 & c_{44} \end{pmatrix} \begin{pmatrix} \varepsilon_1 \\ \varepsilon_2 \\ \varepsilon_3 \\ \varepsilon_4 \\ \varepsilon_5 \\ \varepsilon_6 \end{pmatrix}. \tag{3.36}$$

The tensor of elastic compliance coefficients has all non-zero $c_{\alpha\beta}$ in eq. (3.36) replaced by $s_{\alpha\beta}$ (i.e. c_{11} replaced by s_{11} etc.).

In anisotropic crystals, a specimen twists and bends at the same time, even if only a bending (or twisting) moment is applied. Some relations below refer to this situation. See Schreiber et al. (1973) or Hearmon (1946) for a discussion of other load situations.

6.2. Bulk modulus

K refers to hydrostatic pressure, and is an isotropic quantity with

$$K = (c_{11} + 2c_{12})/3 = [3(s_{11} + 2s_{12})]^{-1}. \tag{3.37}$$

The relative volume change $\Delta V / V$, under pressure p, is

$$\Delta V / V = -p/K = -3p/(c_{11} + 2c_{12}) = -3p(s_{11} + 2s_{12}). \quad (3.38)$$

6.3.   Shear modulus

A shear stress τ_{yz} gives a shear in the (100) plane and the [010] direction. The corresponding shear modulus is

$$G(100)[010] = c_{44} = 1/s_{44}. \tag{3.39}$$

Similarly, for shear in the (110) plane and the $[1\bar{1}0]$ direction,

$$\{G(110)[1\bar{1}0]\}^{-1} = 2(s_{11} - s_{12}) = 2/(c_{11} - c_{12}) = 1/C', \quad (3.40)$$

where C' is Zener's shear constant.

If we let $G(hkl)$ refer to torsion around $[hkl]$, then shear occurs in all directions in the plane (hkl). The general expression for that shear modulus is (Hearmon 1946), with N defined in (3.45),

$$\{G(hkl)\}^{-1} = s_{44} + 2(2s_{11} - 2s_{12} - s_{44})N^4. \tag{3.41}$$

In an isotropic system, the term containing N^4 vanishes and

$$G = c_{44} = 1/s_{44}. \tag{3.42}$$

A general expression for $G(hkl)[h'k'l']$ is found, for instance, in Schreiber et al. (1973) and Turley and Sines (1971).

6.4.   Young's modulus

E is defined as the ratio of uniaxial stress to strain measured along the same axis, when the body is unconstrained perpendicular to that axis. Let σ_1 be along the [100] axis, and $\sigma_i = 0$ ($i \neq 1$). Furthermore, $\varepsilon_2 = \varepsilon_3$ and $\varepsilon_4 = \varepsilon_5 = \varepsilon_6 = 0$. Then, from eq. (3.36), we obtain Young's modulus in the [100] direction:

$$E[100] = \sigma_1/\varepsilon_1 = (c_{11} - c_{12})(c_{11} + 2c_{12})/(c_{11} + c_{12}) = 1/s_{11}.$$

$$(3.43)$$

In an arbitrary direction $[hkl]$, Young's modulus is best given in terms of s_{ij}. One has (Hearmon 1946, Schreiber et al. 1973)

$$\{E[hkl]\}^{-1} = s_{11} - (2s_{11} - 2s_{12} - s_{44})N^4, \tag{3.44}$$

where

$$N^4 = n_1^2 n_2^2 + n_1^2 n_3^2 + n_2^2 n_3^2, \tag{3.45}$$

and n_1, n_2, n_3 are direction cosines for the direction $[hkl]$, i.e. $n_1 = h/(h^2 + k^2 + l^2)^{1/2}$ etc. Uniaxial tension in the [110] direction gives $n_1 = n_2 = 1/\sqrt{2}$ and, by eq. (3.44),

$$\{E[110]\}^{-1} = (2s_{11} + 2s_{12} + s_{44})/4. \tag{3.46}$$

In an elastically isotropic medium, $2s_{11} - 2s_{12} - s_{44} = 0$ and the term containing N^4 in eq. (3.44) vanishes. Then

$$E = 1/s_{11} = (c_{11} - c_{12})(c_{11} + 2c_{12})/(c_{11} + c_{12}). \tag{3.47}$$

Example: direction of largest E. N^4 varies between 0 (in $\langle 100 \rangle$ directions) and 1/3 (in $\langle 111 \rangle$ directions). Usually, $2s_{11} - 2s_{12} - s_{44} > 0$ (cf. table 3.3, $A_Z > 1$). Then E has its largest value in $\langle 111 \rangle$ directions. In a few elements of cubic structure (V, Nb, Cr, Mo) and in, for example, alkali halides, $2s_{11} - 2s_{12} - s_{44} < 0$ and E has its largest value in $\langle 100 \rangle$ directions.

6.5. Poisson ratio

The Poisson ratio v is defined as the negative ratio of transverse strain to longitudinal strain, for the case of uniaxial stress. If the stress is along [100] one gets

$$v[100] = -\varepsilon_2/\varepsilon_1 = c_{12}/(c_{11} + c_{12}) = -s_{12}/s_{11}. \tag{3.48}$$

More generally, v must be specified both with respect to the direction $[hkl]$ of the longitudinal strain and the direction $[h'k'l']$ of the transverse strain. Then (Schreiber et al. 1973)

$$v[h'k'l'][hkl] = -\frac{s_{12} + (s_{11} - s_{12} - s_{44}/2)M^4}{s_{11} - (2s_{11} - 2s_{12} - s_{44})N^4}. \tag{3.49}$$

Table 3.3

Materials with noteworthy anisotropy, given by A_E and A_Z. Elastic stiffnesses in GPa

Material	c_{11}	c_{12}	c_{44}	A_E	A_Z	Comment
BaF$_2$	91	41	25	0.0	1	Isotropic
CaO	224	60	81	0.01	0.99	Almost isotropic
Al	108	62	28	−0.12	1.22	Almost isotropic
Cr	348	67	100	0.33	0.71	Anisotropic; $A_E > 0$
Fe (bcc)	230	135	117	−1.2	2.46	Anisotropic
^{3}He	0.024	0.020	0.012	−1.7	6.0	Note large A_Z
Th	77	51	46	−2.1	3.5	Note rather small A_Z
β-brass	130	102	74	−2.1	5.3	Very anisotropic
Li (bcc)	13.6	11.4	9.8	−4.6	8.9	Extremely anisotropic
Pu (fcc)	36	27	34	−30	7.6	Extremely anisotropic
KCl	40.5	6.9	6.27	0.63	0.35	Very anisotropic, $A_E > 0$
TaC	505	73	79	0.64	0.37	Very anisotropic, $A_E > 0$

N^4 was defined in eq. (3.45) and

$$M^4 = n_1^2 m_1^2 + n_2^2 m_2^2 + n_3^2 m_3^2, \tag{3.50}$$

where m_1, m_2, m_3 are direction cosines for $[h'k'l']$. In an elastically isotropic crystal

$$\nu = -s_{12}/s_{11}. \tag{3.51}$$

Example: anisotropic and negative Poisson ratios. Consider a single crystal of cubic elastic symmetry, under tension in the [110] direction. We want to calculate ν referring to contractions in the [1$\bar{1}$0] and [001] directions, respectively. Equation (3.49), with $n_1 = n_2 = 1/\sqrt{2}, n_3 = 0$ and $m_1 = -m_2 = 1/\sqrt{2}, m_3 = 0$ or $m_1 = m_2 = 0, m_3 = 1$, gives

$$\nu[1\bar{1}0][110] = -\frac{2s_{11} + 2s_{12} - s_{44}}{2s_{11} + 2s_{12} + s_{44}}, \tag{3.52}$$

$$\nu[001][110] = -\frac{4s_{12}}{2s_{11} + 2s_{12} + s_{44}}. \tag{3.53}$$

In an elastically isotropic material, $\nu < 0.5$. Negative ν are thermodynamically allowed, but seem not to have been observed with certainty. However, the *anisotropic* Poisson ratio often exceeds these limits. Iron in bcc lattice structure has $s_{11} = 7.67$, $s_{12} = -2.83$ and $s_{44} = 8.57$ (in $(TPa)^{-1}$); from Every and McCurdy (1992). This yields $\nu[1\bar{1}0][110] = -0.06$ and $\nu[001][110] = 0.62$. Extreme values of ν arise for elastically very anisotropic materials (Kitagawa et al. 1980, Date and Andrews 1969, Baughman and Galvão 1993). The intermediate-valence-state compounds $Sm_{1-x}Y_xS$ show anomalies in ν and may have $c_{12} < 0$ (Tu Hailing et al. 1984).

7. Hooke's law in single crystals of non-cubic symmetry

The matrix c_{ij} for a *hexagonal* symmetry is

$$\begin{pmatrix} c_{11} & c_{12} & c_{13} & 0 & 0 & 0 \\ c_{12} & c_{11} & c_{13} & 0 & 0 & 0 \\ c_{13} & c_{13} & c_{33} & 0 & 0 & 0 \\ 0 & 0 & 0 & c_{44} & 0 & 0 \\ 0 & 0 & 0 & 0 & c_{44} & 0 \\ 0 & 0 & 0 & 0 & 0 & (c_{11} - c_{12})/2 \end{pmatrix}. \tag{3.54}$$

Examples of solids with this symmetry are Mg, Zn, Ti, Zr, ice, graphite and β-quartz (SiO_2). The matrix of compliances for a hexagonal symmetry have all c_{ij} in eq. (3.54) replaced by s_{ij} (i.e. c_{12} replaced by s_{12} etc.), except that $(c_{11} - c_{12})/2$ is replaced by $2(s_{11} - s_{12})$. The corresponding matrix for *tetragonal* symmetry has $(c_{11} - c_{12})/2$ in the lower right corner replaced by c_{66}. Examples of solids with that symmetry are In, β-Sn (white tin) and $BaTiO_3$. The matrix of compliance coefficients has all $c_{\alpha\beta}$ replaced by $s_{\alpha\beta}$. Matrices of stiffness and compliance coefficients for other symmetries are given, for example, by Nye (1957), Fedorov (1968) and Schreiber et al. (1973).

The compressibility κ, expressed in s_{ij} for a solid of *arbitrary elastic symmetry*, is (e.g. Nye 1957)

$$\kappa = K^{-1} = s_{11} + s_{22} + s_{33} + 2(s_{12} + s_{13} + s_{23}). \tag{3.55}$$

In a cubic structure, $s_{11} = s_{22} = s_{33}$, and $s_{12} = s_{13} = s_{23}$, and we recover eq. (3.37). Crystals of hexagonal, tetragonal and trigonal symmetry have $s_{11} = s_{22} \neq s_{33}$ and $s_{13} = s_{23} \neq s_{12}$. One then obtains (Thurston 1965)

$$K = \frac{(c_{11} + c_{12})c_{33} - 2c_{13}^2}{c_{11} + c_{12} + 2c_{33} - 4c_{13}}. \tag{3.56}$$

The volume change under a hydrostatic pressure is $\Delta V = -pV/K$, but the strains ε_i are not equal. Then ε_1 ($= \varepsilon_2$) and ε_3 are given by (cf. Nye 1957, Musgrave 1970)

$$\varepsilon_{1(2)} = -p\frac{c_{33} - c_{13}}{(c_{11} + c_{12})c_{33} - 2c_{13}^2} = -p(s_{11} + s_{12} + s_{13}), \tag{3.57}$$

$$\varepsilon_3 = -p\frac{c_{11} + c_{12} - 2c_{13}}{(c_{11} + c_{12})c_{33} - 2c_{13}^2} = -p(2s_{13} + s_{33}). \tag{3.58}$$

Analogous results for other crystal symmetries are found, e.g. in Nye (1957). As a partial check of eqs. (3.55) and (3.56) we restrict the discussion to elastic isotropy. Then $c_{11} = c_{33}$ and $c_{12} = c_{13}$ (eqs. (3.63)–(3.66)), and we recover the result in a cubic structure.

It should be pointed out that eqs. (3.55) and (3.56) give the bulk modulus for a single crystal and not for a statistically isotropic polycrystal. In the Reuss approximation to the elastic properties of polycrystals, one assumes uniform stress. This is the situation that holds above, and eq. (3.55) is seen to agree with the Reuss expression K_R (Chapter 18, §3.2). A deformation under uniform strain, e.g. constant c/a ratio in hexagonal lattice structures, is described by the Voigt bulk modulus K_V (Chapter 18, §3.2).

Expressions for $E[hkl]$, referring to various non-cubic lattices, are found in Hearmon (1946), Boas and Mackenzie (1950) and Nye (1957). They also give explicit relations between c_{ij} and s_{ij}. The anisotropic Poisson ratio has been derived for hexagonal (Li 1976), tetragonal (Chung et al. 1975) and trigonal (Gunton and Saunders 1972) lattices. In analogy to the example in §6, a negative ν is reported for α-SiO_2 (Kittinger et al. 1981).

Example: Poisson ratio $\approx$ 0 in polycrystalline beryllium. Using c_{ij} from table 3.4 and the Voigt–Reuss–Hill approximation (Chapter 18, §3.3)

Table 3.4
Elastic stiffnesses in In, Be, Mg, Zr, Zn, ice and graphite, in units of GPa

Material	c_{11}	c_{33}	c_{12}	c_{13}	c_{44}	c_{66}[a]
Indium (tetragonal)	45.1	44.6	40.0	41.0	6.51	12.0
Beryllium (hcp)	292	349	24	6	163	134
Magnesium (hcp)	59.3	61.5	25.7	21.4	16.4	16.8
Zr (hcp)	144	166	74	67	33.4	35
Zinc (hcp)	165	61.8	31.1	50.0	39.6	67.0
Ice (hexagonal)	13.7	14.7	7.0	5.6	3.0	3.4
Graphite (hexagonal)	1060	36.5	180	15	4	440

[a] For hexagonal symmetry, $c_{66} = (c_{11} - c_{12})/2$.

for K and G of a statistically isotropic polycrystalline specimen, we get $K_{VRH} = 111.5 \pm 0.1$ GPa and $G_{VRH} = 151.0 \pm 0.8$ GPa, and thus $\nu = 0.03$. This is consistent with a theoretical calculation (Cohen 1982) which gives a slightly negative ν.

8. Elastic anisotropy in single crystals

A crystal may have elastic coefficients $c_{\alpha\beta}$ ($s_{\alpha\beta}$) which, accidentally, yield an isotropic behaviour. For a cubic lattice structure, the isotropy condition is

$$c_{11} - c_{12} - 2c_{44} = 0, \tag{3.59}$$

or, equivalently,

$$2s_{11} - 2s_{12} - s_{44} = 0. \tag{3.60}$$

Zener (1948) introduced, as a measure of anisotropy,

$$A_Z = \frac{2c_{44}}{c_{11} - c_{12}}. \tag{3.61}$$

In the equation for sound propagation in cubic lattices, the quantity

$$A_E = \frac{c_{11} - c_{12} - 2c_{44}}{c_{11} - c_{44}}, \tag{3.62}$$

is a more relevant measure of anisotropy than A_Z (Every 1980). It is this combination of c_{ij} that gives the anisotropic variation of the sound velocity and of the angle between the displacement vector $\mathbf{u}$ and the wave vector $\mathbf{q}$ of the sound wave. A_E also gives the direction for a maximum in the shear mode Grüneisen parameter (Brassington and Saunders, 1983). On the other hand, the difference between the Voigt and Reuss bounds to the shear modulus G of a statistically isotropic polycrystal with elastically anisotropic grains is a function of Zener's measure A_Z. Note that A_Z and A_E are not trivially related, i.e. A_Z cannot be expressed in terms of A_E. Thus, there is no unique measure of elastic anisotropy even in the simple case of cubic lattice symmetry. For isotropic systems, $A_Z = 1$ and $A_E = 0$. Table 3.3 shows data for some materials with noteworthy anisotropy, with c_{ij} from the Landolt–Börnstein tables (Every and McCurdy 1992). The extreme anisotropy of Pu has been discussed by Ledbetter and Moment (1976). Figure 3.1 shows the anisotropy in a plot of $c_{11} - c_{44}$ versus $c_{12} + c_{44}$. Since Every's anisotropy parameter can be written $A_E = 1 - (c_{12} + c_{44})/(c_{11} - c_{44})$, the dashed line in the figure, with slope 1, is the locus of elastic isotropy.

Since the hcp lattice has five independent elastic coefficients, three equations are required to reduce them to the two independent elastic parameters that characterise an elastically isotropic system. The isotropy condition for a *hexagonal symmetry* is

$$c_{11} = c_{33}; \quad c_{12} = c_{13}; \quad c_{11} - c_{12} = 2c_{44}. \tag{3.63}$$

Similarly, a lattice with *tetragonal symmetry* is elastically isotropic if

$$c_{11} = c_{33}; \quad c_{12} = c_{13}; \quad c_{11} - c_{12} = 2c_{44} = 2c_{66}, \tag{3.64}$$

A lattice with *trigonal symmetry* is isotropic if

$$c_{11} = c_{33}; \quad c_{12} = c_{13}; \quad c_{11} - c_{12} = 2c_{44}; \quad c_{14} = 0, \tag{3.65}$$

and a lattice with *orthorhombic symmetry* is isotropic if its nine independent elastic coefficients reduce to two, through the seven relations

$$c_{11} = c_{22} = c_{33}; \quad c_{12} = c_{13} = c_{23};$$

$$(c_{11} - c_{12})/2 = c_{44} = c_{55} = c_{66}. \tag{3.66}$$
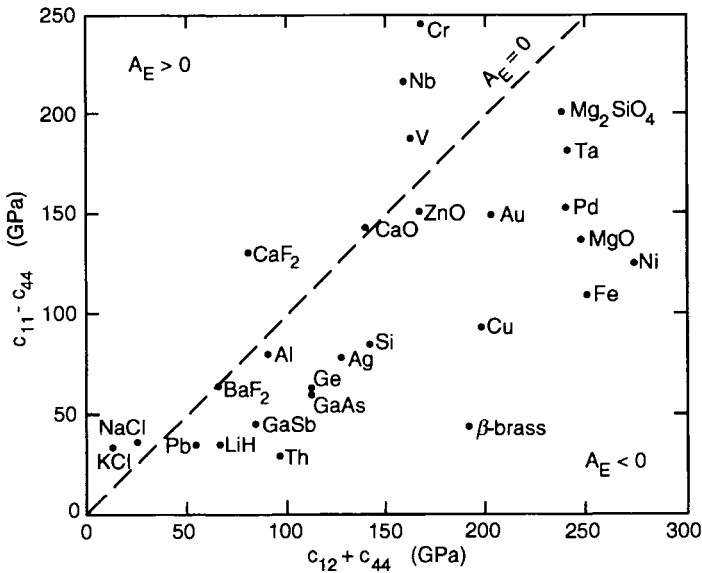
Fig. 3.1. Elastic constants of some materials with cubic lattice symmetry, plotted as $c_{11} - c_{44}$ versus $c_{12} + c_{44}$: The dashed line in the figure, with slope 1, is the locus of elastic isotropy. Data of c_{ij} from Every and McCurdy (1992).

Table 3.5

Elastic stiffnesses in orthorhombic structures, in units of GPa

Material	c_{11}	c_{22}	c_{33}	c_{44}	c_{55}	c_{66}	c_{12}	c_{13}	c_{23}
Rb_2SO_4	50	51	48	16	16	14	20	20	19
Na_2SO_4	80	105	67	15	18	24	30	26	17
Ga	100	90	135	35	42	40	37	33	31
α-U	215	199	267	124	73	74	46	22	108
Mg_2SiO_4[a]	329	200	235	67	81	81	68	69	73
Propylene (cr.)	10	10	325	3.2	1.8	5.5	5.0	1.7	3.2

[a] Forsterite.

Table 3.4, with data from the Landolt–Börnstein tables (Every and McCurdy 1992), shows that the isotropy conditions are approximately fulfilled for hcp Mg, hcp Zr and ice, but not for hcp Zn. The latter fact may be compared with the anisotropy in the vibrational displacements of the atoms due to thermal vibrations, fig. 7.3.

Table 3.6

Anisotropic hydrostatic compression in hexagonal-structure materials, in units of $(TPa)^{-1}$

	Be	Mg	Zr	Zn	Ice	Graphite
$-\varepsilon_{1(2)}/p$	3.1	9.2	3.7	1.8	39	0.49
$-\varepsilon_3/p$	3.0	9.7	3.2	13.7	38	26.9

Table 3.5, with data for orthorhombic structures from Every and McCurdy (1992), shows that Rb_2SO_4 is quite isotropic, in contrast to the chemically related compound Na_2SO_4, while Ga is moderately anisotropic. The latter behaviour may be compared with the highly anisotropic electrical (and hence also thermal) conductivity properties of gallium (Bass 1982). Crystalline polypropylene, with data from Boyd (1983), is highly anisotropic.

Fedorov (1963, 1968) described elastic anisotropy by the mean-square deviation of the matrix $\sigma_{\alpha\beta}$ from a certain average $\bar{c}_{\alpha\beta}$. That makes it possible to assign an anisotropy measure in a lattice of arbitrary symmetry. However, Fedorov's parameter (denoted Λ'_m) for a cubic lattice is more complicated than A_E.

The *third-order* elastic coefficients, for the case of isotropy in cubic lattice structures, obey

$$c_{112} = c_{123} + 2c_{144}; \quad c_{155} = c_{144} + 2c_{456};$$

$$c_{111} = c_{123} + 6c_{144} + 8c_{456}, \tag{3.67}$$

i.e. there are only three independent third-order elastic coefficients in this case.

Example: hydrostatic compression of hexagonal structures. The strains ε_1 ($= \varepsilon_2$) and ε_3 in eqs. (3.57) and (3.58) are equal only if

$$s_{11} + s_{12} = s_{13} + s_{33}. \tag{3.68}$$

We noted above that Mg, Zr and ice are elastically quite isotropic while Zn and graphite are very anisotropic. With s_{ij} from the Landolt–

Börnstein tables (Every and McCurdy 1992), and the formulae (3.57) and (3.58) we get $\varepsilon_{1(2)}/p$ and ε_3/p as in table 3.6.

Example: expansion of tellurium under pressure. Tellurium has a trigonal chain-like structure. Under a hydrostatic pressure p, the strains are (Boas and Mackenzie 1950)

$$\varepsilon_j/p = (s_{11} + s_{12} - s_{13} - s_{33})n^2 - (s_{11} + s_{12} + s_{13}), \qquad (3.69)$$

where $n^2 = 1$ for strain along the chain axis ($j = 3$) and $n^2 = 0$ for an axis perpendicular to the chain. Thus,

$$\varepsilon_3/p = -(2s_{13} + s_{23}). \qquad (3.70)$$

With data from the Landolt–Börnstein tables (Every and McCurdy 1992), we obtain for tellurium $\varepsilon_3/p = -[2(-14.2) + 24.6]$ [TPa]$^{-1}$ = 3.8 [TPa]$^{-1}$, i.e. a positive value. Hence, the crystal *expands* along the chain direction when a hydrostatic pressure is applied. Physically, this is analogous to the elongation of a zigzag shaped chain when it is compressed from its sides.

WHAT VALUES DO THE ELASTIC CONSTANTS TAKE?

1. Introduction

The magnitudes of the elastic constants span over more than an order of magnitude, for instance if one compares the strongly bonded bcc transition metals Cr, Mo and W with the free-electron like bcc alkali metals Li, Na, K, Rb and Cs. They are not sensitive to lattice defects, moderate variations in alloying etc. Obviously the elastic constants reflect the strength of the interatomic forces in the solid, but being elastically "hard" should not be confused with mechanical hardness in its usual sense. Mechanical hardness measures the resistance to plastic deformation, i.e. permanent changes in atomic positions, while elasticity refers to deformations under a load such that the atoms return to their original equilibrium positions when the specimen is unloaded. Mechanical hardness may depend crucially on lattice defects and the detailed chemical composition and there is a very significant temperature dependence. As an example, lead is a soft metal not only because the forces between the atoms are weak, but even more so because the temperature is high on a relative scale (room temperature compared with the melting temperature) and because the lattice structure (fcc) is favourable for plastic deformation through the motion of dislocations. (See Chapter 19, §9, for additional comments on hardness).

We noted in the preceding chapter that a lattice of cubic symmetry has three single-crystal elastic constants. An orthorhombic structure has nine, while an elastically isotropic material has two. Even though these constants are linearly independent in a given solid, they cannot take arbitrary relative values. A solid in equilibrium must be mechanically stable under small deformations and this imposes restrictions, in the form of inequalities, for the elastic constants. We start this chapter with such considerations. Then follow sections which present experimental

data for the elastic properties, pointing out regularities as well as materials with exceptional properties. For instance, although the covalently bonded carbon, in the form of diamond, has the largest known values of c_{11} and c_{44} among the elements, it is a metal, iridium, that has the largest value of c_{12}. The chapter ends with a discussion of temperature, chemical composition, and some other factors that may affect the elastic properties. Such aspects are also dealt with in Chapter 6, on phonons, since the elastic constants are directly related to the low frequency acoustic branch of phonons.

2. Stability requirements

Consider the elastic energy U for an arbitrary but small deformation given by strains ε_α;

$$U = (1/2)V_0 \sum_{i,j=1}^{6} c_{ij}\varepsilon_i\varepsilon_j, \tag{4.1}$$

where V_0 is the volume of the unstrained sample. Lattice stability requires that U is positive for any small deformation. This implies restrictions on c_{ij} which are mathematically expressed by the requirement that the principle minors of the determinant with elements c_{ij} are all positive. For the *engineering elastic constants* this leads to

$$K, G, E > 0, \tag{4.2}$$

$$0.5 > \nu > -1. \tag{4.3}$$

It follows from eq. (3.9) that

$$3G > E. \tag{4.4}$$

The limit $\nu = 0.5$ is obtained for an incompressible material ($K \to \infty$). It is also obtained for an ideal liquid, i.e. a liquid with no shear resistance ($G = 0$), but this does not imply that the liquid is incompressible.

The stability criteria for c_{ij} in systems of *cubic symmetry* are (e.g. Born and Huang 1954, Alers and Neighbours 1957)

$$c_{11} > |c_{12}|; \quad c_{11} + 2c_{12} > 0; \quad c_{44} > 0. \tag{4.5}$$
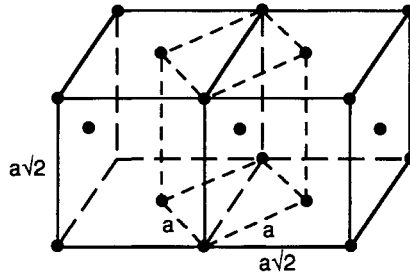
Fig. 4.1. The fcc lattice results when a bcc lattice (central part with short-dashed sides in the figure) has been strained in one direction by a factor $c/a = 2^{1/2}$.

For an isotropic cubic system, i.e. when $c_{11} - c_{12} = 2c_{44}$, and with the identification $K = (c_{11} + 2c_{12})/3$ and $G = c_{44}$, eq. (4.5) is equivalent with eqs. (4.2)–(4.3). Note that $c_{11} + 2c_{12} > 0$ together with the isotropy condition $c_{11} - c_{12} = 2c_{44}$ implies that $3c_{11} > 4c_{44}$.

In a system of *hexagonal symmetry* the stability requirements are

$$c_{11} > |c_{12}|; \quad c_{33}(c_{11} + c_{12}) > 2(c_{13})^2; \tag{4.6}$$

$$c_{11}c_{33} > (c_{13})^2; \quad c_{44} > 0. \tag{4.7}$$

3. Bain paths and lattice instabilities

Bain (1924) pointed out that an fcc lattice can be transformed into a bcc lattice by stretching the sides in the cubic unit cell by factors of 1, $2^{1/2}$ and $2^{1/2}$. Conversely, if the axes of the bcc lattice are stretched by factors of $2^{1/2}$, 1 and 1, it transforms into an fcc lattice (cf. fig. 4.1). The intermediate stretched lattice has a tetragonal structure, with a certain c/a ratio. Going from the bcc to the fcc lattice then corresponds to c/a varying from 1 to $2^{1/2}$. There are many such deformation modes, usually called Bain paths, that connect the fcc and bcc structures. For instance, they may refer to constant volume, uniaxial deformation or uniaxial load. In theoretical calculations, one often allows c and a to vary independently, so that the total crystal energy is minimised as one proceeds along the Bain path.

The first part of the Bain path in the bcc lattice can be described by a distortion towards a tetragonal structure (i.e. a tetragonal strain)

through a multiplication of the lengths of the x- and y-axes by a factor of $1 + \delta$ and a contraction of the z-axis by a factor of $(1 + \delta)^{-2}$. That corresponds, in Voigt's notation, to $\varepsilon_1 = \varepsilon_2 = \delta, \varepsilon_3 = 1 - (1 + \delta)^{-2} \approx -2\delta, \varepsilon_4 = \varepsilon_5 = \varepsilon_6 = 0$. We then obtain, from eq. (4.1), a change ΔU in the energy given by

$$\Delta U = 6V_0 \left(\frac{c_{11} - c_{12}}{2} \right) \delta^2. \tag{4.8}$$

Here we recognise the shear modulus $C' = (c_{11} - c_{12})/2$. With the strains chosen above, the next term in the expansion (eq. (4.8)) of ΔU contains the power δ^3. With strains $\varepsilon_1 = \delta, \varepsilon_2 = -\delta, \varepsilon_3 = \delta^2/(1 - \delta^2)$ instead, we still get unchanged volume and $\Delta U \sim (c_{11} - c_{12})\delta^2$ but the next term in eq. (4.8) containing second-order elastic coefficients c_{ij} is of the order δ^4.

In an analogous way we can apply a shear around the z-axis with $\varepsilon_{12} = \varepsilon_{21} = \delta$ (i.e. $\varepsilon_4 = 2\delta$) and change the z-axis by a factor of $1 + \varepsilon_3 = 1/(1 - \delta)^{-2}$ so that the volume is conserved. Then the change in energy, for an infinitesimal δ, is

$$\Delta U = 2V_0 c_{44} \delta^2. \tag{4.9}$$

Deformations of this kind are used routinely in ab initio electron structure calculations of the total energy, in order to get the elastic constants; (cf. pioneering work on transition metals by Dacorogna et al. 1982, and extensive calculations for $5d$-transition metals by Wills et al. 1992). Figure 4.2 shows the result of similar calculations for $U(c/a)$ along the Bain path for tungsten. The curvature of $U(c/a)$ at the bcc and fcc structures is directly related to the elastic constant $C' = (c_{11} - c_{12})/2$ of these structures (see eq. (4.8)). In fcc W there is no energy barrier (i.e. $C' < 0$) for a small deformation along the Bain path. Therefore, this structure is dynamically unstable. Actually, it is common that the fcc structure is unstable under shear in metals that crystallise in the bcc structure, and vice versa (e.g. Wills et al. 1992). The fcc–bcc Bain path transformation has been reviewed by Milstein et al. (1994). Analogous paths can be defined for transformations between other lattice structures. They may involve a uniform lattice deformation, as in the case above, or atomic motions described by short-wavelength phonons. An example of the latter case is the longitudinal $\mathbf{q} = [2/3, 2/3, 2/3]$
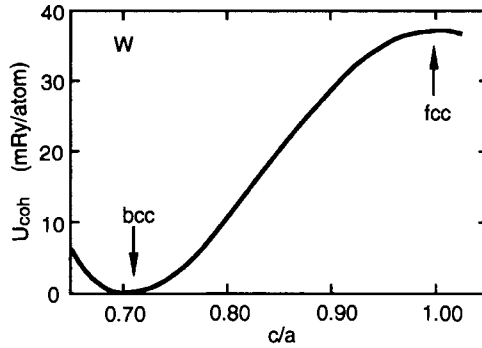
Fig. 4.2. The energy $U(c/a)$ for tungsten, as calculated along the Bain path that connects the bcc and fcc lattice structures. Data from Einarsdotter et al. (1997).

phonon mode in the bcc structure that takes this lattice into the so-called "omega-phase" (see also Chapter 6, §13, for further comments on lattice instabilities).

In this context we note that a central potential $\phi(r)$ may lead to lattice instabilities. Misra (1940) (see also Born and Huang (1954)) showed that with $\phi(r) = ar^{-m} - br^{-n}$, simple cubic lattices are never stable, fcc lattices are always stable and bcc lattices are stable for certain small m and n. As another example, a bcc lattice with only nearest-neighbour and central interactions is unstable against shear (Zener 1948).

4. Cauchy relations and central interatomic forces

If the interatomic forces can be described by a potential $\phi(r)$ which only depends on the distance r between atoms, and if all atoms of an unstrained crystal occupy centres of inversion symmetry in the lattice, c_{ij} obeys the *Cauchy* (1828) *relations*, see also Voigt (1910)

$$c_{23} = c_{44}; \quad c_{13} = c_{55}; \quad c_{12} = c_{66}; \tag{4.10}$$

$$c_{14} = c_{56}; \quad c_{25} = c_{46}; \quad c_{36} = c_{45}. \tag{4.11}$$

This form of the potential ϕ excludes torsional, or bending, forces (present in covalent crystals) and interatomic forces which vary with the atomic volume (present in metals). When eqs. (4.10) and (4.11)

are fulfilled, the maximum number of linearly independent elements c_{ij} is reduced from 21 to 15. For cubic lattices, the three independent elastic coefficients c_{11}, c_{12} and c_{44} are reduced to two since the Cauchy relations in that case can be summarised by

$$c_{12} = c_{44}. \tag{4.12}$$

The Cauchy relations need not be valid in non-Bravais lattices, or in a specimen under pressure. For instance, the atomic sites in the diamond structure do not have inversion symmetry and, hence, an accidental fulfilment of eqs. (4.10) and (4.11) does not imply central forces. This is exemplified by GaAs in table 4.1, showing that $c_{12} \approx c_{44}$ as in eq. (4.12). GaAs has covalent bonding with strong angular forces. Another example is provided by numerically simulated glasses, in which the atoms interact through a central potential (Wearie et al. 1971). Such a material is macroscopically isotropic. If we neglect internal displacements under stresses and shears, the Cauchy relations plus the isotropy condition gives $K = (5/3)G$. However, there *are* internal displacements and K and G must be calculated separately.

The Cauchy (central force) conditions for the *third-order elastic coefficients* in cubic lattices are

$$c_{112} = c_{155}; \quad c_{144} = c_{123} = c_{456}. \tag{4.13}$$

5. Ranges for elastic constants in real materials

Experimental values of second-order elastic coefficients $c_{\alpha\beta}$ and $s_{\alpha\beta}$ and also some higher-order elastic coefficients are found in the Landolt–Börnstein tables (Every and McCurdy 1992). This reference is the main source of data for the discussions below. In cubic lattice structures the inequality $c_{11} < c_{44}$ is very unusual, but not physically impossible, and has been reported for some Mn–Cu and Mn–Ni alloys. It is not unusual that $c_{12} < c_{44}$, but negative c_{12} are very rare. Intermediate-valence-state compounds $Sm_{1-x}Y_xS$ seem to have $c_{12} < 0$. Some reported negative c_{12} values in other systems may be due to indirect effects, e.g. twinning. Table 4.1 lists c_{ij} from the Landolt–Börnstein tables (Every and McCurdy 1992) for some cubic materials with noteworthy elastic properties.

Table 4.1

Materials with noteworthy elastic stiffnesses, in units of GPa

Material	c_{11}	c_{12}	c_{44}	A_E	Comment
W	523	203	160	0.0	High c_{ij}
TiC	513	106	178	0.15	High $c_{11}, c_{44}; c_{12} \ll c_{44}$
Ir	600	260	270	−0.60	Highest known c_{12}; Highest c_{11}, c_{44} in metals; Cauchy relation well obeyed
Diamond	1077	125	577	−0.40	Highest $c_{11}, c_{44}; c_{12} \ll c_{44}$
Mo	465	163	109	0.24	High c_{11}
Cr	348	67	100	0.33	$c_{12} \ll c_{44}$
Cu_2O	121	105	12.1	0.08	$c_{12} \gg c_{44}$
^{3}He	0.024	0.020	0.012	−1.7	Very low c_{ij}
NaCl	49.1	12.8	12.8	−0.36	Cauchy relation obeyed
AgCl	59.6	36.1	6.22	0.21	Cauchy relation violated
GaAs	118	53.5	59.4	−0.93	Accidental Cauchy relation
$Sm_{0.75}Y_{0.25}S$	12.7	−5.1	3.2	1.20	$c_{12} < 0$

There are very few tables of critically assessed experimental data for the engineering elastic constants K, G, E and v. Often, the best values are obtained from the microscopic elastic coefficients c_{ij} (or s_{ij}). Simmons and Wang (1971) have published extensive tables based on the Voigt–Reuss and Hashin–Shtrikman bounds (cf. Chapter 18).

Figure 4.3 shows the shear modulus G plotted versus the bulk modulus K for some solids with cubic or hcp lattice structures. Data for the single-crystal elastic constants (Every and McCurdy 1992) are used to obtain K of cubic structures through an exact relation (eq. (18.18)), and G and remaining K as the average of the upper and lower Hashin–Shtrikman bounds (Chapter 18, §3). Figure 4.4 is a corresponding plot for G versus Young's modulus E, calculated as $E = 9KG/(3K + G)$. The figures show the bounds (dashed lines) implied by the inequality $0.5 > v > 0$ for the Poisson ratio, i.e. $G < 3K/2$ and $2G < E < 3G$. The bulk modulus refers to deformations that change the volume but not the shape of the lattice, while the shear modulus refers to a deformation of the lattice without any overall volume change. As shown in fig. 4.3
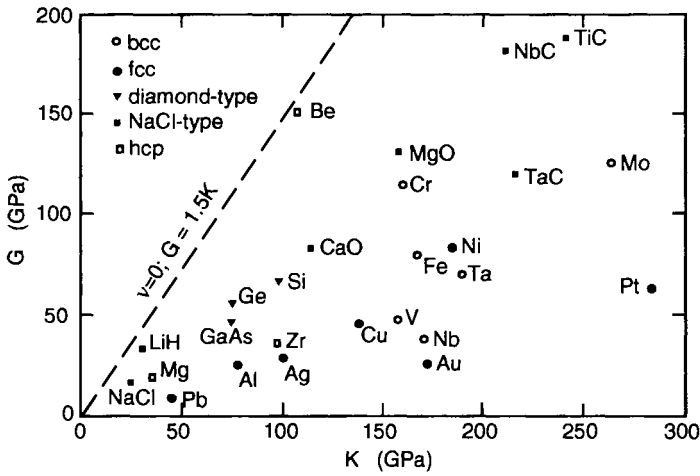
Fig. 4.3. The shear modulus G plotted versus the bulk modulus K for some solids of cubic or hcp lattice structures, with G and K calculated from experimental values of the single crystal elastic constants c_{ij}.

the parameters K and G describing these two independent deformation modes are not very well correlated. We also see that the bcc lattice structure does not show a significantly lower shear modulus, in spite of the fact that the bcc lattice tends to have a phonon shear mode of low frequency in the [110] direction (cf. Chapter 6, §12). The Young's modulus describes a deformation that involves both a volume change and a change in the shape of the lattice, and there is a rather strong correlation between E and G (fig. 4.4). The barely positive Poisson ratio of Be (having a value $\nu < 0$ is not unphysical) was considered in Chapter 3, §7.

Example: rubber-like materials. Rubber is easy to shear, but has a low compressibility, i.e. a high bulk modulus K. Writing the Poisson ratio as eq. (3.11), $\nu = (3K - 2G)/(6K + 2G)$, and with $G \ll K$, we see that $\nu \approx 0.5$ for rubber-like materials, i.e. approximately at the upper theoretical limit for ν. Cork, on the other hand, has $\nu \approx 0$.
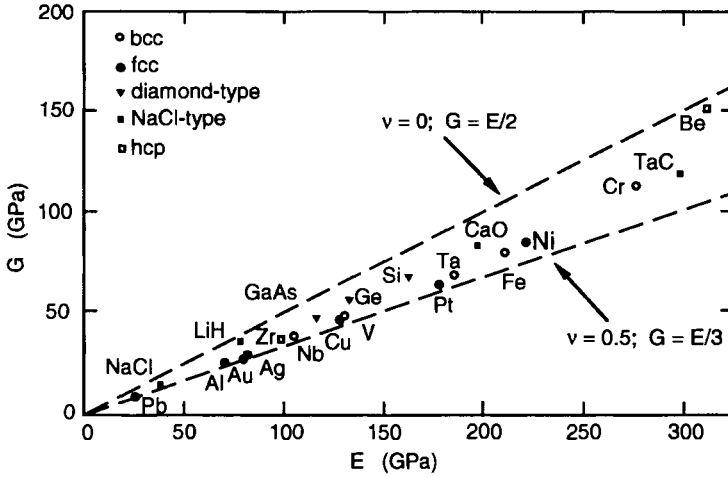
Fig. 4.4. As in fig. 4.3, but with the shear modulus G plotted versus Young's modulus
E.

6. Pressure dependence of elastic constants

In a strict application of Hooke's law, the total energy U has no terms
of higher order than $c_{ij}\varepsilon_i\varepsilon_j$. In a real material, higher-order terms are
present, thus causing the elastic constants to depend on pressure (strain)
(Chapter 3, §4). Furthermore, when a crystal is under pressure the ex-
pansion of U in terms of small strains refers to a crystallographic unit
cell that is smaller than that at zero pressure, which also affects c_{ij}
defined from derivatives of U.

The elastic constants are often determined from ultrasonic wave ex-
periments. Then it is natural to speak of *effective* elastic constants, to be
distinguished from the *thermodynamic* definition, as in eq. (3.15). As an
example, we consider the pressure dependence of c_{11} determined from
experiments as the ratio

$$(\partial c_{11}/\partial p) = [\rho C_L^2(\text{at } p) - \rho_0 C_L^2(\text{at } p = 0)]/p. \tag{4.14}$$

Here C_L is the sound velocity of the longitudinal branch in the [100]
direction of a cubic lattice, and ρ and ρ_0 are the mass densities at p and
$p = 0$, respectively. For *cubic lattice symmetry*, one has (Thurston and
Brugger 1964, Brugger 1965b)

$$-(\partial c_{11}/\partial p)_{p=0} = 1 + (1/3K)(c_{11} + c_{111} + 2c_{112}), \tag{4.15}$$

$$-(\partial c_{12}/\partial p)_{p=0} = -1 + (1/3K)(c_{12} + c_{123} + 2c_{112}), \qquad (4.16)$$

$$-(\partial c_{44}/\partial p)_{p=0} = 1 + (1/3K)(c_{44} + c_{144} + 2c_{155}), \qquad (4.17)$$

Then, by $K = (c_{11} + 2c_{12})/3$, it follows that

$$-(\partial K/\partial p)_{p=0} = (c_{111} + 6c_{112} + 2c_{123})/9K. \qquad (4.18)$$

The difference in the pressure dependence of adiabatic and isothermal elastic constants is discussed by Barsch (1967), with numerical applications to 25 materials (Barsch and Chang 1967). Typically, the two pressure derivatives differ by a few percent at ambient temperature. See also table 13.1 for values of $(\partial K/\partial p)$. In materials showing invar-effects elastic properties may have an anomalous pressure dependence (see §13).

Example: $\partial c_{ij}/\partial p$ for aluminium and iron. With experimental values inserted from the Landolt–Börnstein tables (Every and McCurdy 1992), eqs. (4.15)–(4.17) take the following form for aluminium;

$$\partial c_{11}/\partial p = -1 - (108 - 1080 - 2 \times 315)/232 = 5.9,$$

$$\partial c_{12}/\partial p = 1 - (62 + 36 - 2 \times 315)/232 = 3.3,$$

$$\partial c_{44}/\partial p = -1 - (28 - 23 - 2 \times 340)/232 = 1.9. \qquad (4.19)$$

For bcc iron, we get $\partial c_{11}/\partial p = 6.7$, $\partial c_{22}/\partial p = 4.5$, $\partial c_{33}/\partial p = 2.7$. Furthermore, $(\partial K/\partial p) = 5.2$ (Al) and 5.1 (Fe) (table 13.1).

7. Volume dependence of elastic constants

The volume dependence of elastic properties is, of course, closely related to their pressure dependence. In the theory of anharmonic lattice vibrations (Chapter 8), we introduce the Grüneisen parameter $\gamma(\mathbf{q}, s) = -(\partial \ln \omega(\mathbf{q}, s)/\partial \ln V)$, where $\omega(\mathbf{q}, s)$ is the frequency of a phonon with wave vector $\mathbf{q}$ and mode index s. In the long-wavelength limit, $\omega(\mathbf{q}, s) = C_s(\mathbf{q})|\mathbf{q}|$, where $C_s(\mathbf{q})$ is the sound velocity. Consider now a longitudinal sound wave ($s = \text{L}$) in the [100] direction of a cubic lattice. Then $C_\text{L} = (c_{11}/\rho)^{1/2}$, where ρ is the mass density. Because

$|\mathbf{q}|/\rho^{1/2}$ varies with the volume V as $V^{1/6}$, we get for the corresponding Grüneisen parameter (cf. Brugger and Fritz 1967)

$$\gamma_L[100] = -\left(\frac{d \ln \omega_L}{d \ln V}\right) = -\frac{1}{2}\left(\frac{d \ln c_{11}}{d \ln V}\right) - \frac{1}{6}$$

$$= \frac{K}{2c_{11}}\left(\frac{\partial c_{11}}{\partial p}\right) - \frac{1}{6}. \tag{4.20}$$

From the sound velocities expressed in c_{ij} (table 5.1), we can define Grüneisen parameters $\gamma_L[hkl]$, $\gamma_{T1}[hkl]$ and $\gamma_{T2}[hkl]$, referring to the longitudinal and the two transverse modes, respectively. If the system is isotropic, we are left with only two Grüneisen parameters:

$$\begin{aligned}\gamma_L &= (K/2c_{11})(\partial c_{11}/\partial p) - 1/6 \\ &= -K/2c_{11} - (c_{111} + 2c_{112})/6c_{11} - 1/3, \end{aligned} \tag{4.21}$$

$$\begin{aligned}\gamma_T &= (K/2c_{44})(\partial c_{44}/\partial p) - 1/6 \\ &= -K/2c_{44} - (c_{144} + 2c_{155})/6c_{44} - 1/3. \end{aligned} \tag{4.22}$$

Furthermore, we can write

$$\begin{aligned}\left(\frac{\partial \ln K}{\partial \ln V}\right)_T &= \frac{V}{K_T}\left(\frac{\partial K}{\partial V}\right)_T \\ &= \frac{V}{K_T}\left(\frac{\partial K}{\partial p}\right)_T\left(\frac{\partial p}{\partial V}\right)_T = -\left(\frac{\partial K}{\partial p}\right)_T. \end{aligned} \tag{4.23}$$

Note that for an elastically *isotropic* system, a knowledge of the two sound velocities suffices to determine the two linearly independent elastic constants (e.g. c_{11} and c_{44}). There are only three linearly independent third-order elastic coefficients and only two Grüneisen parameters. In the general anisotropic case, and in order to obtain all c_{ijk}, one has to measure the sound velocities not only for varying crystal volume but also for, say, uniaxial tension (cf. Thurston and Brugger 1964). Elastic Grüneisen parameters in non-cubic systems have been calculated by Gerlich (1969).

The accidental equality $c_{11} - c_{12} = 2c_{44}$ makes the single crystal of cubic symmetry elastically isotropic, but such an isotropy does not imply that the Grüneisen parameter is isotropic. On the other hand, there

Table 4.2

Sound velocity (unit: m/s) and sound wave Grüneisen parameters in aluminium and iron

$[hkl]$		C_L	γ_L	C_{T1}	γ_{T1}	C_{T2}	γ_{T2}
[100]	Al	6320	1.95	3240	2.44	3240	2.44
	Fe	5420	2.17	3860	1.66	3860	1.66
[110]	Al	6480	2.05	3240	2.44	2920	2.03
	Fe	6180	2.05	3860	1.66	2460	1.65
[111]	Al	6530	2.10	3030	2.19	3030	2.19
	Fe	6420	2.03	3000	1.65	3000	1.65

are truly isotropic systems, e.g. glasses, for which eqs. (4.21) and (4.22) hold.

Example: sound-velocity Grüneisen parameters in aluminium and iron. Using the relation (4.20), and the analogous results for other directions $[hkl]$ and for the two transverse modes, and with the data for c_{ij} and c_{ijk} from Every and McCurdy (1992), we obtain the sound velocities C_s and the Grüneisen parameters γ_s of table 4.2. Note that although C_T is almost isotropic for Al, γ_{T1} and γ_{T2} vary considerably with $[hkl]$.

8. Temperature dependence of elastic constants

8.1. Normal temperature dependence, caused by anharmonicity

Wachtman et al. (1961) (see also Durand 1936) noted empirically that the temperature dependence of Young's modulus E of several oxides could be well fitted to

$$E(T) = [1 - bT \exp(-T_0/T)]E(0). \tag{4.24}$$

An expansion of the exponential term for $T \gg T_0$ gives, to leading order,

$$E(T) \approx [1 - b(T - T_0)]E(0). \tag{4.25}$$
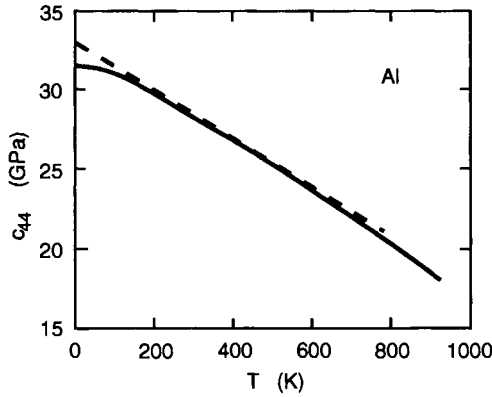
Fig. 4.5. Temperature dependence of c_{44} in Al (solid curve), with data from Every and McCurdy (1992). The dashed line is an extrapolation to low T of the low-order anharmonic correction. Its intercept with the vertical axis gives the value of c_{44} in a "harmonic" system. The measured c_{44} is lower, because of the zero-point vibrations.

This temperature dependence is observed for many systems other than oxides, and for elastic constants other than E (see, for instance, fig. 4.5). Anderson (1966a) has shown how eq. (4.24) can be understood from the quasi-harmonic model of lattice vibrations. We shall partly follow that work but also make contact with the treatment in Chapter 8, of anharmonic lattice vibrations. The elastic constants can be related to the long-wavelength limit of phonons. Anharmonicity shifts a phonon frequency $\omega(\mathbf{q}, s)$ by an amount $\Delta\omega(\mathbf{q}, s)$. In an Einstein model, we may write for shifts $\Delta\omega$ relative to ω at $T = 0$, (eq. (8.27)),

$$\frac{\Delta\omega(\mathbf{q}, s)}{\omega(\mathbf{q}, s)} = \frac{k(\mathbf{q}, s)}{\exp(\theta_E/T) - 1}. \qquad (4.26)$$

Here $\mathbf{q}$ is the wave vector of the phonon, s is a mode index (longitudinal or transverse modes etc.), $k(\mathbf{q}, s)$ is a dimensionless proportionality constant and θ_E is an Einstein temperature characteristic of the entire phonon spectrum. Let Y be an elastic constant. A dimensionally correct relation between Y and ω is $(Y/\rho)^{1/2} = \omega/|\mathbf{q}|$. The mass density ρ varies as $1/V$ and $|\mathbf{q}|$ as $V^{-1/3}$, where V is the sample volume (per mole etc.). Within our simple model, the thermal expansion $V(T) - V(0)$ has the same temperature dependence as $\Delta\omega/\omega$. (In fact, $\Delta\omega$ is to a large extent due to the thermal expansion.) Thus, an expression of the type $(\omega/|\mathbf{q}|)\rho^{1/2}$ has a temperature-dependent shift which varies with T

as $[\exp(\theta_E/T) - 1]^{-1}$. In our model the same temperature dependence enters all (small) shifts in the elastic constants. We summarise this by the relation

$$\frac{\Delta Y}{Y} = \left(\frac{a_Y}{\theta_E}\right) \frac{\theta_E}{\exp(\theta_E/T) - 1},\tag{4.27}$$

where a_Y is a dimensionless proportionality factor varying with the elastic parameter Y under consideration. Comparing the high temperature expansions $T \exp(-T_0/T) = T - T_0 + T_0^2/2T - \cdots$ and $\theta_E[\exp(\theta_E/T) - 1]^{-1} = T - \theta_E/2 + (1/12)\theta_E^2/T + \cdots$, we note that the two leading terms are identical if $T_0 = \theta_E/2$. This gives a theoretical justification for the empirical rule (eq. (4.25)) at intermediate and high temperatures, and for the fact that T_0 was observed to be about 1/3 of the Debye temperature. Since the Debye temperature is less than 500 K for most solids, we also understand why the linear temperature dependence expressed by the series expansion (eq. (4.25)) is such a good approximation at ambient and higher temperatures. (Close to the melting temperature, high-order anharmonic effects usually give a stronger temperature dependence than linear in T, cf. Chapter 8, §6.)

Our shifts $\Delta\omega(\mathbf{q}, s)$ were taken relative to $T = 0$ K. In fact, there is a shift even at $T = 0$, due to the anharmonicity related to the zero-point vibrations. The intercept of the linear portion of $c_{ij}(T)$ with the c_{ij}-axis at $T = 0$ K gives the "harmonic" c_{ij} (see Appendix E and fig. 4.5).

The temperature-dependent part of the energy U (or enthalpy H, Helmholtz energy F, Gibbs energy G) of an insulator varies as T^4 at low T (since C_p and $C_V \sim T^3$). From the fundamental relations of the elastic coefficients expressed as derivatives of U, H, F or G (Chapter 3, §3), it follows that $dY/dT \sim T^3$ at low T. The Einstein model used above to account for the temperature-dependent factor in the empirical relation (eq. (4.24)) gives too rapid (exponential) a temperature dependence at low T. However, the absolute magnitude of the shift ΔY at these temperatures is so small that this discrepancy is of little practical importance. In metals, U, H, F and G vary as T^2 due to the excitation of electron states, but this term is important only at such low T that it is of no interest in the present context.
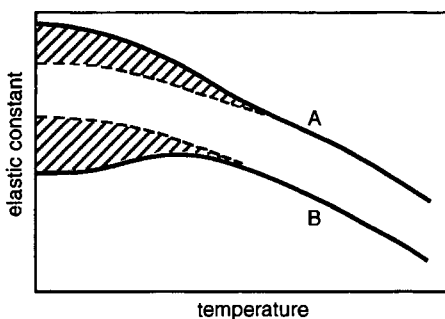
Fig. 4.6. A schematic illustration of an anomalous temperature dependence of an elastic coefficient, caused by features in the electron band structure close to the Fermi level. The smooth dashed curve shows the extrapolation to low T that would result if anharmonic effects is the only cause of a temperature dependence. The hatched parts correspond to the additional electronic contribution. It may increase or decrease the elastic coefficient.

8.2. Anomalous temperature dependence, caused by electronic structure

In some cases, one or several of the elastic coefficients c exhibit a marked temperature dependence also at relatively low temperatures, often below room temperature. Figure 4.6 shows schematically such a behaviour. The smooth decrease with increasing temperature, shown as a dashed curve for low T and a solid curve for high T, is the normal variation of c due to anharmonic effects. Superimposed is a variation illustrated by the shaded area, leading to a low-temperature dependence of c on T as given by the solid curve. Although the "anomalous" contribution at low T is not yet fully understood, it is naturally explained by features in the electron band structure in the immediate vicinity of the Fermi level, which can be reached by thermal excitations. The temperature dependence then has its roots in Fermi–Dirac statistical factors for the electrons. The "normal" variation in the elastic constants at high T, related to anharmonicity, has its roots in the increased vibrational displacement, i.e. in the Bose–Einstein factors for the phonons. (The most important result of anharmonicity is to cause thermal expansion, which affects the elastic constants through their volume dependence.) There is a close connection between an anomalous temperature dependence of c_{ij} as discussed here, and a dependence of c_{ij} on the composition of certain alloys (see §11).

9. Dependence on lattice structure and order

9.1. Polymorphs

Some materials occur in two or several different crystal structures, when the temperature or pressure is varied. There are only few measurements of the engineering elastic constants (K, G, E, v) on such polymorphic phases. E and G in iron and in some Fe–Ni alloys change by less than 10% when the crystal structure changes from bcc to fcc (Ledbetter and Reed 1973). There seem to be no direct measurements of c_{ij} in pure fcc iron (γ-Fe), which is stable in the temperature interval 1173–1660 K. Indirectly, c_{ij} could be inferred from the slope of phonon dispersion curves, derived from inelastic neutron scattering experiments, but the c_{ij} obtained in this way are rather uncertain.

Figure 4.3, where G is plotted versus K, shows no conspicuous difference between the bcc and the close-packed lattice structures. In particular, G of the bcc metals is not systematically smaller, in spite of the tendency for a bcc lattice to have a low frequency vibrational shear mode in [110] direction (Chapter 6, §12). However, fig. 4.3 may be misleading, since it only refers to phases that are actually observed. In §3, we noted that there are many cases when a common lattice structure is in fact dynamically unstable under shear, even though the observed structure is very stable. One example is tungsten, that crystallises in a bcc lattice but is unstable under all shear in the hypothetical fcc lattice (fig. 4.2).

9.2. Order-disorder transformations

Some compounds have an order-disorder transformation. Experiments on Cu_3Au (Flinn et al. 1960) and β-CuZn (McManus 1963) show that the elastic constants c_{ij} of the ordered and the disordered states typically differ by a few percent at most. An isotopic disorder has negligible effect on the electronic structure, and hence also on c_{ij}—see experiments on ^6Li and ^7Li (Felice et al. 1977). See also Chapter 6 (§15) for comments on phonons in disordered lattices.

9.3. Martensitic transformations

Martensitic transformations originally referred to transformations accompanying the quenching of certain steels. The concept is now used in a much wider context, as a description of diffusionless crystallographic transformations that are almost reversible. The elastic constants may show a dramatic discontinuous change as one passes the critical temperature (or critical composition) of some transformations. A soft-mode behaviour may also occur, as is well known from, e.g. $SrTiO_3$. Nakanishi (1979) reviewed elastic constants in relation to martensitic transformations in ionic solids, oxides, metallic alloys and other materials.

9.4. Molecular crystals

The molecular crystal KCN has a NaCl-type lattice with a dumb-bell-like $[CN]^{-1}$ ion that is orientationally disordered at high temperatures, but orders partially at lower T, eventually leading to a rhombic phase for KCN. The elastic coefficient c_{44} of the cubic lattice decreases strongly as T is lowered (Haussühl 1973). There has been much interest in the elastic properties of this and similar molecular crystals, e.g. Rowe et al. (1978), Sahu and Mahanti (1983) and Strössner et al. (1983).

9.5. Glasses

Metallic glasses are statistically isotropic, and therefore described by two independent engineering elastic constants. We consider K and G. The bulk modulus of the glass is usually at most a few percent lower than in the crystalline phase. The shear modulus G, on the other hand, may be typically 30% lower in the glassy state (Logan and Ashby 1974). For instance, in $Pd_{0.775}Si_{0.165}Cu_{0.06}$, Golding et al. (1972) found that K was lower by 6% and G was lower by 35% in the amorphous state. The small change in K is consistent with the small volume difference, i.e. a few percent lower mass density in the amorphous state (cf. table 19.1). If only the volume difference is considered, we expect that $\Delta K / K \approx -2\gamma_G(\Delta V / V)$, where γ_G is a Grüneisen parameter of the order of 2. The large shift in G may be understood from the fact that the atoms in the glass do not take positions in deep symmetric potential wells, but can be displaced a substantial amount under shear forces. This qualitative picture is supported by numerical simulations using a

Morse interaction between the atoms (Weaire et al. 1971). The relation $E = 3G[1 + G/3K]^{-1}$, and the fact that usually $G < K$, implies that E and G covary. Hence, also Young's modulus may be substantially lower in the amorphous than in the crystalline state. A similar but much larger effect has been observed in amorphous films. The transverse sound velocity in a gallium film was smaller by a factor of 2.8 in the amorphous state, while there was no significant change in the longitudinal sound velocity (Dietsche et al. 1980). The heat capacity Debye temperature in amorphous films of Si and Ge is lower than the bulk value by $\sim$20% (Mertig et al. 1984). This is due to a lowering of the transverse acoustic modes, i.e. a lowering of G.

10. Influence of solute atoms

We shall take several different approaches to an estimation of how the elastic properties are affected by point defects; an atomistic nearest-neighbour force constant description, an elastic continuum theory, and an electron-band consideration in metals.

Atomistic force-constant models. In a simple picture of a solid, atoms are connected by springs. The introduction of a small number of point-like defects means that certain springs are changed. The elastic properties depend on some average over all the springs and therefore should vary smoothly with the defect concentration. Let there be N atoms in a monatomic solid, with p_i springs of type i and force constant f_i attached to each atom. A small fraction, c, of all atoms are replaced. Then, cNp_i springs have their strength changed by Δf_i. Averaged over the crystal, the force constant of type i is

$$\bar{f}_i = f_i[1 + 2c(\Delta f_i/f_i)]. \tag{4.28}$$

For a vacancy, we can take $\Delta f_i = -f_i$, and get $\bar{f} = (1 - 2c)f_i$. Such considerations can be put on a firmer mathematical basis. Consider an fcc lattice with only nearest-neighbour central interactions. The force constants attached to a substitutional defect change from f to $f + \Delta f$. Neglecting relaxation around the defects, one obtains (Dederichs and Zeller 1980, Leibfried and Breuer 1978)

$$\frac{\Delta(c_{11} + 2c_{12})}{c_{11} + 2c_{12}} = \frac{\Delta K}{K} = \frac{2c(\Delta f/f)}{1 + 0.24\Delta f/f}, \tag{4.29}$$

with the analogous results $\Delta(c_{11} - c_{12})/(c_{11} - c_{12}) = 2c(\Delta f/f)/(1 + 0.38\Delta f/f)$ and $\Delta c_{44}/c_{44} = 2c(\Delta f/f)/(1 + 0.33\Delta f/f)$. For a vacancy, $\Delta f/f = -1$. Then all relative shifts of c_{ij} are of the order of $3c$.

In our simple model it was assumed that the positions of the atoms are not affected when the forces between them are altered, but in a real solid there are relaxations. We can identify two contributions. First, there is an inhomogeneous relaxation in the immediate neighbourhood of the defect. For a statistical distribution of defects, there is also a uniform volume change (V_{def} per defect) of the sample. From a knowledge of V_{def}, the bulk modulus K and the anharmonic parameters $\partial c_{ij}/\partial p$ and with eq. (4.15) we get a shift $(\Delta c_{11})^*$ per defect, where

$$
\begin{aligned}
(\Delta c_{11})^* &= V_{\text{def}} \left(\frac{\partial p}{\partial V} \right) \left(\frac{\partial c_{11}}{\partial p} \right) \\
&= V_{\text{def}} \frac{K}{V} \left(1 + \frac{c_{11} + c_{111} + 2c_{112}}{3K} \right),
\end{aligned}
\tag{4.30}
$$

with similar expressions for the shifts in c_{12} and c_{44}.

Elastic-continuum model. The elastic-sphere model of Eshelby (1975) is another approach to the influence of small defects on the elastic properties. In a homogeneous material, characterised by any two of the parameters K, G, E and v, there are randomly distributed spherical inclusions with elastic properties given by K', G', E' and v'. In the dilute limit ($c \ll 1$ where c is the volume fraction of inclusions) one obtains

$$
\frac{1}{K} \frac{dK}{dc} = \left[\frac{1 + v}{3(1 - v)} + \frac{K}{K' - K} \right]^{-1},
\tag{4.31}
$$

$$
\frac{1}{G} \frac{dG}{dc} = \left[\frac{2}{15} \frac{4 - 5v}{1 - v} + \frac{G}{G' - G} \right]^{-1}.
\tag{4.32}
$$

This model is now applied to inclusions as small as a single atom. With the typical value $v \approx 1/3$ and very stiff ($K' \gg K$, $G' \gg G$) or very soft ($K' \ll K, G' \ll G$) inclusions, we get relative changes $|(dK/dc)|/K$ and $|(dG/dc)|/G$ that are numerically similar to those in the previous paragraph. We note that eqs. (4.31) and (4.32) follow directly from the relations (17.31) and (17.32) for the elastic properties of composite materials.

Table 4.3

The isentropic c_{ij} at 298 K, in units of GPa

	c_{11}	c_{12}	c_{13}	c_{33}	c_{44}
Pure Mg	59.28	25.90	21.57	61.35	16.32
Mg-1.35 at.% In	59.55	26.26	22.01	61.48	16.25
$\Delta c_{ij}/c_{ij}$, per at.% In	0.003	0.010	0.015	0.002	−0.003

Example: c_{ij} in dilute alloys. Eros and Smith (1961) measured the isentropic (adiabatic) stiffnesses c_{ij} in hcp magnesium alloys with up to a few at.% of Ag, In or Sn. Table 4.3 gives typical results. The relative shifts $\Delta c_{ij}/c_{ij}$, are less than 0.01 per at.% solute. This can be compared with the relative shift ~0.03 per at.% of vacancies for the model in eq. (4.29). Note that the shift in c_{44} is opposite in sign to that of c_{11} and c_{12} for Mg–In. Greiner et al. (1977) measured c_{ij} in cubic Th and $ThC_{0.063}$. They obtained $\Delta c_{ij}/c_{ij} = +0.039$ for c_{11}, −0.004 for c_{12} and −0.052 for c_{44}, i.e. <0.01 per at.% carbon added.

11. Band structure effects in metallic alloys

The elastic constants ultimately depend on the electronic structure of a solid. Normally, the electronic structure varies slowly and smoothly with the composition of an alloy. However, there are cases when the Fermi surface is significantly affected by a small change in the composition. Pockets or holes of electrons in reciprocal space may appear or disappear, necks on the Fermi surface may open or close, etc. This is known as *electronic topological transitions*. A drastic effect would be a metal-to-insulator transition, but here we consider only the metallic state. Effects on elastic constants have been dealt with by, e.g. Vaks and Trefilov (1988, 1991), and the field has been reviewed by Bruno et al. (1994).

Figure 4.7 shows how the room-temperature value of c_{44} depends on the concentration c in bcc $Nb_{1-c}Mo_c$ alloys. If an electron band structure has features close to the Fermi level that will lead to elec-
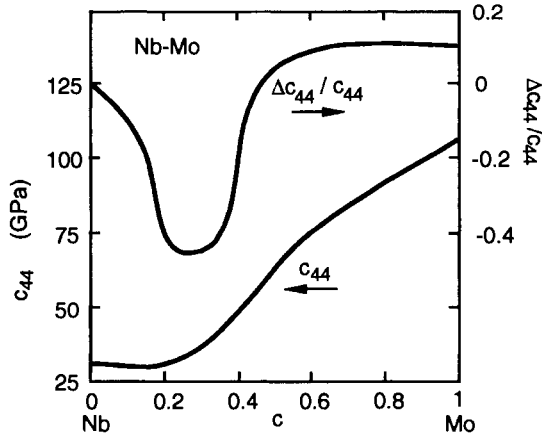
Fig. 4.7. The measured elastic constant c_{44} at room temperature, as a function of the composition, in $Nb_{1-c}Mo_c$ alloys (left scale), and the temperature dependence of c_{44} expressed as $[c_{44}(T) - c_{44}(0)]/c_{44}(0) = \Delta c_{44}/c_{44}$ evaluated with $T = 1000$ K (right scale). Based on experimental data in Every and McCurdy (1992).

tronic topological transitions with changing composition, it will also tend to show temperature induced anomalies of the kind discussed in §8.2. The simple physical picture is that if a feature in the electronic structure is close enough to the Fermi level to be reached through a moderate change in the electron concentration on alloying, it could also be reached (at fixed concentration) by thermal smearing of the Fermi–Dirac function. This is illustrated in fig. 4.7 by the plot of $[c_{44}(T) - c_{44}(0)]/c_{44}(0)$ evaluated at $T = 1000$ K. Anomalies of this kind have been observed in many metallic alloys. In cubic alloys they may be seen in c_{44} as well as in $C' = (c_{11} - c_{12})/2$, but are usually not pronounced in c_{44} and C' at the same time (Every and McCurdy 1992, Bruno et al. 1994).

12. Effect of dislocations and grain boundaries

Measurements of the constants G and E in a cold-worked material (i.e. a material with a high dislocation density) may be typically 5–20% lower than in the annealed state. The bulk modulus, on the other hand, is not much changed on cold working. Even with a dislocation density Λ as high as 10^{16} m^{-2}, less than 1% of all atoms (on the average) are adjacent

to the dislocation cores. Therefore, the decrease in G and E is not related to "bond cutting" or volume changes (as is the effect of vacancies on elastic properties). Instead it is caused by the reversible motion of the dislocations (Read 1940, Eshelby 1949, Mott 1952, Friedel 1953, Koehler and deWit 1959). The shift in Young's modulus can be written

$$\frac{\Delta E}{E} = -k\Lambda L^2. \tag{4.33}$$

Here, k is a dimensionless constant ~ 0.1, Λ is the dislocation density and L the dislocation line length. Since L depends on the pinning of dislocations, impurities may have an appreciable indirect effect on G and E. There may also be reversible grain boundary sliding, which affects the apparent G and E.

In this context we should remark on the measurement of elastic parameters. Young's modulus is defined as the ratio of uniaxial stress to strain. In many experiments, the stress varies sinusoidally with the frequency ω. If the material is strictly elastic, the strain will follow the stress without phase lag. In anelastic (i.e. dissipative) materials, the strain still varies with the frequency ω, but there is a phase difference between stress and strain. Then E is not uniquely defined. The measured G (or E) has one truly elastic part E_0 and one anelastic part (Zener 1948). We can write

$$E(\omega) = E_0 - \frac{E_0 - E_R}{1 + (\omega\tau)^2}. \tag{4.34}$$

E_R includes relaxations and τ is a characteristic time for stress and strain relaxation. The reader is also reminded of the difference between isothermal and adiabatic elastic constants (see Chapter 3, §3 and Chapter 13, §9).

When a polycrystalline material is deformed, it may develop a texture, i.e. a statistically anisotropic distribution of the crystallographic orientation of the individual crystallites. If the single-crystal elastic properties are anisotropic, this leads to an apparent change in the engineering elastic constants of the polycrystal which may completely mask the change due to dislocations (Weiner et al. 1975). It may also yield an apparent Poisson ratio $\nu > 1/2$, in violation of the condition (4.3) on ν (Ledbetter and Reed 1973). See Chapter 18 for further aspects of polycrystalline materials.

In nanocrystalline materials, the grain boundary regions occupy a significant fraction of the solid volume. This can lower the Young's modulus by 15–25% (Schiøtz et al. 1998). Kluge et al. (1990) considered local elastic constants at grain boundaries, through atomistic simulations.

13. Dependence on magnetic state and magnetic fields

An external magnetic field affects Young's modulus of ferromagnetic materials. This is often referred to as the ΔE *effect*, a name given by its discoverers, Honda et al. (1902). Since E and G covary, G is also affected, while the bulk modulus K depends only weakly on magnetic fields. The physical basis for the effect is the same as for magnetostriction. A (non-saturated) magnetic material has more or less randomly oriented magnetic domains. The magnetic energy of these domains couples to the elastic strain energy. Typically, E and G of an annealed specimen (i.e. with very low residual elastic strains) may be 10–20% less than in the unannealed state (Ledbetter and Reed 1973). This is also the order of magnitude of the shifts in E and G when a strong magnetic field is applied. In some metallic glasses, Young's modulus may change by more than a factor of two. The ΔE effect is unusually large in some Fe–B amorphous alloys (Kikuchi et al. 1978, Mitchell et al. 1979). The ΔE effect decreases as the temperature is increased, and is zero above the Curie temperature.

It may happen that the magnetoelastic effect cancels the decrease in E caused by anharmonicity. The result is a Young's modulus which is almost temperature independent over a certain temperature interval. This is the *elinvar* effect (Guillaume 1920). Invar alloys have a very small thermal expansion (of any sign) in a certain temperature range, but show a positive expansion at other temperatures (Chapter 14, §9). This may be viewed as due to a cancellation of the thermal expansion caused by anharmonicity in the lattice vibrations, and a magnetic term that tends to shrink the material with increasing temperature. The elastic constants behave anomalously in the invar-region. For instance, $(\partial c_{11}/\partial p)$ and $(\partial K_S/\partial p)$ are negative for $Fe_{72}Pt_{28}$ (Mañosa et al. 1992, Saunders et al. 1993). The dependence of c_{ij} on composition, temperature and magnetic field in fcc Fe–Ni alloys has been investigated by Hausch and Warlimont (1973). They find an elinvar behaviour at $\sim 45\%$
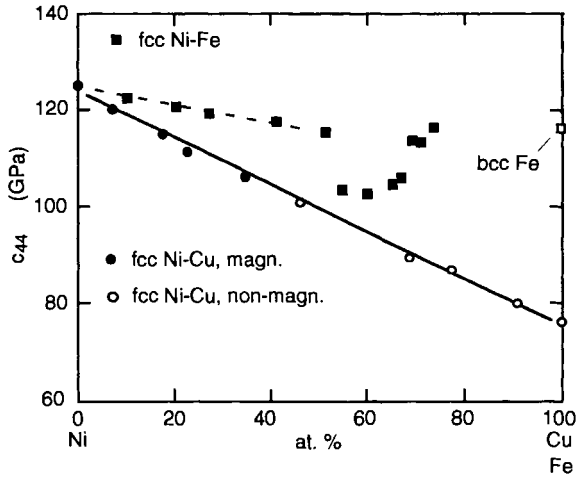
Fig. 4.8. The measured elastic constant c_{44} at room temperature, as a function of the composition, in Ni–Cu and Ni–Fe alloys. Based on experimental data in Every and McCurdy (1992).

Ni; see fig. 4.8, which also shows c_{44} in Ni–Cu alloys that are magnetic in the Ni-rich end. Magnetoelastic phenomena have been reviewed by Steinemann (1978, 1979).

Some metals are strongly paramagnetic, i.e. they almost satisfy the Stoner criterion for an ordered magnetic state (Chapter 10, §3.5). The Debye temperature $\theta_D(-3)$, and hence the elastic parameters, were found to be insensitive to an external magnetic field of strength ≈ 10 T, for $LuCo_2$ (Ikeda and Gschneidner 1980) and Pd (Hsiang et al. 1981). Similarly, the difference in c_{ij} in ferromagnetic nickel in zero magnetic field and in a saturation field is less than 2% at room temperature, i.e. well below the Curie temperature $T_C = 627$ K (Epstein and Carlson 1965). In the vicinity of the critical temperature of magnetic ordering, the elastic constants may show pronounced anomalies. They are particularly large in Cr near the Néel temperature (Every and McCurdy 1992).

SOUND WAVES

1. Introduction

In an isotropic engineering material, e.g. a texture-free piece of poly-crystalline iron, there are two kinds of sound waves, corresponding to *longitudinal* and *transverse* vibrations. The longitudinal mode has the velocity $C_L = \{[K + (4/3)G]/\rho\}^{1/2}$ and the transverse mode has the velocity $C_T = \{G/\rho\}^{1/2}$. Here ρ is the mass density of the medium. In this case there is no distinction between *phase velocity* and *group velocity*. The transverse mode is degenerate; its vibrations can be along any of two (arbitrary) directions perpendicular to the velocity vector.

In a single crystal there are still three modes for sound waves, with velocities expressed in the elastic constants of the medium and the crystallographic direction of the wave vector. However, they can no longer be classified as pure longitudinal and transverse waves, and the phase velocity is not parallel to, or equal in magnitude to, the group velocity except in certain symmetry directions of the lattice. Our approach is related to the treatment of lattice vibrations in Chapter 6, and sound waves may be viewed as the long-wavelength limit of phonons.

2. Formulation of the secular equation

Let the displacement vector $\mathbf{u} = (u_x, u_y, u_z)$ of a sound wave be

$$u_j = A_j \exp[i(q_1 x + q_2 y + q_3 z - \omega t)]. \tag{5.1}$$

The index j refers to Cartesian coordinates. We will write $j = x, y, z$ or $j = 1, 2, 3$, alternatively. The displacement in eq. (5.1) is a complex quantity, while the actual displacement is, of course, real. However, both

the real and imaginary parts of **u** are solutions to the equation of motion. It is convenient to lump the two solutions together, as in eq. (5.1). The sound wave has the frequency ω and the wave vector $\mathbf{q} = (q_1, q_2, q_3)$. The (phase) velocity of the mode s is

$$C_s(\mathbf{q}) = \omega(\mathbf{q}, s)/|\mathbf{q}|. \tag{5.2}$$

When there is no risk of confusion with the Cartesian index j, we let the label s have any of the values 1, 2 or 3. The wave properties are obtained from the equation

$$\begin{pmatrix} \Gamma_{11} - \rho\omega^2 & \Gamma_{12} & \Gamma_{13} \\ \Gamma_{21} & \Gamma_{22} - \rho\omega^2 & \Gamma_{23} \\ \Gamma_{31} & \Gamma_{32} & \Gamma_{33} - \rho\omega^2 \end{pmatrix} \begin{pmatrix} A_1 \\ A_2 \\ A_3 \end{pmatrix} = 0. \tag{5.3}$$

This is known as the *Christoffel* (1877) (also Christoffel–Kelvin or Green–Christoffel) equation. The quantities Γ_{ij} are related to $\mathbf{q}$ and the elastic coefficients by

$$\Gamma_{ij} = \sum_{k,l=1}^{3} (1/2)(c_{kijl} + c_{kilj})q_k q_l, \tag{5.4}$$

and ρ is the mass density of the material. There are non-trivial solutions (A_1, A_2, A_3) to eq. (5.3) only if ω is a solution to the *secular equation*

$$|\Gamma_{ij} - \rho\omega^2 \delta_{ij}| = 0. \tag{5.5}$$

Here $|\ldots|$ is a 3 × 3 determinant and $\delta_{ij} = 0$ for $i \neq j$ and 1 for $i = j$. Often, eq. (5.5) is written as an equation for the sound velocity C, i.e. with ω^2 replaced by $C^2 q^2$. We shall now consider the solution to the secular equation, first in a general mathematical formulation, then in terms of the engineering elastic constants for an elastically isotropic system, for a single crystal of cubic symmetry, and finally for hexagonal lattice symmetry.

3. General solution of the secular equation

Since eq. (5.5) is a cubic equation in C^2 (or ω^2), it has solutions in a closed mathematical form, for any lattice symmetry. A convenient expression for C_s is (Every 1979, 1980)

$$3\rho C_s^2 = T + 2\sqrt{G}\cos[\Psi + (2\pi/3)(s-1)]; \quad s = 1, 2, 3. \quad (5.6)$$

The quantities T, G and Ψ contain the elastic constants and the direction cosines of $\mathbf{q}$, and s also serves as a mode index. If $\Psi = 0$, the cosine term in the last part of eq. (5.6) is the same for $s = 2$ and $s = 3$, i.e. these modes then have equal velocities. Appendix D gives the explicit solution for cubic lattice symmetry.

From a well-known mathematical relation between the sum of eigenvalues, $\Sigma\omega_s^2$, and the trace of the determinant we get from eq. (5.5)

$$3\langle C_s^2 \rangle = \sum_{s=1}^{3} C_s^2 = (\Gamma_{11} + \Gamma_{22} + \Gamma_{33})/\rho\mathbf{q}^2, \quad (5.7)$$

for any lattice symmetry. In a cubic lattice (cf. eq. (5.14)).

$$\langle C_s^2 \rangle = (c_{11} + 2c_{44})/3\rho. \quad (5.8)$$

Explicit expressions for C_s in various lattice symmetries are given by Every (1980). The relation (eq. (5.8)) for cubic lattice symmetry is isotropic, i.e. it holds for each direction $\mathbf{q}$. Still, the separate velocities C_s for $s = 1, 2, 3$ may be more (Fe) or less (Al) anisotropic, as exemplified in table 4.2.

4. Secular equation for isotropic polycrystalline materials

In an isotropic material we can identify $(c_{11} + 2c_{12})/3$ and c_{44} with K and G, respectively (cf. eqs. (3.37) and (3.42)). Then the secular equation yields, for the longitudinal wave,

$$\begin{aligned}
\rho C_L^2 &= K + \frac{4}{3}G = \frac{3K(1-\nu)}{1+\nu} = \frac{G(4G-E)}{3G-E} \\
&= \frac{E(1-\nu)}{(1+\nu)(1-2\nu)} = \frac{2G(1-\nu)}{1-2\nu} = \frac{3K(3K+E)}{9K-E}. \quad (5.9)
\end{aligned}$$

The velocity C_T of transverse sound waves is given by

$$\rho C_T^2 = G. \tag{5.10}$$

Since $K > 0$ and $G > 0$,

$$C_L > \sqrt{(4/3)}C_T. \tag{5.11}$$

This inequality may be sharpened because, almost universally, the Poisson ratio $\nu > 0$ and then $C_L > \sqrt{2}C_T$. Also, when $K > G$, one has $C_L > \sqrt{(7/3)}C_T \approx 1.53C_T$. The result that the longitudinal sound velocity is higher than the transverse sound velocity holds for isotropic materials, e.g. polycrystalline materials without texture, but not necessarily for each direction in an anisotropic lattice (see the example in §5).

Example: an important average of sound velocities. In the Debye theory of the lattice heat capacity, one encounters an average sound velocity $C_{\text{sound},D}$ defined by

$$\frac{3}{C_{\text{sound},D}^3} = \frac{1}{C_L^3} + \frac{2}{C_T^3}. \tag{5.12}$$

By eqs. (5.9) and (5.10), the average velocity $C_{\text{sound},D}$ can be written

$$C_{\text{sound},D} = C_T \left\{ \frac{2}{3} + \frac{1}{3} \left[\frac{1 - 2\nu}{2(1 - \nu)} \right]^{3/2} \right\}^{-1/3}. \tag{5.13}$$

The factor in the parenthesis varies slowly with the Poisson ratio ν, e.g. $C_{\text{sound},D} = (1.12 \pm 0.02)C_T$ if $\nu = 0.31 \pm 0.14$. Since $C_T = (G/\rho)^{1/2}$, one may in this way connect G with the Debye temperature (see Chapter 6, §4, and Schreiber et al. 1973).

5. Secular equation for cubic symmetry

Among all c_{ijkl}, (i.e. $c_{\alpha\beta}$) there are only three independent parameters for a cubic lattice structure; c_{11}, c_{12} and c_{44}. The explicit form of eq. (5.5) is

Table 5.1

$\rho C^2 = \rho \omega^2 / q^2$ in three directions $[hkl]$ in a cubic lattice

Mode	[100]	[110]	[111]
Longitudinal	c_{11}	$(c_{11} + c_{12} + 2c_{44})/2$	$(c_{11} + 2c_{12} + 4c_{44})/3$
Transverse	c_{44}	c_{44}[a]	$(c_{11} - c_{12} + c_{44})/3$
		$(c_{11} - c_{12})/2$[b]	

[a] Polarised along [001].
[b] Polarised along [1$\bar{1}$0].

$$\begin{vmatrix} (c_{11} - c_{44})q_1^2 + c_{44}q^2 - \rho\omega^2 & (c_{12} + c_{44})q_1q_2 & (c_{12} + c_{44})q_1q_3 \\ (c_{12} + c_{44})q_2q_1 & (c_{11} - c_{44})q_2^2 + c_{44}q^2 - \rho\omega^2 & (c_{12} + c_{44})q_2q_3 \\ (c_{12} + c_{44})q_3q_1 & (c_{12} + c_{44})q_3q_2 & (c_{11} - c_{44})q_3^2 + c_{44}q^2 - \rho\omega^2 \end{vmatrix} = 0. \tag{5.14}$$

When the solution to this equation is expressed in the general form eq. (5.6), the angle Ψ only depends on the direction cosines of $\mathbf{q}$ and on the combination $A_E = (c_{11} - c_{12} - 2c_{44})/(c_{11} - c_{44})$ of the elastic parameters. For this reason, A_E is a natural parameter to measure the anisotropy in cubic lattices (Chapter 3, §8). The solutions to eq. (5.14) have very simple forms when $\mathbf{q}$ is along the principle crystallographic directions. Table 5.1 gives the quantity $\rho C^2 = \rho \omega^2 / q^2$ for these cases. Numerical results for Al and Fe are given in table 4.2.

Example: transverse sound velocity being highest. We noted in §4 that in a material described by the isotropic engineering elastic constants K and G, the sound velocity C_L of the longitudinal mode is always larger than C_T of the transverse mode. From table 5.1 we see that in the [111] direction, $C_T > C_L$ if $c_{12} < -c_{44}$. Lattice stability requires that $c_{44} > 0$, so $C_T > C_L$ implies that $c_{12} < 0$. This is extremely unusual, but happens for the so called intermediate-valence compound $Sm_{0.75}Y_{0.25}S$ (cf. table 4.1). Table 5.2 gives the sound velocities, calculated from data in Tu Hailing et al. (1984) (cf. with C_L and C_T in Al and Fe, table 4.2). Similarly, in the [100] direction the transverse mode has the highest velocity if $c_{44} > c_{11}$. This inequality has been reported for some Mn–Cu and Mn–Ni alloys (see Chapter 4, §5).

Table 5.2
Longitudinal and transverse sound velocities (unit m/s) in $Sm_{0.75}Y_{0.25}S$

Mode	[100]	[110]	[111]
Longitudinal	4567	3390	2894
Transverse	2292	2292; 3823	3390

6. Secular equation for hexagonal symmetry

The secular equation for an hcp lattice is easier to solve than for a cubic lattice, since it separates into a linear and a quadratic equation in ω^2. The sound velocities (phase velocities) are (Hearmon 1961, Musgrave 1970)

$$\begin{aligned}
\rho[C_{1,2}]^2 &= c_{44} + (1/2)[n^2 P + (1 - n^2)Q] \\
&\pm (1/2)\{[n^2 P + (1 - n^2)Q]^2 \\
&+ 4n^2(1 - n^2)(R^2 - PQ)\}^{1/2},
\end{aligned} \tag{5.15}$$

$$\rho[C_3]^2 = c_{44} + (1/2)(1 - n^2)(c_{11} - c_{12} - 2c_{44}), \tag{5.16}$$

with n being related to the angle θ between $\mathbf{q}$ and the crystallographic c-axis; $n = q_3/|\mathbf{q}| = \cos\theta$. Furthermore,

$$P = c_{33} - c_{44}; \quad Q = c_{11} - c_{44}; \quad R = c_{13} + c_{44}. \tag{5.17}$$

In the basal plane of the hcp lattice, $n = \cos\theta = 0$. The sound velocities are isotropic, with

$$\rho[C_1]^2 = c_{11}; \quad \rho[C_2]^2 = c_{44}; \quad \rho[C_3]^2 = (c_{11} - c_{12})/2. \tag{5.18}$$

When $\mathbf{q}$ is parallel to the crystallographic c-axis, we have $n = 1$ and

$$\rho[C_1]^2 = c_{33}; \quad \rho[C_2]^2 = \rho[C_3]^2 = c_{44}. \tag{5.19}$$

The sound velocities $C_{1(2)}$ and C_3 in eqs. (5.15) and (5.16) are isotropic, i.e. independent of the angle θ, if

$$c_{11} - c_{12} - 2c_{44} = 0; \quad P = Q; \quad PQ = R^2. \tag{5.20}$$

These relations follow from the isotropy conditions (3.63).

Example: sound velocities in zinc. The hcp single crystal of Zn is in many respects very anisotropic (see figs. 7.3 and 15.3). The elastic constants are $c_{11} = 165$, $c_{12} = 31.1$, $c_{13} = 50.0$, $c_{33} = 61.8$, $c_{44} = 39.6$ (unit GPa; data from Every and McCurdy 1992). This gives the sound velocities 2940 and 2360 m/s along the crystallographic c-axis. In the basal plane, perpendicular to the c-axis, the velocities are 4810, 3060 and 2360 m/s.

7. Phase and group velocity

We define phase velocities

$$\mathbf{C}_{\text{phase}}(\mathbf{q}, s) = \hat{\mathbf{q}}\omega(\mathbf{q}, s)/|\mathbf{q}|, \tag{5.21}$$

and group velocities

$$\mathbf{C}_{\text{group}}(\mathbf{q}, s) = \nabla_{\mathbf{q}}\omega(\mathbf{q}, s). \tag{5.22}$$

When $\mathbf{C}_{\text{phase}}$ and $\mathbf{C}_{\text{group}}$ are isotropic, the label $\mathbf{q}$ can be dropped. Then the angle ϕ between $\mathbf{C}_{\text{phase}}(\mathbf{q}, s)$ and the displacement vector $\mathbf{u}(\mathbf{q}, s) = (u_x, u_y, u_z)$ for the atomic vibrations is either zero (the longitudinal mode), or 90° (the two transverse modes). In this case, one speaks of *pure modes*. The longitudinal pure mode has the phase velocity $C_L = (c_{11}/\rho)^{1/2}$ and the two degenerate transverse pure modes have velocities $C_T = (c_{44}/\rho)^{1/2}$.

A single crystal often has quite anisotropic elastic properties. Then the three vectors $\mathbf{C}_{\text{phase}}(\mathbf{q}, L)$, $\mathbf{C}_{\text{group}}(\mathbf{q}, L)$ and $\mathbf{u}(\mathbf{q}, L)$ are not parallel (except for $\mathbf{q}$-vectors in certain symmetry directions) and $\mathbf{C}_{\text{phase}}$ and $\mathbf{C}_{\text{group}}$ also differ in magnitude. Still it is customary to call the modes "longitudinal" (or *quasilongitudinal*) and "transverse" (or *quasitransverse*). The label of a branch is then retained as one moves with the $\mathbf{q}$-vector away from a symmetry direction where the mode is pure. Since eigenvectors referring to different eigenvalues are normal to each other, the vectors $\mathbf{u}(\mathbf{q}, s)$ for $s = 1$, 2 and 3 are orthogonal. Brugger (1965a) has listed cystallographic directions of pure modes, and the corresponding phase velocities expressed in elastic constants, for cubic, hexagonal, orthorhombic, tetragonal and rhombohedral lattice symmetries.
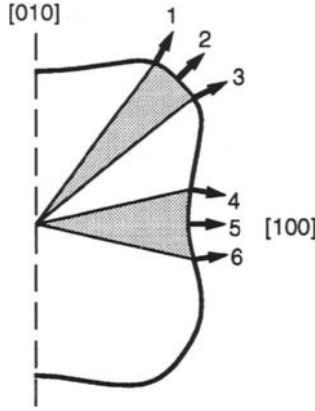
Fig. 5.1. A schematic illustration of "phonon focussing". The solid curve gives $\omega(\mathbf{q}, T_2)$ = constant for the low-velocity transverse mode (T_2) in the (001) $\mathbf{q}$-plane in Ge. $\mathbf{C}_{group}(\mathbf{q}, T_2)$ is exemplified by arrows 1–6.

Every (1980) has shown that the proper anisotropy parameter for sound waves in a cubic lattice structure is $A_E = (c_{11} - c_{12} - 2c_{44})/(c_{11} - c_{44})$, rather than the often used parameter due to Zener (1948), $A_Z = 2c_{44}/(c_{11} - c_{12})$ (see Chapter 3, §8).

8. Energy transport by sound waves

The energy transport by an elastic wave can be described by a *ray velocity*, analogous to the Poynting vector in electromagnetism. In a non-dissipative medium, the ray velocity equals the group velocity (cf. Every 1980). The group velocity $\mathbf{C}_{group}$ can be derived from eqs. (5.21) and (5.22), and the explicit relations for the phase velocity given by Every (1980). However, $\mathbf{C}_{group}(\mathbf{q}, s)$ does not have as simple a form as $\mathbf{C}_{phase}$. The wave vector $\mathbf{q}$, the phase velocity $\mathbf{C}_{phase}$ and the group velocity $\mathbf{C}_{group}$ are, for small $\mathbf{q}$, related by

$$\mathbf{C}_{group} \cdot \mathbf{q} = |\mathbf{q}||\mathbf{C}_{phase}|. \tag{5.23}$$

Hence, $|\mathbf{C}_{group}| \geq |\mathbf{C}_{phase}|$, with equality only in pure modes.

Calculations of group velocities have been performed for, e.g., LiF, KCl, and Al_2O_3 (Taylor et al. 1971), α-SiO_2 and Al_2O_3 (Farnell 1961, Rösch and Weis 1976a), and diamond, Si and Ge (Rösch and Weis

1976b). Among experiments, emphasis has been on germanium (e.g., Hensel and Dynes 1979, Dietsche et al. 1981).

Example. anisotropic group velocities and phonon focussing. The group velocity $\mathbf{C}_{group}(\mathbf{q}, s) = \nabla_{\mathbf{q}} \omega(\mathbf{q}, s)$ is a vector normal to the surface $\omega(\mathbf{q}, s) = $ constant. Figure 5.1 shows the shape of $\omega(\mathbf{q}, T_2)$ for the low-velocity transverse mode (T_2) in germanium when $\mathbf{q}$ is in the (001) plane. $\mathbf{C}_{group}$ tends to be directed along "channels", when $\mathbf{q}$ lies near a point where the curve $\omega(\mathbf{q}, s) = $ constant has an inflection point in $\mathbf{q}$-space. The energy flow is either decreased (arrows 1–3), or increased (4–6) in certain $\mathbf{q}$-directions. This is the physical basis for "phonon focussing" in crystals (Wolfe 1980).

THE PHONON SPECTRUM

1. Introduction

The simplest description of lattice vibrations is the Einstein model (Einstein 1907). All atoms are assumed to vibrate as independent harmonic oscillators with the frequency ω_E. In such a model the heat capacity C_E per atom (subscript E for Einstein) is

$$C_E = 3k_B \left(\frac{\hbar\omega_E}{k_B T}\right)^2 \frac{\exp(\hbar\omega_E/k_B T)}{[\exp(\hbar\omega_E/k_B T) - 1]^2}. \tag{6.1}$$

Figure 6.1, redrawn after Einstein (1907), shows that this extremely simple one-parameter model may account qualitatively for the heat capacity of diamond. The fact that diamond did not have a heat capacity in agreement with the classical Dulong and Petit (1819) rule was a major problem at that time. Einstein's paper can be viewed as the beginning of today's condensed matter theory, that is based on an atomistic approach combined with quantum physics. Within the same model we can also get a good description of the entropy $S(T)$ and the enthalpy $H(T)$ (see fig. 6.2 for Al_2O_3 and fig. 6.3 for TiC).

A closer comparison between experiments and the Einstein-model result reveals discrepancies which are of various origins. A first step towards an improvement would be to model the phonon frequency spectrum better. This is discussed in this chapter. The thermodynamic properties resulting from such descriptions of the spectrum are treated in the Chapter 7. However, there is a close connection between the ways to describe the phonon spectrum, and the thermodynamic properties that can then be calculated. Therefore, some relations from Chapter 7 will be referred to already in this chapter. But even a very accurate description of the phonon spectrum is not sufficient to remove the discrepancies
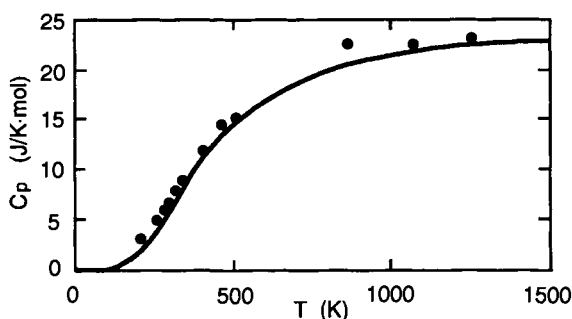
Fig. 6.1. The measured heat capacity $C_p(T)$ of diamond, as it was known in 1907 (symbols), could be accounted for with Einstein's (1907) one-parameter model for the lattice vibrations. After Einstein's original paper.
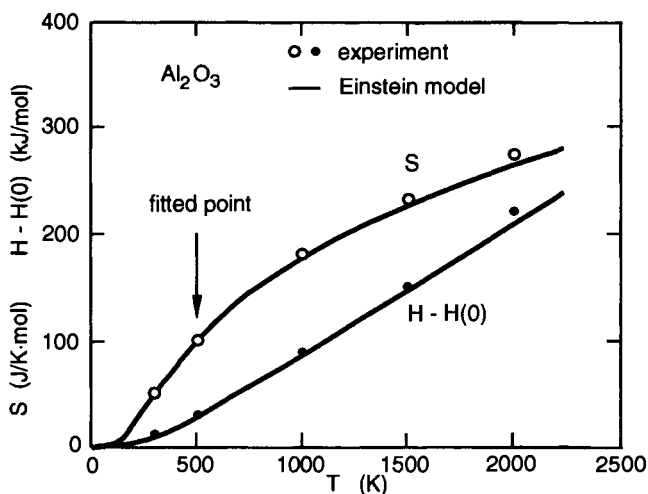
Fig. 6.2. The measured entropy $S(T)$ and enthalpy $H(T)$ of Al_2O_3 (symbols) may be qualitatively represented by an Einstein (1907) model for the lattice vibrations (solid curve). The Einstein temperature is determined by a fit to the measured entropy at 500 K. Experimental data from Barin (1989).

between theory and experiments in figs. 6.2 and 6.3. Anharmonic effects cannot be neglected at high temperatures. They are treated in Chapter 8. Non-vibrational contributions to the thermodynamic properties may also be important. These are discussed in Chapter 10 (electrons) and Chapter 11 (magnetism). A summary of various contributions to the heat capacity of real materials is given in Appendix F.

Fig. 6.3. As in fig. 6.2 but showing the measured entropy $S(T)$ and heat capacity $C_p(T)$ for TiC. The Einstein temperature is determined by a fit to the measured entropy at 600 K. Experimental data from Barin (1989).

2. Phonon dispersion curves

It is assumed that the reader is familiar with elementary aspects of phonons in solids. We first recapitulate some important results to introduce the notation. The reader who wants a more thorough presentation of gene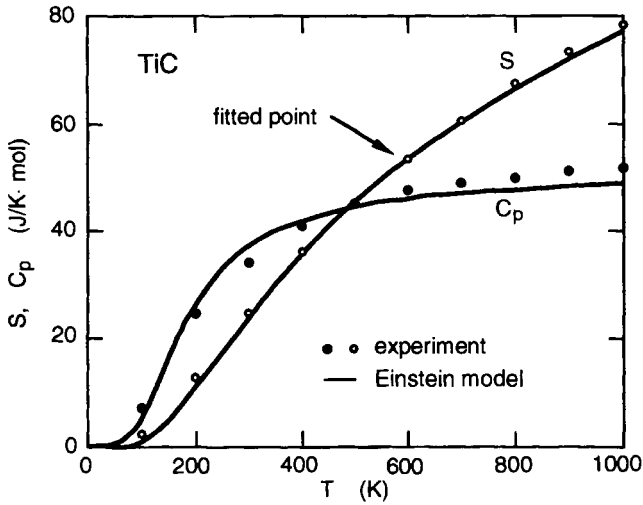ral lattice dynamics is referred to reviews by, e.g. Maradudin et al. (1963), Maradudin (1974), Reissland (1973), Brüesch (1982), Srivastava (1990) and Dove (1993). Plots of dispersion curves and the density-of-states function for insulators are found in Bilz and Kress (1979) while the Landolt–Börnstein tables (Schober and Dederichs 1981, Kress 1983) have similar data for a large number of solids. Brüesch (1986, 1987) reviewed the role of phonons in various experiments.

A phonon state is labelled $(\mathbf{q}, s)$, where $\mathbf{q}$ is a wave vector in the first Brillouin zone and s is an index which refers to longitudinal and transverse branches, as well as to acoustic and optical branches. (Sometimes we call s a mode index, but in other cases $(\mathbf{q}, s)$ is called a phonon mode. The context makes the use of the word "mode" clear.) The *phonon frequencies* $\omega(\mathbf{q}, s)$ and the corresponding *eigenvectors* $\boldsymbol{\varepsilon}(\mathbf{q}, s)$ are obtained from the *dynamical matrix* $\mathbf{D}$ (Appendix C);

$$\omega^2(\mathbf{q}, s)\varepsilon_\alpha(\mathbf{q}, s) = \sum_\beta D_{\alpha\beta}(\mathbf{q})\varepsilon_\beta(\mathbf{q}, s). \tag{6.2}$$

Indices α and β denote Cartesian components (x, y, z). The eigenvectors are orthonormal;

$$\sum_\alpha \varepsilon_\alpha(\mathbf{q}, s)\varepsilon_\alpha(\mathbf{q}, s') = \delta_{ss'}. \tag{6.3}$$

Theoretical accounts of phonon dispersion curves may have two different aims—to reproduce experimental data or to give an ab initio calculation with a minimum of input information (e.g. only atomic numbers and assumed lattice structure). In the first case, one has some experimental knowledge about $\omega(\mathbf{q}, s)$, perhaps only through elastic constants, and the aim is to map $\omega(\mathbf{q}, s)$ for all $\mathbf{q}$ and s as accurately as possible so that the phonon density of states, for example, can be calculated. The standard procedure is to fit a set of force constants which represent the interatomic forces. Such models may be elementary, e.g. the Born–von Kármán model, or more elaborate such as shell models describing ionic compounds. Ab initio calculations are steadily becoming more reliable. In some cases they are of an accuracy comparable to that of direct experiments. This is a field of strong development that lies outside the main scope of this book.

3. Phonon density of states

Several thermophysical properties may be calculated without any detailed knowledge of the phonon dispersion curves and the phonon eigenvectors. The only information needed about the phonons then may be the *phonon density of states* $F(\omega)$. The quantity $F(\omega)\Delta\omega$ measures the number of phonon states with frequencies in the interval $[\omega, \omega + \Delta\omega]$, irrespective of which wave vectors $\mathbf{q}$ and modes s the frequencies in this interval refer to. We must then specify how $F(\omega)$ is normalised. Some authors let it be per mole of a substance, or per lattice primitive cell. In this book we shall take

$$\int_0^{\omega_{max}} F(\omega)\,\mathrm{d}\omega = 3. \tag{6.4}$$

The choice is motivated by the fact that each atom is a three-dimensional oscillator (although coupled to the oscillations of other atoms). In a solid with N atoms, there are in total $3N$ phonon states $(\mathbf{q}, s)$. $NF(\omega)\Delta\omega$ is the number of phonon states with frequencies in the interval $[\omega, \omega + \Delta\omega]$. Our $F(\omega)$ can be said to be normalised "per atom". However, in a solid with several kinds of atoms $F(\omega)$ does not refer to a particular atom but is an average over all vibration modes $(\mathbf{q}, s)$. From a knowledge of the dispersion curves $\omega(\mathbf{q}, s)$ one obtains $F(\omega)$ by

$$
\begin{aligned}
F(\omega) &= \frac{V}{(2\pi)^3} \frac{1}{N} \sum_s \int \mathrm{d}^3\mathbf{q}\, \delta(\omega(\mathbf{q}, s) - \omega) \\
&= \frac{V}{(2\pi)^3} \frac{1}{N} \sum_s \int_{S_\mathbf{q}} \frac{\mathrm{d}S}{|\nabla_\mathbf{q}\omega(\mathbf{q}, s)|},
\end{aligned}
\tag{6.5}
$$

where V is the crystal volume and $\delta(x)$ is the Dirac δ-function. The last integral is over that surface $S_\mathbf{q}$ on which $\omega(\mathbf{q}, s) = \omega$.

Most theoretical calculations of phonon dispersion relations $\omega(\mathbf{q}, s)$ are limited to $\mathbf{q}$-vectors in the directions of high lattice symmetry, e.g. the [100], [110] and [111] directions of fcc or bcc lattices. That information is usually insufficient for an accurate evaluation of the integral in eq. (6.5), but if $\omega(\mathbf{q}, s)$ is known in a mesh of $\mathbf{q}$-points, interpolation procedures may yield $F(\omega)$ with a high numerical accuracy.

Example: $F(\omega)$ of an fcc lattice with nearest-neighbour interaction. Consider an fcc lattice, with only central nearest-neighbour interaction and atomic mass M. The dispersion curves, expressed by a single force constant f, take a very simple form. For instance, we get for the longitudinal (L) and the two degenerate transverse (T) branches in the [100] direction in reciprocal space, for $q_x \leq 2\pi/a$, where a is the lattice parameter (fig. 6.4a):

$$
\omega(q_x, \mathrm{L}) = 4\sqrt{f/M}\,\sin(aq_x/4),
\tag{6.6}
$$

$$
\omega(q_x, \mathrm{T}) = 4\sqrt{f/(2M)}\,\sin(aq_x/4).
\tag{6.7}
$$

Similar relations are obtained in other directions. In spite of this simple form, it is not trivial to evaluate $F(\omega)$. In fact it must be calculated by numerical integration (Leighton 1948, Maradudin et al. 1958). Figure 6.4b shows the density of states thus obtained.
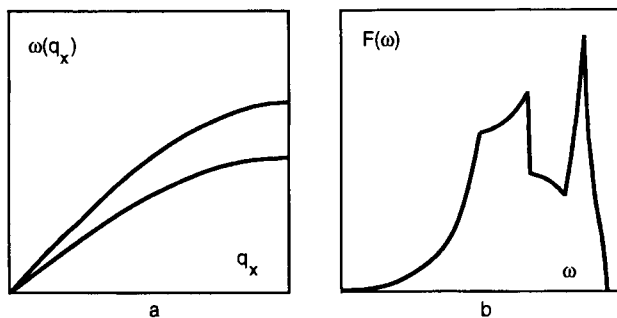
Fig. 6.4. (a) Phonon dispersion curves $\omega(q)$ in the [100] direction of an fcc lattice with central nearest-neighbour interactions, and (b) the phonon density of states $F(\omega)$ obtained by integration over all phonon modes.

4. Debye spectrum

Only a few years after the Einstein model, Debye (1912) introduced his famous model. It is widely used, and sometimes misused. We therefore give a detailed treatment, and comment in several later chapters on its virtues and shortcomings. Here it suffices to note that concepts such as Debye temperatures can be generalised and given useful and precise meanings that go far beyond the simple original ideas described here.

In the long-wavelength limit, i.e. for small $\mathbf{q}$, we can write

$$\omega(\mathbf{q}, s) = C(\mathbf{q}, s)|\mathbf{q}|. \tag{6.8}$$

$C(\mathbf{q}, s)$ is a directional-dependent velocity, defined for the three s-values corresponding to the acoustic branches. The simplest *Debye model* (Debye 1912) assumes a constant value $C(\mathbf{q}, s) = C_{\text{sound,D}}$ for all $(\mathbf{q}, s)$ with $\omega(\mathbf{q}, s)$ linear in $|\mathbf{q}|$ for all wave numbers $|\mathbf{q}| \leq \mathbf{q}_D$. The maximum frequency (the *Debye frequency*) in the model is $\omega_D = C_{\text{sound,D}}q_D$. (In this book $C_{\text{sound,D}}$ denotes the sound velocity in the Debye model, and C_D denotes the heat capacity in the Debye model.) From the general expression (6.5) we get the Debye density of states

$$F_D(\omega) = \frac{3V}{(2\pi)^3 N} \frac{4\pi q^2}{C_{\text{sound,D}}}\bigg|_{q=\omega/C_{\text{sound,D}}} = \frac{3V\omega^2}{2\pi^2 N C_{\text{sound,D}}^3}. \tag{6.9}$$

The value of the *Debye wave number* q_D is fixed by the normalisation condition

$$\int_0^{C_{\text{sound,D}}q_D} F_D(\omega)\, d\omega = 3. \tag{6.10}$$

This yields

$$q_D = (6\pi^2 N/V)^{1/3} = (6\pi^2/\Omega_a)^{1/3}. \tag{6.11}$$

In applications to thermophysical properties, it is convenient to introduce the *Debye temperature* θ_D as a measure of the maximum frequency ω_D. The two parameters are related by

$$\hbar\omega_D = k_B\theta_D. \tag{6.12}$$

In a real solid $C(\mathbf{q}, s)$ is anisotropic, and different for the longitudinal and the transverse acoustic branches. We write $C(\mathbf{q}, s) = C_s(\theta, \phi)$ and $dS = q^2\, d\Omega = [\omega^2/C_s^2(\theta, \phi)]d\Omega$ where (θ, ϕ) are angular coordinates for $\mathbf{q}$ and $d\Omega = \sin\theta\, d\theta\, d\phi$. Equation (6.5) becomes

$$\begin{aligned}
F(\omega) &= \frac{V}{(2\pi)^3 N} \sum_{s=1}^{3} \int \frac{\omega^2\, d\Omega}{C_s^3(\theta, \phi)} \\
&= \frac{\Omega_a\omega^2}{2\pi^2} \sum_{s=1}^{3} \int \frac{1}{C_s^3(\theta, \phi)} \frac{d\Omega}{4\pi}.
\end{aligned} \tag{6.13}$$

This agrees with eq. (6.9) if we define the *Debye sound velocity* $C_{\text{sound,D}}$ by

$$\frac{3}{C_{\text{sound,D}}^3} = \sum_{s=1}^{3} \int \frac{1}{C_s^3(\theta, \phi)} \frac{d\Omega}{4\pi}. \tag{6.14}$$

If C_s is isotropic, but different, for the longitudinal (L) and the two degenerate transverse (T) branches, one has

$$\frac{3}{C_{\text{sound,D}}^3} = \frac{1}{C_L^3} + \frac{2}{C_T^3}. \tag{6.15}$$

The Debye temperature θ_D can now be expressed as

$$\theta_D = \frac{\hbar}{k_B} \left(\frac{6\pi^2 N}{V} \right)^{1/3} C_{\text{sound,D}}$$

$$= \frac{\hbar}{k_B} \left(\frac{6\pi^2 r N_A \rho}{M} \right)^{1/3} C_{\text{sound,D}}. \tag{6.16}$$

Here r is the number of atoms in a molecule ($r = 1$ for an element, 2 for NaCl, 5 for Al_2O_3), M is the mass of a mole of the material, N_A is Avogadro's number, and ρ is the mass density of the material. Since $\omega_D = C_{\text{sound,D}} q_D = C_{\text{sound,D}} (6\pi^2 N/V)^{1/3}$ we can also write the Debye density of states (eq. (6.9)) as

$$F_D(\omega) = \frac{3 V q_D^3 \omega^2}{2\pi^2 N \omega_D^3} = \frac{9\omega^2}{\omega_D^3}. \tag{6.17}$$

The Debye model assumes that $\omega(\mathbf{q}, s) = C_s(\theta, \phi)|\mathbf{q}|$ is linear in $|\mathbf{q}|$ for all wave numbers. The linearity always holds in the small-$|\mathbf{q}|$ limit, for the acoustic phonon branches of any solid, but with increasing $|\mathbf{q}|$ there will be deviations from this simple relation. With the inclusion of only the first correction term, we can write

$$\omega(\mathbf{q}, s) = c_1(\theta, \phi, s)|\mathbf{q}| + c_2(\theta, \phi, s)|\mathbf{q}|^2. \tag{6.18}$$

Then one may prove that $F(\omega)$ has the form

$$F(\omega) = a_1\omega^2 + a_2\omega^4 + \cdots, \tag{6.19}$$

that is, $F(\omega)$ only contains even powers of ω, for small ω. For larger ω there are of course drastic deviations from such a power law, as is illustrated later in this chapter.

Finally some common misconceptions should be clarified. The cut-off frequency ω_D is the highest frequency in the Debye *model* spectrum. But this does not mean that ω_D is the highest frequency in the *actual* spectrum of a solid (cf. fig. 6.5). The cut-off frequency follows from the normalisation condition (6.4), and the connection to the actual spectrum is through the sound velocities, i.e. through the low-frequency part of $F(\omega)$. Since the sound velocities are determined by the elastic properties, one sometimes refers to the low ω part as the *elastic limit*. It may
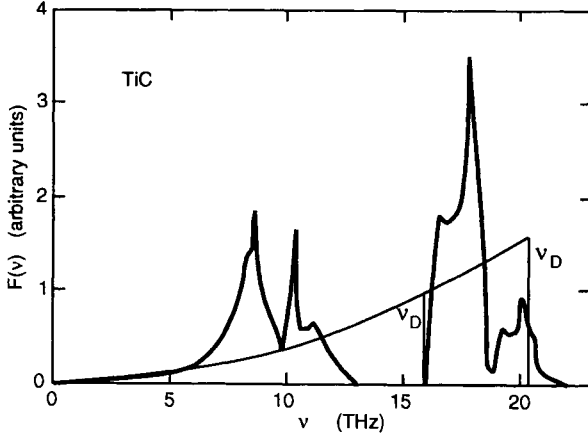
Fig. 6.5. The phonon density of states $F(v)$ for TiC, based on neutron scattering experiments, and two Debye model representations of $F(v)$; $\omega = 2\pi v$.

also be called the *long-wavelength part*, because the wavelength of an elastic wave is $\lambda(\mathbf{q}, s) = 2\pi/|\mathbf{q}| = 2\pi C(\mathbf{q}, s)/\omega(\mathbf{q}, s)$. Sound velocities vary as $\rho^{-1/2}$ where ρ is the mass density, while the highest frequency in a solid with different masses tends to vary as $M^{-1/2}$ where M is the lightest atomic mass. In solids with two or more kinds of atoms, and with large mass ratios, the Debye cut-off frequency ω_D, therefore, may be significantly lower than the highest frequency.

Another confusion may arise in the description of the low temperature heat capacity of solids characterised by a phonon density of states that has clearly separated acoustic and optical parts, as in the example of TiC below. The Debye model heat capacity at very low T can be written $C_D = Nk_B(12\pi^4/5)(T/\theta_D)^3$ (eq. (7.29)). Since only the low frequency phonons (the acoustic branches) contribute significantly to the heat capacity at low T, one could get a very good fit to experiments by modelling only that part. But one must now be careful with the normalisation condition for $F(\omega)$. Comparison of the expression (7.29) for the heat capacity C_D with eq. (6.16) for the Debye temperature θ_D yields $N = N_A r$, when $\int F(\omega)\,d\omega = 3$. If *only* the acoustic part of $F(\omega)$ is considered, we should take $r = 1$ in eq. (6.16). The two approaches yield identical C_D at low T since r cancels in N/θ_D^3, but

the proper $r(>1)$ must be used when the model is considered at higher temperatures.

Example: $F(\omega)$ and a Debye model for TiC. Figure 6.5 shows the phonon density of states $F(\omega)$ obtained from neutron scattering experiments (Pintschovius et al. 1978) and two Debye model representations. The Debye models have the same ω-dependence at low ω, and therefore equally well account for the low temperature heat capacity. However, the one with the lower cut-off $\omega_D = 2\pi\nu_D$ assumes one atom per primitive cell, while the model with the higher cut-off correctly assumes two atoms per primitive cell in TiC. Only the latter model gives a reasonable description of the heat capacity at high temperatures. Note that ω_D is not exactly equal to the highest frequency ω in the true $F(\omega)$.

Example: Debye temperature from approximate sound velocities. From a knowledge of the elastic coefficients c_{ij}, one obtains the velocities $C_s(\theta, \phi)$ as eigenvalues of a secular equation (5.5), and then $C_{\text{sound,D}}$ and θ_D after a numerical integration over angles θ and ϕ (eq. (6.14)). A much simpler, but approximate, method is to estimate the bulk modulus K and the shear modulus G of a polycrystalline material by the Voigt–Reuss–Hill (VRH) approximation (Chapter 18, §3.3), then obtain the longitudinal sound velocity from $\rho C_L^2 = K + (4/3)G$ and the transverse sound velocity from $\rho C_T^2 = G$, and apply eqs. (6.15) and (6.16) to get θ_D. Anderson (1963, 1965) investigated how well a calculation of $C_{\text{sound,D}}$ and θ_D by the latter method approximates the exact θ_D. For Al_2O_3 (trigonal lattice) he obtained $C_{\text{sound,D}} = 7190$ m/s ("exact" numerical calculation) and $C_{\text{sound,D}} = 7093$ m/s (Voigt–Reuss–Hill approximation), while for $CaCO_3$ (orthorhombic lattice) $C_{\text{sound,D}}$ = 3942 m/s ("exact") and $C_{\text{sound,D}}$ = 3991 m/s (VRH). Calculations on a large number of other systems showed that the typical error in θ_D is less than 2% when the approximate method is used. This also means that an accurate value of θ_D may be obtained from the measured longitudinal and transverse sound velocities of (statistically isotropic) polycrystalline materials, without recourse to the elastic constants c_{ij} of a single crystal. When the single crystal is isotropic, θ_D is given exactly by the VRH expression because then $K_V = K_R = K_{\text{VRH}}$ and $G_V = G_R = G_{\text{VRH}}$. Using the quantity $A_{\text{VRH}} = (G_V - G_R)/(G_V + G_R)$ as a measure of elastic anisotropy in a single crystal, Anderson (1963) found that when $A_{\text{VRH}} < 0.2$, the error in the predicted θ_D is $\lesssim 2\%$. In

Table 6.1

Vibrational properties described by a single parameter

Physical property	Moment frequency	Debye temperature
Heat capacity, low T	–	$\theta_D^C(T \to 0) = \theta_D(-3)$
Entropy, low T	–	$\theta_D^S(T \to 0) = \theta_D(-3)$
"Elastic limit", any T	–	$\theta_D^E(T \to 0) = \theta_D(-3)$
Thermal displacement, high T	$\omega(-2)$	$\theta_D^M(T \gtrsim \theta_D) = \theta_D(-2)$
Thermal displacement, low T	$\omega(-1)$	$\theta_D^M(T = 0) = \theta_D(-1)$
Entropy, high T	$\omega(0)$	$\theta_D^S(T \gtrsim \theta_D) = \theta_D(-0)$
Zero-point energy $(T = 0)$	$\omega(1)$	$\theta_D^Z(T = 0) = \theta_D(1)$
Zero-point velocity $(T = 0)$	$\omega(1)$	$\theta_D^Z(T = 0) = \theta_D(1)$
Heat capacity, high T	$\omega(2)$	$\theta_D^C(T \gtrsim \theta_D) = \theta_D(2)$

the example in Chapter 5 (§4) it is argued that θ_D can be well estimated if only G is known.

5. Frequency moment representations of $F(\omega)$

5.1. Definitions

In the limit of low or high temperatures, it may happen that only a certain average of $F(\omega)$, in the form of a frequency moment, is needed to calculate a certain thermophysical property (table 6.1). We define such moments μ_n by

$$\mu_n = \langle \omega^n \rangle = \int_0^{\omega_{max}} \omega^n F(\omega) \, d\omega \Big/ \int_0^{\omega_{max}} F(\omega) \, d\omega. \tag{6.20}$$

Usually it is more convenient to work with a frequency $\omega(n)$ which is related to the nth moment by

$$\omega(n) = [\mu_n]^{1/n}. \tag{6.21}$$

As regards terminology, we will call $\omega(n)$ *moment frequencies* because they have the dimension of frequency, while μ_n are called *frequency moments*, because they are moments, in a mathematical sense. There is
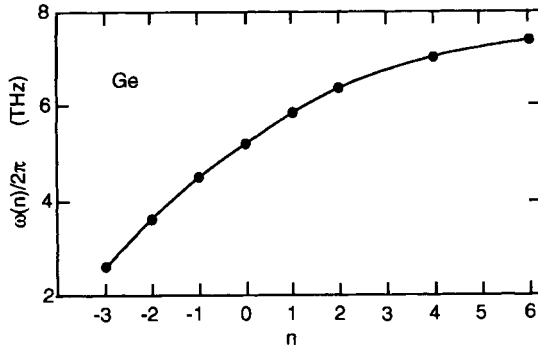
Fig. 6.6. The moment frequencies $\omega(n)$, as a function of n, for Ge. Data from Flubacher et al. (1959).

no restriction on n to be an integer, but since $F(\omega) \sim \omega^2$ for small ω, (eq. (6.20)) converges only if $n > -3$. The limiting value $\omega(0)$, i.e. for $n \to 0$, is defined by

$$\ln[\omega(0)] = \int_0^{\omega_{\max}} \ln \omega F(\omega) \, d\omega \Big/ \int_0^{\omega_{\max}} F(\omega) \, d\omega. \qquad (6.22)$$

It is easy to prove that $\omega(n)$ increases monotonically with n,

$$\omega(n') > \omega(n); \quad n' > n, \qquad (6.23)$$

and asymptotically approaches the maximum phonon frequency $\omega_{\max}$ of $F(\omega)$ when $n \to \infty$. Figure 6.6 shows $\omega(n)$ for Ge.

5.2. Moment frequencies $\omega(n)$ for a Debye spectrum

A Debye spectrum, with $F(\omega)$ given by eq. (6.17), yields

$$\mu_n = \frac{\int_0^{\omega_D} \omega^{2+n} \, d\omega}{\int_0^{\omega_D} \omega^2 \, d\omega} = \frac{3\omega_D^n}{n+3}, \qquad (6.24)$$

which then gives

$$\omega(n) = \left(\frac{3}{n+3}\right)^{1/n} \omega_D. \qquad (6.25)$$

When $n = 0$, eq. (6.22) leads to

$$\ln[\omega(0)] = \int_0^{\omega_D} \omega^2 \ln \omega \, d\omega \bigg/ \int_0^{\omega_D} \omega^2 \, d\omega = \ln \omega_D - 1/3, \quad (6.26)$$

or

$$\omega(0) = \omega_D e^{-1/3}. \tag{6.27}$$

Using the well-known result $(1 + 1/N)^N \to e$ when $N \to \infty$, one easily confirms that $\omega(n)$ in eq. (6.25) has the limit of eq. (6.27) when $n \to 0$.

5.3. Mass dependence of $\omega(0)$

For any $\mathbf{q}$, the phonon frequencies $\omega(\mathbf{q}, s)$ are related to the trace (Tr) of the dynamical matrix $\mathbf{D}$ by

$$\sum_s \omega^2(\mathbf{q}, s) = \sum_{i=1}^{3r} D_{ii}(\mathbf{q}) = \mathrm{Tr}\mathbf{D}(\mathbf{q}). \tag{6.28}$$

Here r is the number of atoms in a primitive cell, and s (which includes any optical branches) runs from 1 to $3r$. Normally, the atomic masses and the interatomic force constants are not separable in $\omega(\mathbf{q}, s)$ if there is more than one kind of atomic mass. However, the masses do separate from the forces in the quantity $\omega(0)$ (Grimvall and Rosén 1983). A general theorem in mathematics gives the roots $\omega(\mathbf{q}, s)$ to the secular equation as a product

$$\prod_{s=1}^{3r} \omega^2(\mathbf{q}, s) = \det \mathbf{D}(\mathbf{q}), \tag{6.29}$$

where det $\mathbf{D}$ is the determinant of the dynamical matrix. Using eq. (6.29), and the fact that the logarithm of a product is a sum of logarithms, one obtains

$$\ln[\omega(0)] = (1/6N) \sum_{\mathbf{q}} \ln[\det \mathbf{D}_0(\mathbf{q})] - (1/2) \ln M_{\mathrm{eff}}, \tag{6.30}$$

where N is the number of atoms, $\mathbf{D}_0$ is the force-constant part of the dynamical matrix and M_{eff} is an *effective atomic mass* defined as the

logarithmic average of all masses in the system. For instance, for a compound or an alloy $A_x B_y$, with atomic masses M_A and M_B, one has $(x + y) \ln M_{\text{eff}} = x \ln M_A + y \ln M_B$. Apart from the trivial case of an element, and also in the elastic-limit quantity $\omega(-3)$, $\omega(0)$ is the only moment frequency among $\omega(n)$ that allows such a general separation of the mass effect. We shall see in Chapter 19, (§§4, 8), that this is a result of practical importance.

6.   Moment frequencies expressed as equivalent Debye temperatures

A moment frequency $\omega(n)$ is a single parameter giving some averaged information about the phonon density of states $F(\omega)$. A Debye temperature θ_D is another single parameter that contains information about the vibration frequencies. In the standard Debye model, θ_D is chosen such that it correctly describes the low frequency, or elastic, part of $F(\omega)$. However, we could also choose θ_D such that the corresponding Debye spectrum correctly yields a particular moment frequency $\omega(n)$, and denote it $\theta_D(n)$. Thus, knowing $\theta_D(n)$ for a certain n we also know $\omega(n)$, and vice versa. However, we will see that there are some advantages in using $\theta_D(n)$, rather than $\omega(n)$. For instance, $\theta_D(n)$ usually varies much less than $\omega(n)$, with n. These ideas will now be given a precise definition.

For a Debye spectrum, $\omega(n) = [3/(n+3)]^{1/n} \omega_D$ (eq. (6.25)). When $F(\omega)$ is not of the Debye form, we *define* Debye frequencies $\omega_D(n)$, and corresponding Debye temperatures

$$\theta_D(n) = \hbar \omega_D(n)/k_B, \tag{6.31}$$

by

$$\int_0^{\omega_D(n)} \omega^n \omega^2 \, d\omega \bigg/ \int_0^{\omega_D(n)} \omega^2 \, d\omega$$

$$= \int_0^{\omega_{\text{max}}} \omega^n F(\omega) \, d\omega \bigg/ \int_0^{\omega_{\text{max}}} F(\omega) \, d\omega. \tag{6.32}$$

Thus, we let $\omega_D(n)$ be the cut-off frequency in a Debye model which reproduces correctly the nth moment of ω for a given density of states

$F(\omega)$. The righthand side of eq. (6.32) is, by definition, equal to $[\omega(n)]^n$. The lefthand side is $3[\omega_D(n)]^3/(n+3)$. Then, if $n > -3$ and $n \neq 0$,

$$\omega_D(n) = \left(\frac{n+3}{3}\right)^{1/n} \omega(n). \tag{6.33}$$

When $n = 0$, ω^n is replaced by $\ln \omega$. The righthand side of eq. (6.32) is given by eq. (6.22) and the lefthand side by eq. (6.26). Hence,

$$\omega_D(0) = e^{1/3}\omega(0). \tag{6.34}$$

If $n = -3$, the integral (eq. (6.20)) for $\omega(n)$ diverges at $\omega = 0$. We then use the fact that $F(\omega) = a_1\omega^2 + a_2\omega^4 + \cdots$, (eq. (6.19)), and define $\omega_D(-3)$ so that it has the same divergent behaviour as $\omega(-3)$ in eq. (6.20). If we replace the lower integration limit 0 in eq. (6.20) by an infinitesimal quantity ε, take $n = -3$ and recall the normalisation $\int F(\omega)\,d\omega = 3$, the righthand side of eq. (6.32) diverges as $(a_1/3)\ln(1/\varepsilon)$ and the lefthand side diverges as $\{3/[\omega_D(-3)]^3\}\ln(1/\varepsilon)$. Thus, $\omega_D(-3) = (9/a_1)^{1/3}$. In a strict Debye model, a_1 follows from eq. (6.17), giving as expected

$$\omega_D(-3) = C_{\text{sound,D}}q_D. \tag{6.35}$$

$C_{\text{sound,D}}$ is the average (eq. (6.14)) over the acoustic branches, and the Debye wavenumber is $q_D = (6\pi^2/\Omega_a)^{1/3}$.

It is now natural to ask what is the use of the Debye parameters $\omega_D(n)$ and $\theta_D(n)$, since they are just other ways of expressing the magnitude of the frequency moments, and do not contain any information that is not already in μ_n or $\omega(n)$. We note that in a strict Debye model, all $\omega_D(n)$ are constant, equal to the cut-off frequency ω_D, and all $\theta_D(n)$ are equal to a single Debye temperature θ_D. In a real solid, $\omega(n)$ varies considerably, while $\omega_D(n)$ and $\theta_D(n)$ are still fairly constant. Figure 6.6 shows $\omega(n)$ for Ge and figs. 6.7 and 6.8 show $\theta_D(n)$ for Ge, CsCl, Al, Mg, Mo and Nb. Often $\theta_D(n)$ has a minimum near $n = 0$.

In conclusion, the density of states of a real solid may be far from that of a Debye spectrum, but still some averages over $F(\omega)$, expressed by $\omega_D(n)$ or $\theta_D(n)$, are fairly well represented by a single parameter, ω_D or θ_D, for a range of n-values. This is one reason for the wide applicability of the Debye model. However, there are examples when
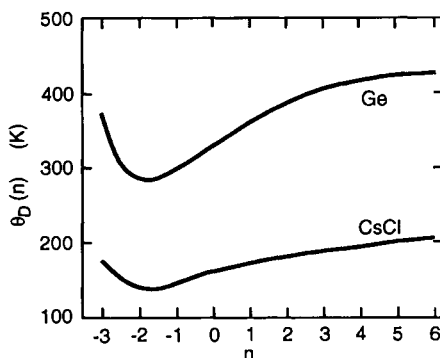
Fig. 6.7. The experimentally determined Debye temperature $\theta_D(n)$, as a function of n,
for Ge (Flubacher et al. 1959) and CsCl (Bailey and Yates 1967).
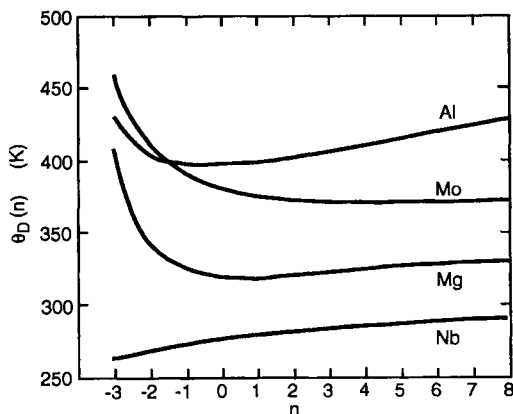

Fig. 6.8. The experimentally determined Debye temperature $\theta_D(n)$, as a function of n,
for Al, Mo, Mg and Nb. Data from Schober and Dederichs (1981).

$F(\omega)$ is so different from a Debye spectrum that the concept of a Debye temperature is less useful. For instance, in graphite and boron nitride, $\theta_D(n)$ increases from about 500 K when $n = -3$ to about 2200 K for large n (Yates et al. 1975).

7. Representing experimental data by Debye models

A Debye model is often assumed to give a reasonable representation of vibration-related properties. Of course we cannot get an exact match,

not even if anharmonic effects are absent, since the true vibrational properties, e.g. the entropy S_{vib}, depend on $3N$ frequencies $\omega(\mathbf{q}, s)$ and we try to describe that by a single Debye frequency ω_D (or Debye temperature θ_D). But for any temperature T, we can derive Debye temperatures θ_D such that the Debye-model description agrees with the true value at that particular T. Thus, if $C_{vib}(T)$ and $S_{vib}(T)$ are the "true" vibrational heat capacities and entropies (includes anharmonic effects), and $C_D(T; \theta_D^C)$ and $S_D(T; \theta_D^S)$ are the corresponding Debye model expressions, we may formally obtain a *heat capacity Debye temperature* θ_D^C and an *entropy Debye temperature* θ_D^S from

$$C_D(T; \theta_D^C) = C_{vib}(T), \tag{6.36}$$

$$S_D(T; \theta_D^S) = S_{vib}(T). \tag{6.37}$$

Similarly, a Debye model can be fitted to the true vibrational displacement $\langle \mathbf{u}^2 \rangle$,

$$\langle \mathbf{u}^2(T; \theta_D^M) \rangle_D = \langle \mathbf{u}^2(T) \rangle, \tag{6.38}$$

and yield a *displacement Debye temperature* θ_D^M that is related, e.g. to the term $\exp(-2M)$ in the Debye-Waller factor (eq. (7.46)).

The Debye temperature $\theta_D(T)$ derived from the low temperature heat capacity is the same as one would get from the sound velocities, i.e. from the elastic constants. Since elastic constants can be measured at various temperatures, it is useful to define an *elastic Debye temperature* labelled $E; \theta_D^E(T)$.

Figure 6.9 shows the entropy and elastic Debye temperatures for corundum (α-Al_2O_3), based on heat capacity and elastic constant data, respectively. The temperature dependence of $\theta_D^S(T)$ at low T is due to the fact that the true phonon spectrum is not of the exact Debye form, and the gradual decrease at high temperatures is due to anharmonic softening of the phonon frequencies. The elastic Debye temperature $\theta_D^E(T)$ only represents the long-wavelength part of $F(\omega)$ and therefore does not show the strong temperature dependence at low T caused by a non-Debyelike $F(\omega)$. The gradual decrease in $\theta_D^E(T)$ with T is due to anharmonic softening of the elastic coefficients.

Whenever a Debye model is used to describe a certain phenomenon, a comparison with a "true" or measured result may yield a corresponding Debye temperature. For instance, a fit to the zero-point vibrational
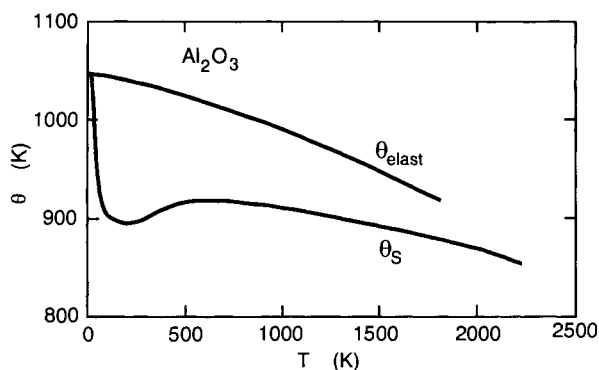
Fig. 6.9. The entropy Debye temperature $\theta_D^S(T)$ and the elastic Debye temperature $\theta_D^E(T)$ for α-Al_2O_3. After Grimvall and Fernández Guillermet (1992).

energy defines the Debye temperature θ_D^Z, of course without a temperature dependence in this case. In Chapter 15 we will introduce the Bloch–Grüneisen (BG) formula $\rho_{BG}(T; \theta_D^{BG})$ for the electrical resistivity. If $\rho(T)$ is the true phonon-limited resistivity we can define a BG Debye temperature $\theta_D^{BG}(T)$ by

$$\rho_{BG}(T; \theta_D^{BG}) = \rho(T). \tag{6.39}$$

(Actually, one must fit to ρ_{BG} at two temperatures, because ρ depends not only on the frequency spectrum but also on the strength of the electron-phonon interaction.)

It will be seen in Chapter 7 that, in the limit of high or low temperatures, some vibrational properties of a harmonic system depend on only one particular moment frequency $\omega(n)$. Table 6.1 summarises those results and also gives the corresponding Debye temperatures $\theta_D(n)$. In some cases the values of $\theta_D(n)$ for a material vary significantly with n, cf. the comment on boron nitride and graphite in §6.

In conclusion, we note that the frequencies $\omega(\mathbf{q}, s)$ are differently weighted in quantities like C, S and $\langle \mathbf{u}^2 \rangle$. Thus, the price one has to pay for a description of thermal properties in terms of a Debye model is that the Debye temperature depends on the temperature as well as on the property one is modelling. In order to stress this fact we will use superscripts C, S, M and E to denote if $\theta_D(T)$ refers to the heat capacity, the entropy, the vibrational displacement or is derived from elastic properties. This set of Debye temperatures should not be con-

fused with the Debye temperatures $\theta_D(n)$. The latter are independent of temperature (for harmonic vibrations) and serve to describe the density of states $F(\omega)$ through its moment frequencies $\omega(n)$, without reference to any particular thermophysical property.

It follows from the discussion in this section that there is no such thing as *the* Debye temperature for a particular solid. One has to specify which physical property one is interested in, and at which temperature. On the other hand, the various Debye temperatures usually differ by less than 10–20%. This is one reason why they are at all used. In the absence of more detailed information, any Debye temperature may give valuable insight. For instance, it roughly gives the temperature below which classical physics should be replaced by a quantum mechanical description of properties which depend on the lattice vibrations. It also gives the temperature below which anharmonic effects may be regarded as insignificant. When we refer to a Debye temperature in this general sense, we usually write it as θ_D, without superscripts. Debye temperatures for some elements and compounds are found in Appendix I.

8. Debye temperatures as functions of temperature

8.1. Harmonic phonons

All the Debye temperatures θ_D^C, θ_D^S and θ_D^M are temperature dependent. This behaviour will now be considered in some detail. If $F(\omega)$ had been exactly of the Debye-model shape, and without any anharmonic effects, all Debye temperatures for a given solid would have been equal, and independent of temperature. We first discuss the temperature dependence of various Debye temperatures at low T, and then how they asymptotically approach their high temperature limits.

Equation (7.30) gives an expression for $C_{\text{har}}(T)$ when the phonon density of states has the low frequency expansion $F(\omega) = a_1\omega^2 + a_2\omega^4 + \cdots$. The heat capacity Debye temperature at $T = 0$ K then follows from $[\theta_D^C(0)]^3 = [\theta_D(-3)]^3 = 9\hbar^3/a_1 k_B^3$. The temperature dependence of θ_D^C at very low T can be written (Grimvall 1986)

$$\theta_D^C(T) = \theta_D(0)[1 - (20\pi^2/21)(a_2/a_1)(k_B T/\hbar)^2]. \tag{6.40}$$

For almost all solids, but with the exception of Au and some of its dilute alloys (Bevk et al. 1977), a_2 is positive and hence $\theta_D^C(T)$ decreases
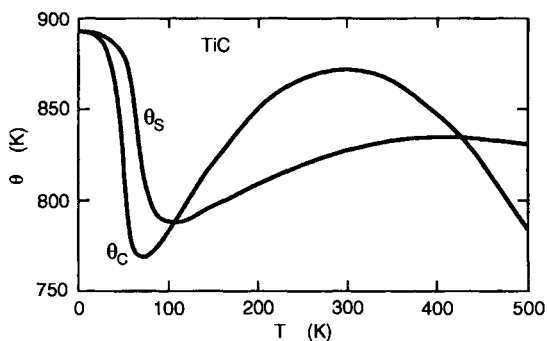
Fig. 6.10. The heat capacity Debye temperature $\theta_D^C(T)$ and the entropy Debye temperature $\theta_D^S(T)$, calculated from the measured $C_p(T)$ of TiC.

quadratically in T at very low T. A more complicated temperature dependence sets in at higher T.

Example: θ_D^C *and* θ_D^S *in TiC.* Figure 6.10 shows Debye temperatures calculated here from the measured heat capacity $C_p(T)$ for TiC (JANAF thermochemical tables (1985) with denser dataset obtained from the table editors). One can prove mathematically that the curves cross at the minimum of θ_D^S.

We will next analyse how rapidly θ_D^C, θ_D^S and θ_D^M approach their high temperature limits, in the case of harmonic vibrations. Recall that the Debye temperatures $\theta_D(n)$, without a superscript, refer to the moment frequencies $\omega(n)$ and are independent of temperature, while θ_D^C, θ_D^S and θ_D^M are obtained by a fit to the (harmonic) heat capacity, entropy and vibrational displacement of an actual system, and therefore vary with the temperature at which the fit is done. For θ_D^C we can write (Tosi and Fumi 1963, Domb and Salter 1952)

$$[\theta_D^C(T)]^2 = \theta_D^2(2)\{1 - (1/28)[\theta_D^4(4) \\ -\theta_D^4(2)]/[T\theta_D(2)]^2 + \cdots\}. \tag{6.41}$$

The analogous expression for θ_D^S is (Tosi and Fumi 1963)

$$\theta_D^S(T) = \theta_D(0)\{1 - (1/40)[\theta_D^2(2) - \theta_D^2(0)]/T^2 + \cdots\}. \tag{6.42}$$

For θ_D^M we have (Barron et al. 1966)

$$\theta_D^M(T) = \theta_D(-2)\{1 + b_2[\theta_D(-2)/T]^4 + \cdots\}, \tag{6.43}$$

with

$$b_2 = (1/7200)\{[\theta_D(2)/\theta_D(-2)]^2 - 1\}. \tag{6.44}$$

Thus, unlike θ_D^C and θ_D^S at high T, θ_D^M has no $1/T^2$-term. Furthermore, $\theta_D^M(0) \to \theta_D(-1)$ when $T \to 0$, a value which is usually not very different from the high-temperature limit $\theta_D(-2)$ of θ_D^M. This means that $\theta_D^M(T)$ usually varies very little with T, as has been illustrated in explicit calculations (Barron et al. 1966). Another way of expressing this fact is that the Debye model, with a constant Debye temperature, may be a better model for the vibrational displacement than for the heat capacity and the entropy, at temperatures $T \lesssim \theta_D$ where anharmonic effects are still rather small.

8.2. Anharmonic effects

At high temperatures anharmonicity affects the various Debye temperatures, and very differently so, as is shown in fig. 6.9 for Al_2O_3, fig. 6.11 for Al_2SiO_5 and fig. 6.12 for ThO_2. The heat capacity Debye temperature behaves unphysically at high T because there is no solution θ_D^C to eq. (6.36) when anharmonic effects make C_p larger than the classical limit $3k_B$ per atom. This is shown in fig. 6.11 as the strongly bent thin curve. It is sometimes, incorrectly, thought that C_V for the lattice vibrations asymptotically approaches $3k_B$ per atom at high T, and therefore θ_D^C calculated from C_V would be well behaved. However, anharmonic effects are present also in C_V and they may be large (cf. fig. 8.3). The "elastic" Debye temperature θ_D^E in fig. 6.9 shows a gradual change with temperature, given by how the elastic constants c_{ij} vary with T. Of course there is no rapid variation at low temperatures because θ_D^E only depends on the low frequency limit of $F(\omega)$, where the spectrum is Debye-like. Unlike θ_D^C, the entropy Debye temperature is mathematically well defined by eq. (6.37) at all temperatures. We shall see in Chapter 8 that the temperature dependence of θ_D^S at high T (usually a decrease) can be given a simple and accurate interpretation in terms of anharmonic shifts in the phonon frequencies $\omega(\mathbf{q}, s)$.

Example: a series expansion for θ_D^S in terms of the entropy. The solution of eq. (6.37) may be obtained by interpolation in tables of the Debye functions (e.g. in American Institute of Physics Handbook 1972). There
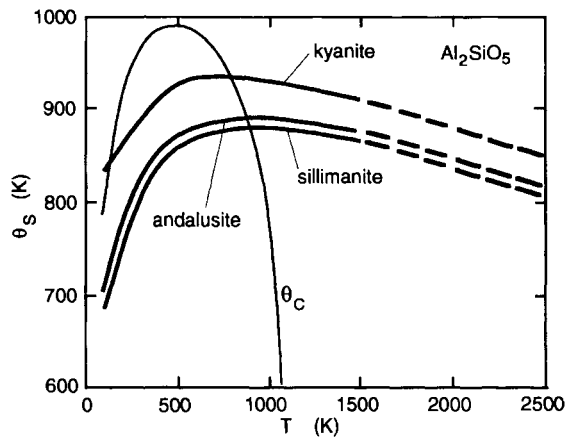
Fig. 6.11. The entropy Debye temperature $\theta_D^S(T)$ for three phases of aluminium silicate, Al_2SiO_5: andalusite, kyanite and sillimanite. Experimental (solid curves) and estimated (continuing dashed curves) data from the JANAF thermochemical tables (1985). The strongly bent thin curve shows the unphysical behaviour of $\theta_D^C(T)$ for andalusite. After Grimvall and Fernández Guillermet (1992).
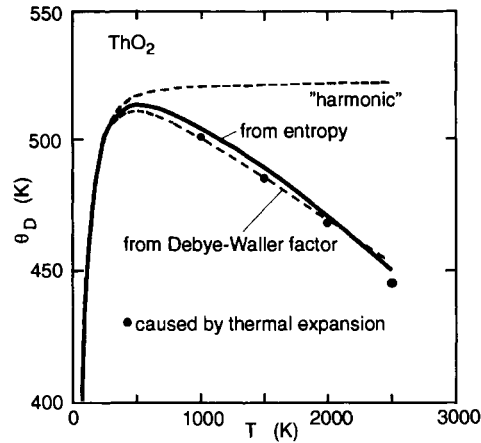

Fig. 6.12. The entropy Debye temperature $\theta_D^S(T)$ for ThO_2, deduced from heat capacity measurements, and various accounts of anharmonicity (see the main text). After Shian Peng and Grimvall (1994a).

is also a rapidly converging series expansion at high T (Shian Peng and Grimvall, 1994a);

$$
\begin{aligned}
\theta_D^S(T) &= T[\varepsilon + (1/49)\varepsilon^3 + (1/896)\varepsilon^5 \\
&\quad + (1/17046)\varepsilon^7 + \cdots],
\end{aligned} \tag{6.45}
$$

where $\varepsilon = \exp[(4/3) - S_{\text{vib}}(T)/(3rNk_B)]$. Figure 6.12 shows θ_D^S obtained in this way for ThO_2. The upper dashed curve represents θ_D^S in the absence of anharmonic effects. The lower dashed curve is an anharmonic softening deduced from the Debye–Waller factor. The symbols represent the effect of thermal expansion, accounted for by the thermodynamic Grüneisen parameter γ_G.

9. $F(\omega)$ from the inverted heat capacity

When the density of states $F(\omega)$ has been obtained, theoretically or from experiments (e.g. by neutron scattering), it is common to calculate the heat capacity $C_{\text{har}}(T)$ and compare with its measured value. One may ask if it would not be possible to reverse this scheme and derive $F(\omega)$ from the measured $C_{\text{har}}(T)$. Mathematically this is a straightforward task but in practice it is usually a futile idea. The expression for the heat capacity,

$$
C_{\text{har}}(T) = (1/3) \int_0^\infty F(\omega) C_E(\hbar\omega/k_B T) \, d\omega, \tag{6.46}
$$

can be regarded as an integral equation for the density of states $F(\omega)$, when $C_{\text{har}}(T)$ is known. It can be "inverted", for instance by the method of Fourier transforms (Montroll 1942). Many other inversion procedures have been devised, e.g. by Lifshitz (1954), Loram (1986) and Regan and Morgan (1992), to mention just a few. However, the heat capacity is so insensitive to details in $F(\omega)$ that such features are not accurately resolved in an inversion for real solids. Furthermore, the high frequency parts of $F(\omega)$ are mainly reflected in the high temperature $C_{\text{har}}(T)$. There anharmonic effects may severely affect the inverted $F(\omega)$ and non-vibrational contributions to the heat capacity may also be important.

In this context we note that $F(\omega)$ is formally specified by an expansion in terms of the even positive frequency moments μ_{2n} (Montroll

1943, 1944). Theoretically, μ_{2n} can be obtained directly from the dynamical matrix $\mathbf{D}$ as $\mu_{2n} \sim \text{Tr}(\mathbf{D}^n)$, but large values of n are required to resolve details in $F(\omega)$, which makes the method less useful. Matsushita and Matsubara (1978) used the real-space version of $\text{Tr}\,\mathbf{D}$ to estimate $F(\omega)$ for small particles. Experimentally, $\omega(0)$ may be obtained accurately from heat capacity data integrated to yield the entropy and then using, e.g. eq. (6.45). Loram (1986) describes other procedures that allows $\omega(n)$ to be obtained from heat capacity data, and gives references to the numerous earlier works along the same lines. We recall that several physical properties, when considered in certain limits, depend on only a single $\omega(n)$, (table 6.1).

10. Comparison between Einstein and Debye models

The Einstein model fails to describe the heat capacity at low temperatures, where $C_E(T)$ decreases exponentially with decreasing T, while the Debye model $C_D(T)$ always shows the correct T^3 dependence. However, this does not mean that the Einstein model always gives a poorer desciption of thermal phenomena. In fact, the two models are often equally good. In both cases, we have a one-parameter description of the frequency spectrum, expressed as frequencies ω_E or temperatures θ_E (Einstein), and ω_D or θ_D (Debye). We will see in Chapter 7 that, in certain limits, a thermophysical property may depend on only one moment frequency $\omega(n)$. Both the Einstein and the Debye models can be fitted to yield such a frequency $\omega(n)$.

For instance, consider the high T expansion of the harmonic heat capacity (eq. (7.31)),

$$
\begin{aligned}
C_{\text{har}}(T) \; = \; & 3Nk_B\{1 - (1/12)[\hbar\omega(2)/k_BT]^2 \\
& +(1/240)[\hbar\omega(4)/k_BT]^4 - \cdots\},
\end{aligned}
\tag{6.47}
$$

We get the same $1/T^2$-term if we either take $\omega_D = (20/12)^{1/2}\omega(2)$ in the Debye model (eq. (7.32)) or take $\omega_E = \omega(2)$ in the Einstein model, i.e. if θ_E and θ_D are related as

$$
\theta_E = \sqrt{(3/5)}\theta_D \approx 0.77\theta_D.
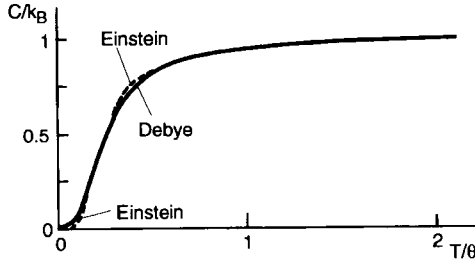\tag{6.48}
$$

Fig. 6.13. The heat capacities in the Debye model (solid line) and Einstein model (dashed line and also nearly coinciding with the solid line) can be made to closely agree if the characteristic temperatures θ_D and θ_E are properly chosen.

Figure 6.13 compares the heat capacities $C_E(T)$ and $C_D(T)$ with this θ-ratio. Similarly, the vibrational entropy at high T is (eq. (7.23)),

$$S_{\text{har}}(T) = 3Nk_B\{1 + \ln[k_B T/\hbar\omega(0)] + (1/24)[\hbar\omega(2)/k_B T]^2$$
$$-(1/960)[\hbar\omega(4)/k_B T]^4 + \cdots\}. \tag{6.49}$$

The same behaviour is obtained in the Debye, (eq. (7.24)), and Einstein models, in the high temperature limit, if either $\omega_E = \omega(0)$ or $\omega_D = \exp(1/3)\omega(0)$, i.e. if

$$\theta_E = \exp(-1/3)\theta_D \approx 0.72\theta_D. \tag{6.50}$$

Some other properties that have contributions from an integration over the entire phonon spectrum can be reproduced equally well with suitably chosen Einstein or Debye parameters, even at 0 K. Such examples are the zero-point energy per atom, $\hbar\omega(1)/2$, and the average zero-point vibrational displacement, $\langle \mathbf{u}^2 \rangle \sim 1/\omega(-1)$.

11. Other few-parameter models for $F(\omega)$

The Debye model, which assumes that $\omega(\mathbf{q}, s)$ is linear in $q = |\mathbf{q}|$ for all $\mathbf{q}$, does not give a good representation for the high frequency part. A relation $\omega(\mathbf{q}, s) \sim \sin q$ would often come closer to reality (cf. the example in §3). Assuming this, or similar, dispersion relations one can express $F(\omega)$ in some general mathematical form that depends on one or several parameters to be fitted. For instance, assuming that $\omega(\mathbf{q}, s) =$
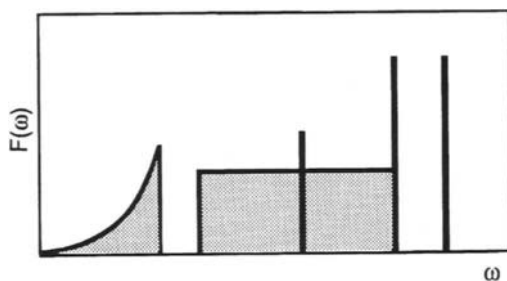
Fig. 6.14. An example of a complex model for $F(\omega)$ which may give a good represen-
tation for a certain compound with several optical phonon branches. The figure is just
an illustrating example and does not refer to a particular material.

$\omega_0 \sin(q/q_D)$ for all q up to the usual Debye cut-off wave vector $q_D = (6\pi^2 N/V)^{1/3}$ would leave us with only one free parameter, ω_0. It could be identified with a temperature $\theta_0 = \hbar\omega_0/k_B$ that would be analogous to the usual Debye temperature. When the model is fitted to, e.g. the heat capacity at different temperatures, one gets a solution $\theta_0(T)$. If the new model gives a better representation of $\omega(\mathbf{q}, s)$ than a standard Debye model, we also expect that $\theta_0(T)$ does not vary as much as $\theta_D(T)$ with T.

There are two main reasons why the Debye model is still so widely used, in spite of its shortcomings. One is tradition, and the connection to a vast amount of information expressed in Debye temperatures. The other is its mathematical simplicity. Figure 6.14 shows, schematically, a model spectrum that is much more complicated than the Debye model, and is of a type that may describe solids with many atoms per primitive cell. It has a low frequency Debye-like part which represents the acoustic branches. The optical branches are in this example described by a rectangular $F(\omega)$ and several sharp peaks as in an Einstein model. Experimental information on, e.g. optical resonance frequencies and elastic constants may be combined with the knowledge of the atomic masses in the solid and other information to fix the characteristic frequencies of such a spectrum. Then, having a model for $F(\omega)$, one may proceed to derive, e.g. thermodynamic properties like the heat capacity and the Helmholtz energy. Kieffer (1982) used complex representations of $F(\omega)$ to model thermodynamic properties of minerals. Westrum and Komada (1986) used another complex model for $F(\omega)$ that has only one free-fitting parameter θ, analogous to the Debye temperature. That

is a useful approach when one wants to isolate, e.g. a Schottky-type anomaly of crystal-field origin in the heat capacity by subtracting a large phonon contribution from the total C_p. It should be remarked that one may still have the problem with an anharmonic contribution, when the lattice part of C_p is modelled. We also recall that the simplest of all the one-parameter models, the Einstein model, may give an adequate description of $F(\omega)$ in many practical applications.

12. Structure dependence of $F(\omega)$ and Debye temperatures

More than 25 of the metallic elements have a low temperature close-packed (fcc or hcp) structure and a high temperature bcc phase. This may be explained if $\theta_{D,bcc}(0)$ is lower than $\theta_{D,fcc}(0)$ or $\theta_{D,hcp}(0)$, since the larger vibrational entropy will then tend to stabilise the bcc phase at high T (cf. Chapter 7, §6). Zener (1948) noted that with only nearest-neighbour central forces, the bcc lattice in unstable against shear in the (110) plane. This, he argued, would tend to give the bcc lattice a low-lying transverse mode and hence, a low Debye temperature. Figure 6.15 shows $F(\omega)$ of bcc, fcc and hcp potassium, calculated in a pseudopotential model. The low-lying [110] shear mode does give a strong weight to $F_{bcc}(\omega)$ at low ω, but because $\theta_D(0)$ is an average over the entire $F(\omega)$, Zener's argument is not sufficient. However, a large number of calculations (Grimvall and Ebbsjö 1975) suggest that for a wide class of interatomic potentials there *is* a tendency for $\theta_{D,bcc}(0)$ to be lower than $\theta_{D,fcc}(0)$ or $\theta_{D,hcp}(0)$ by several percent. A difference of this magnitude is sufficient to explain much of the observed allotropy among the elements (cf. Chapter 7, §6).

Friedel (1974) related $\theta_D(0)$ of transition metals to the coordination number z of their crystal structures. With a tight-binding nearest-neighbour interaction, taken to be independent of the crystal structure,

$$\theta_{D,bcc}(0)/\theta_{D,fcc}(0) = \theta_{D,bcc}(0)/\theta_{D,hcp}(0) = \sqrt{8/12} \approx 0.82. \quad (6.51)$$

This is too low a ratio. Moraitis and Gautier (1977) extended Friedel's (1974) model to include also next-nearest neighbours, but $\theta_{D,bcc}(0)/\theta_{D,hcp}(0)$ is still not satisfactorily accounted for.

A relative volume change by $\Delta V/V$ gives rise to a relative change $\gamma(0; V)(\Delta V/V)$ in $\theta_D(0)$ (cf. Chapter 8, §3.3). The Grüneisen parameter typically is $\gamma(0; V) = 1.5 \pm 1$. If the bcc phase has an atomic
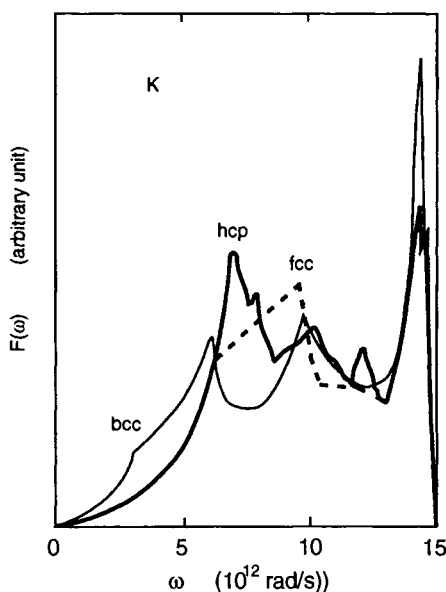
Fig. 6.15. The phonon density of states $F(\omega)$ for potassium in bcc, fcc and hcp lattice structures, as obtained in pseudopotential calculations. After Grimvall and Ebbsjö (1975).

volume Ω_a that is significantly higher than that of the close-packed fcc and hcp phases, the allotropy of the metallic elements might be due to a lowering of $\theta_{D,bcc}(0)$ associated with the larger Ω_a. A model with atoms represented by rigid spheres of fixed radius would make Ω_a of bcc lattices 9% larger than for fcc and hcp lattices. However, the actual volume change usually is too small to be of significance in this context (Chapter 19, §2).

The rather weak dependence of a certain Debye temperature on the lattice structure, that is suggested above for bcc, fcc and hcp lattices, may hold also in more complicated cases. See, for instance, the comparison of three structures of Al_2SiO_5 in fig. 6.11. Of course we expect a large difference in θ_D between structures of the same chemical composition if the chemical bonding is very different. Carbon in the forms of diamond and graphite provides a good example. Another is tin, where the low temperature phase α-Sn is a semiconductor and β-Sn is a metal (see Chapter 7, §6.2). Lattice instabilities (see below) also show that one should use with caution the rule of thumb that Debye temperatures vary
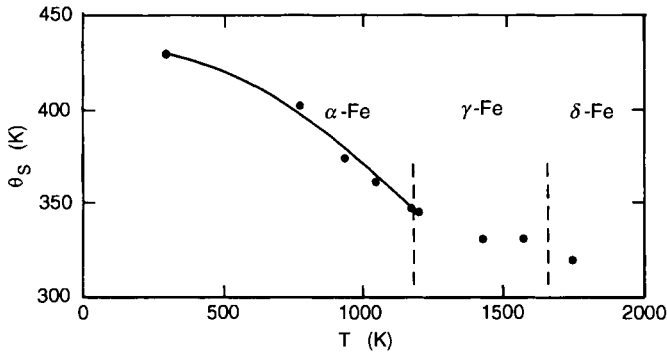
Fig. 6.16. The entropy Debye temperature $\theta_D^S(T)$ for iron (symbols), calculated from the phonon densities of states $F(\omega)$ which are based on neutron scattering experiments at various temperatures. The solid curve is a guide to the eye.

less than a few percent with the lattice structure, for a given chemical composition.

Example: $\theta_D^S(T)$ for bcc and fcc Fe. Iron transforms from a bcc lattice structure to an fcc structure at 1184 K, and then transforms back again to a bcc structure at 1660 K, before melting at 1808 K. Phonon frequencies have been measured by neutron scattering at several temperatures. From a fit of force constants to the measured phonon dispersion curves, a temperature dependent $F(\omega)$ can be derived. Neuhaus et al. (1997) and Neuhaus (1999) analysed such information and calculated the vibrational entropy. Figure 6.16 shows the entropy Debye temperature $\theta_D^S(T) \approx \theta_D(0; T)$ derived here from their data. Note that the transition to a paramagnetic state in the bcc lattice at the Curie temperature 1042 K seems to give a depression in $\theta_D^S(T)$, which is superimposed on the general decrease due to anharmonic effects. Note also how small is the change in $\theta_D^S(T)$ at the bcc-to-fcc and fcc-to-bcc transitions.

13. Lattice instabilities

The discussion in the previous section took for granted that the lattice vibrations are well defined in, for instance, bcc, fcc and hcp lattices. However, it is quite common that a hypothetical structure of a solid is dynamically unstable. For instance, tungsten is stable in the observed

bcc lattice structure but is unstable in the fcc structure at ambient pressure (see the example below). Magnesium, with an hcp structure, is unstable in the bcc lattice (Althoff et al. 1993). Other examples are Os and Ir (Wills et al. 1992) and Cu (Kraft et al. 1993), with an observed fcc structure but a dynamically unstable bcc structure, and Ni–Cr alloys with fcc Ni and bcc Cr being stable phases while bcc Ni and fcc Cr are dynamically unstable (Craievich and Sanchez 1997). Covalent $A^N B^{8-N}$-type semiconductors (e.g. GaAs) are dynamically unstable in the NaCl-type lattice structure (Ozoliņš and Zunger, 1999).

A dynamical instability may appear in the long-wavelength limit of the phonon spectrum (i.e. for small ω), but also for frequencies corresponding to wave vectors well into the first Brillouin zone. In the former case, the instability is often related to a negative value of the elastic constant $C' = (c_{11} - c_{12})/2$. Tungsten shows instabilities for a large range of **q**-vectors. Ti and Zr have unstable longitudinal phonon modes in the bcc structure at $T = 0$ K, close to $\mathbf{q} = [2/3, 2/3, 2/3]$. Those modes are stabilised at high T and the lattice transforms from the hcp to the observed bcc structure. The stabilisation of bcc Mg under pressure is considered in the example in Chapter 7 (§6.4). Grimvall (1998) has reviewed the steps leading to an understanding of unstable lattice structures of the metallic elements, in particular the apparent discrepancies (cf. fig. 1.8) when ab initio electron structure calculations were confronted with thermodynmic interpretations of measured binary phase digrams. See also the discussion of the Bain paths in Chapter 4 (§3).

Example: $\theta_D^S(T)$ for Ti and Zr in hcp and bcc structures. Figure 6.17 shows $\theta_D^S(T)$, calculated here from entropy data that are based on $F(\omega)$ from inelastic neutron scattering. The bcc structure is dynamically unstable at very low temperatures. The data for the hcp phases are smoothly extrapolated in the figure to high T, following what one would expect from anharmonic effects. We note that close to the melting temperature, θ_D^S is the same for the bcc and hcp structures, to within a few percent, in spite of the considerable difference at lower temperatures. The results indicate that at high temperatures θ_D^S is larger for the bcc structure than for the hcp structure, i.e. opposite to the trend discussed above that the bcc phase has a slightly lower Debye temperature.
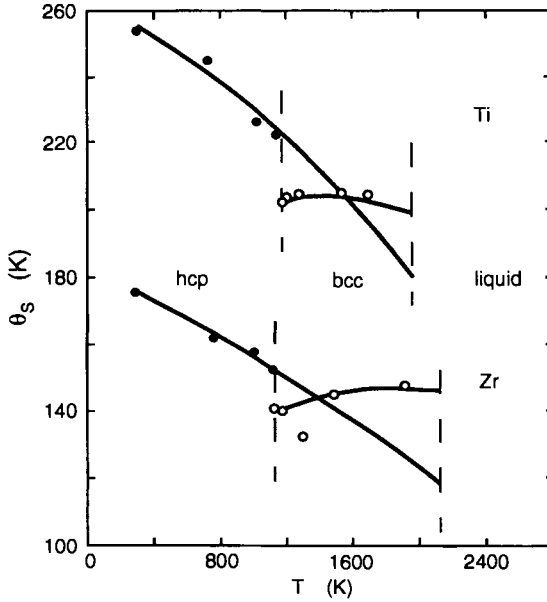
Fig. 6.17. The entropy Debye temperature $\theta_D^S(T)$ for Ti and Zr in hcp and bcc structures, derived from neutron scattering data for the phonons at certain temperatures (symbols). Solid curves are guides to the eye. Data from Heiming et al. (1991) and Petry et al. (1991).

14. Amorphous systems

In amorphous materials the lattice periodicity is lost, and we no longer have eigenmodes $(\mathbf{q}, s)$ for the vibrations in the form of propagating un-damped waves. However, for harmonic interactions between the atoms, there are still well defined eigenfrequencies and hence, a well-defined $F(\omega)$. Most of the quantities introduced in this chapter, therefore, remain valid in an amorphous system. In particular, we may consider the elastic-limit Debye temperature $\theta_D(-3)$. It is typically lower by 15–30% when compared with the crystalline state. This is well established, both experimentally (e.g. Golding et al. (1972) for $Pd_{0.775}Si_{0.165}Cu_{0.06}$, Mizutani and Massalski (1980) for $Pd_{0.80}Si_{0.20}$, Suck et al. (1981) for $Mg_{0.70}Zn_{0.30}$) and theoretically (e.g. Hafner 1983). See also the discussion on the elastic shear modulus G in Chapter 4 (§9). However, it is only the low frequency part of $F(\omega)$ that is significantly different in the amorphous and the crystalline states. The Debye temperature $\theta_D(2)$,

which measures ω^2 averaged over the entire density of states $F(\omega)$, is essentially the same in both structures (e.g. Suck et al. 1980, 1981) in the case of "dense" amorphous materials, i.e. where the density is close to that of the crystalline state. The *electronic* states in strongly disordered systems may be localised, i.e. their wave functions do not extend far beyond a region of atomic size. In contrast to this, most of the vibrational modes in glasses are not localised but propagate through the solid, although with considerable damping (Nagel et al. 1984).

15. Effect of order-disorder transitions

Some compounds, for instance CuZn, Cu_3Au and Ni_3Al, exist at low temperatures in an ordered structure, with the two kinds of atoms taking positions in two different sublattices. At a certain critical temperature there is an order–disorder transition. One may ask if the vibrational spectrum of the ordered and the disordered phases are so different that it affects the entropy difference, and therefore must be considered in an account of the transition temperature. This is a question which has been difficult to resolve, experimentally as well as theoretically. It has been claimed (e.g., Fultz et al. 1995) that experiments give an increased vibrational entropy as large as about $0.3k_B$ per atom in the disordered state of Ni_3Al. On the other hand, there are theoretical calculations that yield a much lower value (van de Walle et al. 1998). For comparison, we note that an entropy increase by $0.3k_B$ per atom corresponds to a moment frequency $\omega(0)$, or entropy Debye temperature θ_D^S, that is lowered by about 10% in the disordered state. It implies that the interatomic force constants are lowered (on the average) by over 20%. Such large variations are usually not observed when the type of chemical bonding (here metallic) is unaltered. We note that the mass disorder does not affect the difference in entropy between the disordered and the ordered states at high temperatures, because in both cases the atomic masses enter as the logarithmic average over the constituent atoms (§5.3). Of course the *static* disorder is associated with an entropy. For a random distribution of atoms in a compound A_cB_{1-c} over a lattice, the entropy per atom is $-k_B[c \ln c + (1 - c) \ln(1 - c)]$. As an example, for a binary compound like CuZn we have $c = 0.5$, and an entropy $k_B \ln 2 \approx 0.69k_B$ at complete static disorder.

16. Effect of magnetism and magnetic fields

In the example above on bcc and fcc iron it was noted that passing through the Curie temperature T_C has only a moderate effect on θ_D^S, which averages over all frequencies. On the other hand, electron structure calculations (Ekman et al. 1998) have shown that strictly non-magnetic bcc Fe would be dynamically unstable under shear. It is necessary in this case to have magnetic moments, rather well localised on the Fe atoms, but the moments can be disordered like in the paramagnetic state well above T_C without making the lattice structure dynamically unstable. We have also noted (Chapter 4, §13) that there may be pronounced anomalies in the elastic constants near a critical temperature for magnetic ordering.

The Debye temperature of ferromagnets, subject to an external magnetic field, is affected in a complicated way (see, for example, Wohlfarth 1974). The Debye temperature of non-magnetic materials (as opposed to magnetic materials in the paramagnetic state) seems usually not to be affected by an external magnetic field, not even in the case of strongly paramagnetic materials (Ikeda and Gschneidner 1980, Hsiang et al. 1981). However, there are also cases where θ_D *is* affected by a magnetic field, probably due to induced magnetic moments (e.g. in Sc and YCo_2) (see Gschneidner and Ikeda 1983).

THERMAL PROPERTIES OF HARMONIC LATTICE VIBRATIONS

1. Introduction

Lattice vibrations give the key to many temperature dependent properties of solids. If we know the quantum mechanical energy eigenvalues of these vibrations, we can easily model thermodynamic quantities such as the Gibbs energy and the heat capacity. If we also know the eigenfunctions corresponding to the eigenvalues, we can calculate, e.g. the vibrational displacements of the atoms and connect that to properties such as the electrical resistivity. In applications to materials science the temperature is often so high that a *classical description* agrees very well with the more fundamental *quantum mechanical approach*. We therefore start with a brief comparison of these two descriptions.

Consider a one-dimensional oscillator in classical mechanics. If the restoring force constant is k, and the mass is M, the frequency is

$$\omega = \sqrt{\frac{k}{M}}. \tag{7.1}$$

The potential energy E_{pot} is

$$E_{\text{pot}} = \tfrac{1}{2}kx^2 = \tfrac{1}{2}M\omega^2 x^2. \tag{7.2}$$

The *equipartition theorem* says that, in thermal equilibrium, the potential energy $\bar{E}_{\text{pot}}$ and and the kinetic energy $\bar{E}_{\text{kin}}$ are equal;

$$\bar{E}_{\text{pot}} = \bar{E}_{\text{kin}} = \frac{1}{2}k_{\text{B}}T. \tag{7.3}$$

Here " $\bar{}$ " denotes thermal average. It follows that the thermally averaged squared displacement is

$$\overline{x^2} = \frac{k_B T}{k} = \frac{k_B T}{M\omega^2}. \tag{7.4}$$

The heat capacity $C = \partial E / \partial T$ is

$$C = \frac{\partial}{\partial T}(\bar{E}_{pot} + \bar{E}_{kin}) = k_B. \tag{7.5}$$

The absolute value of the Helmholtz (free) energy $F = E - TS$ is undefined since classical physics only deals with entropy *differences* and not their absolute values.

These classical properties can be contrasted with the quantum mechanical description. There the Helmholtz energy can be obtained as

$$F = -k_B T \ln Z. \tag{7.6}$$

Z is the partition function, containing a sum over all quantum states i with energies E_i;

$$Z = \sum_i \exp(-E_i / k_B T). \tag{7.7}$$

In our case with a single oscillator, the quantum energies are $\hbar\omega(n + 1/2)$ with $n = 0, 1, 2, 3, \ldots$, and Z takes a simple closed form;

$$Z = \sum_{n=0}^{\infty} \exp[-\hbar\omega(n + 1/2)/k_B T] = \frac{\exp(-\hbar\omega/2k_B T)}{1 - \exp(-\hbar\omega/k_B T)}, \tag{7.8}$$

which yields

$$\begin{aligned} F &= \hbar\omega/2 + k_B T \ln[1 - \exp(-\hbar\omega/k_B T)] \\ &= k_B T \ln[2\sinh(\hbar\omega/2k_B T)]. \end{aligned} \tag{7.9}$$

From a knowledge of $F = E - TS$, ordinary thermodynamics gives, e.g. the energy E and the entropy S. The third law of thermodynamics implies that $S = 0$ at $T = 0$ K, and the entropy has a well-defined value. There is also an "equipartition" theorem for each quantum state

of a harmonic oscillator, saying that the expectation values $\langle H_{\text{pot}} \rangle$ and $\langle H_{\text{kin}} \rangle$ of the potential and kinetic parts of the Hamiltonian H are equal. Hence, this equipartition of energies also holds in thermal equilibrium for the statistical distribution over quantum states, i.e.

$$\overline{\langle H_{\text{pot}} \rangle} = \overline{\langle \tfrac{1}{2} M\omega^2 x^2 \rangle} = \tfrac{1}{2}\bar{E}(T). \tag{7.10}$$

A quantum mechanical description is necessary at "low" temperatures, i.e. at temperatures such that $k_B T \lesssim \hbar\omega$. Expressed in terms of some characteristic Debye temperature θ_D for a solid, this condition can be written $T \lesssim \theta_D$. Since for many materials of practical importance $\theta_D \lesssim$ 300 K, a classical description is often adequate at room temperature and above.

This chapter gives a systematic presentation of thermodynamic properties in the quantum mechanical description, and with series expansions at high temperatures showing the approach to classical behaviour.

2. Thermal energy of phonons

In thermal equilibrium, the energy associated with a harmonic phonon mode $(\mathbf{q}, s)$ with frequency $\omega = \omega(\mathbf{q}, s)$ is (for simplicity we write $E(\mathbf{q}, s)$ instead of $\bar{E}(\mathbf{q}, s)$ etc.)

$$E(\mathbf{q}, s) = \hbar\omega[n + 1/2] = (\hbar\omega/2)\coth(\hbar\omega/2k_B T). \tag{7.11}$$

where n is the Bose–Einstein statistical factor

$$n(\mathbf{q}, s) = \frac{1}{\exp(\hbar\omega/k_B T) - 1}. \tag{7.12}$$

The total vibrational energy of a crystal with N atoms is

$$E_{\text{har}}(T) = \sum_{\mathbf{q},s} E(\mathbf{q}, s) = N \int_0^{\omega_{\text{max}}} \hbar\omega$$
$$\times \left[\frac{1}{\exp(\hbar\omega/k_B T) - 1} + \frac{1}{2}\right] F(\omega)\, d\omega. \tag{7.13}$$

Here we have introduced a subscript "har" to stress that this an expression for harmonic lattice vibrations. In a real system anharmonic

corrections may be important. If $F(\omega)$ has the form of a Debye spectrum, the harmonic vibrational energy is E_D;

$$E_D(T) = (9/8)N\hbar\omega_D$$
$$+ \frac{9N\hbar}{\omega_D^3} \int_0^{\omega_{max}} \frac{\omega^3}{\exp(\hbar\omega/k_BT) - 1} \, d\omega. \qquad (7.14)$$

At high temperatures, $E_{har}(T)$ has the expansion

$$E_{har}(T) = 3Nk_BT\{1 + (1/12)[\hbar\omega(2)/k_BT]^2$$
$$- (1/720)[\hbar\omega(4)/k_BT]^4 + \cdots\}. \qquad (7.15)$$

Expressed in the Debye temperatures $\theta_D(n)$, this expansion becomes

$$E_{har}(T) = 3Nk_BT\{1 + (1/20)[\theta_D(2)/T]^2$$
$$- (1/1680)[\theta_D(4)/T]^4 + \cdots\}. \qquad (7.16)$$

The Einstein-model result at high temperatures is obtained from eq. (7.15) with all $\omega(n)$ replaced by the Einstein frequency ω_E, and the Debye-model result is obtained from eq. (7.16) with all $\theta_D(n)$ replaced by the Debye temperature θ_D.

Example: the equipartition theorem and the zero-point vibrational energy. The thermal energy of a phonon mode $(\mathbf{q}, s)$ is $\hbar\omega(n + 1/2)$. We note that the high temperature expansion of the Bose–Einstein function n contains a term $-1/2$ that cancels the explicit term $1/2$ in $\hbar\omega(n + 1/2)$ (see Appendix D). Thus, the thermal energy (eq. (7.15)) approaches k_BT per mode $(\mathbf{q}, s)$, which is the well-known result of the equipartition theorem in classical mechanics. This fact can be given a graphical interpretation. The shaded area in fig. 7.1 between the Dulong–Petit value $3k_B$ and $C_{har}(T)$, yields the zero-point energy of the vibrations, for any form of harmonic vibrational density of states $F(\omega)$.

Example: zero-point vibrations and the cohesive energy. The cohesive energy U_{coh} of a solid at $T = 0$ K has contributions from the energy $-U_{stat}$ of a static lattice, with the atoms at their equilibrium positions, and the zero-point vibrational energy, i.e. (averaged per atom)

$$U_{coh} = -U_{stat} - E_{vib} = -U_{stat} - (3/2)\hbar\omega(1)$$
$$= -U_{stat} - (9/8)k_B\theta_D(1). \qquad (7.17)$$
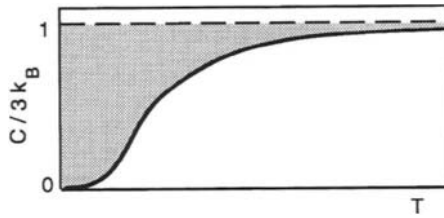
Fig. 7.1. The vibrational heat capacity per atom, plotted as $C/3k_B$. The shaded area yields the zero-point vibrational energy.

The magnitude of U_{coh} depends on the reference state used, but typically $E_{vib}(T = 0)$ is less than 1% of U_{coh} (table 1.1). Furthermore, $\theta_D(1)$ of competing structures with the same type of chemical bonding usually differ by less than 5% (Chapter 6, §12). For a given solid, $E_{vib}(T = 0)$ therefore does not affect the relative thermodynamic stability of different crystal structures. Carbon seems to be an exception (Yin and Cohen 1984). In a static lattice at $T = 0$ K, diamond has a marginally lower energy than graphite. However, $E_{vib}(T = 0)$ in diamond is exceptionally large, while some of the chemical bonds in graphite are of the weak van der Waals type and give a much lower $E_{vib}(T = 0)$. The difference is sufficient to make graphite the stable phase at low temperatures.

3. Entropy of phonons

The vibrational entropy S_{har} plays a particularly important role among the thermodynamic functions for lattice vibrations. There are two main reasons for this. Atomic masses separate from interatomic forces in the high temperature expression for S_{har}. Furthermore, anharmonic effects can be simply incorporated in the description. But in this section we shall focus on the harmonic case. Three convenient expressions for the entropy of a particular mode $(\mathbf{q}, s)$ are

$$S(\mathbf{q}, s) = k_B[(1 + n)\ln(1 + n) - n \ln n], \tag{7.18}$$

$$S(\mathbf{q}, s) = k_B \left\{ \left(\frac{\hbar\omega}{k_B T} \right)(n + 1) - \ln \left[\exp \left(\frac{\hbar\omega}{k_B T} \right) - 1 \right] \right\}, \tag{7.19}$$

$$S(\mathbf{q}, s) = k_B \left\{ \frac{\hbar\omega}{2k_B T} \coth\left(\frac{\hbar\omega}{2k_B T}\right) - \ln\left[2\sinh\left(\frac{\hbar\omega}{2k_B T}\right)\right]\right\},$$

$$(7.20)$$

Here $n = [\exp(\hbar\omega/k_B T) - 1]^{-1}$ and $\omega = \omega(\mathbf{q}, s)$. The total vibrational entropy in a solid with N atoms is

$$S_{har}(T) = \sum_{\mathbf{q}, s} S(\mathbf{q}, s) = N \int_0^{\omega_{max}} S(\omega)F(\omega)\ d\omega. \qquad (7.21)$$

When $F(\omega)$ has the form of a Debye model, we get the Debye-model entropy S_D;

$$\begin{aligned} S_D(T) &= \frac{12Nk_B}{\omega_D^3} \int_0^{\omega_D} \frac{\hbar\omega^3/(k_B T)\ d\omega}{\exp(\hbar\omega/k_B T) - 1} \\ &\quad - 3Nk_B \ln[1 - \exp(-\hbar\omega_D/k_B T)]. \end{aligned} \qquad (7.22)$$

A very important result is the high temperature expansion of eq. (7.21), expressed in moment frequencies $\omega(n)$;

$$\begin{aligned} S_{har}(T) &= 3Nk_B\{1 + \ln[k_B T/\hbar\omega(0)] + (1/24)[\hbar\omega(2)/k_B T]^2 \\ &\quad - (1/960)[\hbar\omega(4)/k_B T]^4 + \cdots\}. \end{aligned} \qquad (7.23)$$

We note that to leading order at high T, the entropy only depends on the logarithmic average $\omega(0)$ of the phonon frequencies, without regard to the detailed shape of $F(\omega)$ or if $F(\omega)$ refers to, e.g. an element, a compound or a disordered alloy. Expressed in the Debye temperatures $\theta_D(n)$, eq. (7.23) takes the form

$$\begin{aligned} S_{har}(T) &= 3Nk_B\{4/3 + \ln[T/\theta_D(0)] + (1/40)[\theta_D(2)/T]^2 \\ &\quad - (1/2240)[\theta_D(4)/T]^4 + \cdots\}. \end{aligned} \qquad (7.24)$$

The Einstein-model result at high temperatures is obtained from eq. (7.23) with all $\omega(n)$ replaced by the Einstein frequency ω_E, and the Debye-model result is obtained from eq. (7.24) with all $\theta_D(n)$ replaced by the Debye temperature θ_D.

4. Heat capacity

Since we now deal with strictly harmonic vibrations, the heat capacities C_p and C_V, taken at constant pressure and constant volume, respectively, are equal ($= C_{har}$).

Thermodynamics gives

$$C_{har} = (\partial E_{har}/\partial T) = T(\partial S/\partial T). \tag{7.25}$$

From expressions for the entropy S and its series expansions in §3, we can derive a number of useful relations. The heat capacity $C_{har}(\mathbf{q}, s)$ of a single phonon mode $(\mathbf{q}, s)$ with frequency $\omega = \omega(\mathbf{q}, s)$ is

$$
\begin{aligned}
C_{har}(\mathbf{q}, s) &= k_B \left(\frac{\hbar\omega}{k_B T} \right)^2 \frac{\exp(\hbar\omega/k_B T)}{[\exp(\hbar\omega/k_B T) - 1]^2} \\
&= k_B \left(\frac{\hbar\omega}{k_B T} \right)^2 \frac{1}{4\sinh^2(\hbar\omega/2k_B T)}.
\end{aligned} \tag{7.26}
$$

The total heat capacity C_{har} in a solid with N atoms and a phonon density of states $F(\omega)$ is

$$C_{har}(T) = N \int_0^{\omega_{max}} C_{har}(\omega) F(\omega) \, d\omega. \tag{7.27}$$

When $F(\omega)$ has the form of a Debye model, with Debye temperature θ_D, we get

$$C_D(T) = 9Nk_B \left(\frac{T}{\theta_D} \right)^3 \int_0^{\theta_D/T} \frac{x^4 e^x}{(e^x - 1)^2} \, dx. \tag{7.28}$$

At very low temperatures, the upper integration limit θ_D/T in the Debye expression (7.28) can be replaced by ∞. Then the integral becomes a constant, $4\pi^4/15$, and

$$C_D(T) = Nk_B \frac{12\pi^4}{5} \left(\frac{T}{\theta_D} \right)^3 \approx 234 Nk_B \left(\frac{T}{\theta_D} \right)^3. \tag{7.29}$$

We recall that θ_D is defined through an average over anisotropic and mode dependent sound velocities, eq. (6.14), so eq. (7.29) is valid for

any solid in the low temperature limit, irrespective of its structure at the atomic level (but see Chapter 11, §5 for a comment on glasses).

We noted in eq. (6.19) that for small ω, $F(\omega) = a_1\omega^2 + a_2\omega^4 + \cdots$, with only even powers of ω. If this form is used in the expression (7.27), and we go to the low temperature limit, the result is

$$
\begin{aligned}
C_{\text{har}}(T) = {} & Nk_B[(4\pi^4/15)a_1(k_BT/\hbar)^3 \\
& + (16\pi^6/21)a_2(k_BT/\hbar)^5 + \cdots].
\end{aligned} \tag{7.30}
$$

Thus, the low temperature expansion of $C_{\text{har}}(T)$ does not have a T^4 contribution.

The high-temperature expansions of $C_{\text{har}}(T)$ in terms of moment frequencies, $\omega(n)$, or the related Debye temperatures $\theta_D(n)$, are

$$
\begin{aligned}
C_{\text{har}}(T) = {} & 3Nk_B\{1 - (1/12)[\hbar\omega(2)/k_BT]^2 \\
& + (1/240)[\hbar\omega(4)/k_BT]^4 - \cdots\},
\end{aligned} \tag{7.31}
$$

$$
\begin{aligned}
C_{\text{har}}(T) = {} & 3Nk_B\{1 - (1/20)[\theta_D(2)/k_B/T]^2 \\
& + (1/560)[\theta_D(4)/T]^4 - \cdots\}.
\end{aligned} \tag{7.32}
$$

The Einstein-model result at high temperatures is obtained from eq. (7.31) with all $\omega(n)$ replaced by the Einstein frequency ω_E, and the Debye-model result is obtained from eq. (7.32) with all $\theta_D(n)$ replaced by the Debye temperature θ_D.

Example: the Dulong–Petit rule. Dulong and Petit (1819) noted empirically that the specific heat (i.e. heat capacity per mass) at room temperature, multiplied by the atomic weight, was approximately constant for 13 solid elements. Their numbers correspond to a heat capacity of about 6.5 cal/mol. This is reasonably consistent with the high temperature limit $3Nk_B$ in eq. (7.31) which yields 5.96 cal/mol. Further aspects of the Dulong–Petit rule are found in the discussion of the Neumann–Kopp rule in Chapter 19 (§5).

Example: heat capacity of fullerite. At room temperature C_{60} molecules can form an fcc structure called fullerite, with transitions to other structures at lower temperatures. Figure 7.2 shows the heat capacity as it results from low temperature (<20 K) heat capacity measurements
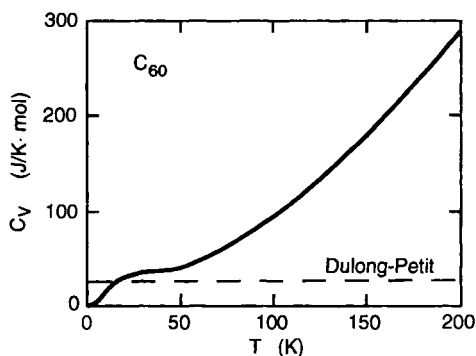
Fig. 7.2. The heat capacity of C_{60} fullerite from experiments. After Jin Yu et al. (1994).

(Beyermann et al. 1992), from information about the atomic dynamics through neutron scattering (Pintschovius et al. 1992) and from the theoretical modelling of those excitations (Jin Yu et al. 1994). Each C_{60} molecules contributes 3×60 modes vibration modes. When placed in a lattice, six of these modes refer to intermolecular motions (three vibrations and three rotations of the molecule). The remaining modes refer to intramolecular motions. The two sets of modes are well separated in energy. At ambient temperature only the intermolecular motions contribute significantly to C_p. The force constants for the intramolecular motions are almost as strong as in the diamond form of C. We therefore expect that C_p of fullerite (in a hypothetically stable state) would not reach the classical (Dulong–Petit) limit until around 2000 K.

5.   Thermal atomic displacements

5.1.   General relations

Much of the material in the following discussion of thermal atomic displacements has been developed in relation to thermal effects in X-ray crystallography. The monograph by Willis and Pryor (1975) covers these aspects in depth. Some additional formulae are given in Appendix D. Butt et al. (1988, 1993) have tabulated displacements for many solids with cubic lattice structure.

The instantaneous position $\mathbf{R}(\kappa, l; t)$ of the κth atom in the lth unit cell is written

$$\mathbf{R}(\kappa, l; t) = \mathbf{R}^0(\kappa, l) + \mathbf{u}(\kappa, l; t), \tag{7.33}$$

where $\mathbf{u}$ is the displacement vector from the equilibrium position $\mathbf{R}^0$. We wish to calculate the thermal averages $\langle \mathbf{u}^2 \rangle$ and $\langle u_\alpha^2 \rangle$, of $\mathbf{u}(\kappa, l)$ and its Cartesian components $u_\alpha(\kappa, l)$, respectively. Let there be N_c primitive cells in the lattice, with r atoms in each cell. From (D.10),

$$\langle u_\alpha^2(\kappa, l) \rangle = \frac{1}{N_c M_\kappa} \sum_{\mathbf{q},s} \frac{E(\mathbf{q}, s)}{\omega^2(\mathbf{q}, s)} \varepsilon_\alpha(\mathbf{q}, s; \kappa) \varepsilon_\alpha^*(\mathbf{q}, s; \kappa). \tag{7.34}$$

Here $\boldsymbol{\varepsilon}(\mathbf{q}, s; \kappa)$ is the κth part of the total phonon eigenvector $\boldsymbol{\varepsilon}$, i.e. the component of $\boldsymbol{\varepsilon}(\mathbf{q}, s)$ which refers to the displacement of the κth atom. M_κ is the mass of the atom of type κ, and $E(\mathbf{q}, s) = \hbar\omega(\mathbf{q}, s)[n(\mathbf{q}, s) + 1/2]$. The total mean-squared displacement is

$$\langle \mathbf{u}^2(\kappa, l) \rangle = \langle u_x^2(\kappa, l) \rangle + \langle u_y^2(\kappa, l) \rangle + \langle u_z^2(\kappa, l) \rangle. \tag{7.35}$$

If the site (κ, l) has cubic symmetry, the average displacement is isotropic, with

$$\langle \mathbf{u}^2(\kappa, l) \rangle = 3 \langle u_x^2(\kappa, l) \rangle. \tag{7.36}$$

Thus, it is worth stressing that in the approximation of harmonic lattice vibrations and cubic symmetry, the displacements are the same in all directions, e.g. the [100], [110] and [111] directions of an fcc (or bcc) lattice, although this may seem counter-intuitive.

The distribution function $P(u_\alpha, \kappa l)$ for the displacement of the (κl)-atom in the α-direction is Gaussian, i.e.

$$P(u_\alpha) = [2\pi \langle u_\alpha^2(\kappa, l) \rangle]^{-1/2} \exp[-u_\alpha^2 / 2 \langle u_\alpha^2(\kappa, l) \rangle]. \tag{7.37}$$

This relation was proved in the classical limit by Debye (1914) and Waller (1925), and shown by Ott (1935) to be true also in a quantum mechanical treatment. From the distribution functions $P(u_\alpha)$, we can calculate the probability that an atom is to be found in a certain region near its equilibrium position. For instance, there is a 50% probability that the α-component of the displacement vector $\mathbf{u}$ is larger

than $1.54\langle u_\alpha^2\rangle^{1/2}$. See Nelmes (1969) for details regarding displacement probabilities.

Anharmonic effects have been neglected here. They are pronounced for large displacements, and thus make $P(u)$ less reliable when $\mathbf{u}^2 \gg \langle \mathbf{u}^2\rangle$.

5.2.   Monatomic solid with cubic symmetry

In a monatomic solid with cubic symmetry, the index κ is irrelevant. Then

$$\sum_\alpha \varepsilon_\alpha(\mathbf{q}, s)\varepsilon_\alpha^*(\mathbf{q}, s) = 1, \tag{7.38}$$

and eq. (7.34) gives

$$\langle \mathbf{u}^2\rangle = \frac{1}{M}\int_0^{\omega_{max}} \frac{E(\omega; T)}{\omega^2} F(\omega)\, d\omega. \tag{7.39}$$

Thus, we have the important result that the mean-square thermal displacement in a monatomic solid (i.e. an element) with cubic symmetry can be calculated without knowledge about the eigenvectors $\boldsymbol{\varepsilon}$. We also note that eq. (7.39) converges at the lower integration limit only if $F(\omega) \sim \omega^p$ for small ω, with $p > 1$. In a one-dimensional chain, which is often used to illustrate important concepts in lattice dynamics, $F(\omega)$ tends to a constant for small ω. Then $\langle \mathbf{u}^2\rangle$ diverges at all temperatures.

At high temperatures $E(\omega; T) \to k_B T$, and $\langle \mathbf{u}^2\rangle$ becomes

$$\langle \mathbf{u}^2\rangle = \frac{3k_B T}{M\omega^2(-2)}. \tag{7.40}$$

Because $\omega(-2) \sim M^{-1/2}$ for a monatomic solid, we see that $\langle \mathbf{u}^2\rangle$ at high temperatures does not depend on the atomic mass M.

When $T \to 0$ only the zero-point vibrations remain. Then $E(\omega; T) = \hbar\omega/2$ and eq. (7.39) gives

$$\langle \mathbf{u}^2\rangle = \frac{3\hbar}{2M\omega(-1)}. \tag{7.41}$$

In this case, the mass dependence $\omega(-1) \sim M^{-1/2}$ does not cancel in eq. (7.41), and a heavy mass tends to have a low zero-point vibrational

displacement. We note that the high and low temperature limits of the displacement do not depend on the detailed shape of the density of states $F(\omega)$ but only on a single parameter, $\omega(-2)$ and $\omega(-1)$, respectively.

5.3. Thermal displacements in a Debye model

With a Debye model for $F(\omega)$, eq. (7.39) becomes

$$\langle \mathbf{u}^2 \rangle = \frac{9\hbar^2 T}{M k_B \theta_D^2}[\Phi(\theta_D/T) + \theta_D/4T], \tag{7.42}$$

where Φ is the Debye integral function

$$\Phi(x) = \frac{1}{x} \int_0^x \frac{z}{e^z - 1} \, dz. \tag{7.43}$$

For small x, $\Phi(x) = 1 - x/4 + x^2/36 - \cdots$, which yields the high temperature expansion

$$\langle \mathbf{u}^2 \rangle = \frac{9\hbar^2 T}{M k_B \theta_D^2}[1 + (1/36)(\theta_D/T)^2 + \cdots]. \tag{7.44}$$

In the low temperature limit, $\Phi \to 0$ and hence,

$$\langle \mathbf{u}^2 \rangle = \frac{9\hbar^2}{4M k_B \theta_D}. \tag{7.45}$$

5.4. Debye–Waller factor

The mean-square displacements can be obtained from the temperature dependence of the intensity in X-ray or neutron scattering experiments (Debye 1914, Waller 1923). Let I be the actual intensity, I_0 the intensity when the lattice is rigid, $\mathbf{k}_1$ and $\mathbf{k}_2$ the wave vectors and $\lambda = 2\pi/|\mathbf{k}|$ the wavelength of the photon (or neutron) before and after the (elastic) scattering, $\mathbf{q} = \mathbf{k}_1 - \mathbf{k}_2$ and 2θ the angle between $\mathbf{k}_1$ and $\mathbf{k}_2$. One has

$$I = I_0 \exp(-2M_{DW}). \tag{7.46}$$

In the Debye–Waller factor $\exp(-2M_{DW})$ of a cubic lattice,

$$\begin{aligned} M_{DW} &= (1/2)\langle(\mathbf{u} \cdot \mathbf{q})^2\rangle = (1/6)\langle \mathbf{u}^2 \rangle q^2 \\ &= (1/3)\langle \mathbf{u}^2 \rangle(8\pi^2 \sin^2 \theta/\lambda^2) = B \sin^2 \theta/\lambda^2, \end{aligned} \tag{7.47}$$

where B is called the *B-factor* of the atom. According to eq. (7.46), a plot of $\ln(I/I_0)$ versus $\sin^2 \theta/\lambda^2$ (a Wilson plot) should give a straight line with a slope which, at high temperatures, is linear in T, but anharmonic effects give rise to some non-linearity (Hahn and Ludwig 1961, Maradudin and Flinn 1963, Cowley and Cowley 1966, Mair 1980).

5.5. Interatomic distance

The displacements discussed above refer to the deviation of a particular atom from its equilibrium position. Sometimes one is more interested in how the distance between two specific atoms varies due to the vibrations. Let the instantaneous positions of two atoms, labelled 0 and j, be $\mathbf{R}_0 = \mathbf{R}_0^0 + \mathbf{u}_0$ and $\mathbf{R}_j = \mathbf{R}_j^0 + \mathbf{u}_j$. The distance $\mathbf{d}$ between them differs from the distance $\mathbf{d}_0 = \mathbf{R}_j^0 - \mathbf{R}_0^0$ in the static lattice, such that

$$\mathbf{d} = (\mathbf{R}_j^0 + \mathbf{u}_j) - (\mathbf{R}_0^0 + \mathbf{u}_0) = \mathbf{d}_0 + (\mathbf{u}_j - \mathbf{u}_0). \tag{7.48}$$

The mean-square relative displacement is

$$\begin{aligned} \sigma^2 &= \langle (\mathbf{d} - \mathbf{d}_0)^2 \rangle = \langle (\mathbf{u}_j - \mathbf{u}_0)^2 \rangle \\ &= \langle \mathbf{u}_j^2 \rangle + \langle \mathbf{u}_0^2 \rangle - 2 \langle \mathbf{u}_j \cdot \mathbf{u}_0 \rangle. \end{aligned} \tag{7.49}$$

Consider now the relative displacement along the direction $\mathbf{R}_j - \mathbf{R}_0$, for instance the distance between near-neighbours. Thus, we seek

$$\sigma_{\mathbf{R}}^2 = \langle [\hat{\mathbf{e}} \cdot (\mathbf{u}_j - \mathbf{u}_0)]^2 \rangle, \tag{7.50}$$

where $\hat{\mathbf{e}}$ is a unit vector along $\mathbf{R}_j - \mathbf{R}_0$. If the atoms vibrate independently, like in an Einstein model, one has $\langle \mathbf{u}_j \cdot \mathbf{u}_0 \rangle = 0$. In another extreme limit, that of acoustic long-wavelength vibrations, all atoms move in phase and $\mathbf{d} = \mathbf{d}_0$. In a real solid, we expect correlations between the atomic motions to be significant when 0 and j are near neighbours, but to be small for atoms far apart. A general expression for $\sigma_{\mathbf{R}}$, in a monatomic lattice with atomic mass M, is (Grüneisen and Goens 1924, Warren 1969)

$$\begin{aligned} \sigma_{\mathbf{R}}^2 &= \frac{\hbar}{NM} \sum_{\mathbf{q},s} \frac{[\boldsymbol{\varepsilon}(\mathbf{q}, s) \cdot \hat{\mathbf{e}}]^2}{\omega(\mathbf{q}, s)} \coth \left[\frac{\hbar \omega(\mathbf{q}, s)}{2k_B T} \right] \\ &\quad \times \{ 1 - \cos[\mathbf{q} \cdot (\mathbf{R}_j^0 - \mathbf{R}_0^0)] \}. \end{aligned} \tag{7.51}$$

Without the cosine term in eq. (7.51), $\sigma_{\mathbf{R}}^2 = 2\langle \mathbf{u}^2 \rangle/3$ (cf. eqs. (7.11), (7.34) and (7.49)). That would correspond to $\mathbf{R}_j - \mathbf{R}_0$ being so large (i.e. the atoms 0 and j being so far apart) that the cosine term averages to zero when one sums over $\mathbf{q}$. An accurate treatment of eq. (7.51) requires numerical calculations. Not even in a Debye model is it possible to get a closed-form algebraic expression for $\sigma_{\mathbf{R}}^2$. The quantity $\sigma_{\mathbf{R}}^2$ is accessible in experiments on extended X-ray absorption fine structures, XAFS (e.g. Greegor and Lytle 1979, Böhmer and Rabe 1979 and Marcus and Tsai 1984). Displacement correlation functions have also been calculated from the phonon spectrum, for instance by Beni and Platzman (1976) for Zn, Sevillano et al. (1979) for Cu, Fe and Pt and Zywietz et al. (1996) for SiC. See Appendix D for further comments.

5.6. General expression for the thermal displacement

We now seek a general but tractable expression for $\langle \mathbf{u}^2(\kappa, l) \rangle$ in a lattice of arbitrary structure. It is convenient to introduce a matrix $\mathbf{B}$ with elements (do not confuse $\mathbf{B}$ with the B-factor in eq. (7.47))

$$B_{ij} = \langle u_i u_j \rangle. \tag{7.52}$$

Let the r atoms in the primitive cell be numbered by $\kappa = 1, \ldots, r$. Then u_i is a component of the vector $(u_{1x}, u_{1y}, u_{1z}, u_{2x}, \ldots, u_{rz})$. From a result in matrix theory (Born 1942) we can write (for brevity restricted here to high temperatures)

$$B(\kappa\kappa) = \frac{k_B T}{N_c M_\kappa} \sum_{\mathbf{q}} \left[\mathbf{D}^{-1}(\mathbf{q}; \kappa\kappa) + \frac{1}{12} \left(\frac{\hbar}{k_B T} \right)^2 \mathbf{I} \right. $$
$$\left. - \frac{1}{720} \left(\frac{\hbar}{k_B T} \right)^4 \mathbf{D}(\mathbf{q}; \kappa\kappa) + \cdots \right]. \tag{7.53}$$

$\mathbf{D}$ is the $3r \times 3r$ dynamical matrix and $\mathbf{I}$ is a unit matrix. $B(\kappa\kappa)$ refers to the displacement of atoms of kind κ. This expression is useful since it allows the evaluation of $\langle \mathbf{u}^2 \rangle$ directly from the inverted dynamical matrix $\mathbf{D}$.

5.7.   Two atoms per primitive cell

An interesting special case is a lattice with a primitive cell containing two atoms, denoted by 1 and 2. Let their masses be $M(1)$ and $M(2)$. From eq. (7.34) we cannot obtain the displacements of each kind of atom without knowing the 6-component eigenvectors $\boldsymbol{\varepsilon}(\mathbf{q}, s) = [\boldsymbol{\varepsilon}(\mathbf{q}, s; 1), \boldsymbol{\varepsilon}(\mathbf{q}, s; 2)]$. However, we can obtain the weighted sum

$$M(1)\langle\mathbf{u}_1^2\rangle + M(2)\langle\mathbf{u}_2^2\rangle = 2\int_0^{\omega_{\max}} [E(\omega; T)/\omega^2]F(\omega)\,d\omega. \quad (7.54)$$

Here $E(\omega, T)$ is the Einstein thermal energy. To obtain the displacement of each atom we turn to eq. (7.53). $\mathbf{D}(\mathbf{q})$ is now a 6×6 matrix. It can be blocked into four parts, $\mathbf{D}(\kappa\kappa') = \mathbf{D}_0(\kappa\kappa')/[M(\kappa)M(\kappa')]^{1/2}$ (cf. eq. (C.3)). Then eq. (7.53) yields the high temperature result

$$M(1)\langle\mathbf{u}_1^2\rangle_\alpha = (k_BT/N_c)\sum_\mathbf{q}\mathbf{D}_\alpha^{-1}(\mathbf{q}; 11), \quad\quad\quad (7.55)$$

$$M(2)\langle\mathbf{u}_2^2\rangle_\alpha = (k_BT/N_c)\sum_\mathbf{q}\mathbf{D}_\alpha^{-1}(\mathbf{q}; 22). \quad\quad\quad (7.56)$$

The index α refers to a Cartesian component in the displacements and in the block $\mathbf{D}(\kappa\kappa)$. At high temperatures, we only keep the first term on the righthand side of eq. (7.53). Then, since $\mathbf{D}^{-1}(\mathbf{q}, \kappa\kappa) \sim M(\kappa)$, the atomic masses cancel on each side of eqs. (7.55) and (7.56), respectively. It follows that $\langle\mathbf{u}_1^2\rangle$ and $\langle\mathbf{u}_2^2\rangle$ do not depend on the masses but only on the forces between the atoms.

If the force-constant part obeys $\mathbf{D}_0(11) = \mathbf{D}_0(22)$, one has the important result that the mean-square thermal displacements in a diatomic solid at high temperatures are the same for both kinds of atoms, irrespective of their mass ratio. The condition $\mathbf{D}_0(11) = \mathbf{D}_0(22)$ is fulfilled if there are only nearest-neighbour interactions, but also for direct Coulomb forces in an ionic compound A^+B^-. In the low temperature limit, on the other hand, only zero-point vibrations remain. Then the average displacement amplitudes are unequal for the two kinds of atoms (cf. the analogous result in eq. (7.41)).

The *monatomic hexagonal close-packed lattice* is a special case of diatomic lattices. The **B**-matrix has the form

$$\mathbf{B} = \begin{pmatrix} \langle u_a^2\rangle & 0 & 0 \\ 0 & \langle u_a^2\rangle & 0 \\ 0 & 0 & \langle u_c^2\rangle \end{pmatrix}, \quad\quad\quad (7.57)$$

where u_a refers to vibrations along an a-axis, and u_c to vibrations perpendicular to that axis. $\mathbf{D}_0(11) = \mathbf{D}_0(22)$ and $M(1) = M(2) = M$. From eq. (7.54) we obtain the average $\langle \mathbf{u}^2 \rangle$ over all directions,

$$
\begin{aligned}
\langle \mathbf{u}^2 \rangle &= 2\langle u_a^2 \rangle + \langle u_c^2 \rangle \\
&= (1/M) \int_0^{\omega_{max}} [E(\omega; T)/\omega^2] F(\omega)\, d\omega.
\end{aligned}
\tag{7.58}
$$

In an arbitrary direction $\mathbf{q}$, making an angle θ with the c-axis, one has

$$
\langle (\mathbf{u} \cdot \hat{\mathbf{q}})^2 \rangle = \langle u_c^2 \rangle \cos^2 \theta + \langle u_a^2 \rangle \sin^2 \theta.
\tag{7.59}
$$

Example: mean-square displacements in NaCl-type lattices. Since the essential interatomic forces in alkali halides, A^+B^-, are Coulomb forces plus interaction from overlap of atomic wave functions on neighbouring ions, we expect that $\langle \mathbf{u}^2(A) \rangle \approx \langle \mathbf{u}^2(B) \rangle$ at high temperatures. Calculations confirm this result (Huiszoon and Groenewegen 1972). For work on thermal displacements in $NbC_{0.95}$ (which has NaCl-structure), see Kaufmann and Meyer (1984), citing Müllner, Reichardt and Christensen. Butt et al. (1993) have tabulated atomic displacements in 52 diatomic cubic compounds, based on diffraction experiments.

Example: anisotropic vibrations in zinc. Zinc has unusually anisotropic thermal displacements. According to eq. (7.57) it suffices to find $\langle u_c^2 \rangle$ and $\langle u_a^2 \rangle$. A strict treatment requires not only the frequencies $\omega(\mathbf{q}, s)$ but also the corresponding eigenvectors. However, it is a useful approximation (Grüneisen and Goens 1924) to introduce two effective density-of-states functions of the Debye type, $F_a(\omega)$ and $F_c(\omega)$, and choose Debye temperatures θ_a and θ_c such that the temperature dependence of the displacements is well described. Figure 7.3 shows that this gives a good account of $\langle u_c^2 \rangle$ and $\langle u_a^2 \rangle$ in zinc. The normalisation of $F_a(\omega)$ and $F_c(\omega)$ is defined by fitting theory and experiment at $T = 0$ K. The inset shows the actual $F(\omega)$ and the two Debye spectra used here.

5.8. Combined static and dynamic displacements

In a random alloy $A_x B_{1-x}$, the atoms may take the positions of an ordered lattice but show displacements relative to the ideal lattice positions, because of the randomness and different atomic sizes. Such static
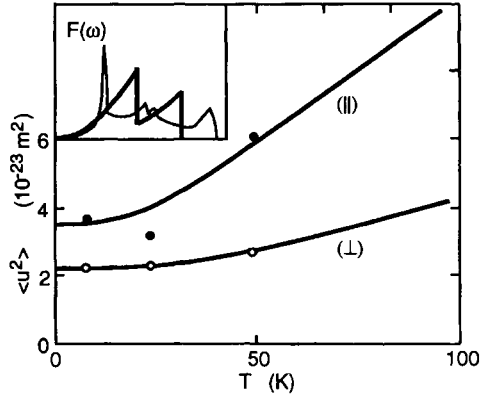
Fig. 7.3. Anisotropic thermal displacements in zinc, calculated with separate Debye models (shown in the inset together with the full $F(\omega)$) for directions parallel ($\parallel$) and perpendicular ($\perp$) to the hcp c-axis. Filled and open circles are measured values. After Potzel et al. (1984).

displacements are superimposed on the dynamic (vibrational) displacements. Static displacements affect the vibration frequencies, but that would enter as higher-order corrections in this case. Then it is reasonable to consider static and dynamic displacements as uncorrelated and get, for the total displacement,

$$\langle \mathbf{u}^2 \rangle_{\text{total}} \approx \langle \mathbf{u}^2 \rangle_{\text{static}} + \langle \mathbf{u}^2 \rangle_{\text{dynamic}}. \tag{7.60}$$

For an example of this approach, see Dernier et al. (1976) in an analysis of the mixed-valence compound $Sm_{0.7}Y_{0.3}S$.

5.9. Vibrational velocity

The instantaneous velocity $v_\alpha(\kappa, l; t)$ of an atom (κl) in the direction α is obtained from $\partial u_\alpha(\kappa, l; t)/\partial t$ (cf. Appendix D). Then, in analogy to eq. (7.34), we get the thermal average

$$\langle v_\alpha^2(\kappa, l, t) \rangle = \frac{1}{N_c M_\kappa} \sum_{\mathbf{q}, s} E(\mathbf{q}, s) \varepsilon_\alpha(\mathbf{q}, s; \kappa) \varepsilon_\alpha^*(\mathbf{q}, s; \kappa). \tag{7.61}$$

In a monatomic lattice with cubic symmetry, $\langle \mathbf{v}^2 \rangle = \langle v_x^2 \rangle + \langle v_y^2 \rangle + \langle v_z^2 \rangle$ is isotropic;

$$\langle \mathbf{v}^2 \rangle = \frac{1}{M} \int_0^{\omega_{\text{max}}} E(\omega, T) F(\omega) \, d\omega, \tag{7.62}$$

with the low and high temperature limits

$$\langle \mathbf{v}^2 \rangle = 3\hbar\omega(1)/2M = (9k_B/8M)\theta_D(1), \quad T = 0, \tag{7.63}$$

$$\langle \mathbf{v}^2 \rangle = 3k_B T/M, \quad k_B T \gg \hbar\omega_{max}. \tag{7.64}$$

See Chapter 19, §3 for comments on bounds to $\langle \mathbf{v}^2 \rangle$.

Example: Heisenberg's uncertainty relation in solids. In a monatomic lattice with cubic symmetry, the zero-point vibrational displacement and velocity are given by

$$\langle u_x^2 \rangle_{T=0} = \hbar/2M\omega(-1), \tag{7.65}$$

$$\langle v_x^2 \rangle_{T=0} = \hbar\omega(1)/2M. \tag{7.66}$$

The inequality $\omega(1) > \omega(-1)$, eq. (6.23), is equivalent with the Heisenberg uncertainty relation

$$\langle u_x^2 \rangle_{T=0} \langle v_x^2 \rangle_{T=0} > \hbar^2/4M^2. \tag{7.67}$$

For a single one-dimensional oscillator the relation (7.67) becomes an equality, while the Debye model gives $(9/8)(\hbar^2/4M^2)$ for the lefthand side of eq. (7.67). An analogous inequality holds for the displacement and velocity of a particular atom in a lattice with several different atoms (Housley and Hess 1966).

6. Temperature and pressure induced polymorphism

6.1. Introduction

With polymorphism we mean that an element or a compound can exist in several different crystalline forms. (Some authors use the word allotropy in the case of elements. Others use the word polytypism.) We will be interested in the cases when a solid transforms from one thermodynamically stable crystal structure to another, with varying temperature or pressure. A typical example of a temperature-induced transformation is that of tin at 286 K, from the low temperature semiconducting phase (gray tin) to the metallic β-phase (white tin). A typical

Table 7.1

Examples of temperature or pressure-induced polymorphism

Material	Point of transition[a]	Structural change
Fe	1173 K	bcc → fcc
Fe	1660 K	fcc → bcc
Fe	∼10 GPa	bcc → hcp
Ti	1155 K	hcp → bcc
Zr	1136 K	hcp → bcc
Be	1547 K	hcp → bcc
C	∼1.5 GPa	graph.→ diam.

[a]Data from Young (1991).

pressure induced transformation is that of alkali halides, where at least eight of the twelve compounds which crystallise in the B1 (i.e. NaCl-type) structure at zero pressure transform to the B2 (i.e. CsCl-type) structure at pressures below 100 GPa (Kim and Gordon 1974). Table 7.1 gives some additional examples. Data from Young (1991) and the JANAF thermochemical tables (1985).

6.2. Temperature-induced transformations

That structure is the most stable, which has the lowest Gibbs energy $G = U - TS + pV$. We first discuss a temperature-induced transformation and then one induced by pressure. Let us describe the temperature-dependent part of G by harmonic lattice vibrations, and specialise to $p \approx 0$ (i.e. normal atmospheric pressure) and high temperatures ($T > \theta_D$). Then the difference $G_2 - G_1$ between two phases, 1 and 2, is (cf. eq. (D.7))

$$G_2 - G_1 = \Delta H + 3Nk_BT\{\ln[\omega_2(0)/\omega_1(0)] \\ + (1/24)(\hbar/k_B)^2[\omega_2^2(2) - \omega_1^2(2)]/T^2 + \cdots\}, \quad (7.68)$$

where $\Delta H = [G_2 - G_1]_{T=0\ K}$ is the difference in cohesive energy for the static lattice at 0 K. Ignoring the term $\sim 1/T^2$ in eq. (7.68), the condition $G_1(T_t) = G_2(T_t)$ yields the transformation temperature T_t;

$$T_t = \frac{\Delta H}{3Nk_B \ln[\omega_1(0)/\omega_2(0)]}. \quad (7.69)$$
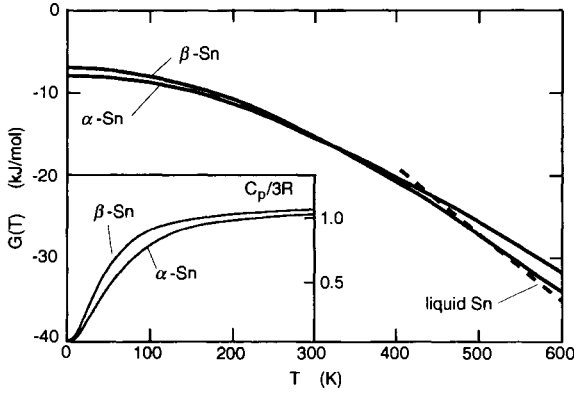
Fig. 7.4. The Gibbs energy $G(T)$ for α-Sn, β-Sn and liquid Sn. The inset shows the heat capacity, normalised as $C_p/3R$. Data from Dinsdale (1991) and Hultgren et al. (1973a).

If the difference $\Delta\omega = \omega_1(0) - \omega_2(0)$ is small compared with $\omega_1(0)$ [$\approx \omega(0)$], we get

$$\frac{\Delta\omega}{\omega(0)} = \frac{\Delta H}{3Nk_BT_t}. \tag{7.70}$$

Example: gray and white tin. Figure 7.4 shows $G(T)$ for gray, white and liquid tin, as derived from experiments at ambient pressure. Gray tin (α-Sn) is a semiconductor with the diamond-type lattice structure and white tin (β-Sn) is a metal with tetragonal structure. The electronic structure, and hence the bonding, is radically different in the two phases. This is reflected in the entropy Debye temperatures evaluated at $T = T_t = 286$ K, where $\theta_D^S(\text{grey})/\theta_D^S(\text{white}) \approx 1.3$.

6.3. Pressure-induced transformations

To illustrate the pressure-induced transformation we consider $T = 0$ K. The relative lattice stability is determined by the enthalpy $H = U + pV$. At the transformation pressure p_t,

$$U_1(V_1) + p_tV_1 = U_2(V_2) + p_tV_2. \tag{7.71}$$

Thus, a transformation occurs at

$$p_t = \frac{U_2(V_2) - U_1(V_1)}{V_1 - V_2}. \tag{7.72}$$
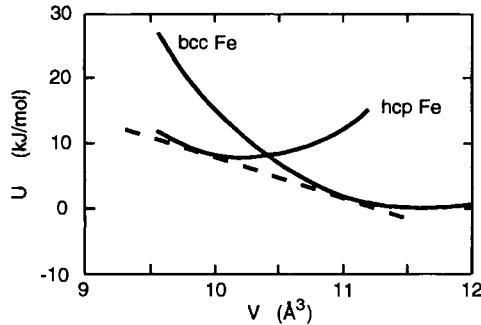
Fig. 7.5. The energy $U(T)$ for bcc and hcp Fe, as a function of the volume per atom. From ab initio electron structure calculations (Ekman 1998, unpublished).

The pressure p_t has a geometrical interpretation as the slope of the common tangent to the $U_1(V)$ and $U_2(V)$ versus V curves (fig. 7.5).

Because our approach only compares the energy difference between two equilibrium structures, we cannot say anything about kinetic aspects, such as nucleation and growth of a phase (Yamada et al. 1984), but see the discussion of dynamic instabilities in §6.4 below and in Chapter 6 (§13).

Example: pressure-induced transformation in Fe. At ambient temperature and pressure, iron has the bcc structure. Under pressure, it transforms to an hcp structure. Figure 7.5 shows the energy U at $T = 0$ K for bcc and hcp Fe, from ab initio electron structure calculations. The transition pressure p_t as given by eq. (7.72) corresponds to the slope of the common tangent to $U(V; \text{bcc})$ and $U(V; \text{hcp})$ in fig. 7.5. The calculation yields $p_t \approx 10$ GPa, in good agreement with experiments, which are uncertain due to hysteresis in p_t. The large difference in atomic volume of Fe between the bcc and hcp lattices is due to magnetic effects. There is no magnetic moment in hcp Fe at the volumes considered here. (In a model with atoms represented by rigid spheres, the atomic volume of the bcc phase would be 9% larger than for the hcp phase, see Chapter 19, §2.)

Example: temperature- and pressure-induced polymorphism in TlI. Thallium iodide has some interesting properties (Samara et al. 1967). At ambient pressure and $T_t = 429$ K, it transforms from a low temperature orthorhombic structure (1) to a more dense cubic CsCl-type structure

(2). The same structural transformation takes place if, at ambient temperature, the pressure is increased to $p_t = 0.29$ GPa (2.9 kbar). The heat of transformation at 0.1 MPa (1 bar) is $\Delta H = 1230 \pm 160$ J/mol. The molar volume is lower by 3.3% in the CsCl structure; $V_1 - V_2 = 1.5$ cm^3/mol. We shall analyse these transformations in a simple model. With $N = 2N_A$ and $T = 429$ K, eq. (7.69) gives $\omega_2(0)/\omega_1(0) = 0.94$. In the pressure-induced transformation, temperature effects cannot be neglected. If the high temperature form of $G_2 - G_1$ in eq. (7.68) replaces $U_2 - U_1$ in eq. (7.72), and the volume dependence of ΔH and $\omega_2(0)/\omega_1(0)$ is ignored, eq. (7.72) yields $p_t = 0.26$ GPa, to be compared with the measured $p_t = 0.29$ GPa.

6.4. Approaching a lattice instability

In the solid-solid phase transformations discussed above, each phase also exists as a metastable phase in a certain temperature or pressure interval beyond the point of equal Gibbs energies. The actual transformation takes place through nucleation and growth of the new phase. We shall now comment on the case when a phase becomes dynamically unstable due to a change in temperature, pressure or chemical composition (cf. Chapter 4, §3, Chapter 6, §13). Then the concept of a vibrational entropy has no physical meaning, and the Gibbs (or Helmholtz) energy is undefined.

For example, consider the behaviour of G when a change in the pressure p takes the solid from a dynamically stable state to one that has an unstable phonon mode. In a strict Debye model, and at high temperatures, the Gibbs energy can be written (eq. (D.8)),

$$G \approx U(V) + pV - 3Nk_B T[1/3 + \ln(T/\theta_D)]. \tag{7.73}$$

If we let θ_D approach 0 in eq. (7.73), G would diverge towards $-\infty$, and hence this phase would be stabilised relative to other phases just before it becomes unstable at a pressure p_c. However, eq. (7.73) assumes that all phonon frequencies tend to zero at the same rate, and become 0 at p_c. In a real material, there will be one particular mode $(\mathbf{q}, s)$ that first reaches $\omega(\mathbf{q}, s) = 0$. The singularity therefore is very weak, and G does not diverge when $p \rightarrow p_c$ (Fernández Guillermet et al. 1995). Hence, on approaching p_c, there is only a small precursor effect in the phase diagram. Figure 7.6 shows this for Mg, which is stable in the bcc structure
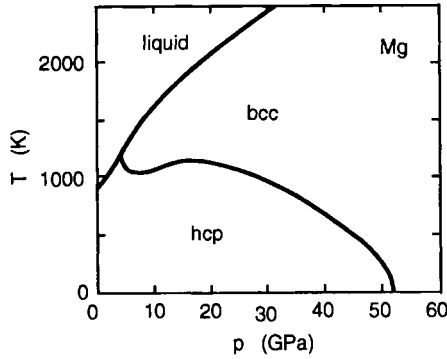
Fig. 7.6. The temperature-pressure phase diagram of magnesium, as obtained through ab initio electron structure calculations. After Moriarty and Althoff (1995).
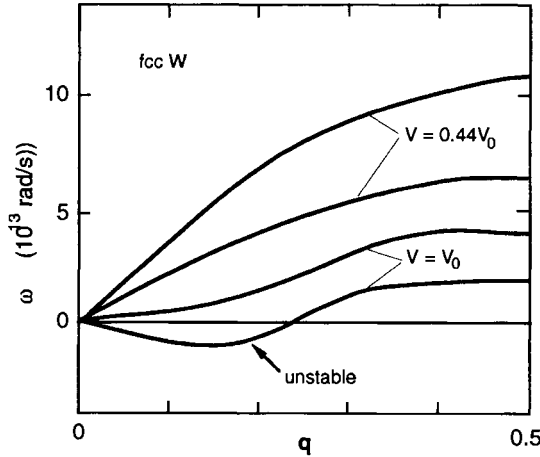
Fig. 7.7. At ambient pressure (volume V_0 per atom) the fcc lattice of tungsten is dynamically unstable under shear, but the phonons are stabilised with increasing pressure, as shown here for phonons in the [100] direction when $V = 0.44V_0$. The figure gives $-|\omega(\mathbf{q}, s)|$ when $\omega^2(\mathbf{q}, s) < 0$. For each V, the upper curve refers to longitudinal and the lower curve to transverse modes. After Einarsdotter et al. (1997).

at high p but with a transverse [110] mode that becomes unstable at low pressures (Moriarty and Althoff 1995). Analogously, the Pt-W phase diagram does not show any feature revealing that the fcc lattice becomes unstable as one goes from Pt towards pure W (Fernández Guillermet et al. 1995). See also Craievich and Sanchez (1997) for calculations on Ni–Cr alloys, showing that the elastic constant $C' = (c_{11} - c_{12})/2$ is

negative for fcc Cr and for bcc Ni (pure Cr has the bcc and pure Ni the fcc lattice structure). Strong anharmonicity in the soft modes will modify the arguments above, but not change the essential point about the singularity in G. Finally, it should be remarked that the actual transformation may take place before the point of instability, and be of the first-order type discussed in §§6.2 and 6.3 above. For instance, the bcc phase of Ti and Zr appears to be dynamically unstable at low temperatures, but the phonons are well defined at the bcc $\leftrightarrow$ hcp transition (see fig. 6.17).

Example: phonon instability in fcc tungsten. Tungsten at ambient conditions has the bcc lattice structure, and the fcc structure is dynamically unstable (Einarsdotter et al. 1997). Under compression, the phonon modes of the fcc lattice are gradually stabilised. Figure 7.7, based on ab initio electron structure calculations, shows this for phonons in the [100] direction. Modes in some other directions are also strongly affected.

PHONONS IN REAL CRYSTALS:
ANHARMONIC EFFECTS

1. Introduction

In the previous chapters we discussed lattice vibrations under very ideal circumstances. The lattice was assumed to be free from defects such as vacancies, impurities, grain boundaries and surfaces. It was also assumed sufficient to retain only the harmonic part of the expansion of the potential energy in the atomic displacements. Although these may be excellent approximations in some cases, they completely leave out certain phenomena. For instance, perfectly harmonic vibrations give no thermal expansion. Furthermore, if the vibrations are harmonic and the lattice is also free from defects, the thermal conductivity is infinite.

As a starting point of our theoretical treatment we take the expansion of the total lattice energy in atomic displacements $\mathbf{u}_i$ and the corresponding momenta $\mathbf{p}_i$. With i, j denoting atoms and α, β Cartesian components, the energy in the harmonic approximation is

$$\sum_i \frac{\mathbf{p}_i^2}{2M_i} + \Phi_0 + (1/2) \sum_{i,j,\alpha,\beta} \Phi''_{\alpha\beta}(i, j) u_{i\alpha} u_{j\beta}. \tag{8.1}$$

Corrections to the simple theory of Chapters 6 and 7 may arise because:
 (i) Higher-order powers of $\mathbf{u}$ are added to the expansion of the potential energy Φ in eq. (8.1).
(ii) The perfect periodicity is destroyed by the presence of vacancies, impurity atoms, dislocations, grain boundaries, free surfaces, etc.

If, in the case of (ii), we only retain quadratic terms in $\mathbf{u}$, the vibrations are still described as harmonic. However, the solutions to the equations of motion are no longer plane waves characterised by the

wave vector $\mathbf{q}$ (although that may be a good approximation for most of the vibrational modes).

The anharmonic effects mentioned under (i) are present even in a lattice without any defects. That is the theme of this chapter. Vibrations in defect lattices, (ii), are considered in Chapter 9. Original work covering the main points in this chapter is due, inter alia, to Leibfried and Ludwig (1961), Maradudin and Fein (1962), Cowley (1963) and Barron (1965). There are several reviews, e.g. by Cowley (1968), Wallace (1972) and Barron and Klein (1974).

2. Weakly perturbed harmonic vibrations

Let $\omega_0(\mathbf{q}, s)$ be the frequency of the phonon mode $(\mathbf{q}, s)$ in the harmonic approximation. In a real system, which we assume does not deviate too far from the harmonic conditions, the frequency $\omega_0(\mathbf{q}, s)$ is shifted to a complex value

$$\omega(\mathbf{q}, s) = \omega_0(\mathbf{q}, s) + \Delta(\mathbf{q}, s) - i\Gamma(\mathbf{q}, s). \tag{8.2}$$

If there had been no imaginary part $-i\Gamma(\mathbf{q}, s)$, the perturbed state $(\mathbf{q}, s)$ would have the exact energy eigenvalue $\omega_0(\mathbf{q}, s) + \Delta(\mathbf{q}, s)$, and a time dependence given by $\exp[-i(\omega_0 + \Delta)t]$. The imaginary term adds a factor $\exp(-\Gamma t)$ to the time dependence. Hence, the state $(\mathbf{q}, s)$ decays, but if Γ is small ($\Gamma/\omega_0 \ll 1$), the lifetime of the state will be long and it is still meaningful to label it by the $(\mathbf{q}, s)$ of the unperturbed state. (The situation is similar to that encountered in atomic physics. The energy levels of the hydrogen atom are well described by the quantum mechanical version of Bohr's simple theory. In a more accurate description, however, there are corrections which shift the energy levels and give them a finite line width.)

In this chapter we assume that Γ is negligible, i.e. we let

$$\omega(\mathbf{q}, s) = \omega_0(\mathbf{q}, s) + \Delta(\mathbf{q}, s). \tag{8.3}$$

An important result is that, within the low-order quantum-mechanical perturbation theory, the shifted frequencies (eq. (8.3)) are those obtained in a neutron inelastic scattering experiment. We will comment on that in §6 when the vibrational entropy is discussed. A significant consequence

of a finite Γ is to limit the phonon part of the thermal conductivity. That problem is dealt with in Chapter 16. Furthermore, a measurable physical property, such as the heat capacity, cannot have an imaginary part. Therefore, one cannot simply insert the perturbed complex energies (eq. (8.2)) in, e.g. Bose–Einstein statistical factors. There is a well-developed theory for how to allow for a finite Γ in an account of thermodynamic properties (see e.g. Pathak and Varshni 1969).

3.   The quasi-harmonic approximation and phonon Grüneisen parameters

3.1.   General aspects and cubic lattice symmetry

The quantities $\Phi''_{\alpha\beta}(i, j)$ in eq. (8.1) have the dimension of force constants, measuring the interatomic forces when the potential Φ is given. The derivatives with respect to the coordinates (α, β) are evaluated for atoms labelled (i, j) that have the position vectors $\mathbf{R}_i$ and $\mathbf{R}_j$. If the lattice is strained, the atoms take new positions where the derivatives of Φ should be evaluated. Therefore, the force constants depend on the state of strain. For instance, they will vary with an external pressure. In the *quasiharmonic approximation* we allow for such a strain dependence of the phonon frequencies $\omega(\mathbf{q}, s)$, but still consider them to be harmonic. This may be a very good approximation to describe physical phenomena, although from a strict mathematical point of view, it is inconsistent for the following reason. If the vibrations are truly harmonic, the third- and higher-order derivatives of Φ are zero. But variations in the second derivative of Φ with small variations in the positions $\mathbf{R}$ are proportional to these high-order derivatives.

The *Grüneisen parameter* $\gamma(\mathbf{q}, s)$ is now introduced as a measure of how the phonon frequency $\omega(\mathbf{q}, s)$ is altered under a small change in the geometry of the crystallographic unit cell. The most commonly encountered Grüneisen parameter is that referring to an isotropic change in the volume V;

$$\gamma(\mathbf{q}, s) = -\frac{V}{\omega(\mathbf{q}, s)}\left(\frac{\partial\omega(\mathbf{q}, s)}{\partial V}\right) = -\left(\frac{\partial\ln\omega(\mathbf{q}, s)}{\partial\ln V}\right). \qquad (8.4)$$

This expression will be the cornerstone in the simplest theory of thermal expansion, (Chapter 14, §4). It is a special case of a more generally defined Grüneisen parameter $\gamma(\mathbf{q}, s; \varepsilon_i)$ that expresses how $\omega(\mathbf{q}, s)$ varies

under a small change in ε_i, where ε_i is a strain parameter specifying the geometry of the unit cell. Here, $i = 1, 2, 3$ refer to the lengths a_i of the cell axes and $i = 4, 5, 6$ refer to the angles between a_i (Chapter 3, §2);

$$\gamma(\mathbf{q}, s; \varepsilon_i) = -\frac{1}{\omega(\mathbf{q}, s)} \left(\frac{\partial \omega(\mathbf{q}, s; \varepsilon_i)}{\partial \varepsilon_i} \right)_{\varepsilon_i'}. \tag{8.5}$$

The derivative is taken with all $\varepsilon_i' \neq \varepsilon_i$ kept constant. Usually γ is calculated at the reference state of zero external tension or shear. For clarity we will sometimes add a label V to the most common Grüneisen parameter, as defined in eq. (8.4), i.e. $\gamma(\mathbf{q}, s; V)$. We remark that other authors often write the Grüneisen parameter as γ_G, with a subscript G. In this book the notation γ_G is used for the *"thermodynamic" Grüneisen parameter* (eq. (13.23)), which is obtained directly from macroscopic thermodynamic quantities. Grüneisen parameters can be defined also for electronic and magnetic contributions to the total free energy of a solid. For brevity the label "phonon" on the Grüneisen parameters in this chapter is suppressed.

If, for $i = 1, 2, 3$, one of the a_i is changed by a relative amount $\Delta a_i / a_i$, the corresponding strain is $\varepsilon_i = \Delta a_i / a_i$. Then, from eq. (8.5),

$$\left(\frac{\Delta \omega(\mathbf{q}, s)}{\omega(\mathbf{q}, s)} \right) = -\gamma(\mathbf{q}, s; \varepsilon_i) \Delta \varepsilon_i = -\gamma(\mathbf{q}, s; \varepsilon_i) \left(\frac{\Delta a_i}{a_i} \right), \tag{8.6}$$

and we can write

$$\gamma(\mathbf{q}, s; a_i) = -\left(\frac{\partial \ln \omega(\mathbf{q}, s)}{\partial \ln a_i} \right). \tag{8.7}$$

In a lattice with cubic symmetry, $a_1 = a_2 = a_3 = a$ and $V \sim a^3$, and therefore $\partial \ln a_i / \partial \ln V = 1/3$ under uniform expansion or contraction of the unit cell. Hence,

$$\begin{aligned} \gamma(\mathbf{q}, s; V) &= -\left(\frac{\partial \ln \omega(\mathbf{q}, s)}{\partial \ln V} \right) \\ &= -\sum_{i=1}^{3} \left(\frac{\partial \ln \omega(\mathbf{q}, s)}{\partial \ln a_i} \right) \left(\frac{\partial \ln a_i}{\partial \ln V} \right) = \gamma(\mathbf{q}, s; a). \end{aligned} \tag{8.8}$$

where we have introduced yet another Grüneisen parameter, $\gamma(\mathbf{q}, s; a)$.

Usually, the Grüneisen parameters are positive and lie in the range 1.5 ± 1. Negative Grüneisen parameters sometimes occur for low-lying frequencies (long-wavelength transverse modes) in open structures like those of Ge, Si and some alkali halides.

3.2. Grüneisen parameters in hexagonal lattice symmetry

The conventional notation for the lattice parameters in hexagonal lattices is $a_1 = a_2 = a$ and $a_3 = c$. Then, for a uniform expansion or contraction of the unit cell (i.e. while keeping c/a fixed)

$$
\begin{aligned}
\gamma(\mathbf{q}, s; V) &= -2 \left(\frac{\partial \ln \omega(\mathbf{q}, s; a_1)}{\partial \ln a_1} \right) \left(\frac{\partial \ln a_1}{\partial \ln V} \right) \\
&\quad - \left(\frac{\partial \ln \omega(\mathbf{q}, s; c)}{\partial \ln c} \right) \left(\frac{\partial \ln c}{\partial \ln V} \right) \\
&= (1/3)[2\gamma(\mathbf{q}, s; a_1) + \gamma(\mathbf{q}, s; c)].
\end{aligned} \tag{8.9}
$$

Here, we have to be careful in the notation. In eq. (8.9) we have written a_1 to denote that we only change the strain in one direction, perpendicular to the c-axis. It is now natural to introduce Grüneisen parameters $\gamma_\parallel$ and $\gamma_\perp$, such that $\gamma_\parallel = \gamma_\perp$ in the special case of cubic symmetry. We define

$$
\gamma_\parallel(\mathbf{q}, s) = \gamma(\mathbf{q}, s; c) = -\left(\frac{\partial \ln \omega}{\partial \ln c} \right)_a, \tag{8.10}
$$

$$
\gamma_\perp(\mathbf{q}, s) = \gamma(\mathbf{q}, s; a_1) = -\frac{1}{2} \left(\frac{\partial \ln \omega}{\partial \ln a} \right)_c, \tag{8.11}
$$

In the last derivative, it is the cell dimension a that is varied (i.e. a_1 and a_2 both vary by the same amount), and this gives rise to the prefactor $1/2$. With the definitions above, and those to follow in this chapter, the various Grüneisen parameters will be equal in the special case that all $\gamma(\mathbf{q}, s)$ of the individual phonon modes are equal and depend only on volume changes, irrespective of shape deformations of the lattice unit cell.

Example: Grüneisen parameter for varying c/a in hcp lattices. Some materials with hcp structures, e.g. Cd and Zn, have a c/a ratio which deviates strongly from the "ideal" value 1.63, but the atomic volume
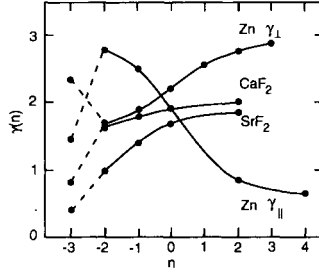
Fig. 8.1. The Grüneisen parameter $\gamma(n; V)$ as a function of n, for CaF_2 and SrF_2 (Bailey and Yates 1967) and for Zn (Barron and Munn 1967). Because the Zn lattice is hexagonal, there are two Grüneisen parameters, $\gamma_\perp$ and $\gamma_\parallel$.

is not abnormal (cf. the example in Chapter 19, §2). It is therefore of interest to consider how the phonon frequencies vary with c/a at fixed volume V. One has

$$
\begin{aligned}
\gamma(\mathbf{q}, s; c/a) &= -\left(\frac{\partial \ln \omega(\mathbf{q}, s)}{\partial \ln(c/a)}\right)_V \\
&= -\left(\frac{\partial \ln \omega(\mathbf{q}, s)}{\partial \ln a}\right)_c \left(\frac{\partial \ln a}{\partial \ln(c/a)}\right)_V \\
&\quad -\left(\frac{\partial \ln \omega(\mathbf{q}, s)}{\partial \ln c}\right)_a \left(\frac{\partial \ln c}{\partial \ln(c/a)}\right)_V \\
&= (2/3)[\gamma_\parallel(\mathbf{q}, s) - \gamma_\perp(\mathbf{q}, s)].
\end{aligned}
\tag{8.12}
$$

Here, we have used the fact that $ca^2 \sim V$ = constant, which yields $c/a = (\text{constant})/a^3$ and, hence, $[\partial \ln(c/a)/\partial \ln a]_V = -3$. Similarly, $[\partial \ln(c/a)/\partial \ln c]_V = 3/2$. In zinc, $\gamma_\perp = 2.50$ and $\gamma_\parallel = 1.28$ when all modes are given equal weights ($n = 1$, fig. 8.1). Then $\gamma(c/a) = -0.81$. In the special case of isotropy, $\gamma_\parallel = \gamma_\perp$, we would get $\gamma(\mathbf{q}, s; c/a) = 0$ as expected, since it was assumed that c/a varied under constant volume.

3.3. Grüneisen parameters for moment frequencies and Debye temperatures

Grüneisen parameters can be defined also for the moment frequencies $\omega(n)$ and the corresponding Debye temperatures $\theta_D(n)$. For instance,

$$
\gamma(n; V) = -\left(\frac{\partial \ln \theta_D(n)}{\partial \ln V}\right) = -\left(\frac{\partial \ln \omega(n)}{\partial \ln V}\right).
\tag{8.13}
$$

In the strict Debye model, $\omega_D = C_{\text{sound,D}}q_D = k_B\theta_D/\hbar$, where $C_{\text{sound,D}}$ is the sound velocity and $q_D = (6\pi^2 N/V)^{1/3}$. Then

$$\gamma(\theta_D; V) = -\left(\frac{\partial \ln \theta_D}{\partial \ln V}\right) = -\left(\frac{\partial \ln C_{\text{sound,D}}}{\partial \ln V}\right) + \frac{1}{3}. \tag{8.14}$$

Only if all $\gamma(\mathbf{q}, s; V)$ are equal, is $\gamma(n; V)$ independent of n. Often $\gamma(\mathbf{q}, s; V)$ of different modes $(\mathbf{q}, s)$ differ by as much as a factor of two. The corresponding variation of $\gamma(n; V)$ is shown in fig. 8.1. The value of $\gamma(2; V)$ has a simple relation to the trace of the dynamical matrix (see Appendix C).

It is not unusual to approximate $\gamma(n)$ by the thermodynamic Grüneisen parameter γ_G (see eq. (13.23)). This may be too crude an approximation. For instance, in the very anisotropic graphite, $\gamma(n)$ varies very strongly with n (Bailey and Yates 1970).

If $\gamma(n; V)$ depends only weakly on the volume, we can integrate eq. (8.13) and obtain

$$\frac{\theta_D(n; V)}{\theta_D(n; V_0)} = \left(\frac{V_0}{V}\right)^{\gamma(n)}. \tag{8.15}$$

In hexagonal structures, the corresponding relation is

$$\frac{\theta_D(n; a, c)}{\theta_D(n; a_0, c_0)} = \left(\frac{a_0}{a}\right)^{2\gamma_\perp(n)} \left(\frac{c_0}{c}\right)^{\gamma_\parallel(n)}. \tag{8.16}$$

Example: Slater's form of the Grüneisen parameter $\gamma(-3; V)$. Slater (1940) derived an expression for the Grüneisen parameter, essentially as follows. Expand the volume change $V - V_0$, due to an external pressure p, in powers of p and keep only the first two terms; $V - V_0 = V_0(a_1 p + a_2 p^2)$. The average sound velocity $C_{\text{sound,D}}$ to be used in $\theta_D(-3)$ is given by $3/(C_{\text{sound,D}})^3 = 1/C_L^3 + 2/C_T^3$, eq. (6.15). If we neglect the volume dependence of the Poisson ratio and use eqs. (5.9) and (5.10) for C_L and C_T expressed in the elastic constants, we get $C_{\text{sound,D}} \sim (KV)^{1/2}$. K is the bulk modulus; $K^{-1} = -(1/V)(\partial V/\partial p)_T = -(V/V_0)[a_1 + 2a_2(V - V_0)/(a_1 V_0)]$. Then, as in eq. (8.14), one obtains Slater's expression

$$\begin{aligned}
\gamma(-3; V) &= -(1/2)(\mathrm{d}\ln K/\mathrm{d}\ln V) - 1/6 \\
&= a_2/a_1^2 - 2/3 = (1/2)(\mathrm{d}K/\mathrm{d}p) - 1/6. \tag{8.17}
\end{aligned}$$

The coefficients a_1 and a_2, which yield $\mathrm{d}\ln K/\mathrm{d}\ln V$, can be measured (Gschneidner 1964). At the time of Slater's original derivation, it was unknown to what extent $\gamma(\mathbf{q}, s)$ varies with the phonon mode $(\mathbf{q}, s)$ and no distinction was made between $\gamma(n; V)$ for different n. Here we have stated explicitly that Slater's expression is an estimation of $\gamma(-3; V)$. Thus, it is not equal to the Grüneisen parameter $\gamma(0; V)$ $(\approx \gamma_{\mathrm{G}})$ that is approximately obtained from the thermal expansion coefficient at moderate and high temperatures (Chapter 14, §4.2). The quantity $(\mathrm{d}K/\mathrm{d}p)$ in the last part of eq. (8.17) is discussed in Chapter 13, §2.

Example: internal pressure from zero-point vibrations. Suppose that we have calculated the atomic volume Ω_{a} from a model that considers only the static lattice. We now estimate how much Ω_{a} is changed due to the zero-point $(T = 0)$ lattice vibrations. The pressure p is related to the energy by $p = -(\partial U/\partial V)_S$. If we add to U the zero-point energy $(3/2)\hbar\omega(1)$ per atom, (eq. (7.17)), the pressure is changed by

$$
\begin{aligned}
p_Z &= -(V/\Omega_{\mathrm{a}})(3\hbar/2)[\partial\omega(1)/\partial V] \\
&= [3\hbar\omega(1)\gamma(1)]/[2\Omega_{\mathrm{a}}].
\end{aligned}
\tag{8.18}
$$

V/Ω_{a} is the number of atoms in the solid. An added internal pressure p_Z gives rise to a relative change in the atomic volume;

$$
\frac{\Delta\Omega_{\mathrm{a}}}{\Omega_{\mathrm{a}}} = \frac{p_Z}{K_T} = \frac{3\hbar\omega(1)}{2K_T\Omega_{\mathrm{a}}}\gamma(1),
\tag{8.19}
$$

where a mass dependence (isotope effect) enters through $\omega(1)$. At high temperatures, with $p = -(\partial F/\partial V)_T$ and F as given in eq. (D.7), we find that $\hbar\omega(1)\gamma(1)$ in eq. (8.19) should be replaced by $2k_{\mathrm{B}}T\gamma(0)$. Then p does not depend on the atomic mass. Figure 8.2 shows how the lattice parameter depends on the isotopic composition and the temperature, for lithium hydrides with different lithium and hydrogen isotopes; after Grimvall (1996). See also Johansson and Rosengren (1975) for a discussion of $^6\mathrm{Li}$ and $^7\mathrm{Li}$, and Ramdas (1995) and Haller (1995) for reviews of various isotope effects in semiconductors.
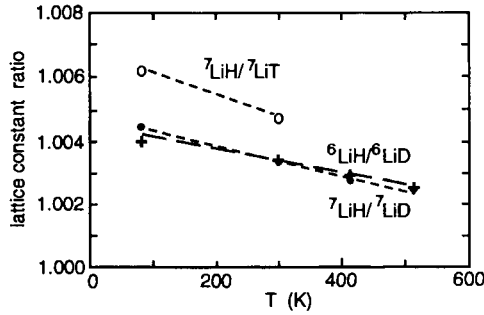
Fig. 8.2. Effect of isotope mass on the lattice parameter of lithium hydrides.

4. Explicit anharmonicity

The frequency shifts discussed above vanish if the crystal volume, or rather all ε_i, remain constant. However, there are also effects that we will refer to as *explicitly anharmonic*. They arise from higher-than-quadratic terms when the potential energy Φ is expanded in powers of displacements **u** from the equilibrium positions of the atoms, (eq. (8.1)). (Due to the zero-point motion they are, to some extent, present also at $T = 0$.) To see the structure of the associated frequency shifts, it is illuminating first to study an anharmonic one-dimensional oscillator. Let the mass M move in a potential

$$V(x) = (1/2)M\omega^2 x^2 + V_3 x^3 + V_4 x^4, \tag{8.20}$$

where V_3 and V_4 are in some sense (decreasingly) small. When $V_3 = V_4 = 0$, the energy eigenvalues are $E_n = \hbar\omega(n + 1/2)$. Quantum mechanical perturbation theory, applied to the state n and at $T = 0$, gives energy shifts ΔE_n. In conventional notation, they can be written

$$\Delta E_n = \langle n|V_3 x^3 + V_4 x^4|n\rangle - \sum_{n'\neq n} \frac{|\langle n|V_3 x^3 + V_4 x^4|n'\rangle|^2}{E_{n'} - E_n}. \tag{8.21}$$

We have $\langle n|V_3 x^3|n\rangle = 0$, since in this term the integrand is an odd function of x and the integration is over negative and positive x. In the last term of eq. (8.21) we only keep the lowest-order part of the numerator, i.e. $\langle n|V_3 x^3|n'\rangle$. Thus, the term $V_4 x^4$ contributes to the first order (in the first term on the righthand side), while $V_3 x^3$ contributes to second

order in the perturbation expansion. It is necessary to keep both these terms, even though $V_4 x^4$ was assumed to be much smaller than $V_3 x^3$ in the relevant range of x-values, because the larger term enters only in a higher-order perturbation contribution. We shall use subscript 2 for the quasiharmonic shift (because only terms quadratic in the atomic displacements are kept), while frequency shifts originating from $\mathbf{u}^3$ and $\mathbf{u}^4$ are denoted Δ_3 and Δ_4. (Other authors may use other conventions for the subscripts of Δ.) Neglecting damping of the phonons, we now get

$$\omega(\mathbf{q}, s) = \omega_0(\mathbf{q}, s) + \Delta_2(\mathbf{q}, s) + \Delta_3(\mathbf{q}, s) + \Delta_4(\mathbf{q}, s). \qquad (8.22)$$

When one adds the explicitly anharmonic shifts Δ_3 and Δ_4 to the quasiharmonic model, but still neglects damping, one sometimes calls it the *pseudoharmonic approximation*. (It should be mentioned that some authors refer to eq. (8.22) as the quasiharmonic approximation, but normally "quasi-harmonic" refers only to $\omega_0 + \Delta_2$.)

The shifts $\Delta_2(\mathbf{q}, s)$, $\Delta_3(\mathbf{q}, s)$ and $\Delta_4(\mathbf{q}, s)$ can be written in condensed form as (e.g. Maradudin and Fein 1962, Cowley 1963, 1968, 1970, Cowley and Cowley 1965, Wallace 1972)

$$\Delta_2(\mathbf{q}, s) = (2/\hbar) \sum_\alpha V_\alpha(\mathbf{q}s, -\mathbf{q}s)\varepsilon_\alpha, \qquad (8.23)$$

$$\Delta_3(\mathbf{q}, s) = -(18/\hbar^2) \sum_{\mathbf{q}_1 s_1, \mathbf{q}_2 s_2} |V(\mathbf{q}s, \mathbf{q}_1 s_1, \mathbf{q}_2 s_2)|^2 R(0, 1, 2),$$

$$(8.24)$$

$$\Delta_4(\mathbf{q}, s) = (12/\hbar) \sum_{\mathbf{q}_1 s_1} V(\mathbf{q}s, -\mathbf{q}s, \mathbf{q}_1 s_1, -\mathbf{q}_1 s_1)$$
$$\times [2n(1) + 1], \qquad (8.25)$$

with

Table 8.1

The relative frequency shifts $-\Delta_{\text{tot}}/\omega_{\text{harm}}(0)$ and $-\Delta\omega(V_0)/\omega_{\text{harm}}(0)$ near T_{fus}. Based on data from Fernández Guillermet and Grimvall (1991a) (for Mo, W) and Rosén and Grimvall (1983)

	Cu	Zn	Al	Pb	K	Mo	W
$-\Delta_{\text{tot}}/\omega_{\text{harm}}(0)$	0.14	0.10	0.15	0.11	0.12	0.30	0.31
$-\Delta\omega(V_0)/\omega_{\text{harm}}(0)$	−0.01	−0.01	0.00	−0.01	0.04	0.17	0.18

$$R(0, 1, 2)$$

$$= [n(1) + n(2) + 1]\left(\frac{1}{\omega_0 + \omega_1 + \omega_2} - \frac{1}{\omega_0 - \omega_1 - \omega_2}\right)$$

$$+ [n(1) - n(2)]\left(\frac{1}{\omega_0 - \omega_1 + \omega_2} - \frac{1}{\omega_0 + \omega_1 - \omega_2}\right). \quad (8.26)$$

In the Bose–Einstein function $n(i)$, as well as in the interaction function $V(i, \ldots)$, in the quantities $\Delta(i)$ and ω_i, and in the summations, the index $i = 0, 1, 2$ is short for $(\mathbf{q}, s)$, $(\mathbf{q}_1, s_1)$ and $(\mathbf{q}_2, s_2)$, respectively. In Δ_2, the thermal strain ε_α is to be calculated as in eq. (14.17). $V_\alpha(0)$, $V(0, 1)$ and $V(0, 1, 2)$ are short for the Fourier transforms of the interatomic potential. The principal value (in the mathematical sense) should be taken in the sum over the singular terms in eq. (8.26). (In a non-primitive lattice there is an additional term in Δ_4.)

One can show that Δ_3 is always negative. Δ_4 may have either sign but often cancels much of Δ_3. Usually, Δ_2 is much larger than $\Delta_3 + \Delta_4$, but see also the elements K, Mo and W in table 8.1. The temperature dependence of Δ_3 and Δ_4 comes from the Bose–Einstein factors n. At high temperatures the factors $(n + 1/2)$, and therefore also Δ_3 and Δ_4, are linear in T (Appendix E). When $T = 0$ there remains the term $1/2$ in $(n + 1/2)$, i.e. the contribution from zero-point vibrations. Hence, Δ_3 and Δ_4 are not zero at $T = 0$ K.

Table 8.1 gives the quantities $\Delta_{\text{tot}}/\omega_{\text{harm}}(0)$ and $\Delta\omega(V_0)/\omega_{\text{harm}}(0)$ near the melting temperature T_{fus} for some metals. Here $\omega_{\text{harm}}(0)$ is approximated by the frequency corresponding to the Debye temperature θ_D^S derived from the experimental entropy at 300 K, and corrected for the
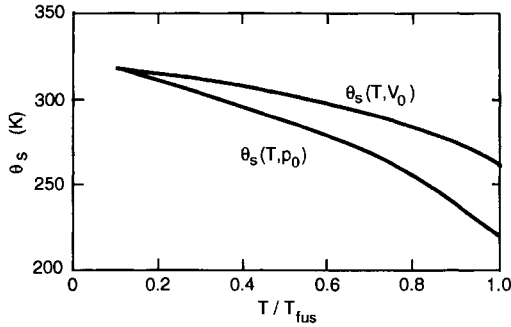
Fig. 8.3. The entropy Debye temperature $\theta_{\mathrm{D}}^{S}(T)$ of tungsten, at constant pressure and at fixed volume, as derived from thermodynamic data.

electronic contribution to S. The total frequency shift Δ_{tot} is obtained from $\theta_{\mathrm{D}}^{S}(T \approx T_{\mathrm{fus}}) - \theta_{\mathrm{D}}^{S}(T = 300\,\mathrm{K})$, and $\Delta\omega(V_0)$ is the frequency shift that results when the thermal data have been reduced to fixed volume V_0. Within low-order perturbation theory, $\Delta_{\mathrm{tot}} = \Delta_2 + \Delta_3 + \Delta_4$ and $\Delta\omega(V_0) = \Delta_3 + \Delta_4$, but close to T_{fus} there are higher-order anharmonic contributions to Δ_{tot} and $\Delta\omega(V_0)$. As shown in table 8.1, the thermal expansion accounts for almost all of the frequency shifts in Cu, Zn, Al and Pb, i.e. $\Delta\omega(V_0)/\omega_{\mathrm{harm}}(0) \approx 0$. However, in Mo and W there are considerable frequency shifts $\Delta\omega(V_0)$ also when the solid is held at a fixed volume V_0 (see also fig. 8.3). In K, the shift $\Delta\omega(V_0)$ is moderate in absolute magnitude, but is not much smaller than Δ_2. A closely related consequence is that the vibrational part of the heat capacity C_V at high T is not approximately given by the classical value $3k_{\mathrm{B}}$ per atom. This fact is worth noting, since it is often assumed that C_V is close to $3k_{\mathrm{B}}$ per atom at high T. Consider, for instance, the three compounds Al_2O_3, MgO and Mg_2SiO_4. These solids are insulators, and therefore C_V has a contribution from lattice vibrations only. C_V of Al_2O_3 and MgO approach the Dulong–Petit limit but C_V of Mg_2SiO_4 steadily increases above this value as T increases. Wallace (1997) got results similar to those of table 8.1 in an analysis of 25 elements.

Example: temperature dependence of frequency shifts in an Einstein model. The summations in eqs. (8.24) and (8.25) cannot be carried out in a closed form, and one is left with a numerical calculation. However, a simple expression results if we replace ω_2 and ω_3 in the Bose–Einstein factors by the same frequency, ω_{E}. If we also take an Einstein represen-

tation of the strain ε_α (cf. eq. (14.17)), including that due to zero-point vibrations, we get

$$\Delta_2(\mathbf{q}, s) = k_2(\mathbf{q}, s)\omega_0(\mathbf{q}, s) \left(\frac{1}{\exp(\hbar\omega_E/k_B T) - 1} + \frac{1}{2} \right), \quad (8.27)$$

with the same expressions for Δ_3 and Δ_4 if $k_2(\mathbf{q}, s)$ in eq. (8.27) is replaced by other functions, $k_3(\mathbf{q}, s)$ and $k_4(\mathbf{q}, s)$, respectively. Although the temperature dependence of Δ_2, Δ_3 and Δ_4 is the same as in an Einstein model for the thermal energy, our description is not that of an ordinary Einstein model since the (dimensionless) quantities $k_i(\mathbf{q}, s)$ $(i = 1, 2, 3)$ may vary with the mode $(\mathbf{q}, s)$.

5.   Thermodynamic functions in anharmonic systems

5.1.   Introduction

In Chapter 7 we derived expressions for the energy $E_{har}(\mathbf{q}, s)$, the entropy $S_{har}(\mathbf{q}, s)$, the Helmholtz energy $F_{har}(\mathbf{q}, s)$ and the heat capacity $C_{har}(\mathbf{q}, s)$ of strictly harmonic systems. In this chapter we have introduced approximate phonon frequencies $\omega_0(\mathbf{q}, s) + \Delta_2(\mathbf{q}, s) + \Delta_3(\mathbf{q}, s) + \Delta_4(\mathbf{q}, s)$ in anharmonic systems. A central question is whether E, S, F and C can be obtained for the anharmonic case simply by replacing ω_0 by $\omega_0(\mathbf{q}, s) + \Delta_2(\mathbf{q}, s) + \Delta_3(\mathbf{q}, s) + \Delta_4(\mathbf{q}, s)$ in the usual expressions for E etc. of harmonic vibrations. One can show (Barron 1965) that the entropy is correctly given in this way, but not the energy, the Helmholtz energy and the heat capacity.

5.2.   The quasiharmonic model

We write

$$\omega(\mathbf{q}, s) = \omega_0(\mathbf{q}, s) + \Delta_2(\mathbf{q}, s; V(T)) \tag{8.28}$$

to indicate that Δ_2 varies implicitly with the temperature through the thermal expansion (or contraction) of the solid. The entropy is, (eq. (7.20)),

$$S(\mathbf{q}, s) = k_B\{(x/2)\coth(x/2) - \ln[2\sinh(x/2)]\}, \tag{8.29}$$

where $x = \hbar\omega(\mathbf{q}, s)/k_B T$. This yields (suppressing the label $(\mathbf{q}, s)$ on S)

$$
\begin{aligned}
\left(\frac{\partial S}{\partial V}\right)_T &= \left(\frac{\partial S}{\partial x}\right)_V \left(\frac{\partial x}{\partial V}\right)_T = \left(\frac{\partial S}{\partial T}\right)_V \left(\frac{\partial T}{\partial x}\right)_V \left(\frac{\partial x}{\partial V}\right)_T \\
&= -\left(\frac{C_V}{\omega}\right)\left(\frac{\partial\omega}{\partial V}\right)_T = -\left(\frac{C_V}{V}\right)\left(\frac{\partial \ln(\omega_0 + \Delta_2)}{\partial \ln V}\right)_T \\
&= \frac{C_V}{V}\gamma(\mathbf{q}, s; V).
\end{aligned}
\tag{8.30}
$$

Thus,

$$
\gamma(\mathbf{q}, s; V) = \left(\frac{V}{C_V}\right)\left(\frac{\partial S}{\partial V}\right)_T.
\tag{8.31}
$$

We can generalise eq. (8.31) to arbitrary deformations of the crystallographic unit cell and write, for strains ε_i ($i = 1$ to 6)

$$
\gamma(\mathbf{q}, s; \varepsilon_i) = \frac{1}{C_\varepsilon}\left(\frac{\partial S}{\partial \varepsilon_i}\right)_{T,\varepsilon_i'},
\tag{8.32}
$$

where C_ε is the heat capacity taken at constant strain. The heat capacity at constant pressure, C_p, is

$$
\begin{aligned}
C_p &= T\left(\frac{\mathrm{d}S}{\mathrm{d}T}\right)_p = T\left(\frac{\partial S}{\partial T}\right)_V + T\left(\frac{\partial S}{\partial V}\right)_T\left(\frac{\partial V}{\partial T}\right)_p \\
&= C_V + T\left(\frac{C_V}{V}\right)\gamma(V)\left(\frac{\partial V}{\partial T}\right)_p,
\end{aligned}
\tag{8.33}
$$

that is

$$
C_p(\mathbf{q}, s) = C_V(\mathbf{q}, s)[1 + \beta T\gamma(\mathbf{q}, s; V)],
\tag{8.34}
$$

where β is the cubic expansion coefficient.

5.3. Third- and fourth-order anharmonicity

Let ΔF_3 and ΔF_4 be the perturbation corrections due to explicit anharmonicity in the Helmholtz energy F, i.e. terms analogous to the frequency shifts Δ_3 and Δ_4. The general form of ΔF_3 and ΔF_4, at

arbitrary temperatures, is given in Appendix E (cf. the work by Ludwig 1958, Maradudin et al. 1961, Cowley 1963, 1968 and Barron and Klein 1974). With the notation from §4 one has the high temperature forms

$$\Delta F_3 = -24(k_B T/\hbar)^2 (1/\hbar)$$

$$\times \sum_{\mathbf{q}s, \mathbf{q}_1 s_1, \mathbf{q}_2 s_2} \frac{|V(\mathbf{q}s, \mathbf{q}_1 s_1, \mathbf{q}_2 s_2)|^2}{\omega(\mathbf{q}, s)\omega(\mathbf{q}_1, s_1)\omega(\mathbf{q}_2, s_2)}, \tag{8.35}$$

$$\Delta F_4 = 12(k_B T/\hbar)^2 \sum_{\mathbf{q}s, \mathbf{q}_1 s_1} \frac{V(\mathbf{q}s, -\mathbf{q}s, \mathbf{q}_1 s_1, -\mathbf{q}_1 s_1)}{\omega(\mathbf{q}, s)\omega(\mathbf{q}_1, s_1)}. \tag{8.36}$$

The next-order contributions to F, which are proportional to T^3 at high temperatures, have been written down by Shukla and Cowley (1971) and evaluated numerically for simple models by Shukla and Wilk (1974). They are too complicated to calculate in a realistic treatment of real solids.

6. Thermodynamic functions related to frequency shifts

We may express ΔF and ΔS in the frequency shifts Δ_2, Δ_3 and Δ_4 as (Barron 1965, Cowley and Cowley 1966, Wallace 1972)

$$\Delta F = (\hbar/2) \sum_{\mathbf{q}s} [n(\mathbf{q}, s) + 1/2][2\Delta_2(\mathbf{q}, s) + \Delta_3(\mathbf{q}, s) + \Delta_4(\mathbf{q}, s)],$$
$$\tag{8.37}$$

$$\Delta S = -\hbar \sum_{\mathbf{q}s} \left(\frac{\partial n(\mathbf{q}, s)}{\partial T} \right) [\Delta_2(\mathbf{q}, s) + \Delta_3(\mathbf{q}, s) + \Delta_4(\mathbf{q}, s)].$$
$$\tag{8.38}$$

Equation (8.38) has the very important interpretation that the entropy S is correctly obtained, within the low-order perturbation theory considered here, if one takes the harmonic-model expression for S and replaces all frequencies $\omega_0(\mathbf{q}, s)$ by the shifted frequencies $\omega_0(\mathbf{q}, s) + \Delta_2(\mathbf{q}, s) + \Delta_3(\mathbf{q}, s) + \Delta_4(\mathbf{q}, s)$ (see Appendix E). Within low-order quantum-mechanical perturbation theory, these shifted frequencies are also those measured in a neutron inelastic scattering experiment (see, e.g. Maradudin and Fein 1962 and Cowley 1968). Such experiments

are often analysed to give phonon dispersion curves, and the related phonon density of states $F(\omega)$ through a fit of force constants in order to generate $\omega(\mathbf{q}, s)$ for all modes $(\mathbf{q}, s)$. When the frequencies $\omega(\mathbf{q}, s)$ are measured at different temperatures, one also obtains a temperature dependent $F(\omega)$ which can be used to evaluate the vibrational entropy $S_{vib}(T)$, with anharmonic effects included. As we shall see in the examples below, the high temperature frequency shifts vary more rapidly than linearly with T. Obviously anharmonic effects beyond the low-order perturbation contributions Δ_3 and Δ_4 may become significant well below the melting temperature. It is not known to what extent one may then use the frequencies obtained in neutron scattering experiments to calculate the vibrational entropy, but assuming such a connection to be valid seems to give a useful description. Finally, we stress again that its is only for the entropy that one can account for the anharmonicity by inserting the anharmonically shifted frequencies in the mathematical expressions derived for a harmonic model (cf. eqs. (8.37) and (8.38)).

The heat capacity is obtained from $T (dS/dT)$. This yields

$$
\begin{aligned}
\Delta C_p = -\hbar T \sum_{\mathbf{q}s} &\{[\partial^2 n(\mathbf{q}, s)/\partial T^2] \\
&\times [\Delta_2(\mathbf{q}, s) + \Delta_3(\mathbf{q}, s) + \Delta_4(\mathbf{q}, s)] + [\partial n(\mathbf{q}, s)/\partial T] \\
&\times [d\Delta_2(\mathbf{q}, s)/dT + d\Delta_3(\mathbf{q}, s)/dT \\
&+ d\Delta_4(\mathbf{q}, s)/dT]\}.
\end{aligned}
\tag{8.39}
$$

At constant volume,

$$
\Delta C_V = \Delta C_p + \hbar T \sum_{\mathbf{q}s} [\partial n(\mathbf{q}, s)/\partial T][\partial \Delta_2(\mathbf{q}, s)/\partial V][dV/dT].
$$

$$
\tag{8.40}
$$

This is equivalent (Appendix E) to the well-known relation (neglecting the volume dependence of Δ_3 and Δ_4)

$$
\begin{aligned}
C_p - C_V &= (C_{p,har} + \Delta C_p) - (C_{V,har} + \Delta C_V) \\
&= \Delta C_p - \Delta C_V = \beta \gamma_G C_V T.
\end{aligned}
\tag{8.41}
$$

Example: frequency shifts in tungsten at fixed volume. The total entropy S_{tot} obtained from heat capacity data at constant pressure can be reduced to a fixed volume V_0, using the formalism in Chapter 13 (§7).

Subtraction of an electronic term S_{el} yields the vibrational contribution $S_{\text{vib}} = S_{\text{tot}} - S_{\text{el}}$, from which the entropy Debye temperature $\theta_{\text{D}}^S(T)$ can be calculated. At fixed volume $\theta_{\text{D}}^S(T)$ contains only the shift $\Delta_3 + \Delta_4$ while $\theta_{\text{D}}^S(T)$ at constant pressure contains the shift $\Delta_2 + \Delta_3 + \Delta_4$. Figure 8.3 shows the result for tungsten; from Fernández Guillermet and Grimvall (1991a).

7. Factors influencing the Grüneisen parameter

Point defects, dislocations, grain boundaries etc. have only a small effect on the Debye temperature (Chapters 6 and 9). It is then not surprising that also the Grüneisen parameters are rather insensitive to such defects. More specifically, consider the thermodynamic Grüneisen parameter

$$\gamma_{\text{G}} = \beta V K_T / C_V, \tag{8.42}$$

where β is the thermal expansion coefficient, V the specimen volume, K_T the isothermal bulk modulus and C_V the heat capacity at constant volume. None of the quantities on the righthand side of eq. (8.42) depends strongly on lattice defects. In concentrated alloys, one expects that γ_{G}, like θ_{D}, varies smoothly with the composition (cf. Chapter 9, §4). This has also been found in experiments on solid solutions of Zr, Nb and Mo at 300 K (Smith and Finlayson 1976), where γ_{G} lies in the range 1.5 ± 0.5. Nagel et al. (1984) noted that although the Grüneisen parameter in glassy materials is affected by phonon localisation, so few modes are localised that the overall Grüneisen parameter is within 10% of its value in the crystalline material.

Concerning the volume (i.e. pressure) dependence of the Grüneisen parameters, Moriarty et al. (1984) found, in theoretical calculations for Al, that γ_{G} decreases smoothly from about 2.0 to about 1.0 when the material is compressed to half its original volume. Analysis of C_p data gave $(\text{d} \ln \gamma / \text{d} \ln V) = 3.2 \pm 0.8$ for Ge (Leadbetter and Settatree 1969), 2.1 ± 0.3 for Pb (Leadbetter 1968), 1.4 ± 0.5 for KCl, 1.1 ± 0.4 for NaCl and 0.9 ± 0.6 for KBr (Leadbetter et al. 1969). For NaCl, see also Boehler et al. (1977). In Chapter 4 (§7) we showed that the third-order elastic constants are related to the elastic-limit Grüneisen parameter. The fourth-order coefficients c_{ijkl} are related to the volume dependence of γ.

ATOMIC VIBRATIONS IN DEFECT LATTICES

1. Introduction

We have seen in previous chapters that many thermophysical proper-
ties depend on some average of the vibrational density of states $F(\omega)$.
Such properties are usually insensitive to the presence of lattice de-
fects like impurities, vacancies, dislocations, grain boundaries etc. At
very low temperature, however, only modes of low energies are excited.
Then, low-frequency defect modes may give a significant contribution
to the thermophysical properties of the sample. At room temperature
and above, one does not expect that a low concentration of imperfections
in the lattice causes any spectacular features in static properties like the
heat capacity and thermal expansion. But of course even a low concen-
tration of defects may have a profound effect on transport properties like
electrical and thermal conduction and diffusion. In concentrated alloys
and mixed crystals, some vibration modes may be very different from
those of the host material, but properties which depend on an average of
$F(\omega)$ are still expected to vary smoothly with the composition.

2. General aspects

It is convenient to introduce a density of states $\Delta F_{\text{def}}(\omega)$ which de-
scribes the changes in the atomic vibrations when a defect is created
in a lattice. Consider a solid with N lattice sites, of which N_{def} are
associated with the creation of a defect. For instance, if the defect is
a vacancy, $N_{\text{def}}/(N + N_{\text{def}}) \approx N_{\text{def}}/N$ is the vacancy concentration. In
the case of a surface, N_{def} may be loosely identified with the number of
surface atoms, but see the discussion below. We now write

$$F_{\text{tot}}(\omega) = F_{\text{bulk}}(\omega) + (N_{\text{def}}/N)\Delta F_{\text{def}}(\omega), \tag{9.1}$$

where $F_{tot}(\omega)$ is the total density of states of the actual specimen and $F_{bulk}(\omega)$ is its density of states in the absence of the defect under consideration, in both cases as an average per atom. The normalisation relations are $\int F_{tot}(\omega)\,d\omega = 3 = \int F_{bulk}(\omega)\,d\omega$. Then

$$\int_0^{\omega_{max}} \Delta F_{def}(\omega)\,d\omega = 0, \qquad (9.2)$$

i.e. $\Delta F_{def}(\omega)$ varies in sign.

From $\Delta F_{def}(\omega)$ we can calculate, for example, the change in the vibrational heat capacity;

$$\Delta C_{har,def}(T) = \int_0^{\omega_{max}} C_{har}(\hbar\omega/k_B T)\Delta F_{def}(\omega)\,d\omega, \qquad (9.3)$$

where ω_{max} is the maximum frequency in the presence of lattice defects. It may be larger than ω_{max} of the defect-free solid. C_{har} is the heat capacity of a single harmonic oscillator. The high-temperature limit $(k_B T \gg \hbar\omega_{max})$ of (9.3) is

$$\Delta C_{har,def}(T) = k_B \int_0^{\omega_{max}} \Delta F_{def}(\omega)\,d\omega = 0. \qquad (9.4)$$

This relation simply reflects the fact that the vibrational heat capacity at high temperatures has the classical value of $3k_B$ per atom, for a perfect crystalline atomic arrangement as well as for a structure with defects. Note that there may also be an additional heat capacity associated with the *formation* of the defect, such as the two-level description of vacancies, eq. (11.7).

Except for point defects, the number N_{def} in eq. (9.1) is usually not exactly defined, but there is a strict operational definition of, e.g. the surface contribution to the thermodynamic functions as (half) the difference between the properties of two well separated blocks of a material, and the same blocks joined with perfect atomic matching. Even though N_{def} may be poorly defined, it gives a measure of the size, or amount, of defect regions, e.g. the area of an interface, and can be used to estimate how vibrations at defects affect thermodynamic quantities.

Example: surface states in TiN. Rieder and Drexel (1975) found, from neutron scattering experiments, that $\Delta F_{def}(\omega)$ due to surface effects in
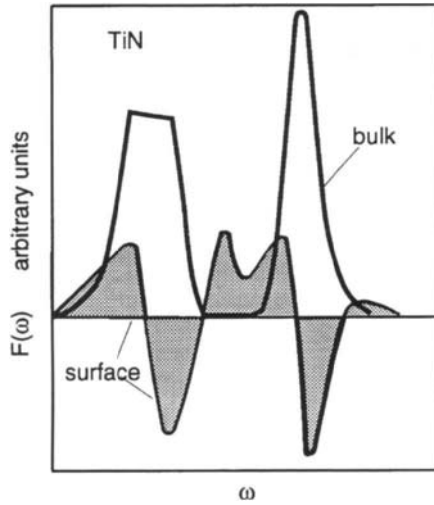
Fig. 9.1. The defect-related vibrational density of states $F_{\mathrm{def}}(\omega)$ for surface states in TiN, expressed as the change in the bulk density of states caused by the surface states (shaded regions), compared with $F(\omega)$ in the bulk. Arbitrary units and arbitrary scale factors for $F(\omega)$ and $F_{\mathrm{def}}(\omega)$. After Rieder and Drexel (1975).

TiN has three positive and two negative regions when plotted versus ω. Their result is schematically shown in fig. 9.1. A similar result for $\Delta F_{\mathrm{def}}(\omega)$ has been obtained by Loram et al. (1993) in an analysis of heat capacity data for the high temperature superconductor $YBa_2Cu_3O_{6+x}$ for varying x.

3. Surfaces

3.1. Elastic waves in a semi-infinite elastic continuum

In an ordinary Debye model, the lattice vibrations are described by elastic waves propagating in an infinite medium. In a semi-infinite medium, bounded by a free surface, the classical wave equation $\partial^2 u_\beta / \partial t^2 - c_\beta^2 \nabla^2 u_\beta = 0$ has solutions u_β which are the usual bulk waves, but also solutions with an amplitude localised to the surface region. The latter modes, known as *Rayleigh waves* (Rayleigh 1900), propagate with their wave vector $\mathbf{q}$ in the surface plane. Their frequency is

$$\omega = C_{\mathrm{T}}|\mathbf{q}|\xi, \tag{9.5}$$

where C_T is the transverse sound velocity in the bulk. The dimensionless parameter ξ depends on the ratio C_T/C_L and lies between 0.874 and 0.955. For a given $\mathbf{q}$, the frequency of the Rayleigh wave is thus less than that of the transverse elastic bulk wave. (In a real solid the sound velocity is anisotropic (Gazis et al. 1960).) A brief general discussion of elastic surface waves is found in Landau and Lifshitz (1959). Maradudin (1981) has reviewed the entire field of surface waves.

3.2. Thermal properties of an elastic-continuum surface

We shall calculate the heat capacity in the low temperature limit, i.e. when only elastic waves are excited. The allowed (q_x, q_y) for wave propagation parallel to the surface give a density of states which varies linearly with ω. The number of (Rayleigh) states is proportional to the area A of the surface. Their density of states is

$$F_R(\omega) = Ak_1\omega. \tag{9.6}$$

We note that the frequencies of both the bulk and the surface states are linear in the wave number q (for small q). The fact that $F_R(\omega)$ is linear in ω, while the bulk $F(\omega)$ varies as ω^2, reflects the difference in possible $\mathbf{q}$-vectors sampled in a two- and three-dimensional system. The low frequency part of the density of states, for the states *not* localised to the surface, is of the bulk form plus a correction $Ak_2\omega^2$. Hence, approximately,

$$F_{tot}(\omega) = (1 - Ak_3)F_{bulk}(\omega) + Ak_4\omega. \tag{9.7}$$

This is the "Debye model" in the presence of a surface. For mathematical details, see Wallis (1975), Stratton (1953, 1962), Dupuis et al. (1960), Maradudin et al. (1963) and Maradudin and Wallis (1966). From eq. (9.7) we obtain the low temperature heat capacity

$$C_{tot}(T) = (1 - Ak_3)C_{bulk}(T) + Ak_5T^2, \tag{9.8}$$

where $C_{bulk} \sim T^3$. The parameters $k_1, \ldots, k_5$ depend on the elastic parameters and the mass density of the material. The T^2-term in eq. (9.8) can be observed only at low temperatures and if the surface-to-volume ratio is large enough, i.e. for very small particles. But then the finite size of the particle is important (§3.4), which gives corrections

to our model of vibrations in an elastic continuum instead of the true discrete atomic lattice. Therefore, eq. (9.8) can only be used for very qualitative estimations.

3.3. Thin slabs

Consider a thin slab formed by N layers of atoms. This is the three-dimensional generalisation of a finite monatomic linear chain. Such a model system has been extensively studied by Allen et al. (1971). The solutions to the equation of motion are of the form

$$\mathbf{u} = \mathbf{u}(R_{j(z)}) \exp[i(\mathbf{q} \cdot \mathbf{R}_{j(xy)} - \omega t)]. \tag{9.9}$$

$R_{j(z)}$ denotes the z-component (i.e. perpendicular to the surfaces) of the position vector $\mathbf{R}_j$ of the jth atom. $\mathbf{R}_{j(xy)}$ is a position vector along the slab and $\mathbf{q} = (q_x, q_y)$ is a two-dimensional wave vector. Almost all of the modes of the form eq. (9.9) have amplitudes $\mathbf{u}(R_{j(z)})$ which are appreciable throughout the width of the slab. However, a mode corresponding to a Rayleigh wave has a displacement $\mathbf{u}(R_{j(z)})$ which decreases rapidly as $\mathbf{R}_j$ moves inward from either surface. Allen et al. (1971) also discovered new surface modes which do not exist in the limit of small $\mathbf{q}$ and thus have no elastic-wave counterpart. Similar results have been obtained in a study of the TiN(001) surface (Benedek et al. 1984).

3.4. Small particles

The bulk material has a phonon density of states which is quasicontinuous and varies as ω^2 for small ω. In a very small sample, on the other hand, the eigenfrequencies form a discrete spectrum. In particular, there is a lowest eigenfrequency ω_{min} which can be estimated crudely as follows. In the bulk, $\omega = Cq$, where C is a sound velocity. In a small particle, of diameter d, it is unphysical to consider wavelengths larger than d, i.e. $q > 2\pi/d$. With $\omega_D = Cq_D \sim 2\pi C/d_0$, where d_0 is the diameter of an atom, we get $\omega_{min} \sim (d_0/d)\omega_D$. The discrete nature of the low frequency part of the vibrational spectrum means that we must write out explicitly the first terms in the partition function when $T \lesssim (d_0/d)\theta_D$, instead of applying the usual integral approximation. This has been recognised by Burton (1970), Chen et al. (1971) and Baltes and Hilf (1973). Nishiguchi and Sakuma (1981) made an

accurate study of the vibrations of a small elastic sphere. The excess heat capacity (above the bulk value) has been measured for ionic solids (NaCl; Barkman et al. (1965)) and metals (Pb, In; Novotny and Meincke (1973)). The theory referred to above is in reasonable agreement with the experiments. Dobrzynski and Leman (1969) developed a frequency-moment representation of the surface phonons, and calculated their contribution to the heat capacity.

4. Point imperfections

4.1. The mass-defect model

The mass defect is the simplest point imperfection in a vibrating lattice. One then assumes that the mass of a particular atom in the perfect lattice is altered from M to M', without any change of the force constants. That is the case if an atom is replaced by one of its isotopes, and one therefore also speaks of an *isotope defect*. The important parameter characterising the impurity is the relative mass difference ε;

$$\varepsilon = \frac{M - M'}{M}. \tag{9.10}$$

In the case of a light impurity $(M' < M; \varepsilon > 0)$, there may be a *localised mode*, with a frequency $\omega_{\text{imp}} > \omega_{\text{max}}$, i.e. above the highest frequency of the host lattice. When the impurity is much heavier than the host atoms $(M' \gg M; \varepsilon < 0)$ there is a pronounced resonance at a frequency ω_i which is "embedded" in the quasicontinuous spectrum of the host lattice.

Starting from a general expression for ω_i (Kagan and Iosilevskii 1962, 1963, Lifshitz 1956, Brout and Visscher 1962, Dawber and Elliott 1963, Mannheim 1968, Dederichs and Zeller 1980), we restrict the discussion to the case of cubic symmetry and one atom per primitive cell. The impurity-mode frequencies ω_i are threefold degenerate (equivalent x, y and z directions) and obtained from

$$\varepsilon \omega_i^2 \int_0^{\omega_{\text{max}}} \frac{F(\omega)\, d\omega}{\omega_i^2 - \omega^2} = 3, \tag{9.11}$$

where $F(\omega)$ and ω_{max} refer to the unperturbed vibrations of the host.

For a light impurity, $\omega_i > \omega_{\text{max}}$. We then expand the integrand in eq. (9.11) in powers of ω/ω_i and consider $\varepsilon \approx 1$ (i.e. $M' \ll M$). Keeping only the first two terms in the expansion gives

$$\omega_i \approx (1 - \varepsilon)^{-1/2}\omega(2) = (M/M')^{1/2}\omega(2), \tag{9.12}$$

where $\omega(2)$ is the unperturbed second-moment frequency (eq. (6.21)).

When the impurity is very heavy ($|\varepsilon| \gg 1; \varepsilon < 0$) there is a resonance mode $\omega = \omega_i$, where ω_i has a small imaginary part. A Debye model for the host lattice, $F(\omega) = 9\omega^2/\omega_{\text{D}}^3$, in eq. (9.11) gives, to lowest order in the limit that $\omega_{\text{D}} \gg \omega_i$,

$$\omega_i^2 = \frac{\omega_{\text{D}}^2}{3|\varepsilon|}[1 - i(\omega_i/\omega_{\text{D}})(\pi/2)]. \tag{9.13}$$

We now see explicitly that the heavy impurity gives rise to a frequency with an imaginary part, i.e. a damped mode. When $\omega_i/\omega_{\text{D}} \ll 1$ we can neglect the imaginary term in eq. (9.13) and treat the resonance as if it were a true eigenstate with a frequency $[3|\varepsilon|]^{-1/2}\omega_{\text{D}}$.

4.2. Thermal displacement in the mass-defect model

The theory for the thermal displacement, $\langle \mathbf{u}_{\text{def}}^2 \rangle$, of impurity atoms is complicated, but in an approximate theory one just scales the displacement of the replaced host atom;

$$\langle \mathbf{u}_{\text{def}}^2 \rangle / \langle \mathbf{u}_{\text{host}}^2 \rangle = (M/M')^{1/2}, \quad T \ll \theta_{\text{D}}; \tag{9.14}$$

$$\langle \mathbf{u}_{\text{def}}^2 \rangle / \langle \mathbf{u}_{\text{host}}^2 \rangle = 1, \quad T \gg \theta_{\text{D}}. \tag{9.15}$$

Equations (9.14) and (9.15) may be compared with the result in Chapter 7 (§5.2), that $\langle \mathbf{u}^2 \rangle$ in the high temperature limit does not depend on the atomic mass M, and varies as $M^{-1/2}$ at 0 K. Calculations by Dawber and Elliott (1963), using a Debye model for the host lattice, showed eq. (9.15) to be exact and eq. (9.14) to be correct to within about 5%. These authors also give an expression for the velocity of the defect as $\langle \mathbf{v}_{\text{def}}^2 \rangle$. Both $\langle \mathbf{u}_{\text{def}}^2 \rangle$ and $\langle \mathbf{v}_{\text{def}}^2 \rangle$ can be measured in Mössbauer experiments.

4.3. Debye temperature in the mass-defect model

Consider a crystal with a low concentration, c, of impurities. When their vibrations are described by the mass-defect model, i.e. with all force constants unchanged, the Debye temperatures $\theta_D(n; c)$ are related to $\theta_D(n)$ of the pure host lattice as

$$\theta_D(-3; c) = \theta_D(-3)[1 - c\varepsilon]^{-1/2} \approx \theta_D(-3)[1 + c\varepsilon/2], \qquad (9.16)$$

$$\theta_D(0; c) = \theta_D(0)[1 - \varepsilon]^{-c/2} \approx \theta_D(0)[1 + c\varepsilon/2], \qquad (9.17)$$

$$\theta_D(2; c) = \theta_D(2)[1 + (c\varepsilon)/(1 - \varepsilon)]^{1/2} \approx \theta_D(2)[1 + c\varepsilon/2]. \quad (9.18)$$

These relations easily follow from the fact that $\theta_D(n; c) \sim [M_{eff}(n)]^{-1/2}$, where $M_{eff}(-3)$ varies as the mass density of the specimen (cf. eq. (6.16)), $M_{eff}(0)$ is the logarithmic average of the atomic masses (cf. eq. (6.30)), and $M_{eff}(2)$ follows from $\Sigma\omega^2 = \mathrm{Tr}\,\mathbf{D}$ (Appendix C) as $1/M_{eff}(2) = (1 - c)/M + c/M'$.

4.4. Force constant changes

The equation (9.11) for the localised or resonance-mode frequencies ω_i can be generalised to include force constant changes at the impurity (Kagan and Iosilevskii 1962, Mannheim 1968). Work by Tiwari and Agrawal (1973a, b, c) and Tiwari et al. (1981) exemplify theoretical calculations of resonance states, with allowance for both mass and force constant changes.

   Let the force constants associated with an impurity atom be changed by a relative amount $\Delta f/f$ (cf. Chapter 4, §10). The elastic-limit Debye temperature $\omega_D(-3)$ depends predominantly on the shear modulus, as $\omega_D(-3) \sim G^{1/2}$ (cf. Chapter 6, §4). The relations in Chaper 4 (§10) for the elastic shear moduli $c_{11} - c_{12}$ and c_{44} now give, approximately,

$$\theta_D(-3; c) \approx \theta_D(-3)\left[1 + \frac{2c(\Delta f/f)}{1 + \Delta f/(3f)}\right]^{1/2}$$
$$\approx \theta_D(-3)[1 + c(\Delta f/f)]. \qquad (9.19)$$

Then it has been implicitly assumed that the lattice coordinates are unaltered. However, there are two kinds of relaxations in the atomic positions; an overall change of the volume of the specimen and a "local"

change in the vicinity of an impurity atom. We write the first type of volume change ΔV as $\Delta V / V = c \Delta \Omega_a / \Omega_a$, where $\Delta \Omega_a$ is the defect formation volume. With a Grüneisen parameter approach we get, as a crude estimate for the effect of the overall volume change,

$$\theta_{\text{dilated}} = \theta_{\text{undilated}}[1 - c\gamma_G(\Delta \Omega_a / \Omega_a)]. \tag{9.20}$$

With the realistic values $\gamma_G = 1.5$ and $\Delta \Omega_a / \Omega_a = 0.2$, we see that this type of relaxation effect may be significant (cf. Tiwari et al. 1981, on Cu–Sn).

4.5. *Heat capacity*

We now turn to the relative change, $\Delta C_{\text{har}} / C_{\text{har}}$, in the vibrational heat capacity associated with a low concentration of impurity atoms. Consider first *heavy* impurities. Very roughly, one obtains a contribution from the $3Nc$ localised or resonance modes, superimposed on a change in the heat capacity of the $3N(1 - c)$ extended modes. Heavy impurities lead to a $\Delta C_{\text{har}} / C_{\text{har}}$ that is peaked at low temperatures (below $T = [3|\varepsilon|]^{-1/2}\theta_D$, cf. eqs. (9.13) and (9.3)). This effect has been observed, e.g. for Pb in Mg (Panova and Samoïlov 1965, Cape et al. 1966). To achieve a quantitative account of such measurements one must go beyond our simple idea of a sharp resonance mode (e.g. Tiwari and Agrawal 1973a, b, c).

The effect ΔC_{har} of a *light* impurity will be difficult to see directly in heat capacity measurements since the heat capacity of the host has already reached its (large) classical value at the temperatures when the localised modes of the impurity start to be significantly excited.

Although it is very difficult to obtain a precise expression for ΔC_{har}, there is an integral relation which links ΔC_{har} to the excess entropy ΔS_{har}. By using (7.24) we can write for the high temperature limit $S_{\text{har}}(\infty)$:

$$\begin{aligned}
\Delta S_{\text{har}}(\infty) &= \int_0^\infty \frac{\Delta C_{\text{har}}(T)}{T} dT \\
&= 3N k_B \ln[\theta_D(0)/\theta_D(0; c)],
\end{aligned} \tag{9.21}$$

where $\theta_D(0)$ refers to the logarithmically averaged phonon frequencies of the host material.

5.   Concentrated alloys and mixed crystals

In this section we go beyond the dilute limit of impurities or defects that was considered above, and discuss (one-phase) concentrated alloys and mixed crystals (e.g. $Na_cK_{1-c}Cl$). The lattice vibrations are assumed to be harmonic, but since there is no translational invariance, the eigenstates are no longer plane waves, and the eigenfrequencies cannot be mapped as sharp dispersion curves $\omega(\mathbf{q}, s)$. Even if the dispersion curves are strongly modified, or give a completely inadequate description, there is still a well-defined density of states $F(\omega)$. In the long-wavelength limit, $\omega(\mathbf{q}, s) = C_{\text{sound}}(\mathbf{q}, s)|\mathbf{q}|$, implying that $F(\omega) \sim \omega^2$ for small ω. A strict Debye model, which assumes that the elastic limit is extrapolated to the frequency ω_D, may be an equally good approximation in a pure element as in a concentrated alloy or a mixed crystal. In, say, a substitutional alloy with a bcc or fcc lattice, $F(\omega)$ usually retains the general shape with two humps, corresponding to longitudinal and transverse modes. However, the sharp structures in $F(\omega)$ characteristic of a perfect periodic lattice are smoothed out.

Consider a compound or a solid solution with the composition A_cB_{1-c}. Here $0 < c < 1$, but it is not required that c or $1 - c$ is small. The masses of the constituents are M_A and M_B. Then the first equalities in eqs. (9.16)–(9.18) hold exactly, within the mass-defect model (i.e. without allowance for changes in the interatomic forces). Thus,

$$\theta_D(-3; c) = \theta_D^A(-3)[(1 - c) + cM_B/M_A]^{-1/2}, \tag{9.22}$$

$$\theta_D(0; c) = \theta_D^A(0)[M_A/M_B]^{c/2}, \tag{9.23}$$

$$\theta_D(2; c) = \theta_D^A(2)[(1 - c) + cM_A/M_B]^{1/2}. \tag{9.24}$$

These relations can also be written as *interpolation formulae* between the Debye temperatures θ_D^A and θ_D^B of the pure components:

$$[\theta_D(-3; c)]^{-2} = (1 - c)[\theta_D^A(-3)]^{-2} + c[\theta_D^B(-3)]^{-2}, \tag{9.25}$$

$$\theta_D(0; c) = [\theta_D^A(0)]^{(1-c)}[\theta_D^B(0)]^c, \tag{9.26}$$

$$[\theta_D(2; c)]^2 = (1 - c)[\theta_D^A(2)]^2 + c[\theta_D^B(2)]^2. \tag{9.27}$$

Within the mass-defect model (i.e. without force constant changes), the interpolation formulae are excact. They are also exact if the masses M_A
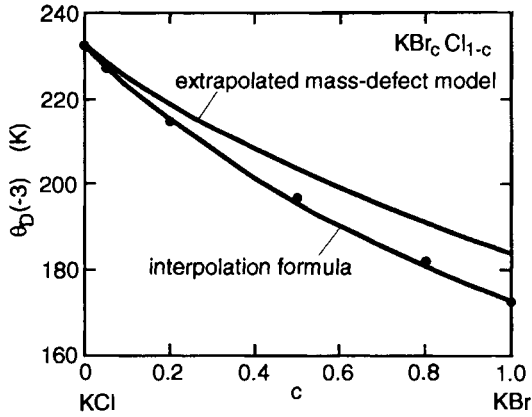
Fig. 9.2. The measured Debye temperature $\theta_D(-3) = \theta_D^C(T = 0\,K)$ in KBr_cCl_{1-c} (symbols), the interpolation formula (9.25) and an extrapolation from $\theta_D(-3)$ of pure KCl using the mass-defect model only (eq. (9.22)).

and M_B are equal but the properly averaged interatomic force constants vary as $1/f(c) = c/f_B + (1-c)/f_B$ in eq. (9.25), as $f(c) = [f_B]^c[f_A]^{1-c}$ in eq. (9.26) and as $f(c) = cf_B + (1-c)f_A$ in eq. (9.27). Thus, eqs. (9.25)–(9.27) go beyond the mass-defect model and may give a good account of the concentration dependence of the Debye temperatures in many real systems, but there are also exceptions (cf. the two examples below).

Example: interpolation formulae in KBr_cCl_{1-c}. Figure 9.2 shows the interpolation formula (9.25) for KBr_cCl_{1-c}, fitted at the two ends of pure compounds, and compared with experimental $\theta_D(-3)$ from low temperature heat capacity experiments by Karlsson (1970). Also shown is $\theta_D(-3)$ as extrapolated from pure KCl, using only the mass-defect model (eq. (9.22)). It is seen that the extended mass-defect model (the interpolation formula) gives a good description. This is expected because the bonding (ionic in character) is not very different in KCl and KBr. This should be contrasted with the following example of Nb–Mo alloys.

Example: the Debye temperature $\theta_D(-3)$ in Nb–Mo alloys. Niobium and molybdenum form a solid solution with bcc lattice structure over the entire composition range of Nb_cMo_{1-c} alloys. The atomic masses
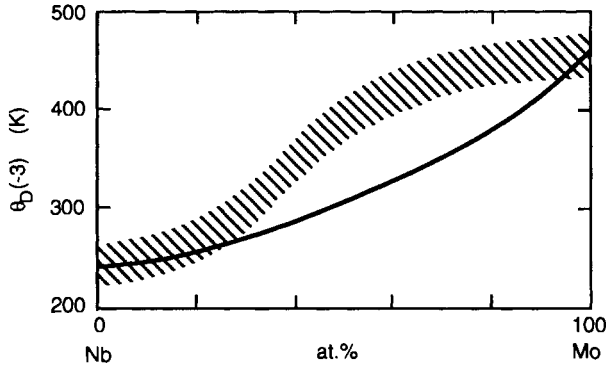
Fig. 9.3. The measured Debye temperature $\theta_D(-3)$ in the alloy Nb–Mo. Data points, from White et al. (1978), lie scattered in the shaded region. The lower solid curve is the interpolation formula (9.25).

of Nb and Mo differ by only 3%, and thus have almost negligible effect on the concentration dependence of the phonon frequencies. In spite of the fact that Nb and Mo are located next to each other in the Periodic Table, there are large variations in the interatomic forces. Figure 9.3 shows experimental results for $\theta_D(-3)$, from White et al. (1978). The data are scattered in the shaded band. The interpolation formula (9.25), given as a solid curve, fails to give a good account of the variation in $\theta_D(-3)$.

6. Vacancies

The atoms surrounding a vacant site are more loosely bound than those in the bulk and therefore give an increased vibrational entropy. At high temperatures, we have

$$S_{vac} = k_B \int_0^{\omega_{max}} \ln(k_B T / \hbar \omega) \Delta F_{vac}(\omega) \, d\omega$$

$$= -k_B \int_0^{\omega_{max}} \ln(\omega) \Delta F_{vac}(\omega) \, d\omega, \qquad (9.28)$$

where we have used the result that $\ln(k_B T / \hbar) \int \Delta F(\omega) \, d\omega = 0$, by eq. (9.2). The physical dimension (the unit) of ω in $\ln(\omega)$ in the last part of eq. (9.28) is of no concern since by eq. (9.2), $\ln(\omega/\omega_1) \Delta F(\omega) \, d\omega$ is independent of the choice of the frequency unit ω_1.

We crudely estimate S_{vac} as follows. If a certain vibration mode has the frequency ω_{bulk} in the perfect crystal and ω_{vac} when a vacancy has been introduced, the vibrational entropy is changed by $k_B \ln(\omega_{\text{bulk}}/\omega_{\text{vac}})$. Consider a simple cubic lattice with central nearest-neighbour interactions. The 6 atoms adjacent to the vacancy have their force constants reduced by a factor of 2, for vibrations towards the vacant site. Because vibration frequencies vary as [force constant]$^{1/2}$, we reduce the corresponding frequencies by a factor of $1/\sqrt{2}$. Then the vibrational excess entropy in the high temperature limit becomes (per vacant site)

$$S_{\text{vac}} \approx 6k_B \ln(\sqrt{2}) = 3k_B \ln 2 \sim 2k_B. \tag{9.29}$$

This is, of course, a much too simplified picture, but it gives the right order of magnitude of S_{vac}. Similar bond-cutting models have been applied to an fcc lattice (Stripp and Kirkwood 1954), a simple cubic lattice (Mahanty et al. 1960) and fcc Cu (Huntington et al. 1955). They all give $S_{\text{vac}} \approx 1.7k_B$ to $2.0k_B$ per vacant site. Experimental values of S_{vac}/k_B, compiled by Brudnoy (1976) and Wollenberger (1996) usually lie in the range 1–3, but with a large scatter between different measurements on the same element. The data given in the Landolt–Börnstein tables (Ullmaier 1991) confirm the picture of a large uncertainty in S_{vac}/k_B. See also Harding and Stoneham (1981) and Sahni and Jacobs (1982) for similar data in ionic crystals.

An accurate calculation of S_{vac} must include several features, in addition to the bond-cutting approach. First, the atoms near the vacancy will relax to new equilibrium positions which changes the effective force constants acting on them. Then there is a dilatation of the lattice even far from the vacant site. The correponding shifts can be handled using the Grüneisen model (see, for example, Mott and Gurney 1940, Vineyard and Dienes 1954, Huntington et al. 1955 and §4.4 above). The dilatation term may also be obtained (Huntington et al. 1955) from the macroscopic relations

$$(\partial S/\partial V)_T = (\partial p/\partial T)_V = K_T\beta = C_V\gamma_G/V. \tag{9.30}$$

If we take the values $C_V = 3Nk_B$, $V = N\Omega_a$, $\gamma_G = 1.5$ and $\Delta V = V_{\text{vac}} = 0.5\Omega_a$, the dilatational term gives $S_{\text{vac}} \sim 2k_B$, per vacancy.

7. Dislocations

 The dislocation core has a more open structure than the perfect lattice.
One therefore expects a softening of the atomic vibrations near the core.
Simple estimates (Friedel 1982) show that, for the core of a dislocation,
the vibrational entropy $S_{\text{disl}} \sim 0.5k_{\text{B}}$ (or less) per atom in the core. The
strain field surrounding a dislocation is of long range and has regions
of compression as well as expansion, where the Grüneisen description
should be applicable. There seems to be no estimation of the overall
effect of dislocations on the vibrational spectrum.
     Vibrations of the dislocations as such should also be considered.
When a dislocation line is pinned at its ends, it can vibrate much
like a string under tension. Granato (1958) and Ohashi and Ohashi
(1980) developed a theory for the contribution of such vibrations to
the heat capacity of a solid, and Bevk (1973) performed experiments
on copper. The corresponding heat capacity C_{disl}, which varies lin-
early with the temperature T, is exceedingly small compared to the
lattice part of the total heat capacity C_p, except at very low tem-
peratures. Theory (Granato 1958) and experiments (Bevk 1973) show
that $C_{\text{disl}}/C_p \sim 10^{-3}$ at $T/\theta_{\text{D}} \sim 10^{-2}$ in heavily cold-worked
samples (dislocation density 10^{15} m^{-2}).

8. Grain boundaries

The thermodynamics of grain boundaries is similar to that of solid-
vacuum interfaces, but much more complex. The grain boundary energy
(per area) is usually determined from the surface tension. The temper-
ature is high and in the surface tension $\gamma_{\text{grainb}} = E_{\text{grainb}} - TS_{\text{grainb}}$, the
entropy-related part TS_{grainb} may amount to $E_{\text{grainb}}/4$ or more. There is
both a configurational (static) and a dynamic (vibrational) contribution
to S_{grainb}. They may be of the same order of magnitude (Ewing 1971,
Ewing and Chalmers 1972, Hasson et al. 1972). The structure of grain
boundaries has often been studied through numerical simulations with
an assumed interatomic potential, see, e.g. Schiøtz et al. (1998). In very
fine-grained material, a substantial part of the atoms are affected by
the grain boundaries, which may lead to a large effect in the vibra-
tional entropy. For instance, in nanocrystalline Ni$_3$Fe (grain size $\sim$9
nm) the reported excess vibrational entropy is $0.18k_{\text{B}}$ per atom (Frase
et al. 1997), which corresponds to a lowering of the average vibrational
frequency by about 6%.

THERMODYNAMIC PROPERTIES OF CONDUCTION ELECTRONS

1. Introduction

Many thermophysical properties which are related to the electronic structure of metals and alloys depend on the electron density of states $N(E)$ at the Fermi level E_F. For instance, the Sommerfeld formula for the electronic heat capacity, which appears in almost all textbooks on solid state physics, reads (some authors let $N(E)$ refer to both spin directions and then the prefactor of 2 is absent)

$$C_{el} = \gamma T = \frac{2\pi^2}{3} N(E_F) k_B^2 T. \tag{10.1}$$

This expression is qualitatively correct, for simple (i.e. free-electon-like) metals as well as for transition metals and alloys. However, it neglects some important features. There should be an electron-phonon many-body enhancement factor $1 + \lambda_{el-ph}$, which typically is 1.4 but occasionally (e.g. Pb, Hg) can be as large as 2.5. That correction is temperature dependent and vanishes at high temperatures. Equation (10.1) also assumes that the electron states are probed in such a narrow energy interval around the Fermi energy that the density of states can be regarded as a constant and equal to $N(E_F)$. Near the melting temperature, this leads to an error in C_{el} by a factor of two or more, for some transition metals. It is obvious from what has just been said that an accurate account of the thermal properties of conduction electrons has to go beyond the simple textbook formula (10.1). This chapter primarily deals with such aspects.

2. Thermodynamic functions

2.1. Fermi–Dirac function and the chemical potential

The electrons in a solid can be divided into two groups; those that form
the closed electron shells of the constituent atoms (the core electrons),
and the remaining electrons of higher energy (the *valence electrons*). In
metals the valence electrons can move more or less freely through the
lattice. One usually refers to them as the *conduction electrons.*

We first consider the *Sommerfeld model* (Sommerfeld and Bethe
1933) in which the conduction electrons are assumed to form a gas
of fermions with energies E_k and a density of states $N(E)$. The
Fermi–Dirac distribution function is

$$f(E) = \frac{1}{\exp[(E - \mu)/k_B T] + 1}, \tag{10.2}$$

where $\mu = \mu(T)$ is the chemical potential. We shall frequently
encounter $\partial f/\partial E$ or $\partial f/\partial T$. Some useful expressions are

$$\begin{aligned}
-\frac{\partial f}{\partial E} &= \frac{1}{k_B T} f(E)[1 - f(E)] \\
&= \frac{1}{4 k_B T} \frac{1}{\cosh^2[(E - \mu)/2 k_B T]},
\end{aligned} \tag{10.3}$$

and

$$\frac{\partial f}{\partial T} = -k_B \left(\frac{E - \mu}{k_B T} \right) \left(\frac{\partial f}{\partial E} \right). \tag{10.4}$$

The function $-\partial f/\partial E$ is symmetrically peaked around $\mu(T)$, with an
approximate width of a few $k_B T$ (fig. 10.1).

The chemical potential $\mu(T)$ is determined by the condition that the
total number of conduction electrons, N_{el}, is conserved, i.e.

$$2 \int_{-\infty}^{\infty} N(E) f(E)\, dE = N_{el}. \tag{10.5}$$

The integration limits in eq. (10.5) mean that the integration is over all
energies for which the integrand is nonvanishing. Often one takes $E = 0$
to be the bottom of the conduction band, i.e. $N(E) = 0$ for $E < 0$. The
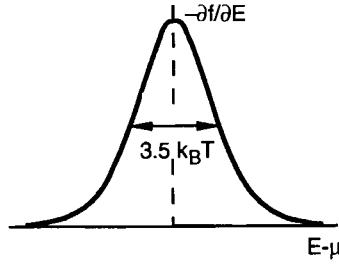
Fig. 10.1. The peaked shape of $-(\partial f/\partial E)$ around the Fermi level.

lower integration limit then is 0. The *Fermi energy* (*Fermi level*) E_F is defined to be the chemical potential at zero temperature, $E_F = \mu(0)$. Sometimes the energies are counted relative to E_F instead, i.e. $E = 0$ at the Fermi level. It even happens, in theoretical calculations, that still another reference level is chosen for the energies, e.g, the zero-level for the so-called muffin-tin potential. It is common to express E_F through the *Fermi temperature* T_F;

$$k_B T_F = E_F. \tag{10.6}$$

From what has just been said about the various conventions for the reference level of E_F, it is obvious that the Fermi temperature T_F is not a unique quantity. However, in free-electron-like systems, one almost invariably takes $E = 0$ at the bottom of the conduction electron band, and textbook values of T_F then refer to this case.

It is a standard technique (Ashcroft and Mermin 1976) to evaluate integrals such as eq. (10.5) in the form of a series expansion in powers of T. Then, to lowest order in T^2,

$$
\begin{aligned}
\mu(T) - \mu(0) &= \mu(T) - E_F = -(\pi^2/6)(k_B T)^2 \\
&\times (dN/dE)_{E=E_F}/N(E_F),
\end{aligned} \tag{10.7}
$$

where dN/dE is evaluated at $E = E_F$. Because $\partial f/\partial E$ is peaked around $\mu(T)$ with an approximate width $\sim 4k_B T$ (fig. 10.1), it is of interest to know how large is the shift $\mu(T) - \mu(0)$ expressed in units of $k_B T$. From eq. (10.7)

$$\frac{\mu(T) - \mu(0)}{k_B T} = -k_B T \frac{\pi^2}{6}\left(\frac{N'}{N}\right) \approx -\frac{T}{T_v}\mathrm{sgn}(N'). \tag{10.8}$$

Table 10.1

The Fermi temperature T_F in a free-electron description

Element	Na	Cu	Mg	Zn	Al	Pb	β-Sn
T_F [K]	37,000	81,000	83,000	109,000	135,000	109,000	116,000

The function sgn(x) is ± 1, depending on the sign of x. T_v is a characteristic temperature such that $N(E)$ varies significantly (e.g. a variation comparable to $N(E)$ itself) when E is altered by an amount $k_B T_v$. For free electrons, $T_v \sim T_F \sim 10^5$ K (table 10.1). With T lower than the melting temperature T_{fus}, the shift $\mu(T) - \mu(0)$ therefore is negligible in free-electron-like metals. In transition metals, however, $N(E)$ may vary considerably over energies $k_B T_{fus}$ around the Fermi level. Then one cannot neglect the temperature dependence of $\mu(T)$ in the calculation of high temperature properties. See also the related discussion of the heat capacity (eqs. (10.13) and (10.14)).

2.2. Heat capacity

The total conduction-electron energy is (in the single-particle description, i.e. with the neglect of explicit many-body corrections)

$$E_{el} = 2 \int_{-\infty}^{\infty} E N(E) f(E) \, dE, \tag{10.9}$$

which gives the heat capacity

$$C_{el} = \frac{\partial E_{el}}{\partial T} = 2 \int (E - E_F) N(E) \left(\frac{\partial f(E)}{\partial T} \right) dE$$

$$= 2 k_B^2 T \int \left(\frac{E - E_F}{k_B T} \right)^2 N(E) \left(-\frac{\partial f(E)}{\partial E} \right) dE. \tag{10.10}$$

In the integrand, a term $0 = \partial(2 E_F N_{el})/\partial T$ was subtracted, and a higher-order correction from the temperature dependence of $\mu(T)$ was ignored. The integration is over all energies where $N(E)$ is non-vanishing, but as we shall see below only a narrow energy interval around E_F gives a significant contribution. If $N(E)$ is slowly varying

with E near the Fermi level, $N(E) \approx N(E_F)$ can be taken outside the integral. Then

$$C_{el} = \frac{2\pi^2}{3} N(E_F) k_B^2 T. \tag{10.11}$$

It is common to write $C_{el} = \gamma T$. This form allows for electron-phonon many-body corrections etc. in the parameter γ. For the Sommerfeld result (eq. (10.11)) we use the notation

$$C_{el} = \gamma_b T = (m_b/m) C_{fe}. \tag{10.12}$$

The subscript b means that electron band structure effects are included. C_{fe} is the heat capacity calculated in the free-electron model. The band mass m_b is defined in Appendix B.

If the density of states around the Fermi level is expanded in a series in $E - E_F$, one obtains ($N' = dN(E)/dE$; $N'' = d^2N(E)/dE^2$)

$$C_{el} = \frac{2\pi^2}{3} N(E_F) k_B^2 T$$
$$\times \left\{ 1 - (k_B T)^2 \frac{\pi^2}{2} \left[\left(\frac{N'}{N}\right)^2 - \frac{7}{5}\frac{N''}{N} \right] \right\}. \tag{10.13}$$

For a free-electron density of states, $N(E) \sim E^{1/2}$, and $(N'/N)^2 = 1/(4E_F^2)$ and $N''/N = -1/(4E_F^2)$. Then eq. (10.13) becomes the well-known result from textbooks (e.g. Wilson 1965)

$$C_{el} = \frac{2\pi^2}{3} N(E_F) k_B^2 T \left\{ 1 - \frac{3\pi^2}{10} \left(\frac{T}{T_F}\right)^2 \right\}. \tag{10.14}$$

It is not an unusual mistake that the $(T/T_F)^2$-term in C_{el} is neglected in transition metals, invoking an argument that $T_F = E_F/k_B$ is of the order of 100,000 K (cf. table 10.1). A correct treatment has to consider what is the energy interval ΔE around E_F over which $N(E)$ varies significantly, and replace T_F in the low temperature expansion (eq. (10.14)) by $\Delta E/k_B$, a quantity which may be <1000 K when E_F falls at a sharp structure in $N(E)$.

Example: C_{el} for a realistic density of states $N(E)$. This example serves to give an idea about corrections to eq. (10.11) in a real metal. The inset
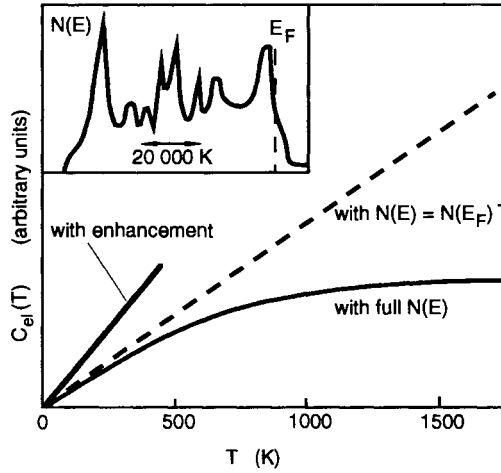
Fig. 10.2. The inset shows a density of states $N(E)$ for d-electrons characteristic of Pd. The main part of the figure shows the corresponding heat capacity $C_{\text{el}}(T)$ in three models, as described in the text. The arrow marks the energy width ΔE that corresponds to
$$\Delta E / k_B = 20{,}000 \text{ K}.$$

in fig. 10.2 shows the gross features of $N(E)$ for Pd. The main figure shows the heat capacity $C_{\text{el}}(T)$ calculated from this $N(E)$ in three models. The two straight lines refer to a constant $N(E) = N(E_F)$ for all E; the full-drawn line with a tentative constant many-body enhancement parameter $\lambda = 0.7$ (allowance for electron-phonon and other corrections, see below), and the dashed line with $\lambda = 0$. The full-drawn curve is based on the full $N(E)$ and therefore reflects the true behaviour at high T (where electron-phonon effects are small).

2.3. Entropy

A useful expression for the entropy is

$$S_{\text{el}} = -2k_B \int_{-\infty}^{\infty} \{ f(E)[\ln f(E)] \\ + [1 - f(E)] \ln[1 - f(E)]\} N(E) \, dE. \tag{10.15}$$

The function inside the braces { ... } in eq. (10.15) is an even function of $E - \mu(T)$ and is sharply peaked at $\mu(T)$. When the density of states

varies slowly with E near the Fermi level, $N(E)$ can be taken outside the integral, as a constant $N(E_F)$. We get

$$S_{el} = \frac{2\pi^2}{3} N(E_F) k_B^2 T. \tag{10.16}$$

Thus $S_{el} = C_{el}$, a result which also follows immediately from the general thermodynamic relation

$$S_{el}(T) = \int_0^T \frac{C_{el}(T')}{T'} \, dT' \tag{10.17}$$

when $C_{el}(T')$ is linear in T'. However, we noted above that structure in the energy dependence of $N(E)$ near E_F may be important. Then $S_{el} \neq C_{el}$ at high T (cf. Chapter 19, §12).

3. Electronic entropy and heat capacity in real metals

3.1. Introduction

The Sommerfeld electron theory of metals, leading to expressions such as eq. (10.11) for the heat capacity C_{el} and eq. (10.16) for the entropy S_{el}, is not in quantitatively good agreement with experiment, even if one uses an electron density of states $N(E_F)$ determined from accurate electron band calculations. The main reason is that the Sommerfeld model neglects important *electron-phonon many-body corrections*. Their existence was realised by Buckingham (1951) and Buckingham and Schafroth (1954) but their magnitude was unknown until much later (e.g. Ashcroft and Wilkins 1965, Allen and Cohen 1969). The electron-phonon many-body correction to the thermal properties of conduction electrons has been reviewed by Grimvall (1976, 1981).

The complications caused by a rapidly varying density of states $N(E)$ around the Fermi level have already been discussed above. It may be necessary to allow the chemical potential μ to vary with T. In numerical calulations of the electron band-structure term (i.e. without many-body corrections) one may use eq. (10.5) to determine $\mu(T)$, then eq. (10.15) to obtain the entropy, and finally calculate the heat capacity as $C = T(\partial S / \partial T)$. Examples showing the non-linear T-dependence of

C_{el} at high temperatures are given in Eriksson et al. (1992) and in fig. 10.2.

3.2.   Effects of electron scattering

In the treatment of electron states with energies E_k, and a corresponding density of states $N(E)$, it is assumed that the electrons move in a perfect periodic lattice, with sharp energy eigenvalues E_k. In a real solid, scattering against phonons or impurities gives these electron states a finite life time τ which may be described by an imaginary part $-2i\Gamma = -i\hbar/\tau$ in E_k. We can still use the expression (10.15) for the entropy if we replace the density of states $N(E)$ by a "smeared" function $N^*(E)$ defined as

$$N^*(E) = \int_{-\infty}^{\infty} N(\varepsilon) \frac{(\Gamma/\pi)}{(E - \varepsilon)^2 + \Gamma^2} \, d\varepsilon. \tag{10.18}$$

When $\Gamma \to 0$, the Lorentz function in the integrand becomes a δ-function, $\delta(\varepsilon - E)$, and then $N^*(E) = N(E)$. If we expand $N(E)$ around E_F as $N(\varepsilon) = N(E_F) + (\varepsilon - E_F)N'$, (eq. (10.18)) formally diverges, but the contribution from $(\varepsilon - E_F)N'$ vanishes over a symmetric interval around E_F. Therefore, in real cases, it is only when $N(E)$ has a strong non-linear energy dependence near E_F that the finite lifetime of the electrons affects the entropy. Electron states within several $k_B T$ from E_F contribute to the entropy (eq. (10.15)), so the effect of a finite Γ is negligible if $\Gamma \ll k_B T$. For the phonon-limited life time one has (Chapter 15 and Grimvall 1981) $\Gamma = \pi \lambda_{el-ph} k_B T$ at high T, where λ_{el-ph} is the electron-phonon parameter introduced in §3.3. Since λ_{el-ph} is of the order of unity, the phonon-limited Γ could have a significant influence on S_{el}. However, calculations with realistic $N(E)$ (Thiessen 1986) show that the effect is usually small ($<10\%$, any sign). In the case of impurity scattering it is convenient to relate $\Gamma = \hbar/2\tau$ to the electron lifetime as it enters the electrical conductivity, $\sigma = ne^2\tau/m_b$ (eq. (15.9)). It follows that when the electrical resistance due to impurities is less than that due to electron-phonon scattering, as is the case with dilute impurities, the influence of impurity scattering is negligible. Finally, note that even if $N(E)$ is a δ-function, $N^*(E)$ decays as $1/E$ for large E and therefore has an infinite width. Integrals for thermal properties are taken over a finite energy range, and $N^*(E)$ must be multiplied by a renormalisation factor so that eq. (10.5) is still fulfilled.

3.3. Electron-phonon many-body corrections to the electronic entropy

The electron-phonon many-body corrections are significant only at low temperatures ($T < \theta_D$) and may usually be neglected when T is so high that one has to consider the variations in $N(E)$ dealt with above. Therefore, in this section we let the electron density of states be a constant, $N(E_F)$. We also assume that the electron-phonon interaction, expressed through a so-called electron self energy M_{el-ph}, is isotropic. Then (Grimvall 1976, 1981, 1986)

$$S_{el} = \frac{N(E_F)k_B\hbar^2}{(k_BT)^2} \int_{-\infty}^{\infty} \left[\frac{\omega}{\cosh^2(\hbar\omega/2k_BT)}\right] \times [\hbar\omega - \mathrm{Re}M_{el-ph}(\omega, T)] \, d\omega. \tag{10.19}$$

This result holds for all temperatures. In the low temperature limit ($T \ll \theta_D$ where θ_D is a Debye temperature) the integral (10.19) picks up M_{el-ph} very close to the Fermi level, i.e. for small ω. There one may expand M_{el-ph} as $M_{el-ph}(\omega, k_F; T) = -\lambda_{el-ph}\hbar\omega$. The resulting integral has the same form as in the Sommerfeld model, apart from a factor $1 + \lambda_{el-ph}$, and the final low temperature result is

$$S_{el} = (2\pi^2/3)N(E_F)(1 + \lambda_{el-ph})k_B^2T. \tag{10.20}$$

Thus the effect of electron-phonon many-body interactions is easily accounted for, at very low temperatures. The high temperature limit of eq. (10.19) agrees exactly with the Sommerfeld model, since M_{el-ph} goes to zero as $(\theta_D/T)^2$ for $T > \theta_D$. At intermediate temperatures, one has to perform the integration in eq. (10.19) numerically. It is convenient to split S_{el} into two parts; S_b which is the Sommerfeld (or electron-band theory) result, and S_{el-ph} which is the correction caused by electron-phonon many-body interactions;

$$S_{el} = S_b + S_{el-ph}. \tag{10.21}$$

In the low temperature limit,

$$S_{el-ph} = \lambda_{el-ph}S_b. \tag{10.22}$$

If M_{el-ph} is calculated with an Einstein model for the lattice vibrations S_{el-ph} can be expressed as a universal function $S_{el-ph}(T)/(\gamma_b\lambda_{el-ph}T)$ (fig. 10.3).
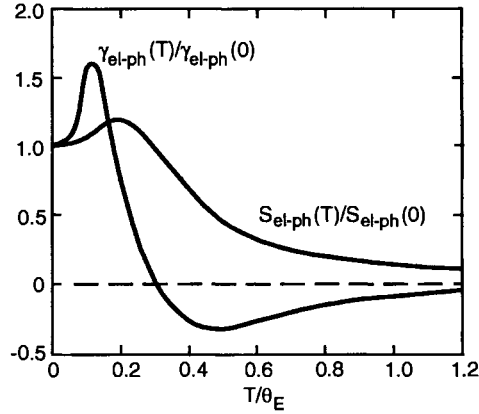
Fig. 10.3. The temperature dependence of the electron-phonon renormalisation contribution to the electronic heat capacity $\gamma_{el-ph}(T)$, and to the electronic entropy, $S_{el-ph}(T)$, calculated in an Einstein model for the phonons. From Grimvall (1981).

The quantity λ_{el-ph} discussed in this section is closely related to the BCS theory of superconductivity. In fact, λ_{el-ph} can be estimated from the critical temperature T_c (Appendix B). Numerical values of λ_{el-ph} are given in Appendix I. Because λ_{el-ph} is anisotropic, the listed values of λ_{el-ph} are averages over the electron states at the Fermi level. There is also a close relation between λ_{el-ph} and the "transport" coupling parameter λ_{tr} that appears in the electrical resistivity of metals (Chapter 15).

3.4.   Electron-phonon many-body corrections to the electronic heat capacity

The electronic heat capacity (at constant volume) is obtained from

$$C_{el} = T \left(\frac{\partial S_{el}}{\partial T} \right)_V .$$ (10.23)

Equation (10.20) gives the low temperature (i.e. $T \ll \theta_D$) result

$$C_{el} = (2\pi^2/3)N(E_F)(1 + \lambda_{el-ph})k_B^2 T = \gamma_b(1 + \lambda_{el-ph})T.$$ (10.24)

We define a *"thermal" effective electron mass m_{th}* by

$$m_{th} = (\gamma/\gamma_{fe})m,$$ (10.25)

where γ is the measured coefficient in $C_{el} = \gamma T$, m is the usual (free) electron mass, and γ_{fe} is the coefficient resulting from the free-electron version of the Sommerfeld model. With the electron-phonon many-body correction written explicitly we have

$$m_{th} = (\gamma_b/\gamma_{fe})(1 + \lambda_{el-ph})m = m_b(1 + \lambda_{el-ph}). \tag{10.26}$$

In analogy to our treatment of the entropy, the electronic heat capacity is split into two parts;

$$C_{el} = [\gamma_b + \gamma_{el-ph}(T)]T, \tag{10.27}$$

where $\gamma_{el-ph}(T=0) = \gamma_b\lambda_{el-ph}$. At high temperatures, γ_{el-ph} tends to zero. There is no temperature dependence in γ_b because we have assumed the approximation that $N(E)$ is a constant, within the energy interval probed by the heat capacity. Figure 10.3 shows $\gamma_{el-ph}(T)$ in an Einstein phonon model. As a rough rule of thumb, we can take $\gamma_{el-ph}(T)/\gamma_b = \lambda_{el-ph}$ for $T < \theta_D/4$ and zero for $T > \theta_D/3$, where θ_D is a characteristic Debye temperature. The temperature dependence of $\gamma_{el-ph}(T)$ and $S_{el-ph}(T)$ given in fig. 10.3 is not much altered if one uses the true phonon spectrum instead of the Einstein model; the peaks in fig. 10.3 will be somewhat broader and with smaller maxima. The decrease, and eventual absence, of the electron-phonon enhancement factor is not easy to see in experiments on C_p because it is difficult to separate it from the temperature dependence of the lattice part. However, there seems to be clear evidence for the effect, including a spin fluctuation part (see below) in Lu and Sc (Tsang et al. 1985, Pleschiutschnig et al. 1991, Swenson 1996).

Heavy fermion systems get their name from the fact that the effective electron mass (quasi particle mass) at the Fermi level is very high; several orders of magnitude larger than in conventional metals. The heat capacity parameter $\gamma = C_{el}/T$ shows a strong temperature dependence, varying with the material. The ground state of a heavy-fermion system may be superconducting (e.g. $CeCu_2Si_2$, UPt_3), magnetic (e.g. UCd_{11}, U_2Zn_{17}) or normal metallic (e.g. $CeAl_3$, $CeCu_6$). We may still write $m_{th} = m_0(1 + \lambda_{el-ph})$ where m_0 is the result in the absence of electron-phonon interactions, but in this case the effect of the electron-phonon interaction is to reduce m_{eff}, i.e. $\lambda_{el-ph} < 0$ (Fulde et al. 1993).

3.5.   Other many-body corrections

Electron-electron interactions: In a uniform electron gas, the electron-electron many-body corrections to the thermal electron mass are small. In free-electron-like metals the corrections are at most a few percent (Grimvall, 1975b). In transition metals there are important electron-electron many-body terms, but to a large extent they are folded into the single-particle density of states $N(E)$ obtained in a band structure calculation. The remaining correction to the thermal mass probably is only a few percent and of uncertain sign. Lacking more detailed information it is therefore best to neglect these effects.

Electron-paramagnon interactions: In metals that are close to a magnetic instability, there are electron-paramagnon many-body corrections. We can write (Gladstone et al. 1969, Burnell et al. 1982, Leavens and MacDonald 1983)

$$m_{\text{th}} = m_{\text{b}}(1 + \lambda_{\text{el-ph}} + \lambda_{\text{el-sp}}), \tag{10.28}$$

where $\lambda_{\text{el-sp}}$ refers to spin fluctuations (i.e. paramagnons). It is difficult to calculate $\lambda_{\text{el-sp}}$ accurately (Daams et al. 1981, Leavens and MacDonald 1983). Among several proposed expressions we quote that of Doniach and Engelsberg (1966);

$$\lambda_{\text{el-sp}} = 3IN(E_{\text{F}}) \left\{ 1 + \frac{\nu IN(E_{\text{F}})}{12[1 - IN(E_{\text{F}})]} \right\}. \tag{10.29}$$

Here we recognise the term $1 - IN(E_{\text{F}})$ from the Stoner model of magnetism, where the susceptiblity $\chi = \chi_0/[1 - IN(E_{\text{F}})]$ diverges when $IN(E_{\text{F}}) \to 1$ which signals a transition to a magnetically ordered state (eq. (19.24)). The parameter ν is roughly of the order of 1/2. In free-electron-like metals $IN(E_{\text{F}}) \ll 1$, and $\lambda_{\text{el-sp}}$ is negligible. Also for most transition metals $\lambda_{\text{el-sp}} < 0.05$. However, there seem to be metals (LuCo$_2$; Ikeda and Gschneidner 1980, MnSi; Taillefer et al. 1986) with $\lambda_{\text{el-sp}}$ of the order of 4, i.e. a larger enhancement than the highest known $\lambda_{\text{el-ph}}$ from electron-phonon interactions.

Electron-magnon interactions: In magnetically ordered materials, there are electron-magnon many-body corrections which add a term analogous to $\lambda_{\text{el-sp}}$ in eq. (10.28). The magnitude of their influence on m_{th} is not very well known, but it may be comparable to $\lambda_{\text{el-ph}}$ in Ni and Co (Phillips 1967, Batallan et al. 1975) and even be the dominating

enhancement in rare earths (Cole and Turner 1967, Nakajima 1967, Kim 1968). Fulde and Jensen (1983) gave a unified theoretical treatment of electron mass enhancements due to electron-phonon, electron-paramagnon and electron-magnon interactions. The corrections may be appreciable near $T = 0$ K, but disappear at high temperatures (cf. fig. 10.3).

Single-particle density of states in magnetic metals: In the Stoner model of ferromagnetic metals, one considers separate density-of-states functions, $N_+(E)$ and $N_-(E)$, for the two spin directions. Relations such as eq. (10.15) for the entropy and eq. (10.1) for the low temperature heat capacity remain valid if we put

$$2N(E) = N_+(E) + N_-(E). \tag{10.30}$$

However, one should note that the splitting of the two spin bands, and hence $N_+(E_F)$ and $N_-(E_F)$, varies with the temperature. The many-body enhancement factor need not be the same for the two spin directions, but this is of no concern if we let the enhancement factor be an average over all electron states, in analogy to the case of anisotropic enhancement referred to earlier.

4. Electron density of states in real metals

The energies $E(\mathbf{k}, s)$ of electron states in a perfectly periodic lattice of an element or a compound, and the corresponding density-of-states $N(E)$, are obtained from electron structure calculations through well-developed methods and in numerous scientific papers. This case will not be further considered here. In materials which lack perfect periodicity, for instance, alloys, amorphous structures and liquids, there are still solutions to the Schrödinger equation which give well-defined energy eigenvalues (in the single-particle description) and, hence, a well-defined $N(E)$. Therefore, the methods described in this chapter still apply. However, we can no longer label the electron energy values with precise wave vectors $\mathbf{k}$, and the sharp structures in $N(E)$ that are associated with the lattice periodicity through certain values of $\mathbf{k}$ will be smeared. When the disturbance of the electron states is only moderate, such as in a dilute alloy, we may keep the labels $(\mathbf{k}, s)$ on the electron states and introduce a smearing of $N(E)$ through a finite electron

lifetime. This was discussed in §3.2. On alloying, the electron-phonon parameter $\lambda_{\text{el}-\text{ph}}$ shows no variation that is particularly different from the variation in $\lambda_{\text{el}-\text{ph}}$ between elements (Grimvall 1976, 1981).

The simple Bohr model of an atom considers a sequence of possible energy states for the electrons. In atoms of increasing atomic number, and hence increasing number of electrons, these energy levels are succesively filled with electrons. Similarly, in a metal, the conduction electrons (valence electrons) go into electron states described by the density-of-states $N(E)$. As one moves, e.g. to the right in a transition-metal row in the Periodic Table, the increasing number of valence electrons succesively fills $N(E)$ to higher energies. The *rigid-band model* assumes that $N(E)$ stays the same along this sequence, and only the Fermi energy increases with the filling of the electron-band states. This is a considerable simplification, but may still give a useful insight into the physics of trends among metals and alloys. If one starts from a pure element whose $N(E)$ is known, and increases the number of electrons only moderately through alloying, it may be a reasonable approximation to use a $N(E)$ of fixed shape and calculate the Fermi level from eq. (10.5), with the new number of electrons N_{el}. The resulting $N(E_{\text{F}})$ is then used to obtain thermodynamic properties of the alloy. In Chapter 1, we used the rigid-band concept in an even more simplified form (Friedel's rectangular $N(E)$) to get a qualitative account of the bulk modulus and cohesive energy of transition metals. However, arguments invoking the rigid-band model must be used with great care, and sometimes the model fails badly.

It is beyond the scope of this book to review the large field of electron band structure calculations. In pioneering work, Moruzzi et al. (1978) calculated $N(E)$ for all metals with atomic number $Z < 49$. In the Landolt–Börnstein tables, Cracknell (1984) presents graphs of $N(E)$ for metallic elements and Sellmyer (1981) gives $N(E)$ for ordered compounds and disordered alloys. Moruzzi and Sommers (1995) published $N(E)$ calculated ab initio for the elements with atomic number $Z < 55$, in assumed fcc and bcc lattice structures, and also graphs of $N(E)$ for their ordered $3d/3d$- and $4d/4d$-transition metal alloys in assumed lattice structures of the CsCl, CuAu, Cu_3Au and AuC_3 types. Papaconstantopoulos (1986) published $N(E)$ and γ_{b} for free-electron-like, $3d$-, $4d$- and $5d$-transition metals.
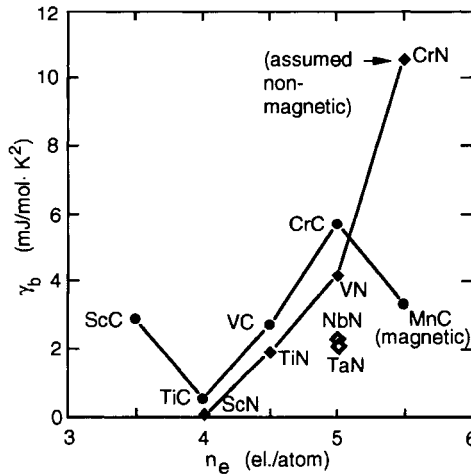
Fig. 10.4. The variation of γ_b in the electronic heat capacity $C_{el} = \gamma T$, as a function of the average number of valence electrons per atom, n_e. After Grimvall (1999), and based on electron-band structure calculations.

Example: heat capacity in transition metal carbides and nitrides. Figure 10.4 shows the electron-band structure parameter γ_b that appears in the "bare" (i.e. without many-body corrections) heat capacity $C_{el} = \gamma_b T$. Thus, $\gamma_b \sim N(E_F)$, with $N(E_F)$ taken from electron-band structure calculations. We see that there is a regular variation of γ_b as a function of the average number n_e of valence electrons per atom in the compounds, which suggests a rigid-band picture. In fact, that crude description with bonding and antibonding electron states below and above $n_e = 4$, respectively, correlates very well with the maximum in cohesion-related properties (melting temperature, elastic constants) for TiC and ScN.

THERMAL PROPERTIES OF FEW-LEVEL SYSTEMS AND SPIN WAVES

1. Introduction

Several important thermophysical properties may be described by simple models with only two, or a few, energy levels. Of particular interest are vacancy formation, localised f-electrons in rare earths, magnetic excitations in insulators and order-disorder transformations in alloys. A dynamical coupling between discrete spins of magnetic atoms in a lattice leads to excitations which are propagating waves, closely analogous to phonons. They are called spin waves, or magnons. Since the scope of this book is mainly to consider thermophysical properties of materials which are of practical importance, we leave out many effects which are mainly significant at a few kelvin and below.

2. Systems with few energy levels

Consider an ensemble of n-level systems. The energy levels are $E_i (1 \leq i \leq n)$, with degeneracies g_i. Its thermodynamic properties are obtained from the partition function Z_n through the Helmholtz energy $F_n = -k_B T \ln Z_n$;

$$Z_n = \sum_{i=1}^{n} g_i e^{-E_i/k_B T}. \tag{11.1}$$

For instance, the contribution to the heat capacity from each of these n-level systems is $C_n = -T(\partial^2 F_n/\partial T^2)$. An important special case is a two-level system with non-degenerate energy levels E_1 and E_2. We let

$$E_2 - E_1 = \Delta E = k_B T', \tag{11.2}$$
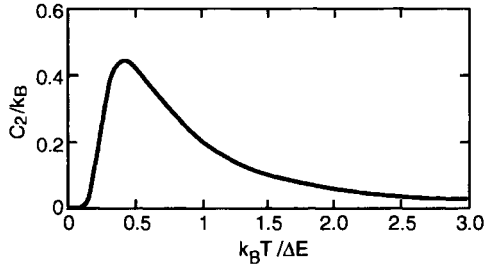
Fig. 11.1. The heat capacity (Schottky peak) for a two-level system with energy spacing ΔE, plotted versus $k_{\rm B}T/\Delta E$.

and get for the heat capacity

$$C_2(T) = k_{\rm B}\frac{x^2 e^x}{[e^x + 1]^2},$$ (11.3)

with $x = \Delta E/k_{\rm B}T = T'/T$. $C_2(T)$ has a characteristic form, known as a *Schottky peak* (fig. 11.1). The behaviour at low and high temperatures is

$$C_2(T) \approx k_{\rm B}(T'/T)^2 \exp(-T'/T), \quad (T \ll T');$$ (11.4)

$$C_2(T) \approx (1/4)k_{\rm B}(T'/T)^2, \quad (T \gg T').$$ (11.5)

At high temperatures, i.e. $T \gg (E_n - E_1)/k_{\rm B}$, all quantum states in the n-level system are equally populated, with a probability $1/G$ where $G = \sum g_i$. Thus, the entropy in the high temperature limit is

$$S = -k_{\rm B}\sum_{i=1}^{n} g_i[(1/G)\ln(1/G)] = k_{\rm B}\ln G.$$ (11.6)

Note that this important sum-rule for the entropy holds irrespective of the detailed nature of the energy levels.

3. Heat capacity from vacancies

Let there be N lattice sites in a solid. A site is either occupied or vacant, and can therefore be described by a two-level model. Hence, we have

N two-level systems. The probability that a site is vacant is $c_{vac}(T)$ (eq. (2.9)). The energy associated with a thermal-equilibrium concentration of vacancies is $E = N E_{vac} c_{vac}$. The heat capacity, $C_{vac} = \partial E / \partial T$, is

$$C_{vac}(T) \approx N k_B \exp(S_{vac}/k_B)(E_{vac}/k_B T)^2 \exp(-E_{vac}/k_B T),$$

(11.7)

that is, of the low temperature form (eq. (11.4)). If there is more than one atom per primitive cell, one may have to consider non-equivalent lattice sites separately, with different N, E_{vac} and S_{vac}. Typically, $E_{vac}/k_B T_{fus} \approx 10$ and $S_{vac}/k_B \approx 3$ for an elemental metal (see tables 2.1 and 2.2). Then $C_{vac}/3N k_B \approx 0.03$ at the melting temperature T_{fus}, but < 0.01 at $T = 0.8 T_{fus}$. The entropy of the solid, which is an integrated property over the heat capacity from $T = 0$, is little affected by the vacancies. Its total value $c_{vac} N S_{vac} < 0.003 N k_B$, which is negligible for all practical purposes, and correponds to the entropy change caused by a shift in the Debye temperature by $< 0.1\%$ (cf. eq. (7.24)). Several aspects of the effect of vacancies on thermophysical properties have been discussed by Kraftmakher (1972, 1978, 1996) and Varotsos and Alexopoulos (1986). Some of their conclusions may be challenged because of the difficulty to quantitatively account for the effect of high-order anharmonicity in the lattice-vibrations of a defect-free crystal.

4. Crystal-field split electron levels in atoms

Rare earth ions in a lattice, for instance Ho^{3+} in the high-T_c superconductor $HoBa_2Cu_3O_{7-\delta}$ and Tm^{3+} in $TmBa_2Cu_3O_{7-\delta}$, give rise to crystalline electric field (CEF) splitting of the Hund's rules ground state $4f$-electron multiplet. These discrete levels contribute to the heat capacity in the form of Schottky-like terms, calculated as shown in §2. The ground state of a free ion, characterised by the quantum number J, has degeneracy $2J + 1$. The crystal field now splits this level. Figure 11.2 shows the low energy part of the split levels, as given by Ferreira et al. (1988a). They calculated the corresponding heat capacity and obtained a good agreement with their experiments for C_p.

7——————— 82 K

3——————— 57 K

1——————— 26 K
1——————— 23 K

                    1——————— 17 K

1——————— 7 K
1——————— 0 K   4——————— 0 K
Ho^{3+} Tm^{3+}
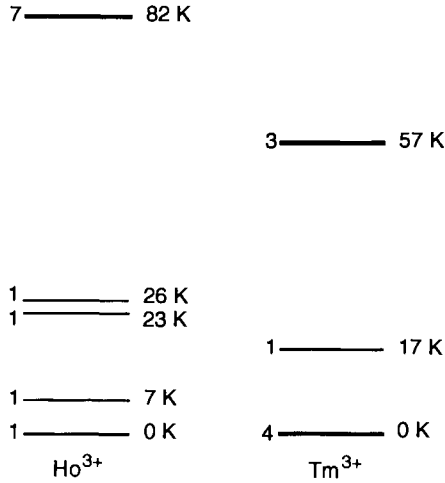
Fig. 11.2. Low energy part of the crystal-field split energy level for the $4f$-electrons in Ho^{3+} and Tm^{3+} in the high temperature superconductors $\text{HoBa}_2\text{Cu}_3\text{O}_{7-\delta}$ and $\text{TmBa}_2\text{Cu}_3\text{O}_{7-\delta}$. The energies are expressed in the equivalent temperature, $E = k_B T$. The number to the left of the levels is the degeneracy. Remaining levels fall at much higher energies.

5. Tunneling states in amorphous materials

Zeller and Pohl (1971) discovered that the low temperature heat capacity of several non-metallic amorphous materials varied linearly in T. This was first surprising, since the Debye T^3-law should hold in the low temperature limit, irrespective of the crystal structure. (The excited phonons have such long wavelengths that they "see" the lattice as an elastic continuum.) The phenomenon, which is present both in insulating glasses and amorphous metals, is still poorly understood (Cibuzar et al. 1984, Graebner and Allen 1983) but it may be qualitatively explained by the two-level tunneling system model (Anderson et al. 1972, Phillips 1972). The idea is that in a glassy material, there are atoms which can be in any of two neighbouring equilibrium positions. Let ε be the spacing between two such levels, and $N(\varepsilon)\Delta\varepsilon$ be the number of two-level systems in the specimen with ε lying in the energy interval $[\varepsilon, \varepsilon + \Delta\varepsilon]$. The total heat capacity is

$$C = \int_0^\infty N(\varepsilon)C_2(\varepsilon/k_B T)\,\mathrm{d}\varepsilon. \tag{11.8}$$

$C_2(\varepsilon/k_B T)$ is negligible when $k_B T \gg \varepsilon$ or $k_B T \ll \varepsilon$, i.e. on either side of the Schottky peak. If $N(\varepsilon)$ is a smoothly varying function of ε we can take $N(\varepsilon^*)$, with $\varepsilon^* \sim k_B T$, outside the integral in eq. (11.8). Then

$$C = (\pi^2/6)k_B^2 N(\varepsilon^*)T. \tag{11.9}$$

The heat capacity in this model is linear in T, in accordance with the experiments.

6. Order-disorder transformations

Order-disorder transformations of various kinds form a central part of statistical physics. The matematical complexity may be enormous, even for very simplified models. Since the field is well covered in many texts (e.g. Ziman 1979), and since it would not be possible to take a discussion to the same depth as in other chapters in this book, we just mention a few important points.

Two problems of prime importance are the order-disorder transitions of spins in magnetic systems, and of atomic configurations in alloy lattices. In the first case we can (in the simplest *Ising model*) assign to each lattice site a spin which is either in a "spin-up" or a "spin-down" state. The spins interact with their nearest-neighbours only, and one introduces different interaction energies for the three possible pairs; spin-up–spin-up, spin-down–spin-down and spin-up–spin-down. In the case of atomic ordering in an alloy with atoms A and B, one again assumes interactions with nearest-neighbours and introduces interaction energies E_{AA}, E_{BB} and E_{AB}. One, of several, approximate mathematical solutions to the statistical mechanics of these models makes use of the *mean-field approximation*. When applied to magnetic systems, it is usually referred to as the *Curie–Weiss theory*, or the *(Weiss) molecular-field theory*. In the atomic ordering case it is known as the *Bragg–Williams model* (although priority should perhaps have been given to Borelius, see Borelius 1934, Domb 1981).

The heat capacity C_{dis} of an order-disorder transformation is very difficult to calculate in its full details for a realistic system. Roughly, it has the form of fig. 11.3. Although C_{dis} is poorly known, it always obeys the sum rule related to the entropy $S_{dis}(T)$,

$$S_{dis}(\infty) - S_{dis}(0) = \int_0^\infty [C_{dis}(T)/T]\,dT. \tag{11.10}$$
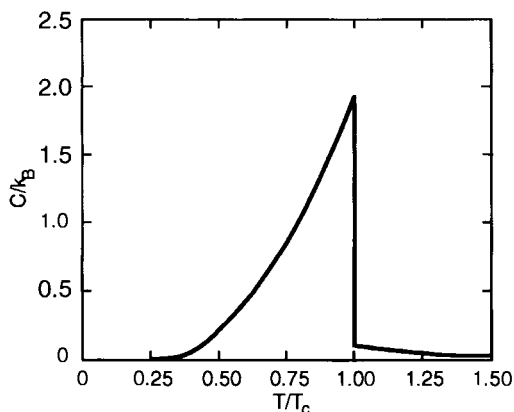
Fig. 11.3. A schematic representation of the heat capacity of a system with an order-disorder transformation at $T = T_c$.

For instance, if an alloy $A_{1-c}B_c$ is completely ordered at low temperatures, the entropy $S_{dis}(0) = 0$. At temperatures so high that the atoms are randomly distributed over the lattice sites, the entropy per site is

$$S_{dis}(\infty) = -k_B\{c \ln c + (1 - c) \ln(1 - c)\}. \tag{11.11}$$

In the special case of an AB alloy (i.e. $c = 0.5$) we get $S_{dis}(\infty) = k_B \ln 2$. An analogous relation holds for the spin-disorder entropy in magnetic insulators. In metals, the question of persistent spin fluctuations above the Curie temperature is a matter of controversy. There seem to be large such fluctuations in Fe.

7. Magnons

In the Ising model of magnetism, mentioned above, magnetic excitations correspond to the reversal of the spin at a particular lattice site (for spin 1/2). Such excited states are separated from the ground state by a rather large energy gap, and hence they are frozen out at low temperatures. However, when the spins of adjacent sites are dynamically coupled to each other, there may be wave-like excitations, called *magnons* or *spin waves*. This is in close analogy to phonons. In an Einstein model, which is reminiscent of the Ising model, the lowest excited state lies at a finite energy level above the ground state. When dynamical coupling between the atoms is introduced, wave-like excitations are

possible, in which each atom is displaced only a small amount relative to its neighbours, and the excitation energy can be very low. It lies outside the scope of this book to discuss magnons in detail and the reader is referred to elementary (Kittel 1996) and more advanced (Kittel 1987) accounts. Below we summarise concepts which are of importance for the thermal properties of solids.

Consider a ferromagnetic insulator, with N regularly ordered atoms which have a spin of magnitude S. (Even for metallic magnetic systems there are several properties which are well described by the model of an insulator.) The lattice may also contain atoms which do not have a magnetic moment, but they are of no concern here. In the ground state ($T = 0$ K) all spins are aligned. The magnons (spin waves) are excitations characterised by a wave vector $\mathbf{q}$, lying in the first Brillouin zone defined by the lattice of magnetic atoms. The energy of a magnon is written $\hbar\omega_{\mathrm{magn}}(\mathbf{q}, i)$. The index i distinguishes between different magnon branches for a given $\mathbf{q}$. The terminology is taken over from phonons and one speaks of the acoustic magnon branch and (in the case of several magnetic atoms per primitive cell) optical magnon branches. However, the three polarisation directions for a given $\mathbf{q}$ in the case of phonons have no magnetic counterpart and there is only one "polarisation" mode for each $\mathbf{q}$. We write for the magnon energy (when i refers to the acoustic mode)

$$\hbar\omega_{\mathrm{magn}}(\mathbf{q}, i) = Da^2q^2. \qquad (11.12)$$

D has the dimension of energy, and measures the strength of the magnetic coupling between adjacent spins, and a is a lattice parameter.

In analogy to the Debye model, we shall assume that eq. (11.12) is valid for all $\mathbf{q}$, and evaluate the magnon contribution $C_{\mathrm{magn}}(T)$ to the heat capacity at low temperatures. The density of states in $\mathbf{q}$-space is the same as for phonons; $V/(2\pi)^3$. The calculations closely follow those of the Debye model for the heat capacity, but with $\omega_{\mathrm{magn}}(q) \sim q^2$ instead of the relation $\omega(\mathbf{q}) \sim |\mathbf{q}|$ for phonons. We get

$$\begin{aligned}
C_{\mathrm{magn}}(T) &= \frac{Nk_{\mathrm{B}}}{4\pi^2}\left(\frac{k_{\mathrm{B}}T}{D}\right)^{3/2}\int_0^\infty \frac{x^{5/2}e^x}{(e^x - 1)^2}\,\mathrm{d}x \\
&= 0.113Nk_{\mathrm{B}}\left(\frac{k_{\mathrm{B}}T}{D}\right)^{3/2},
\end{aligned} \qquad (11.13)$$

with $N = V/a^3$. The integral (11.13) is related to $\zeta(2.5)$, where ζ is Riemann's ζ-function. A similar result is obtained for a ferrimagnet where not all the spins are of equal magnitude (Kouvel 1956).

In an effective-medium model for a simple cubic lattice with nearest-neighbour interactions, the Curie temperature T_c is related to D by (White 1970)

$$k_B T_c = (S + 1)D. \tag{11.14}$$

Within this approximation we can write

$$C_{magn}(T) = 0.113 N k_B (S + 1)^{3/2} (T/T_c)^{3/2}. \tag{11.15}$$

An entropy argument shows that eq. (11.15) cannot hold all the way up to $T = T_c$. We would get, with eq. (11.15),

$$S_{magn}(T_c) = \int_0^{T_c} [C_{magn}/T]\, dT = 0.075 N k_B (S + 1)^{3/2}, \tag{11.16}$$

which is incorrect as the theory only applies at temperatures well below T_c. On the other hand, if there were complete spin disorder at $T = T_C$, we would have an entropy $S_{magn}(T_c) = N k_B \ln(2S + 1)$. For any reasonable magnitude of the spin S, this is much larger than eq. (11.16) and the discrepancy cannot be explained by the relatively small short-range order that still prevails above T_c. Near T_c, the heat capacity must be described by the order-disorder models (§6).

If $\omega_{magn}(\mathbf{q}, i)$ are the magnon frequencies for wave vector $\mathbf{q}$ and mode i, one may form a partition function

$$Z_{magn}(\mathbf{q}, i) = \sum_n \exp\{[-\hbar\omega_{magn}(\mathbf{q}, i)/k_B T][n + 1/2]\}, \tag{11.17}$$

and a corresponding Helmholtz energy

$$F_{magn}(\mathbf{q}, i) = -k_B T \ln Z_{magn}(\mathbf{q}, i). \tag{11.18}$$

Then one could calculate, e.g. the magnetic heat capacity C_{magn} in complete analogy to the case of lattice vibrations. Thus,

$$C_{magn} = N k_B \int \frac{x^2 e^x}{(e^x - 1)^2} F_{magn}(\omega)\, d\omega, \tag{11.19}$$

where $F_{\text{magn}}(\omega)$ is the density of states for the magnon frequencies ω, and $x = \hbar\omega/k_{\text{B}}T$. For a dispersion relation as in eq. (11.12), we recover eq. (11.15). Furthermore, if there is an energy gap Δ up to the lowest magnetic excitation energy, so that $F_{\text{magn}}(\omega)$ is zero for $\hbar\omega < \Delta$, one gets

$$C_{\text{magn}} = C(T; \Delta)\exp(-\Delta/k_{\text{B}}T). \tag{11.20}$$

The formulation in eq. (11.18) can only be used at low temperatures. Actually, if it is formally taken to high T, one double-counts the contribution to the heat capacity. Measurements of the heat capacity in rare earth and yttrium garnets (Harris and Meyer 1962, Guillot et al. 1981) exemplify how the interpretation of the data requires a low temperature collective description (i.e. magnons) and a high temperature (in fact, at 1–10 K) Weiss molecular field approach.

Magnons in *antiferromagnets* (i.e. with alternating spin directions in the ground state) are similar to the magnons of ferromagnetic insulators, but the dispersion relation corresponding to eq. (11.12) has the form

$$\hbar\omega_{\text{magn}}(\mathbf{q}) = [(\hbar\omega_0)^2 + (Daq)^2]^{1/2}, \tag{11.21}$$

where $\hbar\omega_0$ is a characteristic gap energy. In magnetically anisotropic materials, $\omega_0 \neq 0$. Then the lowest excitation energy is finite, $\hbar\omega_0$. The heat capacity at temperatures $k_{\text{B}}T \ll \hbar\omega_0$ will be that of two-level system (§2). When $k_{\text{B}}T \gg \hbar\omega_0$, the thermal properties are dominated by the excitations for which $\hbar\omega_0$ can be neglected compared to Daq, i.e. we can make the approximation that $\hbar\omega_0 = 0$. In that case, the heat capacity varies as T^3. This is the same temperature dependence as for the phonons, a consequence of the fact that $\omega(\mathbf{q}) \sim |\mathbf{q}|$ for both phonons and magnons (in antiferromagentic crystals). At still higher temperatures, it is again necessary to use an order-disorder model.

Example: heat capacity and magnetic entropy in GdCu$_2$Si$_2$. In the compound GdCu$_2$Si$_2$, the Gd ions carry a magnetic moment through their f-electrons. The material is an antiferromagnet with Néel temperature $T_{\text{N}} = 11.9$ K. The isostructural compound LaCu$_2$Si$_2$ is non-magnetic. The extraction of the magnetic part C_{magn} from the total measured heat capacity $C_{\text{tot}} = C_{\text{magn}} + C_{\text{vib}} + C_{\text{el}}$ requires knowledge about the vibrational and electronic contributions. Bouvier et al. (1991) measured C_{tot} of GdCu$_2$Si$_2$ and LaCu$_2$Si$_2$, and assumed that they were essentially
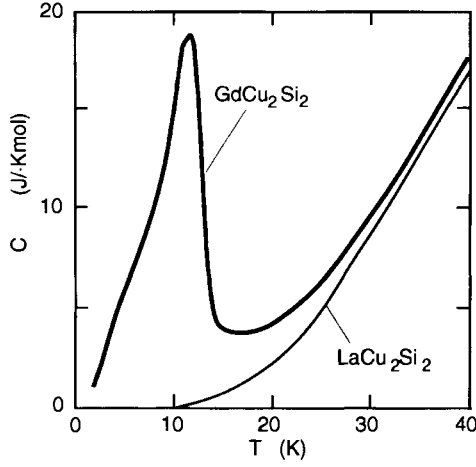
Fig. 11.4. The magnetic part of the heat capacity C of GdCu$_2$Si$_2$ may be estimated as the difference in heat capacities C of GdCu$_2$Si$_2$ and LaCu$_2$Si$_2$. After Bouvier et al. (1991).

the same, except for C_{magn}. Thus, by subtraction, they obtained C_{magn} as in fig. 11.4. A detailed theoretical account of $C_{\text{magn}}(T)$ would be very difficult. However, in spite of such difficulties, the total magnetic entropy at high temperatures,

$$S^{\infty}_{\text{magn}} = \int_0^{\infty} [C_{\text{magn}}(T)/T]\,dT, \tag{11.22}$$

was found to be very close to the expected value $k_B \ln(2J+1) = k_B \ln 8$ per Gd ion, derived from the total angular quantum number $J = 7/2$ for the $4f$-electrons in the Gd ion.

MELTING AND LIQUIDS

1. Introduction

It is a widely held, but erroneous, view that melting occurs at a temperature T_{fus} where the solid structure becomes dynamically unstable. Many different physical reasons have been given for such an instability. For instance, it has been suggested (e.g. Born 1939 and others) that a shear modulus, which normally decreases steadily with T due to anharmonic effects, vanishes at T_{fus}. However, experiments show that elastic constants do not extrapolate to zero at T_{fus}. Another idea is that the free energy for the formation of dislocations becomes zero at T_{fus} (e.g. Kuhlmann–Wilsdorf 1965). The liquid would then be described essentially as a solid penetrated by a very dense network of dislocations. It has also been suggested that the vacancy concentration becomes so high at T_{fus} that the lattice collapses (Gorecki 1974), while the Lindemann (1910) melting criterion (Chapter 19, §6) focusses on the magnitude of the vibrational displacement of the atoms as the cause of a lattice instability. These and other melting mechanisms have been thoroughly reviewed by Boyer (1985) and Poirier (1991).

From a thermodynamic point of view, a theory of melting should consider the Gibbs energy of both the solid and the liquid phases, and find that temperature at which $G_{sol}(T) = G_{liq}(T)$. This does not necessarily exclude a description with contributions to G invoking a dynamical instability. However, a straightforward approach to the free energy gives a good account of T_{fus}, for instance as demonstrated in work on Na (Stroud and Ashcroft 1972, Holian et al. 1983), Al (Straub et al. 1994) and Mg (Moriarty and Althoff 1995). Molecular dynamics calculations, relying on a semiempirical interaction between the atoms, may yield a reasonable value for T_{fus}, e.g. as in calculations for Cu (Sadigh and Grimvall 1996).
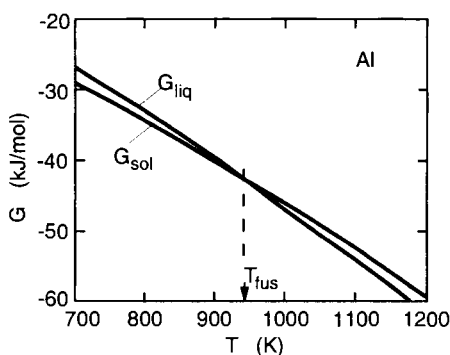
Fig. 12.1. The Gibbs energy $G = H - TS$ for the solid (fcc) and the liquid phases of Al, in the vicinity of the melting temperature T_{fus}.

Figure 12.1 shows the Gibbs energy $G(T)$ of fcc and liquid Al at ambient pressure and in the vicinity of T_{fus}, based on recommended data (JANAF thermochemical tables 1985). The scale is chosen so that $G_{sol} = 0$ at 0 K. It is obvious that the melting temperature, i.e. the point of intersection between G_{sol} and G_{liq}, will move significantly even for small changes in G_{liq}. For a long time, it was therefore difficult to get a good theoretical prediction of the melting temperature, and it is still a demanding task (cf. the references above).

In this context we note that although the Gibbs energies of the solid and the liquid are equal at T_{fus}, there is an energy barrier between the states. The dynamics of the melting process may involve atomic motions that can be described as characteristic of an incipient instability. If T_{fus} actually coincides with the temperature at which the solid phase becomes dynamically unstable, it has no meaning to continue G_{sol} beyond T_{fus}, as in fig. 12.1. In a dynamically unstable structure, the vibrational part of the entropy is undefined, and the Gibbs energy $G = H - TS$ has no interpretation as a quantity describing the energy of a (metastable) state.

2. Entropy of fusion

The entropy of fusion (entropy of melting) ΔS_{fus} is directly related to the difference in slope in the plot of $G(T)$ for the solid and the liquid phases (cf. fig. 12.1);
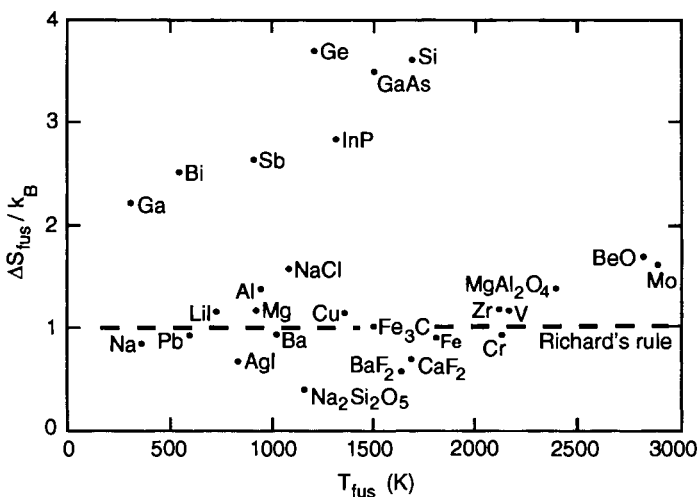
Fig. 12.2. The entropy of fusion ΔS_{fus}, per atom and normalised as $\Delta S_{fus}/k_B$, as a function of the melting temperature T_{fus}. The dashed line is Richard's rule. Data from Barin (1989).

$$\Delta S_{fus} = S_{liq} - S_{sol} = \left(-\frac{\partial G}{\partial T}\right)_{liq} - \left(-\frac{\partial G}{\partial T}\right)_{sol}. \qquad (12.1)$$

The major contribution to ΔS_{fus} usually comes from the positional disorder in the liquid state. It is difficult to account for quantitatively, but is accessible, for instance, through molecular dynamics calculations. Experimentally, it is found that ΔS_{fus} is approximately k_B per atom for many elements (*Richard's rule*), but fig. 12.2 shows that this is not a universally valid result. Some $\Delta S_{fus}/k_B$-values in the figure are considerably smaller than 1. There can be two simple reasons for such a behaviour. The liquid may retain some local ordering near T_{fus}, reminiscent of the solid structure, which gives a lower S_{liq} than in a more disordered phase. Another possibility is the development of partial disorder already in the solid, through some kind of lattice defects, which would increase S_{sol} and, hence, decrease $\Delta S_{fus}/k_B$. CaF_2 exemplifies a solid where there is a transition to a phase of high entropy just prior to melting.

The elements Si, Ge, Sb and Bi and (as examples) the III–V semiconductors GaAs and InP all have exceptionally large $\Delta S_{fus}/k_B$. The essential explanation is the different chemical bonding in the solid and the liquid. The solids are semiconductors (Si, Ge, III–V compounds)

or semimetals (Sb, Bi) while the liquid states are metallic. In fact, if solid Si and Ge had been free-electron-like metals, like Pb in the same column in the Periodic Table, a very crude scaling argument suggests that they would have Debye temperatures θ_D which are about 60% of what is observed in the semiconducting state (Grimvall, 1977). Because vibrational entropies contain a leading term $3k_B \ln(T/\theta_D)$ per atom (eq. (7.24)), such a difference in θ_D would account for about $1.5k_B$ of the anomalous ΔS_{fus}.

Electronic excitations can usually be neglected in ΔS_{fus}. In metals with an electron density of states $N(E)$ which is not varying much within an approximate energy interval $\pm 2k_B T$ around the Fermi energy E_F, one has for the electronic part, (eq. (10.16));

$$(\Delta S_{fus})_{el} = \frac{2\pi^2}{3} k_B^2 T_{fus}[N_{liq}(E_F) - N_{sol}(E_F)]. \tag{12.2}$$

This term gives an essential contribution to $(\Delta S_{fus})_{total}$ only if $N_{sol}(E_F)$ and $N_{liq}(E_F)$ are significantly different and, at the same time, T_{fus} is large. In free-electron-like systems none of these conditions are fulfilled. Furthermore, most transition metals with a high T_{fus} do not show a large difference in $N_{sol}(E_F)$ and $N_{liq}(E_F)$. Noteworthy exceptions are Cr, Mo and W. Their strong bonding in the solid (bcc) phase, and the related high T_{fus}, is due to the fact that the Fermi level E_F lies in a pronounced minimum in $N(E)$. This is an effect that appears in a half-filled electron d-band in the bcc lattice structure, and it is not as pronounced in the atomically disordered liquid. As an illustration, assume that $N_{liq}(E_F)/N_{sol}(E_F)$ as in fig. 12.3. That would give $(\Delta S_{fus})_{el} \sim 0.5k_B$/atom in W. Silicon and germanium, with an anomalously large ΔS_{fus}, have $N_{sol}(E_F) \approx 0$. With a free-electron-like $N_{liq}(E_F)$ (cf. references below), eq. (12.2) contributes only $\sim 0.1k_B$/atom.

The sharp structures found in $N(E)$ in many crystalline metals, caused by the periodic structure of the lattice, are absent in liquid metals. This is illustrated in fig. 12.3 which shows $N(E)$ for bcc W (solid lines; from Einarsdotter et al. (1997)) and a tentative $N(E)$ for liquid W (dotted curve) based on a comparison with calculated $N(E)$ for bcc and liquid Cr (Jank et al. 1991) and Mo (Moriarty 1994). For theoretical calculations of $N(E)$ in liquids, see, e.g. Jank and Hafner (1990) for Be, Mg, Zn, Cd, Hg, Ca, Sr and Ba; Hafner and Jank (1990) for Al, Ga, In and Tl; Hafner and Jank (1992) for As, Sb and Bi; Jank et al. (1991);
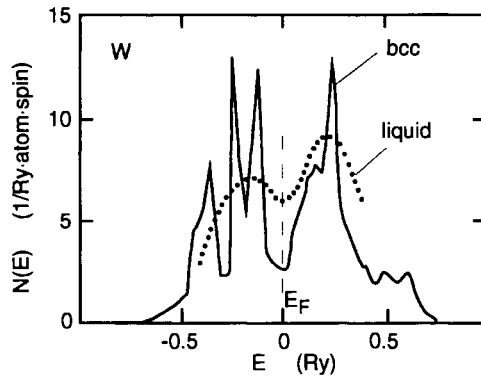
Fig. 12.3. The electron density of states $N(E)$ for bcc and liquid W, in arbitrary units.

Bose et al. (1993) for several $3d$- and $4d$-transition metals; Wang et al. (1992) for Si; Wang et al. (1993) for C; and Kulkarni et al. (1997) for Ge.

Wallace (1997) analysed the entropy of fusion of 25 elements, that are metallic at least in their liquid state. In order to isolate the contribution to ΔS_{fus} that comes from the atomic configurational disorder, he used Grüneisen parameters to convert the experimental entropy S_{sol} in the crystalline state just below the melting temperature to the value S_{sol} would take at the density of the liquid phase. It was found that the disorder, at equal densities for the solid and the liquid, contributes to ΔS_{fus} an almost universal value of $(0.80 \pm 0.1)k_B$ per atom. This is in good agreement with Richard's rule. When the actual value of ΔS_{fus} differs from the universal value caused by disorder, it has other explanations, as discussed above.

Finally we note that for iron $\Delta S_{fus} = 0.9k_B/$atom is about the same as for most non-magnetic elemental metals, in spite of the magnetic entropy $\sim 1k_B/$atom due to spin disorder in bcc as well as fcc Fe (Grimvall 1989). The existence of a magnetic entropy also in the liquid phase explains why ΔS_{fus} is not anomalous for Fe.

3. Liquid heat capacity

At the melting temperature, the difference in heat capacity C_p between the solid and the liquid phases is rather small, and it can be of either

Table 12.1

The discontinuity in the heat capacity at the melting transition, expressed as $(C_{p,\text{liq}} - C_{p,\text{sol}})/3k_B$ (per atom)

Cu	−0.03	Ge	−0.05
Ag	0.06	Si	−0.08
Au	−0.10	GaAs	0.10
Na	0.01	NaCl	0.04
Mg	0.02	KCl	0.13
Al	−0.09	CaF$_2$	−0.34
Pt	−0.01	BaF$_2$	−0.10
Fe	0.14	Na$_2$SiO$_3$	−0.04

sign. See table 12.1 giving $(C_{p,\text{liq}} - C_{p,\text{sol}})/3k_B$ per atom, based on data from Barin (1989).

There is not much experimental information on C_p in liquids well above T_{fus}. Measurements on free-electron-like elements with low melting temperatures and (less accurate) data for elemental transition metals (e.g. Pottlacher et al. 1993) indicate that $C_p(T)$ is usually almost independent of T over a wide range of temperatures. Theoretical calculations using molecular dynamics for Cu (Sadigh and Grimvall 1996) corroborates this result. The heat capacity at constant volume, $C_V(T)$, decreases with T. It approaches $\sim 2k_B$/atom at high T through the gradual loss of shear resistance, which leaves four degrees of freedom (three kinetic energy variables and one term referring to compression potential energy) instead of the six degrees of freedom for three-dimensional harmonic oscillators (Wallace et al. 1982). Figure 12.4 shows the lattice parts of $C_p(T)$ and $C_V(T)$ for Na and Hg. The molecular dynamics calculation for Cu mentioned above gives the same picture.

4. More on lattice instabilities

Figure 12.5 shows, with a full-drawn curve, the experimental heat capacity C_p in solid Cu, including suggested values in the superheated region (JANAF thermochemical tables 1985), and a tentative extrapolation (dashed) to high temperatures. It also shows, with a full-drawn
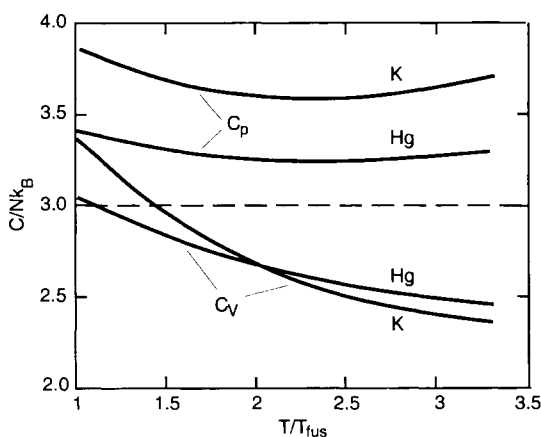
Fig. 12.4. Heat capacities C_p and C_V for K and Hg (per atom) plotted versus the reduced temperature T/T_{fus}, as derived from experimental data. After Grimvall (1975a).
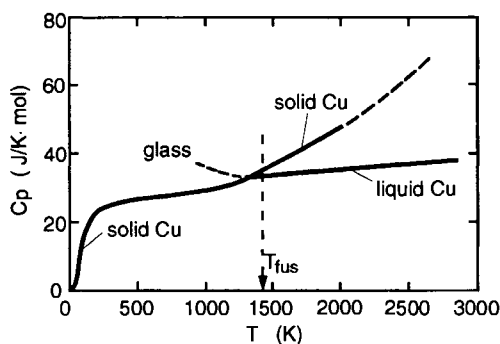
Fig. 12.5. The recommended (JANAF thermochemical tables 1985) heat capacity C_p for solid Cu (solid line) with a tentative extrapolation to higher T (dashed), and the calculated (Sadigh and Grimvall 1996) C_p for liquid Cu with a tentative extrapolation (dashed) into the supercooled region.

curve, the heat capacity in the liquid phase (Sadigh and Grimvall 1996) and a tentative extrapolation (dashed) in the supercooled region.

If C_p of the solid continued to increase with T as in Fig. 12.5, while C_p of the liquid remained essentially constant, the solid phase would become more stable than the liquid at some temperature T_S well above T_{fus}. (The Gibbs energy decreases faster with T for the phase with the larger heat capacity.) A re-entering solid phase is of course unreasonable, and some kind of a lattice instability must occur below T_S. In fact,

there may be several different such instabilities (Stroud and Ashcroft 1972, Pietronero 1987, Fecht and Johnson 1988), but not much is known about them.

The extrapolation of C_p in the liquid to temperatures below T_{fus}, has been the subject of much modelling, but the situation is still unclear. When the liquid has been undercooled to a temperature T_g, there will be a *glass transition*, characterised by an increase of the viscosity by many orders of magnitude, so that the material transforms to a glassy solid state.

EQUATION OF STATE AND THERMAL EXPANSION: MACROSCOPIC RELATIONS

1. Introduction

Arguably, the best known non-trivial relation in thermodynamics is the ideal gas law,

$$pV = Nk_BT. \tag{13.1}$$

This is an *equation-of-state* (EOS), i.e. a relation between the pressure p, the volume V and the temperature T. For gases, pressure is a very important variable. In materials science, on the other hand, pressure may seem to be of little importance, with an obvious exception being geophysical applications. For instance, we noted in Chapter 1 that the standard thermodynamic properties are now recommended to be evaluated at 10^5 Pa (1 bar) while they were previously referring to the "normal" ambient pressure, 101,325 Pa (1 atm). For example, the two reference levels for the pressure lead to a difference in the standard entropy $S^\circ_{298.15}$ of aluminium by $\sim 10^{-6}$ J/(K mol), to be compared with the full value $S^\circ_{298.15} = 28.275$ J/(K mol). Even if we take zero pressure instead of 101,325 Pa, it would increase $S^\circ_{298.15}$ by less than 0.001 J/(K mol). Pressure is a variable that is usually not even mentioned in tables of properties like the electrical and thermal conductivity. Yet almost every textbook on solid state physics contains the formula

$$C_p - C_V = VT\beta^2K_T, \tag{13.2}$$

where C_p and C_V are the heat capacities at constant pressure and volume, β is the cubic expansion coefficient and K_T is the isothermal bulk modulus. The main reason is a fundamental difference between experiments and theory. Experiments are easily performed at constant (e.g.

ambient) pressure and it can be quite difficult to impose the condition of constant volume instead. Theories of solids, on the other hand, are most easily formulated at constant volume. There is a need to convert one set of data to the other. (One may note in this context that "heat capacity at constant volume" is not quite the same as "heat capacity at *fixed* volume"; see §7.)

At a given temperature, the ideal gas law provides a universal relation between the pressure and the volume. When this is not accurate enough one may resort to a vast number of equations-of-state, the best known being the van der Waals equation that contains two parameters specific for the considered gas. For solids there is no universal equation-of-state corresponding to the ideal gas law but there are numerous equations-of-state containing parameters characteristic of the material, for instance the Murnaghan equation.

Finally, it should be remarked that one may distinguish between "*thermal* equations of state" that give a relation of the form $p = p(V, T)$ and "*caloric* equations of state" that give a relation of the form $U = U(V, T)$ or $H = H(p, T)$. Taken together, they give a complete thermodynamic description. Here we will be concerned mainly with the thermal equation of state, and often the temperature dependence will be ignored so that we just formulate a $p - V$ relation.

This chapter presents thermal equations-of-state and closely related thermodynamic relations where the approach is macroscopic, i.e. without any attempt to connect explicitly to lattice vibrations and conduction electrons. Such aspects are considered in the next chapter, on thermal expansion.

2. Power series in pressure or volume

Let $V(p, T)$ be the volume of a specimen and V_0 its volume at $p = 0$ and temperature T. We expand $V(p, T)$ in powers of p;

$$V = V_0\{1 + a_1(T)p + a_2(T)p^2 + a_3(T)p^3 + \cdots\}. \tag{13.3}$$

The isothermal compressibility $\kappa_T = (-1/V)(\partial V/\partial p)_T$ is usually taken in the limit of zero ($\sim$atmospheric) pressure. Then (K is the bulk modulus)

$$\kappa_T = K_T^{-1} = -a_1(T). \tag{13.4}$$

Keeping only the first three terms in the series expansion eq. (13.3) gives

$$V/V_0 = 1 + a_1(T)p + a_2(T)p^2. \tag{13.5}$$

If we consider a fixed temperature and regard $V(p = 0) = V_0$ as known, eq. (13.5) is a two-parameter equation of state. However, there are other two-parameter relations between V and p at fixed T. For instance, we can assume that the isothermal bulk modulus K_T varies linearly with p;

$$K_T(p; T) = K_0(T) + K_0'(T)p. \tag{13.6}$$

Here $K_0'(T) = \partial K_T(p, T)/\partial p$ is evaluated at $p = 0$. As seen in the following example, the dimensionless parameter K_0' typically is between 4–6. (Many authors use the symbol B for the bulk modulus and hence introduce a quantity denoted B_0'.)

In analogy to the approach above we may also expand the pressure in powers of the small quantity $(V_0 - V)/V$;

$$p = b_1(T)\left(\frac{V_0 - V}{V}\right) + b_2(T)\left(\frac{V_0 - V}{V}\right)^2 + \cdots. \tag{13.7}$$

If $V - V_0$ from eq. (13.3) is inserted in eq. (13.7), and the coefficients of equal powers of p on the left- and righthand sides are put equal, we obtain relations between a_1, a_2 and b_1, b_2. In particular, when only the lowest-order terms are kept,

$$K_T = \kappa_T^{-1} \approx b_1. \tag{13.8}$$

Example: the parameter K_0' in real solids. We noted in Chapter 4 (§6) that for cubic lattice symmetry, $(\partial K/\partial p)$ can be expressed in third-order elastic coefficients as

$$\left(\frac{\partial K}{\partial p}\right)_{p=0} = K_0'(T) = -\frac{c_{111} + 6c_{112} + 2c_{123}}{9K}, \tag{13.9}$$

where $K = (c_{11} + 2c_{12})/3$. With experimental data for elastic coefficients from Every and McCurdy (1992) we obtain the results in table 13.1. Here we have ignored the small difference at room temperature between isothermal (K_0') and isentropic (the experimental c_{ij} and c_{ijk}) quantities. For many materials, $K_0' \approx 4$–5. It is worth noting how little

Table 13.1

The dimensionless parameter $K_0' = (\partial K / \partial p)$, and the bulk modulus K (in GPa), as
calculated from experimental second- and third-order elastic coefficients

	Al	Fe	Nb	Ge	C[a]	GaAs	NaCl	MgO	CaF$_2$
K_0'	5.2	5.1	6.8	4.0	4.9	4.6	4.5	3.9	5.3
K	77	167	170	75	442	75	25	160	86

[a] Diamond

K_0' varies from one material to another, when compared with the much
larger variation in the magnitude of the bulk modulus itself.

3. The Murnaghan equation of state

From the definition $K_T(p) = -V(\partial p / \partial V)_T$, and with the notation
$V_0 = V(p=0; T)$, we find from eq. (13.6) Murnaghan's (1944)
logarithmic *equation-of-state*,

$$\ln[V_0 / V] = \frac{1}{K_0'} \ln[1 + (K_0'/K_0)p]. \tag{13.10}$$

Often it is written in the mathematically equivalent form

$$p = \frac{K_0}{K_0'} \left[\left(\frac{V_0}{V} \right)^{K_0'} - 1 \right]. \tag{13.11}$$

It should be remarked that our simple derivation of eq. (13.10) is not
quite satisfying from a physical point of view but a correct treatment
yields the same mathematical expression as eq. (13.10).

At low pressures, the expressions (13.3) and (13.10) are of course
equivalent. (Keep only the term linear in p and use the fact that $K^{-1} = -a_1$.) It has been empirically established (Anderson 1966b) that for
many solids, Murnaghan's equation gives a better representation than
the polynomial expression (13.3), even if p^3 and p^4 terms are included
in the polynomial.

Since $K_T = -V(\partial p / \partial V)_T$ we get, from eq. (13.11),

$$\frac{K_T(V; T)}{K_T(V_0; T)} = \left(\frac{V_0}{V} \right)^{K_0'(T)}. \tag{13.12}$$

We can also use $p = -(\partial U/\partial V)$ and eq. (13.11) to get a relation for U as a function of V, in analogy to the functions $U_{\text{coh}}(V)$ considered in Chapter 1. However, $U(V)$ obtained in this way only contains parameters K_0 and K_0' referring to properties of the solid at the equilibrium volume. Therefore, it only describes $U(V)$ for small $V - V_0$. In fact, this $U(V)$ diverges for large V and does not give a relation to cohesive energies.

The quantity $K_0'(T) = \partial K_T(p, T)/\partial p$ is temperature dependent; often increasing with T but it may also decrease. Fernández Guillermet (1995) has summarised and extended work on this temperature dependence in relation to Murnaghan's equation-of-state.

4. A universal binding energy relation

In Chapter 1 (§2) we introduced a relation $U(\lambda)$ that gives the variation of the total energy of the solid as a function of a parameter λ that can be, for instance, a lattice parameter. From $U(\lambda)$ we get the cohesive energy U_{coh} and the bulk modulus K. The example of $U(\lambda)$ shown in fig. 1.1 used the familiar 6–12 Lennard–Jones potential. We may call $U(\lambda)$ a *cohesive-binding-energy* relation. There is an empirical cohesive-binding-energy relation that has been found to account for a large number of experimental data for cohesive properties (Ferrante et al. 1983, Rose et al. 1981, 1983, 1984). In its three-parameter form it is assumed that the volume V_0 and the bulk modulus K_0 at the equilibrium conditions, and the cohesive energy U_{coh}, are known. Then the binding energy relation has the form of the mathematical Rydberg function;

$$U(\lambda)/U_{\text{coh}}(\lambda) = -(1 + \lambda)\exp(-\lambda). \tag{13.13}$$

The scaled length parameter λ is

$$\lambda = \frac{9V_0 K_0}{E_{\text{coh}}}\left(\frac{R}{R_0} - 1\right), \tag{13.14}$$

where $R/R_0 = (V/V_0)^{1/3}$. From eq. (13.13) and $p = -\partial U/\partial V$ we easily derive an equation-of-state. The relation (13.13) is known as the *universal-binding-energy relation* (UBER). It describes well the shape of the binding-energy curves for a wide class of systems, including

ordinary bulk cohesion of solids, diatomic molecules, chemisorption and adhesion (Ferrante et al. 1983). There is much work discussing this type of relation; see for instance an extension to relations with more parameters (In Ho Kim et al. 1992).

5. Other equations-of-state

There are numerous other equations-of-state (Holtzapfel 1996, Poirier 1991, Anderson 1995). One of the best known is the *Birch–Murnaghan equation-of-state*, in which Birch (1938, 1947, 1952) extends a theoretical basis by Murnaghan (1937). It can be written

$$
p = \frac{3}{2} K_T \left\{ \left(\frac{V_0}{V} \right)^{7/3} - \left(\frac{V_0}{V} \right)^{5/3} \right\}
$$
$$
\times \left\{ 1 + \frac{3}{4} (K_0' - 4) \left[\left(\frac{V_0}{V} \right)^{2/3} - 1 \right] \right\}. \tag{13.15}
$$

The form in eq. (13.15) is called the Birch–Murnaghan equation-of-state of third order. Earlier, and following Birch, the quantity $(3/4)(4 - K_0')$ was denoted ξ. With $K_0' = 4$ we get the corresponding equation of second order.

The *Mie–Grüneisen equation-of-state* is briefly treated in Chapter 14 (§4.1). Thomsen and Anderson (1969) discussed the partial lack of consistency between the Mie–Grüneisen equation and other equations-of-state like the Murnaghan equation, and warn against the simultaneous use of equations-of-state that are not mutually consistent.

6. Some important thermodynamic relations

6.1. Definitions

For later reference we define some important thermodynamic quantities and express them as derivatives of thermodynamic functions. They refer to isotropic systems (including cubic lattice symmetry). Anisotropic quantities are considered in §8 and §9.

The *heat capacities* at *constant volume*, and at *constant pressure*, are defined by

$$C_V = \left(\frac{\partial U}{\partial T}\right)_V = T\left(\frac{\partial S}{\partial T}\right)_V, \tag{13.16}$$

$$C_p = \left(\frac{\partial H}{\partial T}\right)_p = T\left(\frac{\partial S}{\partial T}\right)_p. \tag{13.17}$$

The *isothermal* and the *isentropic* (also called *adiabatic*) *compressibilities* κ and *bulk moduli* K are defined by

$$\kappa_T = (K_T)^{-1} = -\frac{1}{V}\left(\frac{\partial V}{\partial p}\right)_T = \frac{1}{V}\left(\frac{\partial^2 F}{\partial V^2}\right)_T^{-1}, \tag{13.18}$$

$$\kappa_S = (K_S)^{-1} = -\frac{1}{V}\left(\frac{\partial V}{\partial p}\right)_S = \frac{1}{V}\left(\frac{\partial^2 U}{\partial V^2}\right)_S^{-1}. \tag{13.19}$$

Thermal expansion is decribed by the *cubic expansion coefficient*. It can be expressed in the Helmholtz energy F, or the entropy S;

$$\beta = \frac{1}{V}\left(\frac{\partial V}{\partial T}\right)_p = -\frac{1}{V}\frac{(\partial p/\partial T)_V}{(\partial p/\partial V)_T} = \frac{1}{K_T}\left(\frac{\partial p}{\partial T}\right)_V$$

$$= -\frac{1}{K_T}\left(\frac{\partial^2 F}{\partial T\partial V}\right) = \frac{1}{K_T}\left(\frac{\partial S}{\partial V}\right)_T, \tag{13.20}$$

where we have used

$$p = -\left(\frac{\partial F}{\partial V}\right)_T. \tag{13.21}$$

There is a simple expression for βK_T;

$$\beta K_T = -\left(\frac{\partial V}{\partial T}\right)_p\left(\frac{\partial p}{\partial V}\right)_T = \left(\frac{\partial p}{\partial T}\right)_V = \left(\frac{\partial S}{\partial V}\right)_T. \tag{13.22}$$

The *thermodynamic Grüneisen parameter* γ_G is defined by

$$\gamma_G = \frac{\beta V K_T}{C_V}. \tag{13.23}$$

This is a very important quantity, which can also be written

$$\gamma_G = -\frac{V}{C_V}\frac{(\partial V/\partial T)_p}{(\partial V/\partial p)_T} = \frac{V(\partial p/\partial T)_V}{C_V} = \frac{V(\partial S/\partial V)_T}{C_V}. \quad (13.24)$$

The Grüneisen parameter γ_G is sometimes called the Grüneisen constant. However, it may vary by a factor of two or more as a function of T, thus being far from a constant, and should rather be called the Grüneisen function $\gamma_G(T, V)$. Still, γ_G varies much less than C_V and β as a function of T. (The name Grüneisen *ratio* has also been used, for reasons that are obvious; cf. eq. (8.6).)

Besides the Grüneisen parameter there are other useful dimensionless parameters that describe thermoelastic behaviour. One of them is the *Anderson-Grüneisen parameter* δ (Grüneisen 1912, Anderson 1966a, Barron 1979). It was earlier called the second Grüneisen parameter. We define Anderson–Grüneisen parameters δ_T and δ_S by

$$\delta_T = -\frac{1}{\beta K_T}\left(\frac{\partial K_T}{\partial T}\right)_p, \quad (13.25)$$

$$\delta_s = -\frac{1}{\beta K_S}\left(\frac{\partial K_S}{\partial T}\right)_p. \quad (13.26)$$

Using thermodynamic identities we obtain the relations

$$\delta_T = -\frac{1}{\beta K_T}\left(\frac{\partial K_T}{\partial T}\right)_p = -\left(\frac{\partial \ln K_T}{\partial \ln V}\right)_p = \left(\frac{\partial \ln \beta}{\partial \ln V}\right)_T, \quad (13.27)$$

with an analogous relation for δ_S.

In the example in Chapter 8 (§3.3), we considered Slater's (1940) form of the Grüneisen parameter and found (when the Poisson ratio does not vary with the volume V) that $(\mathrm{d}\ln K/\mathrm{d}\ln V) = -2\gamma(-3) - 1/3$. If we, crudely, identify $\gamma(-3)$ with the thermodynamic Grüneisen parameter γ_G we get $\delta = 2\gamma_G + 1/3$. This is not a very precise relation but it supports the experimental result that $\delta \sim 4$ for many materials, and also demonstrates that δ and γ_G are related.

6.2. $C_p - C_V$ and related quantities

Using macroscopic thermodynamics, in particular Maxwell relations, one can derive a number of useful relations between C_p, C_V, K_T, K_S, κ_T, κ_S and β. Most of those quoted below, and several others, are given by Wallace (1972). The well-known relation

$$C_p - C_V = VT\beta^2 K_T \tag{13.28}$$

may be rewritten as

$$C_p - C_V = \frac{V\beta^2 K_T}{C_p^2}C_p^2 T = AC_p^2 T. \tag{13.29}$$

The merit of the last formulation is that the parameter A is often approximately constant, over a wide range of temperatures $T > \theta_D$. Therefore, $AC_p^2 T$ can be used to extrapolate $C_p - C_V$. When A is regarded as a constant, eq. (13.29) is known as the *Nernst–Lindemann relation* (Nernst and Lindemann 1911). Another relation of practical importance is

$$C_p = C_V\left(1 + \frac{\gamma_G^2 T C_V}{V K_T}\right) = C_V(1 + \beta\gamma_G T). \tag{13.30}$$

Often one calculates the bulk modulus from the elastic coefficients c_{ij} (Chapter 18, §3). Because the experimental c_{ij} usually refer to isentropic conditions, it is K_S that is obtained. Then, when reducing C_p to C_V, one may use

$$C_p = C_V\left(1 + \frac{VT\beta^2 K_S}{C_p}\right). \tag{13.31}$$

The compressibilities at constant temperature and at constant entropy are related by

$$\kappa_T - \kappa_S = \frac{VT\beta^2}{C_p}. \tag{13.32}$$

The corresponding bulk moduli obey

$$K_S - K_T = K_T K_S (\kappa_T - \kappa_S),$$ (13.33)

and

$$K_S = K_T \left(1 + \frac{V T \beta^2 K_S}{C_p} \right) = K_T (1 + \beta \gamma_G T).$$ (13.34)

Comparing eq. (13.31) and the first part of eq. (13.34) gives

$$\frac{C_p}{C_V} = \frac{K_S}{K_T} = \frac{\kappa_T}{\kappa_S}.$$ (13.35)

It follows that the thermodynamic Grüneisen parameter may be written

$$\gamma_G = \frac{\beta V K_T}{C_V} = \frac{\beta V K_S}{C_p}.$$ (13.36)

The relations (13.31) and (13.34) imply that

$$C_p > C_V; \quad K_S > K_T.$$ (13.37)

Example: C_p, C_V, K_S and K_T in aluminium. Figure 13.1 shows C_p and $K_S = (c_{11} + 2c_{12})/3$ as obtained from experiments and C_V and $K_T = K_S(C_V/C_p)$, as calculated from the relations above.

7. Thermodynamic properties reduced to fixed volume

Experiments are usually carried out at constant (i.e. ambient) pressure, while theoretical calculations are more conveniently performed at constant specimen volume. However, there is sometimes confusion about what is meant by "constant volume". In the heat capacity $C_V(T)$ one takes the ratio $\Delta U / \Delta T$ of infinitesimal quantities ΔU and ΔT at a certain temperature T_1 while the volume V is kept constant. If the ratio is taken at a different temperature T_2, the volume is again kept constant but normally $V(T_1) \neq V(T_2)$. One therefore must distinguish between
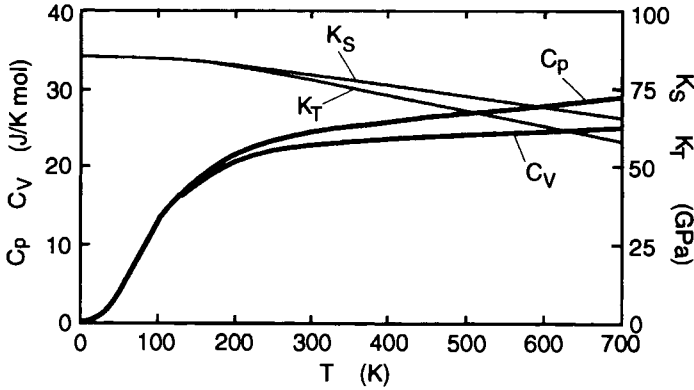
Fig. 13.1. C_p and C_V, and K_S and $K_T = (C_V/C_p)K_S$ for aluminium.

$C_{V_0}(T)$, which is C_V reduced to a fixed volume V_0, and the conventional $C_V(T) = T(\partial S/\partial T)_V$. The relation

$$\left(\frac{\partial C_V}{\partial V}\right)_T = T\left(\frac{\partial^2 S}{\partial T \partial V}\right) = T\left(\frac{\partial^2 p}{\partial T^2}\right)_V \tag{13.38}$$

gives, to lowest order in $(V - V_0)/V_0$ (cf. Wallace 1972),

$$\begin{aligned}
C_V(T) - C_{V_0}(T) &= (V - V_0)T[K_T(\partial\beta/\partial T)_p \\
&\quad + 2\beta(\partial K_T/\partial T)_p + \beta^2 K_T(\partial K_T/\partial p)_T].
\end{aligned} \tag{13.39}$$

Calculations by Wallace (1972) show that there is a strong cancellation among the terms on the righthand side of eq. (13.39). For instance, at $T = 2\theta_D$, C_{V_0} is larger than C_V by 2% in KCl and the difference changes sign at $T \sim 1.4\theta_D$. See also fig. 13.2 for W.

The reduction of the energy and the entropy to fixed volume is given by

$$\begin{aligned}
U(T, V) - U(T_0, V_0) &= \int_{T_0}^{T} C_{V_0}(T')\,dT' \\
&\quad + \int_{V_0}^{V} T^2 \frac{\partial}{\partial T}\left[\frac{p(T, V')}{T}\right] dV',
\end{aligned} \tag{13.40}$$

$$S(T, V) - S(T_0, V_0) = \int_{T_0}^{T} \frac{C_{V_0}(T')}{T'} dT'$$
$$+ \int_{V_0}^{V} \frac{\partial p(T, V')}{\partial T} dV'. \tag{13.41}$$

To lowest order in $(V - V_0)/V$, we may obtain $S(T, V) - S(T, V_0)$ directly from eq. (13.24) as

$$S(T, V) - S(T, V_0) = (V - V_0)\gamma_G C_V / V_0$$
$$= (V - V_0)\beta K_T. \tag{13.42}$$

At room temperature, $S \sim 2Nk_B$ (very roughly). Then, with $\gamma_G \sim 1.5$ and $C_V \sim 3Nk_B$, we obtain, as a crude estimate, $[S(V) - S(V_0)]/S(V_0) \sim 2(V - V_0)/V_0$. Thus, the difference between room temperature values of $S(V)$ and $S(V_0)$ is often $\sim 1\%$ if $V - V_0$ is due to the thermal expansion from 0 K to room temperature.

The expansion coefficient β depends on the volume as (cf. eq. (13.22))

$$\left(\frac{\partial \beta(T, V)}{\partial V}\right)_T = \frac{1}{K_T}\left(\frac{\partial^2 S(V, T)}{\partial V^2}\right)$$
$$- \frac{1}{K_T^2}\left(\frac{\partial K_T}{\partial V}\right)_T \left(\frac{\partial S}{\partial V}\right)_T. \tag{13.43}$$

To lowest order in $V - V_0$ we have

$$\beta(V) - \beta(V_0) = \frac{V - V_0}{V_0} \frac{1}{K_T} \left(\frac{\partial K_T}{\partial T}\right)_p. \tag{13.44}$$

The temperature dependence of elastic constants is discussed in Chapter 4 §8.

Example: heat capacity of tungsten, reduced to fixed volume. Using the formalism above, and available experimental data, Fernández Guillermet and Grimvall (1991a) obtained the heat capacity of tungsten at fixed volume V_0 (the volume at 298 K) (fig. 13.2). An interpretation in terms of anharmonic shifts in the Debye temperature $\theta_D(0)$ is given in the example in Chapter 8 (§6).
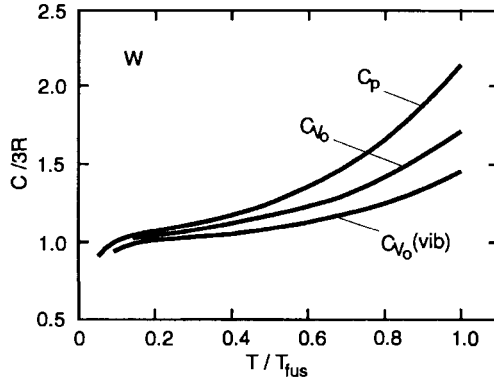
Fig. 13.2. The total heat capacity of tungsten at constant pressure, C_p, and the heat capacity C_{V_0} which is reduced to fixed volume $V_0 = V(300\ \text{K})$, as a function of the reduced temperature T/T_{fus}, where $T_{\text{fus}} = 3695$ K is the melting temperature. Also shown is C_{V_0} with an electronic term subtracted, to yield $C_{V_0}(\text{vib})$.

8.   Thermal expansion in anisotropic solids

Quite generally, the *linear* expansion coefficient, $\boldsymbol{\alpha}$, is a symmetric tensor of rank two. It is related to the symmetric strain tensor $\boldsymbol{\varepsilon}$ by

$$
\begin{pmatrix}
\varepsilon_{11} & \varepsilon_{12} & \varepsilon_{13} \\
\varepsilon_{12} & \varepsilon_{22} & \varepsilon_{23} \\
\varepsilon_{13} & \varepsilon_{23} & \varepsilon_{33}
\end{pmatrix}
=
\begin{pmatrix}
\alpha_{11} & \alpha_{12} & \alpha_{13} \\
\alpha_{12} & \alpha_{22} & \alpha_{23} \\
\alpha_{13} & \alpha_{23} & \alpha_{33}
\end{pmatrix}
\Delta T,
\tag{13.45}
$$

where ε_{ij} are the strains caused by a temperature increment ΔT. The *cubic* (i.e. volume) expansion coefficient, β, is obtained through the relation $\Delta V/V = \varepsilon_{11} + \varepsilon_{22} + \varepsilon_{33}$. One has

$$
\beta = \alpha_{11} + \alpha_{22} + \alpha_{33}.
\tag{13.46}
$$

A general definition of α_{ij} is

$$
\alpha_{ij} = \left(\frac{\partial \varepsilon_{ij}}{\partial T} \right)_{\sigma}.
\tag{13.47}
$$

The derivative is taken with all components σ_{ij} of the stress tensor held constant. Usually, σ refers to constant (ambient) pressure p, and we write

$$
(\alpha_{ij})_p = \left(\frac{\partial \varepsilon_{ij}}{\partial T} \right)_p.
\tag{13.48}
$$

Table 13.2

Non-vanishing α_{ij} and α_μ in different crystal symmetries

Symmetry	Tensor components α_{ij}	In Voigt's notation
Cubic	$\alpha_{11} = \alpha_{22} = \alpha_{33} = \alpha = \beta/3$	$\alpha_1 = \alpha_2 = \alpha_3 = \alpha$
Hexagonal		
Trigonal	$\alpha_{11} = \alpha_{22} = \alpha_\perp; \alpha_{33} = \alpha_\parallel$	$\alpha_1 = \alpha_2 = \alpha_\perp; \alpha_3 = \alpha_\parallel$
Tetragonal		
Orthorhombic	$\alpha_{11}, \alpha_{22}, \alpha_{33}$	$\alpha_1, \alpha_2, \alpha_3$
Monoclinic	$\alpha_{11}, \alpha_{22}, \alpha_{33}, \alpha_{13}$	$\alpha_1, \alpha_2, \alpha_3, \alpha_5/2$
Triclinic	$\alpha_{11}, \alpha_{22}, \alpha_{33}, \alpha_{13}, \alpha_{12}$	$\alpha_1, \alpha_2, \alpha_3, \alpha_5/2, \alpha_6/2$

Table 13.2 gives the independent α_{ij} in different crystal symmetries. It also gives α_{ij} expressed as α_μ, with only one index $\mu = 1$–6, using Voigt's contraction scheme (table 3.1).

The linear expansion coefficient in a certain crystallographic direction $[hkl]$ is

$$\alpha[hkl] = n_1^2\alpha_{11} + n_2^2\alpha_{22} + n_3^2\alpha_{33}. \tag{13.49}$$

Here, n_1, n_2 and n_3 are the direction cosines of $[hkl]$. In axial crystals (hexagonal, trigonal and tetragonal lattices),

$$\begin{aligned} \alpha[hkl] &= (n_1^2 + n_2^2)\alpha_{11} + n_3^2\alpha_{33} = \alpha_\perp \sin^2\theta + \alpha_\parallel \cos^2\theta \\ &= \alpha_\perp + (\alpha_\parallel - \alpha_\perp)\cos^2\theta, \end{aligned} \tag{13.50}$$

where θ is the angle between $[hkl]$ and the c-axis, and we have used the result that $n_1^2 + n_2^2 + n_3^2 = 1$.

Example: thermal expansion in some axial crystals. Table 13.3 gives $\alpha_\perp$ and $\alpha_\parallel$ in some metallic and non-metallic crystals, with data from Touloukian et al. (1975, 1977). The cubic expansion coefficient is

$$\beta = 2\alpha_\perp + \alpha_\parallel. \tag{13.51}$$

Note that magnesium (hcp structure) is almost isotropic in its expansion properties, while hcp zinc, which is also a divalent metal in the same column in the Periodic Table as Mg, is very anisotropic.

Table 13.3

Linear thermal expansion coefficients in some axial crystals (at 293 K)

	Be	Mg	Zn	Zr	β-Sn	RuO$_2$	SiO$_2$	Al$_2$O$_3$
$\alpha_\perp$ [10^{-6} K^{-1}]	12	25	14	4	16	6	12	6
$\alpha_\parallel$ [10^{-6} K^{-1}]	10	26	64	7	33	-2	7	5

9. Grüneisen parameters in non-cubic lattices

9.1. General relations

In an anisotropic solid, Grüneisen parameters $\gamma_{G,i}$ are defined as a generalisation of the relation $\gamma = (V/C_V)(\partial S/\partial V)_T$ for the isotropic case. We have (see, for example, Wallace 1972, Barron et al. 1980 and eq. (8.32))

$$\gamma_{G,i} = \frac{1}{C_\varepsilon}\left(\frac{\partial S}{\partial \varepsilon_i}\right)_{T,\varepsilon_i'}, \tag{13.52}$$

where $C_\varepsilon(T)$ is the heat capacity at constant strain ε, a quantity that is further discussed below. The index ε_i' in the derivative means that all strain components except ε_i are held constant.

The generalisations of the relations $\gamma_G = V\beta K_T/C_V = V\beta K_S/C_p$ are, with Voigt's notation for α_μ,

$$\gamma_{G,i} = (V/C_\varepsilon)\sum_{j=1}^{6}(c_{ij})_T\alpha_j, \tag{13.53}$$

$$\gamma_{G,i} = (V/C_\sigma)\sum_{j=1}^{6}(c_{ij})_S\alpha_j. \tag{13.54}$$

There are six components of the Grüneisen parameter, $\gamma_{G,i}$ ($i = 1$–6). C_σ is the heat capacity at constant stress σ, and c_{ij} are elastic stiffness coefficients. The "inverse" relations to eqs. (13.53) and (13.54) are

$$\alpha_i = (C_\varepsilon/V)\sum_{j=1}^{6}(s_{ij})_T\gamma_{G,j}, \tag{13.55}$$

$$\alpha_i = (C_\sigma/V) \sum_{j=1}^{6} (s_{ij})_S \gamma_{G,j}. \tag{13.56}$$

We also note the following result (e.g. Musgrave 1970);

$$(s_{ij})_T - (s_{ij})_S = \frac{VT\alpha_i\alpha_j}{C_\sigma}. \tag{13.57}$$

When all $\alpha_i > 0$, which is often the case,

$$(c_{ij})_S > (c_{ij})_T, \tag{13.58}$$

$$(s_{ij})_T > (s_{ij})_S, \tag{13.59}$$

which should be compared with the general result that $K_S > K_T, \kappa_S < \kappa_T$ (eq. (13.37)).

Example: reduction of general formulae to cubic symmetry. As an illustration we check that eqs. (13.55) and (13.56) contain the well-known relations (13.36) for a cubic lattice. Then, $\alpha_1 = \alpha_2 = \alpha_3 = \alpha$, while $\alpha_i = 0$ when $i = 4, 5$ and 6. Furthermore, $C_\varepsilon = C_V$. Hence,

$$\beta = 3\alpha = \sum_{i=1}^{6} \alpha_i = (C_V\gamma_G/V) \sum_{i,j=1}^{6} (s_{ij})_T = C_V\gamma_G/(VK_T).$$

$$\tag{13.60}$$

Here we have used the result from eq. (3.21) that $1/K_T = \sum(s_{ij})_T$. Similarly, from eq. (13.56), when $\gamma_{G,i} = \gamma_G$ and with $C_\sigma = C_p$,

$$\beta = 3\alpha = \sum_{i=1}^{6} \alpha_i = (C_p\gamma_G/V) \sum_{i,j=1}^{6} (s_{ij})_S = C_p\gamma_G/(VK_S).$$

$$\tag{13.61}$$

We also easily see that eq. (13.57) for cubic lattices reduces to the correct result, eq. (13.32). Then $\kappa_T - \kappa_S = \sum[(s_{ij})_T - (s_{ij})_S] = 9\alpha^2 VT/C_p = \beta^2 VT/C_p$.

9.2. Grüneisen parameters in hexagonal lattices

An important special case is that of *hexagonal* lattice symmetry. (The same relations hold for *trigonal* and *tetragonal* lattices.) There are only two independent quantities α_{ij}, i.e. $\alpha_\perp$ and $\alpha_\parallel$. Furthermore, there are two independent Grüneisen parameters; $(\gamma_G)_\perp$ and $(\gamma_G)_\parallel$. Performing the summations in eq. (13.54) we obtain, for a stress corresponding to hydrostatic pressure p,

$$(\gamma_G)_\perp = (V/C_p)\{[(c_{11})_S + (c_{12})_S]\alpha_\perp + (c_{13})_S\alpha_\parallel\}, \tag{13.62}$$

$$(\gamma_G)_\parallel = (V/C_p)\{2(c_{13})_S\alpha_\perp + (c_{33})_S\alpha_\parallel\}. \tag{13.63}$$

The "inversion" of these relations gives

$$\alpha_\perp = (C_p/V)\{[(s_{11})_S + (s_{12})_S](\gamma_G)_\perp + (s_{13})_S(\gamma_G)_\parallel\}, \tag{13.64}$$

$$\alpha_\parallel = (C_p/V)\{2(s_{13})_S(\gamma_G)_\perp + (s_{33})_S(\gamma_G)_\parallel\}. \tag{13.65}$$

We may now write the cubic expansion coefficient as

$$\beta = 2\alpha_\perp + \alpha_\parallel = C_p\gamma_{G,\text{hex}}/VK_S, \tag{13.66}$$

with

$$\gamma_{G,\text{hex}} = [2(\kappa_\perp)_S(\gamma_G)_\perp + (\kappa_\parallel)_S(\gamma_G)_\parallel]/\kappa_S, \tag{13.67}$$

i.e. $\gamma_{G,\text{hex}}$ is a weighted average of $\gamma_\perp$ and $\gamma_\parallel$. The quantities $\kappa_\perp$ and $\kappa_\parallel$ are properly defined compressibilities. Analogous relations for *orthorhombic* crystals are found in Barron et al. (1980).

Let the axes of the hexagonal unit cell have the conventional lengths a and c. Then $d\varepsilon_1 = d\varepsilon_2 = da/a$ and $d\varepsilon_3 = dc/c$. Hence, we can write

$$\alpha_\perp = (\partial \ln a/\partial T)_p, \tag{13.68}$$

$$\alpha_\parallel = (\partial \ln c/\partial T)_p. \tag{13.69}$$

Furthermore,

$$(\gamma_G)_\perp = (1/2C_\varepsilon)(\partial S/\partial \ln a)_{T,c}, \tag{13.70}$$

$$(\gamma_{\mathrm{G}})_{\parallel} = (1/C_{\varepsilon})(\partial S/\partial \ln c)_{T,a}. \tag{13.71}$$

Munn (1969) has discussed the thermal expansion of Zn, Cd, Mg, Sn, In, Bi and Sb, which all have axial lattice structures. There is an empirical correlation that $(\gamma_{\mathrm{G}})_{\perp} > (\gamma_{\mathrm{G}})_{\parallel}$ if $(c/a) > (c/a)_{\mathrm{ideal}}$ in the hcp lattices.

9.3. Generalisation of $C_p - C_V$ to non-cubic lattices

For isotropic materials, or crystals of cubic symmetry,

$$C_p - C_V = VT\beta^2 K_T. \tag{13.72}$$

C_p is the heat capacity measured with the stresses $\sigma_i = -p$ $(i = 1, 2, 3)$ and $\sigma_i = 0$ $(i = 4, 5, 6)$. Sometimes, eq. (13.72) is used to find C_V from the measured C_p. However, this C_V is *not* the heat capacity at constant dimensions of the crystallographic unit cell. Instead it refers to constant volume *and* isotropic stress, i.e. there will be changes in the shape of the unit cell. We shall denote this heat capacity $\tilde{C}$. Thus,

$$\tilde{C}_V = C_p - VT\beta^2 K_T, \tag{13.73}$$

for a crystal of any symmetry. The generalisation of eq. (13.72) to anisotropic solids is (Truesdell and Toupin 1960, Barron and Munn 1968)

$$C_{\sigma} - C_{\varepsilon} = VT \sum_{i,j=1}^{6} \alpha_i \alpha_j (c_{ij})_T. \tag{13.74}$$

Here, the heat capacity C_{σ} refers to constant stress and C_{ε} to constant strain. When the specimen is under a hydrostatic pressure p, we have $C_{\sigma} = C_p$. In theoretical calculations, it is attractive to assume that not only the total volume, but also the shape of the unit cell is kept constant. It is therefore of interest to know how much C_{ε} differs from $\tilde{C}$ calculated by eq. (13.73). In axial lattices one has (Barron and Munn 1968)

$$\frac{\tilde{C}_V - C_{\varepsilon}}{C_{\varepsilon}} = \frac{2(TC_{\varepsilon}/V)[(\gamma_{\mathrm{G}})_{\perp} - (\gamma_{\mathrm{G}})_{\parallel}]^2}{(c_{11} + c_{12})_T + 2(c_{33})_T - 4(c_{13})_T}. \tag{13.75}$$

Finally we note the following inequality, valid for any lattice symmetry (Barron and Munn 1968);

$$C_p \geq \tilde{C}_V \geq C_{\varepsilon}. \tag{13.76}$$

Table 13.4

$\tilde{C} - C_\varepsilon$ in hexagonal lattices

Material	$(\gamma_G)_\perp$	$(\gamma_G)_\parallel$	$(\tilde{C} - C_\varepsilon)/3Nk_B$
Magnesium (283 K)	1.54	1.55	0.0000
Zinc (283 K)	2.15	1.98	0.0004
Zinc (600 K)	2.18	1.72	0.0084
Zirconium (300 K)	0.86	1.03	0.0012
Graphite (1000 K)	1.06	0.38	0.0029

The last inequality becomes an equality if and only if $\gamma_1 = \gamma_2 = \gamma_3$.

Example: $\tilde{C} - C_\varepsilon$ in hexagonal lattices. Barron and Munn (1968) investigated $\tilde{C} - C_\varepsilon$ for several cubic solids. Table 13.4 is based on some of their results.

9.4.   Generalisation of $K_T C_p = K_S C_V$ to non-cubic lattices

For an isotropic solid one has the equality $K_T C_p = K_S C_V$, but in an anisotropic solid $K_T C_\sigma \neq K_S C_\varepsilon$ in general. Then the definition of $\gamma_G(T; V)$ is not unique. We may consider

$$\gamma_G(T; \varepsilon) = \beta V K_T / C_\varepsilon = (V/C_\varepsilon)(\partial S/\partial V)_{T, \text{isotropic strain}}, \quad (13.77)$$

or

$$\gamma_G(T; \sigma) = \beta V K_S / C_\sigma = -(V/T)(\partial T/\partial V)_{S, \text{isotropic stress}}. \quad (13.78)$$

The quantity $\gamma_G(T; \varepsilon)$ has been discussed by Collins and White (1964) and $\gamma_G(S; \sigma)$ by Barron and Munn (1967). For an isotropic solid $\gamma(\mathbf{q}, s)$ is a constant, but in the expression above, $\gamma(\mathbf{q}, s; \varepsilon)$ and $\gamma(\mathbf{q}, s; \sigma)$ depend on the temperature unless all ratios $s_{ij}(T)/s_{i'j'}(T)$ remain constant. However, the variations in $s_{ij}(T)/s_{i'j'}(T)$ are due to higher-order anharmonic effects and therefore are small. Barron and Munn (1967) estimate that, in zinc, $\partial \ln \omega(\mathbf{q}, s)/\partial \ln V$ at isotropic stress and constant S varies by a few percent from 0 K to room temperature.

THERMAL EXPANSION: MICROSCOPIC ASPECTS

1. Introduction

Most materials increase their volume as the temperature T is raised. Since also the thermal displacement of atoms increases, one might think that the atoms "push" their neigbours apart. However, this is a misleading argument. A crystal described with perfectly harmonic lattice vibrations shows no thermal expansion at all. Many solids, for instance silicon and germanium and some alkali halides, shrink with increasing T, at low temperatures. Some solids with non-cubic lattice structures, for instance zinc and uranium, shrink in one direction but expand in others so that there is a net volume increase. There are also materials, such as invar alloys, which have a very small or slightly negative coefficient of thermal expansion at ambient temperatures. Figure 14.1 exemplifies how the cubic expansion coefficient β varies with T.

A correct approach to thermal expansion relies on basic thermodynamics, in particular the fact that the volume of a solid in thermal equilibrium is such that it minimises the Helmholtz energy. A temperature dependence of the specimen volume V arises when there are contributions to F which vary with both T and V (under restrictions such as a constant number of atoms and constant pressure).

The field of thermal expansion has been reviewed by Barron et al. (1980), with emphasis on the low-temperature behaviour. Monographs by Yates (1972) and Krishnan et al. (1979) give a general introduction and a detailed survey of experimental data. See also Wallace (1972) for a more theoretical account.
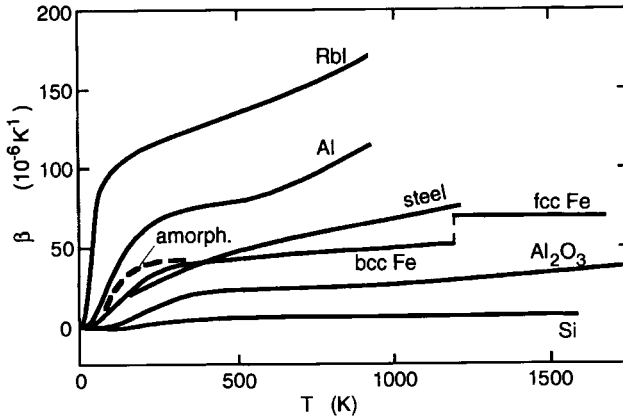
Fig. 14.1. The cubic expansion coefficient $\beta(T)$ of RbI, Al, α-Fe (bcc) and β-Fe (fcc), a stainless steel, amorphous $Pd_{0.775}Si_{0.165}Cu_{0.06}$, Al_2O_3 and Si. Data from Touloukian et al. (1975, 1977) and, for Pd–Si–Cu, from Kaspers et al. (1983). The curves for RbI, Al and Si end at the melting temperatures.

2. General relations

We simplify the problem and assume an isotropic material, or a single crystal with cubic lattice symmetry, so that the thermal expansion is isotropic. (Macroscopic aspects of anisotropy were considered in Chapter 13 (§8). They can be connected to microscopic aspects along the lines of the present chapter.) We also assume that the material is under hydrostatic pressure (including atmospheric pressure, i.e. $p \approx 0$). The *cubic expansion coefficient* β (volume expansion coefficient) is defined by

$$\beta = \frac{1}{V} \left(\frac{\partial V}{\partial T} \right)_p . \tag{14.1}$$

In an isotropic material, the *linear expansion coefficient* is

$$\alpha = \beta/3. \tag{14.2}$$

To evaluate the righthand side of eq. (14.1) we need an equation of state, i.e. a relation between p, V and T. For a comparison, consider

first the equation-of-state of an ideal gas; $pV = Nk_BT$. It yields an expansion coefficient

$$\beta = \frac{1}{V}\left(\frac{Nk_B}{p}\right) = \frac{1}{T}. \tag{14.3}$$

In contrast to this universal behaviour, β of different solids may even vary qualitatively. In many cases, however, $\beta(T)$ of a crystalline solid has a temperature dependence which is remarkably similar to that of the heat capacity. While the previous chapter described thermal expansion in terms of phenomenological relations, the theme of the present chapter is to understand the physical origin of thermal expansion in terms of electron and phonon states. For instance, that will provide an explanation for the covariation of $\beta(T)$ and $C_V(T)$ just referred to.

3. Microscopic models for thermal expansion

Let us assume that the total Gibbs (or Helmholtz) energy, and thus the entropy S, is the sum of independent contributions labelled by r. These terms may originate from atomic vibrations, electronic and magnetic excitations, etc. The relation (13.20) can be generalised as

$$\beta = \sum_r \beta_r = \frac{1}{K_T}\sum_r\left(\frac{\partial S_r}{\partial V}\right)_T. \tag{14.4}$$

Each contribution to the entropy may be associated with a *Grüneisen parameter* $(\gamma_G)_r$, through

$$(\gamma_G)_r = \frac{V}{(C_V)_r}\left(\frac{\partial S_r}{\partial V}\right)_T. \tag{14.5}$$

The total Grüneisen parameter γ_G is a weighted average of $(\gamma_G)_r$,

$$\gamma_G = \frac{\sum_r (C_V)_r (\gamma_G)_r}{\sum_r (C_V)_r}. \tag{14.6}$$

From eqs. (14.5) and (14.6) we get

$$\gamma_G = \frac{\sum_r [V/(C_V)_r](\partial S_r/\partial V)_T (C_V)_r}{\sum_r (C_V)_r} = \frac{V(\partial S/\partial V)_T}{C_V}, \tag{14.7}$$

i.e. we recover eq. (13.24), as expected. The following sections consider various contributions to β_r and $(C_V)_r$. We will see that the dimensionless parameter $(\gamma_G)_r$ in eq. (14.5) is often of the order of 2. Then the expansion coefficient has contributions from those excitations (vibrational, electronic, magnetic etc.) which contribute to a significant fraction of the heat capacity at the temperature of interest.

4. Phonon contribution to the thermal expansion

4.1. The quasiharmonic approximation

The contributions to F in a non-magnetic insulator come from the lattice vibrations. If only the terms corresponding to harmonic vibrations are kept in F, such a system has no thermal expansion. Strictly speaking, the assumption of harmonic vibrations is not quite the same as assuming interactions between the atoms to be represented by ideal springs obeying Hooke's law. In the case of such springs, and with nearest neighbour interactions, the expansion coefficient is negative (Barron 1957). The reason is that the restoring forces from springs perpendicular to the direction of an atomic displacement do depend on the strain state. Furthermore, we will see that there are cases when anharmonicity in the lattice vibrations gives rise to a thermal *contraction*. These introductory remarks serve to stress that there is no a priori reason why a solid should expand on heating, even when only lattice vibrations are considered, although expansion is of course the normal behaviour.

In the quasiharmonic approximation, each phonon mode $(\mathbf{q}, s)$ contributes to the entropy an amount (eq. (7.20))

$$S(\mathbf{q}, s) = k_B\{(x/2)\coth(x/2) - \ln[2\sinh(x/2)]\}, \qquad (14.8)$$

where $x = \hbar\omega(\mathbf{q}, s)/k_B T$. The frequency $\omega(\mathbf{q}, s; V)$ is volume dependent;

$$\left(\frac{\partial \ln\omega(\mathbf{q}, s; V)}{\partial \ln V}\right) = -\gamma(\mathbf{q}, s). \qquad (14.9)$$

(In order to avoid too many indices we write $\gamma(\mathbf{q}, s)$ rather than $\gamma_{G,ph}(\mathbf{q}, s)$ when dealing with the Grüneisen parameter for individual

phonons, and also $C_V(\mathbf{q}, s)$ instead of $C_{V,\text{ph}}(\mathbf{q}, s)$.) Because $\beta = (1/K_T)(\partial S/\partial V)_T$, we are interested in

$$\left(\frac{\partial S(\mathbf{q}, s)}{\partial V}\right)_T = \left(\frac{\partial S}{\partial x}\right)\left(\frac{\partial x}{\partial V}\right) = \frac{\hbar}{k_B T}\left(\frac{\partial \omega}{\partial V}\right)\left(\frac{\partial S}{\partial x}\right). \quad (14.10)$$

Compare this with the expression for $C_V(\mathbf{q}, s)$;

$$C_V(\mathbf{q}, s) = T\left(\frac{\partial S}{\partial T}\right)_V = T\left(\frac{\partial S}{\partial x}\right)\left(\frac{\partial x}{\partial T}\right) = -\left(\frac{\hbar\omega}{k_B T}\right)\left(\frac{\partial S}{\partial x}\right). \quad (14.11)$$

Combining eqs. (14.9)–(14.11) gives

$$\left(\frac{\partial S(\mathbf{q}, s)}{\partial V}\right)_T = [\gamma(\mathbf{q}, s)/V]C_V(\mathbf{q}, s). \quad (14.12)$$

By eq. (14.4), the cubic expansion coefficient due to all phonon modes is

$$\beta_{\text{ph}} = \frac{1}{V K_T}\sum_{\mathbf{q},s} C_V(\mathbf{q}, s)\gamma(\mathbf{q}, s). \quad (14.13)$$

If we assume that $\gamma(\mathbf{q}, s)$ is the same for all modes $(\mathbf{q}, s)$, and neglect the temperature dependence of K_T as well as non-vibrational contributions and the difference between C_p and C_V, we get that the expansion coefficient $\beta(T)$ has the same temperature dependence as the heat capacity C_p. This is sometimes called *Grüneisen's rule*, or Grüneisen's law. Furthermore, since C_V for phonons at low temperatures has the temperature dependence $A_1 T^3 + A_2 T^5 + \ldots$, the same powers of T appear in $\beta_{\text{ph}}(T)$ at low T.

We can express β_{ph} in terms of the Grüneisen parameter $\gamma_{\text{G,ph}}$ as

$$\beta_{\text{ph}} = \frac{C_{V,\text{ph}}\gamma_{\text{G,ph}}}{V K_T}, \quad (14.14)$$

giving

$$\gamma_{\text{G,ph}} = \frac{\sum_{\mathbf{q},s} C_V(\mathbf{q}, s)\gamma(\mathbf{q}, s)}{\sum_{\mathbf{q},s} C_V(\mathbf{q}, s)}. \quad (14.15)$$

At low temperatures, $C_V(\mathbf{q}, s)$ is appreciable only for those phonon modes which have $\hbar\omega(\mathbf{q}, s)/k_B T \lesssim 1$ while at high temperatures all C_V are close to the Dulong–Petit value k_B. Since $\gamma_G(\mathbf{q}, s)$ may vary by a factor of two or more between low frequency transverse modes and high frequency longitudinal modes, for example, the weighted average $\gamma_{G,ph}$ in eq. (14.15) may show a considerable temperature dependence in the range from 0 K to θ_D. At high temperatures, $T \gtrsim \theta_D$, each $C_V(\mathbf{q}, s) \approx k_B$ and $\gamma_{G,ph}$ varies very little with T.

We now turn to the volume change $\Delta V = V(T) - V(0)$. It is obtained as

$$\Delta V = \int_0^T V(T')\beta(T')\,\mathrm{d}T'. \tag{14.16}$$

If $\gamma_{G,ph}$ is approximated by a temperature-independent constant, and if we neglect the temperature dependence of K_T and other anharmonic corrections, eq. (14.16) yields

$$\Delta V = \frac{\gamma_{G,ph}}{K_T} \int_0^T C_{V,ph}(T')\,\mathrm{d}T' = \frac{\gamma_{G,ph}}{K_T}[E_{har}(T) - E_{har}(0)].$$

$$\tag{14.17}$$

$E_{har}(0)$ is the zero-point vibrational energy. When one lacks detailed information about the temperature dependence of $\gamma_{G,ph}(T)$ it may be a useful approximation to take ΔV proportional to the thermal energy, as in eq. (14.17). This, gives essentially the *Mie–Grüneisen equation of state* at zero pressure (Mie 1903, Grüneisen 1912). With an Einstein approximation for $E_{har}(T)$,

$$V(T) - V(0) = \left(\frac{3N\gamma_{G,ph}k_B T}{K_T}\right) \frac{\theta_E/T}{\exp(\theta_E/T) - 1}. \tag{14.18}$$

4.2.   Higher-order anharmonicity

We noted in Chapter 8 (§6) that the third- and fourth-order anharmonic effects are correctly accounted for if, in the harmonic expression for the entropy, one inserts the shifted frequencies

$$\omega(\mathbf{q}, s) = \omega_0(\mathbf{q}, s) + \Delta_2(\mathbf{q}, s) + \Delta_3(\mathbf{q}, s) + \Delta_4(\mathbf{q}, s). \tag{14.19}$$

In the previous section we only considered the quasiharmonic approximation, i.e. $\omega(\mathbf{q}, s) = \omega_0 + \Delta_2$. Those results are easily extended to include Δ_3 and Δ_4. We define generalised Grüneisen parameters γ_2 and γ_{34} by

$$\gamma(\mathbf{q}, s) = \gamma_2(\mathbf{q}, s) + \gamma_{34}(\mathbf{q}, s), \tag{14.20}$$

with (assuming $\Delta_2, \Delta_3, \Delta_4 \ll \omega_0$)

$$\gamma_2 = -\left(\frac{\partial \ln(\omega_0 + \Delta_2)}{\partial \ln V}\right), \tag{14.21}$$

and

$$\gamma_{34} = -\left(\frac{\partial \ln(\omega_0 + \Delta_3 + \Delta_4)}{\partial \ln V}\right), \tag{14.22}$$

where Δ_2 and $(\Delta_3 + \Delta_4)$ may be of the same order of magnitude. However, Δ_2 is directly proportional to the volume change, while $(\Delta_3 + \Delta_4)$ is likely to vary much more slowly with V. We thus expect that $\gamma_{34} \ll \gamma_2$.

From the definition of γ_G, (eq. (13.24)), we have the general relations

$$\gamma_G = \frac{V(\partial S/\partial V)_T}{C_V} = \frac{(\partial S/\partial \ln V)_T}{(\partial S/\partial \ln T)_V}. \tag{14.23}$$

It is convenient to introduce *isothermal* and *isochoric* (i.e. "constant volume") *Grüneisen parameters* (Varley 1956, Barron et al. 1980)

$$\gamma_{T,\mathrm{ph}} = -(\partial \ln \theta_D^S/\partial \ln V)_T, \tag{14.24}$$

$$\gamma_{V,\mathrm{ph}} = -(\partial \ln \theta_D^S/\partial \ln T)_V, \tag{14.25}$$

where $\theta_D^S(T)$ is the entropy Debye temperature, which is here assumed to include $\Delta_2 + \Delta_3 + \Delta_4$. After a few manipulations one obtains

$$\gamma_{G,\mathrm{ph}} = \gamma_{T,\mathrm{ph}}/(1 + \gamma_{V,\mathrm{ph}}). \tag{14.26}$$

At low temperatures, $\gamma_{V,\mathrm{ph}} \neq 0$ because the phonon spectrum is not a Debye spectrum, and this gives a temperature dependent $\theta_D^S(T)$ (Chapter 6, §8). When $T \gtrsim \theta_D^S(T)/2$, this effect is of little importance.

Instead the explicit anharmonicity gives a non-zero $\gamma_{V,\text{ph}}$ through the frequency shifts $\Delta_3 + \Delta_4$. Then, $\gamma_{V,\text{ph}} \approx (\Delta_3 + \Delta_4)/\omega_0$, which is usually less than 5% even close to the melting temperature. Furthermore, $\gamma_{T,\text{ph}} \approx \gamma_2 + \gamma_{34} \approx \gamma_2$. Therefore, the Grüneisen parameter γ_{G} derived from macroscopic thermodynamic quantities ($\gamma_{\text{G}} = \beta V K_S / C_p$) gives information about γ_2, i.e. the quasiharmonic shift. It is then assumed that β and C_p do not have significant contributions of non-vibrational origin.

Leadbetter (1968) has discussed the separation of the quasiharmonic and the explicitly anharmonic parts in S, C_V and β, with an application to Al and Pb, and a similar analysis was performed for Ge (Leadbetter and Settatree 1969), NaCl and KBr (Leadbetter et al. 1969). Rosén and Grimvall (1983) considered non-transition metals.

4.3. High-temperature expansion of $\gamma_{\text{G,ph}}$

We consider $\gamma_{\text{G,ph}}$ within the quasiharmonic approximation. From eq. (14.15) and the high-temperature expansion (eq. (7.31)) of C_V we obtain, after a rearrangement of terms (Barron et al. 1964),

$$
\begin{aligned}
\gamma_{\text{G,ph}}(T) \;=\;& \gamma(0) + (1/12)[\hbar\omega(2)/k_{\text{B}}T]^2[\gamma(0) - \gamma(2)] \\
& + (1/240)[\hbar\omega(4)/k_{\text{B}}T]^4[\gamma(4) - \gamma(0)] \\
& - (1/144)[\hbar\omega(2)/k_{\text{B}}T]^4[\gamma(2) - \gamma(0)] + \ldots . (14.27)
\end{aligned}
$$

Here, $\omega(n)$ are moment frequencies and $\gamma(n)$ corresponding Grüneisen parameters (see Chapter 8, §3.3). When $T \gg \theta_{\text{D}}$, $\gamma_{\text{G,ph}}(T) \rightarrow \gamma(0)$. A plot of $\gamma_{\text{G,ph}}(T)$ versus $1/T^2$ yields $\gamma(0)$ as the intercept at $1/T^2 = 0$. Such an analysis makes use of $\gamma_{\text{G,ph}}(T)$ at intermediate temperatures ($T \sim \theta_{\text{D}}/2$) where anharmonic effects are small. Therefore, the determination of $\gamma(0)$ is quite accurate. After $\gamma(0)$ has been obtained one may plot $[\gamma(0) - \gamma_{\text{G,ph}}(T)]T^2$ versus $1/T^2$ to give $\gamma(2)$ and $\gamma(4)$. One can prove that

$$
\gamma(n) = \frac{\int \gamma_{\text{G,ph}}(T) C_{\text{har}}(T) T^{n-1} \, dT}{\int C_{\text{har}}(T) T^{n-1} \, dT}. \tag{14.28}
$$

The integrals converge for $-3 < n < 0$. Thus, an analysis of $C_{V,\text{ph}}(T)$ may give a good estimate of $\gamma(-2)$, $\gamma(-1)$, $\gamma(0)$, $\gamma(2)$ and $\gamma(4)$. The

pressure dependence of the elastic constants yields $\gamma(-3)$. Values of $\gamma(n)$ obtained in this way are given in fig. 8.1.

5. Electronic contribution to the thermal expansion

The electronic contribution to the cubic expansion coefficient, β_{el}, is (Varley 1956)

$$\beta_{el} = \frac{C_{V,el}\gamma_{G,el}}{V K_T}. \tag{14.29}$$

$V K_T$ refers to the real solid (i.e. with all contributions to K_T included) but $C_{V,el}$ and $\gamma_{G,el}$ contain the electronic contribution only;

$$\gamma_{G,el} = \frac{V}{C_{V,el}}(\partial S_{el}/\partial V)_T. \tag{14.30}$$

Many-body electron-phonon interactions give to $S_{el}(T)$ a complicated temperature dependence at $T \sim \theta_D/5$, but in the limit of low and high temperatures ($T \lesssim \theta_D/10$ and $T \gtrsim \theta_D/2$) the theory is simple. We can write (Chapter 10, §3),

$$S_{el} = (2\pi^2/3)N(E_F)(1 + \lambda_{el-ph})k_B^2 T \quad \text{low } T; \tag{14.31}$$

$$S_{el} = (2\pi^2/3)N(E_F)k_B^2 T, \quad \text{high } T. \tag{14.32}$$

These expressions require that the electron density of states $N(E)$ varies slowly with the energy E in the vicinity of the Fermi level, so that it suffices to consider the value $N(E_F)$ at the Fermi level. The general definition of Grüneisen parameters, (eq. (14.5)), now gives for the electronic part:

$$\gamma_{G,el} = \frac{d \ln N(E_F)}{d \ln V} + \frac{d \ln(1 + \lambda_{el-ph})}{d \ln V} \quad \text{low } T; \tag{14.33}$$

$$\gamma_{G,el} = \frac{d \ln N(E_F)}{d \ln V} \quad \text{high } T. \tag{14.34}$$

In a free-electron system (Appendix B), $N(E_F) \sim (E_F)^{1/2}V \sim V^{2/3}$. Then,

$$\frac{d \ln N(E_F)}{d \ln V} = \frac{2}{3}. \tag{14.35}$$

In transition metals it has sometimes been assumed that the width W_d of the d-band varies as $V^{-5/3}$ (Heine 1967), and that the "shape" of $N_d(E)$ does not depend on V (Lang and Ehrenreich 1968). Since the area under $N_d(E)$ is invariant (5 electrons per atom and spin), it then follows that $N_d(E_F) \sim 1/W_d \sim V^{5/3}$. We get

$$\frac{d \ln N(E_F)}{d \ln V} = \frac{5}{3}. \tag{14.36}$$

The quantity $d \ln(1 + \lambda_{el-ph})/d \ln V$ has been reviewed by Grimvall (1981). A major contribution to the volume dependence of λ_{el-ph} comes from an average over the phonon frequencies; $\lambda_{el-ph} \sim 1/\langle \omega^2 \rangle = 1/[\omega(2)]^2$. If we only include that effect,

$$\begin{aligned}\frac{d \ln(1 + \lambda_{el-ph})}{d \ln V} &= \frac{\lambda_{el-ph}}{1 + \lambda_{el-ph}} \frac{d \ln \lambda_{el-ph}}{d \ln V} \\ &= \frac{2\lambda_{el-ph}}{1 + \lambda_{el-ph}} \gamma(2). \end{aligned} \tag{14.37}$$

Usually $2\lambda_{el-ph}/(1 + \lambda_{el-ph})$ lies in the interval 1/3 to 1, with a typical value of 1/2 for transition metals. An approximate value of $\gamma(2)$ is 2. Then $d \ln(1 + \lambda_{el-ph})/d \ln V \approx 1$, and we conclude that at low temperatures, the electron-phonon many-body interactions give a significant contribution to the electronic Grüneisen parameter $\gamma_{G,el}$. Hence, an account of the thermal expansion at very low temperatures ($T \lesssim \theta_D/20$), where $\beta_{el} \sim T$ dominates over the phonon part $\beta_{ph} \sim T^3$, cannot be based on a discussion of the electron-band density-of-states $N(E)$ alone. The important role of a temperature dependent many-body effect due to electron-phonon interactions and spin fluctuations at low T has been seen in Lu and Sc (Swenson 1996). At high temperatures ($T \gtrsim \theta_D/2$) a description of β_{el} in terms of $N(E_F)$ is sufficient, but then the total expansion coefficient is dominated by the phonon part β_{ph}.

Barron et al. (1980) reviewed experimental values of $\gamma_{G,el}$. Most of them lie in the interval 1.5 ± 0.5. However, $\gamma_{G,el}$ derived from low-temperature thermal expansion data are often very uncertain. Fletcher and Yahaya (1979) obtained $\gamma_{G,el}$ from band structure theory for 22 transition metals, and modern ab initio electron-structure calculations (e.g. Eriksson et al. 1992) usually yield accurate results.

Finally, we comment on the fact that for phonons the Grüneisen parameter $\gamma(\mathbf{q}, s) = -\partial \ln \omega(\mathbf{q}, s)/\partial \ln V$ is expressed as a derivative
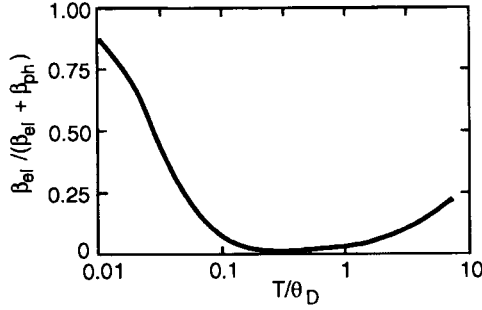
Fig. 14.2. Relative importance of the electronic and the vibrational contributions to the expansion coefficient, β_{el} and β_{ph}, in a typical transition metal and plotted as $\beta_{el}/(\beta_{ph} + \beta_{el})$ versus the temperature T.

of the individual energies (frequencies) $\omega(\mathbf{q}, s)$ while for electrons we used the macroscopic definition (14.5) of γ_G and arrived at $\gamma_{G,el} = d\ln N(E)/d\ln V$. In fact, this $\gamma_{G,el}$ is essentially equivalent with the form $\gamma_{G,el}(\mathbf{k}) = -d\ln(\varepsilon_{\mathbf{k}} - \mu)/d\ln V$ that is based on the individual electron energies $\varepsilon(\mathbf{k})$ (see Appendix B).

Example: comparison between β_{el} and β_{ph} in metals. As a model example, consider a solid described by a Debye phonon spectrum with $\gamma_{G,ph}$ = 1.5. We take $\lambda_{el-ph} = 0.5$, $d\ln(1 + \lambda_{el-ph})/d\ln V = [2\lambda_{el-ph}(1 + \lambda_{el-ph})]\gamma(2) = 1$ and $d\ln N(E_F)/d\ln V = 5/3$. Furthermore, let $C_{V,el} = Nk_BT/T_{fus}$ when $T > \theta_D$ and assume a melting temperature $T_{fus} = 8\theta_D$. These numbers are typical of a transition metal or alloy. We give VK_T an arbitrary fixed value, neglect anharmonic effects in $C_{V,ph}$ and consider only the relative importance β_{el}/β_{ph} of the electron and the phonon contributions to the thermal expansion coefficient. Figure 14.2 shows the result.

6. Magnetic contribution to the thermal expansion

The magnetic contribution to the thermal expansion can be written

$$\beta_{\text{magn}} = \frac{C_{V,\text{magn}}\gamma_{G,\text{magn}}}{VK_T}. \tag{14.38}$$

Here, $C_{V,\text{magn}}$ is the magnetic part of the heat capacity and the "magnetic" Grüneisen parameter is defined by

$$\gamma_{\text{G,magn}} = \frac{V}{C_{V,\text{magn}}(T)} \left(\frac{\partial S_{\text{magn}}}{\partial V} \right)_T . \tag{14.39}$$

In a ferromagnetic insulator at low temperatures, the magnetic part of the heat capacity is described by magnons, or spin waves, of energy $\hbar\omega_{\text{magn}}(\mathbf{q}, i)$ (Chapter 11, §7). The index i distinguishes between acoustic and optical branches (if necessary) and $\mathbf{q}$ is a wave vector in the first Brillouin zone of the lattice defined by the magnetic atoms. Magnons have thermal properties which are similar to those of phonons. From the general entropy expression (7.18), $S(\mathbf{q}, i) = k_B[(1+n)\ln(1+n) - n\ln(n)]$ where $n = \{\exp[\hbar\omega_{\text{magn}}(\mathbf{q}, i)k_B T] - 1\}^{-1}$, we can define a parameter

$$\gamma_{\text{G,magn}}(\mathbf{q}, i) = -\{\partial \ln[\omega_{\text{magn}}(\mathbf{q}, i)]/\partial \ln V\}. \tag{14.40}$$

This is in direct analogy to the mode Grüneisen parameters of phonons. The volume dependence of ω_{magn} is given by how the exchange interaction between adjacent spins varies with the distance between them. However, it may be of more practical use to relate $\gamma_{\text{G,magn}}$ to the volume dependence of the Curie temperature T_c. Within a simple model we have (Chapter 11, §7)

$$\hbar\omega_{\text{magn}} = Da^2 q^2; \quad D = k_B T_c/(1 + S). \tag{14.41}$$

S is the magnitude of the spin on a lattice site and a is a lattice parameter. Then,

$$\gamma_{\text{G,magn}}(\mathbf{q}, i) = -(\partial \ln D/\partial \ln V)_T = -(\partial \ln T_c/\partial \ln V), \tag{14.42}$$

i.e. a common parameter $\gamma_{\text{G,magn}}$ for all $\mathbf{q}$. (The contributions from a^2 and $\mathbf{q}^2$ in eq. (14.41) cancel in eq. (14.42)). The expression (11.15) for C_{magn} now yields, with eq. (14.38),

$$\beta_{\text{magn}} = \frac{0.113 N k_B}{V K_T} \left(\frac{T(S+1)}{T_c} \right)^{3/2} \left(-\frac{\partial \ln T_c}{\partial \ln V} \right). \tag{14.43}$$

The spin wave contribution to the thermal expansion can be observed only at very low temperatures (Lord 1967). At high temperatures, the spin-wave description is inadequate. We should get β from

$(\partial S_{magn}/\partial V)$, but lack a simple and realistic model to evaluate this quantity. For the same reason, we cannot discuss the very intricate question of β_{magn} in iron in this book.

7. Vacancy contribution to the thermal expansion

Let the formation volume of a vacancy be V_{vac} and the atomic volume be Ω_a. In thermal equilibrium, the crystal volume $V(T)$ is

$$V(T) = V(0) + V_{vac}[V(0)/\Omega_a]\exp(S_{vac}/k_B)\exp(-E_{vac}/k_B T).$$

$$(14.44)$$

The term $V(0)/\Omega_a$ is the number of atoms in the solid, and the two exponential factors give the equilibrium concentration c_{vac} of vacancies. Then the vacancies contribute to the cubic expansion coefficient an amount

$$
\begin{aligned}
\beta_{vac} &= (1/V)(\partial V/\partial T) \\
&= (E_{vac}/k_B T^2)(V_{vac}/\Omega_a)\exp(S_{vac}/k_B)\exp(-E_{vac}/k_B T) \\
&= (E_{vac}/k_B T^2)(V_{vac}/\Omega_a)c_{vac}. \qquad (14.45)
\end{aligned}
$$

The vacancy concentration is appreciable only near the melting temperature T_{fus}. Let us take $E_{vac}/k_B T_{fus} \sim 10$ (tables 2.1 and 2.2), $c_{vac}(T_{fus}) \sim 0.002$ and $V_{vac}/\Omega_a \sim 1/2$. Then, $T\beta_{vac} \sim 0.01$. This can be compared with the empirical rule $T_{fus}\beta_{tot} \sim 0.06$. It is obvious that vacancies may in some cases give a significant contribution to the expansion coefficient at high temperatures (i.e. very close to the melting temperature), but because of the sensitivity of the exponential factor to small changes in E_{vac} it is difficult to give an accurate value for β_{vac}. See also Kraftmakher (1972, 1978, 1996) for a detailed discussion of vacancies.
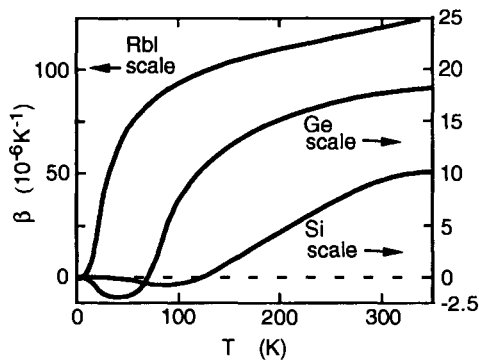
Fig. 14.3. The cubic expansion coefficient $\beta(T)$ of RbI, Ge and Si, shown as a function of temperature, is negative at low temperature. Data from Touloukian et al. (1977).

8. Negative thermal expansion

We noted in the beginning of this chapter that there are solids which shrink on heating, in particular at low temperatures. For a solid of cubic lattice symmetry, a negative expansion is equivalent to a negative Grüneisen parameter $\gamma_G(T)$. We recall that the *phonon contribution* $\gamma_{G,ph}(T)$ is an average over all mode parameters $\gamma(\mathbf{q}, s)$, weighted by the mode heat capacity $C(\mathbf{q}, s)$. Certain solids, e.g. ionic compounds like RbI and RbCl and covalent-bonded solids like Si, Ge, GAs and InSb, have $\gamma(\mathbf{q}, s) = -(\partial \ln \omega(\mathbf{q}, s)/\partial \ln V) < 0$ for some transverse acoustic modes, while $\gamma(\mathbf{q}, s) > 0$ for the longitudinal acoustic modes. At low temperatures, $\gamma_{G,ph}$ is dominated by the transverse modes, because they have the lowest frequencies and hence the largest C_{har} at a given T. Then $\gamma_{G,ph}$, and hence β_{ph}, is negative (fig. 14.3). At high temperatures, $C_{har} \rightarrow k_B$ for all modes (approximately), and the large and positive values of $\gamma(\mathbf{q}, s)$ for the longitudinal mode outweigh the negative $\gamma(\mathbf{q}, s)$ of the transverse branches. That makes $\gamma_{G,ph} > 0$, and we have a positive thermal expansion. There seems to be no nonmagnetic solids with a "common" and simple crystal structure (e.g. bcc, fcc, hcp, NaCl-type, CsCl-type, diamond-type) for which $\gamma_{G,ph} < 0$ when $T > \theta_D$.

Glassy materials usually behave as crystalline solids, but at very low temperatures (<1 K) some of them have $\beta < 0$. That result has been interpreted in terms of two-level *tunneling states* (Chapter 11, §5), but

having $\beta < 0$ is not universal in glasses (Ackerman and Anderson 1982, Kaspers et al. 1983, Piñango et al. 1983).

Some ceramics show a negative expansion coefficient β from low temperatures to T as high as 1000 K. The effect is related to the *rotational motion* of polyhedra of the form SiO_4, PO_4 and WO_4. It has been observed in solids of the form $A_2M_3O_{12}$ and in, e.g. ZrW_2O_8 (Mary et al. 1996).

A special kind of a soft shear mode of vibration, leading to a negative β even at high temperatures (and negative Poisson ratio), is found in *hinged* polyacetylen carbon phases and related systems (Baughman and Galvão 1993). As the name suggests, the structure contains "hinges" that allow for a shear leading to a volume decrease.

Fe_3Si exemplifies a material that has a negative β at low temperatures, caused by a negative *electronic* Grüneisen parameter $\gamma_{G,el}$, and related to a rapidly varying electron density of states near the Fermi level (Miles et al. 1992). Negative expansion coefficient caused by *magnetic* effects are considered in §9 below.

9. Invar-type systems

Some solids, called *invar alloys*, have a very small expansion coefficient in a certain temperature interval. The archetype of such an alloy, with the approximate composition $Fe_{0.65}Ni_{0.35}$, was discovered by Guillaume (1897). Today many similar systems are known, for instance $Fe_{0.72}Pt_{0.28}$, see, e.g. Saunders et al. (1993). Figure 14.4 shows $\beta(T)$ for $Fe_{0.64}Ni_{0.36}$. Obviously it is only in a certain, more or less wide, temperature interval that $\beta \approx 0$. We may understand the behaviour of invar-type systems as follows. The thermal expansion coefficient has one contribution $\beta_{ph}(T)$ from anharmonicity in the lattice vibrations, which is of the normal type described in §4. Then there is a magnetic contribution $\beta_{magn}(T)$, which is negative and happens to be approximately equal to $-\beta_{ph}$. To be more specific, the sum $\beta_{tot}(T) = \beta_{ph}(T) + \beta_{magn}(T)$ may be zero at a certain temperature T, and remain small (with a change in sign) in an interval around that temperature (see fig. 14.4).

The invar-type systems, with a magnetic contribution to the thermal expansion, should be distinguished from materials like Si and C (diamond). The small $\beta = \gamma_G C_V/(V K_T)$ of Si and C at room temper-
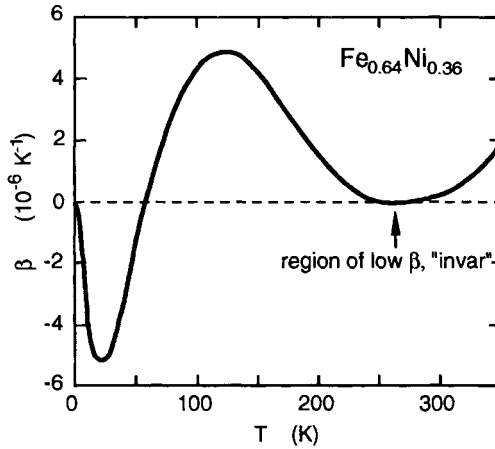
Fig. 14.4. The thermal expansion coefficient in the invar-system $Fe_{0.64}Ni_{0.36}$. Data from Touloukian et al. (1975).

ature can be understood within the usual theory of anharmonic lattice vibrations. It is the result of a small Grüneisen parameter $\gamma_{G,ph}$, a high bulk modulus K_T, and a high Debye temperature so that C_V has not yet reached its classical value.

10. Pressure dependence of the expansion coefficient

Macroscopic thermodynamics gives (Wallace 1972)

$$\left(\frac{\partial \beta}{\partial p}\right)_T = \frac{1}{K_T^2}\left(\frac{\partial K_T}{\partial T}\right)_p.$$
(14.46)

For most materials $(\partial K_T/\partial T)_p < 0$ (Chapter 4, §8) and therefore the coefficient of thermal expansion decreases under an external pressure.

11. Dependence on lattice structure and defects

Usually, the thermal expansion has its major cause in the volume dependence of the phonon frequencies. It has been noted in Chapter 9 that the various Debye temperatures are not much affected by lattice defects. They vary smoothly with the composition in concentrated alloys and

mixed crystals, and do not depend strongly on the lattice structure, provided that the type of bonding is not changed (e.g. metallic to covalent). The same behaviour is expected for the Grüneisen parameter and, hence, also for the expansion coefficient β_{ph}. In particular, we note that a material with disorder, for instance a substitutional alloy or an amorphous material, still has sharp eigenfrequencies for the atomic vibrations if we assume harmonic forces between the atoms. These frequencies can no longer be associated with undampened waves of wave vectors $\mathbf{q}$, but for each of them we can define a Grüneisen parameter, and the theoretical description in this chapter remains valid. An analogous conclusion can be drawn for the electronic contribution to β_{el} in metals (Chapter 10, §3). We conclude that the normal behaviour is a thermal expansion that does not depend strongly on lattice structure or defects. Exceptions may arise, for instance, in magnetic materials or in materials with anomalous bulk moduli.

12. Coupled thermal conduction and expansion

A material, subject to a temperature gradient, is normally in a state of spatially varying strain. The thermal expansion and the thermal conduction are coupled through the equation

$$\nabla(\kappa \nabla T) = \rho c_V (\partial T / \partial t) + \beta T K_T \sum_{i=1}^{3} (\partial \varepsilon_i / \partial t). \qquad (14.47)$$

This is the specialisation to isotropic materials of a general relation (e.g. Fung 1965) for the anisotropic case. The strains correspond to $i = x$, y, z. Furthermore, κ is the thermal conductivity, ρ the mass density, c_V the specific (i.e. per mass) heat capacity, and K_T the isothermal bulk modulus. If the sample is clamped so that the strain is zero, or if the coefficient of thermal expansion is zero, the last term in eq. (14.47) vanishes. Then we recover Fourier's law of heat conduction at constant volume, (eq. (16.9)). If heat flow is prevented, i.e. $\varphi = -\kappa(\nabla T) = 0$, we obtain

$$\left(\frac{\partial T}{\partial t}\right) = -\frac{\beta T K_T}{\rho c_V} \sum_{i=1}^{3} \left(\frac{\partial \varepsilon_i}{\partial t}\right). \qquad (14.48)$$

After integration,

$$\Delta T = -\frac{\beta T K_T}{\rho c_V} \sum_{i=1}^{3} \Delta \varepsilon_i = -\frac{\beta T K_T}{\rho c_V} \left(\frac{\Delta V}{V}\right). \tag{14.49}$$

This is *Kelvin's formula* for the *thermoelastic effect*, i.e. the change in temperature, ΔT, caused by changes in strain, $\Delta \varepsilon_i$. (Cf. the change in temperature when a gas is expanded or compressed.) A uniaxial tension in the x-direction gives, by eq. (3.27), $\varepsilon_1 = \sigma/E$ and $\varepsilon_2 = \varepsilon_3 = -\sigma\nu/E$. Insertion into eq. (14.49) yields

$$\frac{\Delta T}{T} = -\varepsilon_x \gamma_G (1 - 2\nu), \tag{14.50}$$

where γ_G is the Grüneisen parameter and ν is the Poisson ratio. For many materials, $\gamma_G(1 - 2\nu) \approx 1$. A wire which is strained 1% then gets a temperature decrease of about 1%.

ELECTRICAL CONDUCTIVITY OF METALS AND ALLOYS

1. Introduction

There are two formulae for the electrical properties of metals, which are found in almost any textbook on solid state physics. One of them is *Matthiessen's rule* for the resistivity ρ;

$$\rho_{\text{tot}} = \rho_{\text{el-ph}} + \rho_{\text{def}}. \tag{15.1}$$

The other formula expresses the conductivity $\sigma\,(= 1/\rho)$ as

$$\sigma = ne^2\tau/m. \tag{15.2}$$

This relation is often called the *Drude formula* (Drude 1900a, b). Its essential ingredient is the electron scattering time (or lifetime) τ.

Matthiessen's rule says that the total resistivity, ρ_{tot}, is the sum of contributions from the scattering of conduction electrons by the thermal vibrations (to be labelled el–ph for electron–phonon) and the scattering by static lattice defects. The relation (15.1) is well obeyed in many cases, but not for highly resistive systems. For instance, it is not even qualitatively correct for zirconium alloys at high temperatures, or for stainless steels (§11).

In eq. (15.2), e and m are the electron charge and mass, n is the electron number density and τ is an average relaxation time for the conduction electrons carrying the current. Matthiessen's rule follows from eq. (15.2) when

$$\frac{1}{\tau_{\text{tot}}} = \frac{1}{\tau_{\text{el-ph}}} + \frac{1}{\tau_{\text{def}}}. \tag{15.3}$$
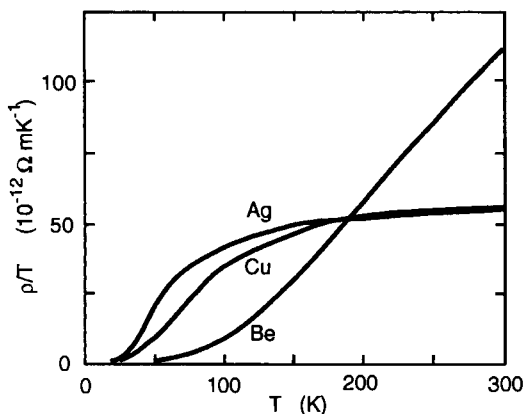
Fig. 15.1. The ratio $\rho_{\text{el-ph}}(T)/T$ for Cu, Ag and Be. Data from Bass (1982).

The relation (15.2) is deceptively simple. It might give the impression that the electron number density n plays a central role. This can be true for doped semiconductors where n varies by many orders of magnitude, but not for metals. The major problem is hidden in the electron relaxation time τ. Let us neglect the effect of impurities on τ and consider the phonon-limited resistivity $\rho_{\text{el-ph}}$ ($=1/\sigma_{\text{el-ph}}$). Grüneisen (1913) noted that, for pure metals, ρ/T and the heat capacity C_p have approximately the same temperature dependence. In fact, an Einstein model for the lattice vibrations leads to proportionality between $\rho_{\text{el-ph}}(T)/T$ and C_V (Chapter 19, §11).

Figure 15.1 shows $\rho_{\text{el-ph}}(T)/T$ for Ag, Cu and Be. Silver is the best elemental conductor at room temperature. We see from the figure that this is partly accidental. Beryllium has such a high Debye temperature ($\sim$900 K) that 300 K is in the low temperature region. Below about 200 K beryllium is a better conductor than the noble metals Cu, Ag and Au. Figure 15.2 gives the resistivity of some other metals. The "normal" high temperature behaviour is that ρ increases somewhat faster than linear in T, as for Al and W. Titanium provides an example of a tendency for "resistivity saturation" (§11). In iron, there is a significant contribution to ρ from scattering of electrons by persisting spin disorder above the Curie temperature.

Monographs by Rossiter (1987), Dugdale (1977), Blatt (1968) and Meaden (1965) give a broad, but mostly elementary, survey of the electrical conductivity of metals.
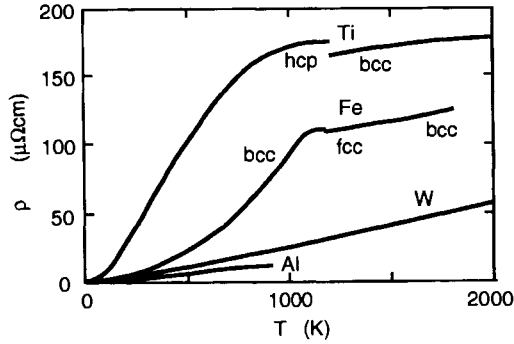
Fig. 15.2. The electrical resistivity $\rho(T)$ of Ti (hcp and bcc), Fe (bcc and fcc) W and Al. Data from Bass (1982).

2. General formulae for the electrical conductivity

We will now start from a general approach to the electrical conductivity (in systems of cubic lattice symmetry) and see how one arrives at $\sigma = ne^2\tau/m$ (eq. (15.2)), and a similar relation, $\sigma = (\omega_{pl}^2/4\pi)\tau$, where for free electrons the plasma frequency ω_{pl} has the well-known form $\omega_{pl}^2 = 4\pi ne^2/m$.

We begin with some expressions to define the notation. An electron with velocity $\mathbf{v_k}$ carries an electric current $-e\mathbf{v_k}$. In equilibrium, for each electron state characterised by the wave vector $\mathbf{k}$, there is also a state $-\mathbf{k}$, with velocity $-\mathbf{v_k}$, so that the total electric current vanishes. In the presence of an electric field $\mathbf{E}$, the Fermi–Dirac function is changed from its equilibrium value $f_\mathbf{k}^0$ to the value $f_\mathbf{k}$. If the field is weak, we can assume that $f_\mathbf{k} - f_\mathbf{k}^0$ is linear in $\mathbf{E}$ and write

$$f_\mathbf{k} - f_\mathbf{k}^0 = e(\mathbf{v_k} \cdot \mathbf{E})\tau(\mathbf{k})(\partial f_\mathbf{k}^0/\partial\varepsilon_\mathbf{k}), \tag{15.4}$$

where $\varepsilon_\mathbf{k} = E(\mathbf{k}) - E_F$. The quantity $\tau(\mathbf{k})$ has the dimension of time. We shall call it a *relaxation time*, although it usually does not fulfill the requirements of such a quantity (namely that the electron states decay exponentially in t/τ as the field $\mathbf{E}$ is turned off at time $t = 0$). In the following we may also write $\tau(\varepsilon_\mathbf{k})$, $\tau(\varepsilon)$, $\tau(\varepsilon_\mathbf{k}, \mathbf{k})$ or $\tau(\varepsilon, \mathbf{k})$ instead of $\tau(\mathbf{k})$, to stress that τ is energy dependent, or both energy dependent and anisotropic. The actual calculation of $\tau(\mathbf{k})$ is difficult, but we can learn much just by assuming that it is a known quantity. The terms multiply-

ing $(\partial f/\partial \varepsilon)$ in eq. (15.4) give the energy acquired by an electron that moves with velocity $\mathbf{v_k}$ in the field $\mathbf{E}$ during the time τ.

The total electric current density is

$$\mathbf{j} = -(2e/V) \sum_{\mathbf{k}} \mathbf{v_k}(f_{\mathbf{k}} - f_{\mathbf{k}}^0). \tag{15.5}$$

The factor of 2 comes from the two spin directions. The current density $\mathbf{j}$ is related to the field $\mathbf{E}$ through the conductivity tensor σ, such that

$$\mathbf{j} = \sigma \mathbf{E}. \tag{15.6}$$

In a system with cubic symmetry, that tensor is diagonal with all the elements $\sigma_{ii} = \sigma$. Then, from eqs. (15.4)–(15.6),

$$\sigma = -(2e^2/3V) \sum_{\mathbf{k}} (\mathbf{v_k} \cdot \mathbf{v_k}) \tau(\mathbf{k})(\partial f_{\mathbf{k}}^0/\partial \varepsilon_{\mathbf{k}}). \tag{15.7}$$

The factor $1/3$ in eq. (15.7) comes from the projection of $\mathbf{v_k}$ along the applied field $\mathbf{E}$ in eq. (15.4).

3. Relations of the type $\sigma = ne^2\tau/m$

Starting from the general relation (15.7) we consider two special cases. First, we let $\mathbf{v_k}$ be isotropic but take an anisotropic $\tau(\mathbf{k})$ and average it over the Fermi surface. In the second case, we let $\tau(\mathbf{k})$ be a constant but take an anisotropic $\mathbf{v_k} \cdot \mathbf{v_k}$ and average it over the Fermi surface.

The usual prescription for turning a sum over $\mathbf{k}$ into an integral brings eq. (15.7) to the form (Appendix B)

$$\sigma = -(2e^2/3)(2\pi)^{-3} \int_{S_F} \frac{\mathbf{v_k} \cdot \mathbf{v_k}}{|\nabla_{\mathbf{k}} E(\mathbf{k})|} \, \mathrm{d}S \int_{-\infty}^{\infty} \tau(\varepsilon, \mathbf{k})(\partial f_{\mathbf{k}}^0/\partial \varepsilon_{\mathbf{k}}) \, \mathrm{d}\varepsilon.$$

$$\tag{15.8}$$

Assume that the first integral can be evaluated with a spherical Fermi surface, but with band structure effects accounted for through an effective band mass m_b, so that $|\mathbf{v_k}|/v_F^0 = m/m_b$, where v_F^0 is the free-electron velocity at the Fermi surface. Furthermore, $n/m =$

$S^0 v_F^0/(12\pi^3 \hbar)$ where S^0 is the area of the free-electron Fermi surface. Then eq. (15.8) can be written

$$\sigma = \frac{ne^2}{m_b} \langle \tau(\varepsilon, \mathbf{k}) \rangle. \tag{15.9}$$

The average relaxation time is defined

$$\langle \tau(\varepsilon, \mathbf{k}) \rangle = \int_{S_F} \frac{dS}{S^0} \int_{-\infty}^{\infty} \tau(\varepsilon, \mathbf{k})(-\partial f_\mathbf{k}^0/\partial \varepsilon_\mathbf{k}) \, d\varepsilon. \tag{15.10}$$

With a constant relaxation time τ, and a free-electron model in eq. (15.10), we recover the familiar form

$$\sigma = ne^2\tau/m. \tag{15.11}$$

Next we replace $\tau(\mathbf{k})$ in eq. (15.8) by a properly averaged constant τ, and also assume that $(-\partial f_\mathbf{k}^0/\partial \varepsilon_\mathbf{k})$ can be replaced by a δ-function $\delta(\varepsilon_\mathbf{k})$ that picks up contributions for $\mathbf{k}$-values, where $\varepsilon_\mathbf{k} = E(\mathbf{k}) - E_F = 0$, i.e. $\mathbf{k}$-values on the Fermi surface. One gets, from eq. (15.7),

$$\sigma = (\omega_{pl}^2/4\pi)\tau. \tag{15.12}$$

Here the *Drude plasma frequency* ω_{pl} is defined by a Fermi-surface average of the squared electron velocity;

$$\begin{aligned} \omega_{pl}^2 &= (8\pi e^2/3V) \sum_\mathbf{k} \mathbf{v}_\mathbf{k}^2 \delta(\varepsilon_\mathbf{k}) \\ &= [8\pi e^2 N(E_F)/3V]\langle \mathbf{v}_\mathbf{k}^2 \rangle. \end{aligned} \tag{15.13}$$

For free electrons, $\omega_{pl}^2 = 4\pi ne^2/m$ and we again recover $\sigma = ne^2\tau/m$. Experimental values of ω_{pl}^2 are reviewed by Foiles (1985). See Appendix H for important comments on the dimensions (units) of σ, e and ω_{pl}.

4. Solutions to the Boltzmann equation

4.1. Relaxation time equations

In the last section, it was not stated how the relaxation time $\tau(\mathbf{k})$ for a particular $\mathbf{k}$ is to be calculated. In a quantum mechanical formulation, one should consider the probabilities for the scattering of an electron from a state $\mathbf{k}$ to other states $\mathbf{k}'$. We describe such processes by

$$P(\mathbf{k}, \mathbf{k}') = P_{\text{el-ph}}(\mathbf{k}, \mathbf{k}') + P_{\text{def}}(\mathbf{k}, \mathbf{k}') + P_{\text{r}}(\mathbf{k}, \mathbf{k}'). \tag{15.14}$$

$P_{\text{el-ph}}$ refers to the scattering of electrons by phonons, P_{def} to the scattering by various kinds of lattice defects (impurity atoms, vacancies, grain boundaries, etc.) and P_{r} refers to remaining scattering mechanisms (e.g. scattering by other conduction electrons and by magnetic excitations).

If one knows the interactions as described by $P(\mathbf{k}, \mathbf{k}')$, the relaxation times $\tau(\mathbf{k})$ follow from a solution of the *Boltzmann equation*, but even without such an information about $P(\mathbf{k}, \mathbf{k}')$ one can derive several useful results. For a system with cubic lattice symmetry, and with some reasonable approximations (Grimvall 1981), one gets

$$\frac{1}{\tau(\mathbf{k})} \left(\frac{\partial f^0}{\partial \varepsilon_{\mathbf{k}}} \right) = -\frac{1}{k_{\text{B}} T} \sum_{\mathbf{k}'} (1 - \cos\theta_{\mathbf{k}\mathbf{k}'}) P(\mathbf{k}, \mathbf{k}'). \tag{15.15}$$

This formulation allows us to state more precisely the difference between a "scattering time" (or "lifetime") of an electron and the quantity $\tau(\mathbf{k})$ to be used in the transport problem. With a factor 1 instead of $(1 - \cos\theta)$ in eq. (15.15), $\tau(\mathbf{k})$ would be the lifetime of an electron state labelled $\mathbf{k}$. It can be calculated by the Golden Rule of quantum mechanics. In that case all scattering processes out of a state $\mathbf{k}$ are of equal importance. In electrical transport problems, we have to ask in which direction the electron goes after the scattering, since "backscattering" of electrons gives the largest contribution to the resistivity. This is expressed by the term $1 - \cos\theta_{\mathbf{k}\mathbf{k}'}$ in eq. (15.15). (In the electron contribution to the *thermal* conductivity the factor $1 - \cos\theta$ does not appear, but instead one must ask what is the change in energy in the scattering process $(\mathbf{k}, \mathbf{k}')$.)

We next assume the presence of different scattering mechanisms, labelled i. Let $\tau_i(\varepsilon_{\mathbf{k}}, \mathbf{k})$ be a solution to the Boltzmann equation, when only a particular scattering mechanism i is present. If the $\tau_i(\varepsilon_{\mathbf{k}}, \mathbf{k})$ thus obtained for different i all have the same dependence on the energy $\varepsilon_{\mathbf{k}}$ and the wave vector $\mathbf{k}$ (i.e. they are just scaled by a factor), it follows that

$$\frac{1}{\tau_{\text{tot}}} = \sum_i \frac{1}{\tau_i}. \tag{15.16}$$

This is equivalent to Matthiessen's rule, cf. eq. (15.3).

4.2. *Variational solution*

The Boltzmann equation is an integral equation which is non-trivial to solve. Therefore, most calculations for real systems rely on an approximate solution, through a variational procedure. The method was outlined by Köhler (1948, 1949) and Sondheimer (1950) and exploited in detail by Ziman (1960). Like other variational calculations, it gives a bound to the exact result. In our case, it can be written

$$
\rho < \frac{(V/2k_{\mathrm{B}}T) \displaystyle\int \mathrm{d}^3k \int \mathrm{d}^3k' (\Phi_{\mathbf{k}} - \Phi_{\mathbf{k}'})^2 P(\mathbf{k}, \mathbf{k}')}{e^2 \left| \displaystyle\int (\mathbf{v}_{\mathbf{k}} \cdot \Phi_{\mathbf{k}})(\partial f^0(\mathbf{k})/\partial \varepsilon_{\mathbf{k}}) \, \mathrm{d}^3k \right|^2}, \tag{15.17}
$$

where $P(\mathbf{k}, \mathbf{k}')$ is the scattering operator introduced in eq. (15.14), and $\Phi_{\mathbf{k}}$ is a trial function to be used in the variational procedure. Since Φ appears squared both in the numerator and the denominator of eq. (15.17), all Φ can be multiplied by the same constant without altering the estimation for ρ. The essence of a variational method is that one can choose Φ to be a function of one or several parameters λ_i. The righthand side of eq. (15.17), i.e. an upper bound to ρ, is then minimised with respect to all λ_i. In most calculations one uses the trial function

$$
\Phi_{\mathbf{k}} = \mathbf{E} \cdot \mathbf{k}. \tag{15.18}
$$

In fact it has no parameters to vary, but since it gives the exact solution under certain idealised assumptions, it is assumed to give a reasonable value of ρ also in real metals.

With Φ as in eq. (15.18), and with the electron states described by an isotropic electron band mass m_{b} as in eq. (B.15), one finds after some manipulations that the variational solution eq. (15.17) gives

$$
\rho < \frac{m_{\mathrm{b}} \langle 1/\tau(\mathbf{k}) \rangle}{ne^2}. \tag{15.19}
$$

This should be compared with the "exact" solution (15.9), $\rho = 1/\sigma = (m_{\mathrm{b}}/ne^2)/\langle \tau(\mathbf{k}) \rangle$. Schwartz' inequality in mathematics implies $\langle 1/\tau \rangle > 1/\langle \tau \rangle$, which is consistent with the inequality in eq. (15.19). In real calculations of ρ from the variational formula (15.17) one has to approximate $P(\mathbf{k}, \mathbf{k}')$, which may introduce errors of unknown sign. Therefore,

formulae such as (15.17), and relations derived from it, are usually (although not correctly) written with an equality sign.

5. Phonon-limited electrical conductivity

5.1.   Resistivity expressed in the Éliashberg transport coupling function

The lifetime τ_{el-ph} for the scattering of electrons by phonons contains quantum-mechanical matrix elements for the electron-phonon interaction, and statistical Bose–Einstein and Fermi–Dirac factors for the population of phonon and electron states, respectively. A very useful quantity in this context is the *Éliashberg transport coupling function* $\alpha_{tr}^2 F(\omega)$. It can, somewhat loosely, be viewed as the product of the squared electron-phonon matrix element, α^2, for all scattering processes where a single phonon of energy $\hbar\omega$ is either emitted or absorbed, and the phonon density of states $F(\omega)$. A similar expression, $\alpha^2 F(\omega)$, arises in the theory of superconductivity and in the effect of electron-phonon interactions on the thermal properties of electrons (see Chapter 10 and Appendix B). The essential difference between $\alpha_{tr}^2 F(\omega)$ and $\alpha^2 F(\omega)$ is a term corresponding to the factor $1 - \cos\theta$.

The Éliashberg coupling function allows us to write the resistivity in a very simple, although approximate, form. In the variational expression for ρ, (eq. (15.17)), we take $\Phi_k = \mathbf{E} \cdot \mathbf{v}_k$. Using eq. (15.13) for the Drude plasma frequency we get

$$\rho = \frac{(4\pi)^2}{\omega_{pl}^2} \int_0^{\omega_{max}} \frac{(\hbar\omega/k_B T)\alpha_{tr}^2 F(\omega)}{[\exp(\hbar\omega/k_B T) - 1][1 - \exp(-\hbar\omega/k_B T)]} \, d\omega.$$

$$(15.20)$$

It is worth commenting on the accuracy of eq. (15.20). First, it requires that the Boltzmann equation is valid. This is true for many metals and alloys, but there are notable exceptions among highly resistive systems (§11). Second, eq. (15.20) is based on the variational method. However, we do not vary anything, but simply take the estimation of ρ that results from the trial function $\mathbf{E} \cdot \mathbf{v}_k$. The accuracy of this procedure is not very well known for transition metals, but it may be acceptable

in free-electron-like metals. Since a true variational approach is very complicated, and still of somewhat uncertain accuracy because its success depends on the choice of trial functions, there is usually no realistic alternative to the use of $\Phi_{\mathbf{k}} = \mathbf{E} \cdot \mathbf{v_k}$ or $\Phi_{\mathbf{k}} = \mathbf{E} \cdot \mathbf{k}$. Furthermore, we have assumed in eq. (15.20) that $\alpha_{\text{tr}}^2 F(\omega)$ and ω_{pl}^2 are well approximated by their values exactly at the Fermi level. Therefore, we do not allow for the effect of a rapidly varying electron density-of-states $N(E)$ around the Fermi level $E = E_{\text{F}}$. (However, there is still an energy dependence of $\tau(\varepsilon)$ arising from the Fermi–Dirac and Bose–Einstein functions, f^0 and n.) In an actual calculation of the resistivity, it remains of course, to find the electron-phonon matrix element that couples an electron in a state $\mathbf{k}$ to an electron in a state $\mathbf{k}'$, through interaction with a phonon of mode s. This is beyond the scope of this book.

5.2. Bloch–Grüneisen resistivity formulae

Ever since the early days of quantum mechanics, the *Bloch–Grüneisen formula* has been used to describe the temperature dependence of the phonon-limited electrical resistivity in metals. It is often given in the form

$$\rho_{\text{BG}}(T) = \frac{c_1}{T} \int_0^{q_{\text{D}}} \frac{q^5}{[\exp(\hbar C q/k_{\text{B}} T) - 1][1 - \exp(-\hbar C q/k_{\text{B}} T)]} \, \mathrm{d}q.$$

(15.21)

Here, c_1 is a constant, specific for the metal under consideration, q is a phonon wave number lying between 0 and the Debye value q_{D}, C is the longitudinal sound velocity and $\hbar C q$ is a long-wavelength phonon energy. The subscript BG stands for "Bloch–Grüneisen". Putting $z = \hbar C q/k_{\text{B}} T$ in eq. (15.21) we have

$$\begin{aligned}
\rho_{\text{BG}}(T) &= \frac{c_2}{\theta_{\text{D}}} \left(\frac{T}{\theta_{\text{D}}}\right)^5 \int_0^{\theta_{\text{D}}/T} \frac{z^5}{(e^z - 1)(1 - e^{-z})} \, \mathrm{d}z \\
&= \frac{c_2}{\theta_{\text{D}}} \left(\frac{T}{\theta_{\text{D}}}\right)^5 J_5(\theta_{\text{D}}/T),
\end{aligned}$$

(15.22)

where c_2 is another constant and J_5 is the Debye integral of order 5. At low temperatures, we need the value $J_5(\infty) = 124.4$, and at high

temperatures $(T \gg \theta_D)$ we need $J_5(T/\theta_D) \approx (1/4)(\theta_D/T)^4$. Then we can write

$$\rho_{BG}(T) = (124.4c_2/\theta_D)(T/\theta_D)^5, \quad T \ll \theta_D, \tag{15.23}$$

and

$$\rho_{BG}(T) = (c_2/4\theta_D)(T/\theta_D), \quad T \gg \theta_D. \tag{15.24}$$

In two famous papers, Bloch (1928, 1930) derived first the high temperature and then the low temperature results (eqs. (15.24) and (15.23)). Grüneisen (1933) noted, empirically, that Bloch's low temperature formula could be matched to the high temperature version and thus provide a good account of the electrical resistivity at all temperatures.

The original derivation of eq. (15.21) rests on a number of assumptions which are usually not very well fulfilled, even for free-electron-like metals. However, it is well known that the Bloch–Grüneisen formula describes $\rho(T)$ for many real systems with a remarkable accuracy. This is easy to explain if we start from the variational estimation of ρ, expressed through the transport electron-phonon coupling $\alpha_{tr}^2 F(\omega)$. The true function $\alpha_{tr}^2 F(\omega)$ contains all complications regarding the phonon spectrum, the electron-phonon matrix elements, coupling to transverse phonons, Umklapp processes etc. Except at very low energies ω, $\alpha_{tr}^2 F(\omega)$ is reminiscent of the phonon density of states $F(\omega)$. Because ρ results from an integration over ω, the resistivity is determined by the gross features of $\alpha_{tr}^2 F(\omega)$ but is insensitive to its finer details. This is analogous to the fact that a Debye model can give a good account of the phonon heat capacity, although $F(\omega)$ may deviate substantially from an ω^2-shape.

As a model approximation, we now represent this function by a power law in ω,

$$\alpha_{tr}^2 F(\omega) = C_n \omega^n, \tag{15.25}$$

for $0 < \omega < \omega_{max}$. It allows us to define generalised Bloch–Grüneisen formulae $\rho_{BG}(T; n)$. They all have $\rho \sim T$ at high temperatures. In the low temperature limit, they yield $\rho \sim T^{n+1}$. Contrary to a widespread belief, the experimental resistivity usually does not vary as T^5 at low temperatures – not even for the free-electron-like metals Na and K. In fact, the full variational formula (15.17) is not quite adequate at low

temperatures because there may be complications due to "phonon drag" and other effects (cf. Grimvall 1981). If we take $n = 4$ and $\hbar\omega_{max} = k_B\theta_D$ in eq. (15.25), the expression (15.20) yields exactly the Bloch–Grüneisen formula (15.21).

5.3. Einstein-model resistivity formula

At intermediate and high temperatures (say $T > \theta_D/4$) any reasonable representation of $\alpha_{tr}^2 F(\omega)$ gives a good account of the resistivity and ρ_{BG} is just one possible choice, which has no deeper justification. In the extreme case of an Einstein model, i.e.

$$\alpha_{tr}^2 F(\omega) = C_0 \delta(\omega - \omega_E), \tag{15.26}$$

where C_0 is a constant, ρ/T becomes proportional to the Einstein heat capacity. Even this crude approximation may give a good description of $\rho(T)$ in many metals, at not too low temperatures (cf. Chapter 19, §11).

5.4. Relation to the electron-phonon coupling parameter λ_{el-ph}

The high temperature limit of eq. (15.20) can be cast in an interesting form. We write

$$\rho = \frac{(4\pi)^2 (k_B T/\hbar)}{2\omega_{pl}^2} 2 \int_0^{\omega_{max}} \frac{\alpha_{tr}^2 F(\omega)}{\omega} \, d\omega = \frac{8\pi^2 k_B T}{\hbar\omega_{pl}^2} \lambda_{tr}, \tag{15.27}$$

where

$$\lambda_{tr} = 2 \int_0^{\omega_{max}} \frac{\alpha_{tr}^2 F(\omega)}{\omega} \, d\omega. \tag{15.28}$$

We noted above that the essential difference between $\alpha_{tr}^2 F(\omega)$ and $\alpha^2 F(\omega)$ is a factor which is approximately $1 - \cos\theta_{kk'}$. Therefore, it is not unreasonable to approximate $\alpha_{tr}^2 F(\omega)$ by

$$\alpha_{tr}^2 F(\omega) = \langle 1 - \cos\theta \rangle \alpha^2 F(\omega), \tag{15.29}$$

where $\langle 1 - \cos\theta \rangle$ is some properly defined average. This leads to the high temperature form

$$\begin{aligned}
\rho &= \frac{8\pi^2 k_B T \langle 1 - \cos\theta \rangle}{\hbar\omega_{pl}^2} \lambda_{el-ph} \\
&= \frac{2\pi m k_B T \langle 1 - \cos\theta \rangle}{\hbar n e^2} \lambda_{el-ph}.
\end{aligned} \tag{15.30}$$

In the last equality we assumed a free-electron expression for ω_{pl}^2. The parameter $\lambda_{el-ph} = 2 \int \alpha^2 F(\omega)(d\omega/\omega)$ is the same as that appearing in the electron-phonon enhancement factor $1 + \lambda_{el-ph}$ of the electronic heat capacity (Chapter 10 and Appendix B). Resistivity data can be used, therefore, to estimate λ_{el-ph} (Grimvall 1981, Allen 1987, 1999). Obviously, we can approximately identify τ_{el-ph} with $\hbar/2\pi\lambda_{el-ph}k_B T$.

6. Electrical conduction in non-cubic lattices

Quite generally, the conductivity σ (or resistivity ρ) is a 3×3 tensor of rank two, with elements σ_{ij} (or ρ_{ij}). If a tensor of rank two has cubic symmetry, it reduces to a scalar, i.e. $\sigma_{ii} = \sigma$, while $\sigma_{ij} = 0$ when $i \neq j$ (similarly, $\rho_{ii} = \rho$ and $\rho_{ij} = 0$). In the general case,

$$\mathbf{j} = \sigma\mathbf{E}, \qquad \mathbf{E} = \rho\mathbf{j}, \tag{15.31}$$

and the current $\mathbf{j}$ is not parallel to the field $\mathbf{E}$ except in certain directions of high symmetry.

We shall exemplify a non-scalar conductivity by a material of *hexagonal* symmetry. (The same relations hold for *trigonal* and *tetragonal* symmetry.) Let θ be the angle between the current $\mathbf{j}$ and the c-axis. The resistivity $\rho(\theta) = E(\theta)/|\mathbf{j}|$ is

$$\rho(\theta) = \rho_\parallel \cos^2\theta + \rho_\perp \sin^2\theta. \tag{15.32}$$

This describes current flow in a wire, for example. Next, we let the field $\mathbf{E}$ have a specified angle θ to the c-axis (e.g. $\mathbf{E}$ is applied across a slab). The conductivity $\sigma(\theta) = j(\theta)/|\mathbf{E}|$ is

$$\sigma(\theta) = \sigma_\parallel \cos^2\theta + \sigma_\perp \sin^2\theta. \tag{15.33}$$

Note that $\sigma(\theta) \neq 1/\rho(\theta)$, although $\sigma_\perp = 1/\rho_\perp$ and $\sigma_\parallel = 1/\rho_\parallel$. A theoretical account of the anisotropy of ρ_{el-ph} is difficult, because it requires a detailed consideration of the scattering process over the Fermi surface (e.g. Chan 1978, Lawson and Guénault 1982). Figure 15.3 shows how $\rho_\parallel/\rho_\perp$ may vary with the temperature in metals. Further aspects of anisotropic conductivity are dealt with in Chapter 18, in connection with the averaging of anisotropic transport coefficients in polycrystalline materials.
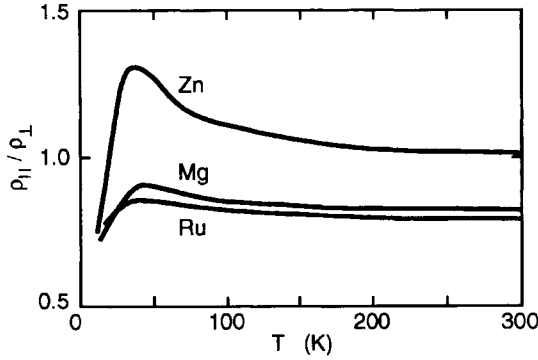
Fig. 15.3. The anisotropy of the electrical resistivity, given as $\rho_\|(T)/\rho_\perp(T)$, for hcp Zn, Mg and Ru. Data from Bass (1982).

7. Matthiessen's rule

Matthiessen and Vogt (1864) noted that the temperature dependence of the resistivity was not affected by small amounts of alloying elements;

$$\mathrm{d}\rho_{\mathrm{tot}}(T, c)/\mathrm{d}T = \mathrm{d}\rho_{\mathrm{el-ph}}(T)/\mathrm{d}T. \tag{15.34}$$

This result, called *Matthiessen's rule*, is usually quoted in the integrated form

$$\rho_{\mathrm{tot}}(T, c) = \rho_{\mathrm{el-ph}}(T) + \rho_{\mathrm{def}}(c). \tag{15.35}$$

Corrections to eq. (15.35) are known as *deviations from Matthiessen's rule* (DMR). Mathematically, we can trace their origin to the relation

$$\frac{1}{\tau_{\mathrm{tot}}(\varepsilon, \mathbf{q})} = \frac{1}{\tau_{\mathrm{el-ph}}(\varepsilon, \mathbf{q})} + \frac{1}{\tau_{\mathrm{def}}(\mathbf{q})}. \tag{15.36}$$

If we consider $\rho \sim \langle 1/\tau_{\mathrm{tot}}\rangle$, as in the expression (15.3), Matthiessen's rule is obtained from eq. (15.36). However, we should rather consider $\rho \sim 1/\langle\tau_{\mathrm{tot}}\rangle = 1/\langle\tau_{\mathrm{el-ph}}\tau_{\mathrm{def}}/(\tau_{\mathrm{el-ph}} + \tau_{\mathrm{def}})\rangle$, which becomes $\langle 1/\tau_{\mathrm{tot}}\rangle$ only if $\tau_{\mathrm{el-ph}}(\varepsilon, \mathbf{k})$ and $\tau_{\mathrm{def}}(\varepsilon, \mathbf{k})$ have the same dependence on ε and $\mathbf{q}$, i.e. if they differ by a (temperature dependent) factor. In this way we see how eq. (15.36) gives rise to a DMR. The fact that $\tau_{\mathrm{el-ph}}(\varepsilon, \mathbf{q})$ is energy dependent, through ε, while $\tau_{\mathrm{def}}(\mathbf{q})$ refers to elastic scattering and is independent of ε, causes a DMR which is peaked at $T \sim 0.1\theta_{\mathrm{D}}$ and

is of the order of $0.1\rho_{\text{def}}$ or (much) less (Engquist and Grimvall 1980). Differences in the anisotropy of $\tau_{\text{el-ph}}$ and τ_{def} also lead to a DMR. A magnetic field may reduce the DMR (Mitchel et al. 1980). Bass (1972) and Cimberle et al. (1974) have reviewed work on DMR. Bass (1982) gives numerical results for the resistivity in dilute alloys, also covering other aspects than DMR.

Impurities not only give a static scattering but they also change the vibrational properties and hence alter $\alpha_{\text{tr}}^2 F(\omega)$. This leads to a DMR at high T which is linear in T, and can have either sign (Engquist and Grimvall 1980). Usually there is no dramatic effect caused by heavy (Kus and Taylor 1980) or light (Kus and Taylor 1982) impurities.

The effect of vacancies and other intrinsic defects is similar to that of impurity atoms. In thermal equilibrium the magnitude of these effects is usually very small. For instance, the resistivity per 1 at.% vacancies (i.e. a very high vacancy concentration) is a few $\mu\Omega$ cm (Wollenberger 1996). The resistivity increase in heavily cold-worked copper is $\sim 2 \times 10^{-4}$ $\mu\Omega$ m (Powell et al. 1959). Still, such small changes in the resistivity are of interest in studies of the recovery of a specimen on anneling, after it has been cold-worked, irradiated etc. Complications in the interpretation arise when point defects migrate to dislocation cores and grain boundaries (e.g. Kasen 1972). Grain boundary scattering is referred to in §9. Rossiter (1987) and Dugdale (1995) give a detailed treatment of the effect of various lattice defects on the electrical resistivity.

8. Concentrated alloys

For low impurity concentrations, c, ρ_{def} varies linearly with c;

$$\rho_{\text{def}}(c) = c\rho_{\text{def}}^*. \tag{15.37}$$

Some values of ρ_{def}^* are given in table 15.1 (Bass 1982). In a system $A_{1-c}B_c$, the linear dependence on the impurity content holds for $c \ll 1$ and $1 - c \ll 1$. The simplest relation that interpolates between these limits is *Nordheim's* (1931) *rule*,

$$\rho_{\text{def}}(c) = c(1 - c)\rho_{\text{def}}^*. \tag{15.38}$$

Qualitatively, this rule is observed in some concentrated alloys, but the transport process is too complicated to allow a more precise, and yet

Table 15.1

Impurity resistance, at low temperatures, in some dilute alloys. Unit: $\mu\Omega$ cm/at.%

Al–Cu	Cu–Al	Al–Fe	Fe–Al	Al–Ti	Ti–Al	Cu–Ag	Ag–Cu	Cu–Au	Au–Cu
0.7	1.3	6.1	5.5	5.9	13	0.08	0.03	0.53	0.43

accurate, relation. For instance, there is no reason to assume that ρ_{def}^* is the same for a dilute solution of A in B, as for a dilute solution of B in A (cf. the pairs in table 15.1). We also note that mutual solubility in a wide range of concentrations c is rather unusual. It requires that the atoms are chemically similar, and then ρ_{def}^* tends to be small. When the concentration c is such that the alloy $A_{1-c}B_c$ forms a two-phase material, one has a transport problem for a composite material, see Chapter 17.

9. Electron mean free path and size effects

If v_F is the velocity of an electron at the Fermi level, and τ is the electron lifetime, we define the *electron mean free path* ℓ as

$$\ell = v_F\tau. \tag{15.39}$$

In a nearly-free-electron model with $v_F = \hbar k_F/m_b$ we get

$$\sigma = ne^2\tau/m_b = ne^2\ell/(m_b v_F) = (3\pi^2)^{-1/3}n^{2/3}(e^2/\hbar)\ell. \tag{15.40}$$

This can be rewritten, with n expressed in terms of the electron density parameter r_s, (eq. (B.11)), and the Bohr radius a_0 (Appendix H), in the form

$$\rho = \pi(16\pi/3)^{1/3}r_s^2 \left(\frac{a_0}{\ell}\right)\left(\frac{a_0\hbar}{e^2}\right). \tag{15.41}$$

Typically, $\pi(16\pi/3)^{1/3}r_s^2 \sim 40$. The quantity $a_0\hbar/e^2 = 0.22$ $\mu\Omega$ m is a *fundamental unit of resistivity* (Appendix H). From eq. (15.41) we can get a rough idea of the mean free path ℓ (in non-transition metals) when
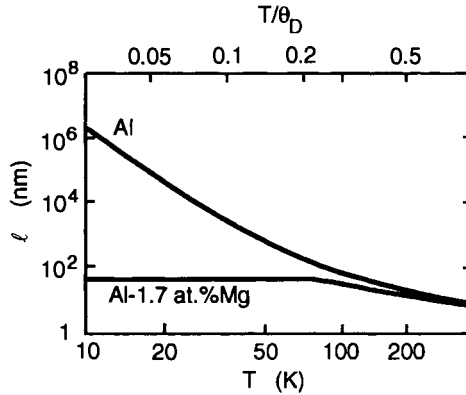
Fig. 15.4. The electron mean free path ℓ in pure aluminium and in Al-1.7 at.% Mg. From Grimvall (1981).

the resistivity is known. Figure 15.4 shows ℓ calculated in this way for pure aluminium and an Al alloy.

When the electron mean free path ℓ becomes comparable with a characteristic dimension of the specimen, surface scattering gives corrections to the bulk resistivity ρ_{bulk}. (This requires pure materials and low temperatures.) For thin films, Fuchs (1938) and Sondheiner (1952) developed a simple model, which gives the first-order correction in the small parameter ℓ_{bulk}/d, where d is the film thickness;

$$\rho_{film} = \rho_{bulk}[1 + (3/8)(1 - p_s)(\ell_{bulk}/d)]. \tag{15.42}$$

The parameter p_s ($0 < p_s < 1$) measures the amount of specular character in the surface scattering. Very similar formulae hold for thin wires. This early theory has been improved (Soffer 1967) to give good agreement with experiments (Stesmans 1982). Thin films may be very fine-grained. Then grain boundary scattering is not negligible (van Attekum et al. 1984, Mayadas et al. 1969). Bass (1982) gives a brief theoretical introduction and an extensive survey of experimental results on size effects in electron scattering.

10. Pressure dependence

We start from the expression for the phonon-limited electrical resistivity at high temperatures (eq. (15.27));

$$\rho_{el-ph} = (8\pi^2 k_B T / \hbar\omega_{pl}^2)\lambda_{tr}. \tag{15.43}$$

In our treatment of the electronic part of the thermal expansion coefficient (Chapter 14, §5), we discussed the volume dependence of the electron-phonon interaction parameter λ_{el-ph}. Because λ_{tr} is closely related to λ_{el-ph} we can take the same approach here, giving

$$d\ln\rho/d\ln V = -2(d\ln\omega_{pl}/d\ln V) + 2\gamma, \tag{15.44}$$

where γ may be (crudely) approximated by the Grüneisen parameter γ_G. In a free-electron model, $\omega_{pl}^2 = 4\pi ne^2/m$, i.e. $d\ln\omega_{pl}/d\ln V = -1/2$. Then the righthand side of eq. (15.44) becomes $1 + 2\gamma_G$. Similar results have been obtained for alkali metals, in pioneering work by Dugdale and Gugan (1962). In transition metals, there are other important terms in $d\ln\lambda_{tr}/d\ln V$ than just $2\gamma_G$, and a detailed consideration of the various contributions to $d\rho_{el-ph}/dV$ is necessary (Sundqvist et al. 1985). Dugdale and Myers (1985) have briefly reviewed the theory of the pressure (i.e. volume) dependence of the electrical resistivity and they give an extensive survey of experiments.

11. Saturation effects

According to the simple theory (eqs. (15.24) or (15.27)), ρ increases linearly in T when $T > \theta_D$. Thermal expansion, combined with the fact that ρ varies with the volume mainly through phonon frequencies, gives an additional slight increase of ρ with the temperature. This is the normal behaviour, shown, for example, by Al (fig. 15.2). Titanium (fig. 15.2) has an anomalous temperaure dependence of ρ which cannot be explained by a rapidly varying $N(E)$ near the Fermi level. Instead, we have an example of what has been termed *resistivity saturation* (Fisk and Webb 1976). Empirically, the shape of $\rho(T)$ is well approximated by the *shunt resistor model* (Wiesmann et al. 1977);

$$\frac{1}{\rho(T)} = \frac{1}{\rho_{ideal}(T)} + \frac{1}{\rho_{sat}}. \tag{15.45}$$

Here ρ_{ideal} is the "normal" resistivity, and ρ_{sat} is a value which the actual resisivity would take when ρ_{ideal} becomes very large (either because T is high or because ρ_{def} is large). A consequence of eq. (15.45)

is that $d\rho/dT < d\rho_{ideal}/dT$. In fact, $d\rho/dT$ is experimentally found to decrease with increasing ρ and becomes negative for most highly resistive metals, such as certain steels and amorphous metals. This is known as *Mooij's rule* (1973). Qualitatively one may understand the phenomenon of saturation as a result of the short electron mean free path ℓ. Obviously, it cannot be shorter than the distance between two scattering centers, i.e. ℓ must at least be larger than the diameter of an atom. This sets a universal (but crude) upper limit to ρ. The resistivity at which $d\rho/dT < 0$ was first thought to have the rather definite value of about 1.5 $\mu\Omega$ m (Mooij 1973), but has later been found to cover a wide range, from 0.3 to 4 $\mu\Omega$ m (Tsuei 1986). In spite of much effort (see Tsuei 1986, and reviews by Allen 1980, 1981, and Lee and Ramakrishnan 1985) there is no generally accepted theory which explains resistivity saturation, and its relation to phenomena like Anderson localisation (e.g. Kaveh and Mott 1982, Howson 1984). Dugdale (1995) has given an elementary review of various aspects of electrical properties in disordered metals.

THERMAL CONDUCTIVITY

1. Introduction

Metals are usually characterised by a high thermal conductivity κ. The heat is carried by the conduction electrons, and an account of the thermal conductivity closely parallels that of the electrical conductivity σ. The Wiedemann–Franz law,

$$\kappa = L\sigma T, \tag{16.1}$$

connects the two phenomena through the Lorenz number L. But it is an insulator—diamond—that has the highest known thermal conductivity of any material at room temperature. In that case, the heat is carried by phonons.

Figure 16.1 exemplifies the temperature dependence of the thermal conductivity in a pure metallic element (Al), a concentrated alloy (steel), a pure insulator (MgO) and a strongly disordered insulator (glass). Pure metals and insulators have a maximum in the thermal conductivity, much below room temperature. With increasing lattice disorder of various kinds, this maximum decreases in height and shifts to somewhat higher temperatures. In very impure or disordered materials, the maximum is absent.

It will be characteristic of our theoretical models, in particular those referring to the lattice part of the conductivity, that they only give qualitative descriptions. Thus, they provide a scheme for semiempirical analysis and for the establishment of trends, but we cannot hope for accurate numerical predictions.

In this book the emphasis is on what affects the thermal conductivity of real materials. More detailed theoretical treatments are found in reviews by Klemens (1958, 1969, 1993) and Beck et al. (1974). Parrot and
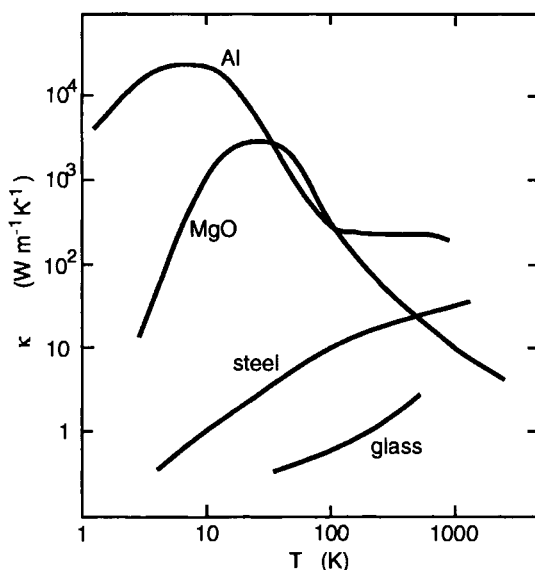
Fig. 16.1. The thermal conductivity $\kappa(T)$ of pure aluminium, pure MgO, a glass and stainless steel. Data from Touloukian et al. (1970).

Stuckes (1975) and Berman (1976) give general reviews of the thermal conductivity, partly along the lines presented here, while Slack (1979) has reviewed the thermal conductivity of insulators at high temperatures. Ziman (1960) gives a detailed account, with ample references to work before 1958.

2. Macroscopic relations

2.1. Thermal conductivity and resistivity

The density of heat flow rate φ in a temperature gradient ∇T is, according to *Fourier's law*,

$$\varphi = -\kappa(\nabla T). \tag{16.2}$$

To be more precise, the *conductivity* κ is a tensor with components κ_{ij} $(i, j = x, y, z)$ and the ith component of the heat-flow vector φ is

$$\varphi_i = -\sum_{j=1}^{3} \kappa_{ij}(\nabla T)_j. \tag{16.3}$$

Table 16.1

Components of the thermal conductivity in some axial crystals (at 300 K), in the unit W/(m K)

	TiO$_2$	SiO$_2$	Cd	Bi	β-Sn	Graphite (pyrolitic)
$\kappa_\perp$	7	6	104	9	74	2000
$\kappa_\parallel$	10	10	83	5	52	10

For a material in which κ_{ij} has cubic symmetry, the conductivity tensor is diagonal, i.e. $\kappa_{ii} = \kappa$ when $i = 1, 2, 3$ and $\kappa_{ij} = 0$ when $i \neq j$. Then the heat flow is parallel to the temperature gradient and eq. (16.3) holds with a scalar κ.

We shall also refer to the *thermal resistivity* **W**. It is the inverse of the conductivity. Thus, for scalar W and κ,

$$W = 1/\kappa. \tag{16.4}$$

In non-cubic lattices, the tensors κ and **W** have the same symmetry properties as the corresponding electrical quantities (Chapter 15, §6). Table 16.1 gives $\kappa_\perp$ and $\kappa_\parallel$ in some axial crystals, with data from Touloukian et al. (1970), and where $\kappa_\parallel$ is the conductivity along the crystallographic c-axis.

In metals, the heat transport by electrons (el) and phonons (ph) can be considered as independent. Then the total thermal conductivity is

$$\kappa_{tot} = \kappa_{el} + \kappa_{ph}. \tag{16.5}$$

Equation (16.5) does not mean that the electron–phonon interaction has been neglected, but only that we may consider separate Boltzmann equations for the electrons and the phonons. Note that the thermal resistivities of different heat carriers are not additive;

$$W_{tot} \neq W_{el} + W_{ph}. \tag{16.6}$$

This should not be confused with the fact that the effects of various scattering mechanisms for electrons may add in W_{el} (Matthiessen's rule), and analogously (but with some restrictions) for the scattering of phonons in W_{ph}.

2.2.   Thermal diffusivity

The physicist is primarily interested in the thermal conductivity κ, while measurements often give the *thermal diffusivity a*. The two quantities are related by

$$a = \frac{\kappa}{c_p \rho}. \tag{16.7}$$

Here, c_p is the specific (i.e. per unit mass) heat capacity at constant pressure and ρ is the mass density. *Fourier's equation* (the *heat equation*) contains the thermal diffusivity;

$$\frac{\partial T}{\partial t} - a(\nabla^2 T) = 0. \tag{16.8}$$

When the thermal conductivity is not uniform throughout the sample, eq. (16.8) is replaced by

$$c_p \rho \frac{\partial T}{\partial t} - \nabla(\kappa \nabla T) = 0. \tag{16.9}$$

Note that κ may be spatially varying not only because of an inhomogeneous material but also because κ is temperature dependent and the sample is in a temperature gradient. The heat equation coupled to the equation of state (i.e. with allowance for thermal expansion) was considered in Chapter 14 (§12).

Example: covarying thermal conductivity and diffusivity. When $T > \theta_D$, the heat capacity is approximately $3k_B$ per atom. If M is the (average) mass of an atom in the specimen, N the total number of atoms, V the specimen volume, and $\Omega_a = V/N$ the volume per atom, we have from eq. (16.7)

$$\frac{\kappa}{a} = c_p \rho \approx \left(\frac{3k_B}{M}\right)\left(\frac{M}{\Omega_a}\right) = \frac{3k_B}{\Omega_a}. \tag{16.10}$$

Since Ω_a does not vary nearly as much as the thermal conductivity between different materials, the material with the higher thermal conductivity usually also has the higher thermal diffusivity, provided that $T > \theta_D$. A later example (fig. 16.8) shows how $a(T)$ varies in a metal (vanadium) from very low to very high temperatures.
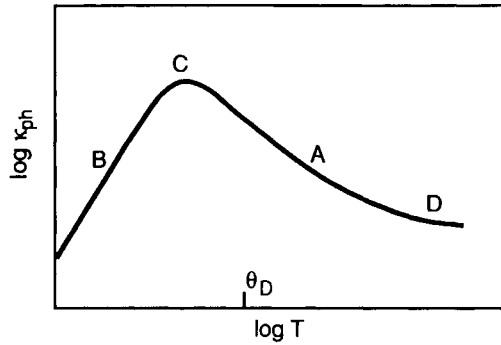
Fig. 16.2. A schematic plot of log(κ_{ph}) versus log(T). The four regions A, B, C and D are discussed in the text.

3. Lattice thermal conductivity: general aspects

The thermal transport by phonons will be referred to as the *lattice thermal conductivity*, and denoted κ_{ph}. In textbooks its mathematical description usually starts from the theory of thermal conduction in a classical gas. This does not mean that one has resorted to a classical description, because the scattering rate is calculated using quantum mechanics. We may think of phonons as a gas of particles, characterised by a momentum $\hbar q$ (q is the wave vector) and an energy $\hbar\omega(q, s)$. In an ideal gas, there are no collisions between the particles. That would lead, in the case of a classical gas, to an infinite thermal conductivity. Likewise, the lattice thermal conductivity is infinite if the phonon mean free path is not limited by collisions—between phonons themselves or between phonons and lattice imperfections. Energy and momentum are conserved in a collision event, but because the phonons are massless particles they may be annihilated or created. The simple picture just outlined allows us to reach a qualitative understanding of the characteristic features in the temperature dependence of κ. Figure 16.2 shows a typical temperature dependence of κ in a non-metallic crystal. There are four regions, denoted A, B, C and D, which we will explain.

In a classical gas one has the well-known formula for the thermal conductivity,

$$\kappa = (1/3)nc_V\bar{C}\ell. \tag{16.11}$$

Here n is the number of particles per volume, c_V is the heat capacity per particle (i.e. nc_V is the heat capacity per volume), $\bar{C}$ is the (aver-

age) velocity of a gas particle in the thermal equilibrium, and ℓ is its mean free path. In a solid, the lattice thermal conductivity is given by an expression of the form (16.11), but we must sum over all phonon modes $(\mathbf{q}, s)$ and let c_V, $\bar{C}$ and ℓ depend on $(\mathbf{q}, s)$. The phonons are not true particles but waves, characterised by a phase and group velocity. In this case, $\bar{C}$ in eq. (16.11) should be replaced by the group velocity $C_g(\mathbf{q}, s) = |\nabla_{\mathbf{q}} \omega(\mathbf{q}, s)|$. Let $c_V(\mathbf{q}, s)$ be the heat capacity of a single mode $(\mathbf{q}, s)$. Then we have for the lattice thermal conductivity $\kappa = \kappa_{ph}$;

$$\kappa_{ph} = (1/3V) \sum_{\mathbf{q},s} c_V(\mathbf{q}, s) C_g(\mathbf{q}, s) \ell(\mathbf{q}, s). \tag{16.12}$$

An accurate evaluation of this expression is a formidable task, but it is easy to draw some qualitative conclusions. The phonon mean free path ℓ is limited by collisions with other phonons and with lattice defects of various kinds. We assume that these mechanisms are additive so that

$$\frac{1}{\ell_{tot}(\mathbf{q}, s)} = \frac{1}{\ell_{ph-ph}(\mathbf{q}, s)} + \sum \frac{1}{\ell_{ph-def}(\mathbf{q}, s)}. \tag{16.13}$$

The first term on the righthand side refers to phonon-phonon collisions and the next terms to phonon scattering by faults such as point defects, dislocations, grain and phase boundaries and the finite size of the sample. The discussion is simplified if only one of the terms in eq. (16.13) dominates at a time and we make that approximation. A calculation of κ_{ph} from eq. (16.12) requires so many simplifying approximations that there is no point in using the precise phonon spectrum. We shall later be content with a Debye model, but we first discuss, qualitatively, the four regions A, B, C and D in fig. 16.2.

Region A. The number of phonons $(\mathbf{q}, s)$ present in thermal equilibrium is given by the Bose–Einstein statistical factor

$$n(\mathbf{q}, s) = \frac{1}{\exp[\hbar\omega(\mathbf{q}, s)/k_B T] - 1} \approx \frac{k_B T}{\hbar\omega(\mathbf{q}, s)}. \tag{16.14}$$

When $T > \theta_D$, we take the leading high temperature term. Phonon collisions that limit the thermal conductivity must involve three or more phonons. The simplest case arises when two phonons combine in a "collision" event, and form one new phonon (fig. 16.3a) or when one
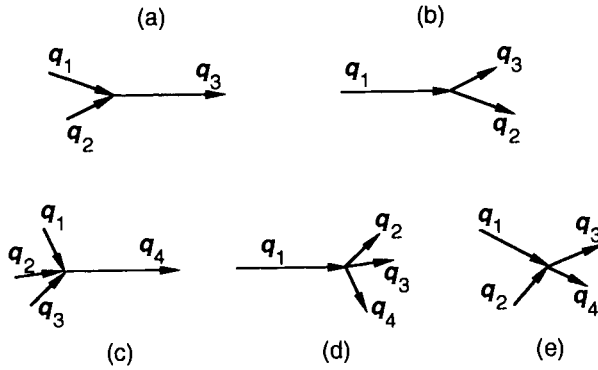
Fig. 16.3. Three-phonon (a, b) and four-phonon (c, d, e) scattering processes.

phonon is annihilated to form two new phonons (fig. 16.3b). It is intuitively clear that the probability for the phonon $(\mathbf{q}_1, s_1)$ to undergo the process depicted in fig 16.3a varies as the number of phonons present to collide with, i.e. as some average n of all $n(\mathbf{q}, s)$. Because $n \sim T$ at high temperatures, we expect that scattering such as in fig. 16.3a (and, it can be argued, such as in fig. 16.3b) leads to $\ell \sim 1/T$. There may also be four-phonon processes (fig. 16.3c, d, e). For them, $\ell \sim 1/T^2$. Usually, the phonon–phonon scattering at high temperatures is dominated by three-phonon processes (fig. 16.3a, b). The heat capacity at high temperature is reasonably well approximated by its classical value, $3k_B$ per atom. Hence, κ_{ph} varies with T as $1/T$. This is close to the observed temperature dependence in region A of fig. 16.2.

Region B. We now turn to region B in fig. 16.2, where $\log(\kappa_{ph})$ varies linearly with $\log(T)$, i.e. $\kappa_{ph} \sim T^n$. Typically, $n \approx 3$. Since there are few phonons excited at low temperatures, collision processes between them are rare. Instead, the mean free path is limited by phonon scattering against defects. Let us take ℓ to be independent of T. Because the heat capacity of phonons at low T varies as T^3 for all crystalline solids, we get the universal result $\kappa \sim T^3$.

Region C. The maximum of $\kappa_{ph}(T)$, region C, occurs roughly where $\ell_{ph-ph} \sim \ell_{ph-def}$. Because ℓ_{def} depends on the nature and number of defects in the crystal, the temperatures covered by region C are characteristic of the specimen rather than of the chemical composition of

the material. As a very crude rule of thumb, the maximum lies at temperatures just below $0.1\theta_D$.

Region D. At very high temperatures, $\kappa_{ph}(T)$ often decreases less rapidly than as $1/T$. There seems to be a "saturation" so that $\kappa_{ph}(T)$ does not fall below a certain value. This is analogous to the saturation of the electrical conductivity in metals and alloys (Chapter 15, §11) and it can be given a similar interpretation. The mean free path decreases with increasing T, but ℓ cannot be shorter than a characteristic distance a between two neighbouring atoms. (In fact, a more restrictive condition holds. A phonon is a wave packet defined by the displacements of discrete atoms. It would be unphysical to consider ℓ shorter than a wavelength.) Hence, from eq. (16.11), κ_{ph} cannot be smaller than of the order of $(1/3)(3Nk_B/V)C_{sound,D}a \sim k_B C_{sound,D}/a^2$, where N is the number of atoms in the volume V, $a^3 \sim V/N$ and $C_{sound,D}$ is the sound velocity in the Debye model. This argument is crude, because the Boltzmann equation and the concept of a mean free path between scattering events breaks down when ℓ approaches a. However, it gives a physical explanation for the observed trend towards a weak temperature dependence of $\kappa_{ph}(T)$ at very high T or in very defect lattices.

In the following sections we will deal separately with the scattering mechanisms which dominate $\kappa_{ph}(T)$ in the regions A, B and D of fig. 16.2. Before that we give a general expression for κ_{ph}, based on the Boltzmann equation for phonon transport.

4. The Boltzmann equation for phonon transport

In Chapter 15 we presented expressions for the electric current **j** and the electrical conductivity tensor σ with components σ_{ij}, in relation to the Boltzmannn equation for electron transport in an electric field **E**. Here we give the corresponding expressions for the density of heat-flow rate φ, and the thermal conductivity components κ_{ij} resulting from the Boltzmann equation for phonon transport in a temperature gradient ∇T. There are close similarities between the two sets of expressions. The thermal transport can be written

$$\varphi = -(1/V) \sum_{\mathbf{q},s} [C_g(\mathbf{q}, s) \cdot \nabla T] C_g(\mathbf{q}, s) \tau(\mathbf{q}, s) C_{har}(\mathbf{q}, s), \quad (16.15)$$

where $\mathbf{C}_g(\mathbf{q}, s) = \nabla_{\mathbf{q}} \omega(\mathbf{q}, s)$ is the group velocity and C_{har} is the heat capacity for a single phonon mode $(\mathbf{q}, s)$, i.e. with the Einstein-model temperature dependence $(x = \hbar \omega(\mathbf{q}, s)/k_B T)$;

$$C_{har} = k_B \frac{x^2 e^x}{(e^x - 1)^2}. \tag{16.16}$$

The tensor components of the thermal conductivity are

$$\kappa_{ij} = (1/V) \sum_{\mathbf{q}, s} [C_g(\mathbf{q}, s)]_i [C_g(\mathbf{q}, s)]_j \tau(\mathbf{q}, s) C_{har}(\mathbf{q}, s). \tag{16.17}$$

In an isotropic system, $\omega(\mathbf{q}, s)$ and $\tau(\mathbf{q}, s)$ depend only on $|\mathbf{q}|$ and s. Then $\mathbf{C}_g(\mathbf{q}, s) = (\mathbf{q}/|\mathbf{q}|) C_g(s)$. When $i \neq j$ the sum over $\mathbf{q}$ in eq. (16.17) yields $\kappa_{ij} = 0$, as expected. The mean free path $\ell(\mathbf{q}, s)$ is

$$\ell(\mathbf{q}, s) = C_g(\mathbf{q}, s) \tau(\mathbf{q}, s). \tag{16.18}$$

With eq. (16.18) in eq. (16.17) we recover the formulation (16.12) of κ_{ph} in terms of ℓ. The prefactor $(1/3)$ in eq. (16.12) arises from eq. (16.17) because, in an isotropic system, $[C_g]_i [C_g]_j = (1/3)[C_g]^2$ on the average.

It is often more natural to express $\tau(\mathbf{q}, s)$ and $\ell(\mathbf{q}, s)$ as a function of the phonon frequencies ω of the modes $(\mathbf{q}, s)$. Then the sums over $(\mathbf{q}, s)$ can be replaced by an integral over ω containing the phonon density of states $F(\omega)$. For instance, from eq. (16.17)

$$\begin{aligned} \kappa_{ph} &= (N/3V) \bar{C}_g \int_0^{\omega_{max}} C_{har}(\omega) \ell(\omega) F(\omega) \, d\omega \\ &= (N/3V) \bar{C}_g^2 \int_0^{\omega_{max}} C_{har}(\omega) \tau(\omega) F(\omega) \, d\omega. \end{aligned} \tag{16.19}$$

Here, $\bar{C}_g$ is some average phonon group velocity, $C_{har}(\omega)$ is the heat capacity of a single phonon mode, (eq. (16.16)), and N/V is the number of atoms per volume. We recall our normalisation convention, $\int F(\omega) \, d\omega = 3$.

5.   Lattice conductivity limited by anharmonic effects

5.1.   General results

If the lattice vibrations are strictly harmonic, the phonons are represented by non-interacting waves. Then there is no mechanism for phonon scattering and the lifetime, $\tau_{\text{ph}-\text{ph}}$, is infinite. In order to have a finite $\tau_{\text{ph}-\text{ph}}$, one must retain anharmonic terms when the potential energy Φ is expanded in the atomic displacements $\mathbf{u}$ (Appendix C);

$$
\Phi = \Phi_0 + (1/2) \sum_{\alpha\beta,ij} \Phi_{ij} u_\alpha u_\beta + (1/3!) \sum_{\alpha\beta\gamma,ijk} \Phi_{ijk} u_\alpha u_\beta u_\gamma
$$
$$
+ (1/4!) \sum_{\alpha\beta\gamma\delta,ijkl} \Phi_{ijkl} u_\alpha u_\beta u_\gamma u_\delta + \cdots. \tag{16.20}
$$

Here, i, j, k and l label atoms and α, β, γ and δ label Cartesian coordinates. It can be shown that terms in eq. (16.20) which are cubic in $\mathbf{u}$ correspond to three-phonon scattering (fig. 16.3a, b). The terms quartic in $\mathbf{u}$ correspond to four-phonon processes (fig. 16.3c, d, e). To calculate the phonon-limited lattice thermal conductivity from eq. (16.17) we first must find the lifetime $\tau(\mathbf{q}, s)$. Consider scattering in and out of a state 1, as shown schematically in fig. 16.3a, b. Let the statistical distribution function of the state 1 be perturbed from its equilibrium value $n(1)$ to $\tilde{n}(1) = n(1) + \Delta n(1)$ but let the states 2 and 3 be described by the equilibrium functions $n(2)$ and $n(3)$. The probability for a scattering event $1 \to 2 + 3$ contains the temperature explicitly through the factors $\tilde{n}(1)[n(2) + 1][n(3) + 1]$. (The term 1 in $n + 1$ arises because of the stimulated emission of bosons, i.e. phonons.) Similar expressions hold for events $2 + 3 \to 1$, etc. One is left with an expression

$$
\frac{1}{\tau(1)} = \frac{2\pi}{\hbar} \sum_{2,3} |H(1, 2, 3)|^2 \frac{n(2)n(3)}{n(1)}, \tag{16.21}
$$

where $|H(1, 2, 3)|^2$ is short for $|\langle 1|\Delta H|2, 3\rangle|^2 \delta(\mathbf{q}_1 - \mathbf{q}_2 - \mathbf{q}_3 - \mathbf{G})\delta(\hbar\Delta_\omega)$, and $\Delta_\omega = \omega_1 - \omega_2 - \omega_3$ or similar terms, $\langle \ldots \Delta H \ldots \rangle$ is a quantum mechanical matrix element for the transition, and delta functions $\delta(\ldots)$ account for wavenumber and energy conservation. Equation (16.21) is a key expression in our subsequent discussion. It is very difficult to evaluate $|H(1, 2, 3)|^2$ accurately but simple assumptions

(e.g. Leibfried and Schlömann 1954, Klemens 1958, 1969), and even dimensional arguments, lead to a form

$$|H(1, 2, 3)|^2 = A\frac{\hbar^2\gamma^2\Omega_a^{1/3}}{3MN}\frac{\omega_1\omega_2\omega_3}{\bar{C}_g^3}. \qquad (16.22)$$

Here, A is a dimensionless constant, roughly of the order of unity. Furthermore, we have assumed a monatomic primitive lattice (fcc or bcc), with atomic volume Ω_a and atomic mass M. The parameter γ in eq. (16.22) is related to the Grüneisen parameters, but it is not equal to any particular $\gamma(n)$. N is the number of atoms and $3N$ is the number of phonon modes. The evaluation of $\tau(1)$ in eq. (16.21) requires a summation over modes 2 and 3. This cannot be done analytically, so it is not possible to give a closed-form expression for the temperature dependence of the thermal conductivity $\kappa_{\mathrm{ph-ph}}(T)$, valid at all temperatures and based on eq. (16.21). Instead we discuss separately the case of high and low temperatures.

The four-phonon processes (fig. 16.3c, d, e), are much less important than the three-phonon processes (Ecsedy and Klemens 1977). This is different from the case of anharmonic shifts in the vibrational entropy (Chapter 8, §5), where the three- and four-phonon interactions are of roughly equal importance.

Because anharmonic effects are always present (contrary to various lattice defects or sample size effects) one may call the lattice conductivity that is limited by anharmonicity the *intrinsic conductivity*. We denote it $\kappa_{\mathrm{ph-ph}}$.

5.2. Low temperatures

The combination $n(2)n(3)/n(1)$ of Bose–Einstein factors in eq. (16.21) must be considered in some detail. At a given (low) temperature, only phonon states with $\hbar\omega_1 \lesssim k_B T$ are sufficiently populated to be of importance in the scattering process $1 \rightarrow 2 + 3$. In this context, Peierls (1929) derived a very important result that only scattering with $\mathbf{G} \neq 0$ in eq. (16.21) contributes to the thermal resistivity. This is termed *Umklapp scattering*, and referred to as U-processes. (The German *Umklapp* means a "flip-over".) If now $\mathbf{q}_1$ is small (because $\hbar\omega_1 \lesssim k_B T$), the δ-function for wave vectors in eq. (16.21) implies that at least one of $|\mathbf{q}_2|$ and $|\mathbf{q}_3|$ is of the order of $|\mathbf{G}|$, i.e. of the order of q_D. This also implies

that at least one of ω_2 and ω_3 is of the order of the Debye frequency ω_D. Hence, when $T \ll \theta_D$, the factor $n(2)n(3)/n(1)$ contains a term of the order

$$\exp(-\hbar\omega_D/k_BT) = \exp(-\theta_D/T). \tag{16.23}$$

Such an exponential term dominates the temperature dependence of $\kappa_{ph-ph}(T)$ and, in a qualitative description, we can neglect any pre-factors containing powers of T. Therefore, at low temperatures, we get approximately

$$\kappa_{ph-ph} = \kappa_0 \exp(-\theta_D/T). \tag{16.24}$$

The prefactor κ_0 is, in principle, to be calculated from $\tau(1)$ in eq. (16.21). In practice, this is not feasible, and we are left with κ_0 as a free parameter. Its order of magnitude may be estimated by joining $\kappa_{ph-ph}(T)$ at high temperature (eq. (16.26)), to the low temperature form (eq. (16.24)), with $T = \theta_D$. The Debye temperature θ_D in eq. (16.24) only measures, in a rough way, the magnitude of typical phonon energies, and θ_D is not equal to any particular $\theta_D(n)$. Sometimes a reasonable account of $\kappa_{ph-ph}(T)$ in the transition region between A and C in fig. 16.2 is obtained with θ_D replaced by $\theta_D(-3)/b$, where b typically is between 2 and 3.

5.3. High temperatures

Let the temperature be much higher than the Debye temperature θ_D, i.e. $k_BT \gg \hbar\omega_i$, for $i = 1, 2, 3$. Then $n(2)n(3)/n(1) \approx (k_BT/\hbar)(\omega_1/\omega_2\omega_3)$. When this is inserted in eq. (16.21) the explicit dependence on ω_2 and ω_3 vanishes, by eq. (16.22). There is still a dependence on the modes 2 and 3 in $H(1, 2, 3)$ but that has been allowed for in an average manner in the constant A in eq. (16.22). The summation over the mode 3 reduces to a single term because of the δ-functions in eq. (16.21). Because $\tau(1)$ now only depends on the frequency $\omega = \omega(\mathbf{q}_1, s_1)$, but makes no explicit reference to the values of $\mathbf{q}$ or s, we write $\tau(1) = \tau(\omega)$ and get

$$\frac{1}{\tau(1)} = \frac{1}{\tau(\omega)} = 2\pi A \frac{\gamma^2 \Omega_a^{1/3} k_B T}{M} \frac{\omega^2}{\bar{C}_g^3}. \tag{16.25}$$

Finally, an integration over all modes 1, i.e. over all frequencies ω, yields κ_{ph-ph} from the expression (16.19). With a Debye phonon spectrum, and using that $\bar{C}_g/a = \omega_D/(9\pi/2)^{1/3}$ and $(4\pi/3)a^3 = \Omega_a$, one obtains

$$\kappa_{ph-ph} = \frac{B}{(2\pi)^3} \frac{M\Omega_a^{1/3} k_B^3 \theta_D^3}{\hbar^3 \gamma^2 T}, \tag{16.26}$$

where B is a dimensionless constant. This is a key result. Formally it is valid when $T \gg \theta_D$, but in practice the $1/T$ dependence is often already well obeyed for $T > \theta_D/3$. A relation of the form (16.26) has been derived by Leibfried and Schlömann (1954) (corrected for an error by a factor of two by Julian (1965)), Klemens (1958, 1969) and others. These theoretical approaches give essentially the same combination of characteristic parameters, but they differ in the numerical prefactor B. This is natural, because an evaluation of B requires a large number of simplifying, and to some extent arbitrary, assumptions. Klemens (1969) suggests that $B = 1.61$, a value that usually gives an adequate description of the measured conductivity of non-metals at high temperatures (Slack 1979). We note that the theory was developed for 1 atom per primitive cell, i.e. with only acoustic branches in the phonon spectrum. In §5.4 it is discussed how θ_D must be redefined in the case of several atoms per primitive cell, i.e. when the phonon spectrum contains optical modes. We also make the important observation that the intrinsic thermal conductivity at high temperatures has an essential contribution from the long-wavelength phonons. This is because $\tau \sim 1/\omega^2$ and $F(\omega) \sim \omega^2$ which makes the product $\tau(\omega)F(\omega)$ in the integrand of eq. (16.19) independent of ω. Finally, we note that κ_{ph-ph} in eq. (16.26) is explicitly linear in the atomic mass M, but there is also an indirect mass dependence in θ_D, which varies as $M^{-3/2}$ (for a monatomic solid). Hence, κ_{ph-ph} varies as $M^{-1/2}$ in this model.

Example: analysing κ_{ph-ph} at high temperatures. In view of the theoretical uncertainties about the absolute magnitude of κ_{ph-ph}, one may choose to analyse high temperature experiments using the semiempirical formula

$$\kappa_{ph-ph} = \kappa^*(T_{fus}/T)^\eta. \tag{16.27}$$

Here κ^* is a fitted prefactor, T_{fus} is a melting temperature and the exponent η is near unity. Neglecting any temperature dependence, other
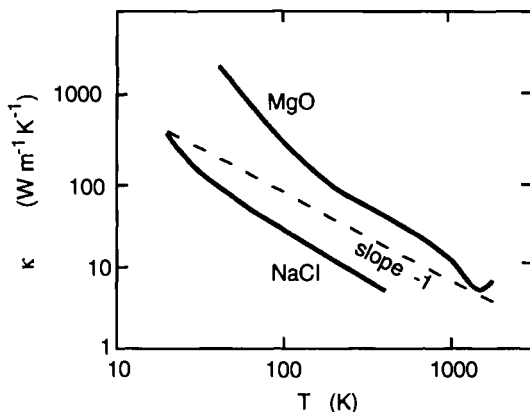
Fig. 16.4. Experimental values (Touloukian et al. 1970) of $\ln \kappa$ versus $\ln T$, in the high-temperature region, for NaCl and MgO. The dashed line has the slope -1, i.e. the slope corresponding to $\kappa \sim 1/T$.

than the explicit factor $1/T$ and the indirect temperature dependence of θ_D due to the thermal expansion, we have from eqs. (16.26) and (16.27) near T_{fus}

$$
\begin{aligned}
\eta &= -(d \ln \kappa_{ph-ph}/d \ln T) \\
&\approx 1 - 3(\partial \ln \theta_D/\partial \ln V)(\partial \ln V/\partial \ln T) \\
&\approx 1 + 3\beta\gamma T_{fus}.
\end{aligned}
\tag{16.28}
$$

For many solids, $\beta T_{fus} \sim 0.06$, and $\gamma \sim 1.5$. Then $\eta \approx 1.3$. Thus, thermal expansion causes η to be somewhat larger than unity. The four-phonon processes (fig. 16.3c, d, e) give a scattering rate for which $\tau \sim 1/T^2$. This would also make η larger than 1, but the effect appears to be small (Ecsedy and Klemens 1977).

Figure 16.4 shows $\ln \kappa_{tot}$ versus $\ln T$, from experiments. Because κ_{tot} for these solids is mainly limited by phonon-phonon scattering, the slopes of the curves give an estimation of the parameter η in eq. (16.27).

5.4.   Several atoms per primitive cell

In the derivation above, we have assumed a Debye spectrum for all phonon modes. This must be modified when there are several atoms per primitive cell in the lattice. Consider the extreme case that the dispersion curves for the optical branches are almost "flat", as in fig. 16.5. The
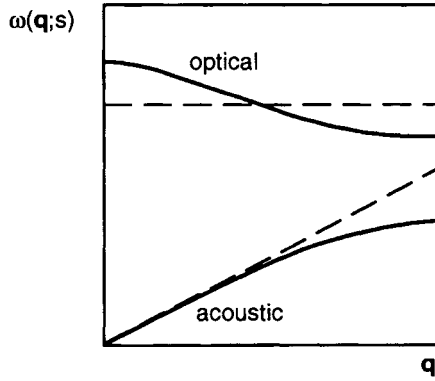
Fig. 16.5. A schematic phonon dispersion curve for a solid with 2 atoms per primitive cell. The dashed line is a model dispersion curve, corresponding to a Debye model for the acoustic branch and an Einstein model for the optical branch.

group velocity $\mathbf{C_g} = \nabla_\mathbf{q}\omega(\mathbf{q}, s) \approx 0$ for these branches, and therefore they do not contribute to the heat flow. Still the optical modes affect the thermal conductivity because they interact with the heat-carrying acoustic modes and thus limit the relaxation time. Slack and Oliver (1971) assumed that one should sum over only the acoustic modes in eq. (16.17) and they neglected the influence of the optical modes on τ for the acoustic branches, while Roufosse and Klemens (1973) included the effect of optical modes on τ. When the high temperature formula (16.26) is applied to lattices with several atoms, p, per primitive cell, one has to be careful in the definition of θ_D. Typical acoustic phonon energies are $k_B\theta_D/p^{1/3}$, and not $k_B\theta_D$. Slack (1979) has considered the thermal conduction in lattices with $p > 1$ in some detail. He finds that a result calculated as if there were 1 atom per cell should be divided by a factor of $p^{2/3}$. This is not a strict rule, but it gives the trend. In an analogous way, θ_D must be reduced in the factor $\exp(-\theta_D/T)$ that accounts for the freezing-out of the Umklapp scattering as the temperature is decreased.

6. Defect-limited lattice conductivity

6.1.   General considerations

We will consider the scattering of phonons by:
  (i)   point defects; substitutional atoms, interstitials, vacancies, isotopic defects etc.;
 (ii)   line defects; thin cylindrical inclusions;
(iii)   planar defects; thin platelets;
(iv)   volume defects; the strain field from dislocations;
 (v)   interface boundaries and sample boundaries.
The scattering cross-section has a different dependence on the phonon wavelength in each of the five cases (i)–(v). It is well known, for example from Rayleigh scattering in acoustics and optics, that the scattering cross-section for a point defect varies as $1/\lambda^4$, where λ is the wavelength. For line defects (ii), the cross-section varies as $1/\lambda^3$; for planar defects (iii), as $1/\lambda^2$; and for the strain field due to dislocations (iv), as $1/\lambda$. In case (v) it is practically independent of λ.

The scattering by defects is of particular importance at low temperatures. Since only phonons with $\hbar\omega(\mathbf{q}, s) \lesssim k_B T$ are excited, it is a good approximation to take $\omega(\mathbf{q}, s)$ linear in $|\mathbf{q}|$. Then $\omega \sim 1/\lambda$. It follows that the scattering cross-sections for cases (i)–(v) vary as ω^n, where $n = 4, 3, 2, 1$ and 0, respectively. The corresponding relaxation times τ vary as ω^{-n}. We now assume an isotropic Debye spectrum for $F(\omega)$, with $k_B\theta_D = \hbar\omega_{max}$, and make the substitution $\hbar\omega/k_B T = x$. Then, from eq. (16.19),

$$\kappa_{ph}(T) = \frac{1}{2\pi^2} \frac{k_B^4 T^3}{\hbar^3 C_g} \int_0^{\theta_D/T} \frac{x^4 e^x \tau(x)}{(e^x - 1)^2} \, dx. \tag{16.29}$$

With $\tau \sim \omega^{-n} \sim x^{-n}$, and at low temperatures, we have

$$\kappa_{ph}(T) \sim T^{3-n} \int_0^\infty \frac{x^4 x^{-n} e^x}{(e^x - 1)^2} \, dx. \tag{16.30}$$

The integral in eq. (16.30) diverges at $x = 0$ when $n = 3$ or 4, i.e. for point and line defects. Therefore, one must introduce a cut-off x_c as the lower integration limit. Physically this cut-off means that the finite size of the specimen, grain boundaries or extended defects, dominate

the scattering of very low frequency phonons. When $n = 0$, 1 or 2, the integrand in eq. (16.30) has its maximum at, very roughly, $x \sim 1$. It follows that those phonons that carry most of the heat have $\hbar\omega(\mathbf{q}, s) \sim k_B T$, i.e. a wavelength $\lambda \sim (\theta_D/T)\lambda_D \sim (\theta_D/T)a$, where a is an atomic diameter.

After this general introduction to defect scattering of phonons, we discuss each defect separately.

6.2. Point defect scattering

It is instructive to first recall Rayleigh's (1894) classical theory of sound wave scattering against small objects. Some complications arise in solids because there are longitudinal as well as transverse modes (Ziman 1960). We can write, for *macroscopic inclusions*,

$$\frac{1}{\tau_{\text{def}}} = n_{\text{def}}A\left(\frac{1}{\lambda^4}\right)\bar{C}_g V_{\text{def}}^2[(\Delta\rho/\rho)^2 + 6(\Delta G/G)^2]. \qquad (16.31)$$

Here, n_{def} is the number of defects per volume, V_{def} is the volume of a single defect (i.e. $n_{\text{def}}V_{\text{def}}$ is the volume fraction occupied by defects), $\bar{C}_g$ is the group velocity of the wave, $(\Delta\rho/\rho)$ is the change in the mass density of the inclusion relative to the matrix, $(\Delta G/G)$ is the corresponding change referring to the shear modulus G (that relates to the sound velocity) and A is a dimensionless constant of the order of $4\pi^3$. Note that $(\Delta\rho/\rho)$ and $(\Delta G/G)$ need not be small.

The archetype of a point defect is a substitutional atom in a lattice. It creates several kinds of disturbances for a propagating phonon. The atomic mass and the interatomic forces are changed, and atoms are more or less displaced (often referred to as lattice relaxation). We first discuss the mass change (*isotope scattering*), because that is the simplest case to treat theoretically.

Klemens (1955) derived an expression for the scattering time $\tau_{\Delta M}$, as limited by a change of an atomic mass from M to $M + \Delta M$. In a monatomic lattice, and with an isotropic Debye model for the phonons, he obtained

$$\frac{1}{\tau_{\Delta M}(\omega)} = c_{\text{def}}\frac{\Omega_a\omega^4}{4\pi\bar{C}_g^3}\left(\frac{\Delta M}{M}\right)^2. \qquad (16.32)$$

This is equivalent to eq. (16.31) when $\Delta G/G = 0$. (Let $A = 4\pi^3$, $\omega\lambda = 2\pi\bar{C}_g$ and $\Delta\rho/\rho = \Delta M/M$.) $V_{\text{def}} = \Omega_a$ is the volume per atom and c_{def}

(with $0 < c_{def} < 1$) is the defect concentration in the lattice (i.e. the volume or site fraction occupied by defects). As in eq. (16.31), eq. (16.32) does not require $\Delta M/M$ to be small. A more detailed formulation of the scattering problem (Takeno 1963, Callaway 1963, Krumhansl 1965, Elliott and Taylor 1964, McCombie and Slater 1964, Klein 1966) leads to essentially the same result.

The combined effect of mass and force constant changes have been studied theoretically by Krumhansl and Matthew (1965) and Yussouff and Mahanty (1966, 1967). In one dimension (a linear chain), Krumhansl and Matthew (1965) found that the factor $(\Delta M/M)^2$ in the scattering rate should be replaced by

$$\left[\frac{\Delta M}{M} + \frac{2(\Delta k/k)}{1 + (\Delta k/k)}\right]^2, \tag{16.33}$$

if the force constants between nearest-neighbours at the defect site are changed from k to $k + \Delta k$. Thus, there is in this model a cancellation of the two effects when $(\Delta k/k) = -(\Delta M/M)/[2 + (\Delta M/M)]^{-1}$. No such simple result seems to be known for a three-dimensional system, but we conclude that the effects of mass and force constant changes are not additive.

An impurity atom may cause a dilatation of the lattice. Its effect on the thermal conductivity can be estimated from the classical theory of Rayleigh scattering, if one relies on some Grüneisen parameter to estimate changes in the group velocity $\bar{C}_g$. Also, in this case there is the possibility of a cancellation between the two effects. In spite of much work (e.g. Carruthers 1961), it is still uncertain how to handle the dilatation term (Klemens 1983a).

In our treatment of point defects, it has been required that $\lambda \gg L$, where L is a characteristic size of the scattering object. Nothing has been said about the distance D between these objects. If the phonon mean free path $\ell_{def} \gg D$, a phonon will "see" very many point-like scattering centres and there may be interference effects. The total scattering amplitude is the sum of amplitudes from each scattering centre. However, the scattered intensity depends on the total scattering amplitude squared. If the scattering centres are randomly distributed, the interference effect averages to zero and the total scattered intensity is the sum of the intensity calculated from each scattering centre separately. (A better known example of this phenomenon is the blue colour of the sky. It is

caused by Rayleigh scattering of light against air molecules, but it is essential that the number-density of molecules is spatially fluctuating.)

Example: vacancy scattering. Vacancies can be regarded as point defects with the mass change $\Delta M/M = -1$ and (less accurate) $\Delta G/G = -1$. The equilibrium number of thermally generated vacancies is much too small (typically $< 10^{-3}$) to have any significant effect on the lattice thermal conductivity. A larger concentration is found in doped ionic solids, e.g. KCl doped with Ca (Slack 1957), where charge neutrality requires that vacancies are formed. The vacancies are often adjacent to the impurity atoms. Their combined effect on κ_{ph} is small, but may be detected in accurate experiments at low temperatures (Schwartz and Walker 1966). The theory of vacancy scattering is in fair agreement with experiments (Klemens 1983a).

Example: clustering of small defects. Assume that clusters are formed, each containing p of the original small defects. Then, n_{def} in eq. (16.31) decreases by a factor p while V_{def}^2 increases by a factor p^2. Thus, within Rayleigh's classical model, τ (and hence κ_{ph}) decreases by a factor of p. However, the Rayleigh formula is not valid when the characteristic size L of the scattering objects becomes comparable to the wavelength. We expect a breakdown of eq. (16.31) when $Lq > 1$, i.e. when $\omega > C_g/L$. The theory describing the transition from Rayleigh scattering to the "geometrical" scattering against large objects is complicated (Schwartz and Walker 1967).

6.3. Dislocation scattering

The influence of dislocations on the lattice thermal conductivity has received continuous interest for a long time (e.g. Klemens 1955, Bross et al. 1963, Eckhardt and Wasserbäch 1978, Anderson 1983). Because of the strain field surrounding a dislocation, they do not scatter like line defects. The effect of dislocations on the thermal conductivity is controversial and theoretical calculations are in poor agreement with experiments. It is only at very low temperatures ($T < \theta_D/10$) that dislocation scattering in heavily deformed materials may be of importance.
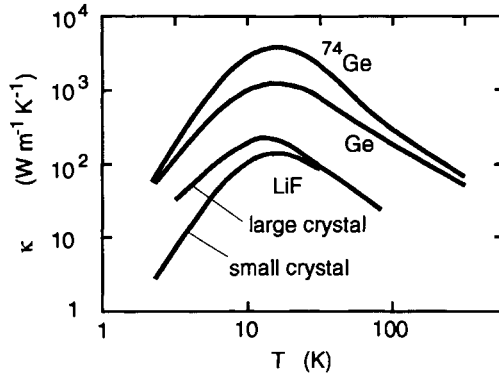
Fig. 16.6. The thermal conductivity κ of a crystal of the pure isotope ^{74}Ge and a crystal of natural Ge. Also shown is κ of irradiated LiF in two crystal sizes.

6.4. Boundary scattering

At very low temperatures, the phonon mean free path ℓ may be comparable to a characterisitic sample dimension d (the diameter of a wire or the diameter of small crystals). Then ℓ is independent of λ (or ω) and κ_{ph} varies as the low temperature lattice heat capacity, i.e. as T^3.

Example: scattering by defects in LiF and Ge. Figure 16.6 shows the measured thermal conductivity of Ge (Geballe and Hull 1958) and LiF (Pohl 1960). For Ge, $\kappa(T)$ is shown for an isotopically almost pure sample of ^{74}Ge and for natural Ge. The difference in κ can be explained by the isotope scattering model (§6.2). At very low temperatures, boundary scattering gives κ a T^3-dependence. The two curves for LiF refer to irradiated samples of different sizes ($6.7 \times 0.8 \times 40$ mm and $0.7 \times 0.8 \times 40$ mm). F-centres, introduced by irradiation, contribute to the scattering at T near the maximum in κ.

6.5. Several scattering processes acting simultaneously

In eq. (16.13) we wrote the inverse phonon mean free path as a sum of inverse mean free paths for each scattering mechanism. This is equivalent to a corresponding relation for the lifetimes $\tau(\omega)$;

$$\frac{1}{\tau_{tot}(\omega)} = \frac{1}{\tau_{ph-ph}(\omega)} + \sum \frac{1}{\tau_{ph-def}(\omega)}. \tag{16.34}$$

Let us assume that there are only two scattering mechanisms, each associated with a constant relaxation time. Then, with $\tau_{tot} = (1/\tau_1 + 1/\tau_2)^{-1}$ inserted in eq. (16.19),

$$
\begin{aligned}
W_{ph,tot} &= 1/\kappa_{ph,tot} \\
&= \left[(N/3V)\bar{C}_g^2 \int_0^{\omega_{max}} C_{har}(\omega)F(\omega)\,\mathrm{d}\omega \right]^{-1} \left(\frac{1}{\tau_1} + \frac{1}{\tau_2} \right) \\
&= 1/\kappa_1 + 1/\kappa_2 = W_1 + W_2.
\end{aligned}
\tag{16.35}
$$

If τ depends on ω, the arguments above can be repeated provided that $\tau_1(\omega)/\tau_2(\omega)$ is independent of ω. Only then can one add phonon-related terms in the thermal resistivity, in analogy to Matthiessen's rule for adding contributions to the electrical resistivity in metals. However, the condition for $\tau_1(\omega)/\tau_2(\omega)$ is usually not fulfilled, but eq. (16.34) is still the natural relation to start from, because it expresses the fact that the total scattering rate is the sum over the various scattering processes that are present.

Erdös and Haley (1969) considered the validity of the relaxation time approximation and eq. (16.34) in an application to point defect scattering in a slab of finite size. Then the point defects contribute to the thermal resistance as $(c_{def})^{3/4}$, i.e. not simply proportional to the point defect concentration c_{def}.

6.6. Concentrated alloys

The electrical resistivity of a concentrated alloy very roughly follows the rule $\rho_{tot} = \rho_{el-ph}(T) + c(1-c)\rho^*$, where the defect resistance $c(1-c)\rho^*$ varies parabolically with the composition $A_{1-c}B_c$ of the alloy and is independent of the temperature. (This behaviour excludes cases with "saturation".) In phonon transport such a simple result does not hold. The reason is to be sought in the point defect scattering, which gives a divergence in κ_{ph} arising from low frequency phonons. The divergence is taken care of by the anharmonic (phonon-phonon) scattering. Because of the very different behaviour of $\tau(\omega)$ for the two scattering mechanisms, Matthiessen's rule is strongly violated. The qualitative result, at high T and not too small c, is (Klemens 1960)

$$
W_{ph,tot} \sim [c(1-c)]^{1/2} T^{1/2} (1/\tau_1 + 1/\tau_2).
\tag{16.36}
$$

Such a behaviour has been observed, e.g. in experiments on Ge–Si (Abeles 1963).

7. Electronic contribution to the thermal conductivity

7.1. Introduction

The expression for the conductivity of a classical gas was the starting point for our discussion of the phonon part of the thermal conductivity in solids. The same fundamental expression can be used in a treatment of the electronic contribution, κ_{el}. One can write

$$\kappa_{el} = \frac{1}{3} n c_{el} v_{el} \ell_{el}, \tag{16.37}$$

where c_{el} is the electronic heat capacity (per electron), n is the number of conduction electrons per volume, v_{el} the electron velocity and ℓ_{el} the electron mean free path. Now let the electrons be described by a free-electron model, i.e. $v_{el} = v_F$ (the Fermi velocity) and $c_{el} = (\pi k_B / v_F)^2 (T/m)$. The mean free path can be expressed in the electron lifetime τ as $\ell_{el} = v_F \tau$. The thermal conductivity then becomes

$$\kappa_{el} = \frac{\pi^2 n k_B^2 T \tau}{3m}. \tag{16.38}$$

Compare this with the result (eq. (15.2)) for the electrical conductivity, $\sigma = n e^2 \tau / m$. We get

$$\frac{\kappa_{el}}{\sigma} = \frac{\pi^2 n k_B^2 T \tau / 3m}{n e^2 \tau / m} = \frac{\pi^2}{3} \left(\frac{k_B}{e} \right)^2 T = L_0 T. \tag{16.39}$$

L_0 (= 2.44×10^{-8} WΩ K^{-2}, or V^{2}K^{-2}) is the *Lorenz number* for a free-electron model in which the lifetime τ is taken to be the same for electrical and thermal transport. The proportionality between κ_{el} and σ was discovered by Wiedemann and Franz (1853). Lorenz (1881) noted that the proportionality constant is linear in T. Therefore, eq. (16.39) is known as the *Wiedemann–Franz* or the *Wiedemann–Franz–Lorenz law*. The first theoretical account of this law is due to Drude (1900a). In a real metal we *define* the Lorenz number L by

$$L = \kappa_{el} / \sigma T. \tag{16.40}$$
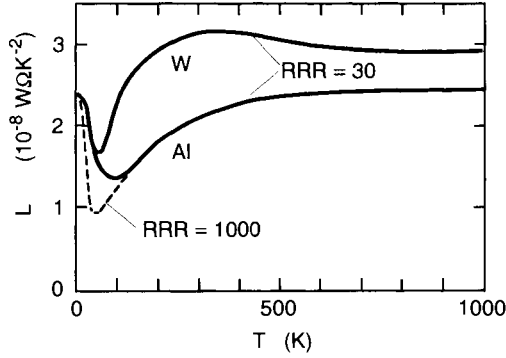
Fig. 16.7. The Lorenz number, as approximated by $L = \kappa_{tot}/\sigma T$, from measured κ_{tot} and σ (Touloukian et al. 1970, Bass 1982). RRR is the residual resistance ratio.

L is temperature dependent, but when $T \gtrsim \theta_D/2$, L often does not deviate more than 20% from L_0 (Laubitz and Matsumura 1972, Laubitz et al. 1976), and normally $L > L_0$. (An exception is Pu, for which $L \approx L_0/2$.) An experimental determination of the Lorenz number requires that the phonon part κ_{ph} is subtracted from the total thermal conductivity $\kappa_{tot} = \kappa_{ph} + \kappa_{el}$. The magnitude of κ_{ph} is very difficult to calculate accurately. In fig. 16.7 we therefore plot the quantity $L(T) = \kappa_{tot}/(\sigma T)$, from experimental data on σ and the total conductivity κ_{tot}. Obviously, the Wiedemann–Franz-law, with $L = L_0$, is approximately obeyed also for these real materials. The minimum in $L(T)$ at low T is discussed in §7.4.

7.2. Fundamental expressions for κ_{el}

In Chapter 15, dealing with the electrical conductivity σ, we obtained the expression

$$\sigma = \frac{ne^2}{m_b}\langle\tau(\varepsilon, \mathbf{k})\rangle. \tag{16.41}$$

Here, m_b is an effective electron band mass and $\tau(\varepsilon, \mathbf{k})$ is an electron lifetime that depends both on the direction of the wave vector $\mathbf{k}$ and on the energy distance ε to the Fermi energy E_F. The brackets $\langle\ldots\rangle$ denote an average over all electron states, with a weight factor $-[\partial f(\varepsilon_\mathbf{k})/\partial\varepsilon_\mathbf{k}]$ which implies that we only sample electron states $\mathbf{k}$ near

the Fermi level. The analogue of eq. (16.41) for the electronic part of the thermal conductivity is

$$\kappa_{\text{el}} = \frac{nk_{\text{B}}^2 T}{m_{\text{b}}} \left\langle \left(\frac{\varepsilon_{\mathbf{k}} - E_{\text{F}}}{k_{\text{B}}T}\right)^2 \tau(\varepsilon, \mathbf{k}) \right\rangle. \tag{16.42}$$

The lifetime $\tau(\varepsilon, \mathbf{k})$ solves the Boltzmann equation in a thermal gradient.

We will now see that eq. (16.42) contains, as a special case, the Wiedemann–Franz law. Let $\tau(\varepsilon, \mathbf{k})$ be isotropic and energy independent, i.e. $\tau(\varepsilon, \mathbf{k}) = \tau$. (This still allows τ to be temperature dependent.) Then, from eq. (16.42),

$$\kappa_{\text{el}} = \frac{nk_{\text{B}}^2 T\tau}{m_{\text{b}}} \int_{-\infty}^{\infty} \left(\frac{\varepsilon_{\mathbf{k}} - E_{\text{F}}}{k_{\text{B}}T}\right)^2 \left(-\frac{\partial f(\varepsilon)}{\partial \varepsilon}\right) \frac{\text{d}\Omega}{4\pi}\text{d}\varepsilon. \tag{16.43}$$

The integral over $\text{d}\Omega$ gives 4π and the integral over ε can be solved exactly, giving $\pi^3/3$. One obtains the desired result

$$\kappa_{\text{el}} = \frac{\pi^2 n k_{\text{B}}^2 T\tau}{3m_{\text{b}}} = \sigma L_0 T. \tag{16.44}$$

7.3. κ_{el} expressed in electron-phonon coupling functions

In Chapter 15 (§5.1), we related the electron lifetime, and the resulting electrical resistivity, in integrals involving the transport Éliashberg coupling function $\alpha_{\text{tr}}^2 F(\omega)$. The corresponding expression for κ_{el} contains both $\alpha_{\text{tr}}^2 F(\omega)$ and the ordinary Éliashberg coupling function $\alpha^2 F(\omega)$. One has (Leung et al. 1977, Tomlinson 1979, Grimvall 1981)

$$\frac{1}{\kappa_{\text{el}}} = \frac{1}{L_0 T} \frac{(4\pi)^2}{\omega_{\text{pl}}^2}$$

$$\times \int_0^{\omega_{\text{max}}} \frac{\hbar\omega/k_{\text{B}}T}{[\exp(\hbar\omega/k_{\text{B}}T) - 1][1 - \exp(-\hbar\omega/k_{\text{B}}T)]}$$

$$\times \left\{ \left[1 - \frac{1}{2\pi^2}\left(\frac{\hbar\omega}{k_{\text{B}}T}\right)^2\right] \alpha_{\text{tr}}^2 F(\omega) \right.$$

$$\left. + \frac{3}{2\pi^2}\left(\frac{\hbar\omega}{k_{\text{B}}T}\right)^2 \alpha^2 F(\omega) \right\} \text{d}\omega. \tag{16.45}$$

We consider this formula in some special cases. It is then convenient to use the thermal resistivity $W_{el} = 1/\kappa_{el}$.

High temperature limit: Let $\hbar\omega_{max}/k_B T \ll 1$ (in practice even $T/\theta_D > 1$ may be enough) and take the free-electron result $\omega_{pl}^2 = 4\pi n e^2/m$. Then

$$W_{el} = \frac{2\pi m k_B}{L_0 n e^2 \hbar} \int_0^{\omega_{max}} \frac{2\alpha_{tr}^2 F(\omega)}{\omega}\, d\omega = \frac{2\pi m k_B \lambda_{tr}}{L_0 n e^2 \hbar}. \tag{16.46}$$

This is now compared with the corresponding expression, (eq. (15.27)), for the electrical conductivity, $1/\sigma = 2\pi m k_B T \lambda_{tr}/(n e^2 \hbar)$. Again, we recover the Wiedemann–Franz law.

Einstein phonon spectrum: Let the phonons be described by an Einstein model. Then

$$\alpha_{tr}^2 F(\omega) = A\delta(\omega - \omega_E), \quad \alpha^2 F(\omega) = B\delta(\omega - \omega_E), \tag{16.47}$$

where A and B are constants. The integral in eq. (16.45) just picks up the δ-function contributions and one obtains

$$W_{el} = k_E C_{har}(T/\theta_E) \left[\frac{A}{B} + \left(\frac{\theta_E}{T}\right)^2 \frac{1}{2\pi^2} \left(3 - \frac{A}{B}\right) \right]. \tag{16.48}$$

Here, k_E is a constant and $C_{har}(T/\theta_E)$ is the lattice heat capacity in an Einstein model. It follows that $W_{el} = 1/\kappa_{el}$ and the heat capacity C_p of a pure metal will tend to have a covarying temperature dependence (cf. Chapter 19, §11).

In Chapter 15 (§5.4), we made the approximation $\alpha_{tr}^2 F(\omega) = \langle 1 - \cos\theta \rangle \alpha^2 F(\omega)$, where $\langle 1 - \cos\theta \rangle$ is a geometrical factor and θ is an electron scattering angle. Typically $\langle 1 - \cos\theta \rangle \approx 1$, i.e. $A/B \approx \langle 1 - \cos\theta \rangle \approx 1$. Motakabbir and Grimvall (1981) discussed W_{el} on the basis of an Einstein model, with A/B as a free parameter. In particular, they were able to account for the minimum in the thermal conductivity of pure metals, which is observed, e.g. for Al, Na and Zn at $T \sim 0.4\theta_D$.

7.4.   The Wiedemann–Franz law

Comparing $1/\kappa_{el}$ in eq. (16.45) with $\rho = 1/\sigma$ in eq. (15.20), it is obvious that the Wiedemann–Franz law is valid if we can make the approximation

$$\left[1 - \frac{1}{2\pi^2} \left(\frac{\hbar\omega}{k_B T} \right)^2 \right] \alpha_{tr}^2 F(\omega) + \frac{3}{2\pi^2} \left(\frac{\hbar\omega}{k_B T} \right)^2 \alpha^2 F(\omega)$$

$$\approx \alpha_{tr}^2 F(\omega), \tag{16.49}$$

i.e. if we can neglect a term

$$\frac{1}{2\pi^2} \left(\frac{\hbar\omega}{k_B T} \right)^2 [3\alpha^2 F(\omega) - \alpha_{tr}^2 F(\omega)] \tag{16.50}$$

in the integrand of eq. (16.45). This is a good approximation when $T > \theta_D$, because then the factor preceding [. . .] in eq. (16.45) is <0.05. At low temperatures (in pure metals), there are large deviations from the Wiedemann–Franz law (fig. 16.7). The prime reason is the inelastic nature of the scattering of electrons by phonons, i.e. the scattering with energy loss or gain. It is often stated that the Wiedemann–Franz law holds in the limit of low and high temperatures. At low T, this is true if T is so low that the (elastic) impurity scattering dominates. At high T, the (dominating) electron-phonon scattering is basically inelastic, but the energy changes, $\sim \hbar\omega_D$, are small compared to the energy $k_B T$, and the scattering therefore appears to be elastic.

For completeness, we remark that we have left out a correction of a few percent or less in κ_{el}, related to the thermoelectric power (e.g. Laubitz and Matsumura 1972).

7.5.   Thermal conductivity in impure metals

We first recall the basic results for the electrical conductivity of impure metals. Let ρ_{tot} obey Matthiessen's rule, $\rho_{tot} = \rho_{el-ph} + \rho_{def}$. We may also write this as $\sigma_{tot} = ne^2\tau_{tot}/m$, with $1/\tau_{tot} = 1/\tau_{el-ph} + 1/\tau_{def}$. The Wiedemann–Franz law gives

$$W_{el,tot} = \frac{m}{ne^2 L_0 T \tau_{tot}} = \frac{m}{ne^2 L_0 T} \left(\frac{1}{\tau_{el-ph}} + \frac{1}{\tau_{def}} \right). \tag{16.51}$$
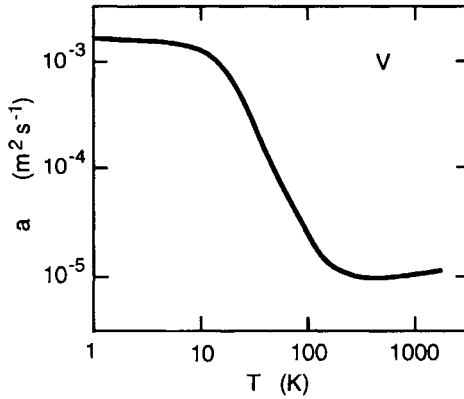
Fig. 16.8. The thermal diffusivity a for vanadium. The residual resistivity is $\rho_{def} = 1.72\ \mu\Omega$ cm. Data as recommended by Touloukian et al. (1973).

Thus, Matthiessen's rule holds also for the electronic thermal resistivity,

$$W_{el,tot} = W_{el-ph} + W_{def}. \tag{16.52}$$

This argument can be repeated with a more fundamental expression than $ne^2\tau/m$ for σ_{tot}.

Assuming that the Wiedemann–Franz law is valid, the effect of various static lattice defects on the electron part of the thermal conductivity follows from our discussion of the electrical conductivity (Chapter 15). See also Motakabbir and Grimvall (1981) for a simple model calculation of $W_{tot}(T)$ in an alloy, with allowance for the energy dependence of $\tau_{el-ph}(\varepsilon)$.

Example: thermal diffusivity in vanadium. In vanadium, the thermal diffusivity $a = \kappa/(c_p\rho)$ is dominated by the electronic contribution. We assume that the Wiedemann–Franz law $\kappa = \sigma L_0 T$ holds. At very low temperatures, $\sigma = \sigma_{def}$. Furthermore, the heat capacity at low T is dominated by the electronic contribution $\sim \gamma T$. It follows that $a \sim \sigma_{def} L_0/\gamma$, i.e. a temperature independent quantity. At high temperatures $(T > \theta_D)$ the heat capacity is dominated by an approximately constant phonon contribution while $\sigma \sim 1/T$. Hence, a is approximately independent of T also in this case. Figure 16.8 shows the measured thermal diffusivity of vanadium (Touloukian et al. 1973).
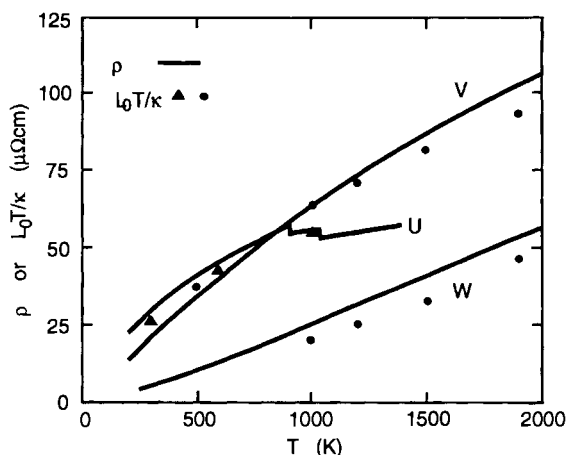
Fig. 16.9. The electrical resistivity ρ (solid lines) and the quantity $L_0 T/\kappa$ (symbols) as obtained from the measured ρ and κ for V, W and U. After Grimvall (1984).

8. Miscellaneous transport mechanisms

8.1. Simultaneous electron and phonon transport

In alloys, heat is conducted by both the electrons and the phonons. It follows from fig. 16.9 that the high temperature conductivity of pure metals is dominated by the electrons, also when the elemental metal is not a very good electrical conductor. Even in a concentrated alloy like stainless steel the electrons carry most of the heat, except in the temperature region of the maximum in the phonon part, i.e. roughly at $T \sim 0.1\theta_D$ (e.g. White 1969) where the phonons give a significant contribution. In particular, this means that metals and alloys have a low temperature limit $\kappa \sim T$. (Use Matthiessen's rule and the fact that impurity resistance always dominates ρ at low enough temperatures.)

8.2. Magnons

Magnons carry heat much like phonons. The effect is significant only at very low temperatures. See, for example, Berman (1976).

8.3. Photons

In materials which are semitransparent to infrared radiation, there is a high temperature contribution to κ which increases with T as T^3. This term is a possible cause of the upturn in κ at high T in MgO (fig. 16.4). The problem has been discussed by Men' and Sergeev (1973) among others. It has been suggested that the mechanism is significant even at room temperature, e.g. for In_2Te_3 (Petrusevich et al. 1960).

8.4. Porous materials

Conduction in inhomogeneous materials is considered in Chapter 17. Here, we only mention that in porous materials both contact resistance, gas conduction and radiation may be important. See, e.g. Furmanski (1994) on porous materials, Larkin and Churchill (1959) on insulating fiber materials and Klemens (1983b) on metal powders.

9. Pressure dependence

The volume (pressure) dependence of the electronic thermal conductivity κ_{el} of metals follows from our discussion of the electrical conductivity and with reference to the Wiedemann–Franz law. The volume dependence of κ_{ph} was, indirectly, discussed in §5.3 where we noted that the thermal expansion affected the high temperature κ_{ph} mainly through θ_D. Many materials, both metals and insulators, have $-d\ln\kappa/d\ln V$ in the range 4–8. For a more detailed discussion, see Ross et al. (1984), Bäckström (1985) and Mooney and Steg (1969).

10. Mean free paths and saturation phenomena

10.1. Phonon transport

A (temperature dependent) characteristic phonon mean free path ℓ_{ph} is sometimes estimated from the measured thermal conductivity and heat capacity by

$$\ell_{ph} = 3\kappa_{ph}V/(\bar{C}_g C_p). \tag{16.53}$$

Here C_p is the lattice heat capacity of a specimen with volume V. A similar expression, $\ell_{ph} = 3a/\bar{C}_g$, involves the thermal diffusivity a. However, eq. (16.53) can be quite misleading. Since ℓ_{ph} and C_g may vary strongly with (q, s), the weighting of modes (q, s) that enter ℓ_{ph} is unclear. Furthermore, ℓ_{ph} has both an explicit temperature dependence from the scattering rate and an indirect variation with T through the heat capacity, which makes an interpretation of ℓ_{ph} difficult (MacDonald and Anderson 1983).

We noted in §3 (in the discussion of region D), that the mean free path $\ell(q, s)$ cannot be shorter than the wavelength of the corresponding phonon, and the wavelength cannot be shorter than the distance a between two neighbouring atoms. Hence, $\kappa_{ph} > k_B C_{sound,D}/a^2$, where $C_{sound,D}$ is the Debye velocity. We rewrite the righthand side of this inequality as

$$(\kappa_{ph})_{sat} \sim \frac{k_B(q_D C_{sound,D})}{a^2 q_D} \sim \frac{k_B \omega_D}{4a} = \frac{k_B \hbar \omega_D}{4a\hbar} = \frac{k_B^2 \theta_D}{4a\hbar}, \qquad (16.54)$$

where we have used the result that $q_D = (6\pi^2)^{1/3}/a$ for a simple cubic lattice. Taking the typical values $\theta_D = 300$ K and $a = 3 \times 10^{-10}$ m, we have for the "saturation" value of the thermal conductivity $(\kappa_{ph})_{sat} \sim 0.5$ W/(m K). This is too crude an estimation of ℓ_{ph}, because we have gone to the extreme limit $\ell \sim a$ for all phonon modes. However, our approach explains why the conductivity of many strongly disordered materials of quite different kinds (alloys, ceramics, ionic solids, polymers), and also the high temperature conductivity of many pure solids, seems to saturate at a rather universal value. Kittel (1949) used these ideas to explain the conductivity of glasses and Slack (1979) has reviewed the field in some detail.

10.2. Electron transport

In Chapter 15 (§11), we discussed saturation effects in the electrical resistivity. Because they suggest a breakdown of the usual Boltzmann equation, one may wonder if the Wiedemann–Franz law still holds. Figure 16.9 shows $L_0 T/\kappa$ and ρ for metals that show saturation (V, U) and those that apparently do not (W). The result is consistent with the idea that the thermal conductivity is almost entirely due to the electrons, and that the Wiedemann–Franz law still holds in the saturation

regime. A closer analysis of tungsten shows that saturation takes place also in that case. As a crude argument for this, we note that $\rho_{\text{el}-\text{ph}}$ at high temperatures varies with typical phonon frequencies as $1/\theta_{\text{D}}^2$, eq. (15.24). Furthermore, the phonon frequencies in W show an extremely large softening with increasing temperature, fig. 8.3. The latter effect alone would give $\rho_{\text{el}-\text{ph}}/T$ a strong increase at high T, but this is partly compensated for by the resistivity saturation.

TRANSPORT, ELASTIC AND THERMAL-EXPANSION PARAMETERS OF COMPOSITE MATERIALS

1. Introduction

Aluminium-silicon alloys are typical two-phase materials, with almost no mutual solubility of silicon and aluminium. A specimen of an Al–Si alloy therefore is a mixture of Al and Si grains. Suppose that the grains are small compared with the size of the specimen, and that they are in a statistically isotropic distribution, on a large scale. Such a material has isotropic electrical and thermal conductivity, bulk modulus, shear modulus, Young's modulus, thermal expansion coefficient etc. Handbook data for these properties are often sparse and not very accurate. One obviously needs methods to estimate the properties of the composite system when the corresponding properties of the constituent phases are known and one has some information about their geometrical distribution. That is the theme of this chapter.

Consider the following well-known relations:

$$\text{electrical conduction} \qquad \mathbf{j} = \sigma \mathbf{E}, \tag{17.1}$$

$$\text{thermal conduction} \qquad \boldsymbol{\varphi} = -\kappa \nabla T, \tag{17.2}$$

$$\text{dielectric displacement} \quad \mathbf{D} = \varepsilon \mathbf{E}, \tag{17.3}$$

$$\text{magnetic induction} \qquad \mathbf{B} = \mu \mathbf{H}, \tag{17.4}$$

$$\text{diffusion} \qquad \mathbf{Q} = -D \nabla c. \tag{17.5}$$

These equations are all of the same mathematical structure. The left-hand side gives the response to a disturbance, and the proportionality

constant (σ, κ, etc.) is a tensor of rank two. For a system of cubic symmetry the tensor reduces to a single constant, which is the case assumed above. Suppose that we have solved the problem of finding the average conductivity σ of a composite material, in terms of the conductivities of the constituent phases and their geometrical distribution. The same mathematical expression can then be used to find, for instance, the average dielectric constant ε, if we know ε of the pure phases. It therefore suffices to consider one of the properties in eqs. (17.1)–(17.5). We shall often choose the electrical conductivity σ, and briefly refer to eqs. (17.1)–(17.5) as "*transport properties*" (although ε and μ do not refer to currents).

The *elastic properties* are more complicated. The counterpart of the transport equations above is

$$\text{Hooke's law} \quad \boldsymbol{\sigma} = \mathbf{C}\boldsymbol{\varepsilon}, \tag{17.6}$$

where now $\boldsymbol{\sigma}$ is the stress and $\boldsymbol{\varepsilon}$ is the strain tensor. The elasticity tensor $\mathbf{C}$ never reduces to a single constant. For a single crystal of a material with a cubic lattice structure, $\mathbf{C}$ has three independent components c_{11}, c_{12} and c_{44}. For an elastically isotropic system, two elastic parameters suffice. In solid mechanics one often chooses them to be the bulk modulus K and the shear modulus G. They are related to Young's modulus E and the Poisson ratio ν through equations given in Chapter 3 (§2). In principle, one may now proceed in analogy to the electrical conductivity, and obtain expressions for the elastic properties of a composite material in terms of the properties of the constituent phases and their geometrical distribution.

The strain $\boldsymbol{\varepsilon}$ associated with a temperature increase ΔT is given by the equation for thermal expansion

$$\boldsymbol{\varepsilon} = \boldsymbol{\alpha}\Delta T. \tag{17.7}$$

The second-rank tensor $\boldsymbol{\alpha}$ reduces to a constant in a material of cubic symmetry ($\alpha = \beta/3$). In a composite material, an estimation of $\boldsymbol{\alpha}$ has to include not only the expansion coefficients of the constituent phases, but also their elastic properties expressed, for example, by K and G.

Methods to find effective properties for a composite follow two main lines—the establishment of *upper and lower bounds* to the quantity of interest, and *direct estimates* through approximate modelling. We shall

consider both approaches in some depth. A case of particular interest is a *dilute suspension*, i.e. a small amount of inclusions embedded in a matrix, for which effective properties can often be exactly obtained.

One of the first extensive treatments of eqs. (17.1)–(17.5) for two-phase materials is that of Bruggeman (1935), who was mainly interested in dielectric properties. Another milestone is papers by Hashin and Strikman (1962a, 1963a). Part of the material in this chapter has been covered in a review by Hale (1976). Reviews by van Beek (1967), Landauer (1978) and Bergman (1978) concentrate on dielectric properties, by Bergman and Stroud (1992) on various electrical and electromagnetic properties, and by Taylor (1991) on thermal transport in materials of practical importance. Christensen (1979), Watt et al. (1976) and Laws (1980) consider elastic properties; Watt et al. (1976) with special reference to geophysical applications. Hashin (1983), Walpole (1981) and Willis (1981) discuss mainly the elastic properties of composites, but also thermal expansion and transport. Torquato (1991) has reviewed mathematical aspects of bounds to the effective properties of composites. Further references are given as we proceed. Figure 17.1 shows schematically some important structures that are dealt with in this chapter. We may characterise them as:

(a) lamellar or fibrous composites (§2.2; Chapter 18, §6);
(b) two- or multiphase composites with no clear matrix phase (§§2.3, 5);
(c) suspension of more or less spherical particles in a matrix (§§3.1, 3.3, 3.4, 5);
(d) suspension of fibres or plate-like particles in a matrix (§§3.2–3.4);
(e) suspension of particles in a matrix, with phase-boundary effects (§8);
(f) weakly inhomogeneous, but statistically isotropic, distribution of phases (§4).

2.   Rigorous bounds

2.1.   General aspects

Consider a composite material of rather complex geometry, such as that shown in fig. 17.2. Its microstructure is characterised by many length scales, and various discernible geometrical arrangements of the phases.
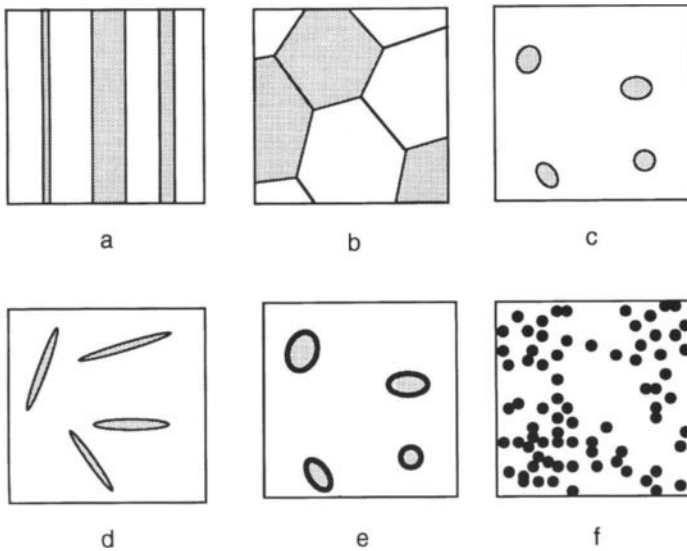
Fig. 17.1. Schematic representation of the microstructure of some composites, here given as two-dimensional cuts through the material.

It is assumed throughout this chapter that the linear dimension of the specimen is much larger than any characteristic and relevant length in the microstructure. The mathematical relations to be presented assume that there are no surface effects caused by the phase boundaries. In transport properties this means that we neglect boundary scattering, contact potentials etc. Ignoring surface effects may be dubious in diffusion problems. In the case of elastic properties and thermal expansion, we neglect grain boundary sliding, formation of cracks and other anelastic behaviour.

2.2. Absolute bounds

In this section we consider bounds which are always valid, whatever is the phase geometry of the composite material. Let phases 1 and 2 occupy the volume fractions f_1 and f_2 ($= 1 - f_1$) and have conductivities σ_1 and σ_2. Then the effective conductivity of the material, measured in any direction, is bounded as (Wiener 1912, Jackson and Coriell 1968)

$$(f_1/\sigma_1 + f_2/\sigma_2)^{-1} \leq \sigma_{\text{eff}} \leq f_1\sigma_1 + f_2\sigma_2. \tag{17.8}$$
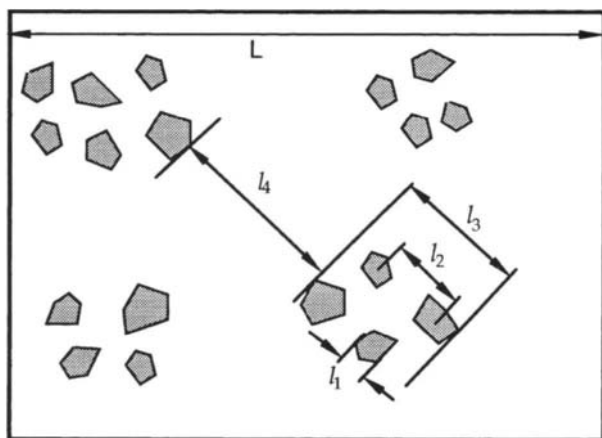
Fig. 17.2. A schematic representation of a composite material with various characteristic length scales.

The lower bound in eq. (17.8) follows from an assumption of a spatially uniform current through the sample and the upper bound from an assumption of a uniform electric field. The bounds in eq. (17.8), sometimes called the *Wiener bounds*, may also be referred to as the *series* and *parallel model*. They are the best possible when only volume fractions are known, because they are attained for conduction in fibrous or lamellar geometries. The generalisation to N phases is

$$\left(\sum_{i=1}^{N} f_i/\sigma_i\right)^{-1} \leq \sigma_{\text{eff}} \leq \sum_{i=1}^{N} f_i\sigma_i. \tag{17.9}$$

Analogous results hold for the bulk modulus K and the shear modulus G (Paul 1960, Hill 1963). Thus,

$$K_{\text{R}} \leq K_{\text{eff}} \leq K_{\text{V}}, \tag{17.10}$$

$$G_{\text{R}} \leq G_{\text{eff}} \leq G_{\text{V}}, \tag{17.11}$$

with

$$K_{\text{V}} = f_1K_1 + f_2K_2, \tag{17.12}$$

$$\frac{1}{K_{\text{R}}} = \frac{f_1}{K_1} + \frac{f_2}{K_2}, \tag{17.13}$$

and corresponding relations for G_V and G_R, when G replaces K in eqs. (17.12) and (17.13). The relations (17.12) and (17.13) have obvious similarities with the series and parallel coupling (eq. (17.8)) that led us to the Wiener bounds. In the lower bound the stress is assumed to be uniform and the strain is the total sum of all the strains in the individual grains coupled in series. Similarly, in the upper bound the strain is assumed to be uniform and the stress is carried by all the individual grains considered in parallel. These assumptions, in the case of one-phase polycrystalline materials, lead to the *Voigt* and *Reuss* bounds (Chapter 18, §3), motivating our use of the subscripts V and R above.

We can obtain bounds to Young's modulus E by the general relation $1/E = 1/(3G) + 1/(9K)$. It is clear that the largest E is obtained with the largest K and G, and vice versa. One has

$$E_R \leq E_{\text{eff}} \leq E_V, \qquad (17.14)$$

with

$$\frac{1}{E_R} = \frac{1}{3G_R} + \frac{1}{9K_R}, \quad \frac{1}{E_V} = \frac{1}{3G_V} + \frac{1}{9K_V}. \qquad (17.15)$$

Note, however, that $E_V \neq f_1 E_1 + f_2 E_2$. After a little algebra one finds that

$$E_V = f_1 E_1 + f_2 E_2 + \frac{27 f_1 f_2 (G_1 K_2 - G_2 K_1)^2}{(3K_V + G_V)(3K_1 + G_1)(3K_2 + G_2)}. \qquad (17.16)$$

The special case $\nu_1 = \nu_2$ for the Poisson ratio implies, (eq. (3.8)), that $G_1 K_2 = G_2 K_1$. Then one recovers the familiar form $E_V = f_1 E_1 + f_2 E_2$ that is often used for fibrous materials. The relation $1/E_R = f_1/E_1 + f_2/E_2$ (which gives E perpendicular to lamellae) holds for any ν_1 and ν_2. From the general relation $\nu = (3K - 2G)/(6K + 2G)$ one finds that ν increases with increasing K (for constant G) but decreases with G (for constant K). No practically useful bounds to ν seem to result from the bounds to K and G (Zimmerman 1992).

2.3. Hashin–Shtrikman bounds

Often one is interested in properties of a composite material which is, in a statistical sense, isotropic and homogeneous. This excludes fibrous and lamellar geometries (with parallel arrangements of fibres or lamellae), for which the bounds of the previous section are relevant. Instead there are more narrow bounds. They are the best possible for σ, K and G in the sense that these bounds are attained in certain geometries (§6.1). Many of the relations below can be cast in a variety of algebraic forms. Although they may look different, they are all equivalent. However, that should not be confused with similar, but less stringent, formulae that are abundant in the literature.

Transport properties: Hashin and Shtrikman (1962a) derived bounds to the conductivity σ. We choose the labelling such that $\sigma_2 > \sigma_1$. The upper bound is

$$\sigma_u = \sigma_2 + \frac{f_1}{1/(\sigma_1 - \sigma_2) + f_2/3\sigma_2}, \tag{17.17}$$

and the lower bound is

$$\sigma_\ell = \sigma_1 + \frac{f_2}{1/(\sigma_2 - \sigma_1) + f_1/3\sigma_1}. \tag{17.18}$$

Note that σ_ℓ is obtained from σ_u if indices 1 and 2 are interchanged. Analogous relations hold for the thermal conductivity, the dielectric constant, the magnetic susceptibility and the diffusion constant. The number 3 in the denominator of the righthand side of eqs. (17.17) and (17.18) is replaced by 2 for a two-dimensional system, for instance in the transverse conductivity of a bundle of cylinders embedded in a matrix (e.g. Milton 1980, Bergman 1982).

Elastic properties: Hashin and Shtrikman (1963a), Walpole (1966) and others have used various mathematical methods to derive bounds to the elastic parameters. One has, for $K_2 > K_1$,

$$K_u = K_2 + \frac{f_1}{1/(K_1 - K_2) + 3f_2/(3K_2 + 4G_2)}, \tag{17.19}$$

and

$$G_{\mathrm{u}} = G_2 + \frac{f_1}{1/(G_1 - G_2) + 6f_2(K_2 + 2G_2)/5G_2(3K_2 + 4G_2)}.$$

(17.20)

The lower bounds, K_ℓ and G_ℓ, are obtained from eqs. (17.19) and (17.20) when indices 1 and 2 are interchanged. However, if $(K_2 - K_1)(G_2 - G_1) < 0$, the bounds to K are reversed (Hill 1963). The bounds to G, when $(K_2 - K_1)(G_2 - G_1) < 0$, are similar to eq. (17.20) (Walpole 1966). Bounds to Young's modulus E are obtained through the relation (3.10) between E, K and G. The absence of useful bounds to ν was noted in connection with the Voigt and Reuss bounds above. Relations such as eq. (17.19) can be written in different, but mathematically equivalent, forms (see Appendix G).

Thermal expansion: Levin (1967) and, independently, Rosen and Hashin (1970) and Schapery (1968) have shown that the linear expansion coefficient of an isotropic two-phase composite can be written in the *exact* form

$$\alpha_{\mathrm{eff}} = f_1\alpha_1 + f_2\alpha_2 + \frac{\alpha_1 - \alpha_2}{1/K_1 - 1/K_2}[1/K_{\mathrm{eff}} - f_1/K_1 - f_2/K_2].$$

(17.21)

If we now use that $K_\ell \le K_{\mathrm{eff}} \le K_{\mathrm{u}}$, eq. (17.21) gives upper and lower bounds to α. The upper bound can be written

$$(\alpha_{\mathrm{eff}})_{\mathrm{u}} = \alpha_2 - f_1(\alpha_2 - \alpha_1)\frac{K_1(3K_2 + 4G_2)}{K_2(3K_1 + 4G_2) + 4f_1G_2(K_1 - K_2)}.$$

(17.22)

Again, the lower bound is obtained if indices 1 and 2 are interchanged. Equation (17.22) holds if $G_2 > G_1$ and $(\alpha_2 - \alpha_1)(K_2 - K_1) < 0$. This is the normal situation, i.e. a stiffer material also has a lower thermal expansion coefficient. If this is not the case, the bounds are reversed so that eq. (17.22) gives $(\alpha_{\mathrm{eff}})_\ell$. When $\alpha_2 = \alpha_1$ or $G_2 = G_1$, the upper and lower bounds to α coincide. $G_2 = G_1(= G)$ implies that $K_{\mathrm{u}} = K_\ell$ and leads to

$$\alpha_{\text{eff}} = f_1\alpha_1 + f_2\alpha_2 - f_1(1 - f_1)(\alpha_1 - \alpha_2)$$

$$\times \frac{4G(K_2 - K_1)}{3K_1K_2 + 4G(f_1K_1 + f_2K_2)}. \tag{17.23}$$

We note that if K_{eff} in eq. (17.21) is replaced by the Reuss expression (17.13) we get exactly $\alpha_{\text{eff}} = f_1\alpha_1 + f_2\alpha_2$. Since K_R is a lower bound to K_{eff}, the expansion coefficient α_{eff} lies below the average $\alpha_{\text{eff}} = f_1\alpha_1 + f_2\alpha_2$ if $(\alpha_1 - \alpha_2)(K_1 - K_2) < 0$, and vice versa.

Properties of multiphase systems: The derivation by Hashin and Shtrikman (1962a, 1963a) allowed for an arbitrary number of phases. To illustrate the mathematical structure of the bounds for this general case we quote two relations. The upper bound to the conductivity is

$$\sigma_{\text{u}} = \sigma_N + A_{N,\sigma}\left[1 - \frac{A_{N,\sigma}}{3\sigma_N}\right]^{-1}, \tag{17.24}$$

where

$$A_{N,\sigma} = \sum_{i=1}^{N-1} f_i\left[\frac{1}{\sigma_i - \sigma_N} + \frac{1}{3\sigma_N}\right]^{-1}. \tag{17.25}$$

The upper bound to the bulk modulus is

$$K_{\text{u}} = K_N + A_{N,K}\left[1 - \frac{3A_{N,K}}{3K_N + 4G_N}\right]^{-1}, \tag{17.26}$$

where

$$A_{N,K} = \sum_{i=1}^{N-1} f_i\left[\frac{1}{K_i - K_N} + \frac{3}{3K_N + 4G_N}\right]^{-1}. \tag{17.27}$$

Here, $i = 1$ to N denotes the phases, numbered so that σ_N, K_N and G_N are largest.

Bounds have also been derived for non-isotropic systems. They are considered in Chapter 18.

Example: comparison of bounds to σ. In fig. 17.3 are shown the Wiener bounds and the Hashin–Shtrikman bounds to the conductivity σ, for
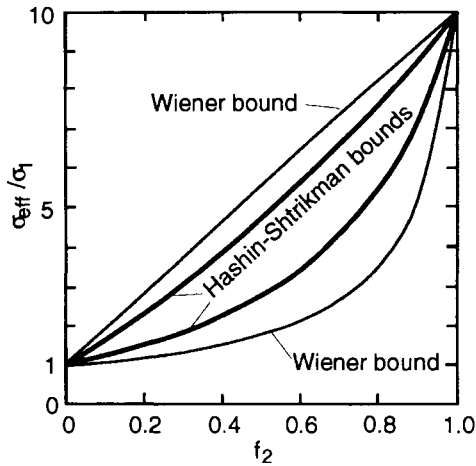
Fig. 17.3. The Wiener bounds and the Hashin–Shtrikman bounds to the conductivity σ of a composite with $\sigma_2/\sigma_1 = 10$, as a function of the volume fraction f_2 of phase 2.

the case $\sigma_2/\sigma_1 = 10$. If the bounds are applied to real materials with phases A and B, one should note that the conductivities of A and B may be significantly influenced, e.g. by the diffusion of (small amounts of) atoms from A to B and vice versa. This complication does not arise in the case of elastic or thermal expansion properties, which depend weakly on variations in the composition of the individual phases.

Example: bounds to the bulk modulus of aluminium–silicon alloys. Aluminium and silicon have very low mutual solubility, and the Al–Si system consists of almost pure Al and Si. Figure 17.4 shows the Voigt, Reuss and Hashin–Shtrikman bounds to the bulk modulus K. Hill (1952) suggested that the arithmetic mean of the Voigt and Reuss limits (the *Voigt–Reuss–Hill approximation*, K_{VRH}) could make a good estimate;

$$K_{VRH} = (1/2)(K_V + K_R),\qquad (17.28)$$

with analogous relations for G and E.

Example: bounds to the expansion coefficient of aluminium–silicon alloys. The two Hashin–Shtrikman bounds to the linear expansion coefficient α in Al–Si lie very close; fig. 17.5. The symbols denote experimental results (Touloukian et al. 1975).
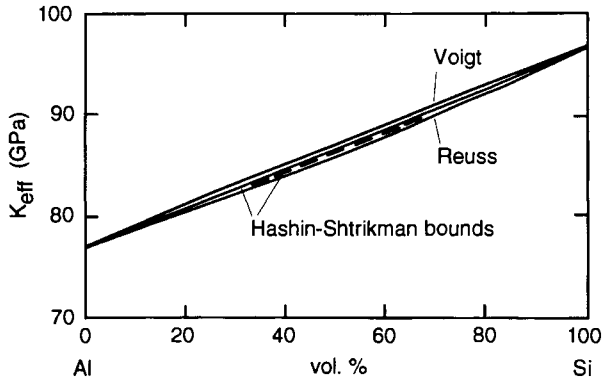
Fig. 17.4. The Voigt, Reuss and Hashin–Shtrikman bounds to the bulk modulus of an aluminium–silicon alloy with no mutual solubility of Al and Si.

Example: thermal expansion in a material with voids. Consider a one-phase material with voids. The voids can be regarded as a second phase with $K_2 \rightarrow 0$. Then, the expression (17.21) for α_{eff} reduces to

$$\alpha_{\text{eff}} = f_1\alpha_1 + f_2\alpha_1 = \alpha_1, \tag{17.29}$$

i.e. the linear expansion coefficent is the same as for the material without voids.

3. Dilute suspensions

We will consider the limiting case when phase 2 is in the form of a dilute suspension, i.e. with a volume fraction $f_2 \ll 1$. The shape of the suspended particles is assumed to be ellipsoidal or, as special cases, spherical, rod- or disc-like. We thus exclude systems for which phase 2 is continuous through the material. Spherical inclusions lead to particularly simple results and we start with them.
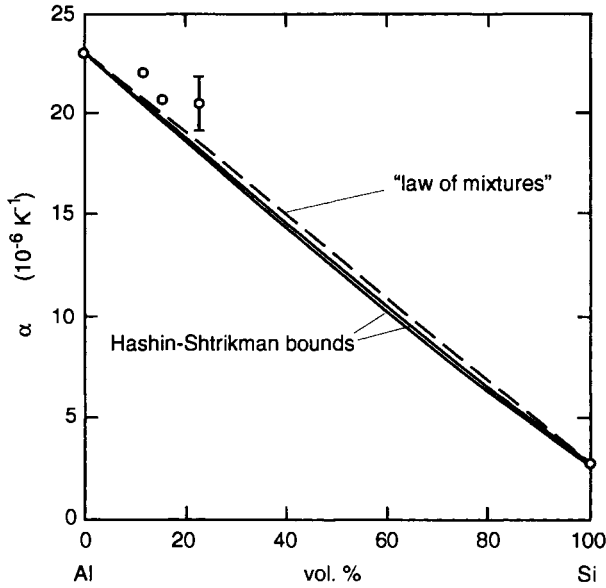
Fig. 17.5. The Hashin–Shtrikman bounds to the linear thermal expansion coefficient α of aluminium–silicon alloys, and the "law of mixtures", $\alpha_{\text{eff}} = f_1\alpha_1 + f_2\alpha_2$.

3.1. Spherical inclusions

Transport properties: Rayleigh (1892) and others (see the review by Grosse and Greffe 1979) considered spherical inclusions in a matrix. In the dilute limit ($f_2 \ll 1$), but for any ratio σ_2/σ_1, one has

$$\sigma_{\text{eff}} = \sigma_1 \left[1 + f_2 \frac{3(\sigma_2 - \sigma_1)}{2\sigma_1 + \sigma_2} \right]. \tag{17.30}$$

Elastic properties: Expressions for the bulk modulus K_{eff} and the shear modulus G_{eff} have been derived, independently, by Dewey (1947), Eshelby (1957) and Hashin (1959). The result is

$$K_{\text{eff}} = K_1 + f_2(K_2 - K_1)\frac{3K_1 + 4G_1}{3K_2 + 4G_1}, \tag{17.31}$$

$$G_{\text{eff}} = G_1 + f_2(G_2 - G_1)\frac{5(3K_1 + 4G_1)}{9K_1 + 8G_1 + 6(K_1 + 2G_1)G_2/G_1}. \tag{17.32}$$

These relations agree with the lower Hashin–Shtrikman bounds when those bounds are considered in the limit $f_2 \ll 1$ and for $K_2 > K_1$, $(K_2 - K_1)(G_2 - G_1) > 0$. If these inequalities are reversed we should compare with the upper Hashin–Shtrikman bound instead.

Thermal expansion: From eqs. (17.21) and (17.31) we obtain the linear expansion coefficient for a suspension of spheres in a matrix. Neglecting $(K_2 - K_1)f_2$ compared with K_1, one has

$$\alpha_{\text{eff}} = \alpha_1 + f_2(\alpha_2 - \alpha_1)\frac{K_2(3K_1 + 4G_1)}{K_1(3K_2 + 4G_1)}. \tag{17.33}$$

3.2. Ellipsoidal inclusions; rods and discs

Rods, needles and fibres can be viewed as limiting cases of elongated ellipsoids of revolution. Similarly, circular discs and plates can be viewed as very oblate ellipsoids.

Transport properties: For a dilute suspension of ellipsoids,

$$\sigma_{\text{eff}} = \sigma_1 + f_2\frac{(\sigma_2 - \sigma_1)}{3}\sum_{i=1}^{3}\frac{\sigma_1}{\sigma_1 + A_i(\sigma_2 - \sigma_1)}, \tag{17.34}$$

where A_i are so-called depolarising factors along the ellipsoid axes $i = x$, y and z. (The name depolarising factor stems from the application to dielectric properties, cf. eq. (17.3).) Tables of A_i have been published by Stoner (1945), Osborn (1945) and Fricke (1953). Some special cases are given in table 17.1. For a sphere, which has all $A_i = 1/3$, we recover eq. (17.30) from eq. (17.34).

In this context, it can be noted that the electric field $\mathbf{E}$ is uniform inside a sphere, or more generally inside an ellipsoid, embedded in a large uniform matrix (e.g., Stratton 1941). If an external field is along the i-axis of the ellipsoid, the average field strength E_i inside the ellipsoid is

$$E_i = E\sigma_1/[\sigma_1 + A_i(\sigma_2 - \sigma_1)]. \tag{17.35}$$

Similarly, in the case of heat conduction, the thermal gradient ∇T is constant inside an ellipsoidal inclusion in a large uniform matrix.

Table 17.1

Depolarising factors

	A_1	A_2	A_3
Sphere, $a_1 = a_2 = a_3$	1/3	1/3	1/3
Very prolate ellipsoid, $a_1 \gg a_2 = a_3$	0	1/2	1/2
Very oblate ellipsoid, $a_1 \ll a_2 = a_3$	1	0	0

The effective conductivity of a dilute suspension of randomly oriented *rods* is obtained from eq. (17.34), and with A_i from table 17.1, as

$$\sigma_{\text{eff}} = \sigma_1 + f_2 \frac{(\sigma_2 - \sigma_1)(5\sigma_1 + \sigma_2)}{3(\sigma_1 + \sigma_2)}. \tag{17.36}$$

The corresponding relation for a dilute suspension of randomly oriented circular thin *discs* is

$$\sigma_{\text{eff}} = \sigma_1 + f_2 \frac{(\sigma_2 - \sigma_1)(\sigma_1 + 2\sigma_2)}{3\sigma_2}. \tag{17.37}$$

Elastic properties: The elastic properties of a matrix with a dilute suspension of randomly oriented ellipsoids have been treated by Wu (1966), Walpole (1969), Watt et al. (1976) and Berryman (1980). The results are more complicated than eq. (17.34) for the transport properties, and we only give a few illustrating examples below. In the low concentration limit of phase 2 one has, for *rods*,

$$K_{\text{eff}} = K_1 + f_2(K_2 - K_1) \frac{K_1 + G_1 + G_2/3}{K_2 + G_1 + G_2/3}. \tag{17.38}$$

The corresponding expression for G_{eff} is algebraically complicated. For *discs*,

$$K_{\text{eff}} = K_1 + f_2(K_2 - K_1) \frac{3K_1 + 4G_2}{3K_2 + 4G_2}, \tag{17.39}$$

$$G_{\text{eff}} = G_1 + f_2(G_2 - G_1) \frac{G_1 + F_2}{G_2 + F_2}, \tag{17.40}$$

where $F_2 = (G_2/6)(9K_2 + 8G_2)/(K_2 + 2G_2)$. The relations (17.39) and (17.40) agree with the upper Hashin–Shtrikman bounds (eqs. (17.19) and (17.20)), in the limit $f_2 \ll 1$, if the discs are stiff, i.e. $K_2 > K_1$, $(K_2 - K_1)(G_2 - G_1) > 0$. Otherwise we should compare with the lower bounds. An expression for the elastic field inside the ellipsoid, analogous to eq. (17.35), has been obtained by Eshelby (1957).

3.3. Inclusions with extreme properties

We first consider the effective conductivity when the inclusions either have a very high conductivity ($\sigma_2/\sigma_1 \gg 1$), or are insulating, with voids as a special case ($\sigma_2/\sigma_1 \ll 1$). In the limit of highly conducting inclusions ($\sigma_2/\sigma_1 \to \infty$),

$$\sigma_{\text{eff}} = \sigma_1[1 + 3f_2] \quad \text{(spheres)}, \tag{17.41}$$

$$\sigma_{\text{eff}} = \sigma_1 + f_2\sigma_2/3 \to \infty \quad \text{(rods)}. \tag{17.42}$$

Similarly, σ_{eff} for thin discs is infinitely large. In the case of insulating inclusions ($\sigma_2 = 0$),

$$\sigma_{\text{eff}} = \sigma_1[1 - (3/2)f_2] \quad \text{(spheres)}, \tag{17.43}$$

$$\sigma_{\text{eff}} = \sigma_1[1 - (5/3)f_2] \quad \text{(rods)}, \tag{17.44}$$

while the interpretation of eq. (17.37) for thin discs is $\sigma_{\text{eff}} = 0$.

Example: elastic and thermal-conduction properties of cast iron. Cast iron has graphite embedded in a matrix, which is itself a composite of ferrite and cementite. Here, we will regard the matrix as a uniform material. When the graphite is mainly in the form of sheets, the material is referred to as grey cast iron, and when it is essentially spherical one refers to ductile cast iron. Graphite is elastically highly anisotropic, but we follow Speich et al. (1980) and Anand (1982), and let each graphite inclusion consist of aggregates of graphite grains for which we take the isotropic values $K_2 = 6.7$ GPa and $G_2 = 3.3$ GPa. For the matrix we take $K_1 = 162$ GPa and $G_1 = 81$ GPa. Figure 17.6 shows experimental data for cast iron of varying graphite concentration. The filled circles refer to ductile cast iron, which has spherical graphite inclusions. The squares refer to gray cast iron, which has flake-like graphite inclusions. In the
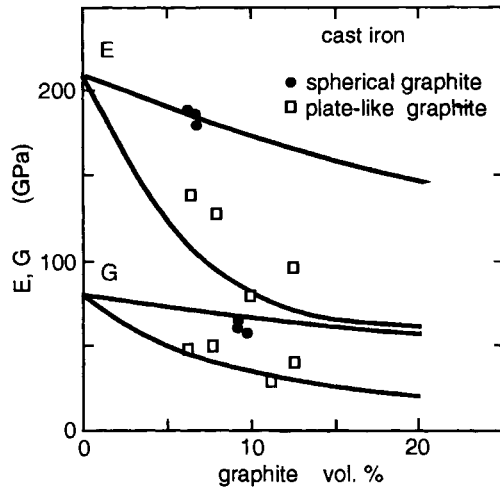
Fig. 17.6. Young's modulus E and the shear modulus G of cast iron. Filled circles and open squares refer to spherical and plate-like graphite inclusions, respectively. After Anand (1982).

dilute limit of inclusions, spheres and plates give properties coinciding with the upper and lower Hashin–Shtrikman bounds, respectively.

Graphite is a very good (although highly anisotropic) thermal conductor (table 16.1). Because spherical inclusions gives the smallest, and plate-like inclusions the largest, effect on the effective conductivity, we expect grey cast iron to have the highest thermal conductivity. This is also observed; $\kappa_{\text{eff}} \approx 45$ W(m·K) for grey cast iron and $\kappa_{\text{eff}} \approx 16$ W(m·K) for white cast iron (Helsing and Grimvall 1991).

Example: elastic properties of porous NbC. Speck and Miccioli (quoted by Toth 1971) measured the shear modulus $G(p)$ and Young's modulus $E(p)$ for sintered $NbC_{0.97}$, as a function of the porosity p. Figure 17.7 shows their data (filled circles) and the expressions for G and E that result from eqs. (17.31) and (17.32) if we take $f_2 = p$ and $K_2 = G_2 = 0$ for the pores.

3.4. Smallest and largest change in effective properties

It is interesting to compare the Hashin–Shtrikman bounds in the limit of small f_2 with the results above for dilute suspensions. One finds that, when the inclusion phase has a higher conductivity than the matrix, the
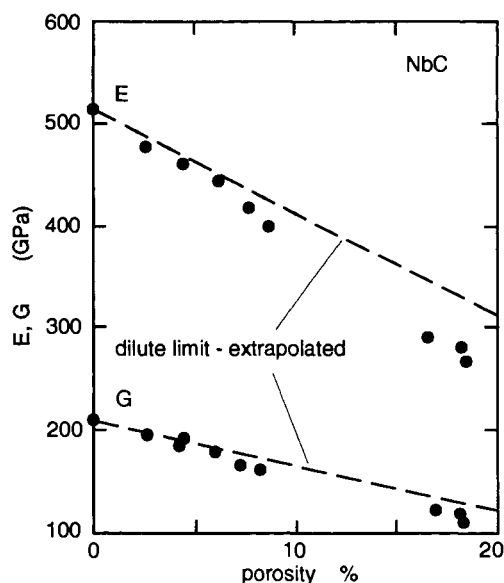
Fig. 17.7. Young's modulus E and the shear modulus G (filled circles) versus the porosity of porous NbC; after data by Toth (1971). The straight lines are extrapolations of the result for a dilute suspension of spherical voids.

upper bound coincides with the result for a dilute suspension of discs, while the lower bound corresponds to a dilute suspension of spheres. If the suspended phase has a lower conductivity than the matrix, the upper Hashin–Shtrikman bound corresponds to spherical inclusions and the lower bound to thin discs. This can be summarised as follows: When a given small amount (f_2) of a phase is added to a matrix in the form of a suspension, one gets the smallest change in σ_{eff} with spherical inclusions, and the largest change with thin discs. Rods fall between these limits. Compared with discs, they do not force the current to make as large "detours" in the composite and therefore affect σ_{eff} less.

Analogous results hold for the elastic properties. The smallest change in the bulk modulus (i.e., when K_{eff} equals a Hashin–Shtrikman bound) is obtained for spherical inclusions, and the largest change (K_{eff} equals the other H–S bound) is obtained for disc-like inclusions.

Example: the aggregate method. One may reverse the procedures discussed above, and determine approximately a property of a material A
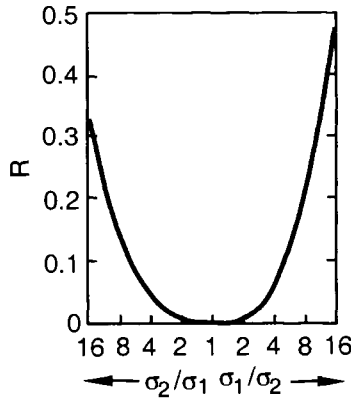
Fig. 17.8. The relative uncertainty $R = \Delta\sigma_2/\sigma_2$ in the conductivity σ_2 derived from measurements of the effective conductivity σ_{eff} of a suspension of sheres of phase 2 in a matrix of phase 1. The experimental uncertainty in σ_{eff} is assumed to be $\pm 1\%$, and $f_2 = 0.1$ in this example. R is given as a function of the contrast σ_1/σ_2 or σ_2/σ_1.

from measurements on a mixture of A and B, where B is a material with known properties. We illustrate the method by first considering a dilute suspension of phase 2 in a matrix of phase 1. Because spherical inclusions have the smallest effect on σ_{eff}, that is the most unfavourable geometry to obtain σ_2 from σ_{eff}. Figure 17.8 shows the relative uncertainty $R = \Delta\sigma_2/\sigma_2$ as a function of the contrast σ_1/σ_2 between the matrix and the inclusions if the experimental uncertainty in σ_{eff} is $\pm 1\%$, $f_2 = 0.1$, and eq. (17.30) is assumed to be exact.

Cementite (Fe_3C) is an important compound in steel. It has been very difficult to make specimens of pure Fe_3C so that its thermal and electrical conductivities could be measured. There are several attempts to derive these conductivities from meaurements of two-phase systems with Fe_3C in ferrite (bcc Fe), and the aggegate method seems to give useful and reliable results (Helsing and Grimvall 1991, Christiansson and Grimvall 1994). See Watt et al. (1976) for further discussions of the aggregate method.

4. Weakly inhomogeneous materials

4.1. Two-phase materials

When the conductivities of the phases are almost equal, the upper Wiener bound $f_1\sigma_1 + f_2\sigma_2 = \langle\sigma\rangle$ (sometimes called the "law of mixtures") gives an approximate but somewhat too large estimation for σ_{eff}. Let the difference in the conductivities, $\delta\sigma = \sigma_2 - \sigma_1$, be a small quantity, and expand the upper and lower Hashin–Shtrikman bounds in powers of δ. Neglecting powers of higher order than δ^2, the two bounds are identical. We take that as an estimation of σ_{eff}, i.e.

$$\sigma_{\text{eff}} \approx \langle\sigma\rangle - f_1 f_2 \frac{(\delta\sigma)^2}{3\langle\sigma\rangle}. \tag{17.45}$$

The corresponding relations for the bulk modulus K, the shear modulus G, and the linear expansion coefficient α, are

$$K_{\text{eff}} \approx \langle K\rangle - f_1 f_2 \frac{3(\delta K)^2}{\langle 3K + 4G\rangle}, \tag{17.46}$$

$$G_{\text{eff}} \approx \langle G\rangle - f_1 f_2 \frac{6(K + 2G)(\delta G)^2}{5\langle G\rangle\langle 3K + 4G\rangle}, \tag{17.47}$$

$$\alpha_{\text{eff}} \approx \langle\alpha\rangle - f_1 f_2 \frac{4(\alpha_1 - \alpha_2)(\delta K)^2}{\langle K\rangle\langle 3K + 4G\rangle}. \tag{17.48}$$

Note that σ_{eff}, K_{eff} and G_{eff} all lie below the arithmetic averages $\langle\sigma\rangle$, $\langle K\rangle$ and $\langle G\rangle$, in agreement with the upper Wiener and Voigt bounds, but $\alpha_{\text{eff}} - \langle\alpha\rangle$ can have either sign. To lowest order, $\alpha_{\text{eff}} - \langle\alpha\rangle$ is independent of δG, which may be compared with the fact that α_u and α_ℓ coincide for any K_1 and K_2 when $G_1 = G_2$.

Series expansions of σ_{eff} to the third and fourth order in $\delta\sigma$ have been worked out by Phan-Tien and Milton (1982), including a generalisation to an arbitrary number of phases. Corresponding results for the elastic parameters are given by Milton and Phan-Tien (1982).

To second order in $\delta\sigma$, eq. (17.45) is equivalent with

$$(\sigma_{\text{eff}})^{1/3} = f_1(\sigma_1)^{1/3} + f_2(\sigma_2)^{1/3}. \tag{17.49}$$

Occasionally, this relation may give a good account of σ_{eff} for real materials even when $\delta\sigma/\sigma_{\text{eff}}$ is not small, but this has no deeper theoretical justification.

4.2. One-phase materials

Consider a one-phase material in which the composition, and therefore also the electrical conductivity, is (isotropically) weakly inhomogeneous. The variations are assumed to be small so that a local conductivity σ can be defined everywhere in the material. Let $\langle\ldots\rangle$ denote a spatial average over the entire specimen. The effective conductivity σ_{eff} is

$$\sigma_{\text{eff}} \approx \langle\sigma\rangle \left\{ 1 - \frac{1}{3} \frac{\langle(\sigma - \langle\sigma\rangle)^2\rangle}{\langle\sigma\rangle^2} \right\}, \tag{17.50}$$

(see Brown (1955), Nedoluha (1957), Herring (1960), Landau and Lifshitz (1960), Beran and Molyneux (1963), Beran (1965), Hori (1973a,b) for proofs and generalisations).

Equation (17.45) is closely related to eq. (17.50) because for a two-phase material we can write $\langle\sigma^2\rangle = f_1(\sigma_1)^2 + f_2(\sigma_2)^2$ and $\langle\sigma\rangle^2 = (f_1\sigma_1 + f_2\sigma_2)^2$, which gives $\langle(\sigma - \langle\sigma\rangle)^2\rangle = f_1 f_2(\sigma_1 - \sigma_2)^2$.

The approach in this chapter relies on a macroscopic description of the conduction. Therefore, in averages such as $\langle(\sigma - \langle\sigma\rangle)^2\rangle$ one should only consider fluctuations on a length scale much larger than the (electron) mean free path.

The bulk modulus in weakly inhomogeneous one-phase materials is (Molyneux and Beran 1965)

$$K_{\text{eff}} \approx \langle K\rangle - \frac{3\langle(K - \langle K\rangle)^2\rangle}{\langle 3K + 4G\rangle}. \tag{17.51}$$

This is obviously another version of eq. (17.46). Analogous results hold for G_{eff} and α_{eff}.

4.3. Clustering

The section above showed that weak inhomogeneities give only a second-order correction to the effective properties, i.e. second order in $\sigma - \langle\sigma\rangle$ etc. A moderate amount of clustering, as in fig. 17.9a, may
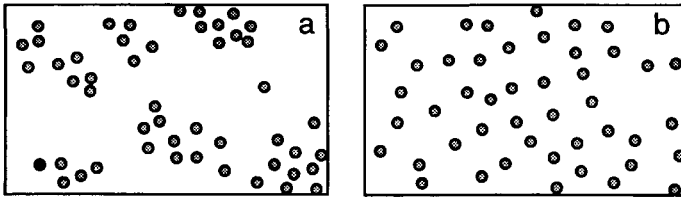
Fig. 17.9. A two-phase material showing clustering (a), and a uniformly random distribution (b), have almost the same effective properties.

therefore give a negligible correction to the properties of a uniformly random distribution, as in fig. 17.9b.

5. Effective-medium theories

5.1. Introduction

In the first part of this chapter we established bounds to σ_{eff}, K_{eff}, G_{eff} and α_{eff} for two-phase materials. These bounds may lie far apart and be of little practical value. It is therefore of interest to have models which give a single estimated value. This has led to a rich literature aiming at approximate but closed-form expressions for σ_{eff}, K_{eff}, etc. Much of that work relies on an empirical fitting to certain functions, or on dubious theoretical assumptions. However, there is one approach, the *effective-medium theory*, which is algebraically simple and yet physically well founded and we focus on that description. (Effective-medium theories can be defined in slightly different ways, leading to different expressions. We shall not dwell on this point but present the simplest and most common version.)

5.2. Transport properties

In §3, we considered a dilute suspension of spheres or ellipsoids in a matrix. If the volume fraction f_2 is not small, one can still use a similar approach but let a sphere of phase 2 be surrounded by a medium with an effective conductivity σ^* instead of σ_1. (We use the notation σ^* because

the effective conductivity obtained here is only an approximation to the true effective conductivity σ_{eff} of the composite.) Then

$$\sigma^* = \sigma_1 + f_2 \frac{3(\sigma_2 - \sigma_1)\sigma^*}{2\sigma^* + \sigma_2}. \tag{17.52}$$

This formula, which can be derived in a much stricter fashion, was given by Böttcher (1952) for the dielectric case. Landauer (1952, 1978) considered dielectric properties of N-phase materials and derived the following relation (here with ε replaced by σ);

$$\sum_{i=1}^{N} \frac{\sigma^* - \sigma_i}{2\sigma^* + \sigma_i} f_i = 0. \tag{17.53}$$

For a two-phase material ($N = 2$) we have

$$\frac{\sigma^* - \sigma_1}{2\sigma^* + \sigma_1} f_1 + \frac{\sigma^* - \sigma_2}{2\sigma^* + \sigma_2} f_2 = 0. \tag{17.54}$$

The latter expression appears first to have been given by Bruggeman (1935) in his treatment of dielectric properties. After a rearrangement of terms, one finds that eq. (17.54) is identical to eq. (17.52). When the relation for σ^* is cast in the symmetric form (17.54), it is obvious that f_2 does not have to be small. If $f_2 \ll 1$, we can approximate σ^* in the denominator by the matrix conductivity σ_2. Then eq. (17.52) is consistent with eq. (17.30), to lowest order in f_2. In the two-dimensional case (e.g. conduction perpendicular to fibres in a matrix), eq. (17.54) retains its form if only $2\sigma^*$ is replaced by σ^* in the two denominators (Bruggeman 1935). Equation (17.53) is of the order N, and has N solutions, but only that σ^* which becomes σ_1 when all $\sigma_i = \sigma_1$ has physical meaning.

The *effective-medium theory* (EMT), or *effective-medium approximation* (EMA), is also known as the *self-consistent method* (SCM). Sometimes it is called the *symmetric* EMT, because eq. (17.53) is symmetric in the phases i, unlike eq. (17.55) below. It is mathematically equivalent to the *coherent potential approximation* (CPA) used to obtain the electron band structure in alloys. The history of EMTs has been reviewed by Landauer (1978).

The EMT result σ^* from eq. (17.54) lies between the upper and lower Hashin–Shtrikman bounds. From eq. (17.52) it is easy to see that

in the dilute limit ($f_2 \ll 1$), σ^* starts out along either the lower or the upper Hashin–Shtrikman bound, depending on the sign of $\sigma_2 - \sigma_1$. With increasing f_2, σ^* then crosses over to the other Hashin–Shtrikman bound at the opposite dilute end ($f_1 \ll 1$).

In this context, it is natural to quote another well-known approximation to σ_{eff}, the *Maxwell Garnett* (MG) expression σ_{MG} that is the solution to the equation (Maxwell Garnett 1904, 1906)

$$\frac{\sigma_{\text{MG}} - \sigma_1}{\sigma_{\text{MG}} + 2\sigma_1} = f_2 \frac{\sigma_2 - \sigma_1}{2\sigma_1 + \sigma_2}. \tag{17.55}$$

Actually, σ_{MG} coincides for all f_2 with either the upper or the lower Hashin–Shtrikman bound, depending on the sign of $\sigma_2 - \sigma_1$. The MG approximation is frequently used in connection with dielectric properties, and textbooks therefore give it with σ replaced by ε, often under the name of the *Clausius-Mossotti approximation*. It is also called the *average t-matrix* or *non-selfconsistent* approximation. We finally note that the MG approximation assumes particles embedded in a continuous matrix while the approach by Bruggeman refers to a random mixture of particles. Therefore, only the latter method shows a percolation threshold (§7); $\sigma_{\text{eff}} = 0$ at $f_2 = 2/3$ for insulating particles ($\sigma_2 = 0$).

5.3. Elastic properties

Budiansky (1965, 1970) and Hill (1965b) independently derived effective-medium results for the elastic properties. Several others have taken similar approaches (see Laws 1980, for a review of the field). One has

$$K^* = K_1 + f_2(K_2 - K_1)\frac{3K^* + 4G^*}{3K_2 + 4G^*}, \tag{17.56}$$

$$G^* = G_1 + f_2(G_2 - G_1)\frac{5(3K^* + 4G^*)G^*}{G^*(9K^* + 8G^*) + 6G_2(K^* + 2G^*)}. \tag{17.57}$$

Thus, K^* and G^* are coupled and one must find their values by numerical iteration. When the Poisson ratio obeys $\nu_1 = \nu_2 = 0.2$, it follows that $3K_1 = 4G_1$ etc., and the relations (17.56) and (17.57) decouple
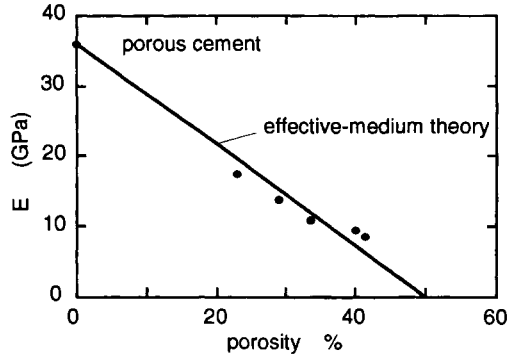
Fig. 17.10. Young's modulus E of porous autoclaved cement, as a function of vol.% porosity. The straight line is the effective-medium result. Symbols give measured values (Beaudoin and Feldman 1975, Feldman and Beaudoin 1977).

(Budiansky 1965). In analogy to how eq. (17.52) could be written in a mathematically equivalent form, (eq. (17.54)), that displays the symmetry between the labels 1 and 2, one can rewrite eqs. (17.56) and (17.57) to symmetric forms (see Appendix G).

Example: cement with voids. Beaudoin and Feldman (1975) and Feldman and Beaudoin (1977) measured Young's modulus E_{eff} for porous autoclaved cement. They also obtained $E_1 = 36$ GPa and $\nu_1 = 0.2$ for pure cement. The pores can be considered as inclusions with $K_2 = G_2 = 0$. The Poisson ratio ν_2 is undefined but it is no restriction to put $\nu_2 = 0.2$. Then the EMT equations for K^* and G^* decouple, giving $K^* = K_1(1 - 2f_2)$ and $G^* = G_1(1 - 2f_2)$ and by eq. (3.10),

$$E^* = E_1(1 - 2f_2). \tag{17.58}$$

The same expression is obtained from eqs. (17.31) and (17.32), i.e. for a dilute suspension of spheres, if we take $K_2 = G_2 = 0$ and note that $3K_1 = 4G_1$ when $\nu_1 = 0.2$. Because one of the phases (the pores) is extreme in its properties we cannot expect the EMT or the dilute suspension model to be adequate when f_2 is not very small. However, fig. 17.10 shows that eq. (17.58) may give a good account of the measured E_{eff} to quite high pore concentrations. Nielsen (1982) has discussed elastic properties of porous cement in some detail.

5.4. Thermal expansion

Because there is an exact result for the linear expansion coefficient α_{eff}, (eq. (17.21)), expressed in terms of the elastic properties of the composite, there is no separate effective-medium theory for α. If one uses the EMT result for K^*, the expression for α is quite complicated, even in the special case that $\nu_1 = \nu_2 = 0.2$, for which K^* and G^* decouple.

6. Exact results in certain geometries

In a few cases, it is possible to give mathematically exact results for the effective properties of a composite material, or they can be calculated numerically to arbitrary accuracy. Although some of these geometries may be far from what is encountered in real materials, the results are of interest because they provide test cases in the assessment of approximate methods.

6.1. Attained Hashin–Shtrikman bounds

The Hashin–Shtrikman conductivity bounds are attained in the "coated sphere" geometry ("composite sphere assemblage"). Choose labelling such that $\sigma_2 > \sigma_1$. Spheres of phase 1 and radius R_1 are coated with shells of phase 2 and radius R_2, with radii such that the volumes of a sphere and of its shell correspond to volume fractions f_1 and f_2, respectively. All space is now filled with such coated spheres, which requires a distribution of radii, including infinitesimally small values. This geometry has an effective conductivity equal to the upper Hashin–Shtrikman bound. If instead spheres of phase 2 are coated by spheres of phase 1, the effective conductivity is equal to the lower Hashin–Shtrikman bound (Hashin and Shtrikman 1962a).

The Hashin–Shtrikman bounds K_ℓ and K_u to the bulk modulus are also attained in the coated-sphere geometry, but not the corresponding bounds to the shear modulus (Hashin 1962, Milton 1981). However, the Hashin–Shtrikman bounds to both K and G are attained in a related geometry with packed spheres (Lurie and Cherkaev 1985), and also in geometries formed by laminate structures (Norris 1985, Milton 1986, Francfort and Murat 1986). Furthermore, when K_{eff} is known, also α_{eff} is known exactly. The analogous result holds in two dimensions. That
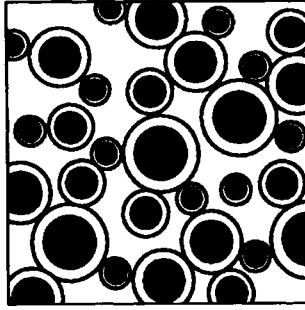
Fig. 17.11. The coated-sphere geometry, here given schematically in its two-dimensional form.

case is schematically shown in fig. 17.11. The fact there exist geometries for which the Hashin–Shtrikman bounds are attained means that these bounds are *optimal*, i.e. they are the best possible under the given assumptions.

6.2. Symmetric cell materials

A two-phase cell material (Miller 1969) is defined as follows: the composite material is subdivided by closed surfaces into closed regions, or cells. Each cell is randomly assigned physical properties with probabilities f_1 and f_2, referring to one or the other of the two phases. The cells are distributed in such a way that the material is statistically isotropic and homogeneous. Figure 17.12 shows schematically a possible phase distribution in 2 dimensions. Let the conductivity of a symmetric cell material be $\sigma_{\text{eff}}(1, 2)$. If now the phases 1 and 2 are interchanged, without altering the phase boundaries, the conductivity is $\sigma_{\text{eff}}(2, 1)$. For a three-dimensional symmetric cell material (Schulgasser 1976)

$$\sigma_{\text{eff}}(1, 2)\sigma_{\text{eff}}(2, 1) \geq \sigma_1\sigma_2. \tag{17.59}$$

In the two-dimensional case, the inequality (17.59) becomes an equality (Dykhne 1970).

6.3. Numerical calculations in periodic geometries

Let a two-phase material have spheres of one phase, forming a periodic lattice, for instance as is schematically shown in fig. 17.13. With such
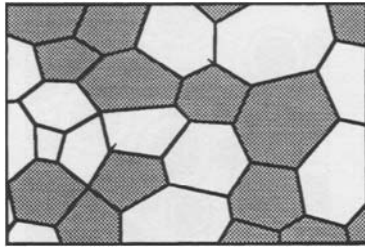
Fig. 17.12. A schematic illustration of a symmetric cell material. The figure also illustrates the concept of percolation, with the gray phase forming a percolating path from the top to the bottom of the frame.

regular phase distributions, the effective conductivity can be calculated numerically with high accuracy, for varying volume fractions and conductivity ratios σ_1/σ_2. Results have been obtained for spheres forming a simple cubic, body-centred cubic and face-centred cubic lattices in a matrix, also close to the percolation threshold. Cheng and Torquato (1997a, b) developed a method that allows the spheres to be coated with a layer that is superconducting, or has a certain resistance. Studies of regular lattice geometries provide accurate results that can be used in the test of approximate methods for less well-ordered composites.

7. Percolation

Consider a dilute suspension of conducting spheres in an insulating matrix. There is no path that lies entirely within the conducting phase and goes through the specimen. Hence, the composite is an insulator. We now increase the volume fraction of the conducting phase. Eventually one reaches a critical concentration f_c, known as the *percolation threshold*, at which a current can pass through the sample. It is obvious that f_c depends strongly on the geometry of the grains of the conducting phase. Examples may be constructed, for which f_c is anywhere in the interval 0 to 1. Figure 17.12 illustrates the idea of percolation.

The percolation phenomenon has been much studied, in particular because of its so-called critical behaviour when f is near f_c. Near f_c, the conductivity varies as $\sigma \sim \sigma_0(f - f_c)^\alpha$, where α is a "critical exponent". The name "percolation" was introduced by Broadbent and Hammersley (1957), with reference to a coffee percolator, in their pio-
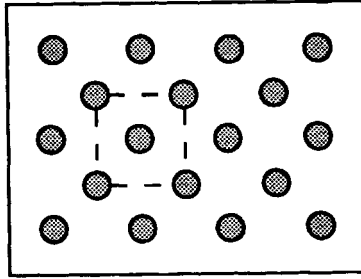
Fig. 17.13. A schematic drawing of a regular phase distribution for which transport
properties can be calculated numerically to arbitrary accuracy.

neering work on the spread of a fluid through a random porous medium.
Such flow problems form a central part of percolation studies (see a
broad review by Sahimi 1993). For further geometrical aspects of perco-
lation, see, e.g. Stauffer (1979) and Stauffer and Aharony (1992). Many
physical properties are covered by Deutscher et al. (1983). Much of the
early work on percolation dealt with resistor networks, along the lines
reviewed by Kirkpatrick (1973). This is because of some nearly univer-
sal features in the critical behaviour, which do not depend crucially on
the kind of system studied.

8. Phase-boundary effects

The presentation in this chapter has assumed perfect interfaces between
the phases. In order to illustrate the possible role of a surface layer cov-
ering the dispersed particles, we consider spherical inclusions (phase 2)
in a matrix (phase 1), with the spheres coated by a thin layer of a surface
phase (s), with thickness δ. Let the conductivities of the three phases be
σ_1, σ_2 and σ_s. When the boundary phase is one with a non-negligible
resistance, we introduce the dimensionless parameter R;

$$R = \left(\frac{\delta}{a}\right)\left(\frac{\sigma_2}{\sigma_s}\right).$$
(17.60)

If we are instead interested in the effect of a non-negligible *conductance*
of the boundary phase, we introduce the dimensionless quantity C;

$$C = \left(\frac{\delta}{a}\right)\left(\frac{\sigma_s}{\sigma_1}\right).$$
(17.61)

Torquato and Rintoul (1995) derived upper and lower bounds to σ_{eff}, containing R or C. They are mathematically elementary but algebraically rather complex. Boundary effects are negligible if $R \ll 1$ or $C \ll 1$.

In the case of elastic properties and thermal expansion, a thin phase-boundary layer has a minor influence. This is in analogy to the almost negligible role of lattice defects for these properties (Chapters 4 and 14). However, the approach in this chapter assumes that there is no grain-boundary sliding. When such effects occur, they may drastically alter the apparent elastic behaviour. For instance, one has to be cautious in the case of cast iron with a graphite phase.

Example: surface effects in particulate and fibre composites. There is a class of ionic conductors called *composite solid electrolytes*, for which surface effects can be dominating. Solid LiCl is a typical ordinary ionic conductor, where the charge is carried by highly mobile ions. If grains of Al_2O_3 are added to LiCl, the effective electrical conductivity may increase by several orders of magnitude, in spite of the fact that Al_2O_3 is insulating. A region of high ionic mobility is formed at the interface between Al_2O_3 and LiCl (see a review by Ce-Wen Nan 1993).

Cracks may arise at phase boundaries or in the surrounding matrix, due for instance, to strains related to the processing of a composite material, and significantly affect transport properties. SiC has five times higher thermal conductivity than that of cold-pressed Ti powder, but still a Ti–SiC particulate composite may have lower conductivity than Ti. Reaction products in the interface zone have a large volume and therefore cause cracking (Turner et al. 1993).

If fibres of high thermal conductivity are given a *coating* of low conductivity, the heat does not penetrate the coating, and the fibres do not affect σ_{eff} of the composite much. Analogously, σ_{eff} can be increased by a highly conducting coating of low conductivity fibres (see a review by Taylor 1991).

9. Resistivity versus conductivity

In this chapter we have referred to the electrical and thermal *conductivities*, σ and κ. We shall now comment on the *resistivities*, and consider

$\rho = 1/\sigma$. The relation between the effective transport coefficients of a composite is

$$\rho_{\text{eff}} = 1/\sigma_{\text{eff}}. \tag{17.62}$$

If we put $\sigma_1 = 1/\rho_1$ and $\sigma_2 = 1/\rho_2$ in the Wiener bounds, (eq. (17.8)), the bounds are reversed. The same substitution in the Hashin–Shtrikman bounds, eqs. (17.17) and (17.18), gives (if $\rho_2 < \rho_1$ in accordance with our assumption in this chapter that $\sigma_2 > \sigma_1$)

$$\rho_2 + \frac{f_1}{1/(\rho_2 - \rho_1) + 2f_2/3\rho_2} \leq \rho_{\text{eff}}$$

$$\leq \rho_1 + \frac{f_2}{1/(\rho_1 - \rho_2) + 2f_1/3\rho_1}. \tag{17.63}$$

We note that the factor 2/3 in the denominators of eq. (17.63) corresponds to 1/3 in the conductivity relation (17.17). Furthermore, although $\rho_{\text{eff}} = 1/\sigma_{\text{eff}}$ one has $\langle\rho\rangle = \langle1/\sigma\rangle \neq 1/\langle\sigma\rangle$. Therefore, in the case of a weakly varying resistivity (or conductivity), the relation analogous to eq. (17.50) for σ_{eff} is

$$\rho_{\text{eff}} \approx \langle\rho\rangle \left\{ 1 + \frac{2}{3} \frac{\langle(\rho - \langle\rho\rangle)^2\rangle}{\langle\rho\rangle^2} \right\}. \tag{17.64}$$

Finally, consider the dilute limit. The smallest influence on ρ_{eff} is obtained when the inclusions in the matrix have spherical shape, and the largest influence when they are plate-like. As an illustration, let phase 1 consist of voids, in a matrix of phase 2. (This labelling is consistent with our convention that $\rho_2 < \rho_1$.) Then, from the lower bound in eq. (17.63) and with $f_1 \ll 1$,

$$\rho_{\text{eff}} = \rho_2[1 + (3/2)f_1]. \tag{17.65}$$

ANISOTROPIC AND POLYCRYSTALLINE MATERIALS

1. Introduction

Fibrous or lamellar composites are typical examples of materials with anisotropic physical properties. More generally, we will be interested in composites in which the properties of each separate phase are isotropic but the geometrical distribution of the phases is anisotropic. We will also treat polycrystalline one-phase materials for which the property of interest is anisotropic in a single crystallite. The two cases are partly related. Consider the microstructure in fig. 18.1. Each grain in the material consists of two phases which form a lamellar structure. If phases 1 and 2 have different isotropic conductivities, the grains may be described by different conductivities perpendicular and parallel to the lamellae. Thus, the entire material can be viewed either as a one-phase poly-crystalline material with anisotropic conductivity in each crystallite or as a two-phase material with isotropic conductivity in each phase. A very important case is that of a polycrystalline material in which the grains are randomly oriented so that the specimen is isotropic on a large scale. One may call this a *quasi-isotropic* material, or a material that is *isotropic in a statistical sense*. Some authors use the word aelotropy for the anisotropy of a single crystal and reserve the use of anisotropy to systems composed of many crystallites. We will not make this distinction.

Much of our discussion parallels that of the preceding chapter. In particular, we are interested in the effective-conductivity tensor components $(\sigma_{\text{eff}})_{ij}$ of an overall anisotropic material, the effective conductivity σ_{eff} of an overall isotropic polycrystalline material and analogous parameters describing elastic and thermal-expansion properties. There are bounds to such quantities, e.g. of the Hashin–Shtrikman (HS) type, and there are effective-medium theories.
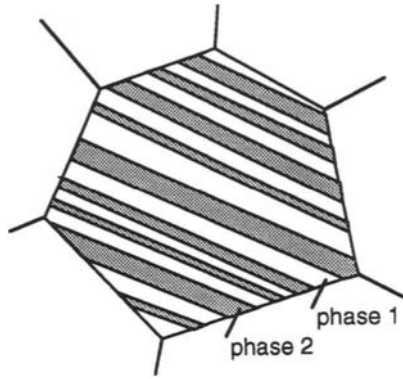
Fig. 18.1. A two-phase material may be viewed as a one-phase polycrystalline material with anisotropic properties in each grain (schematic illustration).

2. Conductivity properties of quasi-isotropic polycrystalline materials

2.1. Bounds

Let the diagonal elements of the conductivity matrix of a single crystal be σ_a, σ_b and σ_c. One can show (Molyneux 1970) that σ_{eff} is bounded by

$$3\left(\frac{1}{\sigma_a} + \frac{1}{\sigma_b} + \frac{1}{\sigma_c}\right)^{-1} \le \sigma_{\text{eff}} \le \frac{1}{3}(\sigma_a + \sigma_b + \sigma_c). \tag{18.1}$$

It was shown by Schulgasser (1977) that one can construct a laminated, statistically isotropic material with the conductivity $\sigma_{\text{eff}} = (\sigma_a + \sigma_b + \sigma_c)/3$. Hence, the upper bound in eq. (18.1) is the best possible, given the condition of overall isotropy. The problem of the best lower bound has been more difficult to solve. Schulgasser (1977) showed that the conductivity is at least $(\sigma_a \sigma_b \sigma_c)^{1/3}$. Avellaneda et al. (1988) and Nesi and Milton (1991) derived a lower bound σ_S which is attainable. That bound is the solution to the equation

$$\sigma_S^3 + (\sigma_a + \sigma_b + \sigma_c)\sigma_S^2 - 4\sigma_a\sigma_b\sigma_c = 0. \tag{18.2}$$

Crystals of axial symmetry (hexagonal, trigonal or tetragonal) have $\sigma_a = \sigma_b = \sigma_\perp$, and $\sigma_c = \sigma_\parallel$. Then eq. (18.2) has a closed-form solution,

$\sigma_S = [(\sigma_\parallel^2 + 8\sigma_\perp\sigma_\parallel)^{1/2} - \sigma_\parallel]/2$, for $\sigma_\parallel > \sigma_\perp$ and with $\sigma_\parallel$ and $\sigma_\perp$ interchanged in σ_S when $\sigma_\parallel < \sigma_\perp$.

Hashin and Shtrikman (1963b) derived bounds which are valid when the grains in the polycrystal are equiaxed, i.e. the grains have no preferred dimension (such as being lamellar; cf. the discussion above) which is a more restrictive condition than requiring overall isotropy of the material. Therefore, these bounds are narrower than the combination of eqs. (18.1) and (18.2). The latter are the best possible, given only the condition of statistical isotropy. In an isotropic material, with grains of axial symmetry, the HS bounds take the form (if $\sigma_\parallel > \sigma_\perp$; otherwise the bounds are reversed)

$$\sigma_\perp \frac{4\sigma_\perp + 5\sigma_\parallel}{7\sigma_\perp + 2\sigma_\parallel} < \sigma_{\text{eff}} < \sigma_\parallel \frac{7\sigma_\perp + 2\sigma_\parallel}{\sigma_\perp + 8\sigma_\parallel}. \tag{18.3}$$

2.2. Effective-medium theory

An effective-medium approach (Stroud 1975, Helsing and Helte 1991) gives σ_{eff} as the solution to ($i = a, b, c$)

$$\sum_i \frac{\sigma_{\text{eff}} - \sigma_i}{2\sigma_{\text{eff}} + \sigma_i} = 0. \tag{18.4}$$

The effective-medium result lies within the H–S bounds. In the special case that $\sigma_a = \sigma_b = \sigma_\perp$ and $\sigma_c = \sigma_\parallel$ (i.e. axial symmetry) we get (see also Bruggeman 1935)

$$\sigma_{\text{eff}} = (1/4)[\sigma_\perp + (\sigma_\perp^2 + 8\sigma_\perp\sigma_\parallel)^{1/2}]. \tag{18.5}$$

We note that eq. (18.4) is identical to the effective-medium result (eq. (17.53)) for a composite made up of equal amounts of three phases with isotropic conductivities.

2.3. Weakly anisotropic material

As an illustration, consider hexagonal (or trigonal, tetragonal) lattice symmetry with

$$\sigma_\parallel = \sigma_\perp(1 + \varepsilon) \tag{18.6}$$

and $|\varepsilon| \ll 1$. Then,

$$\sigma_{\text{eff}} \approx \sigma_{\perp}(1 + \varepsilon/3 - 4\varepsilon^2/27). \tag{18.7}$$

If we keep only terms linear in ε, bounds in eq. (18.1), the HS bounds, and the effective-medium-theory result all agree, and give $\sigma_{\text{eff}} = \sigma_{\perp}(1 + \varepsilon/3)$.

Example: thermal conductivity in pearlite. An Fe–C alloy with 0.8 weight-% C may have the microstructure called pearlite, where ferrite (α-Fe; bcc Fe) and cementite (Fe$_3$C) form lamellae, reminiscent of the geometry in fig. 18.1. The local thermal conductivity, in a region containing many such parallel lamellae, can be viewed as having components $\kappa_{\perp}$ and $\kappa_{\parallel}$ where $\kappa_{\perp}$ and $\kappa_{\parallel}$ are trivially obtained from a parallel and series coupling of α-Fe and Fe$_3$C. (Note that $\kappa_{\parallel}$ denotes the conductivity perpendicular to the lamellae, because this is the direction for axial symmetry.) Using the conductivities (Helsing and Grimvall 1991) $\kappa_{\text{Fe,alloy}} = 30$ W/(m K) and $\kappa_{\text{cementite}} = 8$ W/(m K), and the volume fraction $f_{\text{cementite}} = 0.122$, we get $\kappa_{\perp} = 27.3$ W/(m K) and $\kappa_{\parallel} = 22.5$ W/(m K). If there is no overall preferred orientation of the lamellae, the conductivity properties of a pearlite specimen can be modelled as that of a statistically isotropic one-phase polycrystalline material. Table 18.1 gives results for the bounds in eq. (18.1) and the HS bounds to the thermal conductivity, and also κ^* from an effective-medium theory. The numerical accuracy in the table only serves to show how close bounds are, for given conductivities $\kappa_{\perp}$ and $\kappa_{\parallel}$.

Example: electrical resistivity in yttrium. Yttrium has hexagonal lattice structure with a larger anisotropy ratio $\rho_{\perp}/\rho_{\parallel} = 2.07$ than for most other hcp-structure metals. With $\rho_{\perp} = 71.6\ \mu\Omega$ cm and $\rho_{\parallel} = 34.6\ \mu\Omega$ cm we get bounds and estimates which fall outside the measured value $\rho_{\text{exp}} = 59.7\ \mu\Omega$ cm for polycrystalline specimens. Equation (18.2) yields $\rho_{\text{eff}} < 57.4\ \mu\Omega$ cm. The experimental data, from Hall et al. (1959) and Alstad et al. (1961), are said to refer to a polycrystalline material without texture (cf. §5), corrected for the residual resistivity at low temperatures, and with an uncertainty of about 1%. This example illustrates how bounds can be used to show that not all the assumptions about an experiment may be correct.

Table 18.1

Thermal conductivity of pearlite, in W/(m K), and electrical resistivity of yttrium, in $\mu\Omega$ cm

	$(18.1)_\ell$	$(18.1)_u$	H–S lower	H–S upper	Eff. medium	Experiment
Pearlite	25.488	25.700	25.618	25.627	25.624	
Yttrium	52.8	59.3	54.5	55.6	55.2	59.7

3.   Elastic properties of quasi-isotropic polycrystalline one-phase materials

3.1.   Cubic lattice structures

Voigt and Reuss bounds. We first consider a statistically isotropic polycrystalline one-phase material in which the crystallites have a cubic lattice structure (e.g. fcc, bcc, diamond- or NaCl-type lattice). The elastic properties of the individual crystallites are described by three elastic constants, c_{11}, c_{12} and c_{44}. Our task is to find the effective bulk modulus K_{eff} and shear modulus G_{eff}. Voigt (1910) assumed that the strain is uniform throughout the sample. The bulk modulus then becomes

$$K_V = (c_{11} + 2c_{12})/3. \tag{18.8}$$

Similarly, Reuss (1929) assumed a uniform stress in the sample and obtained the bulk modulus

$$K_R = (c_{11} + 2c_{12})/3, \tag{18.9}$$

i.e. $K_V = K_R$ for cubic lattices. For the shear modulus, the result is

$$G_V = (c_{11} - c_{12} + 3c_{44})/5, \tag{18.10}$$

$$G_R = 5(c_{11} - c_{12})c_{44}/[4c_{44} + 3(c_{11} - c_{12})]. \tag{18.11}$$

Hill (1952) has shown that the assumptions of Voigt (i.e. uniform strain) and Reuss (uniform stress) lead to upper and lower bounds to K and G, for any crystal structure. Thus,

$$K_R \le K_{\text{eff}} \le K_V, \tag{18.12}$$

$$G_R \leq G_{eff} \leq G_V. \tag{18.13}$$

From the general relation (3.10) between E, G and K,

$$\frac{1}{E} = \frac{1}{3G} + \frac{1}{9K}, \tag{18.14}$$

it is obvious that the smallest possible E, denoted E_R, is obtained with G_R and K_R on the right of eq. (18.14). Similarly, the largest value, E_V, is obtained with G_V and K_V on the right. Then

$$E_R \leq E_{eff} \leq E_V. \tag{18.15}$$

Example: Reuss' expression for E. If we solve for E from eq. (18.14) with K_R and G_R given by eqs. (18.9) and (18.11), and use eqs. (3.31)–(3.33), we get

$$\frac{1}{E_R} = s_{11} - \frac{1}{5}(2s_{11} - 2s_{12} - s_{44}). \tag{18.16}$$

In eq. (3.44) it was noted that $\{E[hkl]\}^{-1} = s_{11} - (2s_{11} - 2s_{12} - s_{44})N^4$ where N contains direction cosines for $[hkl]$. Taking an average over all directions $[hkl]$, i.e.

$$\frac{1}{2} \int_0^\pi \{E[hkl]\}^{-1} \sin\theta \, d\theta, \tag{18.17}$$

yields $1/E_R$ as in eq. (18.16). The agreement is not accidental. In Reuss' approach one assumes that the stress σ is uniform in the polycrystalline sample. The effective strain is $\varepsilon_{eff} = \sigma/E_{eff}$. Now, ε_{eff} is the resulting strain from crystallites with a random crystallographic orientation. We have ε_{eff} as an average of $\varepsilon = \sigma/E[hkl]$. Hence, $\varepsilon_{eff} = \sigma/E_R$. A similar argument, with uniform strain, leads to E_V.

H–S bounds. Hashin and Shtrikman (1962b) derived upper and lower bounds to K and G using the same variational method as for their bounds in multiphase materials. It seems not to be known whether, or not, the bounds to G are the best possible (optimal), i.e. if there are quasi-isotropic materials for which they are attained. The bounds to the bulk modulus must coincide in a cubic lattice, since then $K_R = K_V$. Hence,

$$K_u = K_\ell = (c_{11} + 2c_{12})/3. \tag{18.18}$$

The bounds to the shear modulus are algebraically more complicated (Hashin and Shtrikman 1962b). They can be written (when $c_{11} - c_{12} > 2c_{44}$),

$$G_u = c_{44} + \frac{2}{(5/2)[c_{11} - c_{12} - 2c_{44}]^{-1} + 6H_1}, \qquad (18.19)$$

$$G_\ell = \frac{c_{11} - c_{12}}{2} + \frac{3}{(5/2)[2c_{44} - (c_{11} - c_{12})]^{-1} + 4H_2}, \qquad (18.20)$$

where

$$H_1 = \frac{(c_{11} + 2c_{12} + 6c_{44})}{5c_{44}(c_{11} + 2c_{12} + 2c_{44})}, \qquad (18.21)$$

$$H_2 = \frac{2(4c_{11} - c_{12})}{15(c_{11} - c_{12})c_{11}}, \qquad (18.22)$$

When $c_{11} - c_{12} < 2c_{44}$, the upper and lower bounds are reversed. For elastically isotropic crystallites, i.e. when $c_{11} - c_{12} = 2c_{44}$, they simplify to

$$G_u = G_\ell = G_V = G_R = c_{44}. \qquad (18.23)$$

Experimental values of the elastic coefficients of single crystals, and the Voigt, Reuss and HS bounds derived from them, have been tabulated by Simmons and Wang (1971) for essentially all systems with data available at that time.

3.2. Non-cubic lattices

Since the Voigt approach assumes a uniform strain and the Reuss approach a uniform stress, it is natural to use the elastic stiffnesses c_{ij} in the former and the elastic compliances s_{ij} in the latter case. The general expressions for the *Voigt* and *Reuss* bounds to K and G in non-cubic lattices are (Schreiber et al. 1973)

$$K_V = \frac{1}{9}(c_{11} + c_{22} + c_{33}) + \frac{2}{9}(c_{12} + c_{13} + c_{23}), \qquad (18.24)$$

$$\frac{1}{K_R} = (s_{11} + s_{22} + s_{33}) + 2(s_{12} + s_{13} + s_{23}), \qquad (18.25)$$

$$G_V = \frac{1}{15}(c_{11} + c_{22} + c_{33}) - \frac{1}{15}(c_{12} + c_{13} + c_{23})$$

$$+ \frac{1}{5}(c_{44} + c_{55} + c_{66}), \tag{18.26}$$

$$\frac{1}{G_R} = \frac{4}{15}(s_{11} + s_{22} + s_{33}) - \frac{4}{15}(s_{12} + s_{13} + s_{23})$$

$$+ \frac{3}{15}(s_{44} + s_{55} + s_{66}). \tag{18.27}$$

We check that these relations contain the results (eqs. (18.8)–(18.11)) for cubic crystals as special cases. Take $c_{11} = c_{22} = c_{33}$; $c_{12} = c_{13} = c_{23}$; $c_{44} = c_{55} = c_{66}$, with analogous relations for s_{ij}. The results for K_V and G_V follow immediately. Furthermore, $1/K_R = 3(s_{11} + 2s_{12})$ and $1/G_R = (4s_{11} - 4s_{12} + 3s_{44})/5$. With the relations (3.33)–(3.35) between c_{ij} and s_{ij}, we recover eqs. (18.9) and (18.11).

Crystals belonging to one of the seven classes of *hexagonal* lattices have five independent elastic constants; c_{11}, c_{12}, c_{13}, c_{33} and c_{44}. The *Voigt* and *Reuss* bounds, when expressed in c_{ij}, take the form (Watt and Peselnick 1980, Meister and Peselnick 1966)

$$K_V = \frac{1}{9}[2(c_{11} + c_{12}) + c_{33} + 4c_{13}], \tag{18.28}$$

$$K_R = C^2/M, \tag{18.29}$$

$$G_V = \frac{1}{30}[12c_{66} + 12c_{44} + M], \tag{18.30}$$

$$G_R = \frac{5}{2}\left[\frac{c_{44}c_{66}C^2}{(c_{44} + c_{66})C^2 + 3K_V c_{44}c_{66}}\right], \tag{18.31}$$

where $c_{66} = (c_{11} - c_{12})/2$ and the auxiliary moduli C and M are defined

$$C^2 = (c_{11} + c_{12})c_{33} - 2c_{13}^2, \tag{18.32}$$

$$M = c_{11} + c_{12} + 2c_{33} - 4c_{13}. \tag{18.33}$$

The analogous relations for the Voigt and Reuss bounds in trigonal and tetragonal lattices were obtained by Meister and Peselnick (1966).

The *H–S* type bounds to K and G for hexagonal and trigonal (Peselnick and Meister 1965, Watt and Peselnick 1980), tetragonal (Meister and Peselnick 1966, Watt and Peselnick 1980), orthorhombic (Watt 1979) and monoclinic (Watt 1980) lattices are algebraically more complicated than eqs. (18.18)–(18.20). It appears unknown if these bounds are optimal, i.e. the best possible.

3.3.   The Voigt–Reuss–Hill approximation

The Voigt and Reuss estimations are easy to calculate. Hill (1952), having shown that they are rigorous bounds, suggested that one takes their arithmetic average as an estimation of the elastic properties. Usually, one refers to these averages as the *Voigt–Reuss–Hill* (VRH) values, a term introduced by Chung (1963);

$$K_{VRH} = (K_V + K_R)/2, \tag{18.34}$$

$$G_{VRH} = (G_V + G_R)/2. \tag{18.35}$$

Note that E_{VRH} derived by eq. (3.10) from K_{VRH} and G_{VRH}, is not mathematically identical to $(E_V + E_R)/2$, although the latter may be a very good approximation.

There is no particular reason why the arithmetic (VRH) mean should be preferred. Kumazawa (1969) used the geometric mean $(K_V K_R)^{1/2}$ and Shukla and Padial (1973) used the harmonic mean, $2K_V K_R/(K_V + K_R)$. If the material is only weakly anisotropic, they will of course all give good estimations. We can define a measure A_{VRH} of elastic anisotropy by

$$A_{VRH} = \frac{G_V - G_R}{G_V + G_R}. \tag{18.36}$$

This measure has been applied by Chung and Buessem (1967) to crystals of cubic lattice symmetry. The relation between A_{VRH} and Zener's measure, eq. (3.61), $A_Z = 2c_{44}/(c_{11} - c_{12})$ of anisotropy in cubic crystals is

$$A_{VRH} = \frac{(A_Z - 1)}{1 + A_Z^2 + (19/3)A_Z} \approx 0.12(A_Z - 1)^2. \tag{18.37}$$

The last expression refers to almost isotropic materials, $A_Z \approx 1$. We can understand the usefulness of the VRH approximation from the fact that it is accurate to second order in the (small) anisotropy parameter $A_Z - 1$.

The approach discussed above is relevant for the elastic properties measured in short-time (e.g. acoustic) experiments. In long-time (e.g. static compression) experiments, the polycrystalline material may have time to relax so that it is characterised by the Reuss condition of uniform stress. Then K_{eff} is given by K_R (Thomsen 1972).

In analogy to the relation between c_{ij} and the engineering elastic constants, one can derive relations between single-crystal third-order elastic coefficients and the corresponding third-order quantities for the engineering elastic constants (Chang 1967; see also Chung 1967).

Example: VRH and HS estimations of K_{eff} and G_{eff}. Table 18.2 gives VRH- and HS-type estimations of the elastic properties of some poly-crystals. The VRH estimation of K is here defined as $(K_V + K_R)/2 \pm (K_V - K_R)/2$ and the HS type as $(K_u + K_\ell)/2 \pm (K_u - K_\ell)/2$, with analogous definitions for the shear modulus. No uncertainty interval is given when the upper and lower bounds coincide to the number of digits given. The entries (in GPa) for cubic structures are calculated from elastic constants in the Landolt–Börnstein tables (Every and McCurdy 1992), and other entries are from Peselnick and Meister (1965) for Mg and ice, from Watt and Peselnick (1980) for Zn, graphite, Al_2O_3, SiO_2 and Sn, and from Watt (1979) for U and $CaSO_4$. See Watt and Peselnick (1980) for further examples. One notes that in most cases the HS bounds give an estimation that is accurate to within a few percent (provided that the single-crystal elastic constants are accurately known), i.e. better than achieved in many direct experiments. We also note in the table that the VRH approximation lies inside the HS bounds. This is a rule which has few exceptions (Watt et al. 1976, Watt and Peselnick 1980). Even in the very anisotropic case of fcc Pu (cf. table 3.3) one gets a useful estimation of G from the HS bounds. However, the method fails completely in graphite, which has an exceptional anisotropy.

Table 18.2

Voigt–Reuss–Hill (VRH) and Hashin–Shtrikman (HS) estimations of the effective bulk modulus K_{eff} and shear modulus G_{eff}, in units of GPa

	K_{eff} (VRH)	K_{eff} (HS)	G_{eff} (VRH)	G_{eff} (HS)
Al (fcc)	77.3	a	26.1 ± 0.1	26.1
Cu (fcc)	137.7	a	47.3 ± 7.3	47.7 ± 1.7
Th (fcc)	59.6	a	27.7 ± 4.9	27.8 ± 1.2
Pu (fcc)	30.0	a	15.8 ± 6.4	15.3 ± 2.5
α-Fe (bcc)	166.7	a	81.5 ± 7.7	81.8 ± 1.4
Li (bcc, 195 K)	12.1	a	4.34 ± 1.98	4.19 ± 0.85
C (diamond)	442.1	a	534.3 ± 2.4	534.2 ± 0.1
Si (diamond)	97.0	a	66.3 ± 1.5	66.4 ± 0.1
GaAs (diamond)	75.0	a	46.5 ± 2.1	46.6 ± 0.3
NaCl (cubic)	24.9	a	14.7 ± 0.2	14.7 ± 0.1
MgO (cubic)	160.0	a	130.3 ± 2.9	130.3 ± 0.3
TaC (cubic)	217.0	a	119.8 ± 14.0	118.7 ± 2.8
Zn (hcp)	68.3 ± 6.8	69.7 ± 2.2	39.5 ± 5.4	39.7 ± 1.8
Mg (hcp)	36.9	36.9	19.3 ± 0.1	19.3
Ice (hexagonal)	8.14	8.14	3.67 ± 0.02	3.67
Graphite (hexagonal)	161.1 ± 125.3	120.2 ± 84.0	109.2 ± 108.7	73.5 ± 72.7
β-Sn (tetragonal)	60.6	60.6	17.8 ± 2.1	18.2 ± 0.6
SiO_2 (tetragonal)	37.7 ± 0.2	37.7	44.4 ± 3.4	44.2 ± 0.7
Al_2O_3 (trigonal)	251.1 ± 0.2	252.1	163.3 ± 2.7	163.5 ± 0.3
α-U (orthorhombic)	113.1 ± 1.7	112.9 ± 0.3	84.4 ± 3.7	84.2 ± 0.6
$CaSO_4$ (orthorhombic)	54.9 ± 2.7	54.1 ± 1.0	29.3 ± 6.2	29.6 ± 2.2

[a] K_{eff} is given exactly in cubic systems.

4. Thermal expansion of quasi-isotropic polycrystalline one-phase materials

The thermal expansion of a single crystal of hexagonal, trigonal or tetragonal symmetry is described by two expansion coefficients, α_1 ($=\alpha_2$) and α_3. When such single crystals form a statistically isotropic polycrystal, the resulting effective coefficient of thermal expansion takes an *exact* form (Hashin 1984, Schulgasser 1987, 1989, Ballabh et al. 1988, Gibiansky and Torquato 1997) which can be written as

$$\alpha_{\text{eff}} = \frac{2\alpha_1 + \alpha_3}{3} + (\alpha_3 - \alpha_1)$$

$$\times \frac{[1/K_{\text{eff}} - (2c_{33} + c_{11} + c_{12} - 4c_{13})/C^2]}{3(c_{11} + c_{12} - c_{13} - c_{33})/C^2}, \qquad (18.38)$$

where C^2 was defined in eq. (18.32). This relation is sometimes given in a seemingly different, but mathematically equivalent, form. We further note that, by eqs. (18.29), (18.32) and (18.33), $(2c_{33} + c_{11} + c_{12} - 4c_{13})/C^2 = 1/K_R$, so that with the Reuss expression for K_{eff} we get $\alpha_{\text{eff}} = (2\alpha_1 + \alpha_3)/3$.

Because eq. (18.38) is a monotonically varying function of K_{eff} it yields upper and lower bounds to α_{eff} if we insert such bounds for K_{eff}. We remarked in the example in §3.3 that, with very few exceptions, the VRH approximation to K_{eff} lies inside the HS bounds to K_{eff}. Therefore, $K_{\text{eff}}(\text{VRH})$ inserted in eq. (18.38) yields α_{eff} between the HS bounds to α_{eff}. Table 18.3 shows examples when K_{eff} is given by the VRH approximation, i.e. with uncertainties that follow from the bounds K_V and K_R. The unrealistic number of digits in the calculated α_{eff} only serves to show the difference between the bounds that would result if indata had been exact. Expansion data are taken from Touloukian et al. (1975, 1977) and elastic constants from the Landolt–Börnstein tables (Every and McCurdy 1992).

In materials with texture and non-cubic lattice structure, α_{eff} is anisotropic. Dunn and Ledbetter (1995), relying on results by Schulgasser (1987), have given explicit expressions for the generalisation of eq. (18.38) in the Voigt and Reuss limits, when the texture is expressed by coefficients in the orientation-distribution function (ODF).

5. Anisotropic particles in an isotropic matrix

Let a matrix have an isotropic conductivity σ_m, and the grains of a second phase, embedded in the matrix, have anisotropic conductivities characteristic of a hexagonal (or trigonal or tetragonal) lattice structure, i.e. $\sigma_\perp$ and $\sigma_\|$. Levy and Stroud (1997) considered the conductivity of this composite system in the Maxwell Garnett approximation (cf. eq. (17.55)) when the inclusions have spherical shape. The expressions for the effective conductivity are mathematically elementary, but algebraically somewhat complex, and will here be illustrated in two simple

Table 18.3

Linear thermal expansion coefficient α_{eff} (unit 10^{-6} K^{-1}) of statistically isotropic polycrystalline specimens, calculated from eq. (18.38), with K_{eff} in the VRH approximation, and compared with experiments

Material	$\alpha_{\parallel}$	$\alpha_{\perp}$	α_{eff} (VRH)	α_{eff} (exp)
Zn	64	14	28.52 ± 2.15	30
Be	10	12	11.31 ± 0.03	11
Zr	7	4	5.02 ± 0.02	6
β-Sn	33	16	21.63 ± 0.04	22
SiO$_2$	7	12	10.21 ± 0.12	10

cases. First, consider the dilute limit $f_2 \ll 1$ of spherical inclusions which are oriented so that the axes with the conductivity $\sigma_{\parallel}$ are parallel. Let the effective conductivity of the composite in the same direction be $\sigma_{\text{eff},\parallel}$ and the conductivity in any perpendicular direction be $\sigma_{\text{eff},\perp}$. Then

$$\sigma_{\text{eff},\parallel} = \sigma_{\text{m}} \left[1 - 3 f_2 \frac{(\sigma_{\text{m}} - \sigma_{\parallel})}{2\sigma_{\text{m}} + \sigma_{\parallel}} \right], \tag{18.39}$$

$$\sigma_{\text{eff},\perp} = \sigma_{\text{m}} \left[1 - 3 f_2 \frac{(\sigma_{\text{m}} - \sigma_{\perp})}{2\sigma_{\text{m}} + \sigma_{\perp}} \right]. \tag{18.40}$$

As a second example, consider the dilute limit when the spherical inclusions are randomly oriented, so that σ_{eff} is isotropic;

$$\sigma_{\text{eff}} = \sigma_{\text{m}} \left[1 - 3 f_2 \frac{(\sigma_{\text{m}} - \sigma_{\parallel})(2\sigma_{\text{m}} + \sigma_{\perp}) - 2\sigma_{\text{m}}(\sigma_{\perp} - \sigma_{\parallel})}{(2\sigma_{\text{m}} + \sigma_{\parallel})(2\sigma_{\text{m}} + \sigma_{\perp})} \right].$$

$$\tag{18.41}$$

It is easily seen that when $\sigma_{\parallel} = \sigma_{\perp}$, the relations (18.39)–(18.40) become σ_{eff} in the dilute limit of isotropic inclusions, eq. (17.30). Helsing and Helte (1991) derived results similar to those above, but for ellipsoid-shaped inclusions with anisotropic conductivity.

6. Oriented phases

The most important composite materials have more or less parallel fibres in an isotropic matrix, or have a lamellar structure. We have encountered these cases as bounds in some of the expressions in Chapters 17 and 18. There is a vast literature in this field. We shall only make a few comments on fibre composites, that connect to our previous results.

The conduction properties of a fibre composite are described by two parameters, referring to conduction along (σ_L), and transverse (σ_T) to, the fibres. The Wiener bounds in Chapter 17 (§2.2) give the longitudinal conductivity exactly (or to a very good approximation if the individual fibres are shorter than the specimen). For the transverse conductivity, bounds are given by the two-dimensional HS relations, i.e. with 3 replaced by 2 in eqs. (17.17) and (17.18). When the transverse microstructure fulfills the requirements of a symmetric cell material, the result in Chapter 17 (§6.2) is applicable.

A fibre composite which is transversely isotropic has the same symmetry as a single crystal of a hexagonal lattice. Thus we need five independent elastic parameters, to be compared with only two (e.g. K, G) in an elastically isotropic material. We can choose the five parameters to be, e.g. the transverse bulk modulus K_T, the transverse and longitudinal shear moduli G_T and G_L, and the transverse and longitudinal Young's moduli E_T and E_L. Other elastic constants, for instance the transverse and longitudinal Poisson ratios, can be expressed in terms of these five elastic parameters. In analogy to the approaches in this and the previous chapter there are HS-type bounds (Hill 1964, Hashin 1965) and effective-medium results (Hill 1965a). The field has been reviewed by Laws (1980) and Hashin (1983). There is an exact result for the "coated cylinder" analogue of the "coated sphere" aggregate (Hashin and Rosen 1964, Hashin 1983). It should be pointed out that the measured longitudinal effective Young's modulus E_L may be quite different from the approximate value $f_1 E_1 + f_2 E_2$, because fibres are not perfectly straight. If they have a slight sinusoidal shape, and the matrix is not stiff, the fibres may straighten under a load and give a low apparent E_L.

There are two coefficients of thermal expansion, α_T and α_L. If the fibre and matrix materials are isotropic, there is an exact solution (Levin 1967, Rosen and Hashin 1970), in analogy to the case of statistically isotropic materials.

Finally, we briefly comment on materials with a texture, i.e. a preferred orientation for a crystallographic direction $[hkl]$ of the single grains of a one-phase polycrystalline material. The most extreme texture would be when all grains have parallel $[hkl]$, thus effectively making it a single crystal. There are several approaches to a quantitative measure of the degree of texture. Early work often referred to *pole figures*, which give a stereographic representation of the grain orientations. It is now replaced by the concept of an orientation-distribution function, ODF (e.g. Humphreys and Hatherly 1996). See also Dunn and Ledbetter (1995), Hirao et al. (1987) and Schulgasser (1987) for examples of elastic and expansion properties in materials with a texture.

ESTIMATIONS AND CORRELATIONS

1. Introduction

Estimations play an important role in materials science, for instance to provide information when direct experimental data are missing or of low quality. The bases for estimations are of essentially two kinds; *correlations* between different properties of the same material, and *regularities* for a certain property in a group of related materials.

Most of the theories developed in this book centre around some important parameters, such as properly defined Debye temperatures $\theta_D(n)$, Grüneisen parameters $\gamma(n)$ and elastic coefficients c_{ij}. In simplified versions of the theories, one may use a common Debye temperature θ_D and Grüneisen parameter γ_G for all n, and isotropic engineering elastic constants K, G and E instead of c_{ij}. Furthermore, the equipartition theorem for classical harmonic vibrations gives a universal energy $3k_B T$ and heat capacity $3k_B$ at high temperatures. Many properties related to the conduction electrons in metals depend on the electron density of states $N(E)$ in the vicinity of the Fermi level. With relatively few such parameters entering the description, it is not surprising that there are correlations between experimental thermophysical data. For instance, Grüneisen noted already in 1913 that the electrical resistivity (plotted as ρ/T) and the heat capacity C_p of Cu, Ag, Au, Pt and Pb showed almost the same temperature dependence (cf. fig. 19.6). This was long before a theoretical understanding of the temperature dependence of the resistivity, which requires a quantum mechanical model. The Lindemann melting formula is another well known correlation, although of dubious reliability.

Physical properties of solids ultimately depend on the electronic structure, which normally varies in a regular way for a group of chemically related materials. This fact may be used in estimations

through interpolations or extrapolations. Such a regular behaviour is well illustrated by the bulk modulus (see Chapter 1).

This chapter reviews several kinds of correlations and regularities, and critically discusses their theoretical basis and limitations. Some often used relations such as the Lindemann melting criterion, Latimer's rule for standard entropies $S^o_{298.15}$, and the proportionality between defect energies and melting temperatures, have gained their popularity from data on elements. They will lose much of their significance in more complex solids.

2. Rules related to atomic volumes

It is common to define atomic radii based on a lattice model with atomic spheres. For elements, for instance, one may take the radius to be half the distance between nearest neighbours. Several schemes have been devised to define and obtain radii for use in chemical compounds (see, e.g. Pauling 1960). It is meaningful to assign a certain value to the radius r of an atom or ion, only if r is approximately unchanged when one considers different structures or compounds. Depending on the application of interest, this may be a reasonable or a poor assumption. For instance, compare bcc, fcc and hcp lattices. If they are formed by rigid spheres, the atomic volume Ω_a would be 9% larger in the bcc lattice than in the close-packed fcc and hcp lattices. ($\Omega_a = V/N$ where V is the total crystal volume and N is the number of atoms.) Table 19.1 gives the relative change $\Delta\Omega_a/\Omega_a$ in the atomic volume at the transition temperature, for some elements that exist in both bcc and fcc (or hcp) structures. We note the strong tendency to conserve the atomic volume, rather than the radius. Furthermore, theoretical calculations for a large number of intermetallic phases show that Ω_a does not vary much with the crystal structure for given composition (Ferreira et al. 1988b). It should be remarked that the rather large change in volume for the bcc to hcp transition in iron is accompanied by a loss of the magnetic moment that is present also in the paramagnetic states of the bcc and fcc phases of Fe.

As a further warning against the simple interpretation that a bcc lattice has a lower density than the close-packed fcc and hcp lattices, consider Mg. At ambient pressure Mg has the hcp lattice structure. (Actually, the bcc phase is dynamically unstable under long-wavelength

Table 19.1

The relative change in atomic volume when the crystal structure is changed

Transition	$\Delta\Omega_a/\Omega_a$ (%)
Fe(bcc) $\rightarrow$ Fe(fcc), 1184 K[a]	-1.0[b]
Fe(fcc) $\rightarrow$ Fe(bcc), 1660 K[a]	$+0.3$[b]
Fe(bcc) $\rightarrow$ Fe(hcp), $\sim$10 GPa[a]	-6[a]
Co(fcc) $\rightarrow$ Co(hcp), 695 K[a]	0.3[b]
Ti(hcp) $\rightarrow$ Ti(bcc), 1155 K[a]	-0.1[b]
$Ni_{0.76}P_{0.24}$ (amorphous $\rightarrow$ cryst.)	-0.8[c]
$Co_{0.75}P_{0.25}$ (amorphous $\rightarrow$ cryst.)	-1.3[c]
$(FeNi)_{0.8}(BP)_{0.2}$ (amorphous $\rightarrow$ cryst.)	-0.3 to -0.8[d]
Rigid spheres (fcc or hcp $\rightarrow$ bcc)	$+8.9$

[a]Young (1991).
[b]Rudman (1965).
[c]Logan and Ashby (1974).
[d]van den Beukel and Radelaar (1983). Cooling rate to produce the amorphous structure varying from 10^3 to 10^6 K/s.

shear in the [110] mode (Althoff et al. 1993).) At about 50 GPa and 300 K, hcp Mg transforms to bcc Mg, having a volume Ω_a that is lower by $\sim$1% (Olijnyk and Holzapfel 1985).

When an hcp lattice is considered as a stacking of spheres, the c/a ratio for the lattice parameters c and a has the ideal value of $\sqrt{8/3} \approx 1.633$. Magnesium comes close to this, with $c/a = 1.62$, while cadmium has $c/a = 1.89$. The Cd–Mg system forms a solid solution $Cd_{1-x}Mg_x$ with the hcp lattice structure at high temperatures, for all x. Figure 19.1 shows the variation in c/a and the average atomic volume Ω_a. When x increases from 0 to 0.5, c/a decreases by about 13%. This is due to simultaneous variations in c and a, but such that the variation in Ω_a is <1%.

In an alloy, or a mixed crystal such as NaCl–KCl, it is often assumed that a certain lattice parameter a varies linearly with the composition c, i.e. as

$$a = c_1 a_1 + c_2 a_2 \tag{19.1}$$

in a binary system ($c_2 = 1 - c_1$). This relation is known as *Vegard's law*. It was originally applied to solid solutions of ionic crystals (Vegard
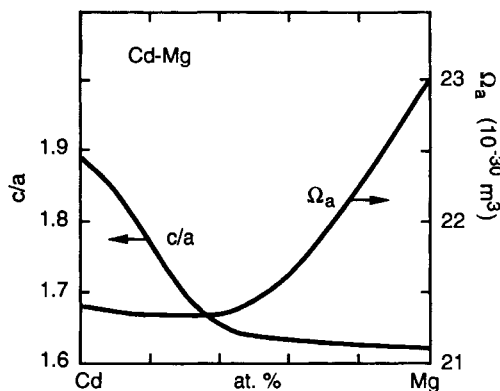
Fig. 19.1. Variation of the ratio c/a of the hcp lattice parameters (lefthand scale) and of the atomic volume Ω_a (righthand scale) of hcp solid solutions of Cd–Mg. Data from Pearson (1972).

1921), but has frequently been used in alloys. However, the "law" is often strongly violated, as exemplified above by the Cd–Mg system, and it must be amended to be useful (Gschneidner and Vineyard 1962). In the light of our discussion of Ω_a above, it may seem better to use the corresponding rule for the atomic volumes;

$$\Omega_a = c_1 \Omega_1 + c_2 \Omega_2. \tag{19.2}$$

This is sometimes called *Zen's rule* (Zen 1956). In eq. (19.2) the solids 1 and 2 need not have the same crystal structure. Note that Vegard's and Zen's relations cannot hold simultaneously. Zen's rule may be of some value, but it should only be used to establish trends. Data on lattice parameters in solids are found in the extensive works by Pearson (1972) and Villars and Calvert (1985).

   In chemistry and metallurgy, one frequently uses the concept of partial molar quantities. The *partial molar volume* $\bar{V}_i$ of component i in a system containing other components j, is defined by

$$\bar{V}_i = \left(\frac{\partial V}{\partial n_i} \right)_{T,p,n_j}, \tag{19.3}$$

where V is the volume of the system and n_i is the number of moles of component i. If Zen's rule holds, and with N_A being Avogadro's number,

$$\bar{V}_i/N_A = \left(\frac{\partial[n_i\Omega_i + n_j\Omega_j]}{\partial n_i} \right)_{T,p,n_j} = \Omega_i. \tag{19.4}$$

Example: interstitial carbon in austenite (fcc Fe). There are cases when the idea of crystals formed by rigid spheres with certain radii gives a very useful insight. Consider, for instance, the bcc and fcc lattices. The bcc structure is usually referred to as "open" while the fcc structure is close-packed. However, the largest "holes" where one can inscribe a sphere are found in the close-packed structure, although the bcc lattice has more volume in the form of void regions. This explains why carbon is almost insoluble in bcc Fe but forms a solid solution in fcc Fe (up to 9 at.% at 1426 K). If carbon atoms could be viewed as rigid spheres which fitted into the "holes" in the lattice, alloying with carbon would not change the lattice parameter of fcc Fe. Then the partial molar volume of C in Fe would be zero. In reality, the iron lattice expands. The measured lattice parameter as a function of the carbon concentration at 900 K (Ridley and Stuart 1970) gives the partial molar volumes

$$\bar{V}_{Fe(fcc)} = 7.20 \text{ cm}^3, \quad \bar{V}_{C \text{ in } Fe(fcc)} = 3.76 \text{ cm}^3.$$

This can be compared with the molar volumes of pure carbon, $\bar{V}_C = 5.31 \text{ cm}^3$ (graphite) and $\bar{V}_C = 3.42 \text{ cm}^3$ (diamond).

3. Bounds to vibrational properties

In a system described by perfectly harmonic lattice vibrations there are simple, but non-trivial, bounds to properties which depend on an average over the vibrational spectrum (Johnson and Kassman 1969, 1972; Johnson et al. 1971). For instance, if the heat capacity $C_{har}(T)$ is fitted to an Einstein model heat capacity $C_E(T)$ at any temperature T_0, one has

$$C_E(T) > C_{har}(T), \quad T > T_0; \tag{19.5}$$

$$C_{\mathrm{E}}(T) < C_{\mathrm{har}}(T), \quad T < T_0. \tag{19.6}$$

It follows that $C_{\mathrm{E}}(T)$ crosses $C_{\mathrm{har}}(T)$ at one and only one temperature. Similarly, if the average squared vibrational displacement $\langle \mathbf{u}^2 \rangle_{\mathrm{har}}$ is fitted at any $T = T_0$ to an Einstein model $\langle \mathbf{u}^2 \rangle_{\mathrm{E}}$, one has that $\langle \mathbf{u}^2 \rangle_{\mathrm{har}}$ at $T > T_0$ lies between $\langle \mathbf{u}^2 \rangle_{\mathrm{E}}$ and another mathematically simple bound, and vice versa. Analogous relations hold for the average squared velocity $\langle \mathbf{v}^2 \rangle$ of an atom. The results just quoted are valid irrespective of lattice structure, range of forces, number of different atoms etc. They are only a consequence of the assumption of harmonic vibrations. Therefore, if accurate experimental data fall outside the bounds it shows the presence of anharmonic effects.

Example: Debye–Waller factor of Fe in Cu. From Mössbauer measurements on ^{57}Fe in Cu (Nussbaum et al. 1968) one can obtain the Debye–Waller factor $\exp(-2M)$, where M is proportional to $\langle \mathbf{u}^2 \rangle$. Let M be described by an Einstein model for $\langle \mathbf{u}^2 \rangle$, fitted at $T_0 = 104$ K. Then $\exp(-2M)$, for any form of the vibrational spectrum of the Fe–Cu system, must lie within the shaded band in fig. 19.2. The fact that the experimental points fall outside that region shows that anharmonic effects influence $\langle \mathbf{u}^2 \rangle$, and hence $\exp(-2M)$.

4. Latimer's rule for standard entropies

Latimer (1921, 1951) noted that the standard entropy per mole, $S^{\mathrm{o}}_{298.15}$, i.e. S at $T = 298.15$ K, is often well described for the elements by the simple expression

$$S_{\mathrm{Latimer}} = 3N_{\mathrm{A}}k_{\mathrm{B}}[k_{\mathrm{L}} + (1/2)\ln M_{\mathrm{r}}]. \tag{19.7}$$

Here, k_{L} is an empirical dimensionless constant of the order of unity, N_{A} is Avogadro's number and $M_{\mathrm{r}} = M/M_0$ is the relative atomic mass (earlier called atomic weight; $12M_0$ is the mass of the atom ^{12}C). Normally, the lattice vibrations account for almost all of $S^{\mathrm{o}}_{298.15}$, and we here consider only that term. From eqs. (7.23) and (6.30), the leading terms of the entropy in the high temperature expansion can be expressed, at $T = T_0 = 298.15$ K, as

$$S^{\mathrm{o}}_{298.15} \approx 3N_{\mathrm{A}}k_{\mathrm{B}}\{4/3 + \ln(T_0/\alpha) + (1/2)\ln M\}, \tag{19.8}$$
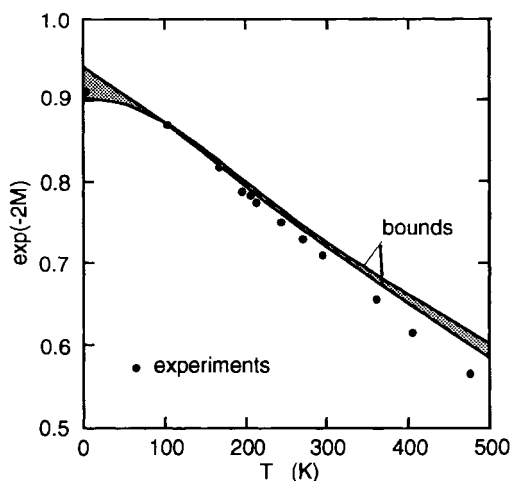
Fig. 19.2. The experimental Debye–Waller factor $\exp(-2M)$ for the vibrations of ^{57}Fe in a Cu host lattice (symbols) is fitted to an Einstein model at 104 K, and also to another simple model which assumes the highest vibrational frequency of the Fe–Cu system to be less than $1.20\omega_{max}$ where ω_{max} refers to the pure Cu host. If the vibration of ^{57}Fe was strictly harmonic, $\exp(-2M)$ would lie in the shaded band. The fact that the experimental data fall outside this band is due to anharmonic effects. After Johnson et al. (1971).

with $\alpha = (\hbar/k_B)(k_S)^{1/2}$, and k_S being an average interatomic force constant (see §8). In analogy to eq. (19.7) we now form the entropy of a compound A_xB_y as

$$
S^o_{298.15}(A_xB_y) \approx 3(x+y)N_Ak_B\left\{\frac{4}{3} + \ln\left[\frac{T_0}{\alpha_A^{x/(x+y)}\alpha_B^{y/(x+y)}}\right]\right.
$$
$$
\left. +\frac{1}{2}\ln[M_A^{x/(x+y)}M_B^{y/(x+y)}]\right\} \tag{19.9}
$$

This form of Latimer's rule gives the correct weight to the atomic masses at high temperatures. If variations in k_S are smaller than variations in M, eq. (19.9) may give a fair estimate of $S^o_{298.15}(A_xB_y)$, but it still has severe limitations (Grimvall 1983). For instance, the high temperature expansion (eq. (19.8)) is not valid at $T_0 = 298$ K for solids with very light atoms, since then $\theta_D(0) \gg 298$ K.

5.   The Neumann–Kopp rule for C_p

The Neumann–Kopp rule expresses the (molar) heat capacity $C_p(A_x B_y)$ of a compound $A_x B_y$ (or an alloy) as the sum of C_p for the elements forming $A_x B_y$,

$$C_p(A_x B_y) = x C_p(A) + y C_p(B).   \qquad (19.10)$$

The rule was formulated by Neumann (1831) and Kopp (1864), as an extension of the Dulong–Petit (1819) rule.

Table 19.2, based on data from the JANAF thermochemical tables (1985), Barin (1989) and Hultgren et al. (1973a, b), suggests that the rule is often astonishingly well obeyed, but in fact its predictive power is rather limited. In systems where the elements A and B and the compound $A_x B_y$ get their major contribution to C_p from the lattice vibrations, and the temperature is higher than, say, the Debye temperatures θ_D of A, B and $A_x B_y$, the Neumann–Kopp rule is just equivalent with the Dulong–Petit rule. To be more precise, consider the first terms in the high temperature expansion $C_{har}/3Nk_B \approx 1 - (1/20)[\theta_D(2)/T]^2$, (7.32). When combined with the interpolation formula (9.27) for $\theta_D(2)$ we recover exactly the Neumann–Kopp rule, so the rule is often reasonable even at temperatures somewhat lower than θ_D of A, B and $A_x B_y$. Furthermore, if the Neumann–Kopp rule is valid at *all* temperatures we may use the expression $S = \int C_p(dT'/T')$ for the entropy and obtain $S(A_x B_y) = x S(A) + y S(B)$, which is exactly Latimer's high temperature rule (eq. (19.9)). On the other hand, Latimer's high temperature relation does not mathematically imply that the Neumann–Kopp rule is valid at low temperatures. In fact, the Neumann–Kopp rule at low T implies that $[\theta_D(-3; A_x B_y)]^{-3} = x[\theta_D(-3; A)]^{-3} + y[\theta_D(-3; B)]^{-3}$. This is not consistent with the interpolation formula (9.25) for $\theta_D(-3)$, which is of the same structure but has exponents -2 instead of -3.

We conclude that the major reason for the apparent success of the Neumann–Kopp rule in many cases is that it expresses the trivial Dulong–Petit results. The rule certainly fails when there are large non-vibrational contributions to the heat capacity (e.g. the magnetic term in C_p for Fe at 1000 K; entries for Fe_3C in table 19.2), when one is well below the Dulong–Petit limit because $T < \theta_D$ (e.g. TiB_2 at 100 K; C in Fe_3C) or when there are large anharmonic effects in one or both of the components (e.g. AlSb at 900 K). Finally we remark that heat

Table 19.2

The experimental heat capacity C_p of elements A and B and compounds $A_x B_y$, and
the result of the Neumann–Kopp rule, $x C_p(A) + y C_p(B)$

Compound $A_x B_y$	T [K]	Heat capacity C_p [J/(K mol)][c]			
		A	B	$xA + yB$	$A_x B_y$ (exp.)
$Cu_{0.8}Zn_{0.2}$	100	16.0	19.5	16.7	16.7
$Cu_{0.8}Zn_{0.2}$	298	24.4	25.4	24.6	24.7
$MgZn_2$	298	24.9	25.4	75.6	74.6
AlSb	298	24.3	25.2	49.6	46.4
AlSb	900	33.1	30.9	64.0	52.2
Mg_2Si	298	24.9	20.0	69.8	67.9
Mg_2Si	900	31.9	25.9	89.7	85.7
B_4Mg	298	11.3	25.4	70.5	70.3
B_4Mg	900	24.2	31.9	128.9	111.0
TiB_2	100	14.3	1.1	16.5	7.5
TiB_2	298	25.2	11.3	47.9	44.3
TiB_2	1000	32.1	25.0	82.0	76.9
WC	298	24.3	6.1[a]	30.4	35.4
WC	1000	27.6	21.6[a]	49.2	50.1
Fe_3C	298	25.0	8.5[b]	83.4	105.9
Fe_3C	1000	54.4	21.6[b]	184.9	119.7
Al_2SiO_5[d]	298	79.0	44.6	123.6	122.2
Al_2SiO_5[d]	1800	135.1	73.8	208.9	220.0

[a]Diamond.
[b]Graphite.
[c]The classical vibrational heat capacity of an element is $3R = 24.94$ J/(K mol).
[d]Al_2SiO_5 considered as $(\alpha\text{-}Al_2O_3)(SiO_2)$.

capacities are sometimes given per mass, e.g. in J/(kg K). Then the Neumann–Kopp rule would of course fail (unless the constituent masses are approximately equal) since the heat capacity per mass does not show the regularity of the Dulong–Petit rule.

6. The Lindemann melting criterion

Lindemann (1910) is often quoted to have suggested that the melting temperature T_{fus} is reached when the root mean square displacement

$[\langle \mathbf{u}^2 \rangle]^{1/2}$ exceeds a certain fraction of the nearest neighbour distance $2a$. Actually, Lindemann never proposed such a rule, but used the melting temperature and other experimental data to derive a vibrational frequency, somewhat analogous to how Einstein fitted a vibrational frequency to heat capacity data. It seems to be Gilvarry (1956) who first gave a criterion for melting in the form usually ascribed to Lindemann. Since $T_{\text{fus}} > \theta_{\text{D}}$, we take the leading term in eq. (7.44) and write the (squared) ratio in Lindemann's rule on the form

$$\xi^2 = \frac{\langle \mathbf{u}^2 \rangle}{4a^2} = \frac{9\hbar^2 T_{\text{fus}}}{4a^2 M k_{\text{B}} \theta_{\text{D}}^2}, \tag{19.11}$$

where $2a$ is some characteristic distance between neighbouring atoms, here defined by $(4\pi/3)a^3 = \Omega_{\text{a}}$. In table 19.3 are given $\xi = [\langle \mathbf{u}^2 \rangle]^{1/2}/2a$ calculated from eq. (19.11), and with $\theta_{\text{D}} = \theta_{\text{D}}(0)$ at $T = T_{\text{fus}}$ from Rosén and Grimvall (1983). (It would be more correct to use $\theta_{\text{D}}(-2)$, which is not easily available at T_{fus}, but typically may be 10% larger than $\theta_{\text{D}}(0)$ in these metals. Furthermore, some authors use θ_{D} from room temperature data and get a smaller ξ because that neglects anharmonic softening of the vibrations.) There have been numerous discussions of Lindemann's rule, trying to give it some theoretical justification (e.g. Enderby and March 1966, Jacobs 1983) or merely examining its validity empirically (e.g. Shapiro 1970, Hansen 1970, Hoover et al. 1971, Young and Adler 1974, Stillinger and Weber 1980, Cho 1982). Equation (19.11) is derived for a monatomic solid with cubic symmetry. In §10, a dimensional argument is given as to why Lindemann's rule may be approximately obeyed for such a simple case, but we do not expect it to hold in more complex materials. A critical assessment by Wolf and Jeanloz (1984) shows that it fails, e.g. for alkali halides. It is obvious that the widespread method of estimating Debye temperatures from melting temperatures is not very reliable. In this context we remark that ordinary melting is not caused by an instability of the lattice at $T = T_{\text{fus}}$ (see Chapter 12).

7. Defect energies related to the melting temperature

The monovacancy formation energy E_{vac} is astonishingly well correlated to the melting temperature (fig. 19.3). A similar correlation is

Table 19.3

The ratio $\xi = [\langle \mathbf{u}^2 \rangle]^{1/2}/(2a)$ at the melting temperature T_{fus}, illustrating Lindemann's rule

Na (bcc)	Cu (fcc)	Pb (fcc)	Al (fcc)	Mg (hcp)	Tl (hcp)
0.13	0.11	0.10	0.10	0.11	0.12
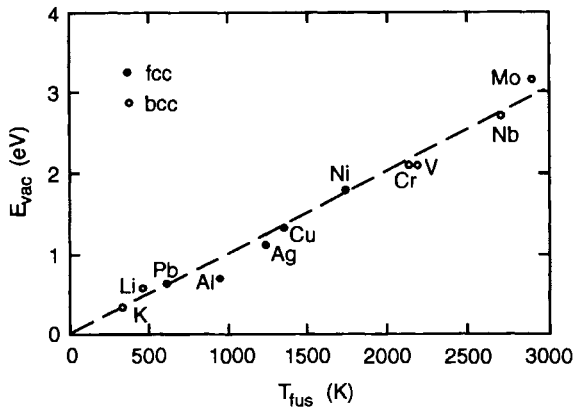
Fig. 19.3. The monovacancy formation energy E_{vac} plotted versus the melting temperature T_{fus}. Data from Ehrhardt (1991) in the Landolt–Börnstein tables. The dashed line is a guide to the eye.

noted for many other defect energies, e.g. dislocations, grain boundaries and surfaces (Grimvall and Sjödin 1974). In §10 we show that such relations follow from dimensional arguments if the interaction between atoms is of a particularly simple form, as may be the case for elements, but they cannot be expected to hold in more general cases.

Diffusion is an important thermophysical phenomenon that we have not dealt with in this book. One reason is that the microscopic aspects of diffusion are still not very well understood. The diffusion process is too complex to be described by accurate expressions without recourse to fitted parameters. On the other hand, there are well-known empirical results. For instance, the activation energy for self diffusion is remarkably well correlated to the melting temperature T_{fus} (e.g. Grimvall and Sjödin 1974).

It has long been known (Carnelley 1879) that the cubic expansion coefficient β tends to be large for materials with a low melting temperature. We can write $T_{\text{fus}}\beta(T_{\text{fus}}) = k$ with $k = 0.059 \pm 0.015$ for the elements with bcc, fcc or hcp lattices. The lowest and the highest values of k among the elements are 0.009 (grey Sn) and 0.15 (Pu) (Gschneidner 1964).

8.   Effective force constants

In classical mechanics, the frequency ω of a harmonic oscillator with force constant k and mass M is

$$\omega = \sqrt{k/M}. \tag{19.12}$$

The same frequency enters the corresponding quantum mechanical energy eigenvalues $\hbar\omega[n + 1/2]$. Thus, knowing ω and M we get the force constant $k = M\omega^2$. We will now see how an effective force constant k_S in a lattice can be obtained from the measured vibrational entropy, and how it can be used to define an energy E_S similar to the cohesive energy. (Labels S here refer to entropy-based quantities.)

The frequencies $\omega(\mathbf{q}, s)$ of a vibrating lattice depend on atomic masses, and on interatomic forces which can be complicated and of long range. But in the logarithmically averaged frequency $\omega(0)$, the masses enter only as a scaling factor $(M_{\text{eff}})^{-1/2}$, where M_{eff} is the logarithmically averaged mass (see Chapter 6, §5.3). There we have also introduced a Debye temperature as $k_B\theta_D(0) = \exp(1/3)\hbar\omega(0)$, and an "entropy Debye temperature" $\theta_D^S(T)$ which has the high-temperature limit $\theta_D(0)$. Thus, knowing the entropy S, we can calculate a high temperature entropy Debye temperature θ_D^S and then obtain a quantity k_S with the dimension of a force constant, through the definition

$$k_S = M_{\text{eff}}(k_B/\hbar)^2[\theta_D^S]^2. \tag{19.13}$$

$\theta_D^S(T)$ is temperature dependent—at low T because the true phonon spectrum is not of the Debye shape, and at high T because of anharmonic effects. In the intermediate temperature region the variation usually is slow. We may now specify θ_D^S by taking its value at, say, $T = \theta_D^S(T)$, and use it in eq. (19.13).

Table 19.4

Effective force constant k_S, derived from the vibrational entropy

	k_S [N/m]		k_S [N/m]		k_S [N/m]		k_S [N/m]
Ti	169	TiC	442	TiB$_2$	477	CaCl$_2$	86
Zr	154	ZrC	398	ZrB$_2$	436	SrCl$_2$	85
Hf	209	HfC	386	HfB$_2$	426	BaCl$_2$	77

In discussions of bonding strengths in solids one usually considers the cohesive energy U_{coh}, or, in more crude comparisons, the melting temperature T_{fus}. The latter quantity can be expressed as an energy through $k_B T_{fus}$. The force constant k_S is also a measure of the bonding strength. To enable comparisons of k_S with U_{coh} and $k_B T_{fus}$, we define a quantity E_S, with the dimension of energy, as

$$E_S = k_S \Omega_a^{2/3}. \tag{19.14}$$

Ω_a is the average volume per atom, i.e. the total crystal volume divided by the total number of atoms. In this way E_S is defined for any solid, be it an element, a compound, or a disordered alloy.

We expect k_S and E_S to show a regular behaviour with the position in the Periodic Table of the atoms in the solid. For instance, elements in the same column, or chemically related compounds, have similar bonding strengths. This is illustrated in table 19.4, based on data in Appendix I. Figure 19.4 shows the corresponding E_S of some metal carbides and nitrides plotted versus the cohesive energy U_{coh}. Regularities such as those displayed here of course require that the nature of the chemical bonding is not drastically changed, as happens in the elements C, Si, Sn, Pb which are in the same column in the Periodic Table and where the bonding changes from covalent to metallic. The ideas in this section have been used to study trends or to estimate vibrational entropies in many systems, for instance metal carbides (Fernández Guillermet and Grimvall 1992), borides (Fernández Guillermet and Grimvall 1991b) and binary ionic compounds (Shian Peng and Grimvall 1994b). Further aspects of the correlations are given in §10.
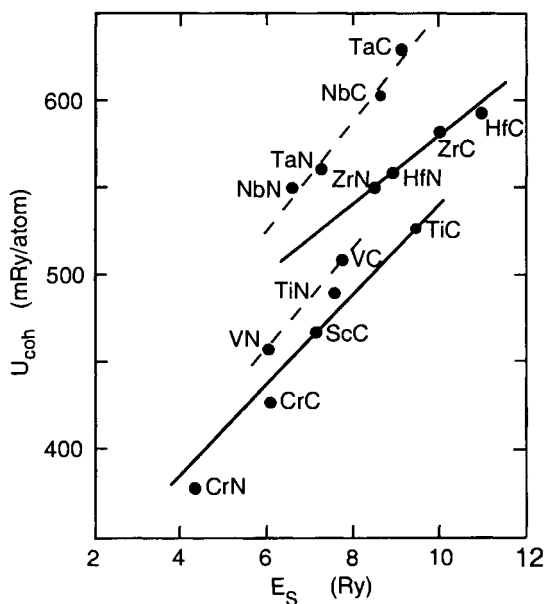
Fig. 19.4. The quantity E_S of transition metals carbides and nitrides shows a regular behaviour as a function of the position of the metal in the Periodic Table and covaries with the cohesive energy U_{coh}. After Grimvall (1999).

9. Hardness

With (mechanical) hardness we mean the resistance of a material to *plastic* deformation. It can be quantified, for instance, by the Brinell or Vickers hardness numbers. They are expressed in pressure unit (e.g. GPa) but must not be confused with the elastic constants, e.g. the bulk modulus K, which is also expressed in this unit. The latter refers to *elastic* deformation, in which the atoms return to their original positions in the lattice on unloading. Mechanical hardness and the bulk modulus may show quite a different behaviour. The mechanical hardness usually decreases very rapidly with temperature at high temperatures (cf., for instance, forging processes) while the bulk modulus typically decreases by only 10–20%, on approaching the melting point. Furthermore, lattice defects and structure are of utmost importance in the mechanical hardness, primarily through the motion and pinning of dislocations. The bulk modulus, on the other hand, depends very weakly on lattice defects. For this reason, a direct comparison between the sample- and
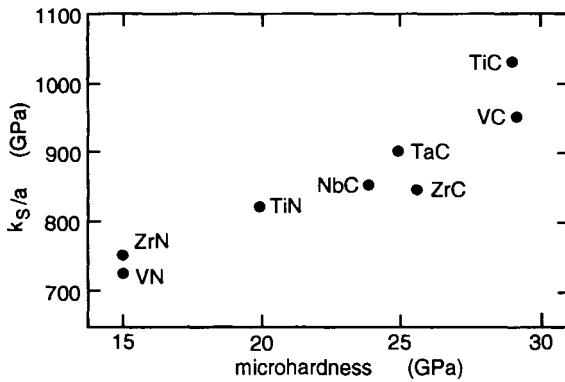
Fig. 19.5. Correlation between the microhardness and the quantity k_S/a, where k_S is the effective interatomic force constant derived from the vibrational entropy. After Grimvall and Thiessen (1986).

temperature-dependent mechanical hardness and the bulk modulus may not be very meaningful. However, hardness ultimately depends on the strength of the interatomic forces, like the bulk modulus or the effective interatomic force constant k_S that was introduced in §8. Therefore, there *is* a correlation between hardness measures and K or k_S/a, if one considers materials which form a well-defined chemical group, similar with respect to structure, and are compared at similar temperatures relative, e.g. to the melting temperature. (We have divided k_S by a lattice parameter a to account correctly for the number of bonds and get a quantity with the dimension of pressure.) Figure 19.5 shows such a correlation between the hardness and the quantity k_S/a for some refractory carbides and nitrides in the NaCl lattice structure.

10. Correlations explained by dimensional analysis

There have been many attempts to account for properties of materials through some simple form of interaction between the atoms. One such interaction is the Lennard–Jones (LJ) potential, also referred to as the 6–12 potential (Lennard–Jones 1924);

$$V_{\text{LJ}}(r) = V_0[(r_0/r)^{12} - 2(r_0/r)^6]. \tag{19.15}$$

It has a minimum at $r = r_0$, where $V_{\text{LJ}}(r_0) = -V_0$. (Note that in a lattice, the distance between nearest neighbouring atoms would not be

r_0 since the minimisation of the total energy also involves more distant atoms.) The LJ potential is an example of a simple interaction which, in more general terms, could be written

$$V(\mathbf{r}) = V_0 \phi(\mathbf{r}/r_0). \tag{19.16}$$

$\phi(\mathbf{r}/r_0)$ is a dimensionless "shape function" and V_0 gives the "strength" of the interaction. The potential acts between pairs of atoms but it is not necessarily a central potential, i.e. it may also describe bending forces, and we let $\mathbf{r}$ be a vector.

When the shape ϕ is fixed, the interaction has only two free parameters which depend on the material, V_0 and r_0, with the dimension of energy and length, respectively. We now seek the energy E_{conf} of certain atomic configurations, e.g. the cohesive energy U_{coh} in different crystal structures, or defect energies such as the vacancy formation energy E_{vac}, the diffusion activation energy E_{diff}, the dislocation line energy E_{disl} and the grain boundary energy E_{grain}. Each of these configurations can be described by a set of parameters r_i which give atomic coordinates, interatomic distances etc. Thus, the problem involves two parameters with the dimension of energy, V_0 and E_{conf}, and parameters r_0, r_i with the dimension of length. In Buckingham's theorem (Appendix A), they are combined in dimensionless ratios; $\Pi_1 = E_{\text{conf}}/V_0$ and $\Pi_i = r_i/r_0$. The theorem states that there is a relation

$$\Omega(\Pi_1, \ldots \Pi_i, \ldots) = 0. \tag{19.17}$$

The form of the function Φ depends on the shape function ϕ and on the defect considered. The quantities Π_i (with $i \neq 1$) take certain values for each type of atomic configuration. For a given ϕ and type of defect, eq. (19.17) then implies that also Π_1 is a constant for each such case with fixed Π_i. By purely dimensional arguments, all energies E_{conf} are therefore proportional to V_0.

We next seek the melting temperature T_{fus} of a material described by eq. (19.16). The temperature is so high that we can use a classical thermodynamic description. Temperatures appear in the combination $k_B T$, with the dimension of energy. The melting temperature, and therefore $k_B T_{\text{fus}}$, is entirely determined by the interaction (19.16) and the considered solid structure that melts. Again, the problem only contains two quantities with the dimension of energy, $k_B T$ and V_0, and a set of length

parameters describing atomic configurations. It follows that $k_B T_{fus}$ is proportional to V_0, and therefore also

$$E_{conf} = C_{conf} T_{fus},\qquad(19.18)$$

where "conf" may refer to, e.g. the cohesive energy and various defect energies.

Given the interaction (19.16) and a certain lattice structure, the classical vibrational displacement $[\langle \mathbf{u}^2 \rangle]^{1/2}$ depends on the temperature T (or, better, $k_B T$), and on V_0 and r_0. We form $\Pi_1 = k_B T / V_0$ and $\Pi_2 = [\langle \mathbf{u}^2 \rangle]^{1/2} / r_0$. According to the discussion above, there is a (new) function Φ such that $\Phi(\Pi_1, \Pi_2) = 0$, where Π_1 has a certain fixed value at $T = T_{fus}$, and hence also Π_2 has a fixed value. Combined with the fact that the lattice parameters scale as r_0, a constant Π_2 is equivalent with Lindemann's melting rule.

Finally we consider phonon frequencies. They are determined by force constants k obtained from the derivatives $\partial^2 \phi(\mathbf{r})/\partial \mathbf{r}^2$ of the interaction between the atoms, evaluated at lattice points which have coordinates that are all proportional to r_0. It follows that all force constants scale as V_0 / r_0^2, and hence all Debye temperatures scale as $\theta_D^2 \sim k/M \sim V_0/(M r_0^2) \sim T_{fus}/(M r_0^2)$.

We can summarise the results of this section as follows. When a group of materials are described by an interaction which is as simple as e.g. eq. (19.16), Lindemann's melting rule, the proportionality between the melting temperature and vacancy energies etc., all follow from dimensional arguments. Such a simple interaction may be reasonable for elements. But in complex materials, the description of the interaction between atoms requires more parameters with the dimensions of energy and length, and then the dimensional argument fails. One should therefore be cautious in extending empirical relations for elements to other solids.

11. Relation between $C_p(T)$, $\beta(T)$ and $\rho(T)$

In the ideal case of harmonic lattice vibrations, the heat capacity (per atom) tends to a universal value at high temperatures, $C_p = C_V \to 3k_B$. Similarly, the thermal expansion coefficient β in the Grüneisen theory, eq. (13.36), tends to the constant $3k_B \gamma_G/(\Omega_a K_S)$, where Ω_a is
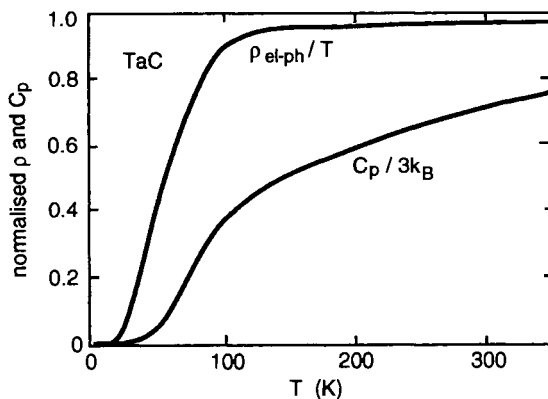
Fig. 19.6. $C_p/(3k_B)$ and the quantity ρ/T normalised to 1 at high temperatures, as a
function of temperature for TaC. After Grimvall (1999).

the volume per atom. The phonon limited electrical resistivity ρ, as
given in the general form (eq. (15.20)), tends to $8\pi^2 k_B T \lambda_{tr}/(\hbar\omega_{pl}^2)$.
Hence, in this description the quantities $C_p/(3k_B)$, $\beta\Omega_a K_S/(3k_B\gamma_G)$ and
$\rho\hbar\omega_{pl}^2/(8\pi^2 k_B T \lambda_{tr})$, vary from 0 at $T = 0$ K to 1 at high temperatures.
In fact, when the phonon density of states is described by an Einstein
model, all three quantities have the same temperature dependence. In
this context, it is interesting to quote what Grüneisen (1913) writes (in
German): "Empirically, I have found the following remarkable result.
(...) That the empirically found agreement between ρ/T (...) and C_p
has a direct theoretical interpretation seems to me doubtful, considering
the complicated processes in the electrical conduction". There now is
such a theoretical interpretation, outlined above. However, there are
examples when the correlation is far from perfect. This is illustrated
in fig. 19.6, that shows C_p and ρ/T for TaC.

12.   Probing electron properties near the Fermi level

According to the Sommerfeld theory, the electronic entropy and heat
capacity are proportional to the electron density of states $N(E_F)$ at the
Fermi level. Many other physical properties are, within simple theo-

ries, related to $N(E_F)$. For instance, the *Pauli spin paramagnetism* is described by the susceptibility

$$
\begin{aligned}
\chi_P &= \mu_B \frac{\partial}{\partial H} \int_{-\infty}^{+\infty} N(E)[f(E - \mu_B H) - f(E + \mu_B H)] \, dE \\
&= 2\mu_B^2 \int_{-\infty}^{+\infty} N(E)(-\partial f/\partial E) \, dE \approx 2\mu_B^2 N(E_F),
\end{aligned}
\tag{19.19}
$$

where $\mu_B = e\hbar/2mc$ is the Bohr magneton. The derivative with respect to H in eq. (19.19) is taken in the weak-field limit, $H \to 0$.

The susceptibility χ_L of the *Landau diamagnetism* is considerably more difficult to calculate, both for free-electron-like systems and transition metals. The free-electron expression is

$$
\chi_L = -\frac{V e^2 k_F}{12\pi^2 mc^2} = -(2/3)\mu_B^2 N_{fe}(E_F).
\tag{19.20}
$$

In Chapter 15 we obtained an expression, $\sigma = ne^2\tau/m$, for the *electrical conductivity*. Another form of σ, which takes the electron velocity v_k to be isotropic but allows the relaxation time $\tau(E)$ to be energy dependent is, from eq. (15.8),

$$
\sigma = (ne^2/m_b) \int \tau(E)(-\partial f/\partial E) \, dE.
\tag{19.21}
$$

Then we have assumed a spherical Fermi surface with a radius $k_F = (3\pi^2 n)^{1/3}$ but allowed electron band effects to be approximately included through an effective band mass m_b.

By the Wiedemann–Franz law, the electronic part of the *thermal conductivity* is

$$
\kappa_{el} = (\pi^2/3)(k_B/e)^2 T\sigma = L_0 T\sigma,
\tag{19.22}
$$

where L_0 is the Lorenz number. However, this relation requires that the relaxation time τ does not vary with the energy E_k of the electron states involved in the transport process. The analogue of eq. (19.21) is, from eq. (16.43),

$$
\kappa_{el} = (nk_B^2 T/m_b) \int \tau(E)[(E - \mu)/k_B T]^2 (-\partial f/\partial E) \, dE.
\tag{19.23}
$$

Table 19.5

Dependence of various properties on the electron density n, electron-band mass m_b and electron-phonon parameter λ_{el-ph}. A, B, C and D are material-dependent constants

Property	Free-electron model	Electron-band effects included through m_b	Electron-phonon mass enhancement included
C_{el}	$Amn^{1/3}$	$Am_b n^{1/3}$	$Am_b(1 + \lambda_{el-ph})n^{1/3}$ (low T)
			$Am_b n^{1/3}$ (high T)
χ_P	$Bmn^{1/3}$	$Bm_b n^{1/3}$	no correction
χ_L	$-(1/3)Bmn^{1/3}$	$-(1/3)Bm(m/m_b)n^{1/3}$	no correction
σ	Cn/m	Cn/m_b	no correction
κ_{el}	Dn/m	Dn/m_b	no correction

We will first let the temperature be so low, or the energy dependence of $N(E)$ so weak, that $(-\partial f/\partial \varepsilon)$ can be considered as a δ-function at the Fermi level. The question now is how band effects (m_b or $N(E_F)$) and electron-phonon many-body corrections enter the physical properties mentioned above. We consider these properties in models at three levels of sophistication: (i) a strict free-electron model; (ii) a nearly-free-electron model in which the Fermi surface is assumed to be spherical with a radius $k_F = (3\pi^2 n)^{1/3}$ and with band effects included through an isotropic effective band mass $m_b = \hbar^2 k_F/|\nabla_k E_F|$; and (iii) electron-phonon many-body corrections to the model (ii), when such effects should enter.

The first column in table 19.5 suggests a strong correlation between C_{el} and χ_P. Since C_{el} and χ_P are both proportional to $N(E_F)$, this correlation may not be limited to free-electron-like systems. However, electron-phonon many-body effects in C_{el}, and also contributions other than χ_P to the measured susceptibility χ, spoil the proportionality between C_{el} and χ in real metals.

It is a non-trivial matter to decide whether, or not, the band density of states $N(E_F)$, the band electron velocity v_k, the band mass m_b etc. should be enhanced by $electron$-$phonon$ $interactions$ (Grimvall 1981). In fact, only the low temperature heat capacity and the effective band masses measured in cyclotron resonance and de Haas–van Alphen experiments should be renormalised by a factor $1 + \lambda_{el-ph}$. In most other
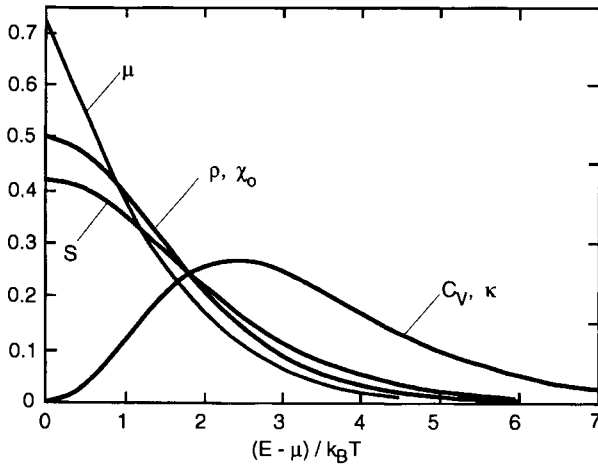
Fig. 19.7. Weight function for Fermi surface averages of some physical parameters. The area under each curve is normalised to unity.

cases, renormalisation effects are either absent or enter in such a way as to cancel. For instance, the renormalisations of τ and m_b cancel in the static electrical conductivity $\sigma = ne^2\tau/m_b$.

There is also an *electron-electron many body effect*. Its influence on C_{el} is small in the simple metals, and it is to a large extent folded into the band structure $N(E_F)$ of transition metals. However, it is essential for the magnetic susceptibility. Within the Stoner (1938) model one can write

$$\chi_P = 2\mu_B^2 N(E_F)/[1 - IN(E_F)], \tag{19.24}$$

where I is the intra-atomic Coulomb interaction between the electrons. When $IN(E_F) > 1$, χ_P is negative, which is interpreted to mean magnetic ordering.

We get from eq. (B.3) that $N(E)$, and hence the electronic heat capacity, contains an average of $\langle 1/v_k \rangle$ over the Fermi surface, while the expression (15.13) for the electrical conductivity contains a product of $\langle 1/v_k \rangle$ and $\langle v_k^2 \rangle$. When the electron states at the Fermi level are described by a single and isotropic band mass, $m_b = \hbar^2 k_F/|\nabla_k E_F|$, any combination of $\langle v_k^n \rangle$ can be expressed in a single m_b. Often this is an oversimplification, and one should introduce different effective band masses $m_b(n)$ for different powers n, in analogy to $\theta_D(n)$ and $\gamma(n)$.

Finally, we consider the case that $(-\partial f/\partial \varepsilon)$ cannot be approximated by a δ-function at the Fermi level. When the electron density-of-states, the electron relaxation time τ, etc. vary strongly with the energy $E - \mu$, the δ-function approximation may be inadequate and one has to state precisely what is the shape and width of the energy "window" around E_F, where the electron states are probed. It follows from eq. (10.10) that C_{el} has contributions from a region defined by the weight function $[(E - \mu)/k_B T]^2(-\partial f/\partial E) \sim [(E - \mu)/k_B T]^2 f(1 - f)$. The susceptibility χ_P of the Pauli paramagnetism, eq. (19.19), and the relaxation time τ in the electrical conductivity, eq. (19.21), have a weight function $f(1 - f)$. The entropy probes the electronic states weighted by $f[\ln f] + [1 - f][\ln(1 - f)]$, eq. (10.15). The chemical potential $\mu(T)$ has a temperature dependence determined by $f[(E - \mu)/k_B T]$ or $1 - f[(E - \mu)/k_B T]$, depending on the sign of $E - \mu$, eq. (10.5). The relaxation time of the electronic contribution to the thermal conductivity has the same weight function as C_{el}, cf. (19.23). Figure 19.7 summarises these cases. It is worth noting that C_{el} and κ_{el} probe the density of electron states in an energy interval of width $\sim 10k_B T$. This is much wider than the width $\sim k_B T$ often alluded to in textbooks.

BUCKINGHAM'S Π-THEOREM

The heat capacity (per atom) in the Einstein model has the form

$$
C_E = 3k_B \left(\frac{\hbar\omega_E}{k_B T} \right)^2 \frac{\exp(\hbar\omega_E/k_B T)}{[\exp(\hbar\omega_E/k_B T) - 1]^2}. \tag{A.1}
$$

It expresses the desired quantity, C_E, in the natural constant k_B and two independent model quantities, $\hbar\omega_E$ and $k_B T$. They may be combined in two quantities Π_1 and Π_2 that are "dimensionless" (more correctly, have dimension 1);

$$
\Pi_1 = \frac{C_E}{k_B}, \quad \Pi_2 = \frac{\hbar\omega_E}{k_B T}. \tag{A.2}
$$

The heat capacity relation in the Einstein model can then be written

$$
\Phi(\Pi_1, \Pi_2) = 0, \tag{A.3}
$$

where Φ is a properly defined function. This example will now illustrate the essential idea in Buckingham's Π-theorem ("pi theorem"). Its name derives from the symbol Π that Buckingham (1914) chose for the dimensionless ratios. The theorem can be formulated as follows. Let a physical quantity a_1 be described by a physical model that contains $r - 1$ linearly independent parameters $a_2, \ldots, a_r$. Assume that these a_i can be expressed using p independent physical units. Then the relation between a_1 and a_i ($i = 2, \ldots, r$) may be written in a general form

$$
\Phi(\Pi_1, \ldots, \Pi_{r-p}) = 0. \tag{A.4}
$$

with $r - p$ linearly independent ratios Π_j ($j = 1, \ldots, r - p$) that have dimension 1 and are formed by all a_i ($i = 1, \ldots, r$).

353

Returning to the Einstein model, as an illustration, we have $a_1 = C_E$, $a_2 = k_B$, $a_3 = \hbar$, $a_4 = \omega_E$, $a_5 = T$. These five quantities a_i can be expressed in the three SI units for mass (kg), length (m) and time (s). However, because we know that ω_E appears in the combination $\hbar\omega$, there are only four linearly independent combinations of a_i. They can be expressed in the two units J and J/K, respectively. Hence, $r = 4$, $p = 2$, and there are $r - p = 4 - 2 = 2$ independent ratios Π_j, in accordance with eq. (A.2).

As another illustration, consider the expression (15.42) for the electrical resistivity ρ_{film} of a thin film of thickness d, when the electron mean free path in the bulk material is ℓ_{bulk};

$$\rho_{film} = \rho_{bulk}[1 + (3/8)(1 - p_s)(\ell_{bulk}/d)]. \qquad (A.5)$$

The dimensionless parameter p_s measures the amount of specular character of the surface scattering. The set $a_i = \{\rho_{film}, \rho_{bulk}, \ell_{bulk}, d, p_s\}$, i.e. $r = 5$. Two independent units suffice in this case, for resistivity and length respectively, i.e., $p = 2$. Hence, we can form $r - p = 5 - 2 = 3$ independent ratios of dimension 1;

$$\Pi_1 = \rho_{film}/\rho_{bulk}, \quad \Pi_2 = \ell_{bulk}/d, \quad \Pi_3 = p_s. \qquad (A.6)$$

Obviously, eq. (A.5) is of the general form $\Phi(\Pi_1, \Pi_2, \Pi_3) = 0$. For a thick film, i.e., a large d, we get $\Pi_2 \ll 1$ and recover the limiting case $\rho_{film} = \rho_{bulk}$. More generally, ignoring certain small effects in a physical description means that there are corresponding ratios Π which we put equal to 0. As an example, ignoring quantum effects in the heat capacity (eq. (A.1)) of a harmonic oscillator means that we take $\hbar\omega/k_B T \ll 1$. In this limit, $\Pi_2 \to 0$ in eq. (A.3) and $\Pi_1 = C_E/k_B \to 3$, i.e. we get the classical Dulong–Petit value. (To be more precise, see below, we get $\Pi_1 \to$ constant.)

When, in physics, we talk about a low (or high) temperature, a low (or high) speed etc., we must always compare with some other parameter (or a combination of parameters) with the dimension of temperature, speed etc. This is equivalent to a corresponding Buckingham Π-ratio being $\ll 1$ (or $\gg 1$).

Finally, consider the case $r - p = 1$, so that the desired relation $\Phi = 0$ can be written

$$\Pi_1 = \text{constant}. \qquad (A.7)$$

When dimensional arguments are invoked, it is often the simple form (eq. (A.7)) that one refers to. We illustrate it by seeking a relation for the frequency ω [s^{-1}] of an oscillator with mass M [kg] and force constant k [N/m = kg s^{-2}]. Then $r = 3$ and $p = 2$, so $r - p = 1$ and only one ratio Π is needed. In line with eq. (A.7) we make the *Ansatz* that $\omega/(M^\alpha k^\beta)$ = constant, or

$$\omega = C M^\alpha k^\beta, \tag{A.8}$$

where C is a constant with dimension 1. Dimensional consistency now implies that $\alpha = -1/2$, $\beta = 1/2$, as expected. Of course, the constant C cannot be determined by dimensional arguments. For instance, we would get the same type of relation if we wanted the frequency $\nu = \omega/2\pi$ instead of the angular frequency ω.

SOME RELATIONS FOR ELECTRON STATES

Summation over **k**-*vectors.* Electron and phonon states in a periodic lattice are, in this book, labelled by a wave vector **k** (electrons) or **q** (phonons). The prescription for turning a sum over all **k** (or **q**) into an integral is

$$\sum_{\mathbf{k}}(\ldots) = \frac{V}{(2\pi)^3} \int (\ldots)\, \mathrm{d}^3\mathbf{k}. \tag{B.1}$$

V is the volume of the crystal and $(\ldots)$ is an arbitrary function of **k**. Let $E(\mathbf{k})$ (or $E_\mathbf{k}$) be the energy of an electron. It is often convenient to write the integral in eq. (B.1) with $E(\mathbf{k})$ as the integration variable. For an isotropic system

$$\sum_{\mathbf{k}}(\ldots) = \int (\ldots)N(E)\, \mathrm{d}E. \tag{B.2}$$

$N(E)$ is the *electron density-of-states* (also called density of levels);

$$N(E) = \frac{V}{(2\pi)^3} \int \mathrm{d}^3\mathbf{k}\,\delta(E_\mathbf{k} - E) = \frac{V}{(2\pi)^3} \int_{S_E} \frac{\mathrm{d}S}{|\nabla_\mathbf{k} E(\mathbf{k})|}. \tag{B.3}$$

The last integral is over that surface S_E in **k**-space for which $E(\mathbf{k}) = E$. Our $N(E)$ refers to one spin direction. Other authors let $N(E)$ refer to both "spin up" and "spin down". The difference will appear as a factor of 2 in our expressions when we sum over all electron states. In an anisotropic system, we can define a directional density of states function $N(E; \mathbf{k})$ as

$$N(E; \mathbf{k}) = \frac{V}{(2\pi)^3} \frac{4\pi k^3}{\mathbf{k} \cdot \nabla_\mathbf{k} E(\mathbf{k})}. \tag{B.4}$$

Then

$$\sum_{\mathbf{k}}(\ldots) = \int dE \int \frac{d\Omega_{\mathbf{k}}}{4\pi}(\ldots)N(E;\mathbf{k}), \tag{B.5}$$

where $d\Omega_{\mathbf{k}}$ is a solid angle.

Free-electron model. For free electrons, $|\nabla_{\mathbf{k}}E(\mathbf{k})| = \hbar^2 k/m$ and $dS = k^2 d\Omega_{\mathbf{k}}$. Equation (B.4) yields

$$N(E) = N_{\mathrm{fe}}(E) = \frac{V}{2\pi^2}\frac{mk}{\hbar^2}, \tag{B.6}$$

or

$$N_{\mathrm{fe}}(E) = \frac{V}{4\pi^2}\left(\frac{2m}{\hbar^2}\right)^{3/2}\sqrt{E}. \tag{B.7}$$

Often, the density of states is given per atom (and spin),

$$N_{\mathrm{a}}(E) = N(E)/N, \tag{B.8}$$

where N is the number of atoms. At the Fermi level, and in the free-electron model,

$$N_{\mathrm{a,fe}}(E_{\mathrm{F}}) = \frac{Z}{2\pi^2}\frac{mk_{\mathrm{F}}}{n\hbar^2} = \frac{3Z}{4}\frac{1}{E_{\mathrm{F}}}, \tag{B.9}$$

where Z is the number of conduction electrons per atom and $n = ZN/V$. In the expression for the Fermi energy, $E_{\mathrm{F}} = (\hbar k_{\mathrm{F}})^2/(2m)$ the Fermi wave number k_{F} is obtained, e.g. from eq. (B.1) as

$$\frac{2V}{(2\pi)^3}\frac{4\pi}{3}k_{\mathrm{F}}^3 = NZ. \tag{B.10}$$

The number of electrons per volume, $n = NZ/V = Z/\Omega_{\mathrm{a}}$, is often expressed through the dimensionless parameter r_{s} that gives the radius, in units of the Bohr radius a_0, of a sphere containing one electron. Thus,

$$\frac{4\pi}{3}(r_{\mathrm{s}}a_0)^3 = \frac{\Omega_{\mathrm{a}}}{Z}, \tag{B.11}$$

$$k_F = \left(\frac{9\pi}{4}\right)^{1/3} \frac{1}{r_s a_0}. \tag{B.12}$$

The average kinetic energy per electron is $(3/5)E_F$, which may be written

$$
\begin{aligned}
\langle E_{kin} \rangle &= \frac{3}{5} E_F = \frac{3}{10} \left(\frac{9\pi}{4}\right)^{2/3} \frac{\hbar^2}{m(r_s a_0)^2} \\
&= \frac{3}{5} \left(\frac{9\pi}{4}\right)^{2/3} \left(\frac{e^2}{2a_0}\right) \frac{1}{r_s^2} = \frac{2.210}{r_s^2} \text{ [Ry]}, \tag{B.13}
\end{aligned}
$$

where we have used that $a_0 = \hbar^2/(me^2)$ and the energy unit 1 Ry = $e^2/(2a_0)$ (see Appendix H).

Electron band mass. For any functional form of $E(\mathbf{k})$ we can define an *effective electron band mass* $m_b(\mathbf{k})$ by

$$\hat{\mathbf{k}} \cdot \nabla_{\mathbf{k}} E(\mathbf{k}) = \frac{\hbar^2 |\mathbf{k}|}{m_b(\mathbf{k})}, \tag{B.14}$$

where $\hat{\mathbf{k}} = \mathbf{k}/|\mathbf{k}|$ is a unit vector along $\mathbf{k}$. If $N(E; \mathbf{k})$ is the density of states of a real metal and $N_{fe}(E)$ is the free-electron density of states we have

$$N(E; \mathbf{k}) = \frac{m_b(\mathbf{k})}{m} N_{fe}(E). \tag{B.15}$$

The average band mass m_b obeys the relations

$$N(E) = \frac{V}{(2\pi)^3} \int_{S_E} \frac{m_b(\mathbf{k})|\mathbf{k}|}{\hbar^2} \, d\Omega_{\mathbf{k}} = \frac{m_b}{m} N_{fe}(E). \tag{B.16}$$

Electronic Grüneisen parameter. In order to illustrate that $\gamma_{el} = d \ln N(E)/d \ln V$ is equivalent with $\gamma_{el} = -d \ln(\varepsilon_{\mathbf{k}} - \mu)/d \ln V$ we assume that the latter quantity is independent of $\mathbf{k}$ for electron states $\varepsilon_{\mathbf{k}}$ near the chemical potential (Fermi level) μ. Under a small volume change ΔV, the energy distance $\varepsilon_{\mathbf{k}} - \mu$ to the Fermi level changes to $\varepsilon_{\mathbf{k}} - \mu + [d(\varepsilon_{\mathbf{k}} - \mu)/dV]\Delta V$, but the *number* of states between the new $\varepsilon_{\mathbf{k}}$ and μ remains the same. Hence, the density of states is changed

by a factor $(\varepsilon_{\mathbf{k}} - \mu)/\{\varepsilon_{\mathbf{k}} - \mu + [d(\varepsilon_{\mathbf{k}} - \mu)/dV]\Delta V\}$. The ratio of the densities of states after and before the volume change can also be written $\{N(E) + [dN(E)/dV]\Delta V\}/N(E)$. Equating the two expressions yields $d \ln N(E)/d \ln V = -d \ln(\varepsilon_{\mathbf{k}} - \mu)/d \ln V$.

Electron-phonon interaction. The quantity $\lambda = \lambda_{\text{el-ph}}$ enters as an enhancement factor $(1 + \lambda_{\text{el-ph}})$ in the low temperature electronic heat capacity. It is also a central parameter in the BCS theory of superconductivity, and it is closely related to the "transport" coupling parameter λ_{tr} that appears in the high temperature electrical resistivity. One can express $\lambda_{\text{el-ph}}$ in the Éliashberg electron-phonon coupling function $\alpha^2 F(\omega)$ (Éliashberg 1962, Grimvall 1981),

$$\lambda_{\text{el-ph}} = 2 \int_0^{\omega_{\max}} \frac{\alpha^2 F(\omega)}{\omega} d\omega. \tag{B.17}$$

McMillan (1968) derived a semiempirical relation which allows $\lambda_{\text{el-ph}}$ to be calculated from the critical temperature T_c of a (strong coupling) BCS-type superconductor (i.e. excluding the oxide high temperature superconductors). Then

$$k_{\text{B}} T_C = \frac{\hbar \omega_{\text{D}}}{1.45} \exp\left[-\frac{1.04(1 + \lambda_{\text{el-ph}})}{\lambda_{\text{el-ph}} - \mu^*(1 + 0.62\lambda_{\text{el-ph}})} \right]. \tag{B.18}$$

Here, ω_{D} is a Debye frequency which may be approximately identified with $(1.45/1.2)\omega(0)$, where $\omega(0)$ is the logarithmic average of the phonon frequencies (eq. (6.22)). The quantity μ^* is an electron-electron interaction parameter; $\mu^* \approx 0.13$.

THE DYNAMICAL MATRIX

Definition. We expand the potential energy Φ of a lattice in the small displacements $u_\alpha(\kappa, l)$ around the equilibrium positions. They refer to the κth atom in the lth cell being displaced an amount u in the α-direction ($\alpha = x, y, z$);

$$\Phi = \Phi_0 + (1/2) \sum_{kl\alpha} \sum_{k'l'\beta} \Phi_{\alpha\beta}(\kappa l; \kappa'l')u_\alpha(\kappa l)u_\beta(\kappa'l') + \cdots. \quad \text{(C.1)}$$

The quantities $\Phi_{\alpha\beta}(\kappa l; \kappa'l')$ are called atomic *force constants.* The physical meaning of $\Phi_{\alpha\beta}(\kappa l; \kappa'l')$ is the force in the α-direction on the atom (κl) that arises when the atom $(\kappa'l')$ is displaced a unit distance in the β-direction while all other atoms are held fixed at their equilibrium positions. From $\Phi_{\alpha\beta}(\kappa l; \kappa'l')$ we define the elements $D_{\alpha\beta}(\kappa\kappa'; \mathbf{q})$ of the *dynamical matrix.* The periodicity and symmetry of a lattice imposes several conditions on $\Phi_{\alpha\beta}$. For instance, $\Phi_{\alpha\beta}$ only depends on $l - l'$. Then

$$\begin{aligned} D_{\alpha\beta}(\kappa\kappa'; \mathbf{q}) &= (M_\kappa M_{\kappa'})^{-1/2} \exp\{i\mathbf{q} \cdot [\mathbf{R}(\kappa) - \mathbf{R}(\kappa')]\} \\ &\times \sum_l \Phi_{\alpha\beta}(\kappa l'; \kappa' 0) \exp[i\mathbf{q} \cdot \mathbf{R}(l)] \end{aligned} \quad \text{(C.2)}$$

$\mathbf{R}(\kappa l)$, $\mathbf{R}(\kappa)$ and $\mathbf{R}(l)$ are position vectors in the lattice, with $\mathbf{R}(\kappa l) = \mathbf{R}(l) + \mathbf{R}(\kappa)$. If there are r atoms per primitive cell, κ and κ' run from 1 to r. Furthermore, $\alpha, \beta = x, y, z$. Thus, we have a $3r \times 3r$ matrix $\mathbf{D}$ with elements $D_{\alpha\alpha'}(\kappa\kappa'; \mathbf{q})$ which are functions of the wave vector $\mathbf{q}$ lying in the first Brillouin zone of the reciprocal lattice. Let $\mathbf{M}$ be a diagonal $3r \times 3r$ matrix with diagonal elements $M_1, M_1, M_1, \ldots, M_r$, M_r, M_r, where M_i is the mass of the atom with $\kappa = i$. Then we can write for the dynamical matrix $\mathbf{D}$;

$$\mathbf{D} = \mathbf{M}^{-1/2}\mathbf{D}_0\mathbf{M}^{-1/2}. \quad \text{(C.3)}$$

$\mathbf{D}_0$ is the force constant part of the dynamical matrix. It does not contain any atomic masses. $\mathbf{D}$ and $\mathbf{D}_0$ are Hermitian matrices; $D_{\alpha\beta}(\kappa\kappa'; \mathbf{q}) = D_{\alpha\beta}(\kappa'\kappa; \mathbf{q})$.

The phonon eigenfrequencies squared, ω^2, are solutions of

$$|D_{\alpha\beta}(\kappa\kappa'; \mathbf{q}) - \omega^2 I_{\alpha\beta}(\kappa\kappa')| = 0, \tag{C.4}$$

where $|\quad|$ denotes a determinant and $I_{\alpha\beta}(\kappa\kappa')$ is the $3r \times 3r$ unit matrix. For each $\mathbf{q}$ there are $3r$ solutions which we label $\omega(\mathbf{q}, s)$.

The expansion of the potential energy in terms of the force constant matrix elements $\Phi_{\alpha\beta}$ does not require a periodic lattice, but is also applicable in a solid with lattice defects. As long as we work within the harmonic approximation there are still $3N$ eigenfrequencies, where N is the number of atoms. (More precisely $3N - 6$ eigenfrequencies since rotation and translation of the entire solid should be excluded.) The frequencies are solutions to

$$|\mathbf{M}^{-1/2}\Phi\mathbf{M}^{-1/2} - \omega^2\mathbf{I}| = 0. \tag{C.5}$$

$\mathbf{M}$, Φ and $\mathbf{I}$ are $3N \times 3N$ matrices. $\mathbf{M}$ is diagonal, with elements M_1, M_1, M_1, ..., M_N, M_N, M_N, $\mathbf{I}$ is a unit matrix and Φ has the elements $\Phi_{\alpha\beta}(\kappa l; \kappa'l')$.

Grüneisen parameter expressed in the dynamical matrix. Since the average $\langle\omega^2\rangle$ is directly related to the trace of the dynamical matrix, it is possible to obtain $\gamma(2; V)$ without the explicit evaluation of all the phonon frequencies. One has

$$\gamma(2; V) = -\frac{1}{2}\frac{d\ln\left[\dfrac{1}{3N}\displaystyle\sum_{\mathbf{q}}\mathrm{Tr}D(\mathbf{q})\right]}{d\ln V}. \tag{C.6}$$

SOME RELATIONS FOR HARMONIC LATTICE VIBRATIONS

Sound velocities in cubic lattice symmetry. The sound velocities C_s ($s = 1, 2, 3$), given by the general form (eq. (5.6)), can be expressed in the case of cubic symmetry (Every 1980) as

$$3\rho C_s^2 = (c_{11} + 2c_{44}) + 2(c_{11} - c_{44})\sqrt{G_0}$$
$$\times \cos[\Psi + (2\pi/3)(s - 1)], \tag{D.1}$$

$$\Psi = (1/3)\arccos(H_0/G_0^{3/2}), \tag{D.2}$$

$$P = n_1^2 n_2^2 + n_1^2 n_3^2 + n_2^2 n_3^2; \quad Q = n_1^2 n_2^2 n_3^2, \tag{D.3}$$

$$G_0 = 1 - 3A_E(2 - A_E)P, \tag{D.4}$$

$$H_0 = 1 - (9/2)A_E(2 - A_E)P + (27/2)A_E^2(3 - 2A_E)Q. \tag{D.5}$$

Here, n_1, n_2, n_3 are direction cosines for the wave vector $\mathbf{q}$. We now see explicitly that the anisotropy of the sound velocities C_s depends on the elastic coefficients only through Every's anisotropy parameter $A_E = (c_{11} - c_{12} - 2c_{44})/(c_{11} - c_{44})$. For an isotropic system we have $A_E = 0$, i.e. $G_0 = H_0 = 1$ and $\psi = 0$, which gives $\rho C_s^2 = c_{11}$ (for $s = 1$) and $\rho C_S^2 = c_{44}$ (for $s = 2, 3$).

High temperature expansion of $n + 1/2$. In theories dealing with harmonic lattice vibrations one frequently encounters the expression $n + 1/2$, where n is the Bose–Einstein function. Then, in the limit of high temperatures,

$$n + \frac{1}{2} = \frac{1}{\exp(\hbar\omega/k_B T) - 1} + \frac{1}{2}$$
$$\approx \frac{k_B T}{\hbar\omega} + \frac{1}{12}\left(\frac{\hbar\omega}{k_B T}\right)^2 - \cdots. \tag{D.6}$$

Thus, we see that the constant $1/2$ in $n + 1/2$ cancels against a term $-1/2$ in the expansion of n.

Helmholtz energy. From the expressions (7.15) for the energy E and (7.23) for the entropy S, we find that the Helmholtz energy $F_{\text{har}} = E_{\text{har}} - T S_{\text{har}}$ of harmonic vibrations has the high temperature expansion

$$
\begin{aligned}
F_{\text{har}}(T) &= 3Nk_{\text{B}}T\{-\ln[k_{\text{B}}T/\hbar\omega(0)] + (1/24)[\hbar\omega(2)/k_{\text{B}}T]^2 \\
&\quad -(1/2880)[\hbar\omega(4)/k_{\text{B}}T]^4 + \cdots\}.
\end{aligned} \tag{D.7}
$$

The corresponding form of F_{har} expressed in Debye temperatures $\theta_{\text{D}}(n)$ is

$$
\begin{aligned}
F_{\text{har}}(T) &= 3Nk_{\text{B}}T\{-1/3 - \ln[T/\theta_{\text{D}}(0)] + (1/40)[\theta_{\text{D}}(2)/T]^2 \\
&\quad -(1/6720)[\theta_{\text{D}}(4)/T]^4 + \cdots\}.
\end{aligned} \tag{D.8}
$$

Atomic displacements. A general expression for the displacement $\mathbf{u}$ of an atom (κ, l) is

$$
\begin{aligned}
u_\alpha(\kappa, l, t) &= \frac{1}{(N_c M_\kappa)^{1/2}} \sum_{\mathbf{q},s} \frac{[E(\mathbf{q}, s)]^{1/2}}{\omega(\mathbf{q}, s)} \varepsilon_\alpha(\mathbf{q}, s; \kappa) \\
&\quad \times \exp\{i[\mathbf{q} \cdot \mathbf{R}^0(\kappa, l) - \omega(\mathbf{q}, s)t]\}.
\end{aligned} \tag{D.9}
$$

The correlation between the displacements $\mathbf{u}$ of an atom (κ, l) and an atom (κ', l') is

$$
\begin{aligned}
\langle u_\alpha(\kappa, l) u_\beta(\kappa', l') \rangle &= \frac{1}{N_c (M_\kappa M_{\kappa'})^{1/2}} \\
&\quad \times \sum_{\mathbf{q},s} \frac{E(\mathbf{q}, s)}{\omega^2(\mathbf{q}, s)} \varepsilon_\alpha(\mathbf{q}, s; \kappa) \varepsilon_\beta^*(\mathbf{q}, s; \kappa') \\
&\quad \times \exp[i\mathbf{q} \cdot (\mathbf{R}^0(\kappa, l) - \mathbf{R}^0(\kappa', l'))].
\end{aligned} \tag{D.10}
$$

The velocity component v_α of an atom (κ, l) is

$$
\begin{aligned}
v_\alpha(\kappa, l, t) &= -\frac{i}{(N_c M_\kappa)^{1/2}} \sum_{\mathbf{q},s} [E(\mathbf{q}, s)]^{1/2} \varepsilon_\alpha(\mathbf{q}, s; \kappa) \\
&\quad \times \exp\{i[\mathbf{q} \cdot \mathbf{R}^0(\kappa, l) - \omega(\mathbf{q}, s)t]\}.
\end{aligned} \tag{D.11}
$$

In the calculation of $\sigma_{\mathbf{R}}^2$ in eq. (7.50) we need to evaluate $\langle \mathbf{u}(\kappa, l) \cdot \mathbf{u}(\kappa', l') \rangle$. In a monatomic cubic lattice and in a Debye model for the lattice vibrations, we get at high temperatures (Brüesch 1986)

$$\langle \mathbf{u}(l) \cdot \mathbf{u}(0) \rangle = \frac{1}{q_{\mathrm{D}} r} \int_0^{q_d r} \frac{\sin t}{t}\, \mathrm{d}t, \tag{D.12}$$

where q_{D} is the Debye wave number and $r = |\mathbf{R}_\ell - \mathbf{R}_0|$. Thus $\langle \mathbf{u} \cdot \mathbf{u}(0) \rangle$ rapidly tends to zero with increasing distance $\mathbf{r}$ between the atoms at $\mathbf{R}(\ell)$ and $\mathbf{R}(0)$.

SOME RELATIONS FOR ANHARMONIC LATTICE VIBRATIONS

Anharmonic Helmholtz energy. The low-order contributions ΔF_3 and ΔF_4 to the Helmholtz energy in quantum-mechanical perturbation theory can be written in the general form

$$\Delta F_3 = -(6/\hbar) \sum_{\mathbf{q}s, \mathbf{q}_1 s_1, \mathbf{q}_2 s_2} |V(\mathbf{q}s, \mathbf{q}_1 s_1, \mathbf{q}_2 s_2)|^2 R_{\mathrm{F}}, \tag{E.1}$$

$$\Delta F_4 = 3 \sum_{\mathbf{q}s, \mathbf{q}_1 s_1} V(\mathbf{q}s, -\mathbf{q}s, \mathbf{q}_1 s_1, -\mathbf{q}_1 s_1)$$
$$\times [2n(0) + 1][2n(1) + 1]. \tag{E.2}$$

where

$$R_{\mathrm{F}} = \frac{[n(0) + 1][n(1) + n(2) + 1] + n(1)n(2)}{\omega(0) + \omega(1) + \omega(2)}$$
$$+ 3\frac{n(0)n(1) + n(0)n(2) - n(1)n(2) + n(0)}{\omega(1) + \omega(2) - \omega(0)}. \tag{E.3}$$

The quantities V are Fourier-transformations of the interaction and n are Bose–Einstein statistical functions. In the high temperature limit, where $n + 1/2 \approx k_{\mathrm{B}}T/\hbar\omega$, cf. eq. (D.6), one obtains eqs. (8.35) and (8.36).

Anharmonic shifts in phonon frequencies and elastic constants. We have written the phonon frequencies, shifted by anharmonic effects to low order in perturbation theory, as

$$\omega(\mathbf{q}, s) = \omega_0(\mathbf{q}, s) + \Delta_2(\mathbf{q}, s) + \Delta_3(\mathbf{q}, s) + \Delta_4(\mathbf{q}, s). \tag{E.4}$$

This is an approximation, and usually a very good one, to the correct (but still within low-order perturbation theory) form (e.g. Cowley 1963)

$$
\begin{aligned}
[\omega(\mathbf{q}, s)]^2 &= [\omega_0(\mathbf{q}, s)]^2 + 2\omega_0(\mathbf{q}, s) \\
&\times [\Delta_2(\mathbf{q}, s) + \Delta_3(\mathbf{q}, s) + \Delta_4(\mathbf{q}, s)].
\end{aligned}
\tag{E.5}
$$

Furthermore, Δ_2, Δ_3 and Δ_4 are all linear in terms of the type $n + 1/2$, where n is a Bose–Einstein occupation number. An expansion of $n + 1/2$ at high temperatures has the form $k_B T / \hbar\omega$, i.e. with cancellation of the term $1/2$ in $n + 1/2$ (cf. eq. (D.6)). Therefore, if the high temperature form of eq. (E.5) is linearly extrapolated to $T = 0$ K, one gets ω_0. It also follows that Δ_2, Δ_3 and Δ_4 are directly linear in T at high T, while shifts taken relative to the frequency at 0 K would vary with T as something like $T - \theta_D/2$. What has now been said about $\omega(\mathbf{q}, s)$ is relevant also for the elastic constants $c_{ij}(T)$, since they give the low-frequency part of ω. For instance, consider a pure transverse mode with $\omega^2 \sim c_{44}$. Then

$$
c_{44}(T) \approx c_{44}(T = 0) - AT
\tag{E.6}
$$

at high T (within low-order perturbation theory, i.e. neglecting higher-order anharmonicity). A is a constant which is specific for the material, and related to anharmonic effects, including thermal expansion. Extrapolation of experimental data from the linear region of $c_{44}(T)$ to $T = 0$ K gives the value of c_{44} for "harmonic" vibrations (cf. fig. 4.5). Of course this assumes that there are no anomalies in $c_{ij}(T)$ of electronic or magnetic origin that would cause a temperature dependence not described by Bose–Einstein factors n.

HEAT CAPACITY CONTRIBUTIONS IN A REAL SOLID
– AN OVERVIEW

Figure F.1 shows contributions to the heat capacity of a typical transition metal, from 0 K to the melting point T_{fus}. Some features are exaggerated for clarity, and the figure mainly serves to identify various contributions. The dashed line gives the classical Dulong–Petit law for the vibrational heat capacity, $C = 3k_B$ per atom. The other contributions are as follows:

(a) C_{har} is the vibrational contribution for perfectly harmonic vibrations. It approaches the Dulong–Petit value asymptotically from below.

(b) $C_{V,\mathrm{ph}}$ is the total vibrational heat capacity, taken at "constant volume", for instance calculated as the vibrational part of $C_V = C_p - VT\beta^2 K_T$. We note that $C_{V,\mathrm{ph}}$ does not strictly approach the classical value $3k_B$ at high T, although this may be a good approximation. Within low order in quantum mechanical perturbation theory, $C_{V,\mathrm{ph}}$ varies linearly with T; in almost all cases an increase. We also remark that $C_{V,\mathrm{ph}}$ is not quite the same as the heat capacity at a fixed volume V_0 (e.g. the volume at 300 K) (see Chapter 13, §7).

(c) The vibrational heat capacity at constant pressure, $C_{p,\mathrm{ph}}$. This term differs from $C_{V,\mathrm{ph}}$ by the addition of the effect of thermal expansion. To low order, anharmonicity causes $C_{p,\mathrm{ph}}$ to increase linearly in T at high T. Normally, higher order anharmonicity gives $C_{p,\mathrm{ph}}$ a more rapid increase above, say, $T_{\mathrm{fus}}/2$.

(d) An electronic contribution C_{el} is added to the vibrational $C_{p,\mathrm{ph}}$. If the electronic density of states $N(E)$ does not vary much within an energy interval $\pm 3k_B T$ around the Fermi level, C_{el} is linear in T. We write $C_{\mathrm{el}} = \gamma T$. Note that γ is not the same as derived directly from low temperature data, because there is an electron-
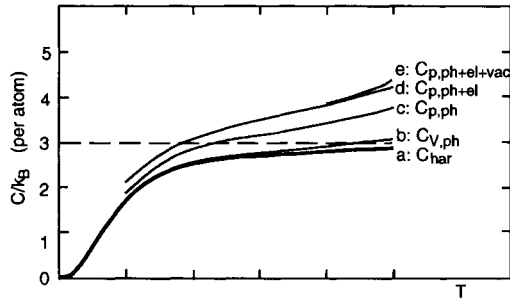
Fig. F.1. Schematic representation of heat capacity contributions in a transition metal.

phonon many-body enhancement to C_{el} at low T only. If $N(E)$ is not approximately constant around the Fermi level, C_{el} has a smooth but complicated temperature dependence. Then C_{el} may vary more rapidly, or less rapidly, than linearly in T (see Chapter 10).

(e) A vacancy contribution is added. It increases with an exponential function in T and is very small until one is close to the melting point.

SOME RELATIONS FOR INHOMOGENEOUS SYSTEMS

Hashin–Shtrikman bounds; an equivalent expression. A mathematically equivalent form of K_u in eq. (17.19) is

$$K_u = f_1 K_1 + f_2 K_2 - \frac{3 f_1 f_2 (K_1 - K_2)^2}{3(f_2 K_1 + f_1 K_2) + 4G_2}. \tag{G.1}$$

Effective-medium theory, equivalent expressions. The effective-medium result (eq. (17.56)) for the bulk modulus may also be written (e.g. Hashin 1983)

$$\frac{f_1}{K^* - K_2} + \frac{f_2}{K^* - K_1} = \frac{3}{3K^* + 4G^*}. \tag{G.2}$$

The shear modulus, (eq. (17.57)), may be written

$$\frac{f_1}{G^* - G_2} + \frac{f_2}{G^* - G_1} = \frac{6(K^* + 2G^*)}{5G^*(3K^* + 4G^*)}. \tag{G.3}$$

UNITS

Energies. Many sources of thermophysical data use non-SI units for energies. Tables H1 and H2 give some examples, with conversion factors. In H1, the temperature (K) is related to energy through $k_B T$. Note that there are several definitions of a calorie. The "thermochemical" calorie has 1 cal = 4.184 J.

Atomic units. Physicists often use so called atomic units (au). The length unit is 1 bohr = $1a_0$, where $a_0 = 5.29177 \times 10^{-11}$ m is the Bohr radius. The unit for energies, in atomic units, is 1 hartree (H) = 2 rydberg (Ry) = 4.359×10^{-18} J. One usually writes $a_0 = \hbar^2/me^2$, 1 H = e^2/a_0 and 1 Ry = $e^2/(2a_0)$. These expressions are not dimensionally correct in SI units. In SI units one has $a_0 = 4\pi\varepsilon_0\hbar^2/(me^2) = 0.5292 \times 10^{-10}$ m (cf. the following section).

Electron charge in transport formulae. The expressions for the electrical resistivity contain the electron charge e. Some of the relations in Chapter 15 refer to the old CGS system of units where e^2 means $e^2/(4\pi\varepsilon_0)$, and $\varepsilon_0 = 8.85419 \times 10^{-12}$ As/(Vm) is the permittivity of free space (vacuum). The SI unit of conductivity is $1/(\Omega m) = A^2s^3/(kgm^3)$. If we write $\sigma = ne^2\tau/m$ we get the correct dimension (unit) for σ when n is number density (unit: m^{-3}), e is charge (unit: C = As), τ is time (unit: s) and m is mass (unit: kg). In eq. (15.12) we replaced ne^2/m by $\omega_{pl}^2/(4\pi)$. However, in the expression $\omega_{pl}^2 = 4\pi ne^2/m$, ω_{pl} does not have the dimension of frequency. A correct form is $\omega_{pl}^2 = 4\pi ne^2/(4\pi\varepsilon_0 m) = ne^2/(\varepsilon_0 m)$. It follows that eq. (15.13) is not dimensionally correct when SI units are used. To get the correct form, e^2 should be replaced by $e^2/(4\pi\varepsilon_0)$. One the other hand, eqs. (15.20), (15.27) and (15.30), which contain a term ω_{pl}^2, are the equivalent of $\sigma = ne^2\tau/m$ and should

Table H.1

Conversion factors for energy units.

K	kcal	J	eV	mRy
1	3.298×10^{-27}	1.3807×10^{-23}	8.617×10^{-5}	6.333×10^{-3}
3.033×10^{26}	1	4.1868×10^{3}	2.613×10^{22}	1.921×10^{24}
7.243×10^{22}	2.388×10^{-4}	1	6.242×10^{18}	4.588×10^{20}
1.160×10^{4}	3.827×10^{-23}	1.6022×10^{-19}	1	73.499
157.9	5.207×10^{-25}	2.180×10^{-21}	0.013606	1

Table H.2

Conversion factors for energies per mole or atom

kJ/mol	kcal/mol	eV/atom	mRy/atom
1	0.2388	0.01036	0.7615
4.187	1	0.04336	3.187
96.49	23.05	1	73.499
1.313	0.3135	0.013606	1

have ω_{pl}^2 calculated from eq. (15.13) as it stands, i.e. without any factor $1/(4\pi\varepsilon_0)$, and hence an ω_{pl} that does not have the dimension of frequency. The fundamental unit of resistivity which we wrote (Chapter 15, §9), $a_0\hbar/e^2 = 0.22 \ \mu\Omega$m comes out correctly with SI units for a_0, $\hbar$ and e.

TABLES OF DEBYE TEMPERATURES AND λ_{el-ph}

Recommended sources of data. Most of the illustrating examples in this book rely on the following sources of data. Sometimes these reference works give carefully assessed data, rather than just a compilation, which makes them very useful.

Heat capacity and directly related properties: JANAF thermochemical tables (1985), Barin (1989), CINDAS tables, Vols. 4, 5 (Touloukian and Buyco 1970).

Elastic constants: Landolt–Börnstein tables (Every and McCurdy 1992).

Phonon dispersion curves, phonon density of states: Landolt–Börnstein tables (Schober and Dederichs 1981).

Electrical conductivity of elements: Landolt–Börnstein tables (Bass 1982).

Thermal conductivity and diffusivity: CINDAS tables, Vols. 1, 2, 10 (Touloukian et al. 1970, 1973).

Thermal expansion: CINDAS tables, Vols. 12, 13 (Touloukian et al. 1975, 1977).

Electron band structure and density of states: Landolt–Börnstein tables (Sellmyer 1981, Cracknell 1984), Moruzzi et al. (1978), Papaconstantopoulos (1986) and Moruzzi and Sommers (1995).

Recommended Debye temperatures and electron-phonon mass enhancement parameters. Tables I.1–I.6 give entropy Debye temperatures θ_D^S evaluated from experimental data for the vibrational entropy at $T \approx \theta_D^S$ (or at $T \approx 298$ K if data at $T \approx \theta_D^S$ are not readily available, except for Table I.1 where the θ-values are corrected to refer to $F(\omega)$ at low T). Entropy values are usually taken from Barin (1989) or the JANAF thermochemical tables (1985). The bulk moduli K and the elastic-

Table I.1
Properties of some free-electron-like metals, including noble metals

At. number	Symbol	$\theta_D(-3)$ K	$\theta_D(0)$ K	λ_{el-ph}
3	Li	350	393	0.4
4	Be	1374	974	0.2
11	Na	152	161	0.16
12	Mg	386	327	0.35
13	Al	429	394	0.43
19	K	88	96	0.13
29	Cu	346	316	0.15
30	Zn	307	225	0.38
31	Ga	296	237	0.4
37	Rb	55	60	0.16
47	Ag	224	215	0.13
48	Cd	182	150	0.38
49	In	108	123	0.8
50	Sn	185	158	0.7
55	Cs	40	44	0.15
79	Au	163	175	0.17
80	Hg	71	92	1.6
81	Tl	80	93	0.8
82	Pb	96	89	1.5

limit Debye temperature $\theta_D^E = \theta_D(-3)$ are from the quoted sources or calculated from elastic constants in the Landolt–Börnstein tables (Every and McCurdy 1992), as explained in Chapters 6 and 17. The electron-phonon mass enhancement parameter λ_{el-ph} is a recommended value from the author's somewhat subjective estimate based on data in Grimvall (1981) and Allen (1987, 1999).

Table I.2

Properties of some transition metals

At. number	Symbol	K GPa	$\theta_D(-3)$ K	θ_D^S K	λ_{el-ph}
22	Ti	105	429	352	0.4
23	V	157	400	384	1.0
24	Cr	160	598	473	0.4
25	Mn	131	409	358	0.4
26	Fe	167	477	413	0.4
27	Co	187	460	365	0.4
28	Ni	184	477	378	0.4
40	Zr	95	299	244	0.4
41	Nb	170	277	282	1.0
42	Mo	264	470	380	0.4
43	Tc	281	454	320	0.4
44	Ru	311	555	384	0.4
45	Rh	267	489	344	0.4
46	Pd	188	275	269	0.4
72	Hf	109	252	203	0.4
73	Ta	193	258	229	0.9
74	W	310	380	319	0.4
75	Re	365	416	264	0.4
76	Os	410	467	320	0.4
77	Ir	355	425	286	0.4
78	Pt	283	237	228	0.4

Table I.3

Entropy Debye temperatures θ_D^S of alkali halides and alkali hydrides (Unit: K)

	θ_D^S		θ_D^S		θ_D^S		θ_D^S
LiF	590	LiCl	354	LiBr	262	LiI	208
NaF	419	NaCl	273	NaBr	204	NaI	161
KF	305	KCl	222	KBr	171	KI	138
RbF	232	RbCl	171	RbBr	130	RbI	110
CsF	199	CsCl	153	CsBr	121	CsI	100
LiH	894	NaH	566	KH	434	RbH	326

All compounds have the NaCl-type crystal structure except CsCl, CsCsBr and CsI which have the CsCl-type structure,

Source: Oberschmidt (1996, unpublished) and, for hydrides, Häglund (1990, unpublished).

Table I.4

Entropy Debye temperatures θ_D^S of alkali-earth-metal halides (Unit: K)

	θ_D^S		θ_D^S		θ_D^S		θ_D^S
BdF$_2$	634	BeCl$_2$	393	BeBr$_2$	303	BeI$_2$	229
MgF$_2$	569	MgCl$_2$	350	MgBr$_2$	244	MgI$_2$	202
CaF$_2$	470	CaCl$_2$	286	CaBr$_2$	204	CaI$_2$	165
SrF$_2$	390	SrCl$_2$	249	SrBr$_2$	170	SrI$_2$	138
BaF$_2$	320	BaCl$_2$	221	BaBr$_2$	156	BaI$_2$	128

Source: Shian Peng and Grimvall (1994b).

Table I.5

Entropy Debye temperatures θ_D^S of transition-metal carbides, nitrides and borides (Unit: K)

	θ_D^S		θ_D^S		θ_D^S		θ_D^S
ScC	654	TiC	805	VC	745	CrC	664
ZrC	650	HfC	581	NbC	634	TaC	551
ScN	755	TiN	710	VN	631	CrN	535
ZrN	582	HfN	521	NbN	539	TaN	489
TiB$_2$	972	ZrB$_2$	834	HfB$_2$	741	VB$_2$	897
NbB$_2$	813	TaB$_2$	740	CrB$_2$	796	MnB$_2$	671

Some of the compounds have a non-stoichiometric composition.
Source: Fernández Guillermet and Grimvall (1989, 1991b).

Table I.6

Entropy Debye temperatures θ_D^S of the elements Si and Ge and III-V compounds (Unit: K)

	θ_D^S		θ_D^S		θ_D^S		θ_D^S
Si	586	Ge	335	BN	1133	BP	898
AlN	954	AlP	482	AlAs	351	AlSb	315
GaN	731	GaP	425	GaAs	322		
InN	524	InP	354	InAs	252	InSb	205

Si and Ge have the diamond structure, AlN, GaN and InN have the ZnO-type structure and the remaining compounds have the ZnS-type structure.
Source: Oberschmidt (1996, unpublished).

REFERENCES

Abeles, B., 1963, Phys. Rev. 131, 1906.

Ackerman, D.A. and A.C. Anderson, 1982, Phys. Rev. Lett. 49, 1176.

Alers, G.A. and J.R. Neighbours, 1957, J. Appl. Phys. 28, 1514.

Allen, P.B., 1980, in: Superconductivity in d- and f-band Metals, H. Suhl and M.B. Maple, eds. (Academic Press, New York) p. 291.

Allen, P.B., 1981, in: Physics of Transition Metals, P. Rhodes, ed. (Inst. Phys. Conf. Ser., No. 55) p. 425.

Allen, P.B., 1987, Phys. Rev. B 36, 2920.

Allen, P.B., 1999, in: Handbook of Superconductivity, C.P. Poole, Jr., ed. (Academic Press, New York).

Allen, P.B. and M.L. Cohen, 1969, Phys. Rev. 187, 525.

Allen, R.E., G.P. Alldredge and F.W. de Wette, 1971, Phys. Rev. B 4, 1661.

Alstad, J.K., R.V. Colvin and S. Legvold, 1961, Phys. Rev. 123, 418.

Althoff, J.D., P.B. Allen, R.M. Wentzcovitch and J.A. Moriarty, 1993, Phys. Rev. B 48, 13253.

American Institute of Physics Handbook, 1972, D.E. Gray, ed. (McGraw-Hill, New York).

Anand, L., 1982, Scripta Met. 16, 173.

Anderson, A.C., 1983, in: Thermal Conductivity, Vol. 16, D.C. Larsen, ed. (Plenum Press, New York) p. 3.

Anderson, O.L., 1963, J. Phys. Chem. Solids 24, 909.

Anderson, O.L., 1965, in: Physical Acoustics, Vol. III B, W.P. Mason, ed. (Academic Press, New York) p. 43.

Anderson, O.L., 1966a, Phys. Rev. 144, 553.

Anderson, O.L., 1966b, J. Phys. Chem. Solids 27, 547.

Anderson, O.L., 1995, Equations of States of Solids for Geophysics and Ceramic Science (Oxford University Press, New York).

Anderson, P.W., B.I. Halperin and C.M. Varma, 1972, Phil. Mag. 25, 1.

Ashcroft, N.W. and N.D. Mermin, 1976, Solid State Physics (Holt, Rinehart and Winston, Philadelphia).

Ashcroft, N.W. and J.W. Wilkins, 1965, Phys. Lett. 14, 285.

Avellaneda, M., A.V. Cherkaev, K.A. Lurie and G.W. Milton, 1988, J. Appl. Phys. 63, 4989.

Bäckström, G., 1985, High Temp.—High Press. 17, 185.

Bailey, A.C. and B. Yates, 1967, Proc. Phys. Soc. 91, 390.

Bailey, A.C. and B. Yates, 1970, J. Appl. Phys. 41, 5088.

Bain, E.C., 1924, Trans. Am. Inst. Min. Metall Engrs. 70, 25.

Ballabh, T.K., T.R. Middya and A.N. Basu, 1988, J. Appl. Phys. 64, 1166.

Baltes, H.P. and E.R. Hilf, 1973, Solid State Commun. 12, 369.

Barin, I., 1989, Thermochemical Data of Pure Substances (VCH Verlag, Weinheim).

Barkman, J.H., R.L. Anderson and T.E. Brackett, 1965, J. Chem. Phys. 42, 1112.

Barron, T.H.K., 1957, Ann. Phys. (NY) 1, 77.

Barron, T.H.K., 1965, in: Lattice Dynamics, R.F. Wallis, ed. (Pergamon Press, Oxford) p. 247.

Barron, T.H.K., 1979, J. Phys. C 12, L 155.

Barron, T.H.K. and M.L. Klein, 1974: in Dynamical Properties of Solids, Vol. 1, G.K. Horton and A.A. Maradudin, eds. (North-Holland, Amsterdam) p. 391.

Barron, T.H.K. and R.W. Munn, 1967, Phil. Mag. 15, 85.

Barron, T.H.K. and R.W. Munn, 1968, J. Phys. C 1, 1.

Barron, T.H.K., A.J. Leadbetter, J.A. Morrison and L.S. Salter, 1966, Acta Cryst. 20, 125.

Barron, T.H.K., J.G. Collins and G.K. White, 1980, Adv. Phys. 29, 609.

Barron, T.H.K., A.J. Leadbetter and J.A. Morrison, 1964, Proc. Roy. Soc. A 279, 62. [Corrigenda A289, 440 (1966)].

Barsch, G.R., 1967, Phys. Stat. Sol. 19, 129.

Barsch, G.R. and Z.P. Chang, 1967, Phys. Stat. Sol. 19, 139.

Bass, J., 1972, Adv. Phys. 21, 431.

Bass, J., 1982, in: Landolt–Börnstein tables, New Series, Vol. III/15a, K.-H. Hellwege and J.L. Olsen, eds. (Springer-Verlag, Berlin).

Batallan, F., I. Rosenman and C.B. Sommers, 1975, Phys. Rev. B 11, 545.

Baughman, R.H. and D.S. Galvão, 1993, Nature 365, 735.

Beaman, D.R., R.W. Balluffi and R.O. Simmons, 1964, Phys. Rev. 134, A532.

Beaudoin, J.J. and R.F. Feldman, 1975, Mag. Concr. Res. 5, 103.

Beck, H., P.F. Meier and A. Thellung, 1974, Phys. Stat. Sol. (a) 24, 11.

Benedek, G., M. Miura, W. Kress and H. Bilz, 1984, Phys. Rev. Lett. 52, 1907.

Beni, G. and P.M. Platzman, 1976, Phys. Rev. B 14, 1514.

Beran, M., 1965, Nuovo Cim. Suppl. 3, 448.

Beran, M. and J. Molyneux, 1963, Nuovo Cim. 30, 1406.

Bergman, D.J., 1978, Phys. Reports (Phys. Lett. C) 43, 377.

Bergman, D.J., 1982, Ann. Phys. 138, 78.

Bergman, D.J. and D. Stroud, 1992, in: Solid State Physics, Vol. 46, H. Ehrenreich and D. Turnbull, eds. (Academic Press, Boston) p. 147.

Berman, R., 1976, Thermal Conduction in Solids (Clarendon Press, Oxford).

Berryman, J.G., 1980, J. Acoust. Soc. Am. 68, 1820.

Bevk, J., 1973, Phil. Mag. 28, 1379.

Bevk, J., T.B. Massalski and U. Mizutani, 1977, Phys. Rev. B 16, 3456.

Beyermann, W.P., M.F. Hundley, J.D. Thompson, F.N. Diederich and G. Grüner, 1992, Phys. Rev. Lett. 68, 2046.

Bilz, H. and W. Kress, 1979, Phonon Dispersion Relations in Insulators (Springer-Verlag, Berlin).

Birch, F., 1938, J. Appl. Phys. 9, 279.

Birch, F., 1947, Phys. Rev. 71, 809.

Birch, F., 1952, J. Geophys. Res. 57, 227.

Blatt, F.J., 1968, Physics of Electronic Conduction in Solids (McGraw-Hill, New York).

Bloch, F., 1928, Z. Physik 52, 555.

Bloch, F., 1930, Z. Physik 59, 208.

Boas, W. and J.K. Mackenzie, 1950, Progr. Met. Phys. 2, 90.

Boehler, R., I.C. Getting and G.C. Kennedy, 1977, J. Phys. Chem. Solids 38, 233.

Böhmer, W. and P. Rabe, 1979, J. Phys. C 12, 2465.

Borelius, G., 1934, Ann. Physik 20, 57.

Born, M., 1939, J. Chem. Phys. 7, 591.

Born, M., 1942, Rep. Progr. Phys. 9, 294.

Born, M. and K. Huang, 1954, Dynamical Theory of Crystal Lattices (Oxford University Press, London).

Bose, S.K., O. Jepsen and O.K. Andersen, 1993, Phys. Rev. B 48, 4265.

Böttcher, C.J.F., 1952, Theory of Electric Polarization (Elsevier, Amsterdam).

Bouvier, M., P. Lethuillier and D. Schmitt, 1991, Phys. Rev. B 43, 13137.

Boyd, R.H., 1983, J. Polymer Sci. 21, 493.

Boyer, L.L., 1985, Phase Transitions 5, 1.

Brassington, M.P. and G.A. Saunders, 1983, Proc. Roy. Soc. A 387, 289.

Broadbent, S.R. and J.M. Hammersley, 1957, Proc. Cambridge Philos. Soc. 53, 629.

Bross, H., A. Seeger and R. Haberkorn, 1963, Phys. Stat. Sol. 3, 1126.

Brout, R. and W. Visscher, 1962, Phys. Rev. Lett. 9, 54.

Brown, Jr., W.F., 1955, J. Chem. Phys. 23, 1514.

Brudnoy, D.M., 1976, J. Phys. Chem. Solids 37, 1109.

Brüesch, P., 1982, Phonons: Theory and Experiments I (Springer-Verlag, Berlin).

Brüesch, P., 1986, Phonons: Theory and Experiments II (Springer-Verlag, Berlin).

Brüesch, P., 1987, Phonons: Theory and Experiments III (Springer-Verlag, Berlin).

Bruggeman, D.A.G., 1935, Ann. Physik 24, 636.

Brugger, K., 1964, Phys. Rev. 133, A1611.

Brugger, K., 1965a, J. Appl. Phys. 36, 759.

Brugger, K., 1965b, J. Appl. Phys. 36, 768.

Brugger, K. and T.C. Fritz, 1967, Phys. Rev. 157, 524.

Bruno, E., B. Ginatempo, E.S. Giuliano, A.V. Ruban and Yu.Kh. Vekilov, 1994, Phys. Rep. 249, 353.

Buckingham, E., 1914, Phys. Rev. 4, 345.

Buckingham, M.J., 1951, Nature 168, 281.

Buckingham, M.J. and M.R. Schafroth, 1954, Proc. Phys. Soc. A 67, 828.

Budiansky, B., 1965, J. Mech. Phys. Solids 13, 223.

Budiansky, B., 1970, J. Compos. Mater. 4, 286.

Burke, J., 1972, J. Less-Common Metals 28, 441.

Burnell, D.M., J. Zasadzinski, R.J. Noer, E.L. Wolf and G.B. Arnold, 1982, Solid State Commun. 41, 637.

Burton, J.J., 1970, J. Chem. Phys. 52, 345.

Butt, N.M., J. Bashir, B.T.M. Willis and G. Heger, 1988, Acta Cryst. A 44, 396.

Butt, N.M., J. Bashir and K.M. Nasir, 1993, Acta Cryst. A 49, 171.

Callaway, J., 1963, Nuovo Cimento 29, 883.

Cape, J.A., G.W. Lehman, W.V. Johnston and R.E. DeWames, 1966, Phys. Rev. Lett. 16, 892.

Carnelley, T., 1879, Ber. Deutsche Chem. Ges. 12, 439.

Carr, W.J., Jr., 1961, Phys. Rev. 122, 1437.

Carruthers, P., 1961, Rev. Mod. Phys. 33, 92.

Catlow, C.R A., J. Corish, P.W.M. Jacobs and A.B. Lidiard, 1981, J. Phys. C 14, L121.

Cauchy, A.L., 1828, Exercis de Mathématique.

Ce-Wen Nan, 1993, Progr. Mater. Sci. 37, 1.

Chadwick, G.A. and D.A. Smith, 1976, Grain Boundary Structure and Properties (Academic Press, London).

Chan, W.C., 1978, J. Phys. F 8, 859.

Chang, R., 1967, Appl. Phys. Lett. 11, 305.

Chen, T.S., G.P. Alldredge, F.W. de Wette and R.E. Allen, 1971, J. Chem. Phys. 55, 3121.

Cheng, H. and S. Torquato, 1997a, Proc. Roy. Soc. (London) A 453, 145.

Cheng, H. and S. Torquato, 1997b, Proc. Roy. Soc. (London) A 453, 1331.

Cho, S.-A., 1982, J. Phys. F 12, 1069.

Christensen, R.M., 1979, Mechanics of Composite Materials (Wiley, New York).

Christiansson, H. and G. Grimvall, 1994, in: Thermal Conductivity, Vol. 22, T.W. Tong, ed. (Technomic Publishing, Lancaster) p. 147.

Christoffel, E.B., 1877, Ann. Mat. Pura Appl. 8, 193.

Chung, D.H., 1963, Phil. Mag. 8, 833.

Chung, D.H., 1967, J. Appl. Phys. 38, 5104.

Chung, D.H. and W.R. Buessem, 1967, J. Appl. Phys. 38, 2010.

Chung, D.Y., J.M. Farley and G.A. Saunders, 1975, Phys. Stat. Sol. (a) 29, K43.

Cibuzar, G., A. Hikata and C. Elbaum, 1984, Phys. Rev. Lett. 53, 356.

Cimberle, M.R., G. Bobel and C. Rizzuto, 1974, Adv. Phys. 23, 639.

Cohen, M.L., 1982, Phys. Scr. T 1, 5.

Cohen, M.L., 1985, Phys. Rev. B 32, 7988.

Cohen, M.L., 1988, Mater. Sci. Eng. A 105/106, 11.

Cole, H.S.D. and R.E. Turner, 1967, Phys. Rev. Lett. 19, 501.

Collins, J.G. and G.K. White, 1964, Progr. Low Temp. Phys. 4, 450.

Cowley, E.R. and R.A. Cowley, 1965, Proc. Roy. Soc. A 287, 259.

Cowley, E.R. and R.A. Cowley, 1966, Proc. Roy. Soc. A 292, 209.

Cowley, R.A., 1963, Adv. Phys. 12, 421.

Cowley, R.A., 1968, Rep. Progr. Phys. 31, 123.

Cowley, R.A., 1970, Rev. Int. Hautes Tempér. et Réfract. 7, 202.

Cracknell, A.P., 1984, in: Landolt–Börnstein tables, New Series, Vol. III/13c, K.-H. Hellwege and J.L. Olsen, eds. (Springer-Verlag, Berlin).

Craievich, P.J. and J.M. Sanchez, 1997, Comp. Mater. Sci. 8, 92.

Daams, J.M., B. Mitrovic and J.P. Carbotte, 1981, Phys. Rev. Lett. 46, 65.

Dacorogna, M., J. Ashkenazi and M. Peter, 1982, Phys. Rev. B 26, 1527.

Date, E.H.F. and K.W. Andrews, 1969, J. Phys. D 2, 1373.

Dawber, P.G. and R.J. Elliott, 1963, Proc. Roy. Soc. A 273, 222.

Debye, P., 1912, Ann. Physik 39, 789.

Debye, P., 1914, Ann. Physik 43, 49.

Dederichs, P.H. and R. Zeller, 1980, in: P.H. Dederichs, R. Zeller and K. Schroeder, Point Defects in Metals II (Springer-Verlag, Berlin).

Dernier, P.D., W. Weber and L.D. Longinotti, 1976, Phys. Rev. B 14, 3635.

Deutscher, G., R. Zallen and J. Adler, eds., 1983, Percolation Structures and Processes, Ann. Israel Phys. Soc., Vol. 5 (Adam Hilger, Bristol).

Dewey, J.M., 1947, J. Appl. Phys 18, 578.

Dietsche, W., H. Kinder, J. Mattes and H. Wühl, 1980, Phys. Rev. Lett. 45, 1332.

Dietsche, W., G.A. Northrop and J.P. Wolfe, 1981, Phys. Rev. Lett. 47, 660.

Dinsdale, A.T., 1991, CALPHAD 15, 317.

Dobrzynski, L. and G. Leman, 1969, J. Physique 30, 116.

Domb, C., 1981, in: Perspectives in Statistical Physics, H.J. Raveche, ed. (North-Holland, Amsterdam) p. 173.

Domb, C. and L. Salter, 1952, Phil. Mag. 43, 1083.

Doniach, S. and S. Engelsberg, 1966, Phys. Rev. Lett. 17, 750.

Dove, M.T., 1993, Introduction to Lattice Dynamics (Cambridge University Press, Cambridge).

Drude, P., 1900a, Annalen der Physik 1, 556.

Drude, P., 1900b, Annalen der Physik 3, 369.

Dugdale, J.S., 1977, The Electrical Properties of Metals and Alloys (Edward Arnold, London).

Dugdale, J.S., 1995, The Electrical Properties of Disordered Metals (Cambridge University Press, Cambridge).

Dugdale, J.S. and A. Myers, 1985, in: Landolt–Börnstein tables, New Series, Vol. III/15b, K.-H. Hellwege and J.L. Olsen, eds. (Springer-Verlag, Berlin) p. 13.

Dugdale, J.S. and D. Gugan, 1962, Proc. Roy. Soc. A 270, 186.

Dulong, P.L. and A.T. Petit, 1819, Ann. Chim. [2] 7, 113, 225, 337.

Dunn, M.L. and H. Ledbetter, 1995, J. Appl. Phys. 78, 1583.

Dupuis, M., R. Mazo and L. Onsager, 1960, J. Chem. Phys. 33, 1452.

Durand, M.A., 1936, Phys. Rev. 50, 449.

Dykhne, A.M., 1970, Zh. Eksp. Teor. Fiz. 59, 110 [Sov. Phys.—JETP 32, 63 (1971)].

Eckhardt, D. and W. Wasserbäch, 1978, Phil. Mag. A 37, 621.

Ecsedy, D.J. and P.G. Klemens, 1977, Phys. Rev. B 15, 5957.

Ehrhardt, P., 1991, in: Landolt–Börnstein tables, New Series, Vol. III/25, H. Ullmaier ed. (Springer-Verlag, Berlin).

Einarsdotter, K., B. Sadigh, G. Grimvall and V. Ozoliņš, 1997, Phys. Rev. Lett. 79, 2073.

Einstein, A., 1907, Ann. Physik 22, 180.

Ekman, M., B. Sadigh, K. Einarsdotter and P. Blaha, 1998, Phys. Rev. B 58, 5296.

Éliashberg, G.M., 1962, Zh. Eksp. Teor. Fiz. 43, 1005 [Sov. Phys.—JETP 16, 780 (1963)].

Elliott, R.J. and D.W. Taylor, 1964, Proc. Phys. Soc. 83, 189.

Emsley, J., 1989, The Elements (Clarendon Press, Oxford).

Enderby, J.E. and N.H. March, 1966, Proc. Phys. Soc. 88, 717.

Engquist, H.-L. and G. Grimvall, 1980, Phys. Rev. B 21, 2072.

Epstein, S.G. and O.N. Carlson, 1965, Acta Met. 13, 487.

Erdös, P. and S.B. Haley, 1969, Phys. Rev. 184, 951.

Eriksson, O., J.M. Wills and D. Wallace, 1992, Phys. Rev. B 46, 5221.

Eros, S. and C.S. Smith, 1961, Acta Met. 9, 14.

Eshelby, J.D., 1949, Proc. Roy. Soc. A 197, 396.

Eshelby, J.D., 1957, Proc. Roy. Soc. A 241, 376.

Eshelby, J.D., 1975, in: The Physics of Metals 2. Defects, P.B. Hirsch, ed. (Cambridge University Press, Cambridge) p. 1.

Every, A.G. and A.K. McCurdy, 1992, in: Landolt–Börnstein tables, New Series III/29, D.F. Nelson, ed. (Springer-Verlag, Berlin) p. 1.

Every, A.G., 1979, Phys. Rev. Lett. 42, 1065.

Every, A.G., 1980, Phys. Rev. B 22, 1746.

Ewing, R.H., 1971, Acta Met. 19, 1359.

Ewing, R.H. and B. Chalmers, 1972, Surf. Sci. 31, 161.

Farnell, G.W., 1961, Can. J. Phys. 39, 65.

Fecht, H.J. and W.L. Johnson, 1988, Nature 334, 50.

Fedorov, F.I., 1963, Kristallographiya 8, 213.

Fedorov, F.I., 1968, Theory of Elastic Waves in Crystals (Plenum Press, New York).

Feldman, R.F. and J.J. Beaudoin, 1977, Mag. Concr. Res. 7, 19.

Felice, R.A., J. Trivisonno and D.E. Schuele, 1977, Phys. Rev. B 16, 5173.

Fernández Guillermet, A., 1995, Int. J. Thermophys. 16, 1009.

Fernández Guillermet, A. and G. Grimvall, 1989, Phys. Rev. B40, 10582.

Fernández Guillermet, A. and G. Grimvall, 1991a, Phys. Rev. B 44, 4332.

Fernández Guillermet, A. and G. Grimvall, 1991b, J. Less-Common Metals 169, 257.

Fernández Guillermet, A. and G. Grimvall, 1992, J. Phys. Chem. Solids 53, 105.

Fernández Guillermet, A., V. Ozoliņš, G. Grimvall and M. Körling, 1995, Phys. Rev. B 51, 10364.

Ferrante, J., J.R. Smith and J.H. Rose, 1983, Phys. Rev. Lett. 50, 1385.

Ferreira, J.M., B.W. Lee, Y. Dalichaouch, M.S. Torikachvili, K.N. Yang and M.B. Maple, 1988a, Phys. Rev. B 37, 1580.

Ferreira, L.G., A.A. Mbaye and A. Zunger, 1988b, Phys. Rev. B 37, 10547.

Fisk, Z. and G.W. Webb, 1976, Phys. Rev. Lett. 36, 1084.

Fletcher, G.C., 1978, Physica 93 B, 149.

Fletcher, G.C. and M. Yahaya, 1979, J. Phys. F9, 1529.

Flinn, P.A., G.M. McManus and J.A. Rayne, 1960, J. Phys. Chem. Solids 15, 189.

Flubacher, P., A.J. Leadbetter and J.A. Morrison, 1959, Phil. Mag. 4, 273.

Foiles, C.L., 1985, in: Landolt–Börnstein tables, New Series III/15b, K.-H. Hellwege and J.L. Olsen, eds. (Springer-Verlag, Berlin) p. 210.

Francfort, G.A. and F. Murat, 1986, Archives Rat. Mech. Analysis 94, 307.

Frase, H.N., L.J. Nagel, J.L. Robertson and B. Fultz, 1997, Phil. Mag. B 75, 335.

Fricke, H., 1953, J. Phys. Chem. 57, 934.

Friedel, J., 1953, Phil. Mag. 44, 444.

Friedel, J., 1969, in: The Physics of Metals I. Electrons, J.M. Ziman ed. (Cambridge University Press, Cambridge) p. 340.

Friedel, J., 1974, J. Phys; Lett. (France) 35, L59.

Friedel, J., 1980, in: Physics of Modern Materials, Vol. I (IAEA, Vienna) p. 163.

Friedel, J., 1982, Phil. Mag. A 45, 271.

Fuchs, K., 1935, Proc. Roy. Soc. A 151, 585.

Fuchs, K., 1938, Cambridge Phil. Soc. 34, 100.

Fulde, P. and J. Jensen, 1983, Phys. Rev. B 27, 4085.

Fulde, P., P. Horsch and A. Ramšak, 1993, Z. Phys. B 90, 125.

Fultz, B., L. Anthony, L.J. Nagel, R.M. Nicklow and S. Spooner, 1995, Phys. Rev. B 52, 3315.

Fung, Y.C., 1965, Foundations of Solid Mechanics (Prentice-Hall, New Jersey).

Furmanski, P., 1994, in: Thermal Conductivity, Vol. 22, T.W. Tong, ed. (Technomic Publishing, Lancaster, PA) p. 771.

Gazis, D.C., R. Herman and R.F. Wallis, 1960, Phys. Rev. 119, 533.

Geballe, T.H. and G.W. Hull, 1958, Phys. Rev. 110, 773.

Gerlich, D., 1969, J. Phys. Chem. Solids 30, 1638.

Gibiansky, L.V. and S. Torquato, 1997, J. Mech. Phys. Solids 45, 1223.

Gilvarry, J.J., 1956, Phys. Rev. 102, 308.

Girifalco, L.A., 1967, Scripta Met. 1, 5.

Gladstone, G., M.A. Jensen and J.R. Schrieffer, 1969, in: Superconductivity, Vol. 2, R.D. Parks, ed. (Marcel Dekker, New York) p. 665.

Golding, B., B.G. Bagley and F.S.L. Hsu, 1972, Phys. Rev. Lett. 29, 68.

Gorecki, T., 1974, Z. Metallkde 65, 426.

Gösele, U., W. Frank and A. Seeger, 1983, Solid State Commun. 45, 31.

Graebner, J.E. and L.C. Allen, 1983, Phys. Rev. Lett. 51, 1566.

Granato, A., 1958, Phys. Rev. 111, 740.

Greegor, R.B. and F.W. Lytle, 1979, Phys. Rev. B 20, 4902.

Greiner, J.D., D.T. Peterson, and J.F. Smith, 1977, J. Appl. Phys. 48, 3357.

Grimvall, G., 1975a, Physica Scripta 11, 381.

Grimvall, G., 1975b, Phys. Scripta 12, 337.

Grimvall, G., 1976, Physica Scripta 14, 63.

Grimvall, G., 1977, Liquid Metals (Inst. Phys. Conf. Series No. 30) p. 90.

Grimvall, G., 1981, The Electron-Phonon Interaction in Metals (North-Holland, Amsterdam).

Grimvall, G., 1983, Int. J. Thermophys. 4, 363.

Grimvall, G., 1984, Physica 127 B, 165.

Grimvall, G., 1986, Thermophysical Properties of Materials (North-Holland, Amsterdam).

Grimvall, G., 1989, Phys. Rev. B 39, 12300.

Grimvall, G., 1996, J. Alloys Compounds 233, 183.

Grimvall, G., 1998, Ber. Bunsenges. Phys. Chem. 102, 1083.

Grimvall, G., 1999, in: Electric Refractory Materials, Y. Kumashiro, ed. (Marcel Dekker, New York).

Grimvall, G. and I. Ebbsjö, 1975, Physica Scripta 12, 168.

Grimvall, G. and A. Fernández Guillermet, 1992, in: Advances in Physical Geochemistry, Vol. 10, Thermodynamic Data Systematics, S.K. Saxena, ed. (Springer-Verlag, Berlin) p. 272.

Grimvall, G. and J. Rosén, 1983, Int. J. Thermophys. 4, 139.

Grimvall, G. and M. Thiessen, 1986, 2nd Int. Conf. Science Hard Mater. (Inst. Phys. Conf. Ser. 75, 61).

Grimvall, G. and S. Sjödin, 1974, Physica Scripta 10, 340.

Grosse, C. and J.-L. Greffe, 1979, J. Chimie Physique 76, 305.

Grüneisen, E., 1912, Ann. d. Phys. 39, 257.

Grüneisen, E., 1913, Berichte Deutsche physikal. Ges. 15, 186.

Grüneisen, E., 1933, Ann. Physik 16, 530.

Grüneisen, E. and E.S. Goens, 1924, Z. Physik 29, 141.

Gschneidner, K.A., Jr., 1964, in: Solid State Physics, Vol. 16, F. Seitz and D. Turnbull, eds. (Academic Press, New York) p. 275.

Gschneidner, K.A., Jr., and K. Ikeda, 1983, J. Magn. Magnetic Materials 31–34, 265.

Gschneidner, K.A., Jr., and G.H. Vineyard, 1962, J. Appl. Phys. 33, 3444.

Guillaume, C.E., 1897, C. R. Acad. Sci. Paris, 125, 235.

Guillaume, C.E., 1920, C. R. Acad. Sci. Paris 170, 1920.

Guillot, M., F. Tchéou, A. Marchand, P. Feldmann and R. Lagnier, 1981, Z. Physik B 44, 53.

Gunton, D.J. and G.A. Saunders, 1972, J. Mater. Sci. 7, 1061.

Hafner, J., 1983, Phys. Rev. B 27, 678.

Hafner, J. and W. Jank, 1990, Phys. Rev. B 42, 11530.

Hafner, J. and W. Jank, 1992, Phys. Rev. B 45, 2739.

Hahn, H. and W. Ludwig, 1961, Z. Physik 161, 404.

Hale, D.K., 1976, J. Mat. Sci. 11, 2105.

Hall, P.M., S. Legvold and F.H. Spedding, 1959, Phys. Rev. 116, 1446.

Haller, E.E., 1995, J. Appl. Phys. 77, 2857.

Hansen, J.-P., 1970, Phys. Rev. A 2, 221.

Harding, J.H. and A.M. Stoneham, 1981, Phil. Mag. B 43, 705.

Harris, A.B. and H. Meyer, 1962, Phys. Rev. 127, 101.

Harrison, W.A., 1966, Pseudopotentials in the Theory of Metals (Benjamin, New York).

Hashin, Z., 1959, in: Nonhomogeneity in Elasticity and Plasticity, W. Olszak, ed. Pergamon Press, New York) p. 463.

Hashin, Z., 1962, ASME J. Appl. Mech. 29, 143.

Hashin, Z., 1965, J. Mech. Phys. Solids 13, 119.

Hashin, Z., 1983, ASME J. Appl. Mech. 50, 481.

Hashin, Z., 1984, J. Mech. Phys. Solids 32, 149.

Hashin, Z. and B.W. Rosen, 1964, J. Appl. Mech. 31, 223.

Hashin, Z. and S. Shtrikman, 1962a, J. Appl. Phys. 33, 3125.

Hashin, Z. and S. Shtrikman, 1962b, J. Mech. Phys. Solids 10, 343.

Hashin, Z. and S. Shtrikman, 1963a, J. Mech Phys. Solids 11, 127.

Hashin, Z. and S. Shtrikman, 1963b, Phys. Rev. 130, 129.

Hasson, G.C., J.-Y. Boos, I. Herbeuval, M. Biscondi and C. Goux, 1972, Surf. Sci. 31, 115.

Hausch, G. and H. Warlimont, 1973, Acta Metall. 21, 401.

Haussühl, S., 1973, Solid State Commun. 13, 147.

Hearmon, R.F.S., 1946, Rev. Mod. Phys. 18, 409.

Hearmon, R.F.S., 1961, An Introduction to Applied Anisotropic Elasticity (Oxford University Press, Oxford).

Hearmon, R.F.S., 1979, in: Landolt–Börnstein tables, New Series III/11, K.-H. Hellwege and A.M. Hellwege, eds. (Springer-Verlag, Berlin).

Hearmon, R.F.S., 1984, in: Landolt–Börnstein tables, New Series III/18, K.-H. Hell-wege and A.M. Hellwege, eds. (Springer-Verlag, Berlin).

Hehenkamp, Th., 1994, J. Phys. Chem. Solids 55, 907.

Hehenkamp, Th., W. Berger, J.-E. Kluin, Ch. Lüdecke and J. Wolff, 1992, Phys. Rev. B 45, 1998.

Heiming, A., W. Petry, J. Trampenau, M. Alba, C. Herzig, H.R. Schober and G. Vogl, 1991, Phys. Rev. B 43, 10948.

Heine, V., 1967, Phys. Rev. 153, 673.

Helsing, J. and G. Grimvall, 1991, J. Appl. Phys. 70, 1198.

Helsing, J. and A. Helte, 1991, J. Appl. Phys. 69, 3583.

Henderson, B., 1972, Defects in Crystalline Solids (Edward Arnold, London).

Hensel, J.C. and R.C. Dynes, 1979, Phys. Rev. Lett. 43, 1033.

Herring, C., 1960, J. Appl. Phys. 31, 1939.

Hill, R., 1952, Proc. Phys. Soc. A 65, 349.

Hill, R., 1963, J. Mech. Phys. Solids 11, 357.

Hill, R., 1964, J. Mech. Phys. Solids 12, 199.

Hill, R., 1965a, J. Mech. Phys. Solids 13, 189.

Hill, R., 1965b, J. Mech. Phys. Solids 13, 213.

Hirao, M., K. Aoki and H. Fukuoka, 1987, J. Acoust. Soc. Am. 81, 1434.

Holian, B.L., G.K. Straub, R.E. Swanson and D.C. Wallace, 1983, Phys. Rev. B 27, 2873.

Holzapfel, W.B., 1996, Rep. Progr. Phys. 59, 29.

Honda, K., S. Shimizu and S. Kusakabe, 1902, Z. Physik 3, 380.

Hoover, W.G., S.G. Gray and K.W. Johnson, 1971, J. Chem Phys. 55, 1128.

Hori, M., 1973a, J. Math. Phys. 14, 514.

Hori, M., 1973b, J. Math. Phys. 14, 1942.

Housley, R.M. and F. Hess, 1966, Phys. Rev. 146, 517.

Howard, R.E. and A.B. Lidiard, 1964, Rep. Progr. Phys. 27, 161.

Howson, M.A., 1984, J. Phys. F 14, L25.

Hsiang, T.Y., J.W. Reister, H. Weinstock, G.W. Crabtree and J.J. Vuillemin, 1981, Phys. Rev. Lett. 47, 523.

Huebener, R.P. and C.G. Homan, 1963, Phys. Rev. 129, 1162.

Huiszoon, C. and P.P.M. Groenewegen, 1972, Acta Cryst. A 28, 170.

Hultgren, R., P.D. Desai, D.T. Hawkins, M. Gleiser, K.K. Kelley and D.D. Wagman, 1973a, Selected Values of the Thermodynamic Properties of the Elements (Am. Soc. for Metals, Metals Park, OH).

Hultgren, R., P.D. Desai, D.T. Hawkins, M. Gleiser and K.K. Kelley, 1973b, Selected Values of the Thermodynamic Properties of Binary Alloys (Am. Soc. for Metals, Metals Park, OH).

Humphreys, F.J. and M. Hatherly, 1996, Recrystallization and Related Annealing Phenomena (Elsevier, Oxford).

Huntington, H.B., 1958, in: Solid State Physics, Vol. 7, F. Seitz and D. Turnbull, eds. (Academic Press, New York) p. 213.

Huntington, H.B., G.A. Shirn and E.S. Wajda, 1955, Phys. Rev. 99, 1085.

Ihm, J. and M.L. Cohen, 1980, Phys. Rev. B 21, 1527.

Ikeda, K. and K.A. Gschneidner, Jr., 1980, Phys. Rev. Lett. 45, 1341.

In Ho Kim, R. Jeanloz, Kyu Soo Jhung, Young Ho Bae and Chul-Kyu Choi, 1992, Phys. Rev. B 46, 3095.

Jackson, J.L. and S.R. Coriell, 1968, J. Appl. Phys. 39, 2349.

Jacobs, R.L., 1983, J. Phys. C 16, 273.

JANAF thermochemical tables, 3rd ed., 1985 (National Bureau of Standards, Washington DC), J. Phys. Chem. Ref. Data 14, Suppl. 1.

Jank, W. and J. Hafner, 1990, Phys. Rev. B 42, 6926.

Jank, W., Ch. Hausleitner and J. Hafner, 1991, J. Phys. Condens. Matter 3, 4477.

Jin Yu, Lingsong Bi, R.K. Kalia and P. Vashishta, 1994, Phys. Rev. B 49, 5008.

Johansson, B. and A. Rosengren, 1975, J. Phys. F 5, L15.

Johnson, D.P., and A.J. Kassman, 1969, Phys. Rev. 188, 1385.

Johnson, D.P., and A.J. Kassman, 1972, Phys. Rev. B 6, 2999.

Johnson, D.P., A.J. Kassman, and W.M. Visscher, 1971, Phys. Rev. Lett. 26, 10.

Julian, C.L., 1965, Phys. Rev. 137, A128.

Kagan, Yu. and Ya. A. Iosilevskii, 1962. Zh. Eksp. Teor. Fiz. 42, 259. [Sov. Phys. JETP 15, 182 (1962)].

Kagan, Yu. and Ya. Iosilevskii, 1963, Zh. Eksp. Teor. Fiz. 45, 819. [Sov. Phys. JETP 18, 562 (1964)].

Karlsson, Å.V., 1970, Phys. Rev. B 2, 3332.

Kasen, M.B., 1972, Acta Met. 20, 105.

Kaspers, W., R. Pott, D.M. Herlach and H. v. Löhneysen, 1983, Phys. Rev. Lett. 50, 433.

Kaufmann, R. and O. Meyer, 1984, Solid State Commun. 51, 539.

Kaveh, M. and N.F. Mott, 1982, J. Phys. C 15, L707.

Kieffer, S.W., 1982, Rev. Geophys. Space Phys. 20, 827.

Kikuchi, M., K. Fukamichi, T. Masumoto, T. Jagielinski, K.I. Arai and N. Tsuya, 1978, Phys. Stat. Sol. (a) 48, 175.

Kim, D.J., 1968, Phys. Rev. 167, 545.

Kim, Y.S. and R.G. Gordon, 1974, Phys. Rev. B 9, 3548.

Kirkpatrick, S., 1973, Rev. Mod. Phys. 45, 574.

Kitagawa, K., M. Ueda and H. Miyamoto, 1980, Acta Met. 28, 1505.

Kittel, C., 1949, Phys. Rev. 75, 972.

Kittel, C., 1987, Quantum Theory of Solids (Wiley, New York).

Kittel, C., 1996, Introduction to Solid State Physics (Wiley, New York).

Kittinger, E., J. Tichý and E. Bertagnolli, 1981, Phys. Rev. Lett. 47, 712.

Klein, M.V., 1966, Phys. Rev. 141, 716.

Klemens, P.G., 1955, Proc. Phys. Soc. A 68, 1113.

Klemens, P.G., 1958, in: Solid State Physics, Vol. 7, F. Seitz and D. Turnbull, eds. (Academic Press, New York) p. 1.

Klemens, P.G., 1960, Phys. Rev. 119, 507.

Klemens, P.G., 1969, in: Thermal Conductivity, R.P. Tye, ed. (Academic Press, London) p. 1.

Klemens, P.G., 1983a, in: Thermal Conductivity, Vol. 16, D.C. Larsen ed. (Plenum Press, New York) p. 15.

Klemens, P.G., 1983b, in: Thermal Conductivity, Vol. 17, J.G. Hust, ed. (Plenum Press, New York) p. 25.

Klemens, P.G., 1993, Thermochim. Acta 218, 247.

Kluge, M.D., D. Wolf, J.F. Lutsko and S.R. Phillpot, 1990, J. Appl. Phys. 67, 2370.

Koehler, J.S. and G. deWit, 1959, Phys. Rev. 116, 1121.

Köhler, M., 1948, Z. Physik 124, 772.

Köhler, M., 1949, Z. Physik 125, 679.

Kopp, H., 1864, Lieb. Ann. Suppl. 3, 290, 307.

Kouvel, J.S., 1956, Phys. Rev. 102, 1489.

Kovács, I. and H. El Sayed, 1976, J. Mat. Sci. 11, 529.

Kraft, T., P.M. Marcus, M. Methfessel and M. Scheffler, 1993, Phys. Rev. B 48, 5886.

Kraftmakher, Y., 1996, Phil. Mag. A 74, 811.

Kraftmakher, Ya. A., 1972, Fiz. Tverd. Tela 14, 392 [Sov. Phys.—Solid State 14, 325 (1972)].

Kraftmakher, Ya. A., 1978, in: Thermal Expansion, Vol. 6, I.D. Peggs, ed. (Plenum Press, New York) p. 155.

Kress, W., 1983, in: Landolt–Börnstein tables, New Series, Vol. III/13b, K.-H. Hellwege and J.L. Olsen, eds. (Springer-Verlag, Berlin).

Krishnan, R.S., R. Srinivasan and S. Devanarayanan, 1979, Thermal Expansion of Crystals (Pergamon Press, Oxford).

Krumhansl, J.A., 1965, in: Lattice Dynamics, R.F. Wallis, ed. (Pergamon Press, Oxford) p. 523.

Krumhansl, J.A. and J.A.D. Matthew, 1965, Phys. Rev. 140, A1812.

Kuhlmann-Wilsdorf, D., 1965, Phys. Rev. 140, A1599.

Kulkarni, R.V., W.G. Aulbur and D. Stroud, 1997, Phys. Rev. B 55, 6896.

Kumazawa, M., 1969, J. Geophys. Res. 74, 5311.

Kus, F.W. and D.W. Taylor, 1980, J. Phys. F 10, 1495.

Kus, F.W. and D.W. Taylor, 1982, J. Phys. F 12, 837.

Landau, L.D. and E.M. Lifshitz, 1959, Theory of Elasticity (Pergamon Press, London).

Landau, L.D. and E.M. Lifshitz, 1960, Electrodynamics of Continuous Media (Pergamon Press, London).

Landauer, R., 1952, J. Appl. Phys. 23, 779.

Landauer, R., 1978, AIP Conf. Proc. 40, J.C. Garland and D.B. Tanner, eds. p. 2.

Lang, N.D. and H. Ehrenreich, 1968, Phys. Rev. 168, 605.

Larkin, B.K. and S.W. Churchill, 1959, AIChE J. 5, 467.

Latimer, W.M., 1921, J. Am. Chem. Soc. 43, 818.

Latimer, W.M., 1951, J. Am. Chem. Soc. 73, 1480.

Laubitz, M.J. and T. Matsumura, 1972, Can. J. Phys. 50, 196.

Laubitz, M.J., T. Matsumura and P.J. Kelly, 1976, Can. J. Phys. 54, 92.

Laws, N., 1980, in: Physics of Modern Materials, Vol. I (Int. Atomic Energy Agency, Vienna) p. 465.

Lawson, N.S. and A.M. Guénault, 1982, J. Phys. F 12, 1407.

Leadbetter, A.J., 1968, J. Phys. C 1, 1489.

Leadbetter, A.J. and G.R. Settatree, 1969, J. Phys. C 2, 1105.

Leadbetter, A.J., D.M.T. Newsham and G.R. Settatree, 1969, J. Phys. C 2, 393.

Leavens, C.R. and A.H. MacDonald, 1983, Phys. Rev. B 27, 2812.

Ledbetter, H.M. and R.L. Moment, 1976, Acta Met. 24, 891.

Ledbetter, H.M. and R.P. Reed, 1973, J. Phys. Chem. Ref. Data 2, 531.

Lee, P.A. and T.V. Ramakrishnan, 1985, Rev. Mod. Phys. 57, 287.

Leibfried, G. and N. Breuer, 1978, Point Defects in Metals I (Springer-Verlag, Berlin).

Leibfried, G. and W. Ludwig, 1961, in: Solid State Physics, Vol. 12, F. Seitz and D. Turnbull, eds. (Academic Press, New York) p. 275.

Leibfried, G. and E. Schlömann, 1954, Nachr. Akad. Wiss. Göttingen Math.-Phys. Kl. 2a(4), 71.

Leighton, R.B., 1948, Rev. Mod. Phys. 20, 165.

Lennard-Jones, J.E., 1924, Proc. Roy. Soc. A 106, 463.

Leung, H.K., F.W. Kus, N. McKay and J.P. Carbotte, 1977, Phys. Rev. B 16, 4358.

Levin, B.M., 1967, Mech. Tverd. Tela 1, 88.

Levinson, L.M. and F.R.N. Nabarro, 1967, Acta Met. 15, 785.

Levy, O. and D. Stroud, 1997, Phys. Rev. B 56, 8035.

Li, Y., 1976, Phys. Stat. Sol. (a) 38, 171.

Lidiard, A.B., 1960, Phil. Mag. 5, 1171.

Lifshitz, I.M., 1954, Zh. Eksp. Teor. Fiz. 26, 551.

Lifshitz, I.M., 1956, Nuovo Cim. 3, Suppl., 716.

Lindemann, F.A., 1910, Z. Physik 11, 609.

Logan, J. and M.F. Ashby, 1974, Acta Met. 22, 1047.

Lomer, W.M., 1958, Vacancies and Other Point Defects in Metals and Alloys, Monograph No. 23 (Institute of Metals, London) p. 85.

Loram, J.W., 1986, J. Phys. C 19, 6113.

Loram, J.W., K.A. Mirza, J.R. Cooper and W.Y. Liang, 1993, Phys. Rev. Lett. 71, 1740.

Lord, A.E., Jr., 1967, J. Phys. Chem. Solids 28, 517.

Lorenz, L., 1881, Ann. Physik 13, 422.

Ludwig, W., 1958, J. Phys. Chem. Solids 4, 283.

Lurie, K.A. and A.V. Cherkaev, 1985, J. Opt. Theor. Appl. 46, 571.

MacDonald, W.M. and A.C. Anderson, 1983, in: Thermal Conductivity, Vol. 17, J.G. Hust, ed. (Plenum Press, New York) p. 185.

Mahanty, J., A.A. Maradudin and G.H. Weiss, 1960, Progr. Theor. Phys. 24, 648.

Mair, S.L., 1980, J. Phys. C 13, 2857.

Mannheim, P.D., 1968, Phys. Rev. 165, 1011.

Mañosa, Ll., G.A. Saunders, H. Rahdi, U. Kawald, J. Pelzl and H. Bach, 1992, Phys. Rev B 45, 2224.

Maradudin, A.A., 1974, in: Dynamical Properties of Solids, Vol. 1, G.K. Horton and A.A. Maradudin, eds. (North-Holland, Amsterdam) p. 1.

Maradudin, A.A., 1981, in: Festkörperprobleme 21 (Advances in Solid State Physics), J. Treusch, ed. (Vieweg, Brunswick) p. 25.

Maradudin, A.A. and A.E. Fein, 1962, Phys. Rev. 128, 2589.

Maradudin, A.A. and P.A. Flinn, 1963, Phys. Rev. 129, 2529.

Maradudin, A.A. and R.F. Wallis, 1966, Phys. Rev. 148, 945.

Maradudin, A.A., P. Mazur, E.W. Montroll and G.H. Weiss, 1958, Rev. Mod. Phys. 30, 175.

Maradudin, A.A., P.A. Flinn and R.A. Coldwell-Horsfall, 1961, Ann. Phys. 15, 337.

Maradudin, A.A., E.W. Montroll and G.H. Weiss, 1963, Solid State Physics Suppl 3, Theory of Lattice Dynamics in the Harmonic Approximation (Academic Press, New York).

March, N.H. and J.S. Rousseau, 1971, Crystal Lattice Defects 2, 1.

Marcus, M. and C.-L. Tsai, 1984, Solid State Commun. 52, 511.

Mary, T.A., J.S.O. Evans, T. Vogt and A.W. Sleight, 1996, Science 272, 90.

Matsushita, E. and T. Matsubara, 1978, Progr. Theor. Phys. 59, 15.

Matthiessen, A. and C. Vogt, 1864, Ann. Physik Chem. 122, 19.

Maxwell Garnett, J.C., 1904, Philos. Trans. Roy. Soc. London, 203, 385.

Maxwell Garnett, J.C., 1906, Philos. Trans. Roy. Soc. London, 205, 237.

Mayadas, A.F., M. Shatzkes and J.F. Janak, 1969, Appl. Phys. Lett. 14, 345.

McCombie, C.W. and J. Slater, 1964, Proc. Phys. Soc. 84, 499.

McManus, G.M., 1963, Phys. Rev. 129, 2004.

McMillan, W.L., 1968, Phys. Rev. 167, 331.

Meaden, G.T., 1965, Electrical Resistance of Metals (Heywood, London).

Meister, R. and L. Peselnick, 1966, J. Appl. Phys. 37, 4121.

Men', A.A. and O.A. Sergeev, 1973, High Temp.—High Press. 5, 19.

Mertig, I., G. Pompe and E. Hegenbarth, 1984, Solid State Commun. 49, 369.

Mie, G., 1903, Ann. d. Phys. 11, 657.

Miedema, A.R. and A.K. Niessen, 1983, Calphad 7, 27.

Miles, J.R., T.F. Smith and T.R. Finlayson, 1992, Phil. Mag. B 65, 1215.

Miller, M.N., 1969, J. Math. Phys. 10, 1988.

Milstein, F., H.E. Fang and J. Marschall, 1994, Phil. Mag. A 70, 621.

Milton, G.W., 1980, Appl. Phys. Lett. 37, 300.

Milton, G.W., 1981, Appl. Phys. A26, 125.

Milton, G.W., 1986, in: Homogenization and Effective Moduli of Materials and Media, J.L. Eriksen et al., eds. (Springer-Verlag, New York).

Milton, G.W. and N. Phan-Thien, 1982, Proc. Roy. Soc. A 380, 305.

Misra, R.D., 1940, Proc. Cambridge Phil. Soc. 36, 173.

Mitchel, W., R.S. Newrock and D.K. Wagner, 1980, Phys. Rev. Lett. 44, 426.

Mitchell, M.A., J.R. Cullen, R. Abbundi, A. Clark and H. Savage, 1979, J. Appl. Phys. 50, 1627.

Mizutani, U. and T.B. Massalski, 1980, J. Phys. F 10, 1093.

Molyneux, J.E., 1970 J. Math. Phys. 11, 1172.

Molyneux, J. and M.J. Beran, 1965, J. Math. Mech. 14, 337.

Montroll, E.W., 1942, J. Chem. Phys. 10, 218.

Montroll, E.W., 1943, J. Chem. Phys. 11, 481.

Montroll, E.W., 1944, J. Chem. Phys. 12, 98.

Mooij, J.H., 1973, Phys. Stat. Sol. (a) 17, 521.

Mooney, D.L. and R.G. Steg, 1969, High Temp.—High Press. 1, 237.

Moraitis, G. and F. Gautier, 1977, J. Phys. F 7, 1841.

Moriarty, J.A., 1994, Phys. Rev. B 49, 12431.

Moriarty, J.A. and J.D. Althoff, 1995, Phys. Rev. B 51, 5609.

Moriarty, J.A., D.A. Young and M. Ross, 1984, Phys. Rev. B 30, 578.

Moruzzi, V.L. and C.B. Sommers, 1995, Calculated Electronic Properties of Ordered Alloys: A Handbook (World Scientific, Singapore).

Moruzzi, V.L., A.R. Williams and J.F. Janak, 1977, Phys. Rev. B 15, 2854.

Moruzzi, V.L., J.F. Janak and A.R. Williams, 1978, Calculated Electronic Properties of Metals (Pergamon Press, Oxford).

Motakabbir, K.A. and G. Grimvall, 1981, Phys. Rev. B 23, 523.

Mott, N.F., 1952, Phil. Mag. 43, 1151.

Mott, N.F. and R.W. Gurney, 1940, Electronic Processes in Ionic Crystals (Oxford University Press, London).

Munn, R.W., 1969, Adv. Phys. 18, 515.

Murnaghan, F.D., 1937, Am. J. Math. 59, 235.

Murnaghan, F.D., 1944, Proc. Nat. Acad. Sci. USA 30, 244.

Musgrave, M.J.P., 1970, Crystal Acoustics (Holden Day, San Francisco).

Nagel, S.R., G.S. Grest and A. Rahman, 1984, Phys. Rev. Lett. 53, 368.

Nakajima, S., 1967, Progr. Theor. Phys. 38, 23.

Nakanishi, N., 1979, Prog. Mater. Sci. 24, 143.

Nedoluha, A., 1957, Z. Physik 148, 248.

Nelmes, R.J., 1969, Acta Cryst. A 25, 523.

Nernst, W. and F.A. Lindemann, 1911, Zeitschr. Elektrochem. 17, 817.

Nesi, V. and G.W. Milton, 1991, J. Mech. Phys. Solids 39, 525.

Neuhaus, J., 1999, to be published.

Neuhaus, J., W. Petry and A. Krimmel, 1997, Physica B 234–236, 897.

Neumann, F.E., 1831, Pogg. Ann. 23, 32.

Nielsen, L.F., 1982, Mater. Sci. Eng. 52, 39.

Nishiguchi, N. and T. Sakuma, 1981, Solid State Commun. 38, 1073.

Nordheim, L., 1931, Ann. Physik 9, 607.

Norris, A.N., 1985, Mech. Materials 4, 1.

Novotny, V. and P.P.M. Meincke, 1973, Phys. Rev. B 8, 4186.

Nussbaum, R.H., D.G. Howard, W.L. Ness, and C.F. Steen, 1968, Phys. Rev. 173, 653.

Nye, J.F., 1957, Physical Properties of Crystals (Oxford University Press, Oxford).

Ohashi, Y.H. and K. Ohashi, 1980, Phil. Mag. A 42, 741.

Olijnyk, H. and W.B. Holzapfel, 1985, Phys. Rev. B 31, 4682.

Osborn, J.A., 1945, Phys. Rev. 67, 351.

Ott, H., 1935, Ann. Physik 23, 169.

Ozoliņš, V. and J. Häglund, 1993, Phys. Rev. B 48, 5069.

Ozoliņš, V. and A. Zunger, 1999, Phys. Rev. Lett., 82, 767.

Panova, G.Kh. and B.N. Samoĭlov, 1965, Zh. Eksp. Teor. Fiz. 49, 456 [Sov. Phys.—JETP 22, 320 (1966)].

Papaconstantopoulos, D.A., 1986, Handbook of the Band Structure of Elemental Solids (Plenum Press, New York).

Parrot, J.E. and A.D. Stuckes, 1975, Thermal Conductivity of Solids (Pion, London).

Pathak, K.N. and Y.P. Varshni, 1969, Phys. Lett. 28A, 539.

Paul, B., 1960, Trans, Met. Soc. AIME 218, 36.

Pauling, L., 1960, The Nature of the Chemical Bond (Cornell University Press, Ithaca, NY).

Pearson, W.B., 1972, The Crystal Chemistry and Physics of Metals and Alloys (Wiley, New York).

Peierls, R.E., 1929, Ann. Physik 3, 1055.

Peselnick, L. and R. Meister, 1965, J. Appl. Phys. 36, 2879.

Petrusevich, V.A., V.M. Sergeeva and I.A. Smirnov, 1960, Fiz. Tverd. Tela 2, 2894 [Sov. Phys.—Solid State 2, 2573 (1961)].

Petry, W., A. Heiming, J. Trampenau, M. Alba, C. Herzig, H.R. Schober and G. Vogl, 1991, Phys. Rev. B 43, 10933.
Pettifor, D.G. 1970, J. Phys. C 3, 367.
Phan-Thien, N. and G.W. Milton, 1982, Proc. Roy. Soc. A 380, 333.
Phillips, J.C., 1967, in: Proc. Int. School of Physics, Enrico Fermi, 37, W. Marshall, ed. (Academic Press, New York) p. 22.
Phillips, W.A., 1972, J. Low Temp. Phys. 7, 351.
Pietronero, L., 1987, in: P. Brüesch, 1987, Phonons: Theory and Experiments III (Springer-Verlag, Berlin) p. 200.
Piñango, E.S., S. Vieira and R. Villar, 1983, Solid State Commun. 48, 143.
Pintschovius, L., W. Reichardt and B. Scheerer, 1978, J. Phys. C 11, 1557.
Pintschovius, L., B. Renker, F. Gompf, R. Heid, S.L. Chaplot, M. Haluska and H. Kuzmany, 1992, Phys. Rev. Lett. 69, 2662.
Pleschiutschnig, J., O. Blaschko, and W. Reichardt, 1991, Phys. Rev. B 44, 6794.
Pohl, R.O., 1960, Phys. Rev. 118, 1499.
Poirier, J.P., 1991, Introduction to the Physics of the Earth's Interior (Cambridge University Press, Cambridge).
Pokorny, M. and G. Grimvall, 1984, J. Phys. F 14, 931.
Pottlacher, G., E. Kaschnitz and H. Jäger, 1993, J. Non-Cryst. Solids 156-158, 374.
Potzel, W., W. Adlassnig, U. Närger, Th. Obenhuber, K. Riski and G.M. Kalvius, 1984, Phys. Rev. B 30, 4980.
Powell, R.L., H.M. Roder and W.J. Hall, 1959, Phys. Rev. 115, 314.
Ramdas, A.K., 1995, Solid State Commun. 96, 111.
Rayleigh, J.W., 1892, Phil. Mag. 34, 481.
Rayleigh, Lord, 1894, Theory of Sound (Dover, New York) (reprinted 1945).
Rayleigh, Lord, 1900, Scientific Papers 2 (Cambridge University Press, Cambridge) p. 441.
Read, T.A., 1940, Phys. Rev. 58, 371.
Regan, S.E. and G.J. Morgan, 1992, J. Phys.: Condens. Matter 4, L195.
Reissland, J.A., 1973, The Physics of Phonons (Wiley, London).
Reuss, A., 1929, Z. Angew. Math. Mech. 9, 55.
Ridley, N. and H. Stuart, 1970, Metal Science J. 4, 219.
Rieder, K.H. and W. Drexel, 1975, Phys. Rev. Lett. 34, 148.
Rösch, F. and O. Weis, 1976a, Z. Physik B 25, 101.
Rösch, F. and O. Weis, 1976b, Z. Physik B 25, 115.
Rose, J.H., J. Ferrante and J.R. Smith, 1981, Phys. Rev. Lett. 47, 675.
Rose, J.H., J.R. Smith and J. Ferrante, 1983, Phys. Rev. B 28, 1835.
Rose, J.H., J.R. Smith, F. Guinea and J. Ferrante, 1984, Phys. Rev. B 29, 2963.
Rosén, J. and G. Grimvall, 1983, Phys. Rev. B 27, 7199.
Rosen, B.W. and Z. Hashin, 1970, Int. J. Eng. Sci. 8, 157.
Ross, R.G., P. Andersson, B. Sundqvist and G. Bäckström, 1984, Rep. Prog. Phys. 47, 1347.
Rossiter, P.L., 1987, The Electrical Resistivity of Metals and Alloys (Cambridge University Press, Cambridge).
Roufosse, M.C. and P.G. Klemens, 1973, Phys. Rev. B 7, 5379.

Rowe, J.M., J.J. Rush, N.J. Chesser, K.H. Michel and J. Naudts, 1978, Phys. Rev. Lett. 40, 455.

Rudman, P.S., 1965, Trans. Met. Soc. AIME, 233, 864.

Sadigh, B. and G. Grimvall, 1996, Phys. Rev. B 54, 15742.

Sahimi, M., 1993, Rev. Mod. Phys. 65, 1393.

Sahni, V.C. and P.W.M. Jacobs, 1982, Phil. Mag. A 46, 817.

Sahu, D. and S.D. Mahanti, 1983, Solid State Commun. 47, 207.

Samara, G.A., L.C. Walters and D.A. Northrop, 1967, J. Phys. Chem. Solids 28, 1875.

Saunders, G.A., H.B. Senin, H.A.A. Sidek and J. Pelzl, 1993, Phys. Rev. B 48, 15801.

Schapery, R.A., 1968, J. Composite Materials 2, 380.

Schiøtz, J., F.D. Di Tolla and K.W. Jacobsen, 1998, Nature 391, 561.

Schober, H.R. and P. H. Dederichs, 1981, in: Landolt–Börnstein tables, New Series, Vol. III/13a, K.-H. Hellwege and J.L. Olsen, eds. (Springer-Verlag, Berlin).

Schreiber, E., O.L. Anderson and N. Soga, 1973, Elastic Constants and their Measurement (McGraw-Hill, New York).

Schulgasser, K., 1976, J. Math. Phys. 17, 378.

Schulgasser, K., 1977, J. Phys. C 10, 407.

Schulgasser, K., 1987, J. Mech. Phys. Solids 35, 35.

Schulgasser, K., 1989, J. Mater. Sci. Lett. 8, 228.

Schwartz, J.W. and C.T. Walker, 1966, Phys. Rev. Lett. 16, 97.

Schwartz, J.W. and C.T. Walker, 1967, Phys. Rev. 155, 969.

Seeger, A., 1973, Crystal Lattice Defects 4, 221.

Sellmyer, D.J., 1981, in: Landolt–Börnstein tables, New Series, Vol. III/13a, K.-H. Hellwege and J.L. Olsen, eds. (Springer-Verlag, Berlin).

Sevillano, E., H. Meuth and J.J. Rehr, 1979, Phys. Rev. B 20, 4908.

Shapiro, J.N., 1970, Phys. Rev. B 1, 3982.

Shian Peng and G. Grimvall, 1994a, J. Nucl. Mater. 210, 115.

Shian Peng and G. Grimvall, 1994b, J. Phys. Chem. Solids 55, 707.

Shukla, M.M. and N.T. Padial, 1973, Rev. Bras. Fis. 3, 39.

Shukla, R.C. and E.R. Cowley, 1971, Phys. Rev. B 3, 4055.

Shukla, R.C. and L. Wilk, 1974, Phys. Rev. B 10, 3660.

Simmons, G. and H. Wang, 1971, Single Crystal Elastic Constants and Calculated Aggregate Properties: A Handbook (MIT Press, Cambridge, MA).

Simmons, R.O. and R.W. Balluffi, 1960, Phys. Rev. 117, 52.

Skriver, H.L., 1985, Phys. Rev. B 31, 1909.

Slack, G.A., 1957, Phys. Rev. 105, 832.

Slack, G.A., 1979, in: Solid State Physics, Vol. 34, H. Ehrenreich, F. Seitz and D. Turnbull, eds. (Academic Press, New York) p. 1.

Slack, G.A. and D.W. Oliver, 1971, Phys. Rev. B 4, 592.

Slater, J.C., 1940, Phys. Rev. 57, 744.

Smargiassi, E. and P.A. Madden, 1995, Phys. Rev. B 51, 129.

Smith, T.F. and T.R. Finlayson, 1976, J. Phys. F 6, 709.

Soffer, S.B., 1967, J. Appl. Phys. 38, 1710.

Sommerfeld, A. and H. Bethe, 1933, Handbuch der Physik 24:2 (Springer-Verlag, Berlin) p. 333.

Sondheimer, E.H., 1950, Proc. Roy. Soc. A 203, 75.

Sondheimer, E.H., 1952, Adv. Phys. 1, 1.

Speich, G.R., A.J. Schwoeble and B.M. Kapadia, 1980, ASME J. Appl. Mech. 47, 821.

Srivastava, G.P., 1990, The Physics of Phonons (Adam Hilger, Bristol).

Stauffer, D., 1979, Phys. Rep. 54, 1.

Stauffer, D., and A. Aharony, 1992, Introduction to Percolation Theory (Taylor and Francis, London).

Steinemann, S.G., 1978, J. Mag. Mag. Mats. 7, 84.

Steinemann, S.G., 1979, J. Mag. Mag. Mats. 12, 191.

Stern, E.A., and Ke Zhang, 1988, Phys. Rev. Lett. 60, 1872.

Stesmans, A., 1982, Solid State Commun. 44, 727.

Stillinger, F.H. and T.A. Weber, 1980, Phys. Rev. B 22, 3790.

Stoner, E.C., 1938, Proc. Roy. Soc. A 165, 372.

Stoner, E.C., 1945, Phil. Mag. 36, 803.

Stratton, J.A., 1941, Electromagnetic Theory (McGraw-Hill, New York).

Stratton, R., 1953, Phil. Mag. 44, 519.

Stratton, R., 1962, J. Chem. Phys. 37, 2972.

Straub, G.K., J.B. Aidun, J.M. Wills, C.R. Sanchez-Castro and D.C. Wallace, 1994, Phys. Rev. B 50, 5055.

Stripp, K.F. and J.G. Kirkwood, 1954, J. Chem. Phys. 22, 1579.

Stroud, D., 1975, Phys. Rev. B 12, 3368.

Stroud, D. and N.W. Ashcroft, 1972, Phys. Rev. B 5, 371.

Strössner, K., W. Henkel, H.D. Hochheimer and M. Cardona, 1983, Solid State Commun. 47, 567.

Suck, J.-B., H. Rudin, H.-J. Güntherodt, H. Beck, J. Daubert and W. Gläser, 1980, J. Phys. C 13, L167.

Suck, J.-B., H. Rudin, H.-J. Güntherodt and H. Beck, 1981, J. Phys. C 14, 2305.

Sundqvist, B., J. Neve and Ö. Rapp, 1985, Phys. Rev. B 32, 2200.

Swenson, C.A., 1996, Phys. Rev. B 53, 3669.

Taillefer, L., G.G. Lonzarich and P. Strange, 1986, J. Magn. & Magn. Mater. 54–57, 957.

Takeno, S., 1963, Progr. Theor. Phys. 30, 144.

Taylor, B., H.J. Maris and C. Elbaum, 1971, Phys. Rev. B 3, 1462.

Taylor, R., 1991, in: International Encyclopaedia of Composites, S.M. Lee, ed., Vol. 5 (VCH, New York) p. 530.

Thiessen, M., 1986, Int. J. Thermophys. 7, 1183.

Thomsen, L., 1972, J. Geophys. Res. 77, 315.

Thomsen, L. and O.L. Anderson, 1969, J. Geophys. Res. 77, 981.

Thurston, R.N., 1965, Proc. IEEE 53, 1320.

Thurston, R.N. and K. Brugger, 1964, Phys. Rev. 133, A1604. (Erratum Phys. Rev. 135, AB3).

Tiwari, M.D. and B.K. Agrawal, 1973a, J. Phys. F 3, 2051.

Tiwari, M.D. and B.K. Agrawal, 1973b, Phys. Rev. B 7, 4665.

Tiwari, M.D. and B.K. Agrawal, 1973c, Phys. Rev. B 8, 1397.

Tiwari, M.D., G. Thummes and H.H. Mende, 1981, Phil. Mag. B 44, 63.

Tomlinson, P.G., 1979, Phys. Rev. B 19, 1893.

Torquato, S., 1991, Appl. Mech. Rev. 44, 37.

Torquato, S. and M.D. Rintoul, 1995, Phys. Rev. Lett. 75, 4067.

Tosi, M.P, 1964, in: Solid Sate Physics, Vol. 16, F. Seitz and D. Turnbull, eds. (Academic Press, New York) p.1.

Tosi, M.P. and F.G. Fumi, 1963, Phys. Rev. 131, 1458.

Toth, L.E., 1971, Transition Metal Carbides and Nitrides (Academic Press, New York) p. 143.

Touloukian, Y.S. and E.H. Buyco, 1970, Specific Heat. Thermophysical Properties of Matter, Vols. 4, 5 (Plenum Press, New York).

Touloukian, Y.S., R.W. Powell, C.Y. Ho and P.G. Klemens, 1970, Thermal Conductivity. Thermophysical Properties of Matter, Vols. 1, 2 (Plenum Press, New York).

Touloukian, Y.S., R.W. Powell, C.Y. Ho and M.C. Nicholaou, 1973, Thermal Diffusivity. Thermophysical Properties of Matter, Vol. 10 (Plenum Press, New York).

Touloukian, Y.S., R.K. Kirby, R.E. Taylor and P.D. Desai, 1975, Thermal Expansion. Thermophysical Properties of Matter, Vol. 12 (Plenum Press, New York).

Touloukian, Y.S., R.K. Kirby, R.E. Taylor and T.Y.R. Lee, 1977 Thermal Expansion. Thermophysical Properties of Matter, Vol. 13 (Plenum Press, New York).

Truesdell, C. and R.A. Toupin, 1960, in: Handbuch der Physik, Vol. 3/1, S. Flügge, ed. (Springer-Verlag, Berlin) p. 226.

Tsang, T.-W.E., K.A. Gschneidner, Jr., F.A. Schmidt and D.K. Thome, 1985, Phys. Rev. B 31, 235, 6095(E).

Tsuei, C.C., 1986, Phys. Rev. Lett. 57, 1943.

Tu Hailing, G.A. Saunders, Y.K.Y. Yoğurtçu, H. Bach and S. Methfessel, 1984, J. Phys. C 17, 4559.

Turley, J. and G. Sines, 1971, J. Phys. D 4, 264.

Turner, S.P., R. Taylor, F.H. Gordon and T.W. Clyne, 1993, J. Mater. Sci. 28, 3969.

Ullmaier, H., ed., 1991, Landolt–Börnstein tables, New Series III, Vol. 25, Atomic Defects in Metals (Springer-Verlag, Berlin).

Vaks, V.G. and A.V. Trefilov, 1988, J. Phys. F 18, 213.

Vaks, V.G. and A.V. Trefilov, 1991, J. Phys. Condens. Matter 3, 1389.

van Attekum, P.M.Th.M., P.H. Woerlee, G.C. Verkade and A.A.M. Hoeben, 1984, Phys. Rev. B 29, 645.

van Beek, L.K.H., 1967, Progr. Dielectrics, Vol. 7, J.B. Birks, ed., p. 69.

van de Walle, A., G. Ceder and U.V. Waghmare, 1998, Phys. Rev. Lett. 80, 4911.

van den Beukel, A. and S. Radelaar, 1983, Acta Met. 31, 419.

Varley, J.H.O., 1956, Proc. Roy. Soc. 237, 413.

Varotsos, P.A. and K.D. Alexopoulos, 1986, Thermodynamics of Point Defects and their Relation with Bulk Properties (North-Holland, Amsterdam).

Vegard, L., 1921, Z. Physik 5, 17.

Villars, P. and L. D. Calvert, 1985, Pearson's Handbook of Crystallographic Data for Intermetallic Phases, Vols. 1–4, 2nd edn. (ASM International, Metals Park, OH).

Vineyard, G.H. and G.J. Dienes, 1954, Phys. Rev. 93, 265.

Voigt, W., 1910, Lehrbuch der Kristallphysik (Teubner, Berlin) (reprinted 1928).

Wachtman, J.B., Jr., W.E. Tefft, D.G. Lam, Jr. and C.S. Apstein, 1961, Phys. Rev. 122, 1754.

Wallace, D.C., 1970, in: Solid State Physics, Vol. 25, H. Ehrenreich, F. Seitz and D. Turnbull, eds. (Academic Press, New York) p. 301.

Wallace, D.C., 1972, Thermodynamics of Crystals (Wiley, New York).

Wallace, D.C., 1997, Phys. Rev. E 56, 1981.

Wallace, D.C., B.L. Holian, J.D. Johnson and G.K. Straub, 1982, Phys. Rev. A 26, 2882.

Waller, I., 1923, Z. Physik 17, 398.

Waller, I., 1925, Dissertation, Uppsala (Sweden).

Wallis, R.F., 1975, in: Dynamical Properties of Solids, Vol. 2, G.K. Horton and A.A. Maradudin, eds. (North-Holland, Amsterdam) p. 441.

Walpole, L.J., 1966, J. Mech. Phys. Solids 14, 151.

Walpole, L.J., 1969, J. Mech. Phys. Solids 17, 235.

Walpole, L.J., 1981, Adv. Appl. Mech. 21, 169.

Wang, C.Z., C.T. Chan and K.M. Ho, 1992, Phys. Rev. B 45, 12227.

Wang, C.Z., K.M. Ho and C.T. Chan, 1993, Phys. Rev. B 47, 14835.

Warren, B.E., 1969, X-ray Diffraction (Addison-Wesley, Reading, MA) p. 238.

Watt, J.P., 1979, J. Appl. Phys. 50, 6290.

Watt, J.P., 1980, J. Appl. Phys. 51, 1520.

Watt, J.P. and L. Peselnick, 1980, J. Appl. Phys. 51, 1525.

Watt, J.P., G.F. Davies and R.J. O'Connell, 1976, Rev. Geoph. Space Phys. 14, 541.

Watts, R.K., 1977, Point Defects in Crystals (Wiley, New York).

Weaire, D., M.F. Ashby, J. Logan and M.J. Weins, 1971, Acta Met. 19, 779.

Weiner, D., A. van den Beukel and P. Penning, 1975, Acta Met. 23, 783.

Westrum, E.F. Jr. and N. Komada, 1986, Thermochim. Acta 109, 11.

White, G.K., 1969, in: Thermal Conductivity, R.P. Tye, ed. (Academic Press, London) p. 69.

White, G.K., J.G. Collins, J.A. Birch, T.F. Smith and T.R. Finlayson, 1978, in: Transition Metals, M.J.G. Lee, J.M. Perz and E. Fawcett, eds. (Inst. Phys. Conf. Ser. No. 39) p. 420.

White, R.M., 1970, Quantum Theory of Magnetism (McGraw-Hill, New York).

Wiedemann, G. and R. Franz, 1853, Ann. Physik 89, 497.

Wiener, O., 1912, Abh. Math.-Physik. Kl. Königl. Sächs. Ges. Wiss. 32, 509.

Wiesmann, H., M. Gurvitch, H. Lutz, A. Ghosh, B. Schwarz, M. Strongin, P.B. Allen and J.W. Halley, 1977, Phys. Rev. Lett. 38, 782.

Willis, B.T.M. and A.W. Pryor, 1975, Thermal Vibrations in Crystallography (Cambridge University Press, London).

Willis, J.R., 1981, Adv. Appl. Mech. 21, 1.

Wills, J.M., O. Eriksson, P. Söderlind and A.M. Boring, 1992, Phys. Rev. Lett. 68, 2802.

Wilson, A.H., 1965, The Theory of Metals, 2nd ed. (Cambridge University Press, Cambridge).

Wohlfarth, E.P., 1974, Phys. Stat. Sol. (a) 25, 285.

Wolf, G.H. and R. Jeanloz, 1984, J. Geophys. Res. 89, No. B9, 7821.

Wolfe, J.P., 1980, Physics Today 33, no. 12, 44.

Wollenberger, H.J., in: R.W. Cahn and P. Haasen, eds., 1996, Physical Metallurgy, 4th ed. (Elsevier, Amsterdam) p. 1621.

Wu, T.T., 1966, Int. J. Solids Struct. 3, 1.

Yamada, Y., N. Hamaya, J.D. Axe and S.M. Shapiro, 1984, Phys. Rev. Lett. 53, 1665.

Yates, B., 1972, Thermal Expansion (Plenum Press, London).

Yates, B., M.J. Overy and O. Pirgon, 1975, Phil. Mag. 32, 847.

Yin, M.T. and M.L. Cohen, 1984, Phys. Rev. B 29, 6996.

Young, D.A., 1991, Phase Diagrams of the Elements (University California Press, Berkeley).

Young, D.A. and B.J. Alder, 1974, J Chem. Phys. 60, 1254.

Yussouff, M. and J. Mahanty, 1966, Proc. Phys. Soc. 87, 689.

Yussouff, M. and J. Mahanty, 1967, Proc. Phys. Soc. 90, 519.

Zeller, R.C. and R.O. Pohl, 1971, Phys. Rev. B 4, 2029.

Zen, E-an., 1956, Amer. Min. 41, 523.

Zener, C., 1948, Elasticity and Anelasticity of Metals (University Chicago Press, Chicago).

Ziman, J.M., 1960, Electrons and Phonons (Clarendon Press, Oxford).

Ziman, J.M., 1979, Models of Disorder (Cambridge University Press, Cambridge).

Zimmerman, R. W., 1992, Mech. Res. Commun. 19, 563.

Zywietz, A., K. Karch and F. Bechstedt, 1996, Phys. Rev. B 54, 1791.

AUTHOR INDEX *

* This list also includes the authors referred to by "et al" in the text.

This Page Intentionally Left Blank

SUBJECT INDEX

This Page Intentionally Left Blank

MATERIALS INDEX *

* Single data points in graphs, and entries in tables on pp. 373–376 non included here.